A Comparative Study of the Pathology and Pathophysiology of Severe Malaria in a Non-Human Primate Model

Thesis

A Comparative Study of the Pathology and Pathophysiology of Severe Malaria in a Non-Human Primate Model

Eric Desombre Lombardini, VMD, MSc, DACVPM, DACVP

OU Student Identifier C5769942

Mahidol-Oxford Tropical Medicine Research Unit (MORU)
3rd Floor, 60th Anniversary Chalermprakiat Building
Faculty of Tropical Medicine, Mahidol University
420/6 Ratchawithi Rd., Ratchathewi District
Bangkok 10400 Thailand

Submitted in total fulfilment of the requirements for the research degree of Doctor of Philosophy

Date: 8 April 2017

The Open University, UK

Declaration of conflicting interests:

E. D. Lombardini is a Lieutenant Colonel in the United States Army. The opinions or assertions herein are those of the author and do not necessarily reflect the view of the United States Department of the Army or The United States Department of Defense.

Language disclaimer:

E.D. Lombardini is a United States citizen, and for the facility of the authorship of this dissertation, “American” English spelling of medical terminology has been employed throughout the text.

Preface:

- Table of Contents
- List of Tables
- List of Figures
- Abstract
- Collaborations
- Published manuscripts, presentations and posters/abstracts in association with dissertation
- Acknowledgements
- Abbreviations

Table of Contents:

List of Figures:

List of Tables:

Abstract:

With the rise in plasmodial drug resistance throughout the world, a dwindling arsenal of anti-malarials and a predilection for use of less than ideal murine models, the need for effective, applicable and established animal models through which to understand severe malarial disease and test potential treatments is becoming increasingly crucial. *Plasmodium coatneyi* was discovered in the Philippines in the early 1960s in Rhesus macaque monkeys and has been evaluated sporadically as a potential platform for comparative studies of *Plasmodium falciparum* induced severe and cerebral malaria in humans. Using 30 years' worth of archival samples at the Armed Forces Research Institute of Medical Sciences in Bangkok, Thailand, compounded with data and material from a series of prospective experimental studies, the work in this thesis sought to fully characterize and describe the pathology and pathobiology of the *P. coatneyi*/Rhesus macaque model. This included a thorough examination of the parasite host interaction, clinical symptomology, hematology and clinical pathology, gross pathology, histopathology, immunohistochemistry, cerebrospinal fluid cytokine profiles, transmission and scanning electron microscopy and atomic force microscopy of the disease in 45 adult rhesus macaques. The study further compared *P. coatneyi* with existing *P. falciparum* infected human material maintained at the National University of Singapore's Vivax laboratory and Oxford University's Ultrastructural Morphology Group, Nuffield Division of Clinical Laboratory Sciences. The study culminated in a successful clinical drug trial which evaluated the efficacy of varying doses of methylene blue as a radical cure for malaria in this non-human primate model. In many ways, the model mirrors *P. falciparum*, however the benefit of this evaluation is that it highlights not only the similarities but also the divergences. The successful completion of this description of the pathology and pathobiology of the *P. coatneyi*/Rhesus macaque model of severe and cerebral malaria adds a complex but effective animal model to the armamentarium in the ongoing war against malaria.

Collaborations/Contributions:

1. Mahidol-Oxford Tropical Medicine Research Unit (MORU), Bangkok, Thailand
2. Armed Forces Research Institute of Medical Sciences (AFRIMS), Department of Veterinary Medicine, Bangkok, Thailand
3. National University of Singapore, Yong Loo Lin School of Medicine, Department of Microbiology and Immunology, Vivax malaria laboratory, Singapore, Singapore
4. Oxford University, John Radcliffe Hospital, Nuffield Division of Clinical Laboratory Sciences, Ultrastructural Morphology Group, Oxford, United Kingdom
5. Chulalongkorn University, School of Veterinary Medicine, Department of Pathology, Bangkok, Thailand
6. Walter Reed Army Institute of Research, Experimental Therapeutics Department, Forest Glen, Maryland, USA
7. Military Malaria Research Program (MMRP), United States Army, Walter Reed Army Institute of Research, Forest Glen, Maryland, USA

A range of individuals assisted in many aspects of the study. Their specific contribution is described in the following, effort prioritized in order of precedence:

a. Study design: Lombardini E, Turner G, Brown A, Ruck R, Imbersbin R
b. Antemortem and Autopsy sample/data collection: Lombardini E, Chumpolkulwong K, Imbersbin R, Rungojn A
c. Retinoscopy: Plewes K, Maude R, Lombardini E
d. Parasitemia calculations/staging: Tayamun S, Inamnuay L, Lombardini E
e. Cytological/Histopathologic slide generation: Tayamun S, Inamnuay L, Lombardini E
f. Cytological/Histopathological slide interpretation: Lombardini E, Turner G
g. IHC slide generation: Sunyakumthorn P, Lombardini E
h. IHC slide interpretation: Lombardini E, Turner G
i. TEM grid generation/image capture: Kaewamatawong T, Lombardini E, Ferguson D
j. TEM image interpretation: Lombardini E, Ferguson D

k. SEM image generation: Malleret B
l. SEM image interpretation: Malleret B, Lombardini E, Ferguson D
m. AFM image generation: Zhao R, Lombardini E
n. AFM interpretation: Lombardini E, Zhao R, Russell B
o. Micropipette assays: Russell B, Zhao R, Lombardini E
p. Biofluidic assays: Russell B, Zhao R, Lombardini E
q. Dissertation writing: Lombardini E
r. Dissertation editing: Turner G, Brown A

The following individuals instructed the author in various technical aspects of the study:

a. Inamnuay L: Parasitemia calculations/staging
b. Sunyakumthorn P: IHC slide generation
c. Kaewamatawong T, Ferguson D: TEM image generation
d. Russell B, Zhao R: AFM; micropipette assay; biofluidic assay
e. Malleret B: SEM image generation

Published manuscripts, lectures and posters/abstracts in association with dissertation:

1. Manuscripts (Published or in preparation):

a. Lombardini ED, Gettayacamin M, Turner GD, Brown AE. A Review of *Plasmodium coatneyi*-Macaque Models of Severe Malaria. Vet Pathol. 2015 Nov; 52(6):998-1011.

b. Lombardini ED, Tayamun S, Inamnuay L, Kaewamatawong T, Im-ersbin R, Sunyakumthorn P, Burke R, Ferguson DJ, Weina P, White NJ, Day NPJ, Brown AE, Turner GDH. The Histopathology of Severe Malaria in the *Plasmodium coatneyi* infected-splenectomized Rhesus Macaque Model. Manuscript draft currently circulated to co-authors.

c. Lombardini ED, Malleret B, Rungojn A, Popruk N, Kaewamatawong T, Brown AE, Turner GDH, Russell B, Ferguson DJP. Ultrastructural characterization of *Plasmodium coatneyi* infection In-Vivo with comparison to *Plasmodium falciparum*. Manuscript draft currently circulated to co-authors.

d. Lombardini ED, Zhao R, Malleret B, Suwanarusk R, Sunyakumthorn P, Im-ersbin R, Inamnuay L, Brown AE, Turner GDH, Russell B. Comparative atomic force microscopy of *Plasmodium coatneyi* infected

erythrocytes with those features described in *Plasmodium falciparum*. Manuscript currently in preparation.

e. Lombardini ED, Ruck R, Paktiya, Im-ersbin R, Inamnuay L, Chumpolkulwong K, Suwit S, Brown AE, Turner GDH, Ohrt C, Weina P, Burke R, Read L, Hickman M, Smith PL, Paris R. Clinical drug efficacy trial of methylene blue as a radical cure anti-malarial compound in the *Plasmodium coatneyi* Rhesus macaque model for severe malaria. Manuscript draft currently circulated to co-authors.

f. Plewes K, Maude R, Brown AE, Turner GDH, Lombardini ED. Retinoscopy in Plasmodium coatneyi infected rhesus macaques, preliminary findings. Manuscript currently in preparation.

2. Lectures

a. Comparative pathology of *Plasmodium coatneyi*-Rhesus macaque model of severe malaria; Invited speaker; Louisiana State University pathobiology Seminar Series, Baton Rouge, Louisiana, USA, 2016

b. Comparative pathology of *Plasmodium coatneyi*-Rhesus macaque model of severe malaria; Invited speaker; Evans Community Army Hospital (EACH) Grand Rounds series, Colorado Springs, Colorado, USA, 2016

c. Comparative pathology of Animal Models of Cerebral Malaria; Invited speaker; United States Army Public Health Command, officer professional development series, Colorado Springs, Colorado, USA, 2016

d. Comparative pathology of *Plasmodium coatneyi*-Rhesus macaque model of severe malaria; Mahidol Oxford Research Unit Seminar Series, Bangkok, Thailand, 2015

e. Comparative Pathology of Animal Models of Cerebral Malaria; Invited speaker; National University of Singapore, Singapore, Singapore, 2014

f. Comparative Pathology of Animal Models of Cerebral Malaria; Trilateral United States, China, Thailand conference on military tropical medicine, Bangkok, Thailand, 2013

g. Comparative Pathology of Animal Models of Cerebral Malaria; Keynote speaker; Asian Society of Veterinary Pathology, Kuala Lumpur, Malaysia, 2013

3. Posters/conference presentations:

a. Immunopathology assessment of central nervous system in *Plasmodium coatneyi*-infected rhesus macaque as a cerebral malaria model. Sunyakumthorn P, Tayamun S, Inamnuay L, Im-erbsin R, Burke RL, Brown AE, Turner GDH, Lombardini ED. American Society for Tropical Medicine and Hygiene, Malaria: Biology and Pathogenesis I. Philadelphia, PA, USA, 2015

b. Ex vivo study of malaria parasite infected blood with Microfluidics. Lombardini E, Russell B. 15th International Congress of Biorheology and 8th International Conference on Clinical Hemorheology. Seoul, Korea, 2015.

c. Diversity of biomechanical and nanostructural changes to human and cynomolgus monkey red cells infected with malaria parasites. Zhang R, Lombardini E, Amir A, Snounou G, Renia L, Cooke BM, Fong MY, Lau YL, Nosten F and Russell B. 15th International Congress of Biorheology and 8th International Conference on Clinical Hemorheology Seoul, Korea 2015.

d. Animal Models of Kidney Injury in Severe Malaria; American Society for Tropical Medicine and Hygiene, Symposium: Acute Kidney Injury in Severe Malaria: Clinical Presentation, Treatment and Pathophysiology, New Orleans, LA, 2014

e. Renal Pathology in the Rhesus Macaque/*Plasmodium coatneyi* model for Severe Malaria. Lombardini E, Im-erbsin R, Weina P, Brown A and Turner G. American Society for Tropical Medicine and Hygiene. New Orleans, LA, 2014.

Acknowledgements:

First and absolutely foremost, I would not have been able to complete even the smallest portion of this study without the extraordinary and unyielding support and love of my wife, Aura, and our son, Tristan. This labor is dedicated to Aura and Tristan. Sei la mia vita, la mia inspiratione, e la mia motivazione.

My supervisory team.

Dr. Gareth Turner is an extraordinary individual, a keen mind and a consummate scientist. This project began from the spark that he lit and from there took flame. I will always be in awe of the effort he has taken in nurturing me, in guiding me and in assisting me in getting this across the finish line. You have been a stalwart and dedicated mentor, a persistent encouragement, a colleague in science and a friend, to whom I am forever indebted.

Dr. Art Brown (Colonel retired), the ideal of the quiet professional, his persistent demonstration of unwavering support and guidance has been a solace throughout this project. A clear mind able to see through the chaos. I could not be more grateful for your support and mentorship.

Colonel Peter Weina, my colleague, mentor and friend in war and peace. Thank you for your dedication to this effort. We have shared the hardship of the desert and I am in your debt for helping me through the jungle of this effort.

My AFRIMS colleagues.

Dr. Piyanate Sunyakumthorn. Yui, with your perpetual smile and your extraordinary work effort, you have been the best possible colleague I could have asked for in shaping, molding and crafting the science of this study as well as in participating significantly in analyzing the data with me. You have been a friend, a collaborator and a teacher.

Mrs. Laksanee Inamnuay. Pi Meow. I could not have done this without your herculean efforts. Thank you.

Khun Sujitra, Khun Artharee and Khun Youee. You were the best staff I could have hoped for. Dedicated, driven, positive, proactive and kind. I am so very grateful to all three of you.

Dr. Rawiwan Im-Erbsin and **Dr. Kesara Chumpolkulwong**. Your professionalism is unparalleled. *P. coatneyi* presented us with extreme challenges, but you surmounted them with seemingly effortless ease.

Lieutenant Colonel Robin Burke. Robin's cool demeanor and even temper helped me drag this project through obstacle after obstacle, challenge after challenge and through the frustrations to this final accomplishment. Thank you.

Colonel William Geesey and **Colonel Christopher Soltis**. The leadership of AFRIMS. Without your permission, this could never have happened. You gave the opportunity to sink or swim, and I hope that this is evidence of my gratitude for your willingness to take a chance in me. You have my enduring thanks.

My Public Health Command leadership.

Major General Thomas R. Tempel, **Colonel Robert von Tersch** and **Colonel Jean Barido**. My sincere thanks for permitting me to tackle the final stages of the dissertation. I endeavored to ensure that the mission never faltered in spite of the having to take so much leave to finish what I had started.

My WRAIR colleagues.

Lieutenant Colonel Lisa Read. Lisa, you have my thanks for helping me find the support I needed at WRAIR and for being a champion for *Plasmodium coatneyi*, in spite of its unpopularity.

Colonel Robert Paris. As the United States Army's lead on malaria, you were willing to invest in the study of a parasite that had gathered cobwebs and lapsed from the limelight, but it is thanks to your support that this project was brought to fruition and so many more opportunities to delve into the secrets of the parasite and the disease have arisen.

<u>My Singapore colleagues</u>.

Dr. Bruce Russell. Bruce deserves an extraordinary recognition. Your unbounded enthusiasm, steadfast and loyal friendship, and extremely keen mind, all were key elements in so many aspects of this project. Your curiosity and scientific acumen is contagious and I am so thankful for having gotten swept along in its current.

Dr. Rossarin Suwanarusk, **Dr. Benoit Malleret** and **Dr. Rosemary Zhao**. Thank you for your dedicated efforts, your consummate collegial support and your partnership.

<u>My MORU and Oxford colleagues</u>.

Professor Nick White and **Professor Nick Day**. You both have my thanks for opening the doors to MORU wide, for your mentorship, guidance and consummate support. I am grateful to you both.

Dr. Stuart Blacksell. A man with whom I would share a beer on the Mekong any day. Stuart is the essence of professionalism, tempered with a kind heart, a diplomatic soul and the burning drive of science. You are a true gentleman and it has been a genuine pleasure to work with you in the field and on this project.

Drs. Richard Maude and **Katherine Plewes**. I only wish we had been able to elaborate the retinal piece further. Thank you for your efforts.

As is always done in the film credits, it is often the last name that deserves distinct recognition. A very special thanks to **Professor David Ferguson**. My short stint at Oxford under your tutelage was a

shining moment in what appeared to be a dark expanse of this dissertation. Yours and Mrs. Ferguson's Scottish hospitality and warmth in sharp contrast to the biting English winter.

Finally, I would like to underscore my sincere and genuine appreciation to the generations of researchers and scientists who have labored towards a greater understanding of *P. coatneyi* malaria, beginning with the discovery of Dr. Eyles, to the extraordinary efforts of the staff of the Veterinary Medicine Department of AFRIMS and to constructive discussions and advice of Professor Nick White, the enthusiasm of personnel at MORU, NUS and the University of Oxford, and grant support from the Wellcome Trust of Great Britain (grant 089275/Z/09/Z).

Ultrastructure: This work was supported with grants from WRAIR-ET, AFRIMS, The British Council (travel award)

Abbreviations:

ACT: Artemisinin-based Combination Therapies

ACVP: American College of Veterinary Pathologists

AFM: Atomic Force Microscopy

AFRIMS: Armed Forces Research Institute of Medical Sciences

AI: Albumin Index

AKI: Acute Kidney Injury

ALP: Alkaline phosphatase

ALT: Alanine transaminase

ARDS: Acute Respiratory Distress Syndrome

AS: Artesunate

AUC: Area under the curve

AV: Attending Veterinarian

β-APP: Beta-amyloid precursor protein

BBB: Blood Brain Barrier

BNP: B-type natriuretic peptide

C: Celsius

CBC: Complete Blood Count

CD3: Cluster of differentiation 3

CD36: Cluster of differentiation 36

CD61: Cluster of differentiation 61

CD68: Cluster of differentiation 68

CM: Cerebral Malaria

CPK: Creatinine phosphokinase

CQ: Quantitation cycle

CQ: Chloroquine

csA: Cell adhesion molecules

CSF: Cerebrospinal Fluid

CTRL: Control

DIC: Disseminated intravascular coagulopathy

DNA: Deoxyribonucleic acid

EDTA: Ethylenediaminetetraacetic acid

ELISA: Enzyme-linked immunosorbent assay

EPO: Erythropoietin

F: Fahrenheit

FAS/ CD95L: Fas ligand

FDP: Fibrin degradation product

FP: Ferriprotoporphyrin IX

G-CSF: Granulocyte-colony stimulating factor

GFAP: Glial fibrillary acidic protein

GLUC: Glucose

GM-CSF: Granulocyte-macrophage colony-stimulating factor

GMP: Good Manufacturing Practices

HE: Hematoxylin and Eosin

HCl: Hydrogen chloride

Hgb: Hemoglobin

HPF: High Powered Fields

HRP-2: Histidine-rich protein II

IACUC: Institutional Animal Care and Use Committee

Iba1: ionized calcium binding adapter molecule 1

ICAM-1: Intercellular adhesion molecule 1

IFNγ: Interferon-gamma

IHC: Immunohistochemistry

IQR: Interquartile Range

IL-1β: Interleukin-1 Beta

IL-1ra: Interleukin-1 receptor antagonist

IL-2: Interleukin-2

IL-4: Interleukin-4

IL-5: Interleukin-5

IL-6: Interleukin-6

IL-8: Interleukin-8

IL-10: Interleukin-10

IL-12/23 (p40): Interleukin-12/23 (p40)

IL-13: Interleukin-13

IL-15: Interleukin-15

IL-17: Interleukin-17

IL-18: Interleukin-18

ILIR: In-House Laboratory Independent Research (Uniformed University of the Health Sciences)

IM: Intramuscular

IND: Investigational New Drug

IQR: Interquartile range

iRBC: Infected Red Blood Cell; equivalent to parasitized RBC

IU: International Units

IV: Intravenous

M. mulatta: *Macaca mulatta* (Rhesus macaque)

M. nemestrina: *Macaca nemestrina* (Pig tailed macaque)

M. arctoides: *Macaca arctoides* (Stump tailed macaque)

M. fascicularis: *Macaca fascicularis* (Cynomolgus macaque)

M. fuscata: *Macaca fuscata* (Japanese Macaque)

MB: Methylene Blue

MCP-1: Monocyte chemoattractant protein-1

MIP-1α: Macrophage inflammatory protein 1 alpha

MIP-1β: Macrophage inflammatory protein-1 beta

M:E: Myeloid Erythroid ratio

Mg: Milligram

Ml: Milliliter

MORU: Mahidol Oxford Research Unit

MRI: Magnetic resonance imaging

NA: Not available

NADPH: Nicotinamide adenine dinucleotide phosphate

ND: Not Determined

NE: Neutrophil elastase

NHP: Non-Human Primate

NSL: No significant lesions

NT-proBNP: N-terminal pro b-type natriuretic peptide

OOR: Out of Range

PAS: Periodic acid–Schiff

PDGF: Platelet-derived growth factor

P. bergei: *Plasmodium bergei*

P. coatneyi: *Plasmodium coatneyi*

P. cynomolgi: *Plasmodium cynomolgi*

P. falciparum: *Plasmodium falciparum*

P. fieldi: *Plasmodium fieldi*

P. fragile: *Plasmodium fragile*

P. hylobati: *Plasmodium hylobati*

P. inui: *Plasmodium inui*

P. knowlsei: *Plasmodium knowlsei*

P. ovale: *Plasmodium ovale*

P. reichenowi: *Plasmodium reichenowi*

P. simium: *Plasmodium simium*

P. vivax: *Plasmodium vivax*

P. yoelli: *Plasmodium yoelli*

PGE-2: Prostaglandin E2

Pg/Ml: Picogram/milliliter

PI: Principal Investigator

QD: Quinidine

qPCR: quantitative real time PCR

RANTES: Regulated on activation, normal T cell expressed and secreted

RBC: Red Blood Cell

RNA-seq: RNA Sequencing

rRNA: Ribosomal ribonucleic acid

sCD40L: Soluble cluster of differentiation 40-ligand

SEATO: South East Asia Treaty Organization

SEM: Scanning Electron Microscopy

SHIV: Simian/Human Immunodeficiency Virus

SI: Sequestration index

SIV: Simian Immunodeficiency Virus

sTNFR1 and sTNFR2: Soluble tumor necrosis factor receptors

Spp.: Species

SRV: Simian Retrovirus

STLV-1: Simian T-Cell Leukemia Virus

TD: Treatment Day

TEM: Transmission Electron Microscopy

TGF-α: Transforming growth factor alpha

TNF-α: Tumor necrosis factor-alpha

TSP: Thrombospondin

Tx: Treatment

USAMRMC: US Army Medical Research and Materiel Command

USP: United States Pharmacopeia

VEGF: Vascular endothelial growth factor

WBC: White Blood Count

WHO: World Health Organization

WTSS: Whole Transcriptome Shotgun Sequencing

WRAIR: Walter Reed Army Institute of Research

Chapter 1: Introduction and Literature Review

1.1 **Overall research aims of this thesis:**

The pathology and pathophysiology of fatal malaria remain areas of active research and controversy. The recent increase in the use of murine models has led to a dynamic and at times controversial discussion as to the relevance of these rodent models, due to differences in the basic pathology of experimental cerebral malaria in the mouse, the undoubted immunopathogenesis of disease in this setting, not reflected in adult human cerebral and severe malaria. Furthermore, the established recognition of ongoing and expanding plasmodial resistance to a range of the few anti-malarial compounds which remain in the arsenal, as well as the ongoing but as yet unfulfilled pursuit of an effective malaria vaccine, underscores the critical need to establish reliable testing platforms for pharmacological and immunomodulatory anti-malarial compounds prior to establishing clinical trials in humans. The paramount importance of the arms race between the various plasmodiae and our dwindling anti-malarial options highlights that the use of murine models to test and propose adjuvant treatments, which then go straight to human trials, has become at best pernicious and at worst unethical.

The Armed Forces Research Institute of Medical Sciences (AFRIMS), in collaboration with various academic institutions worldwide, had conducted studies over the span of 4 decades, using a severe malaria, non-human primate (NHP) model. This thesis began to investigate ways of utilizing NHP models of severe malaria with the following specific aims:

1. To describe in detail, in a systemic and integrated fashion, the cerebral pathology of the *Plasmodium coatneyi*/Rhesus macaque (*Macaca mulatta*) model of severe malaria to determine its representation of the pathophysiology of cerebral malaria in the human, specifically

a. Does the clinical course of fatal malaria in the NHP model involve coma?

b. Is this linked to cerebrovascular iRBC sequestration as is theorized to occur in human malaria cases?

c. Use light and electron microcopy to examine the process of parasitized red blood cell (iRBC) sequestration in the cerebral microvasculature.

2. Compare the non-human primate model with more recently described neuropathological features in human severe and fatal malaria

    a. Is the pathophysiology of cerebral malaria in the NHP model similar to adult or pediatric human cerebral malaria including more recently described secondary neuropathological features such as edema, blood brain barrier leakage (BBB), and axonal injury?

    b. To what extent do host leukocyte and platelet responses contribute to pathology in vital organs?

    c. Does malarial retinopathy occur in the NHP model and if so, what are the pathological correlates of the different patterns of retinal injury?

    d. Can these processes be detected using examination of BBB Leakage, neuroaxonal injury, and cytokine release in the Cerebrospinal Fluid?

3. Recognizing that the select few studies of this model were widely heterogeneous in terms of the criteria of severity and animal protocols, to investigate the clinical, biochemical, parasitological and organ specific histopathology of the model, in order to understand heterogeneity within the model and allow establishment of effective criteria for drug, vaccine and adjuvant treatment trials.

4. Examine the interactions of the *P. coatneyi* parasite with host cells using ultrastructural/ electron microscopic and atomic force microscopic approaches both ex vivo and from tissues.

5. Design prospective experimental approaches to re-invigorate the use of NHP models in understanding the pathophysiology of malaria, based around specific, hypothesis-driven research questions, namely:

    a. What is the incidence of other clinical complications of severe malaria in the NHP model and how do they correlate with those observed in humans, such as anemia, renal dysfunction and hepatic injury?

    b. Is the pathophysiology of severe malaria in this NHP model similar to adult or pediatric human falciparum malaria, primarily focusing on renal, pulmonary, hepatic and cardiac pathology?

    c. Are the clinical pathologic, macroscopic, histopathologic and ultrastructural findings consistent between the *P. coatneyi*/Rhesus macaque model and those observed in humans?

6. Examine the use of the model in an anti-malarial treatment trial of methylene Blue in Severe Malaria.

1.2 **Background and Literature Review:**

1.2.1 The Global Burden of Malaria

Malaria remains one of the most critical public health problems in the world today, and the various responsible plasmodial species are prominent causes of morbidity and mortality in a range of developing nations. Almost half of the world's population is at risk of malaria infection, and vulnerable populations in endemic areas are most commonly children and pregnant women. The human malaria burden worldwide in 2012 was assessed by the World Health Organization to be in excess of 200 million cases, 90% of which were caused by *Plasmodium falciparum*. (WHO 2013) Of the estimated 627,000 fatalities, most occurred in sub-Saharan Africa and about 77% were in children under 5 years of age. (WHO 2013) Though these numbers are high, they represent a worldwide decrease in malaria morbidity and mortality since the start of the current century. Between 2000 and 2012 an estimated 3.3 million deaths due to malaria have been averted, with 90% of them among children younger than five years of age. (WHO 2013) Although phase 3 trials on the latest malaria vaccine RTS,S are promising (RTS,S Clinical Trials Partnership 2014), the current lack of an effective vaccine and increasing plasmodial drug resistance in Southeast Asia to the artemisinin-based anti-malarial drugs (Ashley 2014) threatens to reverse these positive trends. (Aikawa 1992; Ashley 2014; Sá 2009)

Of the *Plasmodium* spp. infecting man, *P. falciparum* is responsible for the vast majority of severe disease and significant morbidity. *Plasmodium vivax* has also been increasingly recognized as causing potentially severe clinical disease (Anstey 2012) to include renal and respiratory syndromes as well as severe anemia and variations of cerebral malaria. (Storm 2014) More recently, *Plasmodium knowlesi* has been shown to cause severe clinical disease including syndromes of anemia, respiratory and renal impairment (Cox-Singh 2015). However, the relative mortality and prevalence of severe disease in vivax and knowlesi malaria is less than falciparum (Barber 2013). Clinical syndromes of

severe falciparum disease vary between semi-immune children and immune naïve adults in non-endemic areas. Severe disease is commonly manifested as cerebral malaria, anemia and metabolic disturbance, with additional complications such as renal and hepatic dysfunction frequent in adults. (WHO 2014)

P. coatneyi has several biological features in common with *P. falciparum* as well as a variety of distinguishing phenotypic traits. Both parasites show 48 hour cycles of intraerythrocytic development, followed by rupture (schizogony), and a resultant fever spike in the host and reinvasion of uninfected erythrocytes. They also both demonstrate microvascular cytoadherence, form rosettes of infected red blood cells with uninfected erythrocytes and develop electron dense knobs on the cell surface which are theorized to play a role in cytoadhesion. (Aikawa 1983; Handunnetti 1989; Kawai 1993; Kawai 1998; Kilejian 1977; Tegoshi 1993; Tongren 2000) Both parasites undergo deep vascular sequestration of trophozoite- and schizont-infected red blood cells and demonstrate a consistent predilection for specific tissues. (Aikawa 1983; Desowitz 1969; Desowitz 1967; Moreno 2013; Sein 1993; Smith 1996)

P. coatneyi was first identified in 1961 in an anophelene mosquito from Malaya. It was experimentally inoculated into a Rhesus macaque monkey and its unique life cycle described. (Eyles 1962) The species was subsequently found in the blood of a cynomolgus macaque (*Macaca fascicularis*) in the Philippines (Eyles 1963) and has since been used as a model for falciparum-like malaria in a variety of macaque species. (Aikawa 1983; Davis 1993; Davison 1998; Davison 2000; Desowitz 1967; Eyles 1963; Kawai 1993; Kawai 1998; Maeno 1993; Matsumoto 2000; Moreno 2013; Moreno 2007; Nakano 1996; Sein 1993; Semenya 2012; Smith 1996; Sullivan 2005; Tegoshi 1993; Tongren 2000; Udomsangpetch 1991; Yang 1999) Foundational work on the parasite and the pathophysiology of infection in macaques was, and continues to be, conducted at the Armed Forces Research institute of Medical Sciences (AFRIMS) in Thailand in collaboration with scientists and

research groups worldwide. (Aikawa 1983; Davis 1993; Desowitz 1969; Desowitz 1967; Desowitz 2008; Maeno 1993; Sein 1993; Smith 1996; Tegoshi 1993; Udomsangpetch 1991)

1.3 **Primate malarias:**

Several animal models of human severe and cerebral malaria have been established over the past 50 years using various *Plasmodium* spp. in both rodent and non-human primate hosts. (Aikawa 1992; Craig 2012; Collins 1988; Davison 1998; de Souza 2010; Kawai 1998; Langhorne 2011; Lou 2001; Maeno 1993; Moreno 2013; White 2010) The histologic and ultrastructural pathology as well as the clinical features and pathophysiology of severe disease have been assessed, in comparison to key features of the human disease, such as sequestration-dependent pathology or immune activation. These animal models are proven platforms for the testing of experimental anti-malarial drugs to determine safety and efficacy, as well as for the evaluation of potential adjuvant therapeutics. (Craig 2012; Maeno 1993) There has however been significant controversy as to the quality and relevance of these various models. The concern has focused primarily on murine models of malaria as not representative of the human disease (Deschamps 2009; Hunt 2010; Langhorne 2011; Stevenson 2010; White 2010), leading to renewed interest in malaria models in non-human primates (NHP).

There is a recent and significant shift in the understanding of falciparum malaria due to the application of molecular techniques, but these have not yet been evaluated in the NHP models. With the increased parasite resistance to various established and newer anti-malarial compounds in our arsenal, therapeutics are required that can be tailored to modulate the immune response to effectively combat plasmodial infection. But in order to fully investigate novel compounds, the pathophysiology of malarial infection in the animal model used needs to be more clearly understood.

Over 250 members of the genus Plasmodium have been described, and both new species and novel host-parasite interactions are reported with regularity. (Guimarães 2012; Levine 1988; Ramiro

2012) Unique plasmodium-vertebrate interactions continue to be discovered in reptiles and birds. (Garamszegi 2009; Howe 2012; Perkins 2009; Poharkar 2009; Woodworth 2005)

The earliest genetic evidence of a malaria plasmodium, dated at approximately 30 million years ago, was obtained through the extraction of DNA from mosquitoes fossilized in amber from the Palaeogene period. (Poinar 2005) The old-world primate plasmodia themselves are polyphyletic and subdivide into 2 major groups. The first of these consists of *Plasmodium ovale*, *Plasmodium malaria*e and sublineages that infect old world monkeys. Parasites of Cercopithecidae monkey species from Asia are more distantly related and comprise 10 species, including *P. coatneyi*. This group also includes *Plasmodium gonderi*, infectious to Cercopithecidae from Africa, *Plasmodium hylobati* which parasitizes Hylobatidae monkeys from Asia, and *P. vivax*, the human plasmodium that is closely related to *Plasmodium simium*, a species of malaria affecting New World monkeys. (Hayakawa 2008) The closest relative *P. coatneyi* appears to be *P. knowlesi*, derived from a single ancestor species, based on evaluation of four different apicoplast genome-encoded genes in the 9 members of the Asian clade. These include a small subunit rRNA, large subunit rRNA and caseinolytic protease C genes. (Mitsui 2010) *P. falciparum* is separate from all of these and is found within the second major group of old world malarias, paired with the chimpanzee parasite: *Plasmodium reichenowi.* (Bray 1958; Hayakawa 2008) Potentially relevant to the debate over models, the rodent malarial parasites are located in a grouping distinct from primate and all other plasmodia. (Escalante 1995; Escalante 1998; Leclerc 2004)

While the various non-human primate species have far greater immunogenic homology to humans than do rodents, complications in both the macaque and murine models include potential variation of the disease progression associated with the route of infection. In humans, the natural route of infection is via dermal injection subsequent to a mosquito bite, in comparison with the experimental murine models receiving predominantly intraperitoneal injections and NHPs inoculated intravenously. Furthermore, the macaque models of severe *P. coatneyi* malaria hitherto reported

typically employ splenectomized animals, which are infected via an IV injection of parasitized blood and parasites which have been harvested from an animal with an intact spleen (hereafter referred to as spleen-intact) or a splenectomized donor animal, or infective stage sporozoites dissected out from infected mosquitoes. Splenectomy results in much higher peripheral parasitemias, circulating mature parasitic stages, and may modulate cytoadhesion and host immune reactions. Therefore, splenectomized experimental animals may be expected to suffer more severe clinical pathologic abnormalities and clinical course of disease. Additionally, many of the studies to date have not had the luxury of using experimentally naïve animals, but instead employed adult animals that had been previously used for studies involving anti-malarial drugs or vaccine candidates in the relapsing malaria model (*Plasmodium cynomolgi*), or animals which have been previously infected with dengue virus, SIV or enteric bacteria, all of which will have had some modulatory effects on the immune status in an individual animal. This presents a significant difference from the highly standardized murine experiments which use inbred mouse strains, but is more in line with the genetic and environmental heterogeneity in affected human populations. (Bruneel 2003; Craig 2012; Deschamps 2009; Dondorp 2008; Hunt 2010; Langhorne 2011; Nagatake 1992; Smith 1982; Yacoub 2010)

1.4 **Ecology of non-human primate malarias:**

The fundamental lifecycle of malaria in non-human primates is quite similar to that of plasmodia infecting humans. This has been underscored with the recent recognition of the simian malaria parasite, *P. knowlesi*, as a previously unrecognized zoonosis and significant cause of malaria in humans. (Cox-Singh 2008) Early taxonomy, based on microscopy, was often complicated by morphological similarities between various species of *Plasmodium* and led to a degree of diagnostic confusion. (Eyles 1962; Ng 2008; Sabbatani 2010; Vythilingam 2010; Vythilingam 2008)

The ecological and environmental requirements for the survival of any plasmodium depends on the parasite reaching a state of “balanced pathogenicity” with the host, whereby the majority of

infections are non-fatal and allow a mosquito to acquire gametocytes through a blood meal and thereby propagate the life cycle. Experimentally, the non-human primate plasmodia of Southeast Asia can be transmitted by a wide range of mosquito species. However, the host-parasite combinations observed in the wild depend on the degree of pathogenicity within specific simian species. This is evidenced by the incompatibility of *P. knowlesi* and the rhesus macaque to cohabitate the same range of forest, because *P. knowlesi* causes a rapidly fatal course of disease in this monkey making malaria persistence impossible. (Rogers 2002; Spangler 1978) This degree of pathogenicity may be the result of recent evolutionary collision between the host and pathogen in which the malaria parasite maintained a high level of virulence due to insufficient evolutionary time to adapt to the host. This particular point is potentially important in selection and interpretation of a model, as differing species of macaques from diverse geographic origins may display differing susceptibility to various plasmodia. At present, only limited comparative studies have been conducted with *P. coatneyi*, examining the pathology in small numbers of animals from different geographic "strains" of either cynomolgus or rhesus macaques. (Fooden 1994; Matsumoto 2000; Migot-Nabias 1999)

Studies in Malaysia in the 1960s examined multiple features of the ecology of the vector mosquitoes, as well as describing and categorizing the malaria parasites found in the local populations of non-human primates. It was established that Anophelene mosquitoes (specifically the *Anopheles leucosphyrus* group of mosquitoes), represented a common vector for *Plasmodium cynomolgi*, *Plasmodium inui*, *Plasmodium fieldi*, *P. knowlesi* and *P. coatneyi*. (Warren 1963) These Anopheles mosquitoes primarily, and apparently preferentially, blood feed on primates. *P. coatneyi* was initially identified in *Anopheles hackeri* (Eyles 1962), a mosquito whose whole life cycle occurs within the forest, and which maintains a high level of endemic malaria within the non-human primates coexisting in the same forested areas. This then translates to high rates of transmission to humans who enter these Southeast Asian rain forests for commerce, warfare or habitation. (Furst 2009)

The epidemiology of transmission of disease within these border areas is especially critical in that the notable emergence of artemisinin-resistant falciparum malaria has come from such ecologic areas. The resistant plasmodia now appear increasingly established within the forests of the Thailand-Cambodian and Thailand-Myanmar borders. (Bhumiratana 2013; Carrara 2013) The importance of this finding cannot be overstated since it holds the potential to reverse the worldwide trend of reduced *P. falciparum* induced morbidity and mortality. (Carrara 2013; Phyo 2012) The arms race between malarial drug resistance and the limited arsenal of effective treatment options, highlights the critical need for the development of a reproducible, reliable animal model which parallels the pathophysiology and tissue pathology of severe falciparum malaria in humans to act as a platform for future vaccine and drug development.

P. coatneyi is considered to be one of the more pathogenic plasmodia in non-adapted hosts, a fact which parallels *P. falciparum* infection in humans. The course of disease in splenectomized macaques is variable, but typically culminates with severe anemia, renal dysfunction, metabolic acidosis, prostration and death. (Desowitz 1967) With *P. falciparum*, clinical presentation is highly heterogeneous, but the most frequently described complications, particularly in older, non-immune, patients, include dyspnea, respiratory distress and eventual coma, with a relatively high mortality rate occurring within hours or days of admission. The literature suggests that the most significant factors leading to death in severe falciparum malaria in both adults and children are metabolic acidosis and coma, as well as severely decreased renal function. (Dondorp 2008; Olliaro 2008; Yacoub 2010)

There are marked differences in the clinical features of severe falciparum malaria in adult humans in comparison with children that bear description. This is a significant field of study in the attempt to further understand the pathobiology of disease in the different age groups. According to the WHO, clinical manifestations of impaired consciousness are more severe in children as is the case with repeated convulsions and dyspnea, while adults demonstrate a greater degree of jaundice in comparison with children. Clinical chemistry and hematological values also differ, with children

having greater severity of anemia, hypoglycemia and metabolic acidosis, while adults typically display far more severe acute renal disease. (WHO 2014)

P. coatneyi has been reported as causing both natural and experimentally-induced disease in a variety of non-human primate species. However, only cynomolgus macaques (*M. fascicularis*) (Eyles 1962; Eyles 1962; Lee 2011; Migot-Nabias 1999), pig-tailed macaques (*Macaca nemestrina*) (Lee 2011), stump-tailed macaques (*Macaca arctoides*) (Seethamchai 2008), and Bornean orangutans (*Pongo pygmaeus*) (Pacheco 2012) have been reported to be susceptible to infection in nature, with or without clinical evidence of disease. In addition to use of those species that are naturally infected, animals in which experimental *P. coatneyi* infection has been studied to various extents include the rhesus macaque (*M. mulatta*) (Aikawa 1992; Arekul 1971; Arekul 1986; Davis 1993; Davison 1998; Davison 2000; Desowitz 1969; Eyles 1963; Maeno 1993; Matsumoto 2000; Migot-Nabias 1999; Moreno 2013; Moreno 2007; Nakano 1996; Semenya 2012; Smith 1996; Tegoshi 1993; Tongren 2000; Udomsangpetch 1989; Yang 1999), black-capped squirrel monkey (*Saimiri boliviensis*) (Sullivan 2005), Japanese macaque (*Macaca fuscata*) (Kawai 1993; Kawai 1998; Kawai 2003; Matsumoto 200), silvery lutung (*Presbytis cristalus*) (Coatney 1971) and white handed gibbon (*Hylobates lar*). (Coatney 1971) The cynomolgus macaque appears to be one of the natural hosts of *P. coatneyi* and is thought to have coevolved with the parasite. Pathology elicited by *P. coatney*i infection in this NHP species is variable and is likely dependent on the genetic heterogeneity of the infected population, since only a subset of animals appear to develop severe disease. The rhesus macaque is far more susceptible to progression of disease than the cynomolgus, but the same heterogeneity appears to apply and may account for the spectrum of pathology and clinical syndromes observed experimentally. The ability to elicit severe disease appears to be more consistent in the rhesus than in the cynomolgus macaques. While both species are used extensively in medical research, and their genomes have been fully sequenced (Yan 2011), it is the experimental reproducibility in the rhesus of the pathological

parameters of falciparum disease in humans, which make the *P. coatneyi*-rhesus macaque model of infection useful for the modeling of severe malaria in humans.

1.5 ***Plasmodium coatneyi* life cycle:**

The stage-specific morphology of *P. coatneyi* was beautifully illustrated in the original Eyles report (1962) and again by Mrs. Gertrude Nicholson in the Primate Malarias text (see Figure 1.1). (Coatney 1971)

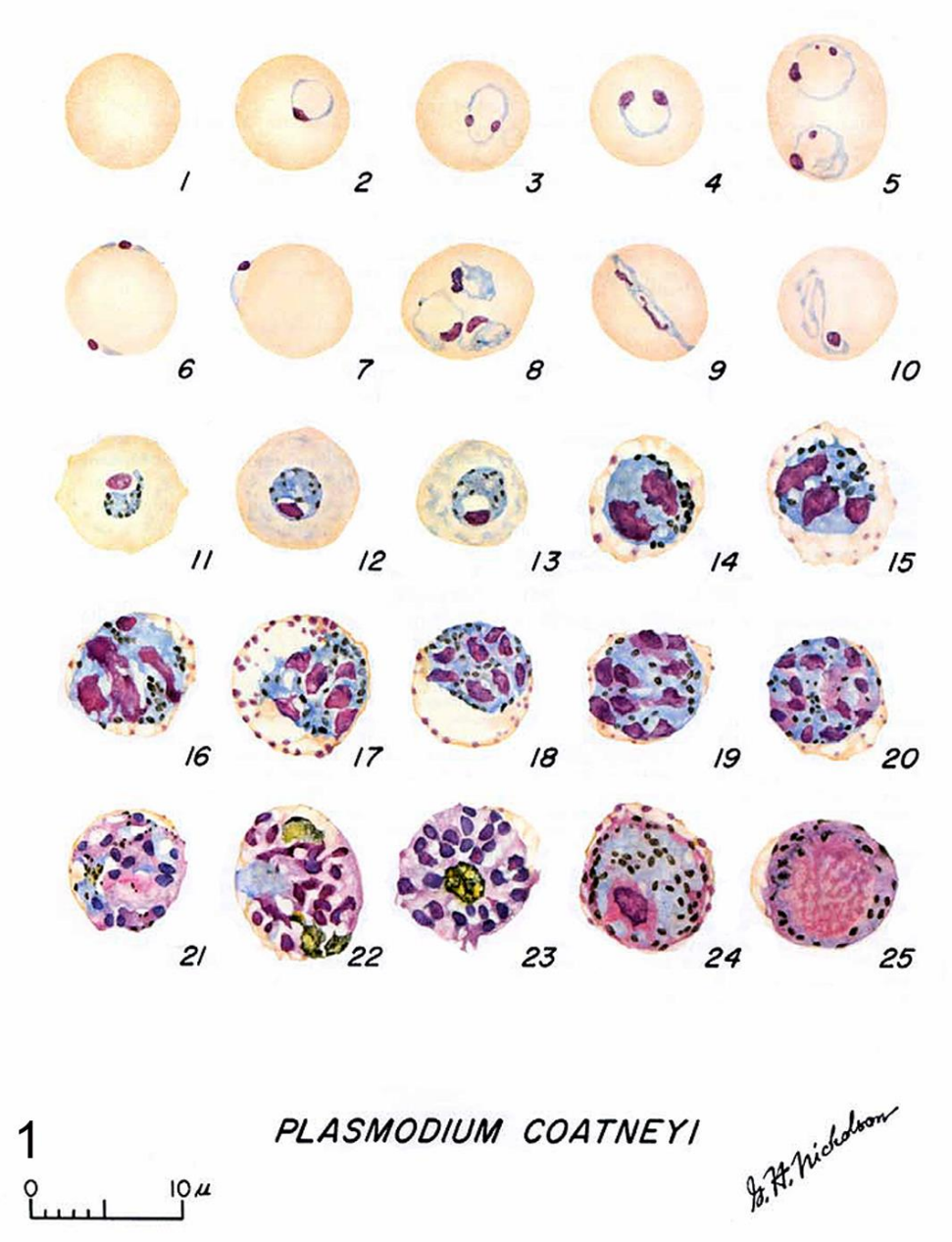

Figure 1.1: This plate is an illustration of the complex intraerythrocytic stages of *Plasmodium coatneyi* with clear demonstration of those diagnostic features which characterize the development of the trophozoites and schizonts. Illustration 1 represents a normal red blood cell, while 2, 3, 6, 7 are examples of young trophozoites demonstrating varying presentations such as rim or displaced types as illustrated in 6. Images 4, 5, 8-11 are examples of growing trophozoites while in 12, 13 the trophozoites are considered to be mature. 14-17 are representative of early schizonts, and 18-21 are stages consistent with developing schizonts. Illustrations 22 and 23 are nearly mature and mature schizonts. The reproductive stages are show in 24 which represents a mature macrogametocyte and in image 25 which is a mature microgametocyte.

Reproduced with permission from Coatney GR, Collins WE, Warren M, Contacos PG. The primate malarias. Washington, D.C.: U.S. Government Printing Office; 1971. Pp. 289–299.

The more immature stages of the species are indistinguishable from *P. falciparum*, and in fact share some diagnostic features with the human malarial parasite. The trophozoite ring form of *P. coatneyi* is smaller than all other simian plasmodia with the exception of *P. knowlsei*. (Coatney 1971) There are frequently 1 to 2 chromatin bodies or nuclei noted within the organism, which are either in close proximity to each other or at polar opposite sides of the ring form (Figure 1.2). Significant morphological variation was observed in the original description but all of the shapes mimicked those that had been described in *P. falciparum*. As with the human parasite, the location of *P. coatneyi* trophozoites within the host erythrocyte varied. Common ring forms were observed as well as a high frequency of marginalized parasites along the periphery of the red blood cell. These forms have been described in *P. falciparum* as “rim” or “displaced’ types (Figure 1.3). (Coatney 1971; Field 1956) The morphological description which was the staple of pathologists and parasitologists before the advent

of molecular technology remains crucial in malaria diagnostics. The variability of location within the host erythrocyte holds true with *P. falciparum* as well, with the peripheralized forms having been called “accolé” or “appliqué”, and considered to be a diagnostic criterion for the human parasite. In these rim forms, the plasmodium typically appears as a continuous thickening of the cell wall, while the displaced form extends beyond the margin of the cell, creating an extruded plaque or bleb which is most noticeable at the point of the trophozoite nuclei (Figure 1.4). (Coatney 1971)

With maturation, both individual and global changes take place within the parasite. As the trophozoites reach more advanced stages, their numbers in the peripheral circulation decrease dramatically, while morphologically, the plasmodia assume a more ovoid form. As with *P. falciparum*, there is a single large food vacuole which decreases in size as time progresses. It is at this stage in development that the highly visible and diagnostic malarial pigment begins to accumulate. In contrast to the pigment of *P. falciparum*, *P. coatneyi* hemozoin crystals, formed as part of hemoglobin consumption by the parasite, do not coalesce until schizogony. Instead, they remain as distinct individual granules which increase in both size and number. It is also at this point of growth that the parasitized erythrocyte begins to display the tinctorial stippling which has been coined Maurer’s spots. These are posited to be secretory organelles, involved in cell signaling and other biochemical processes, which the plasmodium forms within the parasitized erythrocyte, but external to its parasitophorous vacuole. (Lanzer 2006) These require either Giemsa or a modified Leishmann’s staining to properly assess by light microscopy. (Mendiratta 2006) As with the hemozoin crystals, the Maurer’s clefts increase in density with maturation. (Bruce-Chwatt 1985; Eyles 1962)

At a certain point in the development cycle, the trophozoite will transform into a schizont and begin the process of asexual division forming merozoites (Figure 4). As with *P. falciparum,* at this stage the infected erythrocytes become infrequent in the peripheral circulation as they remain in the microvasculature, adhering to the endothelium in a process termed sequestration. This process is felt to underlie the pathophysiology of severe forms of human disease such as cerebral malaria. The

Plasmodium parasite developing within the erythrocyte exports specific parasite-encoded adhesions (Rug 2006) to the surface of the RBC. These proteins, such as PfEMP-1 in *P. falciparum* and its homologs in other plasmodium species, are organized at the electron dense knob protein structures. These mediate specific cytoadhesion to host receptor molecules such as intercellular adhesion molecule 1 (ICAM-1), CD36 and chondroitin sulfate A (CSA) (Almelli 2014). This allows for adhesion not only to the vascular endothelium, but also to host leukocytes, platelets and uninfected erythrocytes (rosetting).

Developing schizonts are round with condensed cytoplasm which contains up to 20 merozoites. Unlike other species of protozoa, the merozoites in *P. coatneyi* do not assume a specific orientation or pattern. At this stage, the malaria pigment crystals begin to coalesce, forming larger irregular granules and the parasitized erythrocyte enlarges and is eventually obscured by the schizont. (Coatney 1971) During this stage, parasitized erythrocytes can still be identified in peripheral blood, but their numbers are significantly decreased in spleen-intact animals. Once the schizont is fully mature, it ruptures, releasing the merozoites into circulation (Figure 1.5). This occurs with relative synchrony and results in the periodicity of parasitemia eliciting the pyrogenic response in the host. In splenectomized monkeys, these late stages of the parasite are also found in peripheral blood, along with the ring forms.

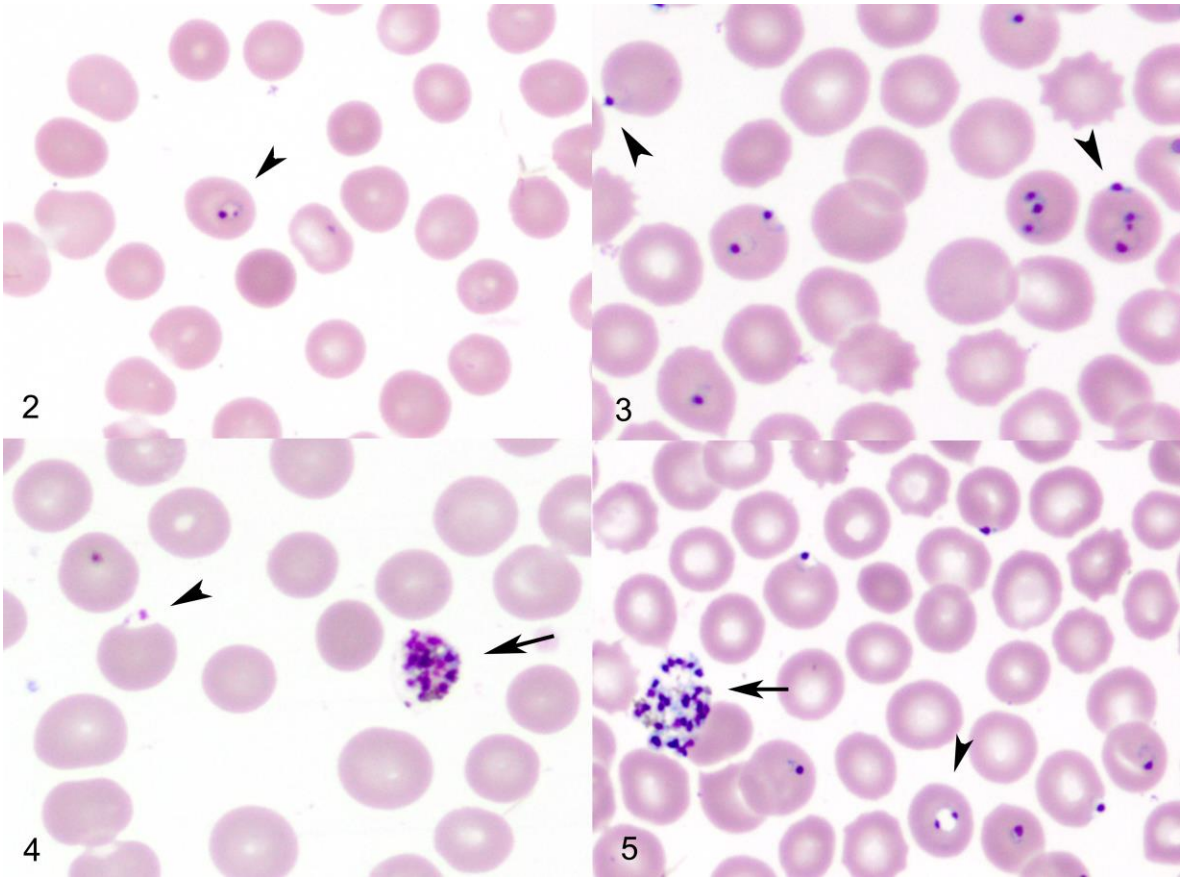

Figure 1.2-5. Intraerythrocytic *Plasmodium coatneyi* trophozoites from peripheral blood smears of the rhesus macaque. (Giemsa staining). Figure 1.2. 1.2% parasitemia: Erythrocytes infected with younger stages of the parasite often contain one or more parasites which have a ring shape and have chromatin bodies which are either in close proximity to each other or are at polar opposite ends of the plasmodium (arrowhead). Figure 1.3. 18% parasitemia: As the parasites develop, they are marginalized in the erythrocyte (arrowheads). Figure 1.4. 1.2% parasitemia: Occasionally, these marginalized parasites expand the cytoplasm of the infected cell, generating a small bleb (arrowhead). At later stages in maturation, the erythrocyte is expanded by a schizont containing high numbers of merozoites (arrow). Figure 1.5. 18% parasitemia: With maturation, the schizont ruptures, releasing the merozoites into the blood stream (arrow). This photomicrograph contains another example of ring stage trophozoite with polar opposite chromatin bodies (arrowhead).

In their initial study, Eyles and colleagues (1962) infected six rhesus macaques (spleen-intact) with *P. coatneyi*. The animals all became clinically ill, displaying marked anemia and severe lethargy. The parasitemia in all of the animals persisted for almost six months post–inoculation, with alternating peaks and troughs of parasite density that differed by 100- to 1000-fold. (Eyles 1962). A second study was conducted in which *P. coatneyi*-naïve animals were inoculated with blood passaged through the first experimental animals. This cohort developed significant malaria-associated mortality causing the authors to question the possibility of multiple stains of *P. coatneyi* with varying levels of virulence. (Eyles 1963)

There have been a variety of studies examining the suitability of *P. coatneyi* in macaques as a model for the cerebral or severe malaria caused in humans by *P. falciparum*, as well as for the evaluation of plasmodium-induced placental pathology. (Davison 1998; Davison 2000) Some of these experiments attempted to describe the pathophysiology of disease through histopathology, immunohistochemistry and transmission electron microscopy (Aikawa 1992; Desowitz 1967; Eyles 1963; Eyles 1962; Kawai 1993; Kawai 2003; Kilejian 1977; Matsumoto 2000; Migot-Nabias 1999; Moreno 2013; Moreno 2007; Nakano 1996; Smith 1996; Tegoshi 1993; Tongren 2000; Udomsangpetch 1991), while others adopted the animal model as a route of drug assessment and testing. (Kyle 1994; Maeno 1993)

1.6 **Clinical course of *P. coatneyi* malaria in the Rhesus macaque model:**

Soon after the original identification of *P. coatneyi*, studies began at the US-Thai South East Asia Treaty Organization (SEATO) labs in Bangkok (now AFRIMS) to characterize the pathobiology of this infection in non-human primates. (Aikawa 1992; Aikawa 1983; Davis 1993; Desowitz 1967; Desowitz 1969; Desowitz 1967; Maeno 1993; Sein 1993; Smith 1996; Tegoshi 1993; Udomsangpetch 1991) Though severe infections often led to death, coma and seizures were not typical of the clinical

picture in macaques, differing from the common pattern associated with severe cerebral malaria in humans. Monkeys progressively lose appetite, develop malaise and lethargy leading to recumbency, and become dehydrated and tachypneic. (Moreno 2013; Smith 1996)

The most consistent pathological effect described in the literature in a *P. coatneyi* infection of rhesus and cynomolgus macaques was anemia, which paralleled the rise in parasite density. In many cases, this was followed by hemoconcentration and rapid deterioration secondary to a shock-like syndrome similar to that described in severe *P. falciparum* and the few reports of *P. knowlesi* malaria. (Cox-Singh 2008; Cox-Singh 2010) This exacerbation is theorized to result in part from a marked decrease in plasma volume concurrent with cytokine-associated increase in vascular permeability. (Arekul 1986; Davis 1993; Desowitz 1967; Desowitz 1967; Moreno 2013; Moreno 2007) These findings are in no way unique to malaria. The infection is more severe in splenectomized animals. Anecdotal evidence from spleen intact donor animals suggests that the parasitemia may even be cleared in immunocompetent animals.

1.7 **Post mortem findings:**

There is only scant information in the literature regarding autopsy findings in *P. coatneyi*-infected animals. Macaques in one particular study consistently were dehydrated and either pale or icteric. There was serous atrophy of fat in multiple organs, and a mild dilation of the ventricles of the heart was noted. Petechiae and coalescing ecchymoses, were described in multiple tissues but most significantly within the epicardium. Concentrated within the kidneys and the liver, much of the viscera was described as having a diffuse brown discoloration (Figure 6) as well as concurrent organ enlargement. This was characterized by splenomegaly (2-3 times normal), hepatomegaly and enlarged lymph nodes. (Aikawa 1992; Davis 1993; Kawai 2006; Smith 1996)

Clinical records of upwards of 60 splenectomized rhesus macaques at AFRIMS provided the foundation of the previously reported pathological data. (Davison 2000; Desowitz 1967; Desowitz 1969; Kawai 1993; Kawai 2006; Lawrence 1986; Moreno 2007; Smith 1996) and corroborated the clinical findings and the autopsy observations in this current study. With parasitemias of 20% and higher, the animals' clinical condition rapidly deteriorated around the 7th day post (intravenous) infection. Clinical signs included hematuria, hemorrhage within the perineum and scrotum, severe depression, recumbency and eventual prostration, progressively worsening anorexia, occasional vomiting and severe dyspnea and tachypnea. Once the animals began to display signs of decreased mentation, death followed rapidly and only rare animals survived beyond the 8th day post infection. Post mortem findings were consistent with the few descriptions in the literature. Animals with higher parasitemias in and around the time of euthanasia or sudden death were observed to have brown discoloration of the liver, lungs, kidneys, heart and brain. (Davis 1993) The discoloration of the organs is due to both vascular congestion and the abundance of malaria hemozoin pigment in erythrocytes and monocytes, both circulating and sequestered. The relationship between malaria infection and the brown discoloration of organs was established by Rudolph Virchow and Friedrich Theodor von Frerichs in the mid-1800s. (Hempelmann 2013) Additional macroscopic findings in this retrospective review conducted at AFRIMS included hepatomegaly with increased friability, heavy congested lungs, and petechiae in the epicardium.

There is a single report in the literature in which a rhesus macaque experimentally infected with *P. coatneyi* developed progressive cutaneous necrosis of the extremities secondary to disseminated intravascular coagulopathy (DIC). This resulted in dermal infarction of the digits and the tail due to thrombosis of the superficial vasculature. (Moreno 2007) A similar unpublished case occurred in Thailand in a rhesus macaque also experimentally infected with *P. coatneyi*. In that instance, the animal developed a necrotizing rhinitis and cheilitis which progressed to erosion and ulceration.

There are occasional reports of gangrenous necrosis in humans secondary to DIC associated with *P. falciparum* infection, but not with any other forms of human malaria. (Chittichai 1991; Liechti 2003; Sharma 2002) While reports of DIC vary in frequency in different human populations, progression to peripheral cutaneous gangrenous necrosis appears to be a rare complication. However, when it does occur, *P. falciparum* is implicated as the causative plasmodium in 95% of human cases and typically the presentation is of ischemia and subsequent necrosis within peripheral tissues. (Bruneel 2003; Ghafoor 2010; McGouran 1977; Mohanty 1985)

1.8 **Clinical pathology:**

Microscopy remains the gold standard of malaria diagnosis in humans and NHPs, both clinically and under experimental settings. Examination is conducted using blood prepared as thin films, in which the sample is prepared with the same methodology as a routine blood smear, and thick films which involves a process of erythrocyte lysis. The latter is more sensitive in plasmodium detection, especially earlier in infection when parasite density is lower; whereas, the former allows for speciation and parasite staging. Although the World Health Organization (WHO) suggests that microscopic slide evaluation in cases of malaria is at best 75% effective based on a range of clinical, geographic and species-specific factors, microscopy has significant advantages over other diagnostic modalities that may be more accurate. (Wilson 2013) The benefits of microscopy for malaria diagnosis are linked to the geography and epidemiology of the various plasmodial diseases. Falciparum malaria is endemic circumferentially along the equator and extends significant distances to the north and south, but still covers a large swath of the poorer and less developed portions of the planet. As such, the most tangible benefits of microscopy are the low cost and the minimal need for infrastructure. However, the technique is also crucial in rapid speciation of parasites, identification of mixed infections, and monitoring treatment. Microscopy has been the mainstay of NHP malaria research as

well, and the bulk of the publications evaluating models of malaria employ microscopic examination to quantitate parasitemias in experimental animals. By using skilled microscopists and associated clinical symptomology, hematologic and blood chemistry data, it is possible to closely map the course of disease.

Up until recently, the clinical pathology of *P. coatneyi* infection in macaques had been poorly elucidated in the literature. A 2013 report by Moreno and colleagues provided more systematic data on the clinicopathological findings of *P. coatneyi* malaria in malaria-naïve, spleen-intact, rhesus macaques. (Moreno 2013) The animals were cured and re-infected at a later date to examine the role of specific acquired immunity in macaques. The study noted that blood chemistry data from the primary infection showed marked azotemia, hypertriglyceridemia, hypoalbuminemia and increased levels of creatinine phosphokinase (CPK) in comparison to pre-infection levels. There was a marked decrease in clinical signs in the second episode of infection which was reflected in the clinical pathology. Triglyceride levels, while elevated, were not significantly different between the first and second *P. coatneyi* infections, suggesting that the release of triglycerides was not directly correlated to the severity of the malaria infection. (Moreno 2013)

Furthermore, the authors observed thrombocytopenia and severe coagulopathy. This was associated with an increase in fibrin degradation product (FDP) levels and concurrent drops in protein C and protein S, suggesting increased consumption of inhibitors of coagulation. (Maeno 1993)

There are several proposed reasons for severe thrombocytopenia occurring in animals during the acute phase of malaria infection. As with the erythrocytic clearance, immune-mediated clearance of platelets may occur as a bystander effect of the presence of the parasitized erythrocytes, stimulating antibody-mediated clearance and upregulation of phagocytic activity in histiocytic cells. (Grau 2003; Jaff 1985) The thrombocytopenia may result from splenic sequestration, peroxidation of the platelet lipid membranes, or platelet consumption from formation of systemic microthrombi.

(Moreno 2007) Metabolic disturbances were evaluated in the rhesus macaque model. (Davis 1993) Animals infected with *P. coatneyi* demonstrated variably increased serum and CSF glucose levels, as well as elevated lactate which increased with parasitemia. This was associated with progressive insulin resistance and a late tendency to lactate acidosis in infected animals, processes observed in human patients with *P. falciparum* infections.

In an early study consisting of a small mixed population of cynomolgus macaques as well as Indian-origin and Thai-origin rhesus macaques, the renal and hepatic clinical pathology associated with severe *P. coatneyi* infection was followed through the course of disease and compared with spleen intact infected animals as well as with uninfected controls. The authors noted concurrent increases in BUN and serum creatinine, both of which initially resolved, only to increase a second time with a concurrent rise in parasite density which continued until death. Furthermore, a slight increase in hepatic alanine transaminase (ALT) was observed immediately following the initial parasitemia peak, but subsequently normalized. Alkaline phosphatase (ALP) remained within reference ranges, though a minor decrease was observed in some of the animals. The animal numbers in the study were insufficient for the purpose of drawing general conclusions as to clinical pathology. The study underscores the absence of adequate data within the literature as a whole. (Desowitz 1967)

Noteworthy amongst these various studies is the significant variability in the level of parasitemia achieved and sustained. Often the degree of acquired immunity is either uncertain or is not reported. This then translates to a degree of variation in the clinicopathological changes observed and reported. There are also significant gaps in the *P. coatneyi* literature as to the impact of the parasite on separate organ systems within the rhesus, much less any of the other NHPs evaluated as models. An example of this can be seen in the absence of adequate studies of the metabolic changes associated with the renal and the hepatic dysfunction.

1.9 **Histopathology and immunohistochemistry:**

The literature contains scant systematic information on the histologic lesions resulting from *P. coatneyi* parasitism in any species. However, a few of the experiments did involve partial autopsies of the infected macaques and subsequent histopathological analysis, which is summarized herein. Chapter 4 of this thesis is dedicated to the histopathological examination of 45 Indian origin rhesus macaques infected with *P. coatneyi* as part of varying experimental protocols conducted at AFRIMS over the past several decades. The results of that study support, reinforce or contrast with the literature review of the histopathology described in the following.

1.9.1 **Central nervous system**:

Sequestration patterns in the infected animals have been the mainstay of the proposal that *P. coatneyi* be used as a model for cerebral malaria in humans. (Desowitz 1969; Nakano 1996; Sein 1993) In *P. falciparum* infections in humans, the sequestration (adherence to endothelium) of parasitized erythrocytes in the microvasculature of the brain often results in partial or complete occlusion of the vessels as characterized by significant congestion with increased margination due to cytoadhesion of infected erythrocytes. These microscopic lesions were correlated with hemorrhage and signs of tissue hypoxia and was theorized to be a significant contributing factor in the development of the symptomology associated with cerebral malaria in humans, namely coma and seizure activity. (Medana 2006) Histological degrees of vascular sequestration differ between different regions of the brain in both humans and non-human primates. (Nagatake 1992; Ponsford 2012; Smith 1996) Reports based on microscopic examination of human brains with cerebral malaria noted a significantly higher degree of parasitized red blood cell sequestration in the cortical grey matter than in the white matter. (Nagatake 1992)

As a result of the human data and building upon previous experiments which evaluated the sequestration patterns in the brains of *P. coatneyi* infected rhesus macaques (Desowitz 1967a;

Desowitz 1967b; Desowitz 1969; Sein 1993), a histopathological and electron microscopic study was conducted in Thailand to examine the distribution of sequestration within the brains of experimentally infected rhesus macaques. (Smith 1996) Animals (5 spleen-intact, 1 splenectomized after infection) were inoculated with a bolus of parasitized blood consisting of 77% trophozoites and 23% schizonts. Parasitemia was assessed daily and parasite staging was also conducted. Between days 7 and 9 post infection, all animals were euthanized, necropsied and evaluated by a veterinary pathologist. At the time of euthanasia, parasitemias ranged from in excess of 200,000 to almost 900,000/mm^3 and consisted primarily of trophozoites. The highest parasitemia was observed in the animal which had been splenectomized at day 5 post inoculation. The presence of sequestration was quantified in the microvasculature of the cortex, the midbrain and the cerebellum, based on histologic examination of 200 microvessels per section. Sequestration was observed in 25% of microvessels in the cerebrum, 24% in the midbrain and 37% in the cerebellum. While not specific to any of the three regions evaluated, the histopathological observations within the central nervous system consisted of congestion, functional obstruction, as characterized by evidence of perivascular edema, hemorrhage and cellular necrosis as well as increased cytoadhesion of parasitized cells (sequestration) of the microvasculature with parasitized and uninfected erythrocytes. In addition, frequent intraerythrocytic and intramonocytic hemozoin pigment and occasional microhemorrhages within the neuropil were described. (Smith 1996)

A window to events within the central nervous system, which has become of increasing clinical interest, and potential histopathological importance, are changes within the retina. Based on recent descriptions of retinal findings in children in East African with severe malaria, retinal hemorrhages are being used as a diagnostic criterion for cerebral malaria in children. (Essuman 2010; Hidayat 1993; Lewallen 1999; Lewallen 2000) Preliminary unpublished histopathological evaluation of two cohorts of animals in prospective studies and the large body of retrospective tissues from various studies conducted at AFRIMS, have failed to show similar hemorrhaging within the retinas of *P.*

coatneyi infected animals. However, based on the diagnostic significance in humans, malaria induced retinopathy should be evaluated in greater depth in animal models.

1.9.2 **Cardiovascular system**:

Two studies conducted in Thailand examined the histopathological sequestration patterns of *P. coatneyi* in the viscera of rhesus macaques with microscopic examination of tissues from multiple organ systems by a veterinary pathologist. (Desowitz 1969; Smith 1996) Overall findings in multiple tissues consisted of congestion and occlusion of small vessels with both parasitized and uninfected erythrocytes. There was also an abundance of phagocytic monocytes containing malaria pigment and varying degrees of lymphocytic inflammation. Frequently, the erythrocytes formed rosettes of uninfected cells bound to a parasitized cell. While this is typically an ultrastructural diagnosis, the authors of this study were able to microscopically identify the rosettes within larger vessels. The study evaluated the degree of sequestration within different organ systems, and noted that the myocardium had the highest degree of histologic sequestration, with individual animals having 84-95% of the myocardial microvasculature showing sequestered parasitized red blood cells. (Figure 7) This was particularly pronounced within the interventricular septum and the left ventricular free wall. Furthermore, the pericardial adipose tissue had a high degree of sequestration and congestion, as did the microvasculature of the pulmonary interstitium and the mesenteric adipose tissue, with an average microvascular sequestration of 85% in and 76% respectively. (Smith 1996) Other studies using macaques report sequestration of *P. coatneyi*-infected erythrocytes in the coronary vasculature, adipose tissue of the omentum, subcutaneous tissues and other sites of fat deposition, the intestinal tract and the skeletal musculature. (Kawai 1993; Levine 1988) This site partiality is consistent with those described in *P. falciparum* infections. (Maeno 1993)

1.9.3 **Hepatic system**:

The liver of infected non-human primates occasionally has a diffuse centrilobular hepatocellular necrosis accompanied by mild increases in serum levels of transaminase. (Desowitz 1967) In addition to the necrosis, mononuclear hepatitis was frequently noted, accompanied by a marked accumulation of birefringent malaria pigment observed within Küpffer cells. (Lawrence 1986; Moreno 2007) (Figure 8).

It is significant that while increases in inducible liver enzymes are a common feature of severe malaria in adult humans, to the extent that a syndrome of 'malaria hepatitis' has been proposed in Indian adult patients, there are only rare reports of centrilobular hepatic necrosis. (Davison 2000; Desowitz 1967)

1.9.4 **Urinary system**:

Kidneys from *P. coatneyi*-infected rhesus macaques in one study had varying degrees of acute tubular necrosis accompanied by hyaline droplet degeneration characterized by expansion of the cytoplasm of the tubular epithelium with eosinophilic globules which are interpreted as possible protein resorption. Furthermore, tubules contained both abundant hemoglobin and cellular casts, and the urinary space contained proteinaceous filtrate with a relative absence of inflammation. (Desowitz 1967) With chronicity there was evidence of glomerular synechiae, interstitial fibrosis, tubular epithelial degeneration, necrosis and regeneration. (Figure 9). Hemoglobinuria has been observed clinically but a formal correlation of clinicopathological and histopathologic findings of renal disease in this model remains to be done.

1.9.5 **Lymphatic system**:

An experimental infection of Japanese macaques observed splenomegaly in all *P. coatneyi*-infected animals. Microscopically, the spleens were characterized with lymphoid follicular hyperplasia, activated macrophages, and red pulp sequestration with parasitized erythrocytes

accompanied by hemozoin pigment (Figure 10). The splenic lesions were considered similar to those noted in humans infected with acute *P. falciparum* infections. (Kawai 2003)

1.9.6 **Reproductive system**:

Studies of placental pathology in the rhesus macaque model were conducted at Tulane University using primiparous and multiparous macaques. The histopathological features of the disease in macaques mirrored that seen in humans infected with *P. falciparum*. The most severe placental lesions consisted of infarction, fibrinoid necrosis, deposition of fibrin and mononuclear and polymorphonuclear fibrinoid necrotizing placentitis. A few of the experimental animals aborted, and fetal death was correlated with the presence of severe placental infarction. The endometrium was typically infiltrated with significant numbers of mixed inflammatory cells and the uterine microvasculature contained parasitized erythrocyte sequestration which increased with proximity to the placental tissues. Furthermore, there was typically infarction of the basal plate with small numbers of neutrophils admixed with pigment laden macrophages. (Davison 2000)

1.9.7 **Other systems**:

Although other organ systems such as the respiratory and hematopoietic systems are involved in the pathophysiology of severe malaria in humans the histopathological examination of these systems in *P. coatneyi* infection in any species of NHP is significantly lacking.

Only a few immunohistochemical studies of the pathophysiology of *P. coatneyi* in macaque models have been conducted. In 1993, Aikawa and colleagues examined rhesus macaques in which the cerebral microvasculature containing sequestered parasitized red blood cells was examined for immunohistochemical reactivity for the endothelial sequestration receptors: CD36, TSP (thrombospondin) and ICAM-1. The cerebral microvasculature of infected animals demonstrated immunoreactivity to all three molecules while that of cerebral endothelial cells in the cerebral microvasculature of uninfected control macaques was negative. (Aikawa 1992) This study mirrored

work that had been conducted in *P. falciparum* infected tissues. The positive immunoreactivity of *P. coatneyi* infected tissues suggests that there is a similar mechanism of cytoadherence in both humans and NHPs. (Oquendo 1989; Roberts 1985; Smith 2000) Subsequently, in 1996, non-cerebral macaque tissues were evaluated using the same molecular markers. All of the experimentally infected animals displayed positive immunohistochemical staining in the heart, lungs, small intestine and the spleen in contrast to the control animals. Additionally, deposition of immunoglobulin G and complement component 3 within the vascular wall (immune complexes) were evaluated using immunofluorescence in all harvested tissues. All of the tissues examined in the *Plasmodium coatneyi*-infected animals were positive for both markers. In contrast, in the uninfected animals, there was immunoreactivity in the spleens and faint immunofluorescence in the kidneys of 2 of the animals, but the brain, heart, lungs and small intestine were universally negative. This microvascular damage in the kidneys is consistent with studies that have been conducted in falciparum malaria infected tissue. (Maeno 1993)

1.10 **Electron Microscopic Findings**:

In contrast with the dearth of histopathological analysis described in the literature, the bulk of the early studies of *P. coatneyi* included transmission electron microscopic examination of the pathological changes in the rhesus macaque. Concentrating on changes associated with the process of sequestration, which is best observed and confirmed using ultrastructural examination to identify specific cytoadhesion, a variety of pathological observations have been reported.

Rosettes, consisting of a central infected erythrocyte, cytoadherent or bound to a variable number of surrounding uninfected erythrocytes, have been described as contributing to the pathogenesis of *P. coatneyi* (Udomsangpetch 1991), *Plasmodium fragile*, and *P. falciparum* infections. They have been observed with cultured *P. falciparum* and in occasional instances with fresh isolates of the human cerebral malaria agent. (Handunnetti 1989; Wahlgren 1992) Rosette formation has

been examined ultrastructurally, and the theorized mechanism of occurrence posits that the uninfected erythrocytes are bound by receptors to the electron-dense knobs found on the cell surface of a centrally located, parasitized red blood cell which contains either a trophozoite or a schizont. (Tegoshi 1993) Rosettes can subsequently begin to recruit and bind to other rosettes or uninfected erythrocytes, forming larger aggregates. *P. vivax*, *P. cynomolgi*, *P. knowlesi* and the ring stage of *P. falciparum* (and *P. coatneyi*) lack the electron dense knobs which mediate cytoadherence and as such are not generally associated with high rates of rosetting. Thus, erythrocyte sequestration, which is considered important for the pathogenesis and clinical outcome of cerebral malaria, is thought to result from a combination of rosette formation between parasitized and uninfected erythrocytes, interactions between distorted erythrocytes and induced pseudopodia of endothelial cells, and direct adhesion between erythrocytes and endothelial cells. (Handunnetti 1989; Howard 1989; Udomsangpetch 1989)

Packed infected erythrocytes are characterized by distortion and prolongation of the cytoplasm, generating irregular forms. These appear to intricate themselves into invaginations and pseudopod-like projections emanating from the adjacent endothelium. Furthermore, the surface of the affected endothelium is crenated, with thickening of the endothelial basal lamina, especially in proximity to the parasitized red blood cells. The infected erythrocytes themselves develop the conical, membrane delineated, electron dense, evenly spaced “knobs” which are involved in binding to unparasitized erythrocytes and potentially to the endothelium as well (Figure 11). (Aikawa 198; Kilejian 1977) Within the red blood cells, in addition to the malaria hemozoin crystals, the plasmodia were described at various stages of development ranging from trophozoites to schizonts, with schizonts predominant. (Sein 1993) Furthermore, infected erythrocytes were noted to be bound to uninfected cells at the point of the electron dense knobs and in doing so formed the described rosette patterns. (Tegoshi 1993)

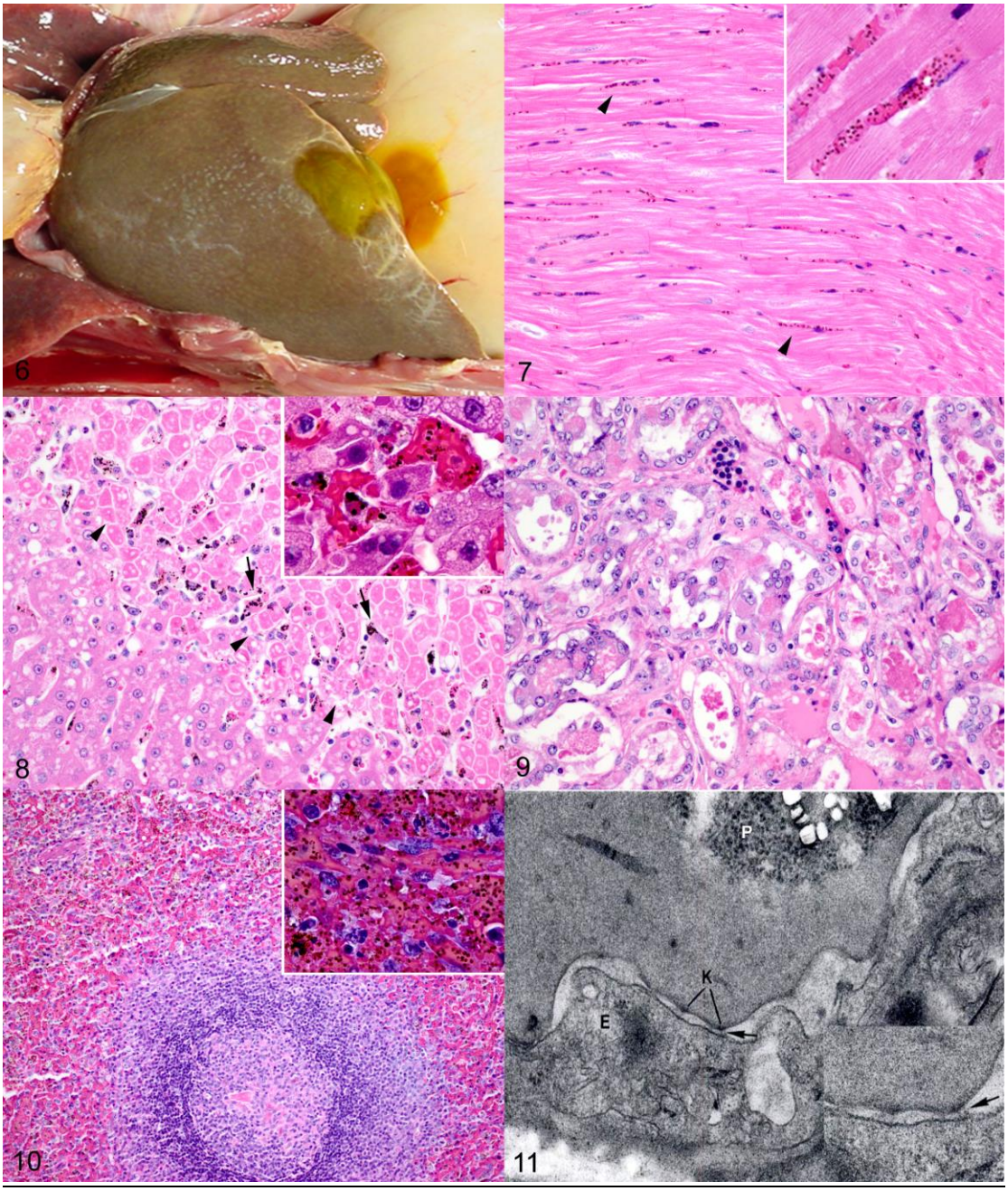

Figure 1.6-11 Rhesus macaque, *Plasmodium coatneyi* infection.

Figure 1.6. Liver. A macroscopic autopsy photograph showing the diffuse pale brown to grey discoloration of the liver from an animal that died of severe *Plasmodium coatneyi* malaria, normally attributed to malaria hemozoin pigmentation.

Figure 1.7. Myocardium. A photomicrograph of the Intravascular, intraerythrocytic trophozoites with microvascular sequestration of both infected and uninfected erythrocytes (inset), associated with

severe *Plasmodium coatneyi* infection. Hematoxylin and Eosin (HE) stain, magnification x 100, inset x 200.

Figure 1.8. Liver. There is severe, focally extensive, centrilobular hepatocellular coagulative necrosis with sinusoidal sequestration, intrasinusoidal pigment and intraerythrocytic *Plasmodium coatneyi* trophozoites (inset), as is occasionally observed in animals with severe *Plasmodium coatneyi* malaria. HE stain. magnification x 100, inset x 200.

Figure 1.9. Kidney. There is severe, multifocal to coalescing tubular necrosis with epithelial degeneration, rare regeneration, cellular casts and proteinosis. HE magnification x 400.

Figure 1.10. Spleen. Splenic histiocytosis is diffuse and marked with innumerable intraerythrocytic *Plasmodium coatneyi* trophozoites and hemozoin pigment. The white pulp is diffusely expanded by activated histiocytes and the red pulp is replete with abundant malaria pigment (inset). HE. magnification x 100, inset x 200.

Figure 1.11. Electron micrograph of cytoadherence (arrow) of parasitized red blood cell knobs (K) to endothelial cells (E) in a cerebral microvessel. P = *Plasmodium coatneyi* (magnification x 36,000). Inset: Cytoadherence (arrow) of knobs to endothelial cells (magnification x 56,000). Transmission electron micrograph. Replicated with permission from Aikawa M et al. A primate model for human cerebral malaria: *Plasmodium coatneyi*–infected rhesus monkeys. Am J Trop Med Hyg: 46: 391-397,1992

The descriptions in the literature suggest that the observed endothelial pseudopodia occur with greater frequency within the microvasculature of the cerebellum than in other regions of the brain. (Sein 1993) Cerebral endothelial pseudopodia have only rarely been described in the literature in diseases other than malaria. Chickens fed a diet high in linoleic acid and deficient in vitamin E were

reported with similar changes (Yu 1974) as were cats with induced endotoxic shock. Rats experimentally manipulated to generate or decrease fluid shear in skeletal muscle microvessels induced formation of endothelial pseudopodia. (Hueck 2008) Furthermore, pigs with experimental *Mycoplasma suis* infections were assessed ultrastructurally and were noted to have similar changes in endothelium throughout multiple organ systems as is described with *P. coatneyi*. (Sokoli 2013)

MacPherson et al. suggested that the endothelial pseudopodia within the cerebral microvasculature, which has also been described in human cases, is a possible pathological manifestation of cerebral vascular insult and a response to endothelial damage. Since these were observed in regions with the slowest blood flow, it was proposed that there was a higher likelihood of trophozoite and schizont-infected erythrocyte deposition. (MacPherson 1985) Ultrastructural lesions in endothelial infections other than malaria have been described in detail including the cytokine-mediated transendothelial migration of leukocytes as well as ligand-receptor connections, suggesting that electron microscopic findings seen in cerebral malaria are multifactorial and not necessarily specific to the plasmodium pathogens. (Gonçalves 2010; Schmidt 2011)

1.11 **Atomic Force Microscopy Studies of Malaria**:

Atomic force microscopy (AFM) or Scanning force microscopy (SFM) is a technology which has shown extraordinary diversity in its application and has been used to successfully map the ultrastructural topography of malaria infected erythrocytes for various different plasmodia, including the human parasites: *P. falciparum* (Aikawa 1996; Aikawa 1997; Akaki 2002; Garcia 1997; Li 2013; Nagao 2000; Olliaro 1997; Quadt 2012), *P. malariae* (Li 2010), *P. vivax* (Malleret 2015) and the rodent parasite: *P. yoelli.* (Claser 2014) The technology is used primarily in the assessment of the forces associated with or in imaging surface ultrastructure of polymer chemistry, semiconductor technology, solid state physics, as well as having applicability in a range of research investigations in medicine,

molecular and cell biology. Our specific use of the technology in this study has been in descriptive imaging, as, through the interface of the probe with the forces generated by the sample, three dimensional images of the topography of the surface of a given sample can be generated. (Binnig 1986; Giessibl 2003) One of the fundamental benefits of this technology is that, as AFM does not use lenses or beam irradiation for imaging, it is not limited by issues of diffraction limit and aberration which affect space resolution, nor does it require a vacuum or particular staining in sample preparation, which are required for either optical microscopy and electron microscopy. The image produced generates a surface map of individual cells and as such is an extraordinary tool in the description and measurement of the structural changes which occur following plasmodial infection of erythrocytes. As such, the final images generate data which provides cross-over and complementary information between both AFM and SEM. The descriptive results of the use of this modality are described in Chapter 6 which discusses the ultrastructural findings in depth.

Transmission Electron Microscopy, Scanning Electron microscopy and Atomic Force Microscopy have all allowed for an in-depth examination of malaria infected erythrocytic surface ornamentation. Knobs (or some variant thereof), caveolae, caveola-vesicle complexes, cytoplasmic clefts, and electron-dense material have all been described in plasmodium infected erythrocyte plasma membranes using various ultrastructural techniques. (Atkinson 1990) The two most important forms of surface ornamentation which are expressed on the plasma membrane of *plasmodium* spp. infected primate erythrocytes, vary in association with the specific species causing the infection, are Knobs and Caveolae.

Knobs or knob like protuberances, have been well described in *P. falciparum* and *P. malariae* (Aikawa 1996; Aikawa 1997; Aikawa 2002; Li 2010) as well as in *P. coatneyi* (Aikawa 1992), while caveolae are seen on the surface of *P. vivax*, *P. ovale*, *P. fragile*, *P. cynomolgi* and one passing report of the structure observed in *P. coatneyi*. (Aikawa 1975; Aikawa 1977) There are sporadic reports which describe knobs on *P. ovale* (Matsumoto 1986) and portrayals of caveolae on the surface of *P.*

malariae infected erythrocytes. (Atkinson 1990; Mackenstedt 1989) Both of these characteristic morphological alterations have been primarily described through the use of transmission electron microscopy and scanning electron microscopy.

P. coatneyi infected Rhesus macaques and Japanese macaques have been employed as animal models for severe and cerebral malaria associated by *P. falciparum*. (Aikawa 1992; Davison 1998; Kawai 1993; Lombardini 2015; Moreno 2013) *P. coatneyi* shares a range of pathophysiological, pathological and ultrastructural features with *P. falciparum*, as well as several distinguishing phenotypic characteristics. Both species of plasmodium have 48 hour intraerythrocytic development cycles, subsequent to which schizogony occurs. The newly released merozoites undergo reinvasion of uninfected erythrocytes and the host has a resultant febrile spike. Both *P. falciparum* and *P. coatneyi* develop rosettes comprising one or multiple infected red blood cells which recruit uninfected erythrocytes (Doumbo 2009; Lombardini 2015; Moreno 2013), they both have well documented microvascular cytoadherence and both parasites appear to share some variation of knob-like structure on the cell surface hypothesized to be involved in the pathogenesis of cytoadhesion. The knobs on erythrocytes infected with mature asexual forms of *P. falciparum* are posited to allow the infected cells to cytoadhere to the vascular endothelium under shear flow conditions and thus avoid splenic clearance. (Malleret 2015)

1.12 **The Pathophysiology of Severe Malaria in human and simian models**:

While there have been remarkable advances, the pathophysiology of both *P. falciparum* and *P. coatneyi* infections remain areas of significant scientific debate. In particular, the pathogenesis of coma in severe malaria is a controversial topic of research. (Turner 1997; Turner 2006; Milner 2011) Previous investigations have tended to split into several camps, the first based around a 'mechanical' theory of coma, in which the pathophysiology of disease is directly linked to microvascular

obstruction by sequestered iRBC and its subsequent effects, whilst other authors view sequestration as an epiphenomenon. This has led to the proposal that the systemic effects of infection, such as soluble cytokine release, nitric oxide or immune dysfunction lead to CNS disease independently of the presence of parasitized erythrocytes in the brain (Clark 1994). This was in part fueled by the observation that murine and hamster models of the disease lacked significant cerebral sequestration. As such, various simian models have been used in pathophysiological studies of severe malaria in an attempt to study and elucidate some of these opposing theories.

Erythrocytic sequestration and cytoadherence have been definitively shown to occur with both parasites through in-vitro studies and electron microscopy (Kawai 1993; Kawai 2003; Smith 1996; Udomsangpetch 1991), and it is this pathological commonality which promoted the use of the *P. coatneyi*-rhesus macaque as a good model of sequestration dependent *P. falciparum* induced cerebral malaria in humans. However, although sequestration is described in the brain, there are a wide range of secondary neuropathological features of the disease which have been recently described in the human disease. Examples include cerebral edema, breakdown of the blood brain barrier, axonal injury, as well as leukocyte and fibrin/platelet thrombus formation. All of these features have been more recently described in both adult and pediatric post mortem studies in human malaria (Turner and Milner 2014), but need to be examined in the macaque model to determine the conformance of the macaque model with the human disease. (Mendiratta 2006)

The role of cytokines in the immunopathogenesis of plasmodium-induced disease has been extensively studied in murine models, however there have been few reports of similar work in non-human primates. One of these studies, undertaken at the U.S. Centers for Disease Control and Prevention, utilized the rhesus macaque-*P. coatneyi* model to evaluate the relationship between serum levels of inflammatory cytokines and prostaglandin with parasitemia levels. Serum interferon-γ levels rose earlier and mirrored the periodicity of the parasitemia, while interleukin-1β and tumor necrosis factor-α increased late in infection. The authors theorized that the change in interferon-γ

was associated with early activation of T-lymphocytes, while the elevated levels of the latter two cytokines correlated with monocyte activation paralleling increased parasitemia. Serum prostaglandin E2 (PGE-2) levels were also elevated. Considering the microvascular insult associated with severe malaria in human disease, the report theorized that the progressive increase in PGE-2 observed in the rhesus was a corollary to the rise in inflammatory cytokines. Finally, the study also evaluated ciliary neurotropic factor, a molecule which is involved in the maintenance of calcium homeostasis in glial cells and neurons, as a means of assessing neural injury in the rhesus. By the later stages of disease, ciliary neurotropic factor had risen in all four of the experimental animals. (Yang 1999)

A more recent study evaluated erythropoietin (EPO) levels in serum and compared the findings with microscopic evaluation of core bone marrow samples. EPO levels in *P. coatneyi*-infected macaques reached a peak of 6 times that recorded in the uninfected control animals, and the EPO zenith coincided with the nadir in hemoglobin levels in the affected monkeys. The increase in renal production of EPO strongly suggests a functional hyperplastic response in the bone marrow to the massive erythrocyte destruction. The bone marrow had a significant shift towards immaturity in both the myeloid and the erythroid lineages during the acute stage of infection. Furthermore, concurrent dyserythropoiesis was morphologically observed, characterized by karyorrhexis and increased nuclear lobulation. Within a week following cure, the nuclear changes in the bone marrow had normalized. (Moreno 2013)

Erythrocyte longevity was also assessed in the infected macaques. A severe anemia was observed approximately 10 days following infection and was correlated with parasitemia. The highest degree of erythrocyte turnover occurred at relatively low parasitemias, suggesting that infected erythrocytes have a bystander effect resulting in concurrent destruction of uninfected red blood cells. Greater than 90% of the cleared erythrocytes were uninfected. (Moreno 2013) Suggested mechanisms of this bystander effect relate to changes in erythrocyte morphology, decreased

longevity and immune-mediated clearance through up-regulated erythrophagocytosis. (Smith 1982; Sri-Hidajati 2005)

1.13 **Controversies surrounding existing animal models of Experimental Cerebral Malaria**:

Partly because of the basic histopathological differences between murine models of experimental CM (ECM) and both those observed in humans and in non-human primate models, the use of these models in an increasing number of adjuvant treatment trials, the status of the mouse model of ECM has been challenged. (White 2010)

One major issue with mouse models is the lack of a basic pathological description of the model and relating this to pathophysiology both in terms of the clinical pattern of disease in the model and comparison of these to the natural host. Additionally, there have been a large number of host/parasite combinations used, characterized to varying degrees, the most popular being the *P. berghei*/ANKA mouse model. This has led to an explosion in the use of this model to represent 'experimental' cerebral malaria. (de Souza 2010; Hunt 2010; Hvid 2010; Langhorne 2011)

The utility of these rodent models tends to be both in their ease of experimental approach, the use of inbred strains and gene knockout strains to study particular pathways of pathogenesis. However, the explosion of research in murine models led to some papers drawing unsustainable conclusions, and the ethically questionable practice of clinical trials in humans being based on minimal data raised solely in animal studies (often underpowered) of unproven relevance.

For instance, human trials of Erythropoietin as an adjuvant treatment in pediatric CM have been conducted (Picot 2009), based on data from murine model studies (Kaiser 2007) despite data in adult PM studies of human CM cases suggesting EPO receptor levels were not significantly different in brainstem tissue of patients with or without coma. (Medana 2009) The use of limited data from

animal models to justify clinical trials is not a minor issue, because results can be misleading since properly controlled large trials with appropriate ethical oversight and safety monitoring are difficult to organize in areas where severe malaria is common, on a par to the logistical challenges of vaccine trials. However, they may have a role in testing potential adjuvant treatments in CM. For instance, the use of Erythropoietin and hypothermia in the treatment of hypoxic-ischemic encephalopathy in Western settings shows some promise. (Rogers 2014) Many such adjuvant or neuroprotective treatments have been proposed in theory for malaria, and those attempted thus far have been in small and overwhelmingly unsuccessful human trials. (John 2010) Therefore, basing decisions for entry into human trials on data from animal models would seem unwise until the models themselves are better characterized.

Other non-human primate models are also employed, with specific focus on vaccine trials. *P. falciparum* itself will infect New World Aotus and Saimiri monkeys, however, neither cytoadherence in the brain nor cerebral malaria develop in those species. Immunohistopathologic studies show no deposition of *P. falciparum* antigen, complement or IgG. (Aikawa 1990; Fujioka 1994) Additionally, the size and frailty of the New World species render them difficult to use for pharmacokinetic or toxicology studies. Sequestration will develop at high parasitemia of *P. fragile* in rhesus, but electron-dense knobs are not seen on parasitized erythrocytes. (Howard 1989) Furthermore, symptoms do not develop until just before death, rendering the *P. fragile* model particularly difficult for use in drug studies of acute malaria. (Miller 1969)

Such controversies led to a period of heated exchanges in the literature and eventually a consensus conference in 2012 in Hinxton, Cambridge UK, which agreed amongst other recommendations that “Development and standardization of animal models, including renewed investment in non-human primate systems, is a priority.” (Craig 2012)

1.13.1 **What positive advantages do animal models of malaria offer?**

The utility of animal models of malaria is unquestionable given the fact that most patients with severe malaria live in resource-poor settings with often limited medical infrastructure in which to base clinical and pathological studies. For instance, gene knockout studies allow close examination of the role of a single specific gene or pathway in the pathogenesis of disease, such as the investigation of gamma interferon related pathology in the mouse brain. (Hunt 2014) This, of course, depends on agreement that the clinical and pathophysiological nature of that disease pattern in the model accurately represents that which is observed in humans.

A second major advantage of animal models is the ability to perform more invasive physiological monitoring or therapeutic studies in controlled circumstances, which would not be ethically acceptable as proof of concept studies in humans – e.g. ex vivo organ based studies such as splenic perfusion as a means to study hemofiltration as a treatment in malaria (Buffet 2011), isolated kidney experiments for examination of reno-protective drugs, or imaging studies of the brain. (Kawai 2010)

Thirdly, as and when basic *in vitro* research or studies from the murine model provide evidence for a promising treatment, a better developed and more relevant model to human physiology and immunology, such as the simian model, could be used as an intervening stage in safety and efficacy testing before moving on to human trials, thereby ensuring maximal and more efficient use of time and funding.

As such, full characterization of animal models is potentially key to understanding the similarities and differences to the human disease which may influence interpretation for specific studies using the model.

1.14 **Discussion**:

It has been over 50 years since the discovery of *P. coatneyi* in the forests of Malaysia, but there remains much to accomplish in describing this potentially valuable model of severe human malaria. Considering the continuing debate as to the suitability of rodent models of experimental severe and cerebral malaria, there remains a significant need to more fully describe the rhesus macaque/*P. coatneyi* model. Animal models of severe and cerebral malaria are being used not only to study pathophysiology but also in drug, vaccine and adjuvant treatment trials, where detailed descriptions of their clinical and pathological characteristics are lacking.

The pathology and pathophysiology of severe and cerebral malaria are still active areas of research and have stimulated significant debate. Conducting such studies in humans poses ethical and logistical difficulties that have resulted in an increasing reliance on murine ECM models, despite basic pathophysiology which differs markedly from that of malaria in humans. Additionally, post mortem based studies of cerebral malaria in adult and pediatric severe malaria cases have led to proposals that these two different patient groups may show pathological differences and have differing pathophysiology in the genesis of similar clinical syndromes.

One of the key areas of controversy has been the degree to which parasite sequestration within the brain can be linked to ante mortem coma. Evidence from Southeast Asian adults seems to clearly support a correlation as is demonstrated in pediatric cases of CM, even though the latter group, in Southeast Asia, has significant rates of coinfection with HIV which may alter secondary aspects of neuropathology. (Hochman 2015; Mbale 2016; Ponsford 2012) However once sequestration is present, which seems to be a process dependent both on parasite load and host immunological responses, it is not inevitable that a patient will develop coma. Patients demonstrating significant levels of cerebral sequestration will not necessarily fall within the clinical criteria of CM, as defined by WHO criteria, and some patients with significant sequestration will not exhibit coma.

Although quantitative recognition of a relationship between sequestration in the brain and coma has been established (by histology and ultrastructural studies) more recently the concept of parasite biomass has been used (Dondorp 2005; Hendriksen 2013) to relate severe disease to indirect measures of pathogen load using serum HRP-2 levels.

A key drawback of murine ECM models is that this process of parasitized erythrocyte sequestration in the cerebral microvasculature does not occur, rather there is localization of host leukocytes mediating an autoimmune meningoencephalitis. Since sequestration is so characteristic of CM in humans, it seems important, when characterizing a putative animal model of severe malaria, that the degree of microvascular sequestration should be determined and the effects of this on clinical course and specific end organ dysfunction examined be in detail.

The simian model of *P. coatneyi*/splenectomized Rhesus macaque had been previously proposed to represent a good model of sequestration dependent pathology and 'cerebral malaria'. Yet we lack a detailed clinical and pathophysiological description of whether this model produces coma, seizure activity or other clinical evidence of the mechanisms of secondary neuropathological injury similar to those more recently described in the humans, such as has been described in associated with blood brain barrier breakdown, host leukocyte responses, cytokine release, astroglial activation, axonal injury, or platelet mediated endothelial cell dysfunction. (Combes 2006; Hora 2016; Medana 2002; Medana 2006; Medana 2007; Storm 2014; Turner 1997)

Fundamentally the question remains as to what represents a substantiated and scientifically valid model of severe or cerebral malaria in humans. Is the macaque model able to replicate falciparum malaria in children as well as adults? In addition to the organ specific complications of severe malaria such as cardiac, renal or hepatic pathology which occur in simian models, can these be linked to sequestration or immune mediated pathology in this model, and are these pathological manifestations consistent with human disease? A clearer understanding of the basic pathology is

critical for understanding the utility of this particular model in both preventive and therapeutic studies.

The macaque model has the potential advantage of a high degree of homology to the human immune system. This evolutionary proximity to human infection, as opposed to the murine models, is only further emphasized by the recent description of *P. knowlesi* infection as a zoonotic human malaria parasite. (Cox-Singh 2015; Vythilingam 2014; Vythilingam 2016) NHP models could address problems involving metabolic and physiologic changes (for instance, the pathogenesis of coma and neurological dysfunction) which are difficult to study in human patients. (Beignon 2013) Functional MRI imaging, intracranial pressure monitoring (Newton 1991) and laser video microscopy of flow and EEG under controlled settings (and in response to potential adjuvant therapies) are difficult to perform, and ethically justify, in human patients with malaria. In comparison with the non-sequestration dependent, immune mediated encephalitis of experimental murine cerebral malaria, the similarities of the pathophysiological tapestry of *P. coatneyi* to human disease should make the simian results more medically relevant.

Thus, using both retrospective pathological studies, and prospective clinical, histopathological and ultrastructural studies this thesis aims to provide data to help determine the validity of the *P. coatneyi* infected rhesus macaque as a model for severe and cerebral malaria in humans. The arms race which is ongoing with this disease is all the more heightened by the parasite's broadening drug resistance, and the search for a strong model of human disease therefore all the more crucial.

1.15 **Summary:**

While there is significant, complex and at times, controversial, ongoing debate as to the validity of murine versus simian models of cerebral and severe malaria, what is constant is the absolute need for effective, replicable, and scientifically confirmed animal models which will serve as a platform for

anti-malaria drug development and vaccine studies moving forward. In-depth examination of the current literature demonstrates extreme heterogeneity of animal based malaria research to date, which is underscored by the controversy as to the murine malaria model focus. Additionally, based on the advent of Artemisinin and Artemisinin Combination Therapy (ACT) drug resistance, the relative absence of effective replacement compounds to combat drug resistance and the sheer epidemiological weight of falciparum malaria susceptible people world-wide, the results of this dissertation gain heightened importance and urgency. Recognizing that the criteria for a model of *P. falciparum* severe or cerebral malaria must include features of cytoadherance, rosette formation, sequestration, similar clinical symptomology to human disease and equivalent immunopathology, this study consists of a thorough, in-depth examination of descriptive clinical, histopathological, ultrastructural and molecular pathology of the rhesus macaque/*P. coatneyi* as an appropriate and replicable animal model for cerebral and/or severe malaria syndromology of *P. falciparum* induced disease in man. In doing so we have attempted to validate its use as a platform for drug and vaccine studies.

Chapter 2: Materials and Methods

2.1 **Introduction**:

2.1.1 **Evolutionary basis for non-human primate modelling**:

Genomic comparison between humans and the various other great apes have noted that chimpanzees display the greatest homology to humans in total DNA sequence, with interspecies sequence differences limited to approximately 1-1.5%. (Page 2001; Stewart 1998) Orangutans and gorillas have similar homology as do chimpanzees, however the next group of animals which demonstrate the closest homologous alignment of whole DNA sequence are the Old World monkeys, to include rhesus macaques. Humans diverged evolutionarily from the great apes approximately 6-7 million years ago. Furthermore, the evolutionary separation of the great apes from Old World monkeys occurred 25 million years ago and the split with New World monkeys is posited to have occurred approximately 35-40 million years ago. (Stewart 1998) Of significant importance to the overall argument as to validity of different animal models, mankind is theorized to have split from rodents and mammals, other than primates, greater than 65-85 million years ago. (Eizirik 2001; Kumar 1998) Based on this relative evolutionary proximity, the rhesus macaque has been employed in a range of comparative biomedical research to include drug development protocols. (Bluemel 2015) The belief that the rhesus macaque metabolism of medication derivatives more closely resembles that of humans in comparison with rodent models remains one of the most significant arguments in the debate as to relevancy of different animal models of severe and cerebral malaria. (Mestas 2004; Perlman 2016; Rhesus Macaque Genome Sequencing and Analysis Consortium 2007) Of significant historical consequence in model selection for drug discovery and applicability research is the failure associated with the Thalidomide safety studies conducted in Europe in the 1950s. In that particular tragic instance, the potential teratogenic effects of the drug were not observed as the

toxicity studies had been limited to research in rodents, lagomorphs, cats and dogs, but excluded the use of non-human primates. The subsequent, disastrous effect of the drug, which resulted in over 10 thousand children being born with severe congenital abnormalities, is paramount to the care which must be given to model selection and the required due diligence in describing the applicability of any animal model. (Bluemel 2015)

2.1.2 **Non-Human primate models**:

The rhesus monkey is one of the hardiest of the established primate malaria models and therefore is considered to be optimal in its ability to tolerate the required procedures for drug evaluation protocols. Although there are New World monkeys that can be infected with *P. falciparum* and *P. fragile* as models of severe malaria (Aikawa 1990; Fujioka 1994; Howard 1989; Miller 1969), the rhesus macaque remains a superior model to the New World Aotus monkey in particular, because sufficient blood volumes can be collected for adequate analysis without causing an adverse iatrogenic anemia.

The model that appears to mimic human severe malaria most closely is the rhesus monkey/*Plasmodium coatneyi* model. The animal protocol employed for this study focused on the methodology of the use of the rhesus monkey/*P. coatneyi* severe malaria model specifically in order to evaluate the use of Methylene Blue (MB) for the treatment of severe blood-stage malaria, the results of which will be described in the subsequent chapter. The experimental model is essentially the same as that which was used in both the retrospective and the prospective studies from which we have drawn data throughout this dissertation. The prospective studies employed a far greater degree of scrutiny and refinement of the data collection to ensure uniformity between the study animals and to maximize the understanding of the pathogenesis of disease progression in this species. The protocol was used primarily for the comparison of two dose levels of MB to intramuscular (IM) Quinine dihydrochloride (QD). After an initial trial of the experiment which proved

to have too few data collection points to adequately monitor the development of severe parasitemia in the animals, the protocol was altered and significantly refined. The original protocol had three primary endpoints: Firstly, to evaluate MB in terms of overall safety. Secondly, to determine if IV MB will be non-inferior to IM QD in terms of efficacy. And finally, to provide efficacy and limited safety data for the selection of an optimal dose of MB for use in planned phase II human clinical trials.

As the animals included in both the retrospective and prospective data were from the AFRIMS closed colony, the degree of inbreeding is a potential confounding factor. To counteract that concern, by Standard Operating Procedure, three generations of the pedigrees of both the male and female monkeys in the AFRIMS Department of Veterinary Medicine's database are reviewed prior pairing or grouping of animals to avoid inbreeding. Furthermore, on a periodic basis (approximately every 15 years), an influx of new, genetically distinct animals are introduced into the AFRIMS colony from suppliers in the United States.

In 2012, the Department of Veterinary Medicine conducted an internal, unpublished study calculating the degree of inbreeding in the rhesus colony through the use of the phylogeny program "Pedigraph" in order to determine the inbreeding coefficient by using the pedigree data of each animal in the colony. 584 rhesus monkeys were examined, and of those, there were 43 monkeys that expressed an Inbreeding Coefficient greater than 0. Throughout the entire population, the Inbreeding Coefficient ranged from 0 to 1.

Table 2.1: Inbreeding coefficient of the AFRIMS rhesus macaque colony

Inbreeding coefficient	**Number of animals out of 584 total**
0.0078125	1
0.03125	6
0.0625	23
0.125	6
0.25	7

2.1.3 **Ethics**:

As part of WRAIR's and AFRIMS's ongoing commitment to the reduction of the number of animals used in medical research, the AFRIMS IACUC put in place a Tissue Sharing Program. This program allows investigators to utilize tissue or other biological materials from ongoing approved research protocols without the need to euthanize additional animals. Furthermore, the AFRIMS comparative pathology division of the Department of Veterinary medicine maintains a comprehensive database of all pathologic samples collected in the 50+ years of medical research conducted in the Institute. Formalin fixed, paraffin embedded tissue blocks from historical protocols dating back over 20 years were used for the application of novel techniques and for histopathological examination. Additionally, medical records were available from the bulk of the retrospective animals, allowing for a consolidation and evaluation of the clinical, experimental and baseline data. Control tissues were harvested post-mortem through the tissue sharing program in association with ongoing IACUC approved infectious disease protocols at AFRIMS, to include renal transplantation studies, *Shigella* sp. drug trials, Simian-Human Immunodeficiency Virus chimera pathogenesis studies, *Plasmodium cynomologi* drug trials and routine attrition within the macaque colony correlated with spontaneous neoplasms or other lesions not associated with experimental protocols. In particular, the animal use protocol for the prospective animals was approved by the AFRIMS IACUC, protocol number 12-08. In all cases, animals were maintained in strict accordance with established principles under the Guide for the Care and Use of Laboratory Animals. (National Research Council 2011) Furthermore, the AFRIMS macaque colony has undergone continuous Association for Assessment and Accreditation of Laboratory Animal Care International (AAALAC) accreditation. Retrospective studies post 1985 were approved by the AFRIMS IACUC, protocol numbers: 90-12; 92-3; 93-6 and 01-05.

2.1.4 **Spleen-intact Donor Monkeys**:

P. coatneyi was inoculated from one rhesus to another through a blood challenge of infected erythrocytes. Inoculation began in an infected donor by intravenous inoculation of freshly thawed cryopreserved *P. coatneyi* strain infected blood. The stabilate stock used was the Hackeri strain of *P. coatneyi* which originated from stocks maintained by cryopreservation at the Centers for Disease Control and Prevention, donated to and archived at AFRIMS (Collins 2001), has been tested and confirmed negative for Herpes B virus, SRV, SIV and STLV-1 to ensure no possibility of adventitious virus transmission into the monkey colony. A 1cc aliquot of a thawed stabilate of *P. coatneyi* infected RBCs (approximately 1 mL equivalent to $5x10^6$ infected RBCs) was administered intravenously into a peripheral vein of the donor monkey as described below. Blood smears were prepared to detect malaria parasites starting on Day 0 before inoculation and continued daily.

Once the blood smear was noted to be positive, either white blood cell (WBC) and/or red blood cell (RBC) counts were performed daily to determine a parasite density (parasitemia). After the parasitemia had reached > 50,000 parasitized RBCs per µL, 10-20 mL of blood was drawn into a heparinized tube, diluted with sterile PBS solution to a concentration of $5x10^6$ infected erythrocytes per 1 mL suspension, and divided into equal 1 mL aliquots. The 1 mL aliquots were subsequently used to infect the study animals and to prepare additional cryopreserved stabilates for future use. The volume and number of times that parasitized blood could be drawn from the donor animals was determined by the attending veterinarian based on calculation of total blood volume in each animal and governed by the IACUC approved protocol, such that at no time would it exceed established guidelines for phlebotomy described below.

After completion of the blood draws, curative treatment was given with CQ 10 mg/kg, PO daily for 7 days. The donor monkeys were considered to be off-study once blood donation had been completed and animals were cleared of parasites. If a blood smear result was positive on day 8 of the CQ treatment, 2-5 additional doses of CQ treatment were continued. Blood smears were collected

daily and continued until the monkey demonstrated 5 consecutive days of negative blood smears. Subsequently, the monitoring schedule was reduced to two times weekly for 2 weeks, and then weekly for 2 more weeks. The donor monkeys were considered to be off-study once they are cleared of parasite, and alternate therapy could have been prescribed as determined by the attending veterinarian. A minimum of 8 weeks recovery period from the last positive smear was required before the donor monkey could be re-infected.

Table 2.2: Donor Inoculation and Treatment Schedule

Day	**Procedures**	**Samples to be collected**
-15	Ketamine restraint 15 mg/kg, weighing, venipuncture 4 ml Complete physical examination	1 ml in EDTA tube for CBC 3 ml in SST tube for ALT, creatinine and total protein
-14	Start pole-collar training and continue for 2 weeks	none
0	Inoculation, IV, cryopreserved *P. coatneyi* infected blood	2 blood smears
1-7	Daily blood collection*	Blood samples for parasite determination
Approximately 7-10	Daily blood collection* At parasitemia >50,000/cu.mm Ketamine restraint 5-10 mg/kg Venipuncture to collect 10-20 ml of blood for inoculum preparation and cryopreservation (if needed). Chloroquine HCl 10 mg/kg, PO after harvest	Blood samples for parasite determination Inoculum preparations: 5 x 10^6 infected RBCs in 1 ml in PBS Submit the rest of blood for cryopreservation
For 6 days after blood harvesting	Chloroquine HCl 10 mg/kg, PO Blood smears follow daily and continue until 5 consecutive negative smears.	2 blood smears for parasite determination
1st to 4th week	Follow up blood smears twice weekly for 2	2 blood smears for parasite

after negative smear	weeks and once weekly for 2 more weeks.	determination

* Blood collection for parasite monitoring and parasitemia determination: Approximately 0.3 ml whole blood were collected in EDTA tube each day (0800-1000 hours) from each monkey by sterile pediatric lancet puncture for WBC count and RBC to determine parasitemia level. Pole-collar restraining was used for this procedure. Hematocrit was occasionally needed.

2.2 **Experimental Monkeys**:

2.2.1 **Splenectomized Experimental Monkeys:**

Splenectomized *P. coatneyi*-naïve rhesus monkeys were used for the severe malaria pathophysiology, pathology and MB studies in this thesis. Splenectomy was necessary to develop and sustain high-grade parasitemia and initiate severe and cerebral malaria effects.

2.2.1.1 **Splenectomy procedure:**

Splenectomies were performed using aseptic technique. The standard midline laparotomy (a surgical procedure involving an incision through the abdominal wall to gain access into the abdominal cavity) was used. A midline incision was made 3 to 4 inches long just cranial to the animal's umbilicus. The spleen was identified and gently exteriorized, avoiding trauma to the pancreas and was held by a piece of damp gauze with sterile normal saline. The surrounding area was examined for accessory splenic tissue. Main blood vessels supplying the spleen were identified and the surrounding adipose tissue was removed by gentle blunt dissection. Triple ligatures of plain catgut No. 3-0 were applied to the splenic blood vessels in close proximity at the hilus roughly 0.5 to 1 cm distal to the splenic capsule. Mosquito forceps were used to clamp the blood vessel group adjacent to the splenic capsule and also to hold the tissue above the ligatures. A scalpel blade or a pair of scissors were used to transect all vessels at the splenic hilus and to remove the entire spleen. The ligatures of the pedicle were observed to ensure hemostasis was intact. The pedicle was returned to the abdomen. The pedicle was observed again for hemostasis and the omentum was re-positioned.

The peritoneum and muscle layer incisions were closed with catgut No. 2-0, with simple interrupted sutures. If loose or excessive subcutaneous tissue was observed, the subcutaneous area was closed with an absorbable suture, Vicryl™ No. 3-0 by subcuticular pattern. The skin was approximated and closed with horizontal mattress sutures of non-absorbable polyamide monofilament (Ethilon™) No. 3-0.

2.2.1.2 **Peri-operative procedures**:

Pre- and Post-Operative Provision, Intra-operative Monitoring and Anesthetic Record for non-human primates. While anesthetized, thermal support was provided by means of an insulated circulating heated water blanket or forced air heating blanket (BAIR hugger). Depth of anesthesia was monitored by testing the strength of response to toe pinch at ten-minute intervals and isoflurane was administered as deemed necessary. Heart and respiratory rate were monitored via esophageal stethoscope and/or pulse oximeter constantly throughout the procedure. Recordings were conducted every five minutes and logged onto the Form: Pre- and Post-Operative Provision, Intra-operative Monitoring and Anesthesia Record for NHP.

2.2.1.3 **Post-operative Provisions:**

As part of post-operative care, splenectomized animals were allowed up to 4 weeks to recover before they were entered into the study. Immediate post-surgical critical care was provided in the Recovery Room. An antiseptic spray was applied to the incision wound. Each individual animal was observed closely for recovery by an assigned technician. Long-acting antibiotics, i.e., Shotapen LA™ (Benzathine penicillin G 100,000 IU, Benzathine penicillin 100,000 IU and Dihydrostreptomycin sulphate 200 mg per ml) at 20,000 IU/kg, IM or equivalent were prescribed. The animals were returned to their home cages once they were fully conscious and limb movement occurred. Observation continued at the animal's home cage until the animal regained consciousness. Food was offered after the animals were fully recovered. The animals and the incision site were observed daily by the staff veterinarian and sutures were removed at 7 to 10 days. Buprenorphine 0.01 mg/kg was

given 1 hour prior to surgery and twice daily (every 12 hours) post surgically by intramuscular injection for the first 48 hours post-operatively, and every 12 hours thereafter as needed as determined by the veterinarian-on-duty.

2.3 **Experimental interventions**:

2.3.1 **Parasite Inoculation**:

On their inoculation day, all monkeys were infected by peripheral vein inoculation with *P. coatneyi*-blood stage parasites (approximately 1 mL equivalent to $5x10^6$ infected RBCs) drawn from the donor monkeys. The blood stage inoculation procedure was conducted using a 22-24 Gauge 1-inch needle.

2.3.2 **Inoculations/Phlebotomy guidelines**:

Monkeys were handled as little as possible. Monkeys were trained in humane restraint with pole-collar devices for all injections or phlebotomy procedures. Chemical restraint with ketamine (5-20 mg/kg ketamine hydrochloride IM) was used for physical examinations and weight determinations and the initial inoculum injections. The ketamine dosage and its use in injection and/or phlebotomy procedures was adjusted by the Attending Veterinarian as necessary to minimize discomfort to the monkey.

An inoculum of *P. coatneyi* parasitized erythrocytes in a volume of 1.0 mL was injected into the saphenous or a peripheral vein of each monkey by 22-23 Gauge, ½-1-inch needle. The monkeys were chemically restrained with ketamine HCl (5-10 mg/kg IM) for this procedure. Injections of MB were administered into a peripheral vein by an intravenous catheter (size: 22 to 24 G). The maximum volume of the IV injection did not exceed 3 ml/kg/day. No chemical restraint was used for phlebotomy or drug administration in these pole-and-collar trained animals, unless deemed necessary by the Attending Veterinarian.

Injections of MB was administered via IV push into a peripheral vein by an intravenous catheter (size: 22 to 24 G). IV injections for MB was drawn directly from 10 mg/mL solutions of 1% USP MB.

The maximum volume of the IM injection did not exceed 1.0 ml/injection site. Compounds given IM included:

1. Ketamine HCl 5-20 mg/kg, IM by 21-23 G needles or smaller.

2. Quinidine (QD), was injected into the thigh muscle. The loading dose was typically a split dose due to volume.

3. The opioid analgesic, buprenorphine, for perisurgical use was prescribed by the veterinarian-on-duty at 0.01 mg/kg, IM, 1hour prior to surgery and every 12 hours post-surgery for 5 to 7 days.

2.3.3 **Dose Formulations Stability and Storage Conditions**:

1. Methylene Blue: Methylene blue was packaged as a USP 1% solution in water for injection at 10 mg/mL pH adjusted with sodium hydroxide and/or hydrochloric acid. The injectable solution was stored in the dark at controlled room temperature (15° - 30°C).

2. Quinine dichloride: Pre-formulated quinine dichloride was sourced from ANB Laboratories, Thailand was stored at controlled room temperature (15° - 30°C) until use.

2.3.4 **Pole and Collar restraint**:

For pole, collar, and chair training, monkeys were trained for 2-3 weeks, such that the animals became familiar with the various procedures involved. This allowed for short term restraint for brief, non-invasive procedures, i.e., venipuncture to obtain blood samples from peripheral veins; test compounds or vehicle administration orally or by IM or IV routes; routine data collection conducted

in conjunction with phlebotomy (i.e. Temperature assessment or electrocardiogram) and palpation or examination of the compound injection sites.

2.4 **Animal protocol Pilot study**:

Initially, the overall study design began with a pilot arm of the study in which a small group of animals were separated randomly into dose groups of 3 animals with a low, mid and high dose of MB at 20% parasitemia. This would allow a characterization of drug efficacy as proof of concept at high parasitemia, and then the intent was to move forward with the rest of the study using the most effective dose. The initial phase required a single donor spleen intact rhesus macaque. The intended subsequent phase was to compare the most effective MB dose level to an established dose of IM QD.

Pitfalls which occurred during the initial trial required a series of amendments to the protocol. Problems which arose were associated with an inadequate understanding of the parasitemia curves in the infected animals and the clinical symptomology in the affected animals using the previous retrospective protocols as a foundation. The blood draws to assess parasitemia were too infrequent and did not adequately capture the spike in parasitemia which occurred in the model and as such, three animals died unexpectedly. Those three animals were autopsied and provided the first data set for use in our histopathological, immunohistochemical and ultrastructural descriptions.

The Pilot phase was intended to comprise of the first experimental cohort and was projected to compare the efficacy of three dose levels of IV MB once 15% parasitemia was reached. This would have been equivalent to a moderately severe case of malaria in a human, but was theorized to have been low enough that the rhesus subjects would not die from the disease prior to initiation of therapy. The mid-level, 10 mg/kg IV bid MB, dose was based on prior pharmacokinetic data collected on MB administered in rhesus monkeys, which showed an area under the curve (AUC) ratio of 3.5:1 for drug levels in rhesus monkeys when compared with human data (Barker et al, unpublished). This

corresponded to an estimated human dose of 3 mg/kg IV bid. The lower dose of MB was planned to be 6 mg/kg IV bid, estimated to be equivalent to just under 2 mg/kg IV bid dose in humans, and the higher 17 mg/kg IV bid dose was estimated to be a dose of 5 mg/kg IV bid in humans. The most effective dose would then have been utilized in Phase II of the protocol.

Any animal which showed criteria of treatment failure at Treatment Day (TD)+72hrs was to be euthanized, and the remaining animals were to be euthanized upon treatment failure or on Day 6 following initiation of treatment (see Criteria for Treatment Success and Treatment Failure below).

A total of 15 monkeys in this portion of the study were randomly assigned to each of three experimental groups with three monkeys in Group 1 and six monkeys per Groups 2 and 3. Group 1 served as the untreated controls. Two additional monkeys were used as donors for inoculum donation. Experimental animals (not including donors) were to be euthanized upon treatment failure or on day six after initiation of treatment. The ultimate goal of this study was to provide efficacy and safety data for the selection of an optimal dose of MB for use in planned phase II human clinical trials, and to support the U.S. Army anti-malarial research program.

As the initial phase failed, the study was restructured and resubmitted to the AFRIMS' IACUC so as to allow for a protocol refinement study and then a subsequent relaunch of the MB pilot, comparing drug dosage levels and parasite clearance in *P. coatneyi* infected rhesus. As animal numbers were restricted by the original protocol, the refinement study and the MB dosing study were limited to an additional experimental 12 animals (three animals included in our prospective data collection were the three *P. coatneyi* infected and untreated animals that died unexpectedly during the initial attempt of the MB dosage study). Of those 12, three were allocated to the refinement study and nine were assigned to the MB dosage study. (Study schedules described in Table 2 and Table 3) The three animals from the failed initial study and the three animals dedicated to the refinement study represented untreated control animals for the subsequent MB dosage study. No

uninfected, MB treated animals were included as drug controls in the study due to limited numbers of available animals.

The MB dosage groups are described in Table 4 and the drug dosing schedule is described in Table 5. Due to the labor intensity of blood sampling, parasitemia assessment, clinical monitoring and eventual autopsy, each of the three MB groups were staggered by a week, and an individual donor macaque was randomly assigned to each group. Equally, a fourth donor animal was dedicated to the refinement study, and that experiment was conducted almost a year prior to initiation of the relaunch of the MB dosage study.

As described above, the model refinement study required three splenectomized, chair trained, experimental animals and one donor macaque. The MB drug dosage study required nine splenectomized, chair trained, experimental animals and three donor macaques. The requirement for four total donors was due to the need to stagger the three separate cohorts of the MB drug dosage phase based on the lessons learned from the failed previous study as well as data derived from the model refinement study which was conducted a year prior to the MB drug dosage study, and which illustrated the significant labor requirements for clinical data collection, parasitemia assessment, drug administration and autopsy timing. The nine experimental animals were splenectomized in accordance with AFRIMS surgical protocols, injected with a microchip temperature recording device (telemetry) in the subcutaneous tissues between the shoulder blades and recovered for one month prior to being infected by peripheral vein inoculation with *P. coatneyi*-blood stage parasites (approximately 1 mL of $5x10^6$ infected RBCs) drawn from the donor monkeys.

Throughout the study, blood draws were calculated using a reference point of a 6.8kg animal as the least common denominator. However, with larger animals, under the purview of the attending veterinarian, blood draws were increased based on their body weight and permissible blood draws

per SOP. All blood drawn was used in accordance with the testing described in the IACUC approved protocol amendments.

Table 2.3: Refinement study schedule

Study Days	Procedures	Specimens
-70	Ketamine restraint 5-20 mg/kg, weighing, venipuncture 1.5 ml Complete physical examination	0.5 ml in EDTA tube[1] 1.0 ml heparin tube for chemistries[2]
-62	Splenectomy and implant transponder	
-14	Withhold morning feed, Ketamine restraint 5-20 mg/kg, weighing, venipuncture 1.5 ml Complete physical examination Place neck collar Start clinical observation with VET-GP-008-F5	0.5 ml in EDTA tube[1] 1.0 ml heparin tube for chemistries[2]
	Start pole-collar training and continue for 2 weeks	
-1	Start Clinical observation three time daily using study specific form#1 (Temperature measurement both rectally and via transponder 3 times) Pole-collar and chair restraint Venipuncture 2.5 ml EKG measurement	0.5 ml in EDTA tube[1] 1.0 ml heparin tube for chemistries[2] 0.5 ml in EDTA for TNF-α[3] 0.5 ml in heparin for nitric oxide[4]

0	Blood smear collection 3 times at 0700 (prior malaria infection), 1100 and 1900 Venipuncture 1.5 ml for CBC and chemistries one time at 1100 Clinical observation 6 time daily using study specific form#1 Temperature measurement from both transponder and rectal temp recorded 6 times at 0700, 1100, 1500, 1900, 2300 and 0300 Ketamine restraint 5-20 mg/kg, weighing Blood inoculation Inoculation 1 ml, IV (5×10^6 infected erythrocytes) (not late than 0800-0830)	0.5 ml in EDTA tube[1] 1.0 ml heparin tube for chemistries[2] Thick and thin blood smears
1 -2	Blood smear collection 3 times at 0700, 1100 and 1900 Venipuncture 1.5 ml for CBC and chemistries at 1100* Clinical observation 6 time daily using study specific form#1 Temperature measurement from both transponder and rectal temp recorded 6 times at 0700, 1100, 1500, 1900, 2300 and 0300	0.5 ml in EDTA tube[1] 1.0 ml heparin tube for chemistries[2] Thick and thin blood smears

Study Days	Procedures	Specimens
3-5	Blood smear collection 3 times at 0700, 1100 and 1900 Venipuncture 1.5 ml for CBC and chemistries twice at 1100 and 1900 Clinical observation 6 time daily using study specific form#1 Temperature measurement from both transponder and rectal temp recorded 6 times at 0700, 1100, 1500, 1900, 2300 and 0300	0.5 ml in EDTA tube[1] 1.0 ml heparin tube for chemistries[2] Thick and thin blood smears
6	Blood smear collection 12 times at 0700, 0900, 1100, 1300, 1500, 1700, 1900, 2100, 2300, 0100, 0300 and 0500 Venipuncture 1.5 ml for CBC and chemistries at 0700, 1500 and 2300 Clinical observation 12 times using study specific form#1 and temperature from both transponder and rectal temp recorded 6 times at 0700, 0900, 1100, 1300, 1500, 1700, 1900, 2100, 2300, 0100, 0300 and 0500. EKG measurement	0.5 ml in EDTA tube[1] 1.0 ml heparin tube for chemistries[2] Thick and thin blood smears

7	Blood smears collected every hour when parasitemia reached 6% or on study day 7 at 0700, 0800, 0900, 1000, 1100, 1200, 1300, 1400, 1500, 1600,1700, 1800, 1900, 2000, 2100, 2200, 2300, 2400, 0100, 0200, 0300, 0400, 0500 and 0600 Venipuncture 1.5 ml for CBC and chemistries at 0700, 1500 and 2300 Clinical observation 24 times daily on study specific form#1 and temperature from both transponder and rectal temp recorded 24 times at 0700, 0800, 0900, 1000, 1100, 1200, 1300, 1400, 1500, 1600,1700, 1800, 1900, 2000, 2100, 2200, 2300, 2400, 0100, 0200, 0300, 0400, 0500 and 0600	Thick and thin blood smears, and 0.3 ml EDTA tube for CBC and parasitemia determination[5]
8	Blood smears collection every hour at 0700, 0800, 0900, 1000, 1100, 1200, 1300, 1400, 1500, 1600,1700, 1800, 1900, 2000, 2100, 2200, 2300, 2400, 0100, 0200, 0300, 0400, 0500 and 0600 Venipuncture 1.5 ml for CBC and chemistries at 0700, 1500 and 2300 Clinical observation 24 times daily on study specific form#1 and temperature from both transponder and rectal temp recorded 24 times at 0700, 0800, 0900, 1000, 1100, 1200, 1300, 1400, 1500, 1600,1700, 1800, 1900, 2000, 2100, 2200, 2300, 2400, 0100, 0200, 0300, 0400, 0500 and 0600	Thick and thin blood smears, and 0.3 ml EDTA tube for CBC and parasitemia determination[5]

Study Days	Procedures	Specimens
	EKG measurements conducted before euthanasia The monkeys euthanized if parasitemia reached 20-25% and/or a combination at least three of the following clinical signs** Collect 2.5 ml blood, blood smear, 3 ml CSF and perform full autopsy	0.5 ml in EDTA tube[1] 1.0 ml heparin tube for chemistries[2] 0.5 ml in EDTA for TNF-α[3] 0.5 ml in heparin for nitric oxide[4]

Monkey ID.NO.: DA831, DA923 and R519

[1] 0.5 ml EDTA blood for complete blood count, reticulocyte count and parasite determination at DVM.

[2] 1.0 ml heparin blood for blood chemistries: BUN, CREA, BUN/CREA ratio, ALT, AST, ALP, GLUC, Total Protein, Na, K, Cl, Serum Lactate, blood pH and methemoglobin by automated hematology analyzer at Department of Veterinary Medicine (DVM).

[3] 0.5 ml EDTA blood for TNF-α level, to DVM lab for centrifuging 20 minutes at 2000 x g. Plasma was either removed and assayed immediately or aliquoted and stored at -20° C. Subsequent use avoided repeated freeze-thaw cycles.

[4] 0.5 ml heparin blood for nitric oxide levels was sent to DVM lab for centrifuging, 20 minutes at 2000 x g. Plasma was either removed and assayed immediately or aliquoted and stored at -20° C. Subsequent use avoided repeated freeze-thaw cycles.

[5]0.3 ml EDTA blood was collected when parasitemia became positive. WBC count and RBC count were also performed for parasitemia determination. CBC was also determined according to clinical indication. A daily blood smear was collected after malaria infected blood inoculation, from day 0 to day 5; blood smears were collected 3 times prior to malaria infection at 0700, 1100 and 1900. On

study day 6, Blood smear collection was increased to 12 times at 2 hourly intervals. On study day 7 and 8, Blood smears were collected every hour when parasitemia reached 6%. Thick and thin blood smears were prepared from capillary blood samples collected from each monkey by sterile pediatric lancet puncture of the lateral auricular vein. The monkeys were physically restrained in the squeeze-cage restraint apparatus or pole-collar restraining for this short procedure.

[6]0.5 ml heparin blood for PK analysis, sent to DVM lab. Whole blood was kept in freezers until analysis.

*In addition to CBC/Chemistry blood collection on day -1, blood was drawn to generate baseline TNF-alpha and NO references. Terminal blood collection allowed repeat sampling for these two assays.

§ Chemistry and CBC measurement increased to 2x daily at day 2 if changes were noted on day 1 and on the day 2 blood draw. In that instance, the total blood draw increased by 1.5mls to a total of 31mls for the experiment. This volume was still within the 1% allowable volume per day for sequential sampling IAW SOP VET VC-301, Nonhuman Primate Phlebotomy.

__Criteria for euthanasia:**__ Parasitemia of 20-25% and/or a combination at least three of the following clinical signs:

- Evidence of severe acute tubular injury (evidenced as both hemoglobinuria/ hematuria combined with elevated creatinine and Blood Urea Nitrogen)
- Hepatic failure (as evidenced by jaundice and significantly elevated ALT, AST, ALK Phos, GGT and decreased albumin)
- Severe anemia as determined by a hematocrit of 15% or less or a precipitous drop as determined by the AV
- Coagulopathy based on improper clotting as well as cutaneous petechiae, and ecchymoses
- Anorexia lasting 3 meals
- Continued recumbency combined with severe lethargy and depression

- Neurological signs such as papillary dilation, lack of a menace response, marked depression and severe weakness characterized by an inability to sit or perch

- Persistent vomiting

- Persistent diarrhea with either frank blood or melena

- Persistent tachycardia or bradycardia

- Marked and persistent dyspnea/tachypnea

- Excessive vocalizing or other signs of significant distress

- Persistent fever of 3 degrees C above baseline or 2 degrees C below baseline in the individual animal

- Ataxia as a feature of neurologic disease (but not specifically due to weakness) as determined by the Attending Veterinarian (AV)

- Progressive cutaneous necrosis

Table 2.4: Procedure schedule

Study Days	Procedures	Specimens
	Screening Ketamine restraint 5-20 mg/kg, weighing, venipuncture 1.5 ml Complete physical examination	0.5 ml in EDTA tube[1] 1.0 ml heparin tube for ALT, AST, BUN, Creatinine, ALP, Glucose, NA, K, Cl and TP
	Splenectomy	NA
	Ketamine restraint 5-20 mg/kg, weighing Implant transponder	NA
	Withhold morning feed, Ketamine restraint 5-20 mg/kg, weighing, venipuncture 1.5 ml Complete physical examination Place neck collar Start clinical observation with VET-GP-008-F5	0.5 ml in EDTA tube[1] 1.0 ml heparin tube for chemistries[2]

	Start pole-collar training and continue for 2 weeks	
-1	Start Clinical observation** 3 times daily using study specific form#1 Temperature measurement via both rectum and transponder 3 times at 0800, 1100 and 1900	NA
0	Clinical observation** 3 times daily with study specific form#1 and measure temperature both via transponder and rectal temp at 0800, 1100 and 1900 Pole-collar restraint Blood smear collection 3 times prior to malaria infected at 0800, 1100 and 1900 Venipuncture 2.5 ml for CBC, chemistries, blood gas, nitric oxide and TNF-α at 0800 Ketamine restraint 5-20 mg/kg, weighing, blood smear collection Inoculation 1 ml, IV (5 x 10^6 infected erythrocytes) (not later than 0800) Pole-collar and chair restraint Venipuncture 1.5 ml for CBC, chemistries and blood gas at 1900	Baseline at 0800 before blood inoculation: 0.5 ml in EDTA tube[1] 1.0 ml heparin tube for chemistries[2] 0.5 ml in EDTA for TNF-α[3] 0.5 ml in heparin for nitric oxide[4] Thick and thin blood smears At 1900: 0.5 ml in EDTA tube[1] 1.0 ml heparin tube for chemistries[2] Thick and thin blood smears

Study Days	Procedures	Specimens
1 – 4	Clinical observation** 3 times daily with study specific form#1 and measure temperature both via transponder and rectal temp at 0800, 1100 and 1900 Pole-collar restraint Blood smear collection 3 times at 0800, 1100 and 1900 Pole-collar and chair restraint Venipuncture 1.5 ml for CBC, chemistries and blood gas at 1900	At 0800 and 1100: Thick and thin blood smears At 1900: 0.5 ml in EDTA tube[1] 1.0 ml heparin tube for chemistries[2] Thick and thin blood smears
5	Clinical observation** 3 times daily with study specific form#1 and measure temperature both via transponder and rectal temp at 0800, 1100 and 1900 Pole-collar restraint Blood smear collection 3 times at 0800, 1100 and 1900 Pole-collar restraint at 1500 Venipuncture 4 ml for nanostructural analysis Pole-collar and chair restraint Venipuncture 1.5 ml for CBC, chemistries and blood gas at 0700 and 1900	At 0800, 1100 and 1900: Thick and thin blood smears At 0700 and 1900: 0.5 ml in EDTA tube[1] 1.0 ml heparin tube for chemistries[2] At 1500 4 ml heparin for nanostructural analysis and atomic force microscopy[5]

6	Weighing by transfer box Clinical observations 8 times/daily on study specific form#1 and temperature measurements both via transponder and rectal temp 8 times at 0700, 1000, 1300, 1600, 1900, 2100, 2400 and 0300 Pole-collar restraint Blood smear collection 8 times at 0700, 1000, 1300, 1600, 1900, 2100, 2400 and 0300 Pole-collar and chair restraint at 0700, 1500 and 2300 Venipuncture 1.5 ml for CBC and chemistries EKG measurement at 0700, 1500 and 2300	Send animal's weight to DVM Lab At 0700, 1000, 1300, 1600, 1900, 2100, 2400 and 0300: Thick and thin blood smears At 0700, 1500 and 2300: 0.5 ml in EDTA tube[1] 1.0 ml heparin tube for chemistries[2]

Study Days	Procedures	Specimens
7	Clinical observation 8 times on study specific form#1 and measure temperature both via transponder and rectal temp 8 times at 0700, 1000, 1300, 1600, 1900, 2100, 2400 and 0300 Pole-collar restraint Blood smear collection 8 times at 0700, 1000, 1300, 1600, 1900, 2100, 2400 and 0300 Pole-collar and chair restraint at 0700, 1500 and 2300 Venipuncture 1.5 ml for CBC and chemistries EKG measurement At 1500 pole-collar and chair restraint Venipuncture 5.5 ml for nanostructural analysis	At 0700, 1000, 1300, 1600, 1900, 2100, 2400 and 0300: Thick and thin blood smears At 0700, 1500 and 2300: 0.5 ml in EDTA tube[1] 1.0 ml heparin tube for chemistries[2] At 1500 or before treatment 5.5 ml heparin for nanostructural analysis and atomic force microscopy[5]
8	Clinical observation 8 times on study specific form#1 and measure temperature both via transponder and rectal temp 8 times at 0700, 1000, 1300, 1600, 1900, 2100, 2400 and 0300 Pole-collar restraint Blood smear collection 8 times at 0700, 1000, 1300, 1600, 1900, 2100, 2400 and 0300 Pole-collar and chair restraint at 0700, 1500 and 2300 Venipuncture 1.5 ml for CBC and chemistries EKG measurement	At 0700, 1000, 1300, 1600, 1900, 2100, 2400 and 0300: Thick and thin blood smears At 0700, 1500 and 2300: 0.5 ml in EDTA tube[1] 1.0 ml heparin tube for chemistries[2]

9	Clinical observation 8 times on study specific form#1 and measure temperature both via transponder and rectal temp 8 times at 0700, 1000, 1300, 1600, 1900, 2100, 2400 and 0300 Pole-collar restraint Blood smear collection 8 times at 0700, 1000, 1300, 1600, 1900, 2100, 2400 and 0300 Pole-collar and chair restraint at 0700, 1500 and 2300 Venipuncture 1.5 ml for CBC and chemistries EKG measurement Day TX 1: 1st Tx around 2000: Pole-collar and chair restraint Place IV catheter, and infuse methylene blue as a slow IV push (3-4 mL/minute) per drug into an IV extension line of D5W Twice daily	At 0700, 1000, 1300, 1600, 1900, 2100, 2400 and 0300: Thick and thin blood smears At 0700, 1500 and 2300: 0.5 ml in EDTA tube[1] 1.0 ml heparin tube for chemistries[2]

Study Days	Procedures	Specimens
10	Clinical observation 8 times on study specific form#1 and measure temperature both via transponder and rectal temp 8 times at 0800, 1100, 1300, 1600, 1900, 2100, 2400 and 0300 Pole-collar restraint Blood smear collection 8 times at 0800, 1100, 1300, 1600, 1900, 2100, 2400 and 0300 EKG measurement at 1100, 1500 and 2300 Day TX 2: 2nd and 3rd Tx (at 0800 and 2000): Pole-collar and chair restraint Place IV catheter Venipuncture 1.5 ml for CBC and chemistries before providing treatment and infuse methylene blue as a slow IV push (3-4 mL/minute) per drug into an IV extension line of D5W Twice daily	At 0800, 1100, 1300, 1600, 1900, 2100, 2400 and 0300: Thick and thin blood smears At 0700 and before providing treatment: 0.5 ml in EDTA tube[1] 1.0 ml heparin tube for chemistries[2]

11	Clinical observation 8 times on study specific form#1 and measure temperature both via transponder and rectal temp 8 times at 0700, 1000, 1300, 1600, 1900, 2100, 2400 and 0300 Pole-collar restraint Blood smear collection 8 times at 0700, 1000, 1300, 1600, 1900, 2100, 2400 and 0300 EKG measurement at 0700, 1500 and 2300 Day TX 3: 4th and 5th Tx (at 0800 and 2000): Pole-collar and chair restraint Place IV catheter Venipuncture 1.5 ml for CBC and chemistries before providing treatment and infuse methylene blue as a slow IV push (3-4 mL/minute) per drug into an IV extension line of D5W Twice daily	At 0700, 1000, 1300, 1600, 1900, 2100, 2400 and 0300: Thick and thin blood smears Before providing treatment and 1900: 0.5 ml in EDTA tube[1] 1.0 ml heparin tube for chemistries[2]

Study Days	Procedures	Specimens
12	Clinical observation 8 times on study specific form#1 and measure temperature both via transponder and rectal temp 8 times at 0700, 1000, 1300, 1600, 1900, 2100, 2400 and 0300 Pole-collar restraint Blood smear collection 8 times at 0700, 1000, 1300, 1600, 1900, 2100, 2400 and 0300 Day TX 4: 6^{th} Tx (at 0800): Pole-collar and chair restraint Place IV catheter Venipuncture 1.5 ml for CBC and chemistries before providing treatment and infuse Methylene blue as a slow IV push (3-4 mL/minute) per drug into an IV extension line of D5W Twice daily At 1900: Venipuncture 1.5 ml for CBC and chemistries	At 0700, 1100 and 1900: Thick and thin blood smears At before providing treatment and 1900: 0.5 ml in EDTA tube[1] 1.0 ml heparin tube for chemistries[2]
13	Clinical observation** 3 times daily using study specific form#1 and measure temperature both via transponder and rectal temp at 0800, 1100 and 1900 Pole-collar restraint Blood smear collection 3 times at 0800, 1100 and 1900 Pole-collar and chair restraint Venipuncture 1.5 ml for CBC and chemistries at 1900	At 0800, 1100 and 1900: Thick and thin blood smears At 1900: 0.5 ml in EDTA tube[1] 1.0 ml heparin tube for chemistries[2]

14	Clinical observation** 3 times daily using study specific form#1 and measure temperature both via transponder and rectal temp at 0800, 1100 and 1900 Pole-collar restraint Blood smear collection 3 times at 0800, 1100 and 1900 Pole-collar and chair restraint Venipuncture 1.5 ml for CBC and chemistries at 1900	At 0800, 1100 and 1900: Thick and thin blood smears At 1900: 0.5 ml in EDTA tube[1] 1.0 ml heparin tube for chemistries[2]

Study Days	Procedures	Specimens
15	6 Days post initiation of treatment, the animals where to be euthanized Ketamine restraint 5-20 mg/kg, weighing, blood collection 2.5 ml *Euthanized all experimental animals, collected exsanguination blood, blood smear, 3 ml CSF and perform full autopsy*	Before scheduled euthanasia 0.5 ml in EDTA tube[1] 1.0 ml heparin tube for chemistries[2] 0.5 ml in heparin for nitric oxide[4] Thick and thin blood smears Exsanguination 50 ml in EDTA tube 50 ml clot tube 100 ml heparin tube

[1] 0.5 ml EDTA blood for complete blood count, reticulocyte count and parasite determination at DVM.

[2] 1.0 ml heparin blood for blood chemistries: BUN, CREA, BUN/CREA ratio, ALT, AST, ALP, GLUC, Total Protein, Na, K, Cl, Serum Lactate, blood pH and methemoglobin by automated hematology analyzer at DVM.

[3] 0.5 ml EDTA blood for TNF-α level, send to DVM lab for centrifuging 20 minutes at 2000 x g. Plasma was either removed and assayed immediately or aliquoted and stored at -20° C. Subsequent use avoided repeated freeze-thaw cycles.

[4] 0.5 ml heparin blood for nitric oxide levels was sent to DVM lab for centrifuging, 20 minutes at 2000 x g. Plasma was either removed and assayed immediately or aliquoted and stored at -20° C. Subsequent use avoided repeated freeze-thaw cycles.

[5] 0.5-2 ml heparin blood for nanostructural analysis and atomic force microscopy.

2.4.1 **Study endpoints**:

Treatment failure was determined by the attending/supervising veterinarian in association with the Principal Investigator and the infected monkeys were considered as having reached study

endpoints if/when the level of parasitemia reached between 20-25% PLUS any THREE of the following clinical criteria post treatment.

1. Activity score of 3 for 2 consecutive clinical sign assessment periods
2. Non-responsive mentation score
3. Anorexia for 3 consecutive feeding periods.
4. Jaundice (by appearance-scleral icterus)
5. Hematuria with frank blood
6. Severe anemia (Hgb <8 mg/dl)
7. Acute renal failure (Persistent rise in BUN and Creatinine as interpreted by the supervising veterinarian and the PI)
8. Marked to severe dyspnea
9. Vomiting
10. Petechiae/ecchymoses on skin or mucous membranes
11. Persistent elevated temperature of 104^{o}F or higher for 3 consecutive assessment periods

Table 2.5: Methylene Blue dosage study – 9 experimental monkeys

Agent	**Group designation**
MB 6 mg/kg IV bid	Group 1 n=3
MB 10 mg/kg IV bid	Group 2 n=3
MB 17 mg/kg IV bid	Group 3 n=3

Table 2.6: Drug Dosing Schedule

Cohort/Group	Monkeys*	Drug/Route	Dose (mg/kg)	Frequency
Donor A, B	2 monkeys	CQ PO	10 mg/kg	Daily for 7 days
Group 1-Pilot	3 monkeys	MB IV	6 mg/kg	Twice Daily for 3 days
Group 2-Pilot	3 monkeys	MB IV	10 mg/kg**	Twice Daily for 3 days

Group 3-Pilot	3 monkeys	MB IV	17 mg/kg	Twice Daily for 3 days

* All available monkeys may have had prior exposure and infections with one or more of the following monkey malaria infections (*P. knowlesi* or *P. cynomolgi*).

** MB dose levels based on data collected from prior pharmacokinetic studies in rhesus monkeys, humans and rats. AUC for rhesus monkey is 3.5 times smaller than in humans. Human doses in clinical trials have ranged from 2-12 mg/kg orally. Single doses up to 20 mg/kg have been tolerated in rhesus monkeys.

2.4.2 **Clinical Observations:**

Observations for signs of clinical toxicity, disease symptomology and evaluation of having reached the treatment window were made at varying timepoints as laid out in the study schedules (Table 2/Table 3). These consisted of a minimum of three times daily and peaked at every other hour over a 24-hour period based on parasitemia. These evaluations included an assessment of appetite, posture, activity, breathing, level of arousal, color of urine and feces, blood pressure, temperature, and signs of painful urination, and were recorded on the Animal Care record as well as in the study specific forms. Electrocardiograms were obtained from chaired, pole and collared animals without sedation.

Each monkey's injection/phlebotomy sites were closely observed for irritation/swelling or other adverse reactions. All unusual observations were recorded. Exact observation times were recorded for each monkey. Any signs of major organ toxicity based on clinical criteria combined clinical chemistry and hematology results were recorded and appropriate actions determined by the Attending Veterinarian in consultation with the PI and co-PIs.

2.5 **Clinical Sign recording**:

Monitoring of the experimental animals in both the refinement study and the MB drug dosing study included Giemsa-stained blood films (thick and thin), clinical and repeated daily hematology and serum chemistry evaluations. On treatment days for the MB drug dosing study, all clinical observations and weights measurements were conducted prior to the scheduled treatment and all phlebotomies were performed prior to treatment as well.

Throughout the study, at each blood draw, clinical signs were assessed and recorded in Study Specific Form #1 (SSF #1) to include neurological signs, activity level, respiratory changes, pulse, level of consciousness, urine characteristics, vomiting/diarrhea, jaundice, dermal petechiae/coagulative abnormalities, anorexia and dehydration. Study Specific Form #2 (not shown) consisted of a spreadsheet which outlined the specific times for blood collection, identified the volumes and the type of collection vial and number of blood smears performed. As temperatures were measured both rectally and via subcutaneous transponder at each blood collection, this data was also recorded on the study specific form. This form followed the individual animal throughout the study, from study day -1 through euthanasia.

Study Specific form #1 assigned values to the clinical signs observed. The additive score was used by the technical staff as a guideline with which to decide when to notify the attending veterinarian and for the veterinary staff as a mechanism in which to determine the need for initiation of fluid therapy. The clinical signs evaluated included activity level, menace response (spontaneous blink and withdrawal reaction to sudden movement near the eyes), mentation, breathing characteristics (bradypnea, tachypnea, dyspnea), presence or absence of vomitus, skin discoloration (to include erythema and petechiation) and turgor, urination facility, volume and color, and appetite. Furthermore, additional features would be annotated such as diarrhea, melena, ataxia, seizure

activity, tremoring, epistaxis, opisthotonus, piloerection, salivation, hemiplegia and inappropriate vocalization.

Study Specific Form #1

Clinical Observation Record for Sever Malaria Study Protocol #: Study Specific Form #1

Animal ID: Group ID: Study Date (Day 0):

Date:	Time:	Study Day:	Activity Level	Menace	Animal Mentation	Animal Breathing	Vomit	Skin color	Skin Turgor	Urine color	Urination	Appetite food	Animal score	**Initial**	Temp (°F)	Animal weight (kg)	**VT int**	Other Observations Treatments

Experimental Animal's Infected Blood), as well as for clinical chemistry evaluation and complete blood count (CBC).

Blood smear samples on glass slides were fixed in methanol and stained with Giemsa. They were examined for the presence or absence of parasites under the oil-immersion objective as well as parasite staging. If no parasites are found in 50 microscopic oil-immersion thick fields or per 1000 white blood cells (WBCs), the smears were considered negative. The parasitemia level was reported as number of parasites per 1µl or mm^3 of whole blood. Parasites were counted per number of WBCs or red blood cells (RBCs), i.e., per 100 –300 WBCs or 500 – 10,000 RBCs. Parasitemia levels were calculated by the appropriate total blood cell count (white or red) per mm^3.

2.5.2 **Parasitemia assessment**:

Using a non-anticoagulant capillary pipette, the blood was drawn from a well-mixed EDTA blood vial and filled the capillary at least two-thirds with blood. The end of the capillary was touched onto the first clean glass slide. The first drop (for thick smears) was placed about 1 cm from the frosted end and another one drop (for thin smears) about 1 cm apart from the first drop.

2.5.2.1 **Thick smear**. Using a second clean slide (as a spreader slide) the first drop of blood was smoothed in a circular motion to cover an area 1-1.5 cm in diameter. Excess blood on the spreader was wiped off with clean dry gauze.

2.5.2.2 **Thin smear**. One end of the spreader slide was placed in front of the second drop of blood at a 35 -45° angle and then pulled back into the drop of blood. The blood film was allowed to spread and fill the angle between the two slides. The spreader slide was then pushed forward until all of the blood had been spread into a moderately thin film.

Note: The blood smear should not cover the entire surface of the slide. In a good thin smear, there was a thick portion and a thin portion and a gradual transition from one to the other. A quality blood

film was determined to have a smooth, even appearance, free from ridges waves, or holes. The feathered edge (an end of smear) was smooth and even. (Figure 1) It was crucial that the edge of the "spreader" slide was absolutely smooth. If it was rough, the blood film had ragged tails containing many leukocytes.

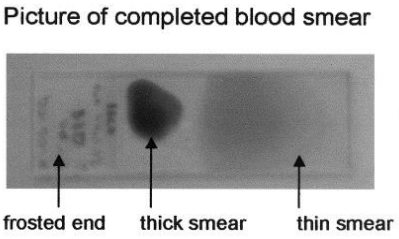

Figure 2.1.

Photograph of a glass slide demonstrating the differences between thick and thin blood smears for malaria parasitemia counts.

The spreader was then alternately used for making the second smear slide with the same animal's blood sample. The first completed slide was used as a spreader slide and prior to making the blood smear on the second slide, the spreader slide was wiped off of excess blood remaining on the edge of slide with a clean gauze.

2.5.2.3 **Parasite staging**:

Parasite stage evaluations were conducted by experienced technicians at AFRIMS. These were performed using the blood smears generated during the study for the purpose of parasitemia assessment, but were evaluated typically weeks following the close of the experiment due to the time requirements for accurate assessments. For the sake of this study, the parasite stages were limited to categories of trophozoites, gametocytes and schizonts.

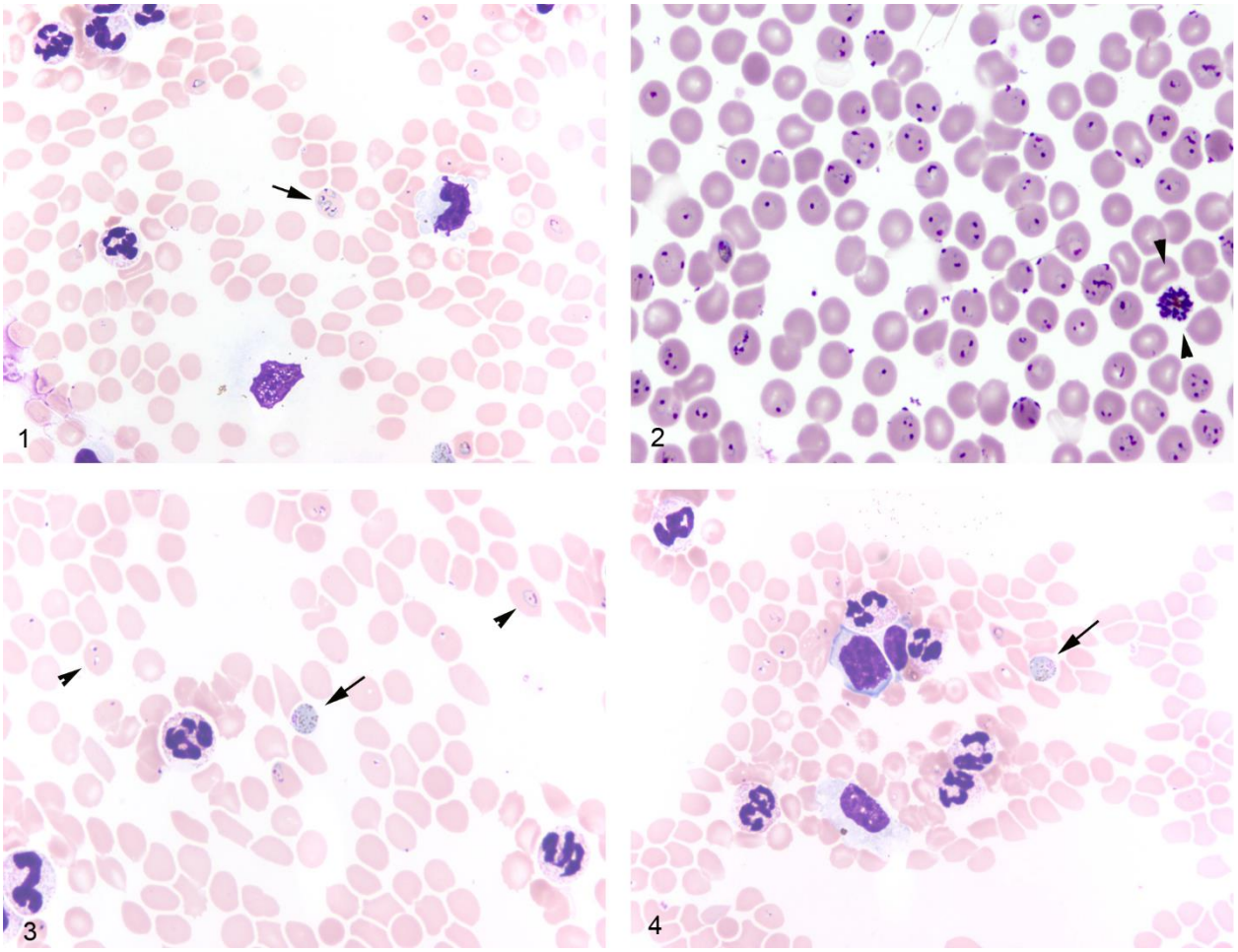

Figure 2.2.1-4. Giemsa stained rhesus macaque blood smears infected with *P. coatneyi* examined under oil immersion at 1000x. Parasite stage examples.

1. Trophozoites, ring stage, multiple infection (arrow)

2. Schizont (arrowheads)

3. Gametocyte (arrow); trophozoites, ring stage (arrowheads)

4. Gametocyte (arrow)

2.5.3 **Blood chemistry and hematology**:

2.5.3.1 **Clinical Chemistry**:

1. Alanine transaminase (ALT)
2. Aspartate aminotransferase (AST)
3. Alkaline phosphatase (ALP)
4. Gamma-glutamyl transferase (GGT)

5. Glucose
6. Blood Urea Nitrogen (BUN)
7. Creatinine (CRE)
8. Albumin
9. Total Protein
10. Bilirubin
11. Lactate
12. Total Cholesterol
13. C-reactive Protein
14. Creatine phosphokinase
15. Sodium (Na^+)
16. Potassium (K^+)
17. Chloride (CL^-)

2.5.3.2 **Hematology**:

1. Total leukocyte count (WBC)
2. Erythrocyte count (RBC)
3. Hemoglobin (HGB)
4. Hematocrit (HCT)
5. Mean corpuscular volume (MCV)
6. Mean corpuscular hemoglobin (MCH)
7. Mean corpuscular hemoglobin concentration (MCHC)
8. Reticulocyte counts (RETIC) by flow cytometry
9. Platelet count (PLT)
10. Differential leukocyte count

2.6 **Blood volume calculations**:

Blood volumes were calculated in adherence with SOP requirements for maximum blood volume draw per week based on each individual animal's weight.

The guidelines for the total volume of blood drawn followed published guidance in the guide for the care and use of laboratory animals (NRC 2011), "Removal of blood from laboratory mammals and birds" (Joint Working Group on Refinement). Accordingly, up to 10% of the circulating blood volume could be safely taken every 3 to 4 weeks without the need for hematologic monitoring. The circulating blood volume was estimated as 54-70 mL/kg (cc/Kg) of body weight.

For a rhesus monkey, circulating blood volume is estimated conservatively to be 54 cc/kg. Thus, using the lowest weight in kg of a monkey eligible for enrollment (6 kg = 324 cc total blood volume), at least 33 cc could be safely drawn every 4 weeks from each monkey.

The recommended 32 cc in a four-week window was at no point exceeded, prior to euthanasia. See Table 6 for listing of blood draws.

Table 2.7: Daily Blood Volumes:

	Parasitemia	CBC	Chemistry	Temperature	Clin. signs	Blood volume
Day 0	3x daily	2x daily	2x daily	3x daily	3x daily	3cc
Day 1	3x daily	1x daily	1x daily	3x daily	3x daily	1.5cc
Day 2	3x daily	1x daily	1x daily	3x daily	3x daily	1.5cc
Day 3	3x daily	1x daily	1x daily	3x daily	3x daily	1.5cc
Day 4	3x daily	1x daily	1x daily	3x daily	3x daily	1.5cc

Day 5	3x daily	2x daily	2x daily	3x daily	3x daily	7.5cc
Day 6*	8x daily	3x daily	3x daily	8x daily	8x daily	4.5cc
Day 7*	8x daily	3x daily	3x daily	8x daily	8x daily	10cc
Day 8*	8x daily	3x daily	3x daily	8x daily	8x daily	4.5cc
Day 9*	8x daily	3x daily	3x daily	8x daily	8x daily	4.5cc
Day 10*	3x daily	2x daily	2x daily	3x daily	3x daily	4cc
Day 11*	3x daily	1x daily	1x daily	3x daily	3x daily	2.5cc
					Total	45.5cc/2 weeks

*Anticipated treatment initiation would be Day 6 and continue through Day 11.

2.7 **Retinoscopy**:

Immediately prior to euthanasia, four animals from the MB study were anesthetized using intramuscular ketamine hydrochloride injection (5-20mg/kg) and underwent ophthalmoscopy to assess retinal changes. Immediately upon sedation, both pupils were dilated using 0.5%/1% tropicamide. Once mydriasis was achieved, digital fundus photography was performed using a portable handheld retinal camera (Kowa Genesis D, Kowa, Japan). A minimum of nine overlapping photographs were captured from each retina to cover the macula, optic disc and peripheral retina. Two masked expert investigators examined the composite photographs for retinal abnormalities. Inter-observer variations were resolved through consensus.

2.8 **Study endpoints**:

2.8.1 **Treatment Outcome Definitions**:

Success:

- Parasitemia decline by ≥ 75% at 48 hours with clinical improvement, *and*
- Parasitemia clearance >99% at the third day after treatment initiation, *and*
- Absence of moribund behavior, stable respiratory status, and stable blood pressure.

Failure:

- Parasitemia decline by < 75% at 48 hours with clinical deterioration, *or*
- Failure to clear parasitemia by 99% by day 3 after treatment initiation, *or*
- Moribund behavior, unstable respiratory status, or unstable blood pressure at the end of three days of therapy.

Further treatment failure was determined by the attending/supervising veterinarian in association with the Principal Investigator and the infected monkeys were considered as having met study endpoints if/when the level parasitemia reached between 20-25% PLUS any THREE of the following clinical criteria are reached post treatment.

1. Activity score of 3 for 2 consecutive clinical sign assessment periods
2. Non-responsive mentation score
3. Anorexia for 3 consecutive feeding periods.
4. Jaundice (by appearance-scleral icterus)
5. Hematuria with frank blood
6. Severe anemia (Hgb <8 mg/dl)
7. Acute renal failure (Persistent rise in BUN and Creatinine as interpreted by the supervising veterinarian and the PI)
8. Marked to severe dyspnea
9. Continued vomiting
10. Petechiae/ecchymoses on skin or mucous membranes
11. Persistent elevated temperature of 104 or higher for 3 consecutive assessment periods

If monkeys were deemed to be in significant pain or distress in the opinion of the Attending Veterinarian, analgesics and/or supportive treatment as required were to be administered using IV

fluids and buprenorphine (0.01 mg/kg IM q12 hours). If the monkeys became moribund or otherwise experienced severe pain or distress that could not be alleviated, they would have been humanely euthanized. Other examples, as described below, of criteria for euthanasia included: unresponsive shock, severe respiratory distress or respiratory failure, severe anemia causing shock symptoms, recurrent or persistent seizures, evidence of stroke, or continued clinical deterioration after 48 hours of therapy.

It was expected, in this severe malaria model, that the animals would display signs of severe malaria at the initiation of therapy, and that they would continue to show these signs during the first 24 hours of therapy regardless of the medication used. Anticipated clinical signs included combinations of the above listed clinical criteria, however these were expected to be transient and reversible once treatment was initiated. Additionally, clinical chemistry and hematological findings were expected to demonstrate organ pathology. These included:

1. Hypoglycemia
2. Metabolic acidosis
3. Severe anemia
4. Hyperparasitemia
5. High blood lactate
6. Renal impairment (elevated BUN and Creatinine)

2.9 **Euthanasia**:

These were terminal experiments, and the intent was for all experimental animals to be humanely euthanized upon reaching euthanasia criteria or their timed study endpoint. Due to the rapid spike in parasitemia in some animals in the first stages of the pilot study, animals died without the benefit of euthanasia. This problem was subsequently managed through increasing the parasitemia

assessments to every other hour. Euthanasia was performed in accordance with AFRIMS Vet Med SOP: Euthanasia of Nonhuman Primates and Other Small Mammals.

Briefly:

1. The person performing euthanasia was required to be technically proficient, use humane handling methods, to understand the reasons for euthanasia, and be trained in the method of euthanasia being employed.
2. Euthanasia was performed in an appropriate area, such as autopsy room or procedure room, that did not contain other animals.
3. Gentle restraint minimizes animal distress, including fear and anxiety. As prescribed by a veterinarian, appropriate chemical restraint was required prior to euthanasia, especially when humane restraint could not be achieved manually or might have posed a risk of injury to the animal or to the person restraining it. As such, the monkeys were chemically restrained with intramuscular ketamine hydrochloride injection (5-20mg/kg).
4. Once sedated, injectable commercial euthanasia agent (Fatal-plus or its equivalent) was given intravenously to induce euthanasia.
5. The euthanizing dose of Fatal-plus use was 100mg/kg. The first half of the dose was given rapidly, with the second half being given more slowly.
6. The animals were observed by the attending veterinarian for a few minutes or until breathing stopped. The complete absence of heartbeats was confirmed by stethoscope before the needle was removed.
7. An additional ¼ dose of euthanasia or anesthetic agent was given if the heartbeat remained.

2.9.1 **Terminal sample collection**:

1. Terminal blood smears were made in order to quantify the parasitemia and for subsequent parasite staging.

2. Sterile urine was collected at autopsy via cystocentesis and a urinalysis was conducted. The remaining volume was spun down and frozen.

3. Cerebral Spinal Fluid was collected immediately post mortem and just prior to autopsy and a drop was placed on a slide for a cellularity assessment. Remaining volume was spun down and frozen. CSF was collected from the cisterna magna at the juncture of the point where the cranial wings of the atlas and the external occipital protruberance bisect. The subarachnoid space was entered using a 22-gauge spinal needle. In rare cases where there was difficulty in collecting CSF in this manner, at autopsy, a cut down was performed and the pathologist collected a CSF sample prior to initiating the autopsy.

2.9.2 **Autopsy guidelines**:

1. Multiple representative tissues were collected from every organ system and photographed.

2. The liver with the gallbladder emptied; brain (cerebrum, cerebellum, brain stem); lungs (without trachea) were weighed.

3. CSF was sampled at euthanasia. As previously described, a drop was placed on a slide for cellularity evaluation and the rest was spun down, aliquoted and frozen at -80°.

4. Terminal blood was taken from the vena cava and the heart. Samples were separated into whole blood and serum. Excess not allocated for use in various tests was aliquoted and frozen at -80°.

5. Both eyes were taken to include a section of optic nerve. Retinal samples were removed from one of the eyes and small sections preserved in Glutaraldehyde and in RNA later. The remaining ocular tissue was preserved in Davidson's solution and in the intact eye, Davidson's was injected at the lateral canthus into the anterior chamber until the globe was firm.

6. Sections of the entire gastrointestinal tract were sampled, 2-3 cm sections were tied off at both end and injected with formalin.

7. The entire spinal cord was removed and preserved whole, a suture was placed in the cervical cord as an identifier.

8. Representative lymph nodes (Mesenteric, popliteal, axillary, inguinal, submandibular and ileocecal), pituitary gland and adrenal glands were identified and labeled.

9. Bone marrow was fixed in-situ in sections of the sternum.

10. Cortical cerebrum samples were made into smears and stained with Giemsa following 30 second fixation in 50% ethanol/methanol mix and air dried.

11. Sterile urine was collected during autopsy directly from the urinary bladder. A urinalysis was conducted, and the remaining volume spun down, aliquoted and frozen at -80°.

12. Tissues for TEM were collected and sectioned into 1 cm cubes and preserved at a volume of 1 mm/1 ml of solution in individual tubes. Tissues for molecular analysis were sectioned at ½ cm and placed in a 1.8 ml Eppendorf tube filled to 1.5ml with RNA later medium. All tubes were clearly labeled as to organ, RNA vs EM and animal accession number. Collection of these tissues were prioritized and ideally were collected within the first 5-10 minutes of the autopsy.

    - The following tissues were preserved in RNA later as multiple (3-5) squares: Central Nervous System (thalamus; hippocampus; fore brain; cerebellum; brain stem; spinal cord), kidney, heart, liver, lung, retina

    - The following tissues were preserved in buffered Glutaraldehyde as multiple (3-5) squares: Central Nervous System (thalamus; hippocampus; fore brain; cerebellum; brain stem; spinal cord), kidney, heart, liver, lung, retina

13. Ante-mortem retinal photographs were taken as possible, immediately prior to euthanasia. Atropine drops were applied during pre-euthanasia blood draw 10 minutes prior to imaging to ensure adequate iridial dilation.

2.9.3 **Fixation, processing and staining**:

1. All tissues collected for histopathology were trimmed into small sections (approximately 2-5 cm), placed into 10% buffered formalin at a tissue:formalin ratio of at least 1:10 within minutes of euthanasia. Formalin was refreshed after 24 hours of fixation to help avoid formation of formalin pigment within tissue sections.

2. For adequate fixation, it was important that tissue sections were no more than 1 cm thick, with the exception of lung and brain. If larger sections were collected, the samples were "bread-loafed" to ensure adequate penetration by the formalin and were preserved with a higher formalin to tissue ratio (up to 1:20) to ensure rapid fixation.

3. In general, sampled lesions involved taking a sample at the margin of any observed lesion that includes adjacent normal tissue as well as one from the center of the lesion. Normal tissue from the affected organ was also sampled for comparison.

4. The fixed tissues were trimmed into 5 mm dice and processed using an automated tissue processor (SLEE medical, Mainz, Germany) as follows: dehydration (70% Isopropanol for 1 h, 95% Isopropanol for 1 h x 3 times, and 100% Isopropanol for 1 h x 3 times), clearing (Xylene substitute (Sigma, St. Louis, MO, USA) for 1 h x 3 times) and paraffin infiltration (molten paraffin for 30 min x 2 times).

2.9.4 **Histological staining**:

Formalin fixed tissue samples were prepared for histopathological evaluation as H&E Sections as described by Prophet et al. Simply, sections were cut at 4µm using a semi-automated rotary

microtome (RM2245, Leica, Buffalo Grove, IL, USA). The tissue sections were mounted onto poly L-lysine coated microscope slides and baked at 60 °C for 14-18 h. Sections were stained with H&E using described techniques. (Harris hematoxylin for 6 min, running tap water for 1 min, eosin Y for 10 min, 70% ethanol for 1 min, 95% ethanol for 1 min, 100% ethanol for 1 min, two rinses in 100% xylene for 1 min each).

2.9.5 **Histopathological analysis and scoring system**:

The H&E stained tissue slides were examined by both a board certified veterinary pathologist (EL) and by a board certified medical pathologist (GT) using Olympus BX43F bright field microscopes (Olympus, Tokyo, Japan). This study reviewed the histopathology from animals within the AFRIMS tissue archives as well as through tissue sharing from an ongoing drug trial protocol using the splenectomized rhesus macaque/*P. coatneyi* model of severe malaria. The selected autopsy cases, which numbered a total of 45, comprised of 30 retrospective and 15 prospective cases where chosen primarily based on experimental history (excluding those cases in which animals had prior clinical infections with either *P. falciparum* or *P. coatneyi*). These were then compared to several spleen-intact animals and 15 malaria naive control animals. Tissues were evaluated qualitatively for histopathologic changes in comparison with control animals and excluding any background lesions observed in the AFRIMS macaque colony through experience or described in the literature. (McInnes 2012)

The spectrum of tissues available for review was constrained in animals from the retrospective cohort by which tissues were collected at the time of those particular studies. In all animals, cerebrum, cerebellum, brain stem, liver, kidneys, heart and lungs were available, while in only some animals were specimens of adrenal and pituitary glands, pancreas, gastrointestinal system, skeletal muscle, eyes, lymph nodes, urinary bladder and reproductive tract obtained and available for review. In contrast, full autopsies were conducted in the prospective study, which included sampling

from multiple areas of the brain and spinal cord. Spinal cord samples were not available from any retrospective study. In 3 animals, splenunculi were identified and evaluated. Once each pathologist had read out the material, consensus relating to any lesion description or scoring discrepancies, was reached through working jointly on a multi-head microscope. Histopathological lesion scoring conducted by both pathologists as follows: 0 = Within Normal Limits, 1= Minimal, 2 = Mild, 3 = Moderate, 4 = Marked, 5 = Severe. Results are discussed in detail in Chapter 4: Cytology and Histopathology.

2.10 **Immunohistochemistry staining**:

2.10.1 **Sample preparation**:

Rhesus tissue samples were fixed in 10% phosphate buffered formalin for at least 48 h. The ratio of tissue: formalin was 1 part tissues to 10 parts formalin. The fixed tissues were trimmed into 5 mm dice and processed using an automated tissue processor (SLEE medical, Mainz, Germany) as follows: dehydration (70% Isopropanol for 1 h, 95% Isopropanol for 1 h x 3 times, and 100% Isopropanol for 1 h x 3 times), clearing (Xylene substitute (Sigma, St. Louis, MO, USA) for 1 h x 3 times) and paraffin infiltration (molten paraffin for 30 min x 2 times). The processed tissues were then embedded into paraffin blocks and sectioned at 5 µm using a semi-automated rotary microtome (RM2245, Leica, Buffalo Grove, IL, USA). The tissue sections were mounted onto poly L-lysine coated microscope slides and baked at 60 °C for 14-18 h.

2.10.2 **Deparaffinization, rehydration, and antigen retrieval**:

To retrieve the epitope in formalin-fixed tissue sections for immune reaction, the heat-induced epitope retrieval (HIER) was used in this study. For CD3, CD20, CD68, Fibrinogen, and Glial Fibrillary Acidic Protein (GFAP) staining, the formalin-fixed paraffin embedded tissues were

deparaffinized, rehydrated, and antigen-retrieved using Pre-treatment module 3-in-1 procedure (PT-link, Dako, Glostrup, Denmark), with Tris/EDTA buffer pH 9 (3-in-1 Target Retrieval solution, Dako, Glostrup, Denmark) at 95 °C for 20 min and then left to cool down to 65 °C. The tissue slides were transferred to incubate in PT-link tank with wash buffer (EnVision™ FLEX Wash Buffer, Dako, Glostrup, Denmark) for 20 min at room temperature.

For CD61 staining, paraffin embedded tissue sections were deparaffinized with Xylene substitute (Sigma, St. Louis, MO, USA) for 5 min 3 times, 100% Ethanol for 2 min twice, 95% ethanol for 2 min twice and an 80% Ethanol for 2 min, and deparaffinized tissue sections were then placed in pressure cooker (Decloaking chamber™ NxGen, Biocare Medical, Concord, CA, USA) and heated at 110ºC for 10 min with citrate buffer, pH6 (Dako, Glostrup, Denmark). The tissue section slices were then removed from the pressure cooker when the chamber temperature decreased to 80 °C and let cool down at room temperature for 20 min.

Before immunostaining, the slides were washed for 3 min in wash buffer bath for 3 times. From this point onwards, tissue sections were always kept moist to avoid non-specific binding and therefore artefactual high background staining.

2.10.3 **Immunohistochemical staining**:

To determine the immunohistopathology of *P. coatneyi* infection in rhesus macaque model, the tissue sections from *P. coatneyi* infected (6 monkeys) and control monkeys (6 monkeys) were immunostained with CD3, CD20, CD61, CD68, Fibrinogen, and GFAP antibodies as primary antibodies. After antigen retrieval, the tissue sections were circled with a hydrophobic barrier pen (Dako, Glostrup, Denmark) to create a barrier for liquids and minimize the amount of reagents required. The optimal dilution of primary antibodies, secondary antibodies, and substrates are shown in Table 1. Primary antibodies and secondary antibodies were diluted with antibody diluent (Dako, Glostrup, Denmark). The diluted primary antibody was added to cover the entire tissue section and incubated

at room temperature in a humidified chamber. Negative control slides included tissue sections incubated with antibody diluent without primary antibody, or omission of the secondary antibody step. The slides were then washed 3 times for 3 min each in a wash buffer bath and incubated with secondary antibodies for 30 min at room temperature in a humidified chamber. After 3 washes in the wash buffer bath, the slides were incubated with prepared substrates for 5 min and washed 3 times in a distilled water bath. The slides were then counterstained for 5 min using hematoxylin solution, Mayer's (Sigma, St. Louis, MO, USA) and washed 3 times in a distilled water bath. The stained slides were dehydrated (95% Ethanol twice, 100% Ethanol three times) and cleared (Xylene twice) before mounting with Toluene based mounting medium (Thermo Fisher Scientific, Drive Kalamazoo, MI, USA).

2.10.4 **Quantitative analysis and scoring system**:

The stained tissue slides were observed under Olympus BX43F bright field microscope (Olympus, Tokyo, Japan). The immunostaining of CD3-, CD20-, CD61-, and CD68-positive cells was quantified as immunoreactive cells per 20 high-power field (HPF) at 400x magnification. Fibrinogen and GFAP immunostaining was quantified using a five point range scoring system; 0 = Within Normal Limits to 5 = Severe. β-APP and Cleaved caspase-3 staining characteristics were assessed qualitatively.

Statistical significance was determined for the following immunohistochemical stains: CD3, CD20, CD68, GFAP and Fibrinogen. Significance was determined based on a comparison between brain stem controls and experimental samples, cerebrum controls and experimental samples as well as in comparing experimental cases of brain stem and cerebrum. Individual slides were evaluated as described above and mean values were calculated so as to regularize the sample size. This was necessary as there were two cerebral slides and a single section of brain stem harvested from each

animal for the purpose of this study. P values were determined using a Mann-Whitney test (GraphPad, La Jolla, CA, USA).

Table 2.8: Immunohistochemistry of paraffin-embedded formalin fixed macaque tissues.

Primary antibody	Primary antibody clone and source	Primary antibody dilution	Primary antibody incubation time	Secondary antibody	Substrate
CD3	Polyclonal rabbit anti-human CD3 (Dako, Glostrup, Denmark)	1:50	30 min	AP labelled polymer conjugated to goat anti-mouse and goat anti–rabbit (Nichirei biosciences inc, Chuo-ku, Tokyo, Japan)	Liquid Permanent Red solution (Dako, Glostrup, Denmark)
CD20	Monoclonal mouse anti-human CD20 clone L26 (Oxford University, Oxford, UK)	1:5	30 min	AP labelled polymer conjugated to goat anti-mouse and goat anti–rabbit (Nichirei biosciences inc, Chuo-ku, Tokyo, Japan)	Liquid Permanent Red solution (Dako, Glostrup, Denmark)
CD61	Monoclonal mouse anti-human CD61 clone Y2/51 (Dako, Glostrup, Denmark)	1:50	60 min	HRP labelled polymer conjugated to goat anti-mouse and goat anti-rabbit (Dako, Carpinteria, California, USA)	3,3'-diaminobenzidine chromogen solution; DAB (Dako, Carpinteria, California, USA)
CD68	Monoclonal mouse anti-human CD68 clone KP1 (Oxford University, Oxford, UK)	1:3	30 min	AP labelled polymer conjugated to goat anti-mouse and goat anti–rabbit (Nichirei biosciences inc, Chuo-ku, Tokyo, Japan)	Liquid Permanent Red solution (Dako, Glostrup, Denmark)
Fibrinogen	Polyclonal rabbit anti-human fibrinogen (Dako, Glostrup, Denmark)	1:200	30 min	AP labelled polymer conjugated to goat anti-mouse and goat anti–rabbit (Nichirei biosciences inc, Chuo-ku, Tokyo, Japan)	Liquid Permanent Red solution (Dako, Glostrup, Denmark)
Glial Fibrillary Acidic Protein (GFAP)	Polyclonal rabbit anti-GFAP, Ready-to-Use (Dako, Glostrup, Denmark)	1:1	30 min	AP labelled polymer conjugated to goat anti-mouse and goat anti–rabbit (Nichirei biosciences inc, Chuo-ku, Tokyo, Japan)	Liquid Permanent Red solution (Dako, Glostrup, Denmark)

AP; Alkaline phosphatase (N-Histofine® Simple Stain alkaline phosphatase (MULTI), Nichirei biosciences inc, Chuo-ku, Tokyo, Japan)

HRP; Horseradish peroxidase (Envision® + Dual Link System-HRP, Dako, Carpinteria, California, USA

2.10.5 **Quantitative enzyme-linked immunosorbent assay for albumin index and brain injury markers**:

Cerebrospinal fluid (CSF) samples were collected from macaques at euthanasia and centrifuged at 10,000 x g for 10 min. CSF supernatant was collected and used for ELISA and multiplex cytokine immunoassay. Plasma samples were also collected on the same day for albumin ratio determination. There were 3 sample groups, uninfected (2 monkeys), 12-week SHIV infected (12 monkeys), and *P. coatneyi* infected (6 monkeys) monkeys. The SHIV group formed a control group of known CNS infected monkeys where it was hoped that any characteristic cytokine signature or BBB injury leading to leakage would differ in pattern to CNS effects on the experimental severe malaria animals. This part of the thesis was conducted in collaboration with Dr. Sandy Vasan and the SHIV model development group at AFRIMS.

2.10.6 **Albumin ELISA:**

To determine albumin index (AI), the plasma samples were diluted at 1:400,000 and the CSF samples were diluted at 1:2,000 using Albumin Monkey Diluent (Abcam, Cambridge, UK). The albumin present in diluted samples was measured using the albumin monkey ELISA kit (Abcam, Cambridge, UK) according to the manufacturer's instructions. Optical density 450 nm values were measured with SPECTRAmax® 340 PC microplate reader (Molecular Devices, Sunnyvale, CA, USA), and the albumin concentration was interpolated from the standard curve using SOFTmaxPRO 4.3.1(Molecular Devices, Sunnyvale, CA, USA) and multiplies by the dilution factor. The AI was calculated using the formula: AI = (CSF albumin/plasma albumin) × 103. The statistical analysis among groups was compared using Kruskal-Wallis test (GraphPad, La Jolla, CA, USA).

2.10.7 **Tau (total) protein ELISA**:

Tau (Total) protein is a biomarker of neuraxonal degeneration in CSF. (Dittrich 2015) To evaluate neuronal injury as a factor of brain pathology, the CSF Tau (total) protein was determined using Human Tau (Total) ELISA kits (Invitrogen, Carlsbad, CA, USA) according to the manufacturer's instructions. Optical density 450 nm values were determined with SPECTRAmax® 340 PC microplate reader (Molecular Devices, Sunnyvale, CA, USA). Background absorbance was subtracted from all data points, including standards, samples, and controls prior to plotting. The concentration of Tau (Total) in samples was calculated from standard curves using a four parameter algorithm by SOFTmaxPRO 4.3.1(Molecular Devices, Sunnyvale, CA, USA) and multiplied by two (dilution factor). The statistical analysis among groups was compared using Kruskal-Wallis test (GraphPad, La Jolla, CA, USA).

2.10.8 **Multiplex cytokine immunoassay**:

Multiplex cytokine immunoassay was conducted as an adjunct to and in collaboration with the ongoing project by the AFRIMS' Simian-Human Immunodeficiency Virus model development project. Through the generosity of the SHIV group, we were able to submit samples for multiplex analysis which were then run in conjunction with the SHIV infected macaque samples and control samples. This was conducted only once and while not a primary feature of the descriptive study, did allow for some fascinating data for both this severe malaria study, but also as a disease comparison for the SHIV group.

To determine specific cytokine involved in *P. coatneyi* infection in rhesus macaques CSF, 23 cytokines, including G-CSF, GM-CSF, IFN-γ, IL-1ra, IL-1β, IL-2, IL-4, IL-5, IL-6, IL-8, IL-10, IL-12/23 (p40), IL-13, IL-15, IL-17, IL-18, MCP-1, MIP-1α, MIP-1β, sCD40L, TGF-α, TNF-α, and VEGF, were screened using MILLIPLEX® MAP Non-Human Primate Cytokine Magnetic Bead Panel (PRCYTOMAG-40K, Millipore, Darmstadt, Germany) according to the manufacturer's instructions. Briefly, 200 microliters of Assay buffer were added into each well of the plate. The plate was sealed and mixed on a plate

shaker for 10 min at room temperature. Assay Buffer was removed from all wells by inverting the plate and tapping it on paper towels. Twenty-five microliters of standard or control were added into appropriate wells, and 25 µl of Assay Buffer was added into sample wells. Then, 25 µl of CSF matrix solution was added into standard and control wells while samples were added into appropriate wells. Mixed beads were then added into all wells. Subsequently, the plate was sealed and wrapped with foil and incubated at 4°C with gentle shaking for 16-18 hr. The following day, the plate was washed twice with 200 µl wash buffer. Detection antibody was added and incubated at room temperature for 1 hr. Streptavidin-Phycoerythrin was added and incubated at room temperature for 30 min. After incubation, plate was washed 2 times, and Sheath Fluid was added into all wells. The plate was run on a Luminex 200™ (Luminex, Austin, USA). The Median Fluorescent Intensity (MFI) data using a 5-parameter logistic method was analyzed. GraphPad software was used for graphing and statistical analysis (GraphPad, La Jolla, CA, USA).

2.11 **Ultrastructural Evaluation of Tissue sections using Transmission and Scanning Electron Microscopy:**

2.11.1 **Transmission Electron Microscopy (TEM) Methodology**:

2.11.1.1 **Transmission electronmicroscopy (Spurr resin) Tissue fixation and processing**:

Examination of the ultrastructural changes in tissues from infected monkeys was performed to determine both the relationship between iRBCs and host cells (such as sequestration within the microvasculature of different organs) and specifically to examine the type of adhesive contacts made by *P. coatneyi* in comparison to that characterized in human tissues in *P. falciparum* infections. (Pongponratn 2003, Promano 2005, Nguangsangiam 2007) This part of the thesis was done in collaboration with Professor David Ferguson, Department of Ultrastructural Morphology, Radcliffe Department of Medicine, Oxford University. EM sections were prepared from tissues as follows:

1. Tissue samples were cut into 6-8 small squares ~ 0.5-1 mm at autopsy, immediately following euthanasia

2. Tissue preservation was in 2.5 % phosphate buffered glutaraldehyde at 4^{o}C until use

3. Prior to processing, tissue samples were washed in 0.1 M phosphate buffer for 20 min; 3-4 times

4. Post fixation: The samples were submerged in 1% osmium tetroxide mixed with 0.1 M phosphate buffer and put on the shaker for 1 hour.

5. 0.1 M phosphate buffer for washing the tissue sample for 20 min; 1 time

6. Normal saline for washing 20 min; 1 time

7. Tissue processing: Dehydration

- 35% alcohol 15-20 min
- 50% alcohol 15-20 min
- 70% alcohol 15-20 min
- 95% alcohol 15-20 min
- 100% alcohol 15-20 min; 3 times
- propylene oxide 15-20 min; 3 times
- infiltrate with Spurr resin with propylene oxide (ratio 1:3) for 3 hours- over night
- infiltrate with Spurr resin with propylene oxide (ratio 1:1) for 3 hours- over night
- infiltrate with Spurr resin with propylene oxide (ratio 3:1) for 3 hours- over night
- infiltrate with Spurr resin for 3 hours- over night; 3 times

8. Embedding with Spurr resin

9. Curling in oven 70^{o} C for 8 hours

10. Section with an ultramicrotome; 70 nm thick

11. Staining with uranyl acetate and lead citrate

12. Grids were examined using JEM-2100 and JEM-1400 Transmission Electron Microscopes; Japan

2.11.2 **Scanning Electron Microscopy (SEM) methodology**:

This part of the thesis was conducted in conjunction and collaboration with Dr. Bruce Russell and Dr. Benoit Malleret at the Vivax Laboratory, National University of Singapore.

In order to further examine the structure of the Knob adhesion proteins on the surface of *P. coatneyi* infected red cells, SEM was performed after magnetic enrichment on ex-vivo infected red blood cell samples from the three splenectomized *P. coatneyi* infected rhesus macaques associated with the model refinement phase of the prospective study. Standard protocols were used as in described in Malleret et al (2013) and outlined in the following section.

2.11.2.1 **SEM tissue fixation and processing**:

1. Sorted cells were coated on a poly-lysine (Sigma) pretreated glass coverslip for 15 mins at room temperature (RT) and were fixed in glutaraldehyde and post-fixed in osmium tetroxide.

2. Cells were washed in deionized water, dehydrated with a graded series of ethanol immersions starting at 25% to 100% and critical point dried (CPD 030, Bal-Tec)

3. Fixed in 2.5% glutaraldehyde 0.1 M phosphate buffer for 1 hours (pH 7.4) at RT

4. The samples were washed twice in PBS and subsequently underwent post-fixation with 1% osmium tetroxide (Ted Pella Inc.) at RT for 1 hour.

5. The glass coverslip surfaces were coated with 5 nm of gold by sputter coating in a high-vacuum sputtering device (SCD005 sputter coater, Bal-Tec)

6. The coated samples were examined with a field emission scanning electron microscope (JSM-6701F, JEOL) at an acceleration voltage of 8 kV using the in-lens secondary electron detector at a working distance of 8 µm.

2.11.3 **Atomic Force Microscopy (AFM) Methodology**:

Atomic Force Microscopy was conducted in collaboration with Dr. Bruce Russell, Dr. Benoit Malleret and Dr. Rosemary Zhao at the Vivax Laboratory, National University of Singapore. Atomic force microscopy was pursued as a mechanism to further describe the comparative nanostructural surface morphology in *P. coatneyi* infected erythrocytes in comparison with both normal cells and *P. falciparum* infections in humans. Results are described in detail in Chapter 6: Ultrastructure.

2.11.3.1 **AFM Slide preparation**:

1. Peripheral venous blood was drawn from the three splenectomized *P. coatneyi* infected rhesus macaques, when their peripheral parasitemia as judged by smear preparation was more than 10% (from the model refinement phase of the prospective study). These were harvested by venipuncture, centrifuged at 5000g for 5 minutes, then resuspended in 1×PBS with 1% BSA medium at 50% to 75% hematocrit.
2. This suspension was then used to make a thin blood smear on microscope slides.
3. The blood smear was air-dried.
4. Dimension FastScan AFM was used to scan the slides. Approximately 100-200 cells were scanned per slide by Bruker AFM probes (FASTSCAN–B). The height images were captured with the samples per line of 512, and scan rate of 3 to 4 Hz. The images were analyzed using NanoScope Analysis (version 1.40), and the details of the nanostructures were measured.

Chapter 3: Clinical, Parasitemic and Macroscopic Autopsy Pathology in the Rhesus Macaque/*P. coatneyi* Severe Malaria Model

3.1 **Introduction to clinical trials**:

The fundamental intent of this dissertation was a complete and coherent description of the Rhesus macaque/*P. coatneyi* model in order to facilitate its use as a legitimate and effective platform on which to conduct anti-malarial drug, adjuvant treatment or vaccine trials. The Armed Forces Research Institute of Medical Sciences (AFRIMS) has long been interested in this model for severe and cerebral malaria, and in collaboration with academics globally, has remained at the forefront of those few experimental studies which have been conducted world-wide. As described in the introduction, there is significant variation in the application of the model and even the definition of severity. In order to study the regenerative impact on the bone marrow as well as the metabolic disturbances, Moreno et al. have used a relapsing version of the model in non-splenectomized monkeys, characterized by a much lower parasitemia as well as having the experimental animals undergo sub-curative treatment with artemether between episodes. (Moreno 2013) Davison et al. examined the placental and fetal pathology secondary to *P. coatneyi* infection and their model involved spleen intact animals whose parasitemias, while significant, did not exceed 150,000 parasites/mm^3 red blood cells. (Davison 1998; Davison 2000; Davison 2005) Other groups have described the model in very limited numbers and have used either Japanese macaques (Kawai 1993; Kawai 1998; Matsumoto 2000) or combined populations of crab-eater macaques and rhesus macaques. (Desowitz 1967)

All of this diversity in the use of *P. coatneyi* as a model for disease in humans highlights not just the heterogeneity of data and reporting in the experimental scientific literature, but to some extent mirrors the heterogeneity of human falciparum infection. In contrast the murine model usually utilizes genetically inbred strains such as the ANKA or CBA mouse, where groups defined as having different disease states such as ‘experimental cerebral malaria’ or ‘severe anemia’ are compared. As

such, our intent in this chapter, is to provide a relatively cohesive description of the clinical and gross findings of *P. coatneyi* infections in a uniform population of adult, Indian origin, splenectomized rhesus macaques from the closed colony at AFRIMS.

This chapter focuses specifically on the disease progression in the 15 prospective animals which were used in the model refinement study and in the methylene blue drug trial. For the purpose of description of the findings associated with temperature and parasitemia, the study concentrates on representative data associated with the refinement protocol as opposed to those that underwent radical cure drug treatment. The primary intent of the refinement study was to establish repeatable and predictable disease progression details. In contrast with other studies, this was done specifically with the resolve of establishing criteria of disease severity similar to those used to define severe malarial disease in humans, as detailed in the WHO criteria. (WHO 2014) This was intended to study the clinical similarities between the model at high levels of parasitemia (maximum 52%), and synchronous severe clinical symptomology. All data was tabulated, graphed, photographed and compared so as to determine the practicality and applicability of the *P. coatneyi*/rhesus macaque model as being adequately representative of cerebral and/or severe malaria in humans.

3.2 **Clinical and gross pathology methodology overview**:

'Signalment' in veterinary medicine refers to systematic identifying criteria that are the foundation of each individual. In this case, the factors considered included species, genetic origin, gender, age, weight and prior clinical/experimental history. Subsequent to intravenous inoculation with approximately 1 mL equivalent to $5x10^6$ infected RBCs of *P. coatneyi* infected blood derived from a parasitemic, spleen intact donor animal, all animals were closely monitored. The animals used in this arm of the study had not been exposed to *P. falciparum* or *P. coatneyi* in any previous studies in the

colony, in order to ensure that infection was on a 'naïve' immunological background. Parasitemia was monitored throughout the experiment either through blood smears generated from an ear nick or concurrent with the larger venous blood draws. The larger volume phlebotomy events evaluated the hematological parameters and a panel of clinical chemistry. Temperatures and clinical signs were monitored throughout the study with frequency increasing in synchrony with the rising parasitemia to a peak of every other hour over 24 hour cycles. Temperatures were recorded via rectum as well as by using a subcutaneous transponder that was injected under the skin between the shoulder blades in all animals. Electrocardiograms were conducted concurrent with blood draws. Immediately prior to death, a subsection of animals had their irises dilated for retinal photography, and all animals had terminal blood, cerebrospinal fluid and urine collected. Complete autopsy was performed in all animals with weighing of select organs (brain, lungs, heart, liver), collection of all tissues in 10% buffered formalin, selected tissues in Glutaraldehyde and RNA-later, as well as photography of all significant lesions.

3.3 **Typical clinical progression**:

Clinical Symptomatology Criteria

Assessment of activity level as determined by moving around the cage and the response to the presence of a veterinarian or a technician; mentation which was evaluated as a response to stimuli outside the cage; menace response in which an animal will blink or withdraw when a sudden movement occurs close to the eyes; breathing, to include both the quantitative number of breaths as well as the quality: labored, shallow, gasping…etc; skin color to include any signs of hemorrhage, jaundice or cyanosis; presence of vomitus; skin turgor as a sign of hydration status; urination characteristics (anuria, dysuria, stranguria), urine color and both quantitative and qualitative

assessment of the urine captured in the pans under the cage; and appetite. All signs were graded, with a maximum score of 24. A normal animal would score 0. (See Study Specific Form #1, Chapter 2)

Additional signs were coded but not scored, included: ataxia; inappropriate vocalization; diarrhea; melena; epistaxis; opisthotonus (abnormal posturing); piloerection; salivation; tremor or twitching of mouth or fingers and/or hemiplegia.

Experimental animals typically began to develop clinical symptomology around day 7 post inoculation, although decreased appetite or anorexia was often noted around day 4 to 5. Initial signs were often found to be associated with activity level and mentation. Parasitemia at this stage would typically be in the range of $10^5 – 10^6/mm^3$. These were closely aligned with the first significant increases in temperature. At this stage, an animal would typically have a total score of around 7, consisting of anorexia (3), some degree of hematuria (1-3), moderate to marked reduction in activity (1-2) and decreased mentation (1). When the hematuria became more significant, changes in skin turgor would typically follow. Immediately prior to death or euthanasia, animals had severely decreased mentation with loss of the menace response. Animals were recumbent in their cages and non-responsive to external stimuli without reaching human criteria of true coma. (Figure 3.1) Animals would typically have been anorexic for 2 days, and at some point, have vomited. Occasionally, there were episodes of dysuria in which animals strained to urinate or were observed to lack sphincter control, and in all animals varying degrees of hematuria was observed. By day 7, most animals were showing signs of dehydration, and in about 30% of animals, prior to death there was evidence of dyspnea. 40% of the animals began to have erythema of the skin concentrated around the perineum, scrotum and the inner thighs. (Figure 3.2)


1


ID NO: DA831
Acc# 14-198 Animal Carcass (perineum)
Date 30 May 14 Photographer Initial:
EN
DATE
2

Figure 3.1: Photograph of a recumbent *P. coatneyi* infected rhesus macaque demonstrating lethargy. While decreased mentation cannot be captured as a static image, these animals were typically poorly or non-responsive to stimuli.

Figure 3.2: Photograph of a *P. coatneyi* infected rhesus macaque demonstrating severe erythema and occasional petechiae on the perineum, scrotum, thighs and legs.

3.4 **Temperature**:

In normal adult animals from the AFRIMS colony, baseline temperatures measured rectally fluctuate between 99.5° F to 102° F (37.5° C to 38.9° C) depending on a range of physiological factors to include gender, feeding schedule, stress, handling time and concurrent procedures.

Experimentally, following the initial temperature spike at day 7, which would often be around 104° Fahrenheit (F) or 40° Celsius (C), the temperature would remain higher than baseline, with peak temperatures reaching up to 107° F or 41.7° C, but fluctuating until death or euthanasia.

3.5 **Parasitemia**:

Parasitemia curves were plotted in all animals in the prospective study. These graphs examined the progression of total parasitemia over time as well as by identifying the life cycle stage of the parasite over the course of the experiment. This allowed for a prediction of specific windows in which there was an anticipated spike in overall parasitemia as well as life cycle stages that were consistent with overlapping clinical symptomology. Previous attempts over the past 30 years to use the model for both pathophysiological studies or drug trials had produced somewhat haphazard results. This was largely due to the fact that the parasitemia spike with *P. coatneyi* is very rapid and subject animal devitalization, collapse and death occurred within a short time frame, frequently

occurring late at night. Specifically, the steep increase in parasitemia observed on day 7, resulted in peak parasitemias of up to 52%. As is described in the demonstrated temperature, clinical chemistry and hematology sections which follow, this spike was associated with severe clinical signs which were likely irreversible after a certain point. Clinical symptomology and the spikes in temperature occurred with a slight lag to the parasitemia increase, however, once established and the animals reached high parasitemias in excess of 15-20%, there was typically significant evidence of multiorgan injury.

Without the development of these graphs and an understanding of the rapidity of development of parasitemia, the model becomes too cumbersome for the use in drug trials. However, by mapping disease progression and overlapping symptomology, parasitemia and temperature data, the model become both manageable as well as relatively predictable.

Beginning on day 1 post inoculation, there was an observable parasitemia which subsequently decreased and by the beginning of day 3 was no longer significant. By the 3rd sampling on day 3, the parasitemia had undergone an initial spike in the range of 10,000 to 30,000 parasites/mm^3 red blood cells corresponding to the first phase of post schizogony in the infected macaque. The cycle then continued and the parasitemia again decreased, implying sequestration, rising again by the end of day 5 at which point the values ranged from 200,000 to 350,000 parasites/mm^3 red blood cells. The next round of intraerythroctytic development, followed by sequestration and a subsequent decrease in peripheral parasitemia occurred over day 6 and was followed by the expected spike by the end of day 7 with calculated parasitemia in excess of 1 million parasites/mm^3 red blood cells. The parasitemia remains sustained at that threshold until death or euthanasia which never exceeded day 8 without some form of medical intervention, due to the severity of clinical symptoms by this stage.

Parasite life cycle stage was a crucial feature in terms of understanding the disease progression as well. The parasitemia spike on day 5 represented a peak of ring stages followed by a predictable spike and peak in trophozoites on day 6 leading to a small spike in schizonts. This was

closely followed by the day 6 (evening) spike in ring forms, a smaller increase in trophozoites and then a schizont increase on day 7. This is followed closely by a dramatic increase in ring forms, which as it began to taper off, yields to the spike in trophozoites at the beginning of day 8. The animals in the refinement protocol typically did not survive beyond this peak, and were euthanized or died naturally. Animals in the methylene blue drug trials showed similar initial parasitemia curves, but once the treatment window was achieved, the parasitemias were significantly controlled, decreased and eventually cleared in the drug study animals.

These results imply a degree of homogeneity both in control of parasitemia in the splenectomized animal, and the development of clinical symptoms in response to infection between different animals.

			Daily Parasitemia Levels		
Study Day	**Date**	**Time**	**DA831**	**DA923**	**R519**
0	**22-May-14**	0800	0	0	0
		1100	0	0	0
		1900	0	0	0
1	**23-May-14**	0800	0	0	0
		1100	0	0	0
		1900	**233**	**348**	**295**
2	**24-May-14**	0800	**83**	**73**	**35**
		1100	**17**	**22**	**12**
		1900	**8**	**7**	**23**
3	**25-May-14**	0800	0	0	0
		1100	**7**	**648**	**64**
		1900	**10,634**	**24,936**	**17,332**
4	**26-May-14**	0800	**1,169**	**2,377**	**1,676**
		1100	**511**	**606**	**718**
		1900	**1,932**	**4,218**	**1,916**
5	**27-May-14**	0800	**386**	**239**	**203**
		1100	**6,443**	**20,905**	**8,302**
		1900	**217,200**	**276,480**	**304,440**
6	**28-May-14**	0700	**144,500**	**47,300**	**71,925**
		0900	**73,984**	**36,850**	**86,100**
		1100	**48,552**	**51,700**	**78,225**
		1300	**36,992**	**26,950**	**50,400**
		1500	**45,645**	**34,140**	**37,157**
		1700	**42,423**	**36,985**	**42,756**
		1900	**27,387**	**38,123**	**47,337**
		2100	**32,220**	**45,520**	**37,666**
		2300	**38,570**	**31,428**	**41,715**
7	**29-May-14**	**0100**	**34,713**	**29,100**	**35,630**
		0300	**28,652**	**26,190**	**27,405**
		0500	**22,591**	**15,132**	**21,378**
		0700	**23,562**	**16,095**	**15,068**
		0800	**21,879**	**38,295**	**26,130**
		0900	**29,733**	**56,610**	**33,462**
		1000	**69,564**	**131,535**	**61,854**
		1100	**291,720**	**549,450**	**375,180**
		1200	**1,009,800**	**1,110,000**	**922,740**
		1300	**992,970**	**1,298,700**	**1,541,280**
		1400	**1,391,280**	**1,737,150**	**1,647,750**
		1500	**1,532,580**	**1,676,080**	**1,433,440**
		1600	**1,623,360**	**1,778,280**	**1,616,960**
		1700	**1,826,280**	**1,737,400**	**1,612,000**
		1800	**1,623,360**	**1,747,620**	**1,507,840**
		1900	**1,543,260**	**1,793,610**	**1,612,000**

		2000	1,701,360	1,823,320	2,140,600
		2100	1,751,400	1,823,320	2,079,440
		2200	1,590,160	1,979,110	2,123,920
		2300	1,536,800	1,950,480	1,936,480
		2400	1,813,650	1,939,140	1,827,800
8	**30-May-14**	**0100**	1,808,000	1,791,720	1,758,640
		0200	1,649,800	1,871,100	1,798,160
		0300	1,389,900	1,587,600	1,600,560
		0400	1,356,000	1,598,940	1,541,280
		0500	1,440,750	1,542,240	1,791,880
		0600	1,175,200	1,496,880	1,501,760
		0700	1,607,040	1,557,300	1,445,520
		0800	1,353,600	1,487,490	1,413,600
		0900	1,192,320	1,315,650	1,409,040
		1000	1,042,560	1,428,420	884,640
		1100	1,013,540	1,514,340	1,249,440
		1200	**END**	1,547,340	1,345,200
		1300		1,401,570	1,190,160
				END	**END**

Table 3.5.1 Parasitemias (p./mm³ RBCs) over the course of the refinement study. Peak parasitemia typically occurs during day 7 post infection, and high parasitemia was maintained through the end of the study.

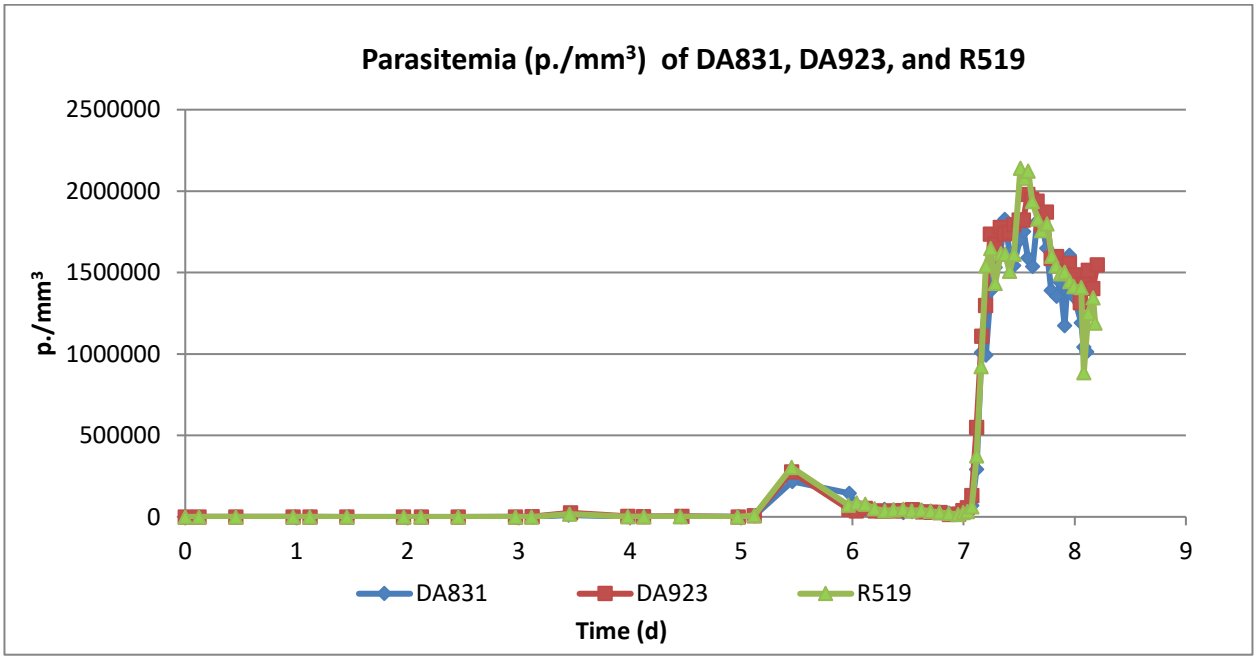

Graph 3.5.1: Representative parasitemia graph demonstrating the spike in parasitemia over time. It is notable that the animals tabulated in this graph demonstrate both a strong correlation in parasitemia

and in terms of disease progression. This trend held true for all 15 prospective animals in the refinement and the drug ranging studies.

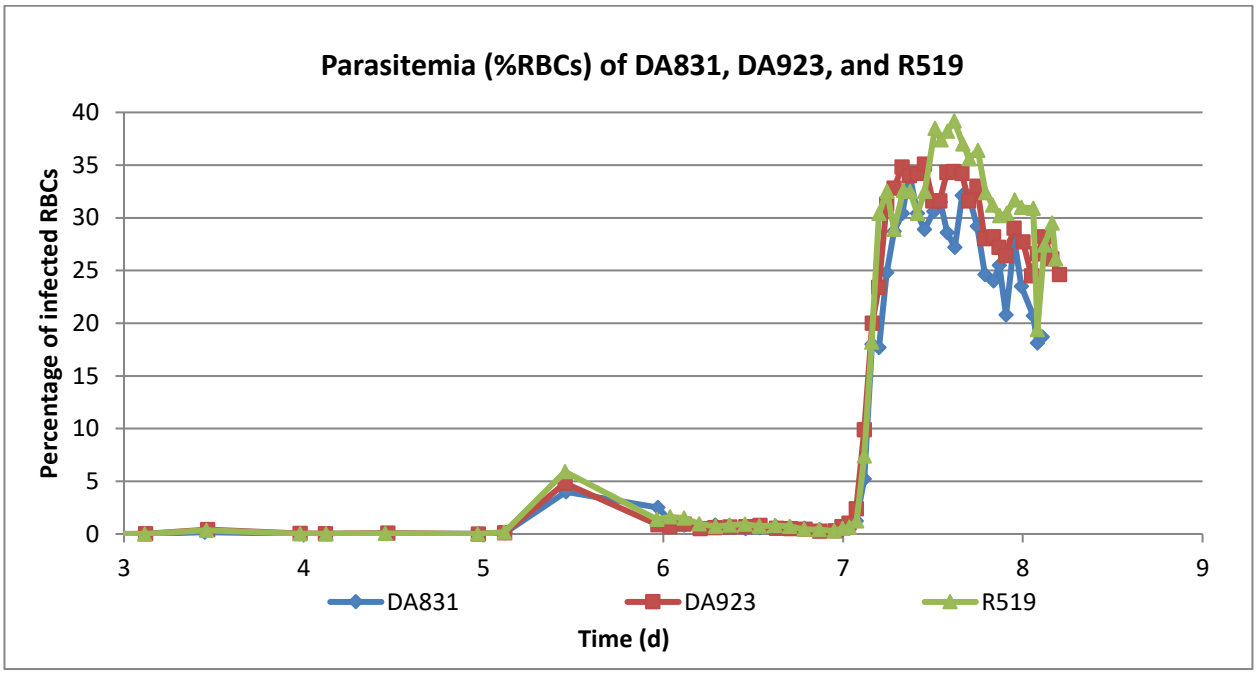

Graph 3.5.2: This parasitemia graph is the same data represented in 3.1, however is represented as percentages of erythrocytes infected.

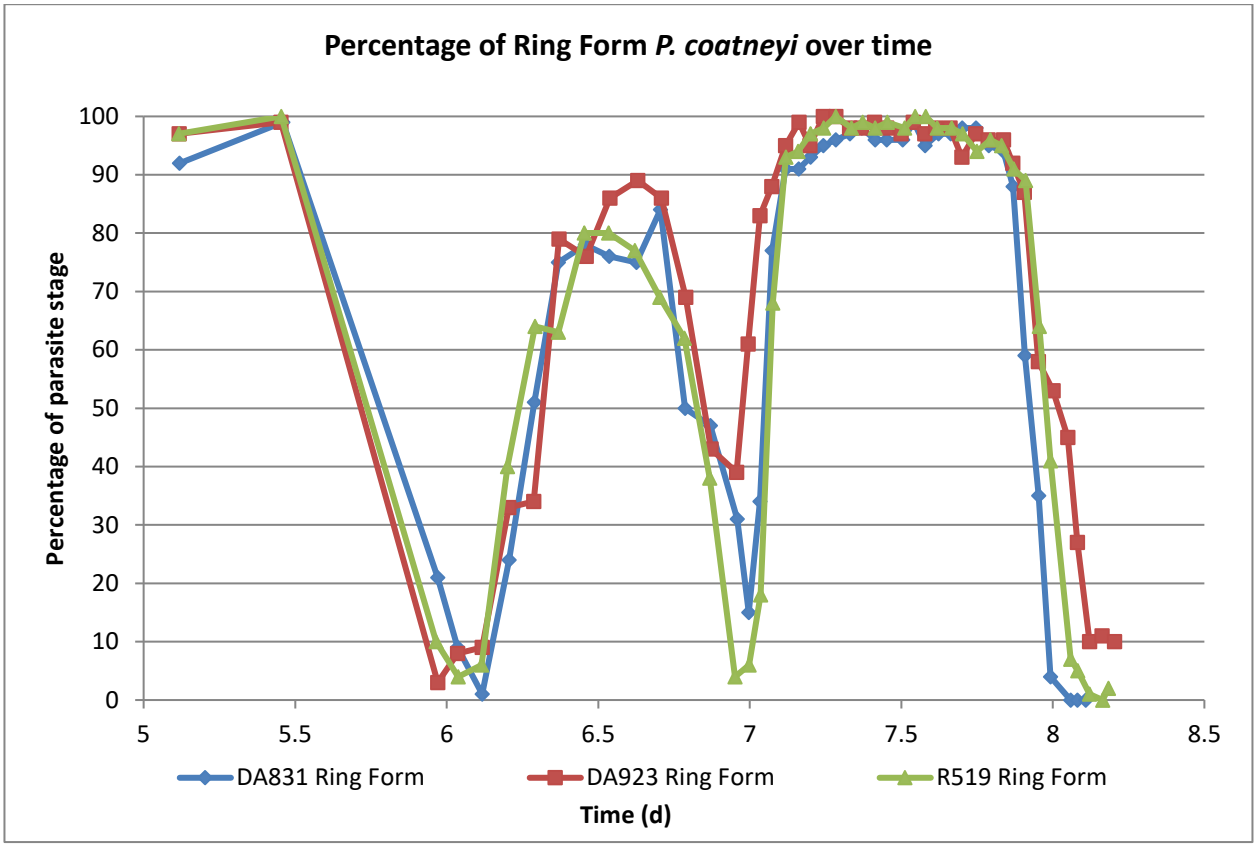

Graph 3.5.3. Percentage of ring forms of *P. coatneyi* staged over the course of the experiment.

The parasitemia for each time point assessed was staged to describe the linear life cycle of the parasite within infected cells over the course of the experiment. (Graph 3.5.3) As with the overall parasitemia, there was extremely close correlation as to parasite developmental stage between infected animals, allowing for a significant degree of prediction as to the anticipated schizogony, spike in febrile disease and resultant clinical symptomology. The ring stage (early trophozoite) of *P. coatneyi* are phenotypically very similar to those of *P. falciparum*. (Figure 3.1.1 arrow) These usually have either a single or double chromatin body, and can present either centrally within the infected erythrocytes or in a marginalized "accolé" or "pliqué" form which are peripheralized but closely associated with the plasma membrane of the erythrocyte and having little impact on the silhouette of the cell. (Figure 3.1.2 arrow) Another form which is described is the vesicular form, in which the peripheralized ring creates a blister elevated from the plasma membrane. (Figure 3.1.5 arrowhead)

With significant infections, there can be multiple young trophozoites or rings infecting individual erythrocytes. (Figure 3.1.3 arrow)

As the trophozoites mature, their cytoplasm intensifies in color and often appears to have a cytoplasmic vacuole. Additionally, the trophozoites being to demonstrate the characteristic hemozoin crystals which stain a golden brown. (Figure 3.1.4 arrow) The younger schizonts are typically round and begin to obscure the host cell. This stage will begin to demonstrate the formation of the merozoites which are comingled with the granular hemozoin pigment. The visible cytoplasm stains a light blue on Giemsa and with maturity the hemozoin granules begin to coalesce. At later stages, the schizont completely fills the erythrocyte making it difficult to distinguish any of the preexisting host cell. Nearing rupture, the schizont is filled with approximately 20 merozoites. (Figure 3.1.5 arrow) The macrogametocytes are highly visible with blue cytoplasm and a red, often peripheralized nucleus. The cytoplasm contains scattered small granules of hemozoin crystals. (Figure 3.1.6 arrow) Microgametocytes are reddish-purple when stained with Giemsa, and often have a large dappled nucleus.

During the course of both the refinement study as well as the methylene blue drug dosage study, each sampling to assess for parasitemia was also analyzed for parasite staging. This provided additional data allowing for a more complete understanding of the projected parasitemia curves. The various stages of maturation of the trophozoites were by far the predominant forms, while for a brief period highlighting the malignant tertian nature of *P. coatneyi* malaria, trophozoites predominate at two points in the course of the disease in this experiment with a separation of 48 hours. Additionally, there is a peak of schizonts on day 7 and it would be anticipated that should the animals not succumb to the severity of the disease, that another larger spike of schizonts would be expected at day 9, however in those animals which participated in the refinement portion of the study, no animal was maintained beyond day 8.

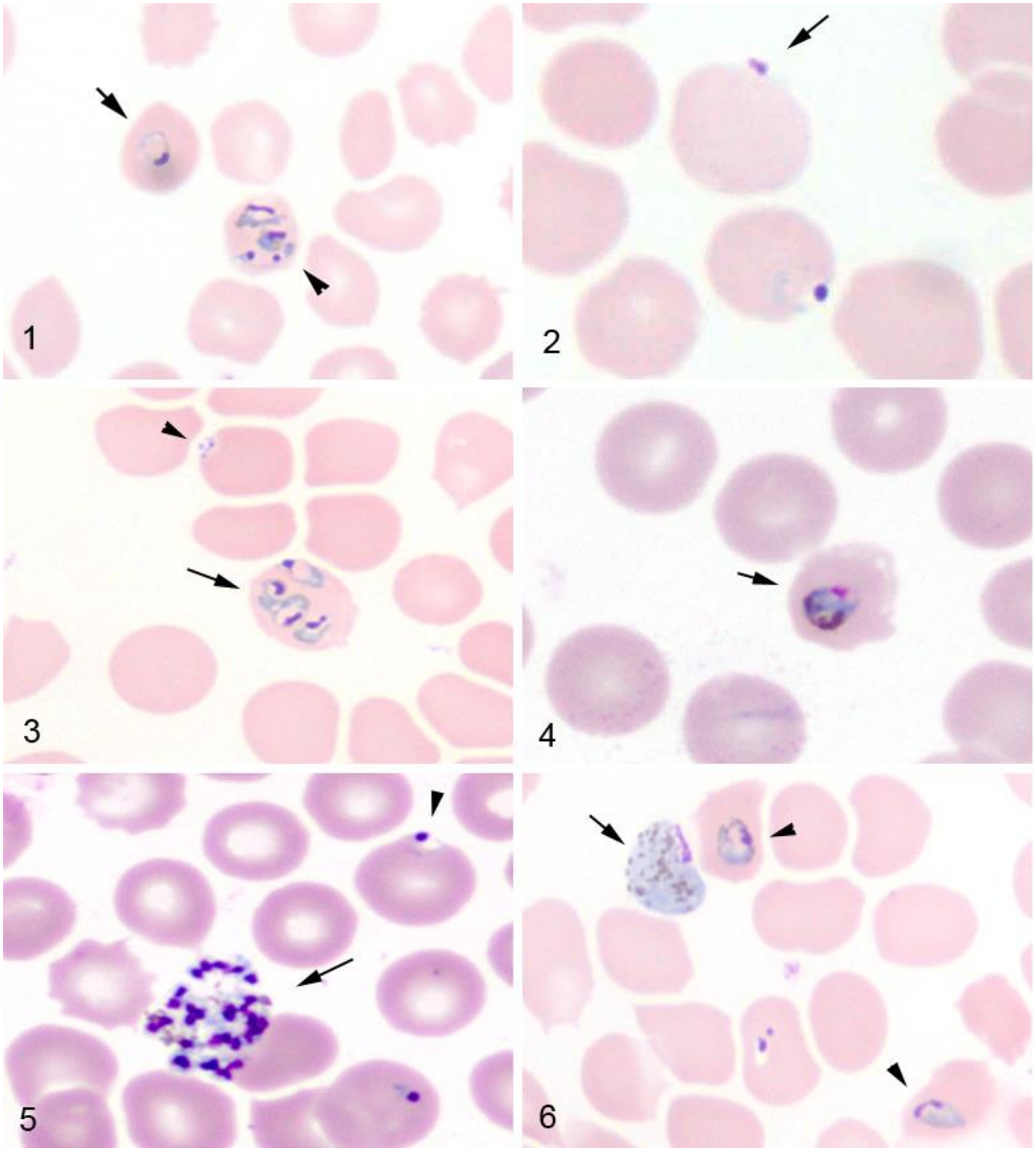

Figure 3.5.1-6 Blood smears from *P. coatneyi* infected rhesus macaques. Each figure within the plate demonstrates progressive developmental stages of the plasmodium within the infected erythrocytes. 3.5.1 illustrates an infected red blood cell containing a single ring stage or young trophozoite (arrow),

while another cell contains 3 or more parasites which appear to be later stage rings. 3.5.2 shows variants of the “accolé” or “pliqué” forms in which the ring stage plasmodium is peripheralized and is essentially confluent with the plasma membrane of the infected cell. These forms are evident in that their cytoplasm is clearer than that of the host cell, and the chromatin body stains brightly and is highly visible (arrow). 3.5.3 demonstrates a single cell infected with 4 parasites all of which are more mature ring forms (arrow) while another cell contains a single accolé ring form (arrowhead). 3.5.4 illustrates a single mature trophozoite which is centralized within the infected erythrocyte (arrow). 3.5.5 has a highly visible mature schizont containing upwards of 20 merozoites (arrow). Additionally, there is an excellent example of the vesicular form of the early trophozoite or ring stage (arrowhead). Finally, in 3.5.6 a macrogametocyte is evident with its blue cytoplasm and speckling of hemozoin granules (arrow). Additionally, within the photomicrograph are two mature trophozoites (arrowheads).

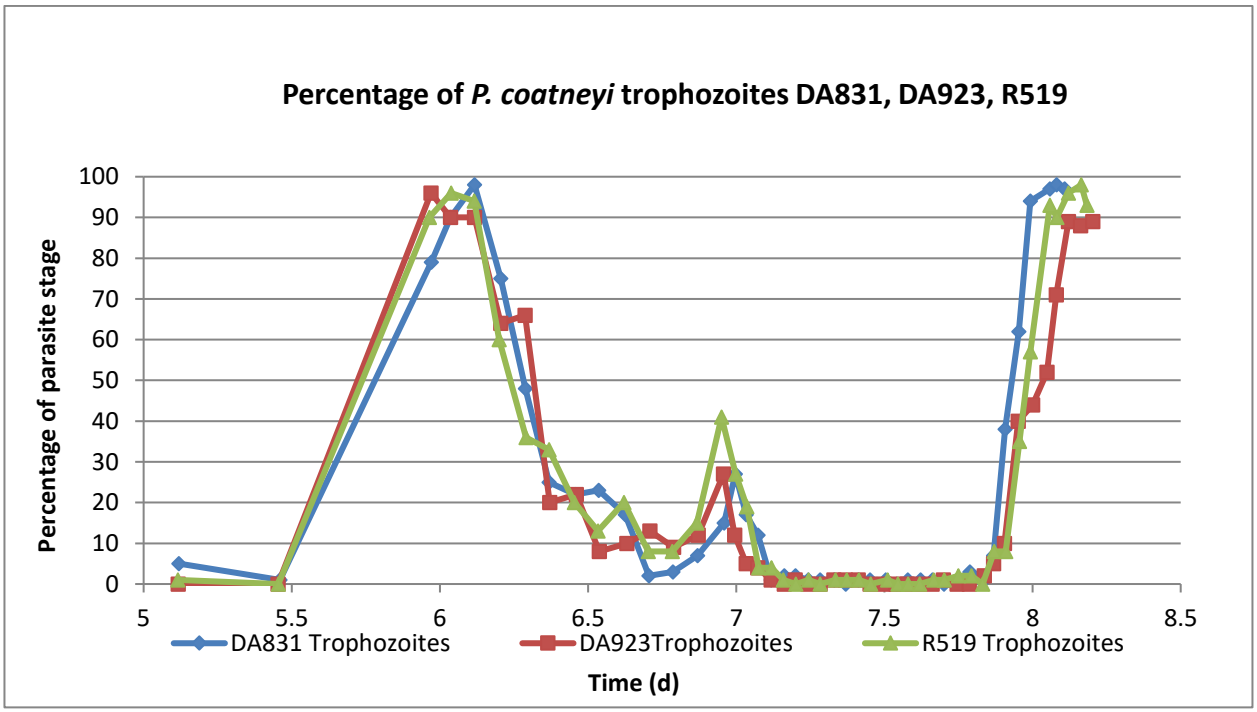

Graph 3.5.4

The mature trophozoites dominate in the blood immediately and predictably following the drop in earlier ring stages.

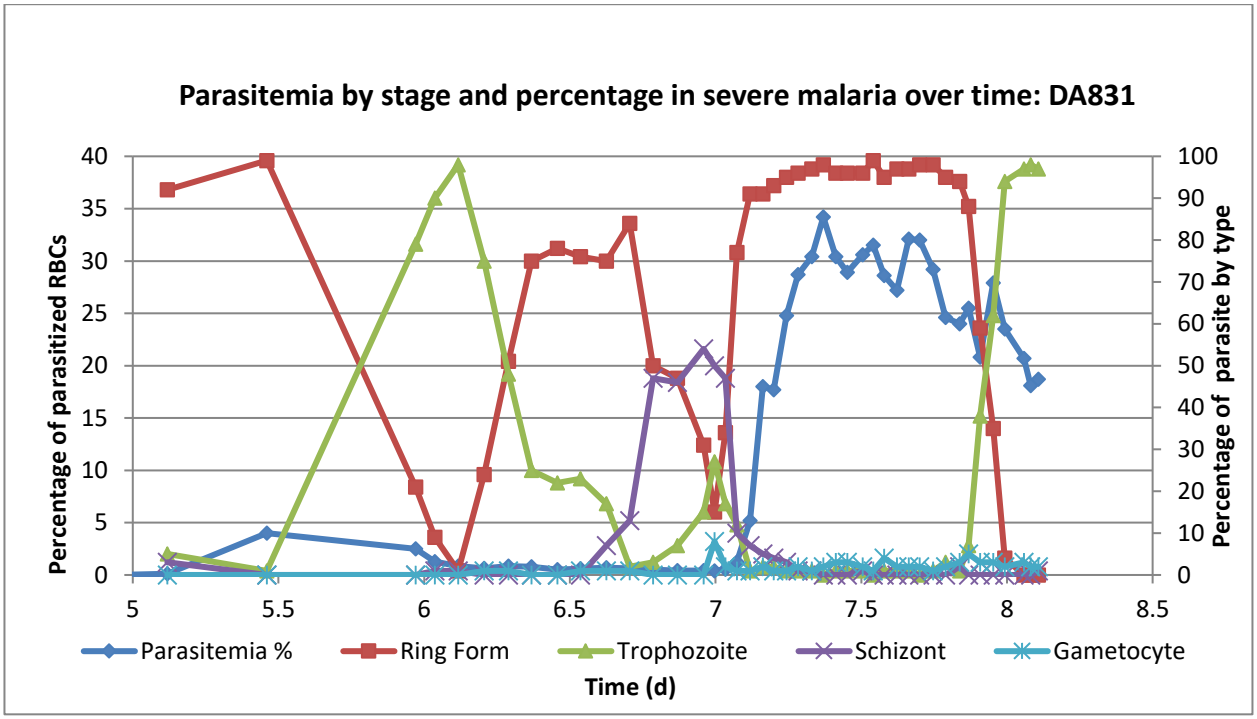

Graph 3.5.5

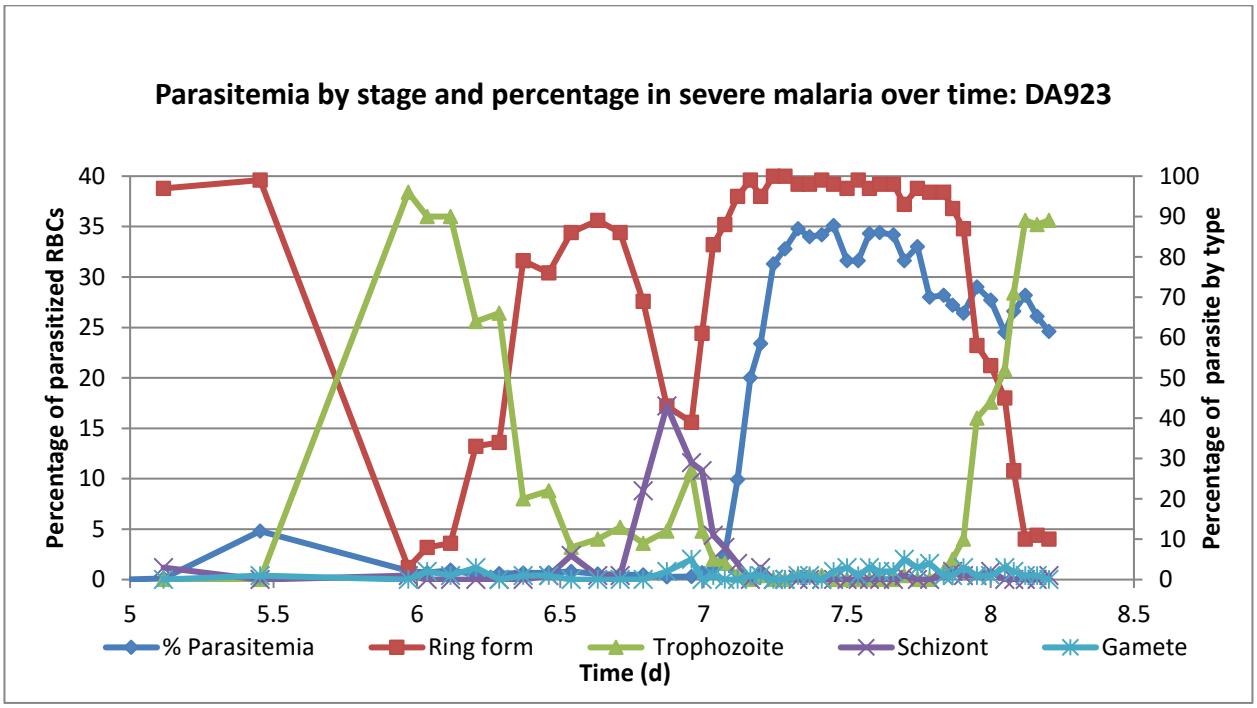

Graph 3.5.6

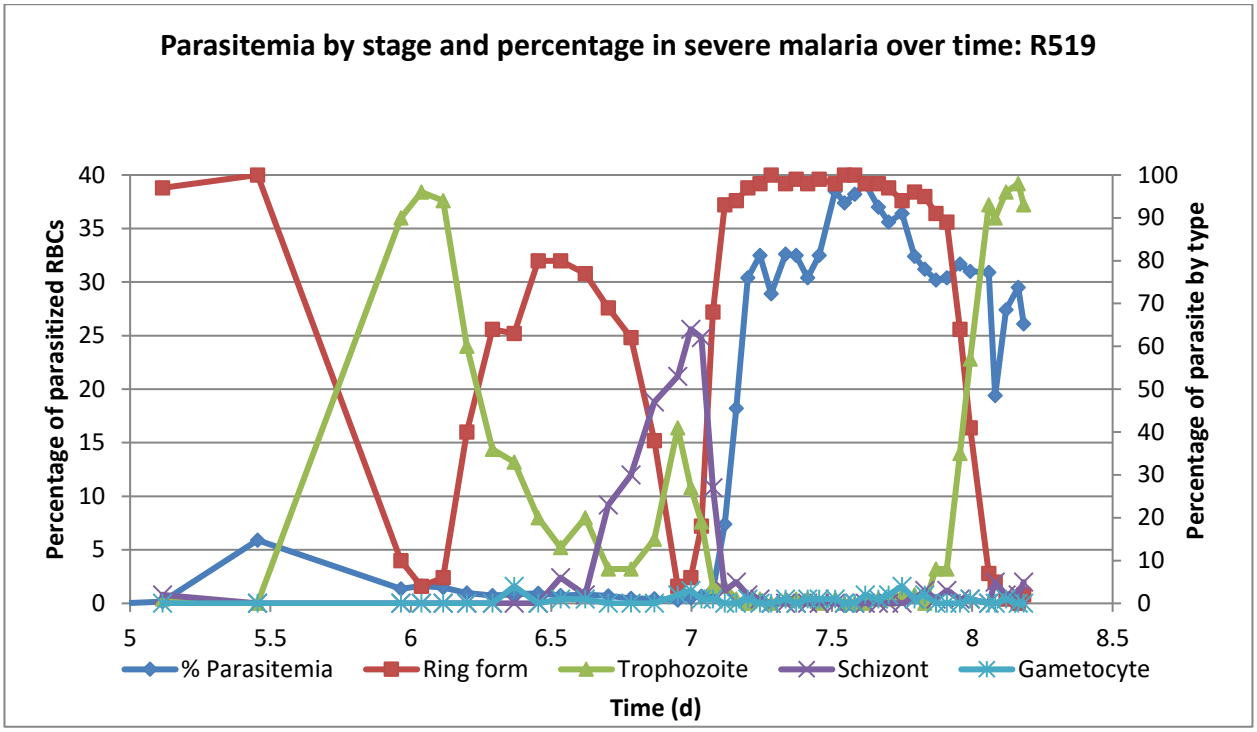

Graph 3.5.7

The preceding 3 graphs, each representing the parasitemia percentage broken out over time as to the specific stage of the erythrocytic life cycle are essentially identical between individual animals. These findings, combined with the parasitemia curves allowed for highly reliable disease progression and subsequently a predictable if brief window in which the animals reached treatment criteria.

3.6 **Temperature versus parasitemia curves**:

Mapping the temperatures against the parasitemia curves across all experimental animals, there was a slight progressive increase in temperatures immediately preceding the initial parasitemia spikes, followed by a predictable, significant and pathological febrile event synchronous with the leap in parasitemia over the course of day 7 and day 8. The initial temperature increases, while notable and allowing for prediction of the critical spike, were not significant due to the range of physiological temperatures noted in pre-experiment data collection and in control animals.

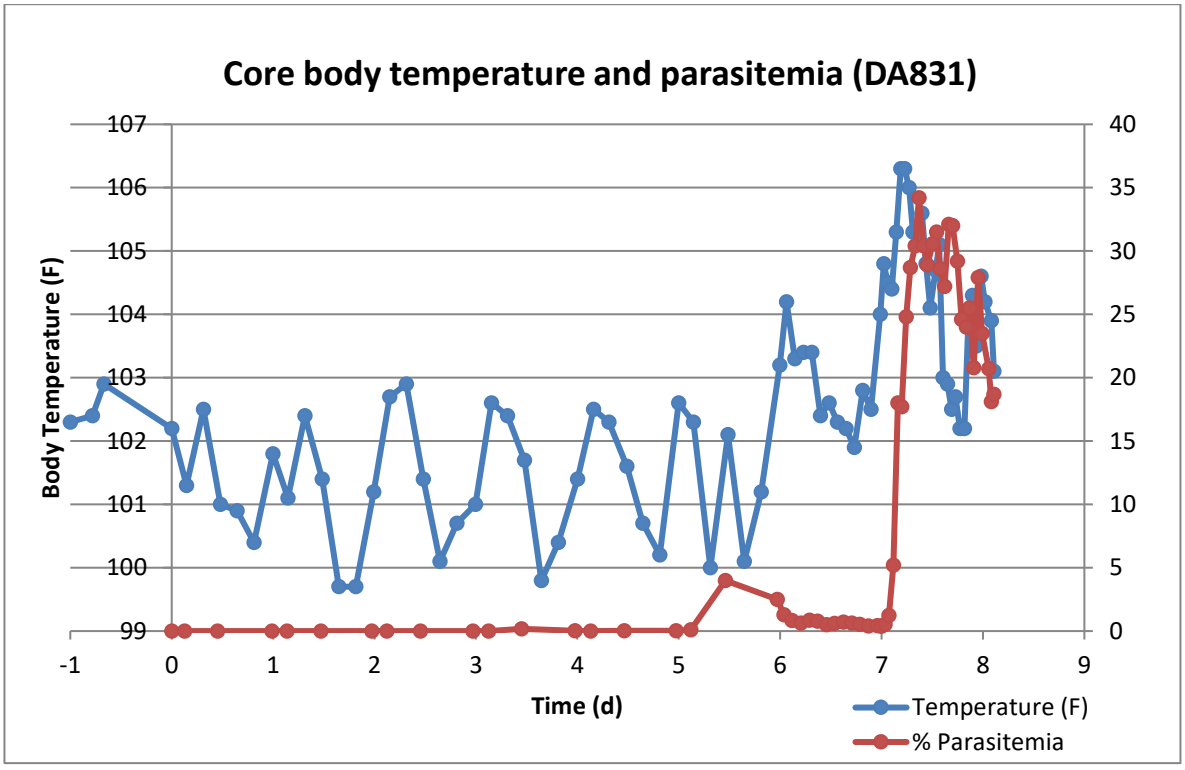

Graph 3.6.1

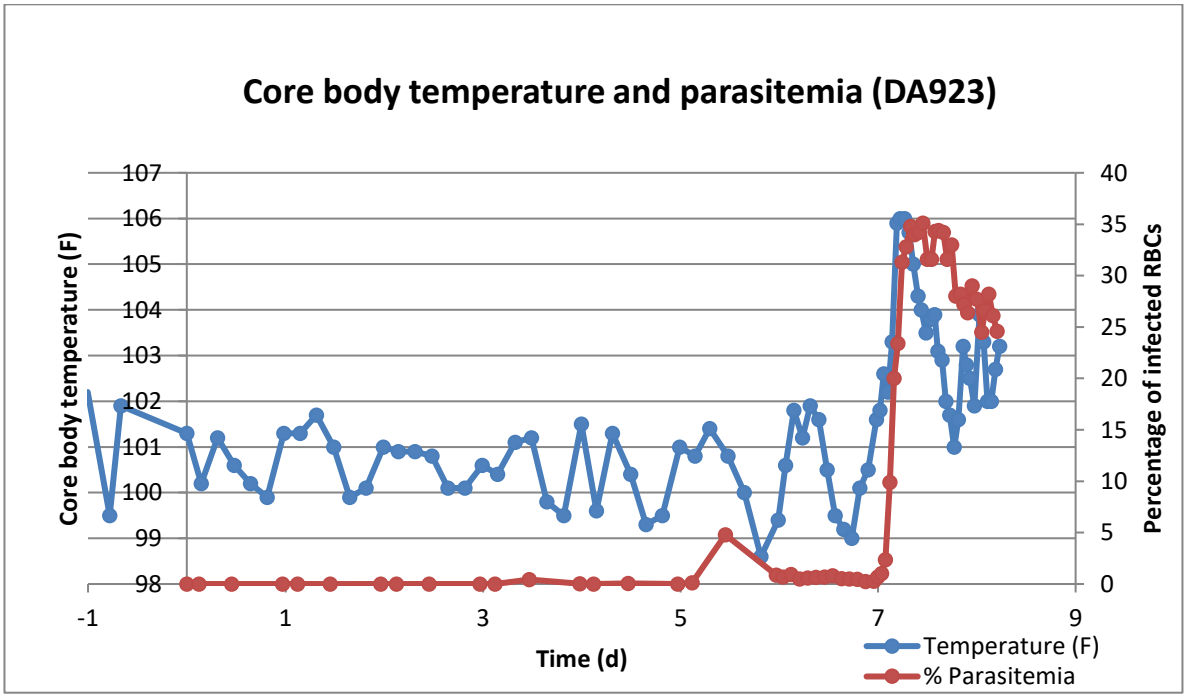

Graph 3.6.2

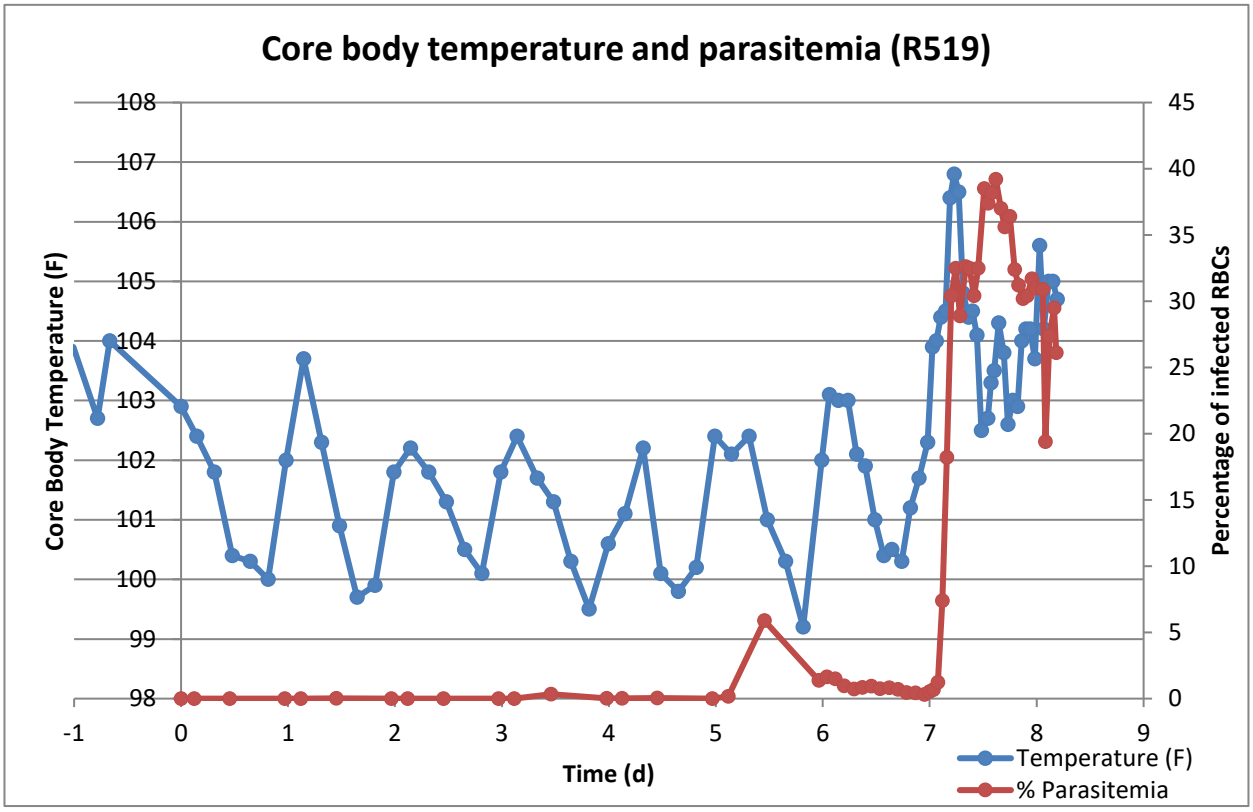

Graph 3.6.3

Graphs 3.6.1-3.6.3 represent the temperature graphed over time further overlain with the percent parasitemia in 3 of the animals from the refinement study. These data were repeatable and predictable over the drug ranging study.

As temperature measurements are far less labor intensive and do not require the specific skill set of microscopic malaria parasite life cycle staging, the use of temperature may represent adequate data collection to map out disease progression in this model, if staggered with parasitemia assessments. If so, the requirement of collecting blood samples every other hour as was done in this study may be excessive. Modern technology and telemetry allows for remote and constant temperature data collection and as such, subsequent studies could employ said technology in order to predict the parasitemia spike. It is important to note that in this study we collected temperature readings both via manual rectal measurement as well as using a subcutaneous microchip. The rectal

temperatures were far more reliable than the microchip readings, and therefore any future studies which choose to employ remote telemetry should first establish their core temperature algorithms and error margin if employing only the superficial temperature rather than a core reading.

3.7 **Hematological Parameters**:

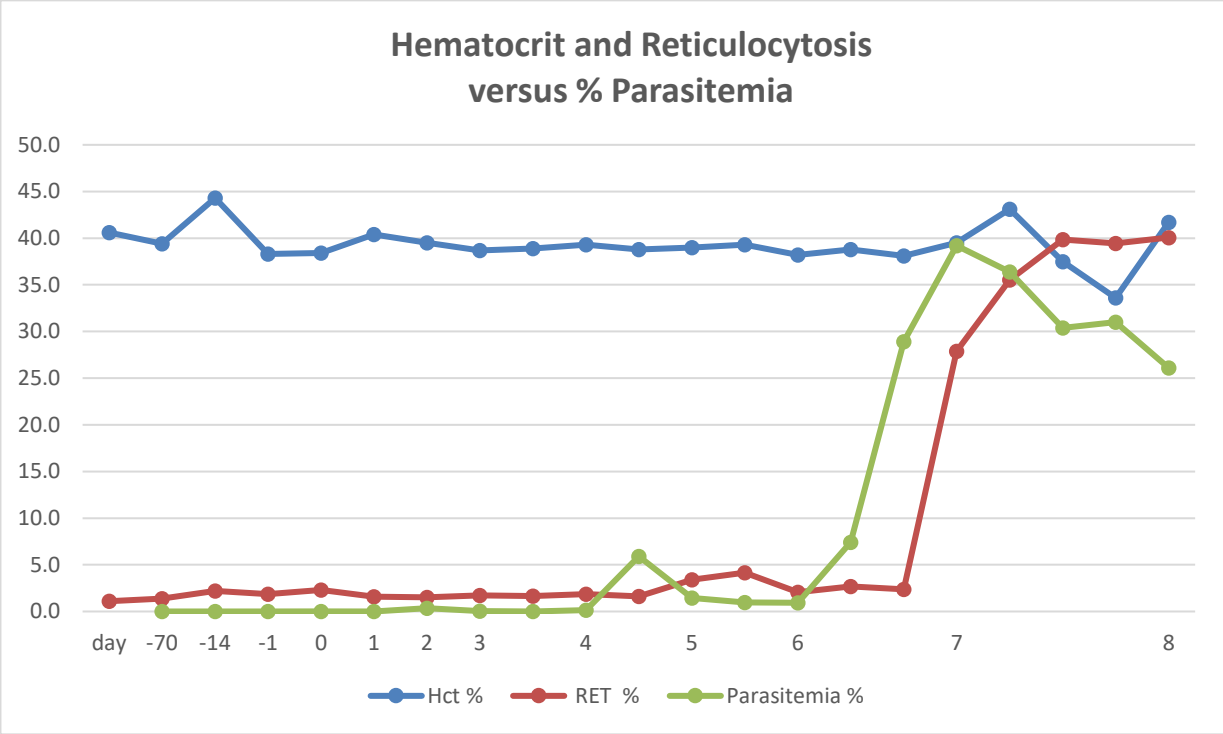

Graph 3.7.1 Mean % Hematocrit and % Reticulocytosis versus % parasitemia from DA831, DA923 and R519. While the mean hematocrit of animals in the acute refinement study remained relatively constant, the reticulocyte count resultant from the regenerative anemia and the upregulation of the bone marrow erythrocyte release demonstrated a steep increase which lagged slightly behind the spike in parasitemia after day 6.

Early studies examining the pathophysiology of *P. coatneyi* in non-human primates noted that the parasite preferentially infects reticulocytes, a trait it shares with *P. vivax*. (Coatney 1971) Additionally, comprehensive evaluation of the bone marrow regenerative response has been described by Moreno et al. (Moreno 2013). In their study, which examined animals over a 30-day period during which they were treated with sub-curative anti-malarial artemether and allowed to

relapse. Bone marrow dyserythropoeisis, characterized by nuclear lobulation and nuclear fragmentation (karyorrhexis) with concurrent erythroid hyperplasia was described using microscopic evaluation of core bone marrow biopsies sampled at various time points in the study. Their results suggest that *P. coatneyi*-infected rhesus macaques develop severe anemia with concurrent coagulopathy, acute renal disease, as well as systemic metabolic dysfunction. These findings are consistent with observations reported in humans with falciparum malaria. (Chang 2004; Dörmer 1983; Planche 2005; von Siedlein 2012) Animals in the refinement study did not demonstrate significant anemia, however this is theorized to be due to the short duration of the study (8 days). In the methylene blue drug dosing study, animals survived up to a maximum of 15 days post infection, and in spite of highly successful radical cure and clearance of the parasites using the drug, there was a progressive anemia observed in all animals with hematocrits dropping to a low of 12%.

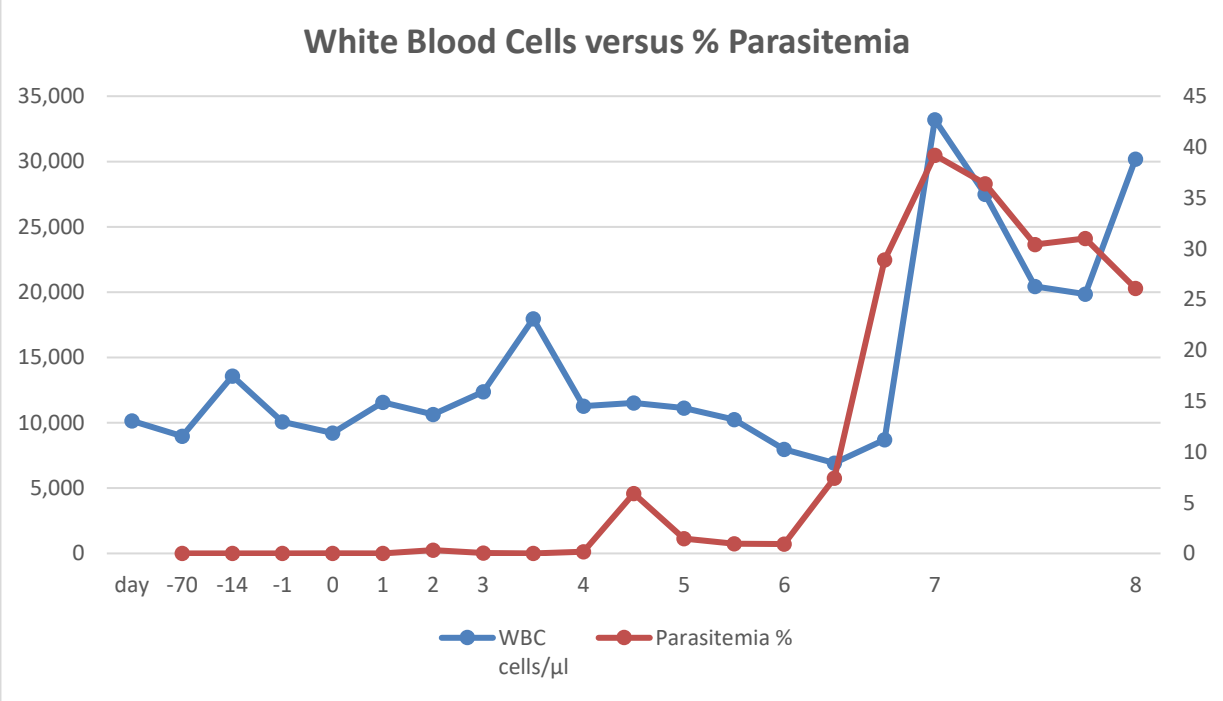

Graph 3.7.2 Mean White Blood Cell count versus % parasitemia from DA831, DA923 and R519. A leukocytosis was observed in the experimental animals which essentially paralleled the spike in parasitemia.

The total white blood cell count shows an increase around day 6 to 7 which parallels the spike in parasitemia. A large, unpublished study of normal blood values of Indian origin rhesus macaques within the AFRIMS colony demonstrated a range in resting total WBC count from 5000-10000 per microliter depending on a variety of physiological factors to include gender, age, experimental history, hierarchical status as well as concurrent disease and environmental stress. Additionally, there are reports of normal blood value ranges in Chinese origin rhesus available. (Chen 2009) Within our study, the white blood cell count was observed to fluctuate over the course of the study, but to reliably decrease at the same point as the parasitemia began to spike, and then with approximately a 12-hour lag, would increase from 2 to 3-fold and the resultant leukocytosis would remain through the end of the study. In the methylene Blue drug ranging study, once the parasitemia began to drop, so too would the WBC count.

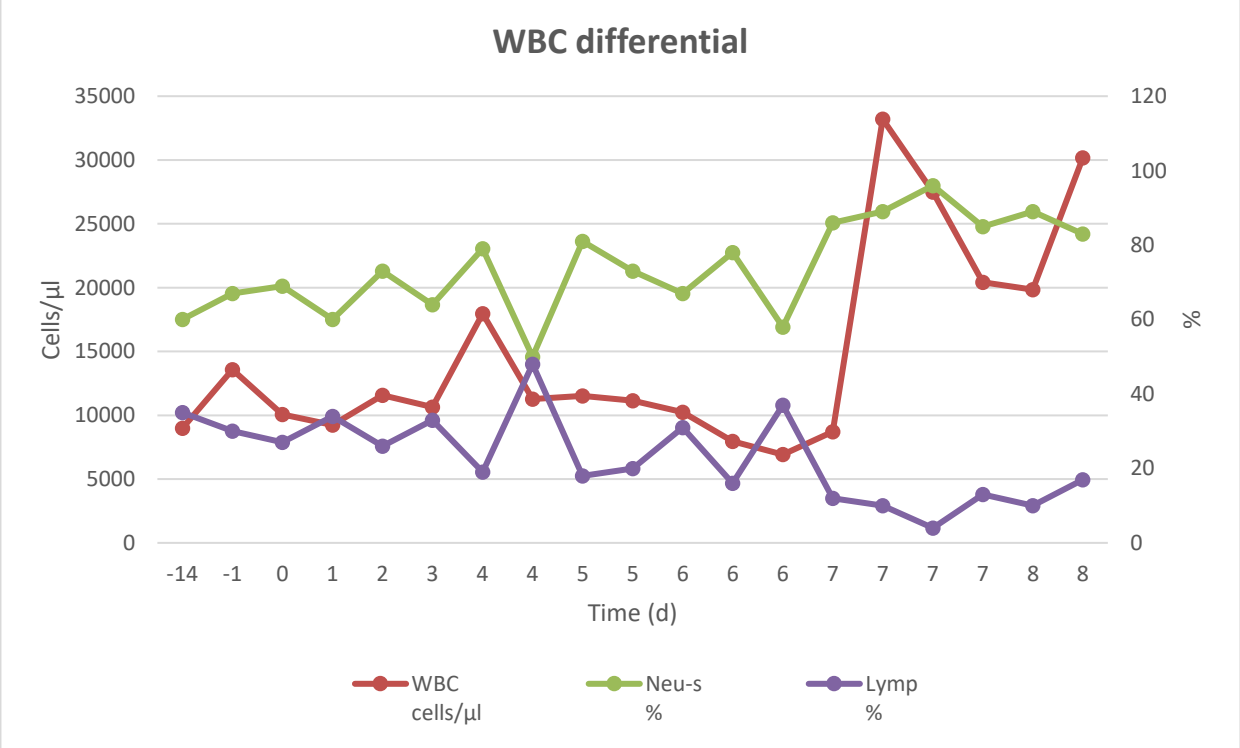

Graph 3.7.3 Mean WBC differentiation over the course of the experiment from DA831, DA923 and R519.

During the peak leukocytosis, there was a concurrent increase in neutrophils while lymphocytes dropped. This circulating leukocytosis does not translate to an infiltration of affected tissues, with the exception of moderate numbers of neutrophils being observed within the sequestered microvasculature of the glomerular tufts. This leukogram mirrors that observed in malignant falciparum malaria with the exception of the monocytosis which is observed in a small percentage of severely affected human victims. (Clark 2003; Fransichetti 2008; Gupta 2015; McKenzie 2005; Tobón-Castaño 2015) The most frequent finding in humans is actually a normal leukogram, with less than 20% of human patients having a leukopenia predominated by lymphopenia. Interestingly, in one study conducted in Colombia by Tobón-Castaño et al, the presence of a leukocytosis, predominated by neutrophils was associated with clinical complications. (Tobón-Castaño 2015)

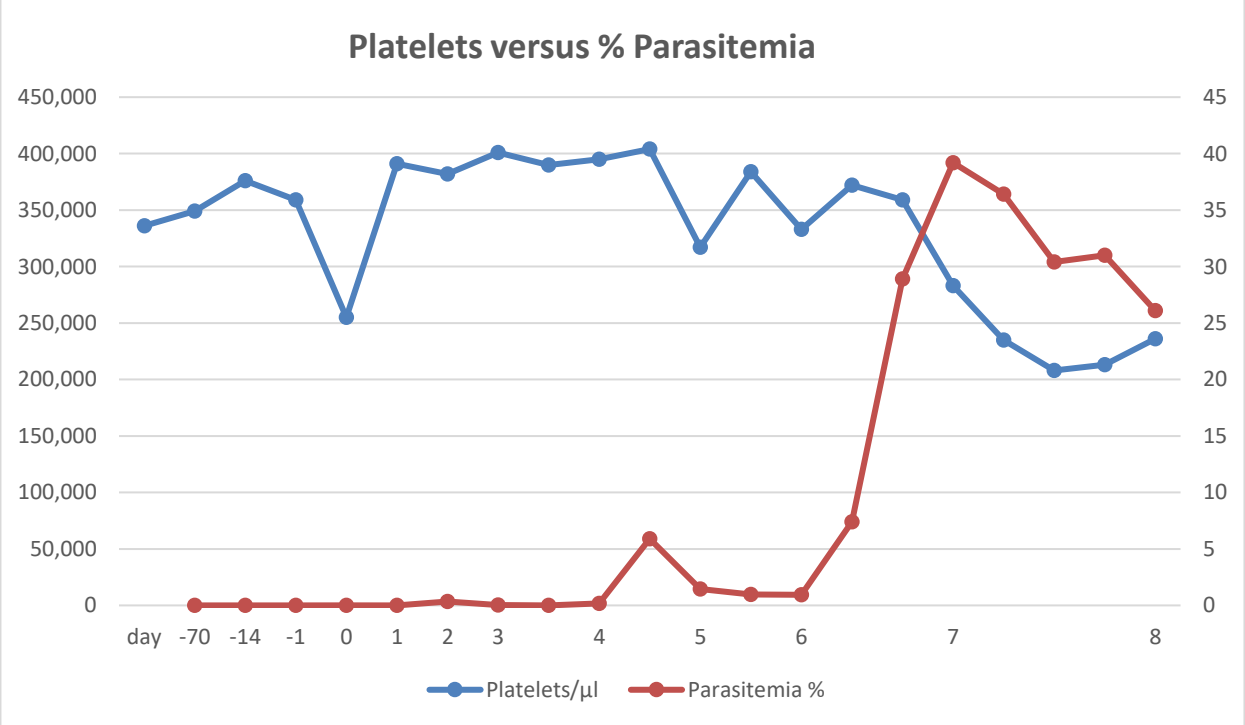

Graph 3.7.3 Mean platelets/microliter versus percent parasitemia from DA831, DA923 and R519.

While still having adequate numbers of thrombocytes, an initial decrease in the total number was observed in all animals. Thrombocytopenia is commonly described in human malaria infection in adults. (Hanson 2015) This finding likely would continue to increase and to accelerate, however euthanasia predates a significant thrombocytopenia in all experimental animals. It is noteworthy to mention that in the histopathology review of both retrospective and prospective cohorts of experimental animals, that fibrin thrombi were not a significant finding except in a few exceptions. Furthermore, special staining using Masson's trichrome did not highlight a primary thrombotic process.

3.8 **Renal and hepatic clinical chemistry**:

Clinical chemistry data supported the clinical symptomology of acute renal disease which was evident in the findings of oliguria, hematuria and dehydration, with hematuria being a common and early clinical sign of disease. The sporadic vomiting observed in some of the animals could be the result of a uremic syndrome, however as it is a relatively non-specific finding, it is not possible to draw a direct correlation and this is unlikely as blood urea nitrogen and the creatinine both increased subsequent to the parasitemia spike on day 7. The increase in blood chemistry abnormalities lagged approximately 12 hours behind the increase in parasitemia. Liver enzymes demonstrated a similar pattern of injury, with elevation of values occurring in a lagged pattern behind the parasitemia. In the case of the hepatic enzymes, Aspartate aminotransferase (AST) showed an initial small increase which was essentially parallel to the parasitemia and temperature increases, while both Alkaline Phosphatase (ALP), and Alanine aminotransferase (ALT) increased approximately 18 hours behind the spike in parasitemia. At that point, AST had a second and significant increase corresponding with the other two enzymes.

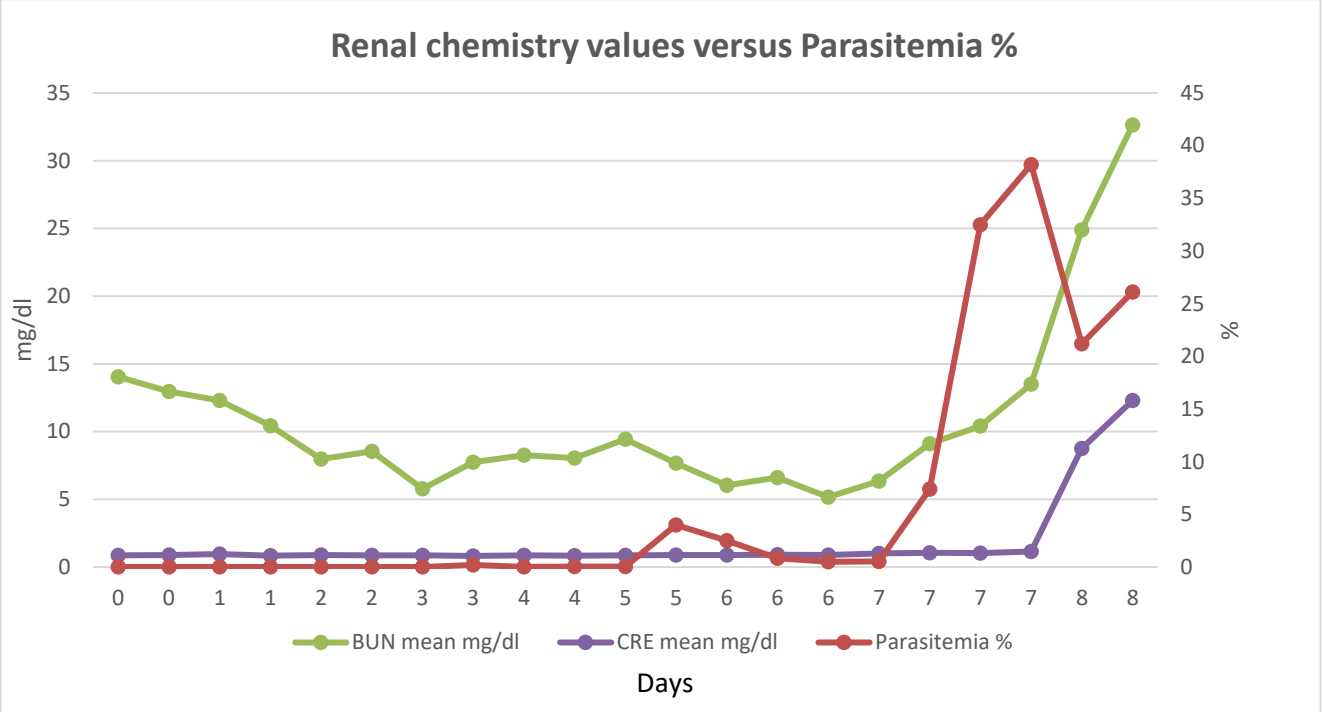

Graph 3.8.1. Mean BUN and CRE versus percent parasitemia from DA831, DA923 and R519.

Date Taken	Parasitemia %	BUN mean mg/dl	CRE mean mg/dl
0	0.00	14.03	0.85
0	0.00	12.97	0.88
1	0.00	12.30	0.95
1	0.00	10.43	0.84
2	0.00	7.97	0.88
2	0.00	8.53	0.87
3	0.00	5.77	0.86
3	0.18	7.73	0.82
4	0.02	8.27	0.85
4	0.03	8.03	0.83
5	0.03	9.43	0.85
5	4.00	7.67	0.89
6	2.50	6.03	0.88
6	0.84	6.60	0.90
6	0.51	5.17	0.87
7	0.52	6.33	1.01
7	7.40	9.10	1.05
7	32.50	10.40	1.03
7	38.20	13.50	1.15
8	21.20	24.90	8.76
8	26.10	32.63	12.29

Table 3.8.1. Mean BUN and CRE values versus percent parasitemia from DA831, DA923 and R519.

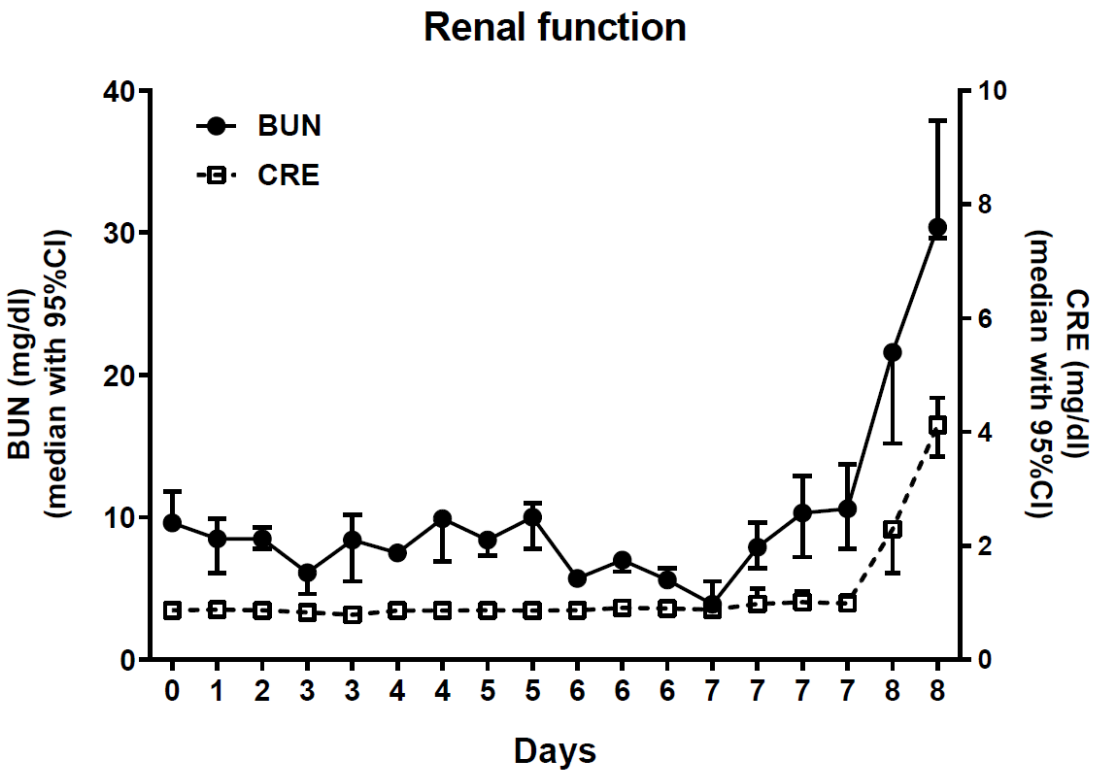

Graph 3.8.2. Median renal values (Blood Urea Nitrogen and Creatinine) from the 3 pilot animals measured over the course of infection.

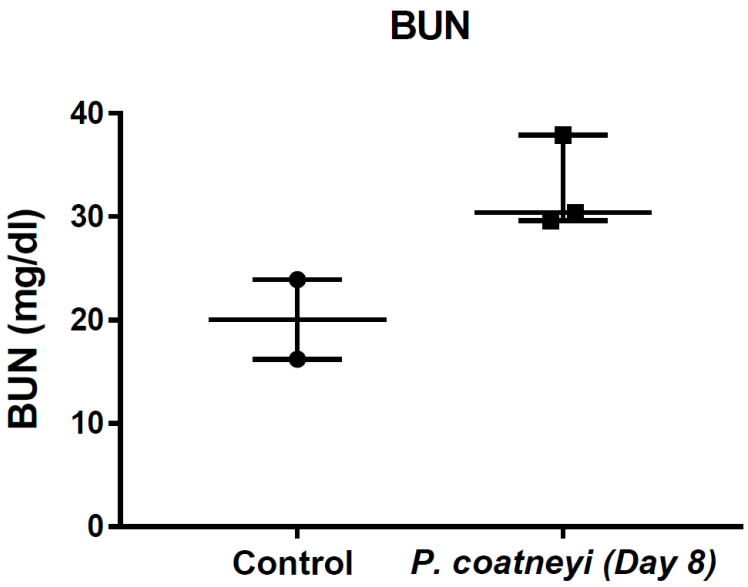

Control	*P. coatneyi (Day 8)*
23.9	30.4
16.2	29.6
	37.9

Table Analyzed	BUN
Column B	***P. coatneyi (Day 8)***
vs.	vs.
Column A	**Control**
Mann Whitney test	
P value	0.2000
Exact or approximate P value?	Exact
P value summary	ns
Significantly different (P < 0.05)?	No
One- or two-tailed P value?	Two-tailed
Sum of ranks in column A,B	3 , 12
Mann-Whitney U	0
Difference between medians	
Median of column A	20.05, n=2
Median of column B	30.4, n=3
Difference: Actual	10.35
Difference: Hodges-Lehmann	13.7

Graph 3.8.3. Median Blood Urea Nitrogen values at peak infection from 3 experimental animals compared with pre-infection median baseline values.

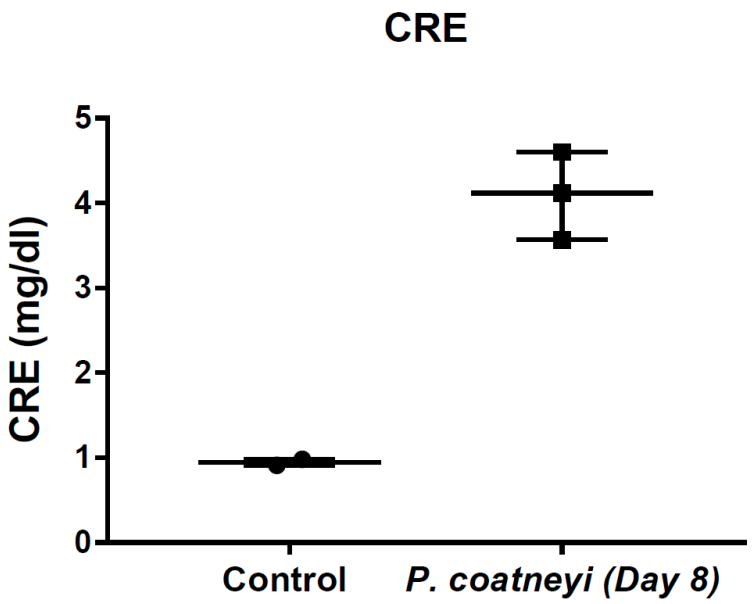

Control	*P. coatneyi (Day 8)*
0.91	3.57
0.98	4.60
	4.12

Table Analyzed	CRE
Column B	***P. coatneyi (Day 8)***
vs.	vs.
Column A	**Control**
Mann Whitney test	
P value	0.2000
Exact or approximate P value?	Exact
P value summary	ns
Significantly different (P < 0.05)?	No
One- or two-tailed P value?	Two-tailed
Sum of ranks in column A,B	3 , 12
Mann-Whitney U	0
Difference between medians	
Median of column A	0.945, n=2
Median of column B	4.12, n=3
Difference: Actual	3.175
Difference: Hodges-Lehmann	3.175

Graph 3.8.4. Median creatinine values at peak infection from 3 experimental animals compared with pre-infection median baseline values.

Median values of both creatinine and blood urea nitrogen were assessed at peak infection in the 3 experimental animals from the pilot study. These values were compared with median baseline values drawn from the same three animals prior to infection. The Mann Whitney test was applied to assess non-parametric significance between baseline and peak values. In both instances, the results were

observed to not be significant. It is important to recognize the small sample size, and the fact that empirically, renal blood chemistry values, as well as the hepatic values described subsequently all demonstrate an observable and marked increase in value lagging behind the spike in parasitemia. Since these values demonstrate acute injury to the renal system (in the case of blood urea nitrogen and creatinine) and to the hepatic system (in the case of ALT, AST and ALP), the empirical increases observed as both median and mean values when compared with internal control baseline values demonstrates that there is a corollary pathological effect of *P. coatneyi* hyperparasitemia on the rhesus.

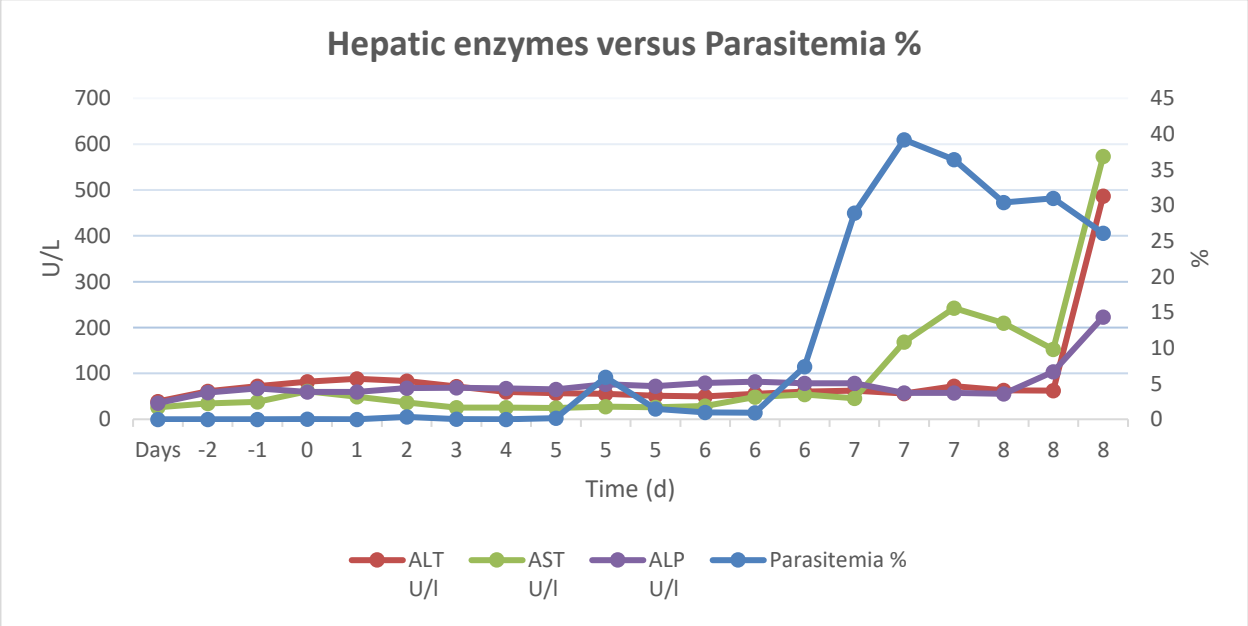

Graph 3.8.5. Mean hepatic enzymes versus percent parasitemia from DA831, DA923 and R519.

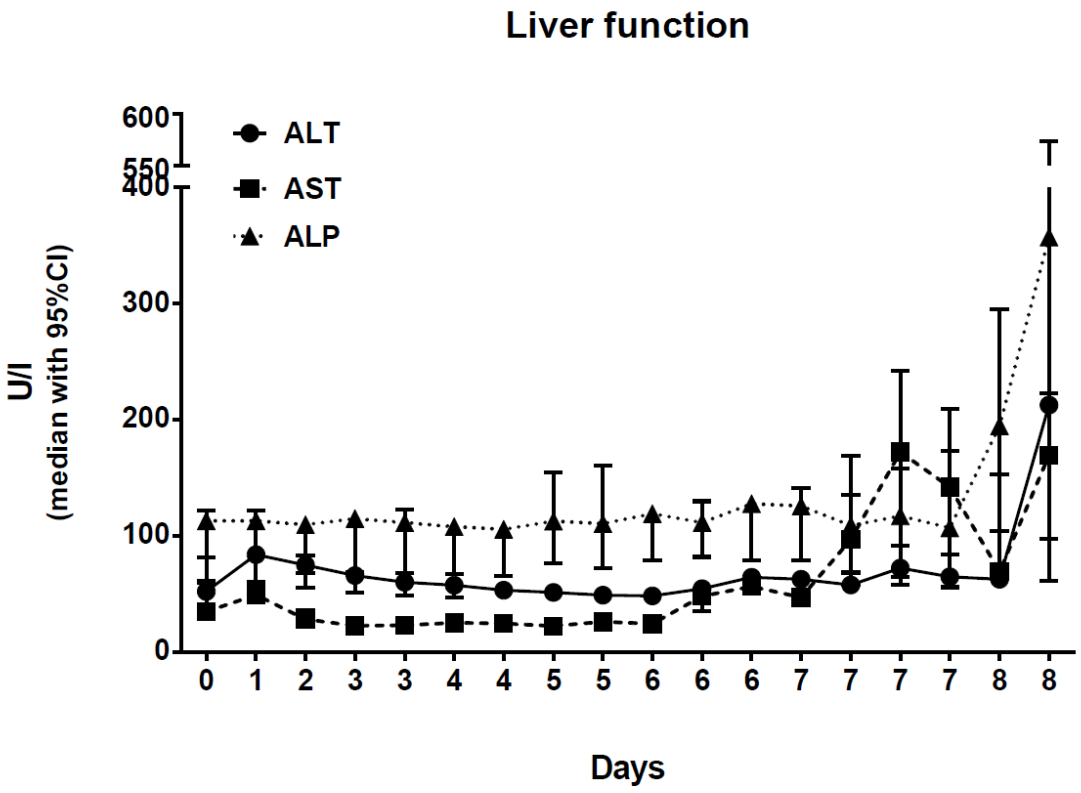

Graph 3.8.6. Median hepatic values (ALT, AST, ALP) from the 3 pilot animals measured over the course of infection.

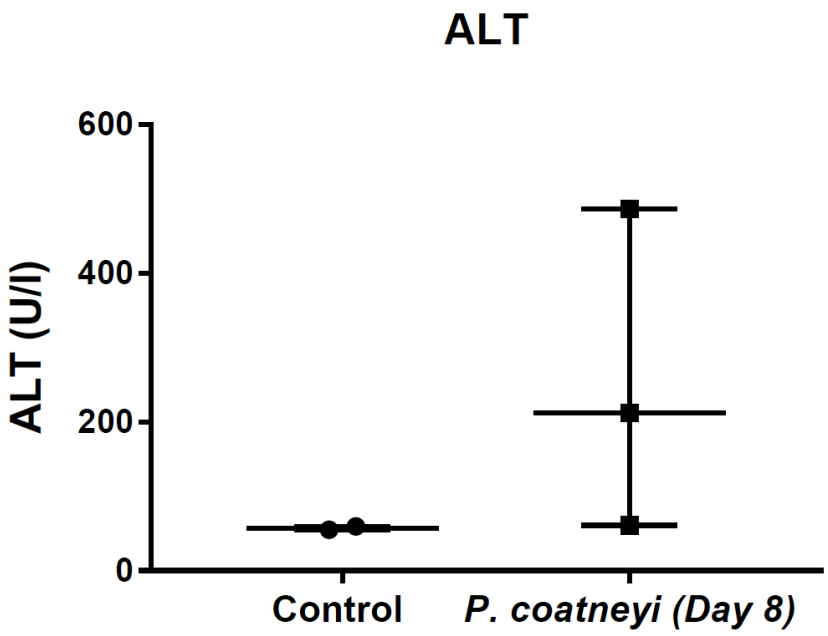

Control	*P. coatneyi (Day 8)*
55.0	212.6
59.6	61.2
	486.5

Table Analyzed	ALT
Column B	***P. coatneyi (Day 8)***
vs.	vs.
Column A	**Control**
Mann Whitney test	
P value	0.2000
Exact or approximate P value?	Exact
P value summary	ns
Significantly different (P < 0.05)?	No
One- or two-tailed P value?	Two-tailed
Sum of ranks in column A,B	3 , 12
Mann-Whitney U	0
Difference between medians	
Median of column A	57.3, n=2
Median of column B	212.6, n=3
Difference: Actual	155.3
Difference: Hodges-Lehmann	155.3

Graph 3.8.7. Median ALT values at peak infection from 3 experimental animals compared with (2) pre-infection median baseline values.

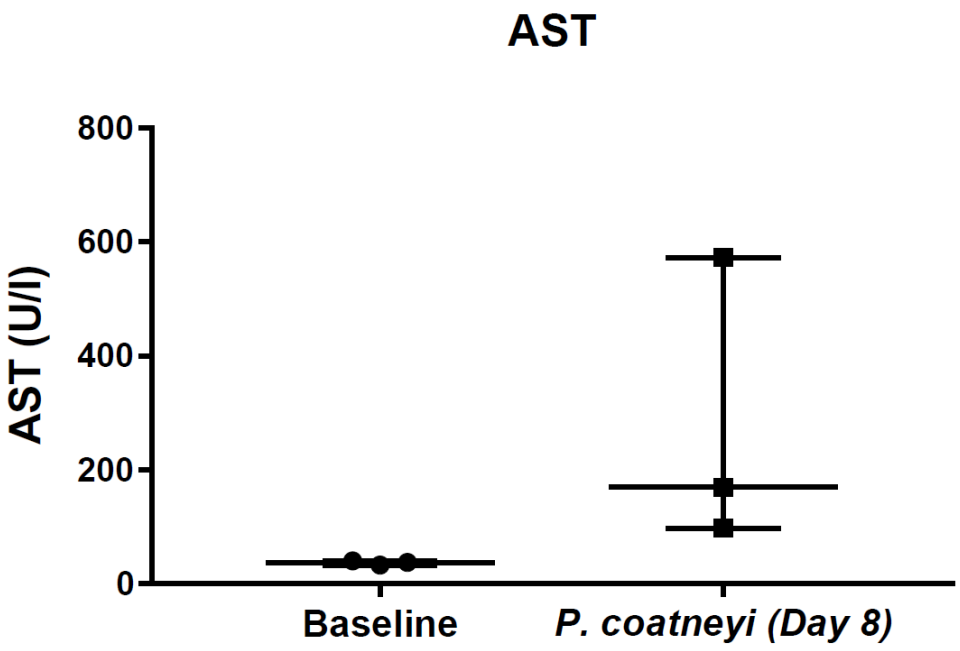

Baseline	*P. coatneyi (Day 8)*
40.0	169.5
32.9	97.5
37.9	573.1

Table Analyzed	AST
Column B	***P. coatneyi (Day 8)***
vs.	vs.
Column A	**Baseline**
Mann Whitney test	
P value	0.1000
Exact or approximate P value?	Exact
P value summary	ns
Significantly different (P < 0.05)?	No
One- or two-tailed P value?	Two-tailed
Sum of ranks in column A,B	6 , 15
Mann-Whitney U	0
Difference between medians	
Median of column A	37.9, n=3
Median of column B	169.5, n=3
Difference: Actual	131.6
Difference: Hodges-Lehmann	131.6

Graph 3.8.8. Median AST values at peak infection from 3 experimental animals compared with pre-infection median baseline values.

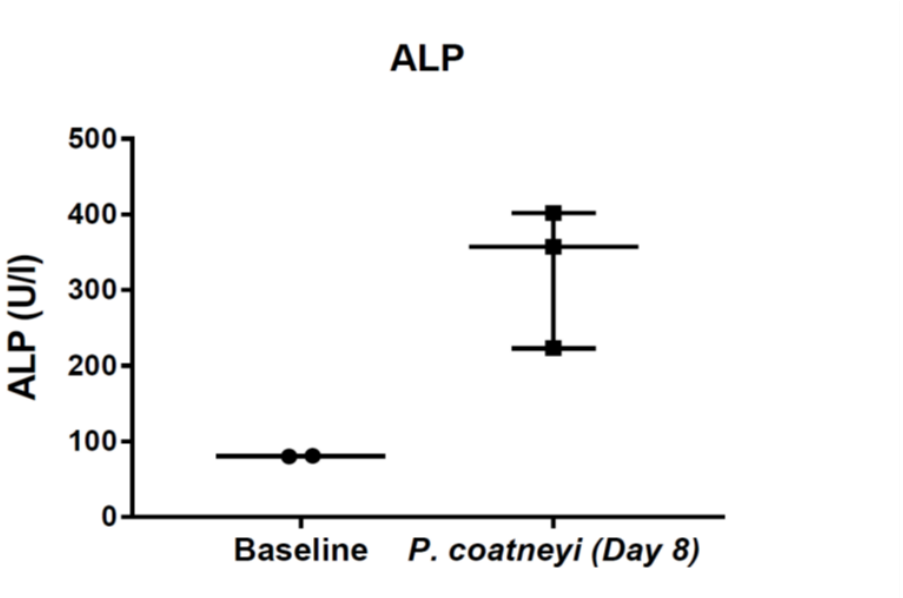

Baseline	*P. coatneyi (Day 8)*
81.2	357.4
80.0	401.9
	223.2

Table Analyzed	ALP
Column B	***P. coatneyi (Day 8)***
vs.	vs.
Column A	**Baseline**
Mann Whitney test	
P value	0.2000
Exact or approximate P value?	Exact
P value summary	ns
Significantly different (P < 0.05)?	No
One- or two-tailed P value?	Two-tailed
Sum of ranks in column A,B	3 , 12
Mann-Whitney U	0
Difference between medians	
Median of column A	80.6, n=2
Median of column B	357.4, n=3
Difference: Actual	276.8
Difference: Hodges-Lehmann	276.8

Graph 3.8.9. Median ALP values at peak infection from 3 experimental animals compared with pre-infection median baseline values.

3.9 **Electrolytes and Glucose**:

Sodium, potassium and chloride remained within normal limits throughout the study in all animals, with no demonstrably significant increases in the values. This argues against significant early acute tubular injury, as this is usually associated with hyperkalemia, although several animals in the terminal phase demonstrated marked abnormalities in renal chemistry just before euthanasia and death.

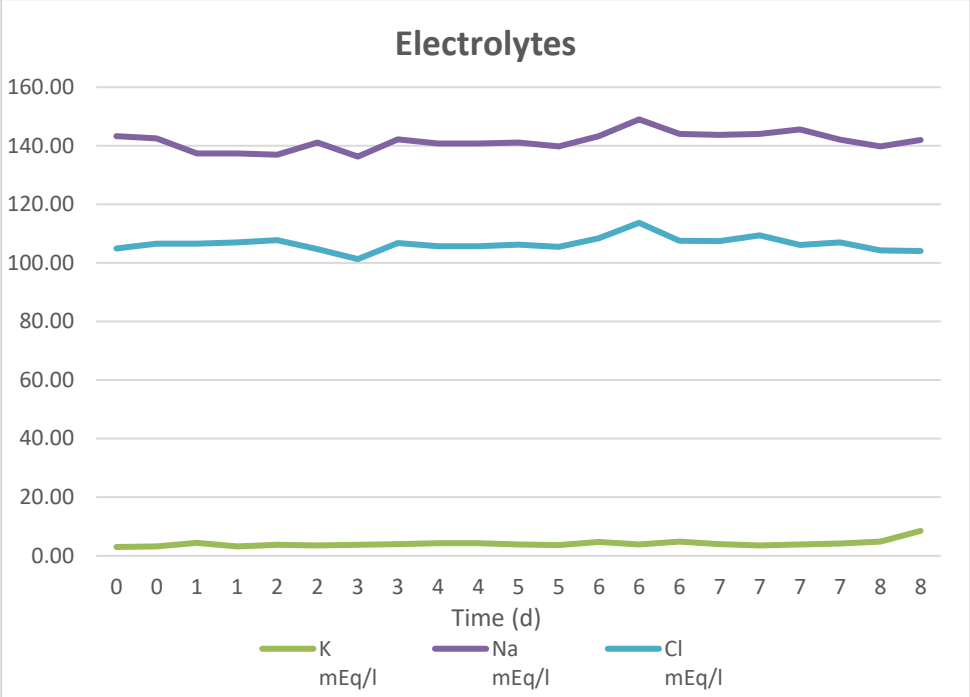

Graph 3.9.1. Mean electrolytes versus percent parasitemia from DA831, DA923 and R519.

Date Taken	K mEq/l	Na mEq/l	Cl mEq/l
0	3.21	141.4	103.7
0	3.19	143.9	105.4
1	3.61	132.2	105.1
1	3.20	143.2	110.6
2	4.34	143.0	111.2
2	3.60	142.5	105.8
3	3.81	143.0	107.3
3	3.58	139.7	105.2
4	3.69	146.5	110.1
4	4.38	144.3	109.8
5	3.07	144.8	108.9
5	4.09	144.2	109.4
6	3.83	143.3	108.7
6	4.10	149.4	113.7
6	4.12	142.9	108.7
7	4.04	144.8	108.9
7	3.98	143.1	109.3
7	4.09	143.3	106.1
7	3.93	141.1	106.4
8	4.03	140.3	103.4
8	16.50	138.0	98.4

Table 3.9.1. Mean electrolyte values from DA831, DA923 and R519.

Hypoglycemia, which is a feature of severe malaria in humans, was not a significant finding in this *P. coatneyi*/Rhesus macaque model. In four of the six animals assigned to the model refinement study, there was a marked decrease in glucose levels the day of either euthanasia or death, however the nine animals in the methylene blue study did not demonstrate any significant change in glucose levels throughout the course of the study. The majority of the animals were both well-muscled and had significant adipose reserves to the point of being overweight in several cases. This may account for their ability to resist the periods of anorexia and the severity of disease by being able to mobilize their fat reserves and maintain normoglycemic levels.

3.10 **Lactate**:

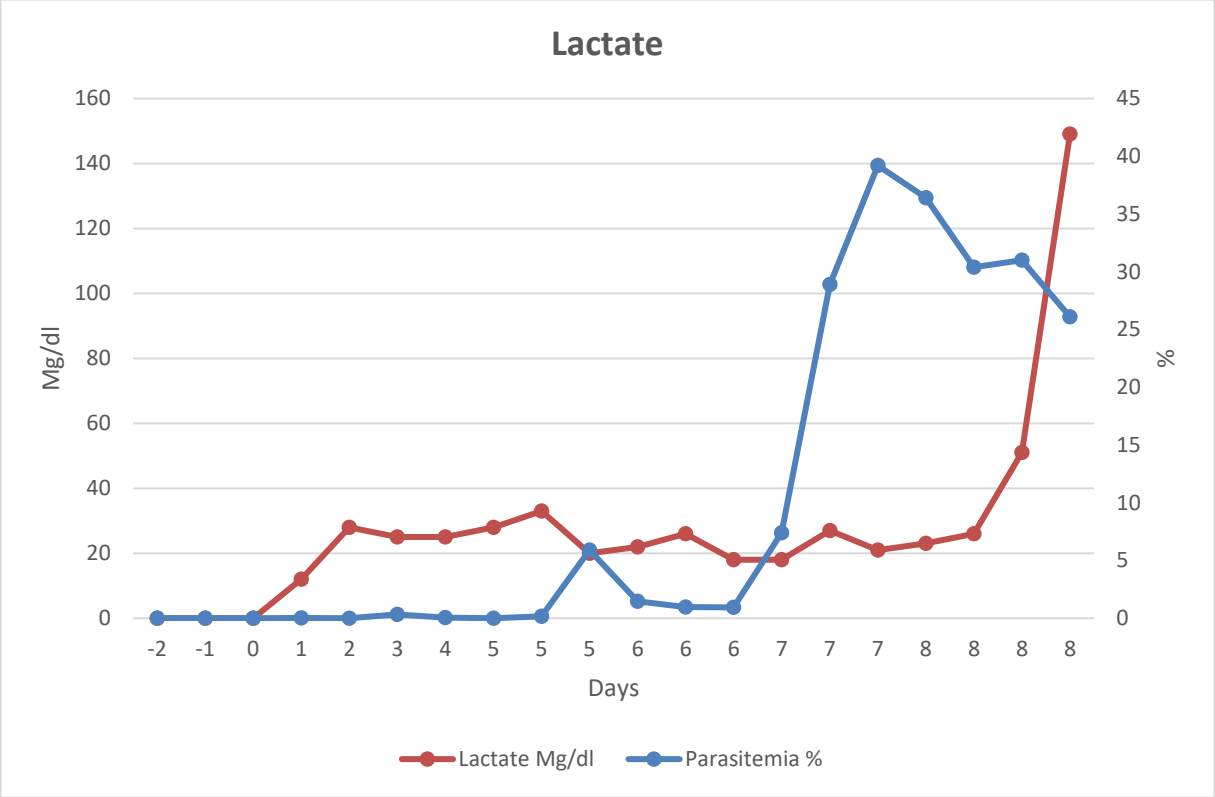

Graph 3.10.1. Mean lactate versus percent parasitemia from *P. coatneyi* infected pilot animals.

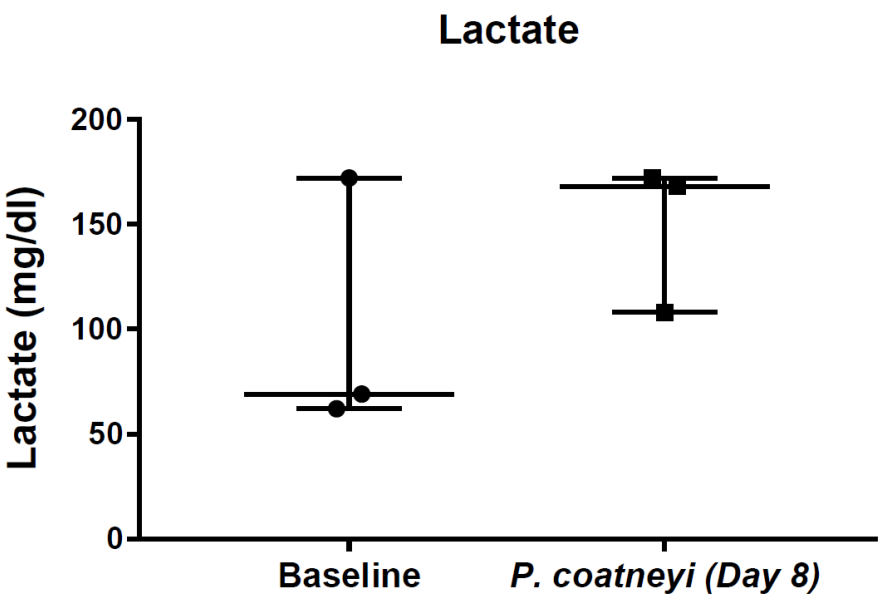

Baseline	*P. coatneyi (Day 8)*
62.0	108.0
172.0	168.0
69.0	172.0

Table Analyzed	Lactate
Column B	***P. coatneyi (Day 8)***
vs.	vs.
Column A	**Baseline**
Mann Whitney test	
P value	0.5000
Exact or approximate P value?	Exact
P value summary	ns
Significantly different (P < 0.05)?	No
One- or two-tailed P value?	Two-tailed
Sum of ranks in column A,B	8.5 , 12.5
Mann-Whitney U	2.5
Difference between medians	
Median of column A	69, n=3
Median of column B	168, n=3
Difference: Actual	99
Difference: Hodges-Lehmann	46

Graph 3.10.2. Median lactate values at peak infection from 3 experimental animals compared with pre-infection median baseline values.

A spike in lactate measurements lagged behind the rise in parasitemia, however with relative consistency, increased just prior to death or euthanasia. These findings were most significant in the prospective, untreated, experimental animals which were used in the model refinement portion of the study. Interestingly, this finding did not occur in the methylene blue study. In those nine animals, the blood lactate remained within normal limits in all animals throughout the course of the study.

Lactic acidosis is a recognized complication of severe malaria, and is one of the primary contributing strong acids in the acidosis observed in severe malaria. (Day 2000) The increased lactate to pyruvate ratio observed demonstrates that anaerobic glycolysis occurs as a result of microcirculatory hypoperfusion in tissues systemically in the patient. In humans, as in the *P. coatneyi*/rhesus macaque model, sequestration of infected erythrocytes by means of cytoadherence, as well as the resultant margination of cells bound to the endothelium, rosette formation, autoagglutination, and endothelial cell injury likely further exacerbates the microcirculatory flow and likely induces regional hypoxia and with additional compromise, anoxia and ischemia. In severe malaria in humans, hyperlactatemia is often correlated with a poor prognosis, especially in children. (Agbenyega 2000; Casals-Pascual 2006; Ishioka 2016) As with analysis of renal and hepatic blood chemistry values, the median lactate at peak parasitemia in the pilot animals was not deemed to be statistically significant in comparison with baseline controls when assessed using the non-parametric Mann-Whitney test, however, empirical assessment of the lactate spike which is slightly delayed behind the marked increase in parasitemia is supportive of lactic acidosis in 2 of the 3 pilot animals.

3.11 **Retinal photography**:

Retinal photography was conducted in a select few animals and the resulting images were evaluated by a human ophthalmologist as well as a specialist in ocular toxicology in rhesus macaques. While no definitive hypotheses can be drawn from the resulting interpretation, the findings do correlate with the absence of retinal hemorrhages noted on microscopic examination of the retinas taken from all of the prospective experimental animals. Furthermore, the retinal edema which is described in one of the three animals appears to correlate with the edema observed histopathologically within the ganglion layer of the retina in multiple of the affected animals.

Number	Fundus	Features
DA977	Left	Normal disc. Marked NFL light reaction. Difficult to see beyond the reflection especially near vessels however no obvious changes
	Right	Normal disc. Again, marked NFL light reflection. No obvious lesions except 3 pale focal lesions just temporal to the disc.
R130	Left	Optic disc enlarged and swollen. Papilloedema and some burying of vessels just superior to the disc. Relatively discrete areas of perifoveal whitening. Thinning of the retina temporal to the fovea. Temporal to fovea multiple small discrete pale lesions
	Right	Optic disc appears swollen. Irregular right foveal border. Multiple temporal discrete pale lesions.
R338	Left	Normal disc, Some generalised whitening along temporal arcade vessels. Single pale focal lesion at inferior temporal arcade
	Right	Normal disc and retina, no additional comments
R761	Left	Normal disc and retina, no additional comments
	Right	Mottled pigmentation of fovea and perifovea with discrete drusen like lesions.

Table 3.11.1 Retinal photography findings. All samples were from P. coatneyi infected animals. Comparison was conducted between animals with normal findings versus those with evidence of injury.

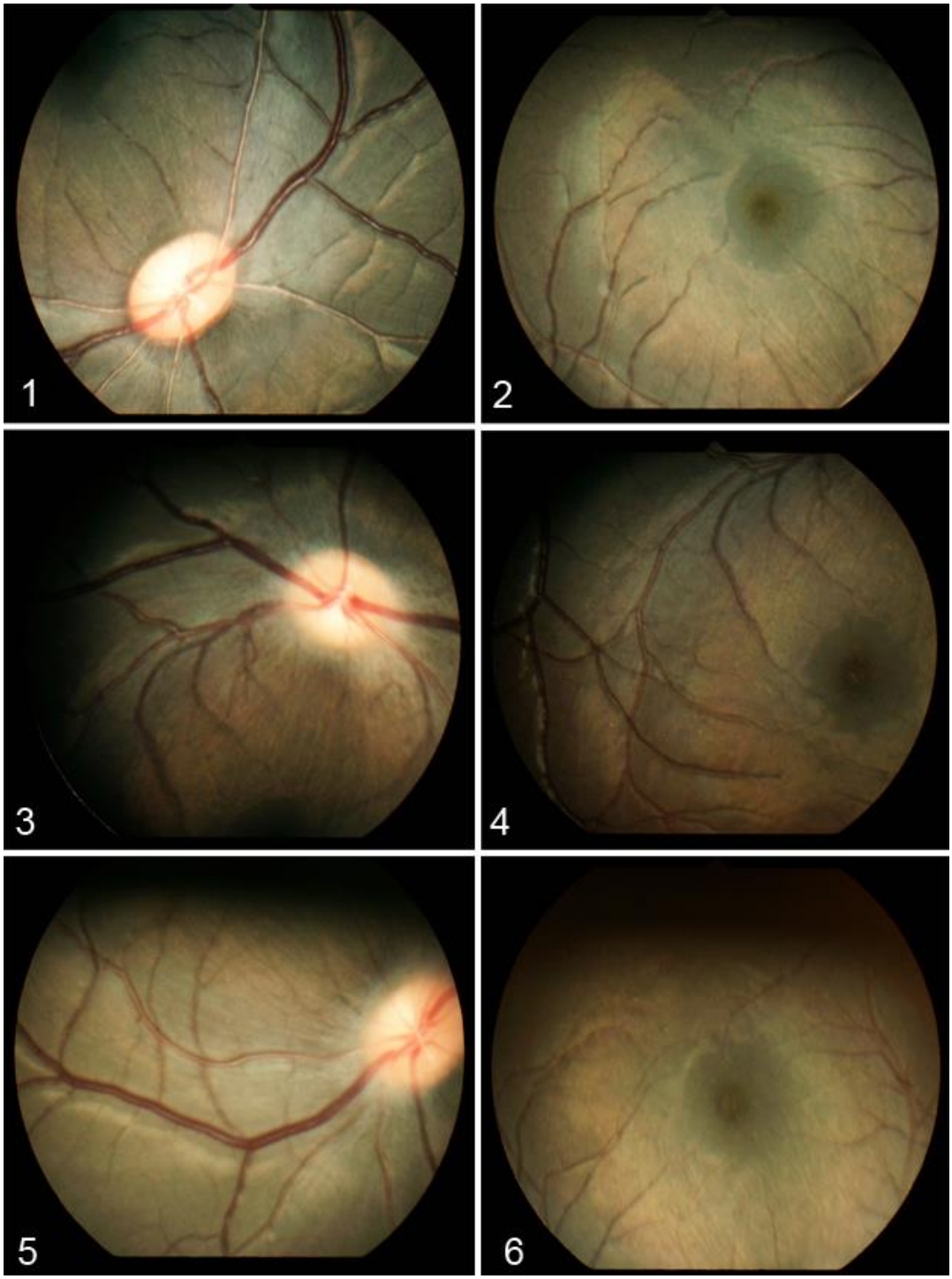

Figure 3.10.1. 1,2: R761 Left eye, Normal; 3,4 R130 Right eye; 5,6 R130 Left eye. In comparison with the normal images at the top of the plate (1,2), in both the right and left eyes of R130 there is evidence of papilloedema which consists of a blurring of the disc margins. This is typically seen as a passive swelling of the optic disc which is predominantly non-inflammatory in nature, rather is often

seen secondary to increased intracranial pressure (3,5). Additionally, the images are illustrative of discrete areas of perifoveal whitening and thinning of the retina temporal to the fovea. (4,6)

The retina can be a 'window' into pathology within the central nervous system, and detailed studies over the past 20 years have led to controversy surrounding how specific retinal changes are in reflecting malaria induced neuropathology. Indirect imaging studies of the brain in CM have proved useful in detailing the variable extent of cerebral edema, which in adults is not a uniform event in coma (Looaresuwan 1983; Looaresuwan 1995; Ponsford 2012), whilst in children the edema has been strongly linked to death in CM. (Seydal 2015)

A spectrum of retinal findings has been reported in malaria, including vascular changes, hemorrhages, white patches related to ischemia, and cloudy exudates. (White 2001; Beare 2003; Beare 2006) While some reports have stated that retinal changes are so strongly linked to malaria that they are being used as a clinical diagnostic criterion for CM in some centers (Beare 2006; Milner 2010), others have reported more variable findings in adult cases. (Abu-Sayeed 2011) Whether retinal changes happen in patients without coma, where neuropathology is less severe, is unclear, and the study of retinopathy in the simian model has not been reported prior to this preliminary examination.

3.12 **Gross findings**:

Autopsy findings described are combined post mortem descriptions from all 45 animals in the study, however these were segregated in terms of those animals who survived the initial insult and were thereby categorized as chronic in comparison with animals whose disease progression was deemed to be acute and in which animals either died spontaneously or were euthanized as a direct result of the *P. coatneyi* infection.

	Acute			Chronic	
	Findings	**Figures**		**Findings**	**Figures**
Brain: Cerebrum	Rare, multifocal parenchymal hemorrhages and congestion	√		NSL	
Brain: Cerebellum	Rare, multifocal parenchymal hemorrhages			NSL	
Brain: Brain stem	Rare, multifocal parenchymal hemorrhages and congestion	√		NSL	
Spinal cord	Rare, multifocal parenchymal hemorrhages and congestion			NSL	
Meninges	Congestion and edema and rare petechiae			NSL	
Eyes	NSL			NSL	
Integument	Erythema with multifocal petechiae and ecchymoses	√		Dermatitis, necroulcerative, multifocal to coalescing, severe	
Lungs	Mild to marked brown discoloration	√		NSL	
Heart	Mild to marked brown discoloration with multifocal white myocardial streaks and rare petechiae and ecchymoses. Cardiac dilatation.	√		NSL	
Liver	Friable hepatomegaly with moderate to severe brown discoloration with sinusoidal congestion	√		Diffuse lobular, zonal pallor and necrosis and hepatomegaly	√
Gallbladder	Choleostasis	√		NSL	
Spleen	Splenomegaly with severe brown discoloration			Brown discoloration	
Kidneys	Moderate to severe brown discoloration with congestion	√		Mild capsular nodularity and diffusely shrunken and severely pale	√
Pancreas	Congestion and edema			NSL	
Adrenal glands	Moderate congestion			NSL	
UB	Moderate to severe hematuria with mucosal hemorrhage	√		NSL	
Reproductive tract	Scrotal and testicular infarction with hemorrhage			NSL	
Gastrointestinal	Multifocal to coalescing, serosal erythema and mucosal hemorrhagic erosive and ulcerative enteritis	√		NSL	
Muscle	NSL			NSL	
Lymph nodes	Draining hemorrhage			NSL	
Thorax	Mediastinal edema			NSL	
Abdominal cavity	Hemoperitoneum and mesenteric edema	√		Peritoneal adhesions and serous atrophy of mesenteric adipose	

Table 3.12.1: Consolidated macroscopic findings from all experimental animals.

The main overall findings in all acute cases are associated with hemozoin deposition in tissues. This presents as a dark brown discoloration of the parenchymal organs. Liver, heart, lungs, kidneys and spleen, when available, all were severely darkened by the presence of the malaria pigment. Additionally, there was enlargement of multiple organs with the liver being the primary organ demonstrating megaly.

Organ specific changes included congestion, rare hemorrhage and edema within multiple sections of the central nervous system, both parenchymal and within the meninges. Integumentary pathology included varying degrees of hemorrhage, as evidenced either by erythema or progressing to petechiae and ecchymoses. The lungs were frequently dark brown and congested. In rare cases, there was consolidation of the interstitum and alveolar collapse, however it was difficult to separate post mortem changes from true malaria induced macroscopic pathology. The heart often demonstrated a spectrum of brown discoloration with multifocal white myocardial streaks and rare epicardial petechiae and ecchymoses. In many cases a flaccid cardiac dilatation was observed within the ventricles. The liver was often noted to be markedly enlarged with rounded edges (hepatomegaly) and was observed to be friable. Furthermore, there was moderate to severe brown discoloration and marked sinusoidal congestion. In cases in which the animal survived beyond the initial acute phase of infection, the liver eventually became very pale, while remaining enlarged. In those instances, the pallor was likely the result of a combination of lipidosis, glycogenosis and zonal coagulative necrosis, patterns of which were subsequently confirmed on histopathology. The gallbladder was often markedly expanded and congested, consistent with cholestasis. Additionally, when the spleen was available, either in spleen intact animals or thanks to the presence of a daughter spleen or splenunculum, the organ was markedly enlarged with bulging edges on cut section and was noted to be very dark. The kidneys were slightly enlarged and dark in the early stages of infection, consistent with severe congestion, resulting in a loss of differentiation between the cortex and the

medulla. Rarely there was superficial cortical pitting. With a degree of chronicity, the kidneys became pale and either remained swollen or became shrunken and nodular with a loss of the smooth superficial surface observed in normal kidneys. The urinary bladder was frequently full of hemorrhagic urine, while the urinary bladder mucosa was often markedly hemorrhagic and edematous. The endocrine organs observed, primarily the adrenal glands and pancreas were noted to be congested and occasionally edematous. In two animals, notably those with scrotal ecchymoses, the testicles often had large areas of acute infarction and had regions which were markedly hemorrhagic. No changes were noted within the uterus or ovaries of the select few female animals included in the study.

All levels of the gastrointestinal tract serosa frequently contained petechiae and ecchymoses while the mucosa was often hemorrhagic and either eroded or ulcerated. The lymph nodes were expanded and dark, resultant from severe draining hemorrhage from multiple organ systems. This was most notable within the mesenteric lymph nodes. Finally, multiple animals were observed to have a combination of pericardial, thoracic and peritoneal accumulation of serosanguinous fluid.

Figures 3.12.1-3. Fig 1. Rhesus macaque, brain. This photograph demonstrates the mildly discolored brain with significant congestion of the superficial vasculature. Note the lack of appreciable cerebral edema. Figure 2. Rhesus macaque, brain. This photograph shows marked hemorrhage within the brain stem and the covering meninges. Figure 3. Rhesus macaque, lungs. The lungs in this images are severely congested and overall the parenchyma of the lungs is markedly darkened.

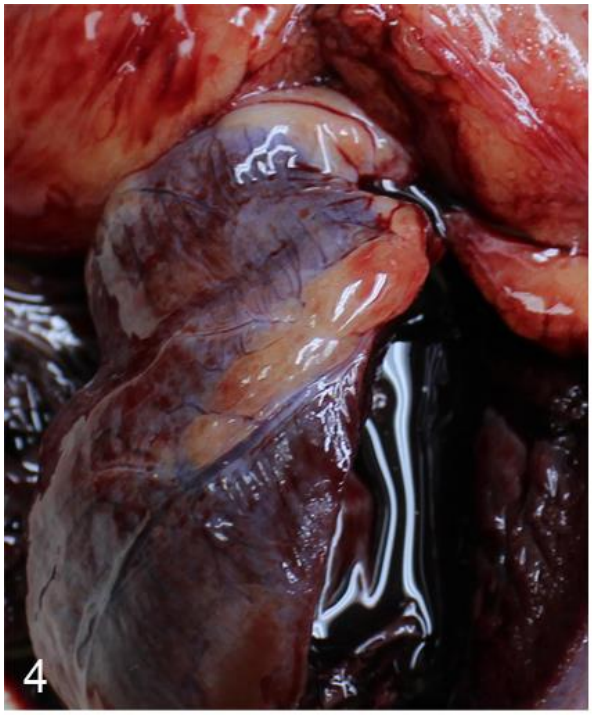

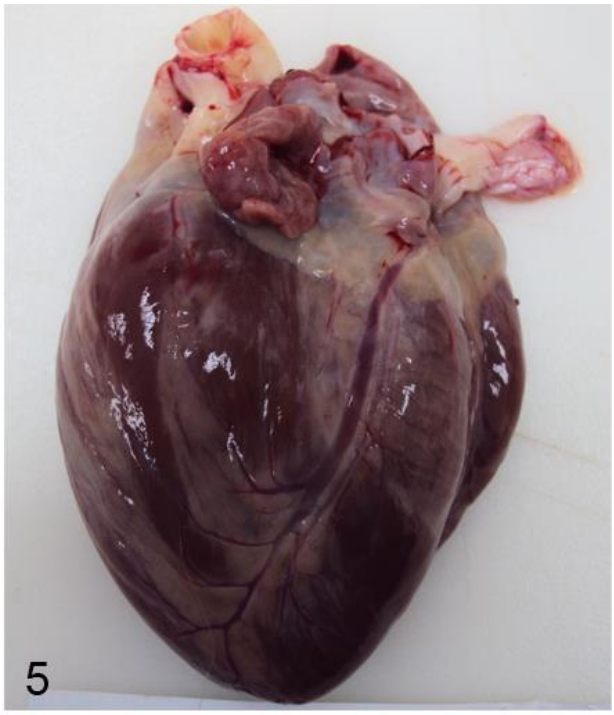

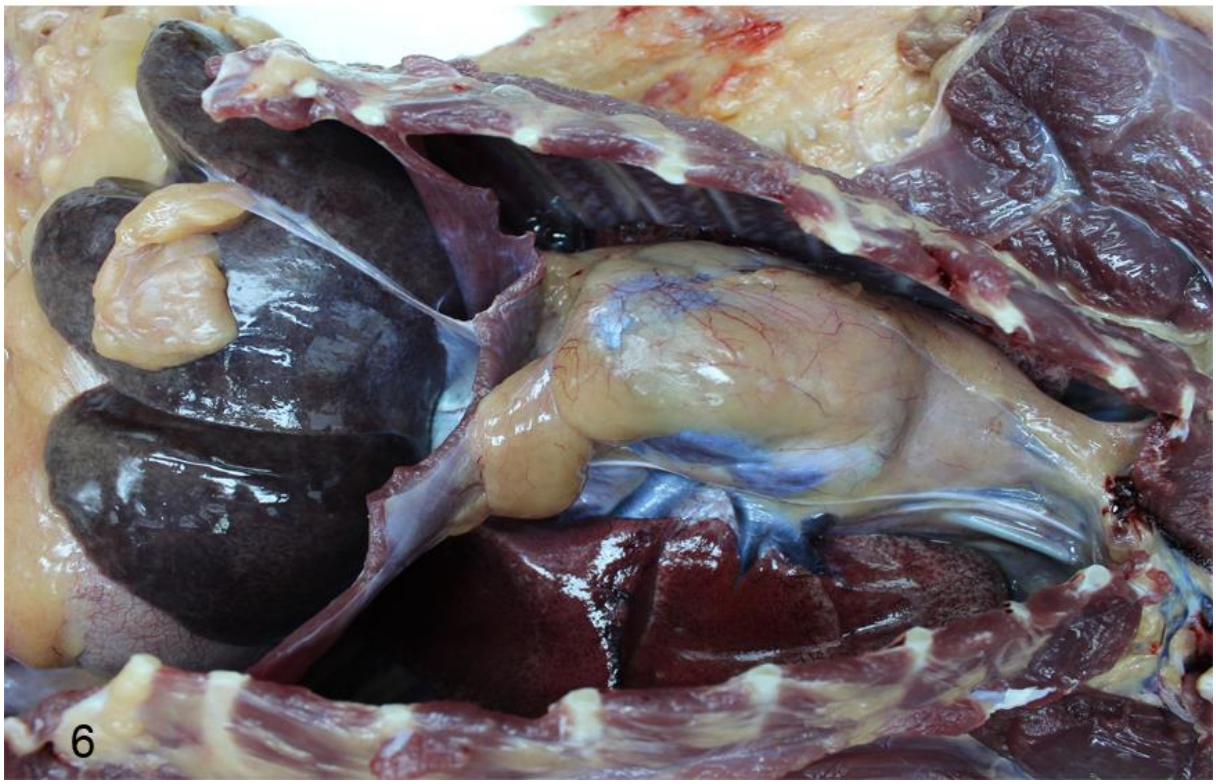

Figures 3.12.4-6. Figure 4. Rhesus macaque, heart. Multifocally within the epicardium of the atrium and the ventricle there is evidence of petechiae and coalescing ecchymoses. Figure 5. Rhesus macaque, heart. Multifocally the epicardium contains streams of white which extend beyond the pericardial adipose and into the myocardium. These are interpreted as early signs of necrosis. Figure

6. Rhesus macaque, thorax and abdomen. The lungs and liver in this photograph are severely discolored, congested and enlarged.

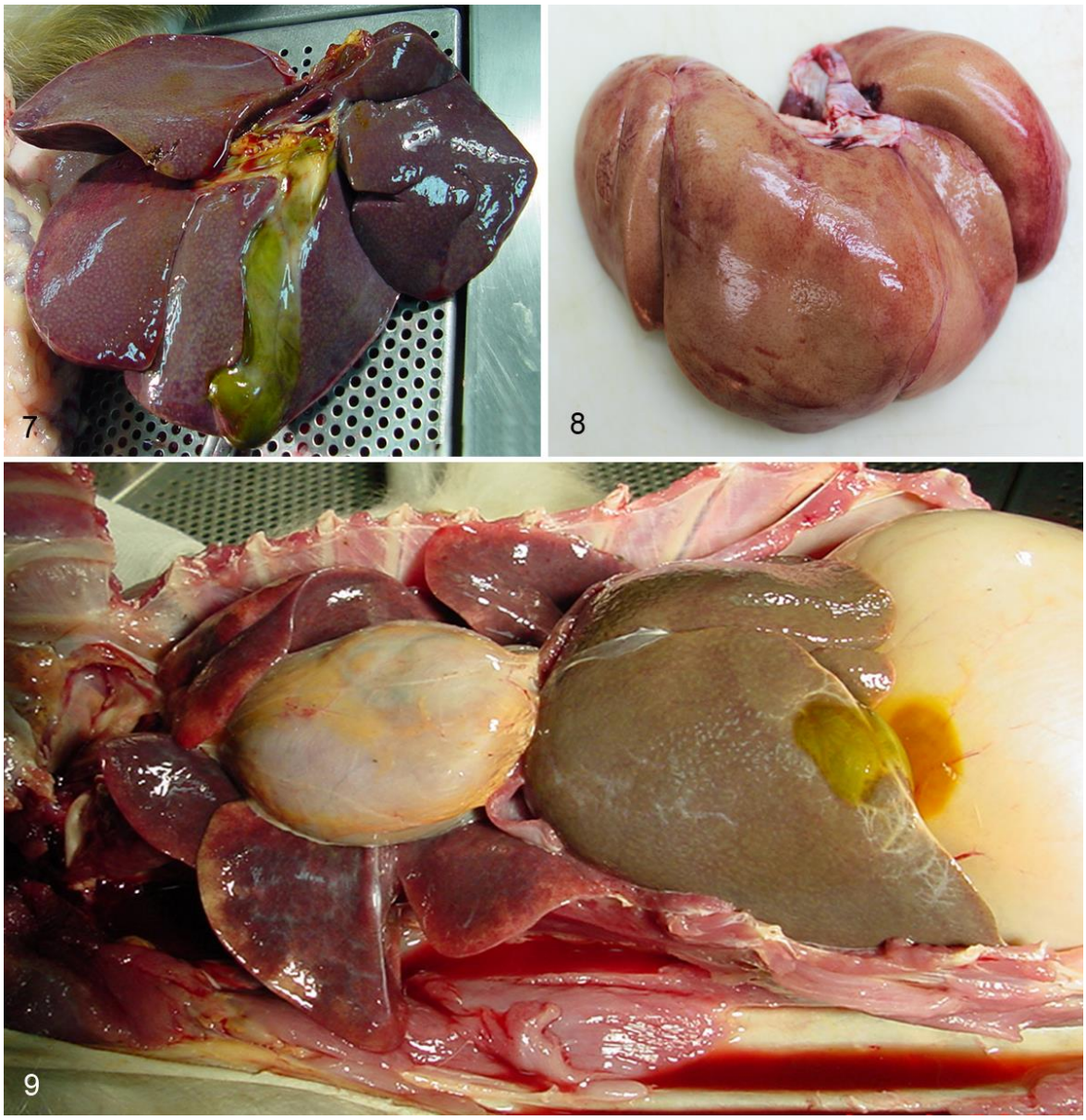

Figures 3.12.7-9. Figure 7. Rhesus macaque, liver. This photograph is representative of the lobular accentuation within the discolored liver secondary to the hepatocellular damage and to the hemozoin pigment accumulation. Additionally, the gallbladder is markedly enlarged, suggestive of cholestasis. Figure 8. Rhesus macaque, liver. This photograph contrasts the acute presentation with that observed with chronicity. In this image, the severely enlarged liver is swollen and pale, suggestive of hepatic lipidosis or zonal necrosis. Additionally, the liver has foci of hemorrhage. When correlated with

microscopy, these macroscopic findings are consistent with a diffuse hepatocellular glycogenosis, regional lipidosis and centrilobular coagulative necrosis. Figure 9. Rhesus macaque, thorax and abdomen. The liver is enlarged and has a brown discoloration. The abdomen contains abundant serosanguinous fluid. Furthermore, the image is demonstrative of the consolidation and pigment accumulation which is observed in the lungs.

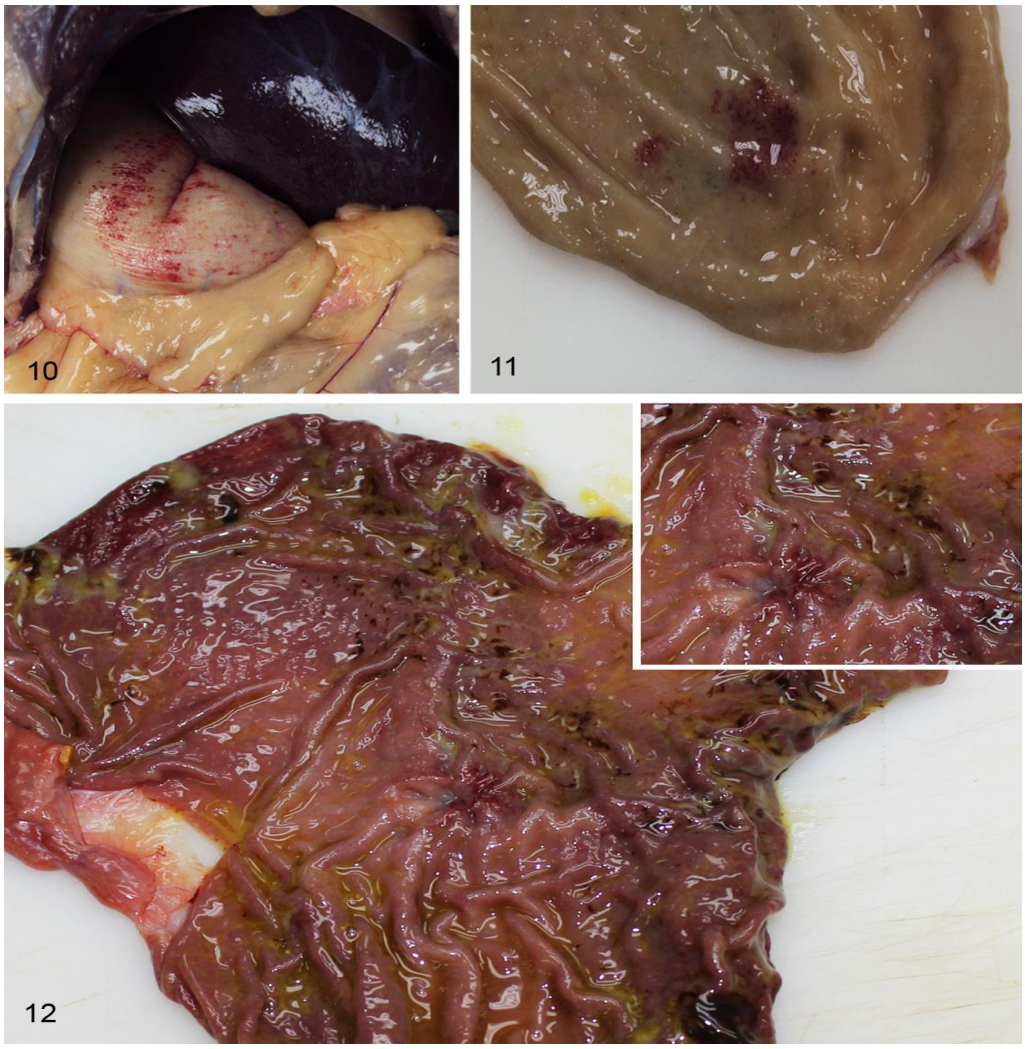

Figures 3.12.10-13. Figure 10. Rhesus macaque, stomach. Multifocally to coalescing, the gastric serosa has streaks of ecchymotic hemorrhage. Figure 11. Rhesus macaque, stomach. The hemorrhage is frequently observed within the mucosa of affected animals, and overlies areas of erosion and rarely, ulceration. Figure 12. Rhesus macaque, stomach. This section of stomach contains multifocal to coalescing necroerosive lesions within the gastric mucosa, overlain with hemorrhage. Inset: Increased magnification of a focus of erosion and hemorrhage within the mucosa. Figure 13. Rhesus macaque, small intestine. Diffusely, the intestinal mucosa is overlain by a layer of mucoid hemorrhage. The mucosa itself is severely erythematous and hemorrhagic.

Figures 3.12.14-16. Figure 14. Rhesus macaque, kidney. This photograph is demonstrative of the severe discoloration observed secondary to hemozoin pigment accumulation within the kidneys. This figure shows a severe highlighting of the medulla by the dark pigment. Figure 15. Rhesus macaque, kidney. This image shows a diffuse discoloration which makes distinction of the cortex and the medulla difficult. Figure 16. Rhesus macaque, urinary bladder. This photograph shows the severe

mucosal hemorrhage frequently noted within the urinary bladder. The small amount of urine found within the bladder in this image is blood tinged.

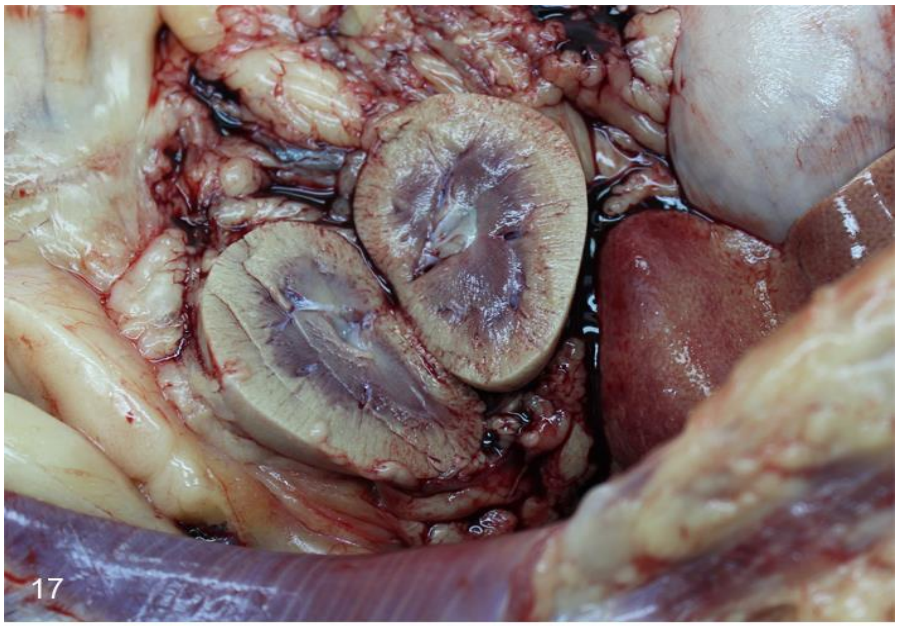

Figure 3.12.17-18. Figure 17 and Figure 18. Rhesus macaque, kidney. These photographs are from animals which survived the initial phase of infection, and are considered to have a chronic form of disease within the kidneys. This manifests grossly as marked pallor of the cortex which is

representative of the loss of parenchyma, interstitial fibrosis and other microscopic aspects of chronic renal injury.

Figure 3.12.19-20. Figure 19. Rhesus macaque. Frequently those animals euthanized during the acute stage of injury with fulminant and high parasitemias demonstrated cutaneous petechiae and ecchymosis. Figure 20. Rhesus macaque. In one case, consistent with another published in the literature (Moreno 2007), the animal developed gangrenous necrosis of the distal digits as well as the upper lip and nasal meatus. The necrosis is theorized to be secondary to the sequestration of the superficial vasculature by infected erythrocytes, causing anoxia, ischemia and necrosis.

3.13 **Discussion**:

While the model proved to be labor intensive, the effort associated with the increased sampling and the close observation of the animals allowed for significant reproducibility both within the experimental animals used in the refinement phase of the study as with the eventual application of the model as a platform for the evaluation of methylene blue as an anti-malarial compound in cases of severe malaria. In all cases, parasitemia, temperatures, clinical symptomology were consistent and reproducible, suggesting that there was a high degree of homogeneity in the model, in

spite of variation in the signalment of the monkeys. Parasitemias were observed to reach extremely high levels of up to 50%. In human disease reports of hyperparasitemia of >20-30% are frequently associated with very severe disease and even death. The parasitemia and temperature curves when combined with the clinical pathology, hematology and clinical symptomology allow for a significant degree of predictability. As such, the potential future application of the model would include a window for therapeutic intervention at an earlier stage in the parasitemia spike noted on day 7, however it is important to note that the sampling frequency is crucial in order to capture the parasite increase and to be able to intervene.

The clinical pathology and hematology described in these experiments both demonstrate certain important similarities to severe human disease. This is particularly notable in regards to the acute hepatic and renal injury as well as some of the hematological changes such as the thrombocytopenia, metabolic disturbances and associated hyperlactatemia. (Carvalho 2014; Barsoum 2000; Taylor 2006; Trampuz 2003; WHO 2014) In humans, the primary complications associated with severe malaria include variations of cerebral malaria, acute renal failure, pulmonary edema, severe anemia, hepatic dysfunction and coagulopathies or bleeding disorders. The most common metabolic abnormalities include acidosis (hyperlactatemia) and hypoglycemia. (Trampuz 2003; WHO 2014)

With particular focus on thrombocytopenia, and as described in chapter 1, frank DIC is rare in adult severe malaria but does occur, and is generally a poor prognostic sign. This appears to either be an area of diversion from falciparum induced disease in pediatric cases, where coagulopathies are relatively well described (Ghosh 2008; Grau 2003; Milner 2014) and disturbances in hemostatic mechanisms have been linked to tissue pathogenesis (O'Sullivan 2016), such as the collection of platelets in cerebral microvessels, although this appears to be increased in HIV-coinfected pediatric cases in Africa. (Hochman 2015) It is possible in this splenectomized model that any coagulopathy driven pathogenesis would occur at a lower parasitemia with increased longevity of the experimental

animals, however without conducting coagulopathy studies, our ability to discuss the role of the coagulation pathway in the pathology of this model is limited.

This hypothesis bears consideration in that the animals which did have evidence of microthrombotic disease or even histopathological and gross evidence suggestive of Disseminated Intravascular Coagulopathy (DIC) appeared to have lower parasitemia counts and to survive the initial insult. In humans, DIC leading to peripheral gangrenous necrosis, while infrequent, is a well reported phenomenon. (Francischetti 2008; Ghosh 2008; Grau 2003; Helbok 2008; Kataki 2004; Lerolle 2007; Liechti 2003; Musoke 2014; Tessier-Marteau 2009; Thanachartwet 2006) As described in Chapter 1, in experimental cases of *P. coatneyi* infection in Rhesus macaques, DIC with gangrene has also been reported (Moreno 2007) and is subsequently illustrated from unpublished data from this study (Figure 3.11.20) in which one of the retrospective animals was treated and survived beyond the first week of infection. In that particular animal, although the peak parasitemia was very high, it was treated with a combination of Artesunate and Quinine and survived almost a month from the initial infection date. In general, the experimental animals decompensate rapidly due to the elevated parasitemia and without radical cure, typically did not survive long enough to demonstrate platelet associated pathology. In the methylene blue drug dosing study, the animals did become moderately thrombocytopenic (±150,000 platelets/µl) by day 9-10, however those animals that were maintained beyond that low point were noted to undergo a significant rebound by the end of the study.

Similarly, while only occurring in a segment of the affected human population, the acute tubular necrosis, interstitial nephritis and glomerulonephrosis described from histopathology of kidney samples from humans suffering from severe malaria are consistent with our findings in macaques. (Das 2008)

The renal malaria syndrome observed primarily in African children consists of the chronic and progressive glomerulopathy which is a crucial factor in therapy and recovery. Acute renal failure observed with *P. falciparum* in Southeast and South Asia as well as in sub-Saharan Africa is associated

with less than 5 percent of the victims of malaria in endemic areas while up to 30% of naïve travelers who become infected present with acute renal failure. (Barsoum 2000; WHO 2014)

Critical differences between human disease and severe *P. coatneyi* infection in splenectomized rhesus macaques include the absence of clinical coma, glucose levels and the lack of severe pulmonary symptoms. Reports of traditional coma in macaques, consistent with the WHO criteria in humans, are vanishingly rare in the literature. A single case report of coma is described in association with experimental pancreatectomy and subsequent diabetic acidosis. (Mirsky 1941) Macaques in this study became so severely lethargic and displayed such a degree of decreased mentation as to come relatively close to the clinical diagnosis, however in keeping with a strict diagnosis, the animals did not meet the WHO criteria of malaria induced unarousable coma. A corollary negative finding included the fact that the macaques did not become hypoglycemic during the course of the infection in spite of severe clinical symptoms. Potentially the stress of severe acute infection in animals with adequate energy reserves compensates for the traditional hypoglycemia observed in humans. (Dungan 2009; Marik 2013) Furthermore, case reports describing abnormal presentations of malaria abound in the literature, to include instances of hyperglycemia. (Chianura 2012; Singh 2014; Trombe 1993; Zaki 2011) In fact, a large retrospective study of children in Kenya noted that almost 50% of children diagnosed with hyperglycemia had concurrent malaria infections. (Osier 2003)

Pulmonary edema is described as a significant factor in severe malaria in humans infected with *P. falciparum*, while in no case was it an important finding in any of the infected macaques participant in this study. Pulmonary edema in humans can occur at any point of the acute stages of infection, however it is reported to happen with much greater frequency later in infection and secondary to other manifestation of disease. The pathogenesis of pulmonary manifestations of falciparum induced disease includes increased pulmonary venous pressure secondary to venous and lymphatic obstruction by sequestration of infected RBCs, increased alveolar capillary permeability

followed by intravascular fluid loss, and associated hypoalbuminemia, resulting in alveolar effusion. (Sirivichayakul 2000; Taylor 2006; WHO 2014) It is possible that the progression of illness in the macaques in this study was too acute to permit pulmonary edema to develop, or that there may be an anatomo-physiological difference in the susceptibility of the pulmonary endothelium between humans and macaques in response to malaria.

The retinoscopic images described in this chapter are purely illustrative and as control images were not taken prior to infection with *P. coatneyi* in these animals, there is no mechanism to infer a correlation of lesions observed with the pathogenesis of *P. coatneyi* induced disease. However, this highlights the fact that the technology employed in human diagnostics can be used effectively in this model, to describe the potential ocular pathology in the *P. coatneyi*/rhesus macaque model. The incidence and clinical significance of retinopathy varies between adult and pediatric cerebral malaria (Maude 2009), and some groups now require retinopathy to a clinical diagnosis of cerebral malaria in pediatric African cases. (Beare 2011) The findings of some changes without marked clinical symptomatology of coma imply that retinopathy in severe malaria infection is not restricted to severe cerebral disease, so interpretation of retinal changes as a 'mirror' onto underlying CNS pathology should be further investigated.

A fundamental question raised by this section and of significant comparative importance is in understanding what the ultimate cause of death was in the experimental animals in this study. Putting aside the fact that the majority of the animals in the study were euthanized, the severe morbidity in all cases combined with the clinical pathology and hematology findings suggests that metabolic acidosis and resultant shock were the main contributing factors leading towards death. Metabolic acidosis is described as a primary feature in the pathogenesis of severe malaria induced disease and is felt to be the most reliable indicator of mortality in humans. (Maitland 2004; Maitland 2005) The pathophysiology of metabolic acidosis is multifaceted in any disease and equally so in severe malaria. Most likely, the absence of pulmonary compromise in these animals does not exclude

the microscopic hypoxic and anoxic damage caused by the microvascular circulatory disruption by the profound cytoadherence of infected erythrocytes, auto agglutination and rosette formation. Subsequently, the hypoxia induced shift within the injured cells toward anaerobic metabolism, with resultant oxidation and lactic acid production may result in the observed metabolic acidosis and progression towards multi-organ failure and death. (English 1997; Maitland 2004; Planche 2005; Planche 2006; Sasi 2007) While at this stage, specific determinants of death in the animals evaluated in both the retrospective and prospective cohorts of this thesis remain unknown, we theorize that the complex interaction with the physical modifications of the infected erythrocytes, the extraordinarily high parasitism, the interactions between parasitized RBCs and both normal RBCs and the microvascular endothelium, resultant vascular damage and leakage, evidence of microscopic cerebral edema, renal, hepatic and cardiac cellular damage, multi-organ hemorrhage, metabolic disturbances, severe pyrexia and inflammatory mediators combine and contribute to fatal outcome.

3.14 **Summary:**

Evaluation of both those ante-mortem findings in retrospective studies which employed the *P. coatneyi*/rhesus macaque model as well as close monitoring and data collection in the 15 prospective animals allowed for a strong comparison and contrasting of the clinical pathology, parasitemia dynamics and macroscopic autopsy findings with those described in falciparum induced disease in humans. Our findings demonstrated a consistently reproducible hyperparasitemia spiking on day 7, correlating with a consistent 48-hour parasite maturation cycle. Additionally, we have established that splenectomized animals infected with *P. coatneyi* undergo a significant febrile spike (up to >106° F) concordant with the observed hyperparasitemia. Affected animals develop respiratory signs of dyspnea as well as urological pathology as observed with unfailing hematuria combined with anuria or stranguria. All animals became severely anorexic, occasionally with evidence of vomiting and diarrhea. The effects on the cardiovascular system suggest development of coagulopathy and multifocal hemorrhage. Neurologically, all infected animals develop severely depressed mentation,

with markedly suppressed menace response and withdrawl. However, and crucially, there was no evidence of either fitting or coma which are deemed to be defining characteristics of human disease. Clinical pathologic findings included reticulocytosis with no statistically significant anemia (within the experimental timeframe), a leukocytosis consisting of a primary mononuclear cell increase. Renal insult was a consistent finding in this model, with BUN and creatinine increases lagging the parasitemia spike. Similar findings occurred within the liver, with hepatic insult resulting in ALT, AST, and Alk Phos increases which lagged behind the parasitemia spike. Of note, hyperlactatemia also occurred consistently, but also appeared to lag after the parasitemia spike. No significant electrolyte abnormalities were observed in any of the infected animals. Similarly, and discordant with human disease, there was a notable absence of hypoglycemia and only mild thrombocytopenia observed (within the experimental timeframe). Finally, in all cases, onset of fatal multiorgan failure occurred by day 8, resulting in either natural death or animals reaching euthanasia criteria. On autopsy, severely affected animal developed cutaneous erythema; petechiae and ecchymoses, multiorgan hyperpigmentation (interpreted to be deposition of malaria pigment). Hepatomegaly and renomegaly, multi-organ hemorrhaging with rare thrombosis and rare gangrenous necrosis were noted. These ante-mortem and autopsy findings in the rhesus macaque display areas which strongly correlate with human syndromology, such as those observed in terms of metabolic acidosis, as well as the hepatic and renal pathology. Severe anemia and thrombocytopenia have both been demonstrated in other studies using this animal-parasite combination and the fact that these were not significant factors in the pathology observed in this series of experiments is likely related to the curtailed experimental timeframe rather than a real absence. Finally, while the neurologic disease in the rhesus is profound, the lack of fitting and coma development is a crucial divergence as are the absences of pulmonary injury, hypoglycemia and retinal changes.

Chapter 4: Cytological and Histopathology

4.1 **Introduction:**

Since the seminal work of Marchiafava and Bignami in the 1880s, numerous significant studies have been conducted using histopathological evaluation of autopsy specimens from fatal human cases of *P. falciparum* induced malaria. (Carlson 1993; Burel 2008; Brown HC 2000; Deaderick 1909; Dorovini-Zis 2011; Dudgeon 1917; Dudgeon 1919; Harnagel 1954; Kean 1944; Kirchgatter 2005; Medana 2002; Menezes 2012; Milner 2013; Milner 2014; Nagatake 1992; Olsson 1969; Patel 2003; Saya 2012; Spitz 1946; Taylor 2004; Taylor 2012; Toro 1978; White 2001; Wilairatawa 2000) These have allowed for generalizations to be made as to the spectrum of pathology within various organ systems in patients dying of falciparum malaria. There are obvious difficulties with such grouped categorization as a wide range of complicating factors must be taken into account. Among these are variability in the immune status and demographics of the subjects, to include the genetic profile of the infected individual, geographic location, pathogenicity and density of the infecting parasite, stage of disease at onset of any therapy, treatment modalities, time to death and co-morbidities to name a few. In essence, the heterogeneity of the parasite and host populations, treatment effects and the varying clinical syndromes of severe and fatal disease all translate to a range of histopathological presentations at autopsy.

Human falciparum malaria presents in a variety of syndromes which have been classified by World Health Organization (WHO 2014) and include cerebral malaria (CM) and associated retinopathy, severe malaria anemia, metabolic derangement with acidosis, shock, acute kidney injury, lung involvement progressing to acute respiratory distress syndrome, disseminated intravascular coagulopathy (DIC) as well as cardiac and hepatic disease. In order to better understand the pathophysiology of these complications, a number of murine and simian models of severe malaria have been developed.

P. coatneyi is one of the parasites that is considered to be an effective correlate to *P. falciparum* and, when infected into the rhesus macaque and similar non-human primates, presents with a parasite periodicity and clinical presentation similar to that observed in human falciparum malaria. The model is not perfect in that there are important features of human falciparum malaria which are absent. For instance, while affected animals may have severely depressed mentation, lethargy and decreased menace response, there is no antemortem neurological syndrome analogous to the coma of human cerebral malaria. In spite of this, the model has been used for pathophysiological investigation of CM (Aikawa 1992; Kawai 1993; Lombardini 2015), renal pathology (Lombardini 2014) and anemia (Moreno 2013). Despite this, to date there has been no comprehensive and systematic survey of the histopathological changes in macaques infected with *P. coatneyi*, beyond small studies with limited numbers of animals from heterogeneous backgrounds and which only evaluated specific target tissues such as the brain, heart or placenta. (Davison 2000; Desowitz 1967; Desowitz 1969; Desowitz & Pavanand 1967; Nagatake 1992; Nakano 1996; Sein 1993; Smith 1996)

As described, this study reviewed the histopathological findings in a large group (n=45, 30 retrospective and 15 prospective) of autopsy cases of *P. coatneyi* infection causing severe malaria in Rhesus macaques (predominantly splenectomized) compared to several spleen-intact animals and 15 non malaria-infected control animals. The histopathological and ultrastructural morphological features of severe and fatal infection were examined and correlated with the clinical features.

4.2 **Clinical and clinicopathology findings:**

Following blood-stage infection the typical course of disease typically presented with a blood stage parasitemia appearing within 2 days, reaching peak of a maximum of 54.6% with severe disease typically at 6-10 days and death/euthanasia generally around 7-12 days post infection depending on the severity of the parasitemia. In synchrony with the periodicity of the parasites' development and with associated schizogony, animals within the prospective cohorts had increasing temperatures

which peaked on average by day 7 at 105-106° Fahrenheit, assessed both by peripheral subcutaneous microchip telemetry as well as rectally.

As described in Chapter 3, animals became anorexic and lethargic with markedly decreased mentation without achieving the criteria of complete non-responsiveness seen in those human patients who develop the coma of cerebral malaria. (Brewster 1990; Clark 2009; Idro 2005; Taylor 2004; WHO 2014) Between days 5 and 7 post infection, all animals developed hematuria and in cases with significant parasitemia, defined as prolonged parasitemias greater than 15%, periods of anuria developed. A smaller percentage of animals had episodes of vomiting or diarrhea. Animals with a significant level of parasitemia displayed mild progressive anemia with reticulocytosis, mild leukocytosis and thrombocytopenia, biochemical evidence of acute renal failure, and hepatic injury which lagged behind clinical signs of hematuria by 24-48 hours. Metabolic acidosis was also seen in the majority of the cases with high parasitemias.

4.3 **Macroscopic findings at autopsy**:

In general terms, the most significant findings at autopsy included vascular congestion in all organs, hepatomegaly with brown discoloration, renomegaly with brown discoloration, brown discoloration of the lungs, a small amount of multifocal white streaking within the epicardium and myocardium interpreted as necrosis, adrenal gland congestion, cerebellar brown discoloration and vascular congestion, and rare hemorrhages within the brain stem and spinal cord. There was rare thrombosis and necrosis within multiple organ system, and soft tissue necrosis most notably within the scrotum and testes in several animals. In one animal from a retrospective study which survived the initial insult and progressed into a chronic infection phase, disseminated intravascular coagulopathy (DIC) developed and led to severe peripheral gangrenous necrosis occurring in the digits, nasal planum and upper lip.

4.4 **Histopathological findings:**

The spectrum of tissues available for review was constrained by which tissues were collected in retrospective studies. In all animals, cerebrum, cerebellum, brain stem, liver, kidneys, heart and lungs were available, while in only some animals were specimens of adrenal and pituitary glands, pancreas, gastrointestinal system, skeletal muscle, eyes, lymph nodes, urinary bladder and reproductive tract available. In contrast, all tissues were collected and evaluated in the prospective study, including multiple areas of the brain and spinal cord samples which were not available from any retrospective study. In three animals splenunculi were identified and evaluated. In all cases, the tissue pathology was evaluated in comparison to archival tissue from normal control rhesus macaques, with attention paid to changes which may represent normal aging or background variation. (Chamanza 2012) A qualitative and for some features a semi-quantitative assessment of histopathological changes was conducted in all available tissues and the results from select key tissues are summarised in Table 1.

Throughout all tissues, there was significant microvascular sludging with parasitized erythrocytes and hemozoin pigment, which appeared to be causing microvascular obstruction, due to an increased congested appearance to many vessels (represented by increased microvascular caliber within a section) and increased numbers of vessels seen in a section, implying opening of collateral vessels. Sequestration is typically interpreted via ultrastructural analysis and is the result of cytoadherance of infected erythrocytes (iRBC) to other infected red cells, uninfected erythrocytes (rosette formation) or to the vascular endothelium (margination), all of which were observed using transmission electron microscopy. This binding, mediated by specific molecular adhesion through parasite encoded adhesins expressed at electron dense membrane knobs on the iRBC surface, results in the formation of rosettes (with uninfected RBC) or autoagglutinates (with other iRBC and platelets) which can contribute to occlusion of small caliber vessels (Figure 4.1.1-4.1.4).

In addition to this apparent disruption of vascular flow, there was light microscopic evidence of infected erythrocytes containing either late ring stage, trophozoites and schizonts stage parasites.

In the case of later stage parasites, food vacuoles containing brown - gold crystalline hemozoin pigment were clearly seen even at low magnification.

Accession #	Acute/ Chronic	Peak parasitemia recorded	Spleen/ Splenunculum Y/N	General sequestration severity	CNS hemorrhage severity and location	CNS edema severity	Cerebellum Purkinje damage severity	Axonal/ neuronal injury severity and location	Renal Injury severity	Renal histopath findings	Cellular/ Hemoglobin casts	Hepatic injury severity	Hepatic histopath findings	Cardiac injury severity	Cardiac histopath findings	Fibrin thrombi Y/N	Mural vascular necrosis Y/N
13-106	A	13.60%	N	5	3; spinal cord	3	1	3/2; cerebrum/ spinal cord	2	H GN; epithelial D/N	Y/Y	2	Hepatocellular individualization; vacuolar degeneration	2	Cardiomyocyte vacuolar D/N	Y	N
13-107	A	10.50%	N	5	3; spinal cord	3	3	3; spinal cord	2	H GN; epithelial D/N	Y/Y	2	Hepatocellular individualization; LP/N portal hepatitis	2	Cardiomyocyte vacuolar D/N	Y	Y
13-108	A	7.50%	N	5	3; spinal cord	3	1	2; cerebrum, spinal cord	2	LP GN; synechiae; epithelial D/N	Y/Y	3	Hepatocellular individualization; vacuolar degeneration	2	Cardiomyocyte vacuolar D/N	Y	N
14-198	A	34.80%	N	5	2; brain stem/ cerebrum	3	3	2/1; cerebrum/ spinal cord, brain stem	3	Synechiae; epithelial D/N	Y/Y	3	Hepatocellular individualization; vacuolar D/N	2	Cardiomyocyte D/N	N	N
14-199	A	39.20%	N	5	1; spinal cord, cerebrum	3	3	2/1; cerebrum/ spinal cord, brain stem	3	Synechiae; epithelial D/N	Y/Y	3	Hepatocellular individualization; vacuolar D/N	2	Cardiomyocyte D/N	N	N
14-200	A	34.20%	Y (DS)	5	2; spinal cord	3	2	2/1; cerebrum/ spinal cord, brain stem	2	LP GN; synechiae; epithelial D/N	Y/Y	3	Hepatocellular individualization; vacuolar D/N	2	Cardiomyocyte D/N	Y	N
15-264	A	16.90%	N	0	3/2; brain stem/ spinal cord	2	3	3/2; cerebrum/ spinal cord	2	LP IN; synechiae; epithelial D/N	Y/Y	3	Coag. N; hepatocellular individualization	1	Cardiomyocyte D/N	N	N
15-265	A	24.50%	N	0	0	3	3	3/2; cerebrum, brain stem/ spinal cord	4	N/H and LP tubulitis/ IN; synechiae; epithelial D/N	Y/Y	4	Sinusoidal H; hepatocellular D/N	3	Cardiomyocyte D/N	N	N
15-266	A	25.40%	N	0	0	1	1	1; cerebrum; brain stem	3	LP IN; synechiae; epithelial D/R	Y/Y	2	Focal N; hepatocellular D/N	1	Cardiomyocyte D/N	N	N
15-271	A	42.50%	N	0	3/2; spinal cord/ brain stem	1	1	3; spinal cord	5	N/LP tubulitis/ nephritis; epithelial D/N	Y/N	2	Sinusoidal H; hepatocellular D/N	1	Cardiomyocyte D/N	Y	Y
15-272	A	40.80%	N	0	1; spinal cord	2	1	1; cerebrum; brain stem	5	N/LP tubulitis/ nephritis; epithelial D/N	Y/N	2	Sinusoidal H; hepatocellular D/N; vasculitis	1	Cardiomyocyte D/N	Y	Y
15-273	A	38.30%	N	0	0	2	0	2; cerebrum	5	N/LP tubulitis/ nephritis; epithelial D/N	Y/N	2	Hepatocellular vacuolar D/N	3	Cardiomyocyte D/N	N	N
15-274	A	42.80%	N	0	0	3	3	3/2; cerebrum/ spinal cord	4	N tubulitis; H/LP IN; synchiae; epithelial D/N	Y/Y	4	Hepatocellular individualization; vacuolar D/N; LP/N portal hepatitis	3	Cardiomyocyte D/N	N	N
15-275	A	45.20%	N	0	0	2	1	2/1; spinal cord/ cerebrum	3	LP IN; epithelial D/N	Y/Y	2	Coag. N; hepatocellular individualization; H/LP hepatitis	3	Cardiomyocyte D/N	Y	Y
15-276	A	42.60%	Y (DS)	0	1; spinal cord	2	1	1; cerebrum, brain stem	5	N/LP tubulitis/ nephritis; epithelial D/N	Y/Y	3	Coag. N; hepatocellular; H/LP hepatitis	2	Cardiomyocyte D/N	Y	N
90-239	A	257,000/ cumm	Y	3	0	0	0	2; cerebrum	1	LP IN	Y/N	NA	Coag. N; (prior pathology report, no tissue available for eval.)	NA	NA	N	N
90-261	A	465,120/ cumm	Y	2 (spleen 4)	0	0	0	2; cerebrum	1	LP IN	Y/N	2	Hepatocellular vacuolar D/N; LP hepatitis	0	NA	N	N
92-523	A	10.50%	Unknown	3	0	3	0	0	0	NA	N/N	0	NA	0	NA	N	N
92-525	A	30.01%	N	5	0	2	NA	1; cerebrum	4	Epithelial D/N	Y/N	4	Coag. N; hepatocellular individualization	0	NA	N	N
92-526	Unk	9.10%	Y	3	1; cerebrum	2	NA	0	NA	NA	NA	1	Hepatocellular individualization; vacuolar degeneration	0	NA	N	N
92-527	Unk	5.20%	Unknown	3	1; cerebrum	1	NA	0	1	Epithelial D/N	Y/N	1	LP hepatitis	0	NA	N	N
92-530	Unk	35.20%	Y	3 (spleen 5)	0	2	NA	1; cerebrum	3	Synechiae; epithelial D/N	Y/Y	3	Hepatocellular individualization; vacuolar D/N	1	Cardiomyocyte D/N	N	N
92-548	C	22.60%	Y	2 (spleen 4)	0	2	3	2; cerebrum	3	Synechiae; epithelial D/N	Y/N	NA	NA	0	NA	N	N
94-380	A	51.30%	N	5	NA	NA	NA	NA	4	Epithelial D/N	Y/Y	2	Hepatocellular individualization; LP portal hepatitis	2	Cardiomyocyte D/N	N	N
94-381	A	49.50%	N	5	NA	NA	NA	NA	2	Epithelial D/N	Y/N	2	Hepatocellular individualization; LH perivascular hepatitis	0	NA	N	N
94-382	A	46.20%	N	5	NA	NA	NA	NA	2	Synechiae; epithelial D/N	Y/N	2	Hepatocellular individualization	1	Cardiomyocyte D/N	N	N
94-383	A	41.70%	N	5	NA	NA	NA	NA	2	LP nephritis; epithelial D/N	Y/N	3	Hepatocellular individualization; LH perivascular hepatitis	2	Cardiomyocyte D/N	N	N

Accession #	Acute/ Chronic	Peak parasitemia recorded	Spleen/ Splenunculum Y/N	General sequestration severity	CNS hemorrhage severity and location	CNS edema severity	Cerebellum Purkinje damage severity	Axonal/ neuronal injury severity and location	Renal Injury severity	Renal histopath findings	Cellular/ Hemoglobin casts	Hepatic injury severity	Hepatic histopath findings	Cardiac injury severity	Cardiac histopath findings	Fibrin thrombi Y/N	Mural vascular necrosis Y/N
02-023	A	35.10%	N	4	2; cerebellum	2	2	2; cerebrum	3	Synechiae; epithelial D/N	Y/Y	2	Hepatocellular vacuolar D/N	2	Cardiomyocyte D/N	N	N
02-042	A	51.01%	N	4	0	2	2	2; cerebrum	4	Epithelial D/N	Y/Y	2	Hepatocellular individualization	2	Cardiomyocyte D/N	N	N
02-043	A	50.01%	N	4	2; cerebellum	2	1	1; cerebrum	4	Epithelial D/N	Y/Y	3	Hepatocellular individualization	1	Cardiomyocyte D/N	N	N
02-044	A	38.50%	N	5	0	2	2	2; cerebrum	5	Epithelial D/N	Y/Y	2	Hepatocellular individualization	2	Cardiomyocyte D/N	N	N
02-045	A	40.01%	N	4	0	2	2	2; cerebrum	4	Epithelial D/N	Y/Y	2	Hepatocellular individualization	1	Cardiomyocyte D/N	N	N
02-046	A	49.50%	N	4	3; cerebrum, spinal cord	2	1	0	5	Epithelial D/N; hemorrhage	Y/Y	5	Coag. N; hepatocellular individualization; H/LP hepatitis	2	Cardiomyocyte D/N	N	N
02-058	C	51.50%	Y (DS)	4	0	0	2	1; cerebrum, spinal cord	5	Cortical infarct; fibrosis; LP IN; epithelial D/R	Y/Y	2	Hepatocellular individualization	0	NA	N	N
02-059	A	39.20%	N	5	2; brain stem	2	0	2; cerebrum	5	Epithelial D/N; hemorrhage	Y/Y	2	Hepatocellular individualization	0	NA	N	N
02-060	A	49.20%	Y (DS)	5	3/2; spinal cord/ cerebrum	3	2	3; spinal cord	4	Epithelial D/N; hemorrhage	Y/Y	3	Coag. N; hepatocellular vacuolar degeneration	2	Cardiomyocyte D/N; interstitial edema/fibrin	Y	N
02-061	A	48.01%	N	5	4/3/2; spinal cord/ brain stem/ cerebrum	3	2	0	4	Epithelial D/N; hemorrhage	Y/Y	5	Coag. N; hepatocellular vacuolar degeneration	1	Cardiomyocyte D/N; interstitial edema/fibrin	Y	Y
02-062	C	50.80%	Y (DS)	0	0	0	2	0	3	Epithelial D/N/R; LH IN	Y/N	0	NA	0	NA	N	N
02-067	A	47.40%	N	5	2; spinal cord	2	2	2; cerebrum	5	Epithelial D/N; hemorrhage	Y/Y	3	Hepatocellular individualization; vacuolar degeneration	NA	NA	N	N
02-068	A	54.60%	N	5	2; cerebellum, spinal cord	2	1	1; cerebrum	5	Epithelial D/N; hemorrhage	Y/Y	5	Coag. N; hepatocellular vacuolar degeneration	2	Cardiomyocyte D/N; interstitial edema/fibrin	Y	N
02-069	A	41.20%	N	5	2; cerebrum	3	2	0	5	Epithelial D/N; hemorrhage	Y/Y	5	Coag. N; hepatocellular vacuolar degeneration	1	Cardiomyocyte D/N; interstitial edema/fibrin	N	N
02-070	A	49.60%	N	5	4; cerebrum	4	2	2; cerebrum	5	Epithelial D/N; hemorrhage	Y/Y	3	Coag. N; hepatocellular vacuolar degeneration	1	Cardiomyocyte D/N; interstitial LH Myocarditis; edema/fibrosis	Y	Y
02-071	A	41.01%	N	5	0	2	1	1; cerebrum	5	Epithelial D/N; hemorrhage	Y/Y	3	Coag. N; hepatocellular vacuolar degeneration	1	Cardiomyocyte D/N; interstitial LH Myocarditis; edema/fibrosis	N	N
02-089	A	20.20%	N	5	3/2; spinal cord/ cerebrum	2	2	1; cerebrum	2	Epithelial D/N	Y/Y	3	Hepatocellular D/N (prior pathology report, no tissue available for eval.)	2	Cardiomyocyte D/N; interstitial LH Myocarditis; edema/fibrosis	N	N
02-090	A	NA	N	4	2/1; cerebrum/ cerebellum	1	1	0	2	Epithelial D/N	Y/Y	3	Hepatocellular D/N	1	Cardiomyocyte D/N	N	N

Key:

A: Acute
C: Chronic
Coag. N: Coagulative Necrosis
D/N: Degeneration/Necrosis
D/N/R: Degeneration/Necrosis/Regeneration
GN: Glomerulonephritis
H: histiocytic
IN: Interstitial Nephritis
LH: Lymphohistiocytic
LP: Lymphoplasmacytic
N: Neutrophilic
NA: Not available or Not applicable

Table 4.4.1. Summary of selected major histopathological features. Severity score is represented as a mean of those semi-quantitative data generated during the reading of the histopathology from all from n=45 Rhesus macaque monkeys infected with *P. coatneyi*. Severity scores consist of a range from 0 to 5. 0=Within normal limits; 1= Minimal; 2= Mild; 3= Moderate; 4= Marked; 5=Severe.

Primary target tissues include the central nervous system, kidneys, liver and heart as well as descriptive evaluation of vascular injury, presence or absence of fibrin thrombi and qualitative evaluation of vascular sequestration.

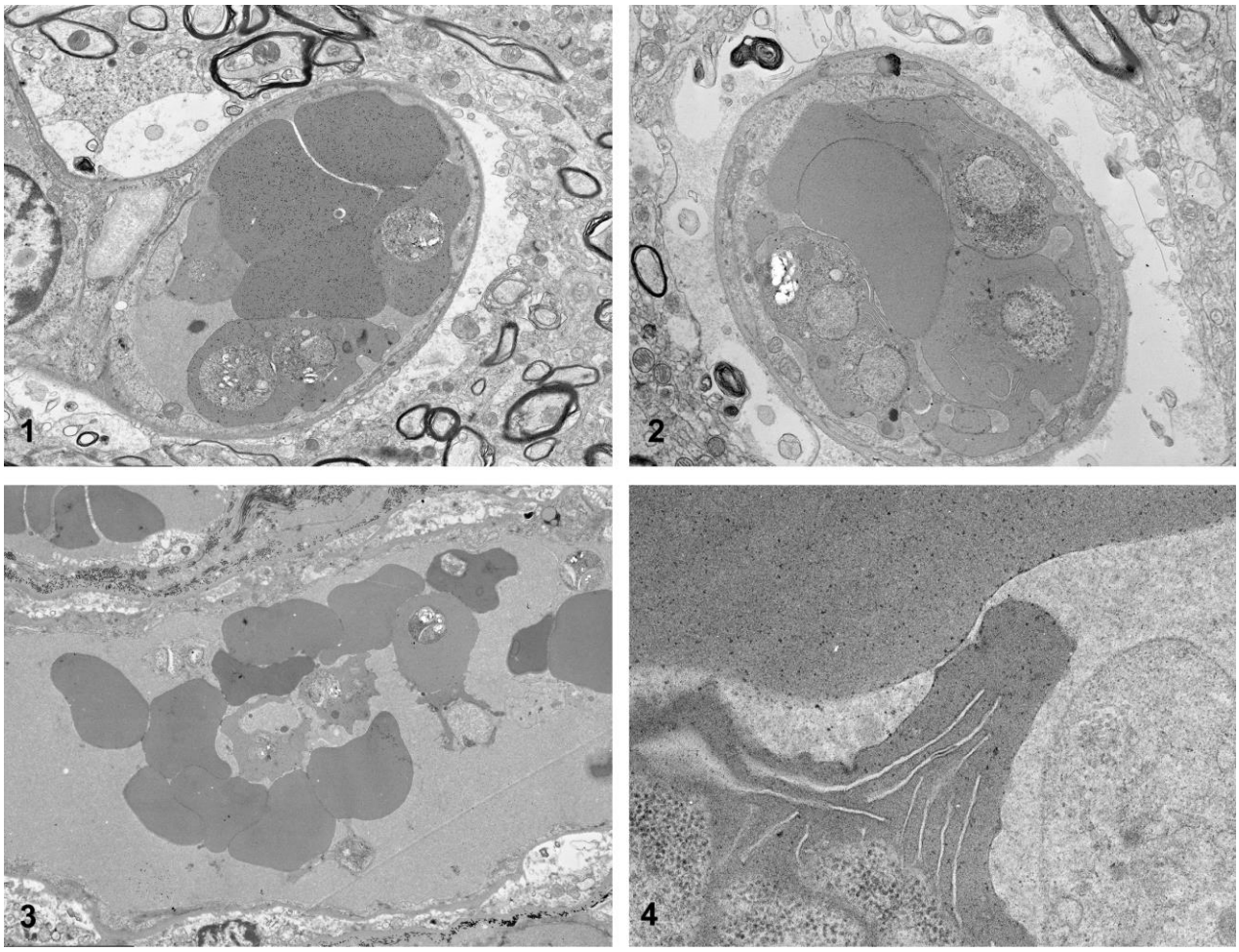

Figure 4.4.1-4: This plate consists of ultrastructural patterns of parasite adhesion in *P. coatneyi* infected rhesus macaque tissues. 4.4.1: Cerebrum with demonstration of microvascular margination of infected erythrocytes to the endothelium within a focal vessel. Additionally, there is mild evidence of perivascular edema. Transmission Electron Microscopy (TEM) 2500x. 4.4.2: Kidney. Similar to 4.4.1, this electron micrograph shows evidence of multiple erythrocytes infected with 1 to 2 plasmodial trophozoites marginated to the vascular wall. TEM 5000x. 4.4.3 Kidney. Within the lumen of this renal vessel are 3 infected erythrocytes forming a rosette with a series of peripheral uninfected erythrocytes. TEM 2500x. 4.4.4 Higher magnification of the binding between iRBC and RBC within a

renal vessel. In this electron micrograph, there is evidence of the surface ornamentation and the cleft-like structures within the cell cytoplasm surrounding the intracellular trophozoite. TEM 12000x.

4.4.1 **Central Nervous System:**

a. Cerebrum: Areas of the cerebrum that were evaluated consisted of the cortex, taken from the frontal lobe and allowing for an evaluation of grey and white matter, thalamus, mid-brain and hippocampus. Microvasculature within both the grey and white matter, but more significantly within the former, was occluded by high numbers of late trophozoite stage infected erythrocytes containing abundant pigment. Levels of sequestration were high and in some cases approached 100% of all vessels seen. The sequestered iRBC appeared to contain predominantly mature trophozoite stages. No significant qualitative difference was observed in sequestration patterns within the different regions of the cerebrum. Frequently surrounding affected vessels, there was an area of clearing or rarefaction within Virchow-Robin space with strands of neuropil connecting to the vessel wall, interpreted as perivascular edema (Figure 4.4.1.1-4.4.1.2).

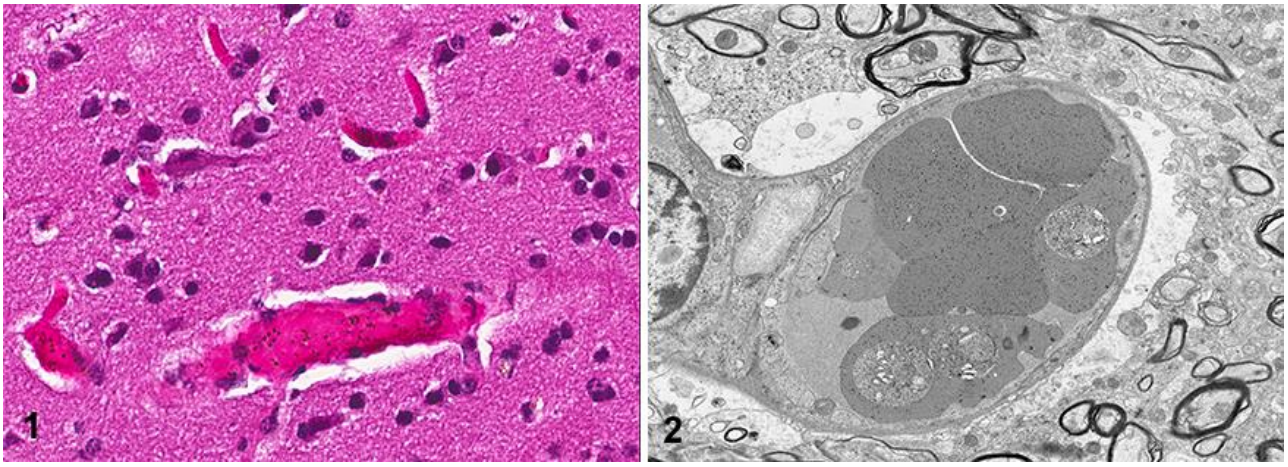

Figure 4.4.1.1-2: Cerebrum. Photomicrograph 4.4.1.1 demonstrates the perivascular edema observed throughout the central nervous system. 400x Hematoxylin and Eosin (HE). This was not observed in control animals and is further supported by the myriad ultrastructural photomicrographs (as in 4.4.1.2) which illustrate the proteinaceous material filling the artificial space surrounding the capillaries. TEM 4000x.

Occasionally, the perivascular space and neuropil contained extravasated erythrocytes or a focal punctate microhemorrhage (Figure 4.4.1.3-4). However, this was a relatively rare finding and no classical ring hemorrhages or reactive astroglial nodules, similar to the Dürck's granulomas described in humans, were observed.

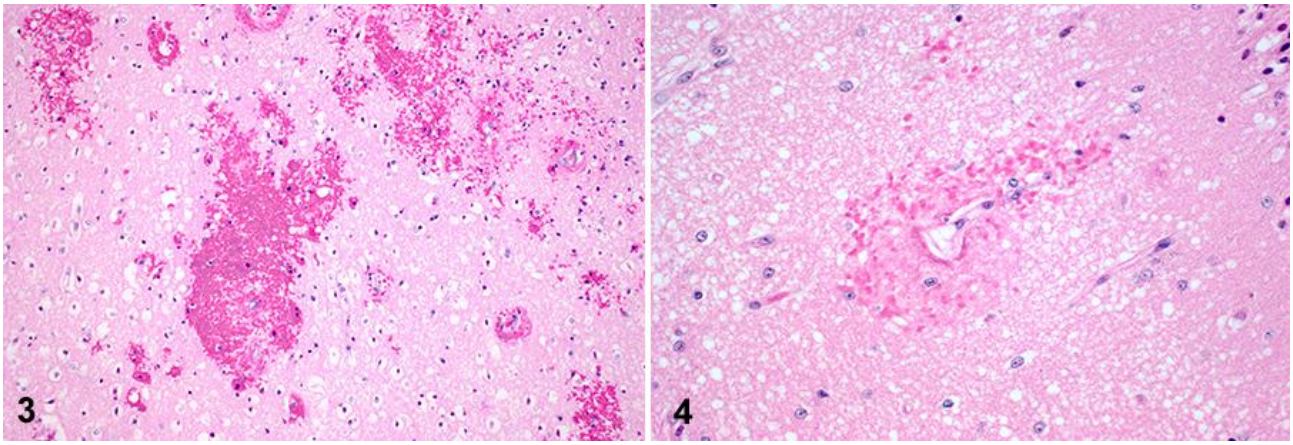

Figure 4.4.1.3-4. 4.4.1.3: Cerebrum. Multifocally the neuropil is expanded by extravasated erythrocytes (hemorrhage), frequently adjacent to or surrounding microvessels with evidence of fibrinoid necrosis to the vascular wall. 200x HE. 4.4.1.4: Cerebrum. Higher magnification of fibrinoid necrosis to the microvascular wall and extravasated erythrocytes expanding and replacing the perivascular neuropil. 400x HE.

Either frank hemorrhage or accumulation of perivascular hemosiderin was noted in the cerebrum in 27% of the animals, but only in 1 case was the hemorrhage a histopathological feature which warranted a severity score of 'marked'. Typically, the score was minimal to moderate. In the spinal cord and brain stem, hemorrhage was noted in 44% of the animals, and in these cases the severity was typically mild or moderate. Occasional neurons were condensed, angular and showed hypereosinophilic cytoplasm which was occasionally microvaculated; distorted nuclei contained consolidated and clumped chromatin (varying stages of degeneration or necrosis). (Figure 4.4.1.5) Affected cells were often bounded by reactive microglial cells (satellitosis). Focal areas of edematous swollen white matter tracts showed features suggestive of acute axonal injury. In addition, there

were some collections of monocytes/macrophages both within vessels and in the perivascular space, although in the large majority of cases little host inflammation (lymphocyte localisation) was seen. Rarely fibrin-platelet thrombi were identified, but typically these were in association with those few cases in which mural vascular necrosis was identified in the brain.

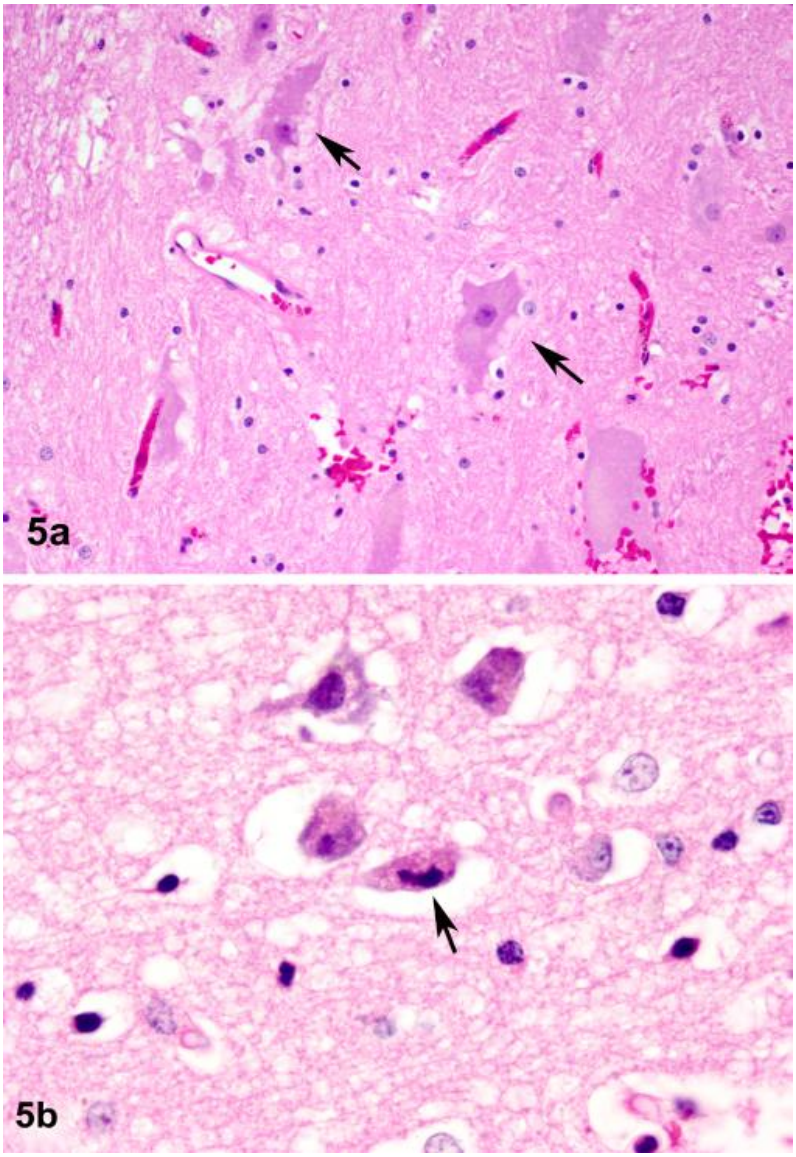

Figure 4.4.1.5a-5b: Figure 4.4.1.5a is representative of degenerative changes within the cerebrum. Multifocally, within this photomicrograph there are examples of neuronal degeneration (neuroplasmic vacuolization) (arrows). Additionally, there is satellitosis of affected neurons and both perivascular/perineuronal edema. 400x HE. Figure 4.4.1.5b illustrates neuronal necrosis characterized by neuronal angulation, nuclear condensation (arrow) and fragmentation. 400x HE.

b. <u>Cerebellum</u>: High levels of microvascular sequestration were seen, consistent with previous reports in this model showing the higher levels in cerebellum than cerebrum. (Sein 1993) In 71% of the cases, there was some degree of Pürkinje cell degeneration, necrosis and loss (Figure 4.4.1.6). Degeneration was characterized by swollen microvacuolated cells with retracted plump dendrites and peripheral edema, while necrosis was comprised of fragmented and angulated cells with hypereosinophilic cytoplasm and disrupted nuclei. Lost cells were in evidence by clear spaces ('empty baskets'), with residual fragments and occasional microgliosis. Foci of microhemorrhage were observed in only 4 cases and the extravasated erythrocytes were typically seen in the perivascular space which is interpreted as a breach of the vessel wall.

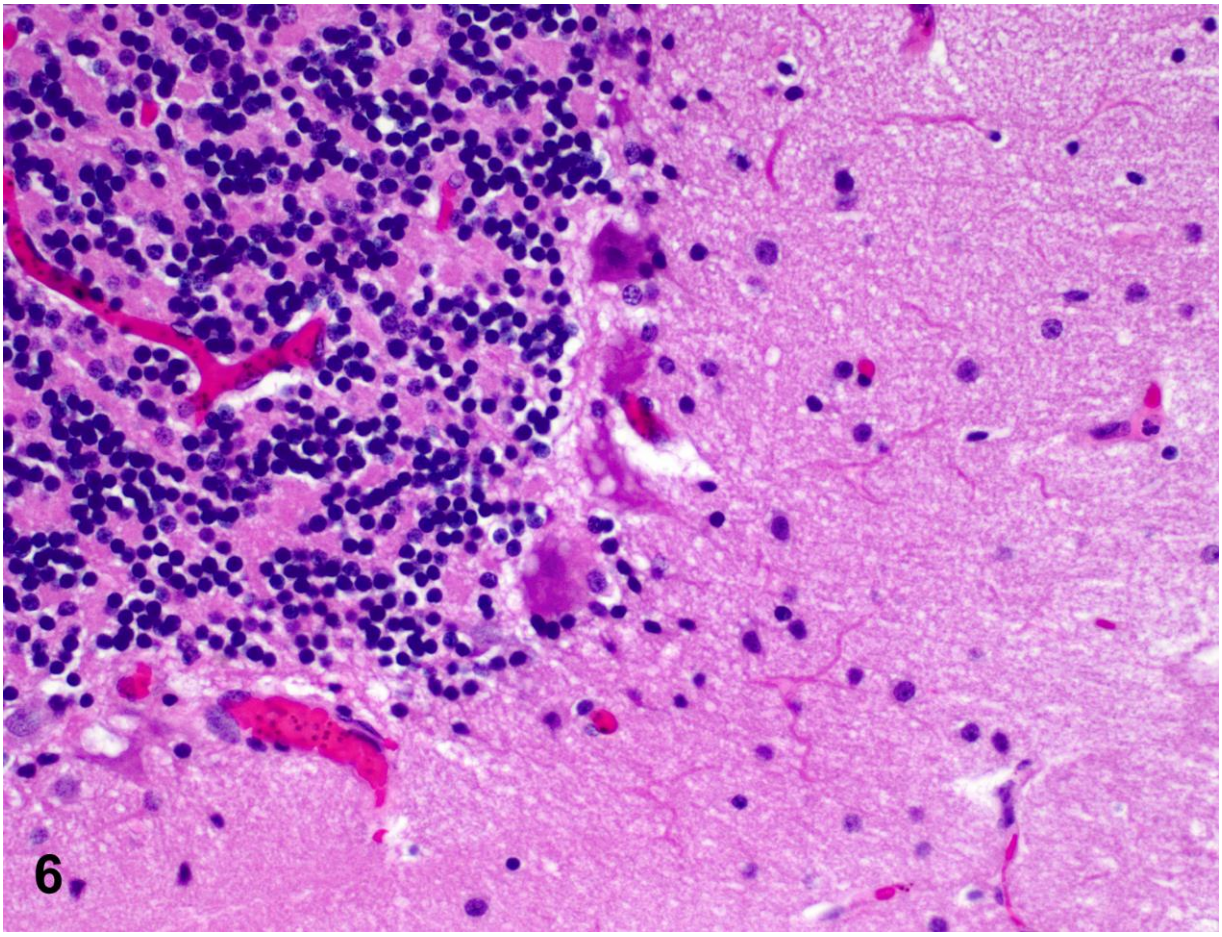

Figure 4.4.1.6: Cerebellum. This photomicrograph illustrates Pürkinje cell degeneration, and necrosis. 400x HE.

c. <u>Brain stem</u>: Microvessels within the brain stem contained moderate to high numbers of sequestered iRBC containing abundant hemozoin pigment. No marked increase in intravascular lymphocytes was seen although monocyte-macrophage numbers did appear increased in both intra- and peri-vascular spaces in individual cases. This was not accompanied by formation of fibrin-platelet thrombi, nor ring hemorrhage formation. Frequently there was perivascular edema, and occasionally small foci of punctate hemorrhage were observed. Furthermore, within the white matter, longitudinal sections of myelin sheaths showed axonal fragmentation and rare digestion chambers. (Figure 4.4.1.7)

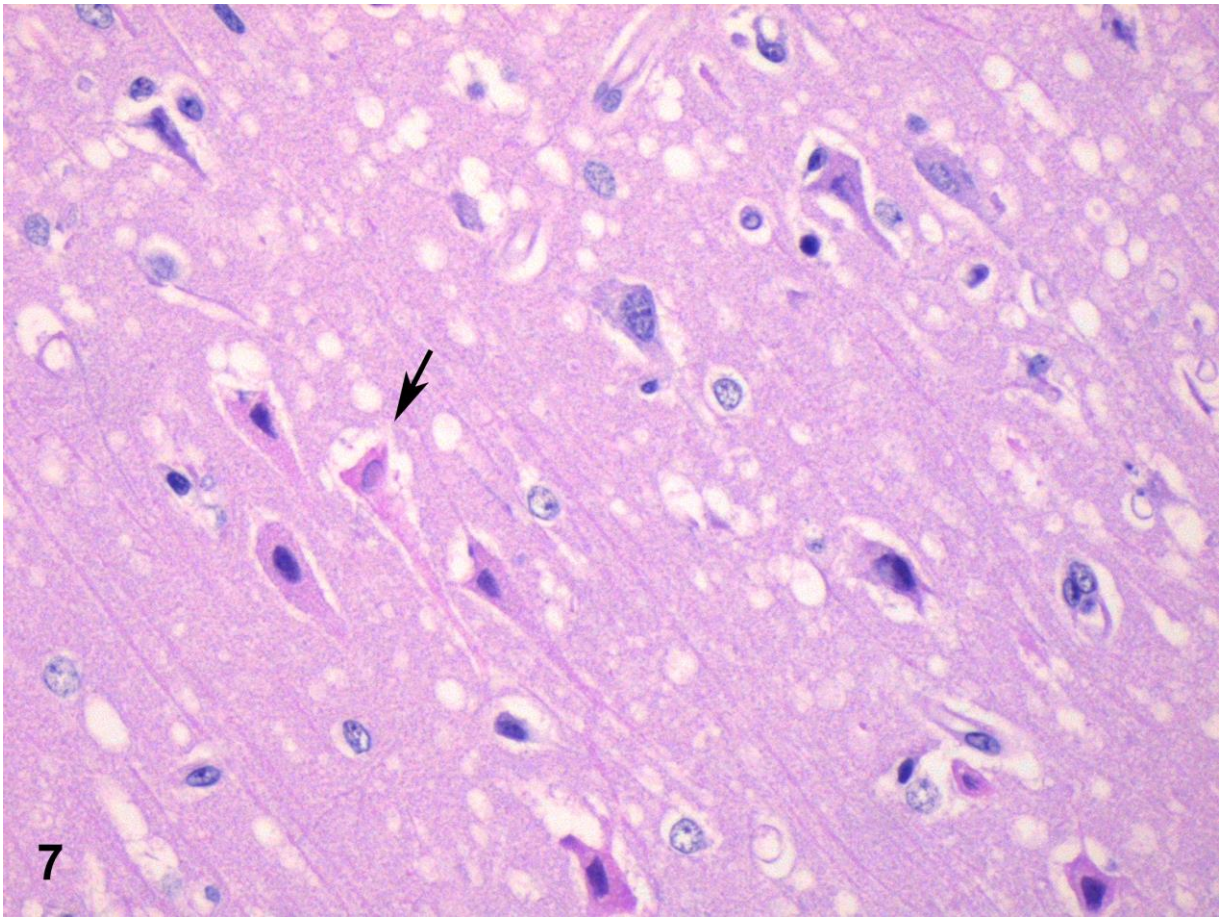

Figure 4.4.1.7: Brain stem. Multifocally throughout this section, the neuropil is replaced by edema, characterized by vacuoles both surrounding degenerate neurons and throughout the neuropil. The

neurons themselves are frequently angulated, shrunken and hypereosinophilic (arrow) suggestive of degenerative and necrotic changes. 400x HE.

d. **Spinal cord**: In 60% of the prospective cases, hemorrhage was observed to be multifocally infiltrating the spinal cord parenchyma surrounding obstructed (due to sequestration) microvasculature. This finding was noted to be more significant within the grey than white matter. Additionally, there were frequent swollen axons (spheroids), rare digestion chambers and dilated myelin sheaths. (Figure 4.4.1.8-9)

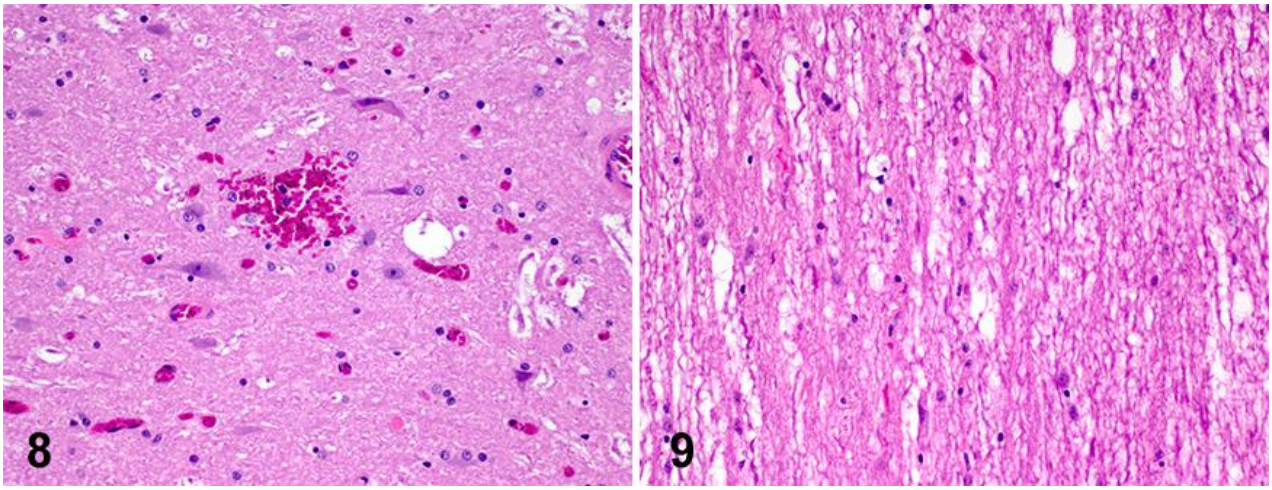

Figure 4.4.1.8-9: Spinal cord. Figure 4.4.1.8 demonstrates the punctate hemorrhages which were frequently observed in sections of the spinal cord. 400x HE. The longitudinal section in 4.4.1.9 demonstrates digestion chambers and dilated myelin sheaths suggestive of axonal injury, necrosis and loss. 400x HE.

4.4.2 **Eyes:**

Microscopic changes were most significant within the ganglion layer of the retina. In that layer, there was increased sequestration of microvasculature, accompanying perivascular edema and multifocally, there was degeneration and loss of ganglion cells (Figure 4.8.1). All other layers of the retina were

unaffected. The remainder of the globe displayed similar changes to those seen universally in all tissues.

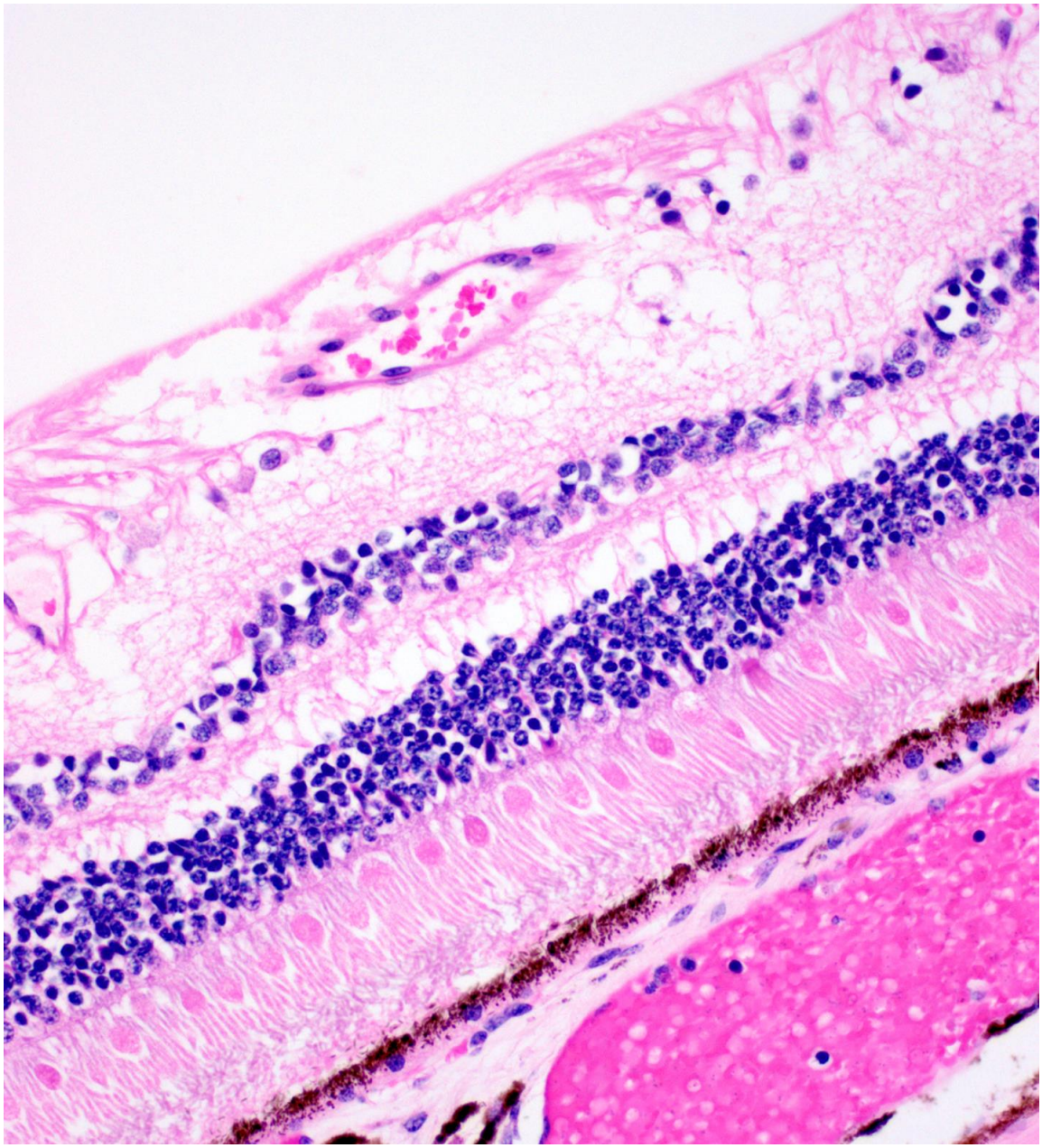

Figure 4.4.2.1: Eye: This photomicrograph of the retina of a *P. coatneyi* infected rhesus macaque shows subtle changes within the outermost layer. Within the ganglion layer there is perivascular edema and ganglion cell loss. 400x HE.

4.4.3 **Sequestration in Brain Microvessels and Calculation of Sequestration Index:**

Brain smears were prepared from cortical grey matter in three prospective animals. (Figure 4.4.3.1-2) In all animals the proportion of vessels showing sequestered iRBC was 100%. The vast majority of iRBC were late trophozoite stage with only occasional schizonts forms. Calculation of sequestration index was performed to compare the number of parasites within vessels (iRBC/100RBC) with those in the peripheral circulation, (as per the method used in human tissues by Silamut et al 1999) which indicated an excess compared to that expected by free mixing with a median of 2.5 times expected parasite levels.

Animal #	Total RBCs Counted	iRBC	Individual parasites	Schizonts	Terminal peripheral parasitemia	Terminal parasitemia %
R519	300	119	133	0	1190160	26.1
DA923	300	181	283	0	1547340	24.6
DA831	300	146	283	1	1013540	18.7

Table 4.2: Summary of the calculated results of brain sequestration in three *P. coatneyi* infected animals.

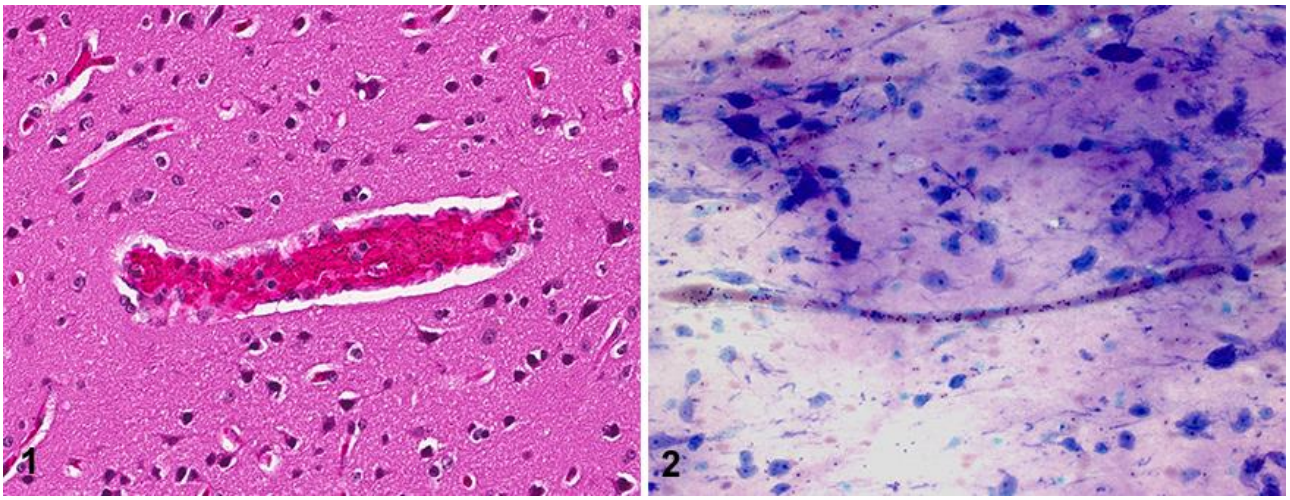

Figure 4.4.3.1-2: Brain: Photomicrograph 4.4.3.1 is an example of the histopathological evidence of vascular sequestration in a medium sized cerebral vessel. 200x HE. Photomicrograph 4.4.3.2 is a brain smear with a central longitudinal section of the cerebral capillary. The malaria pigment and parasites are highly evident in both sections. 400x Giemsa.

4.4.4 **Gastrointestinal tract:**

All sections of the gastrointestinal tract were examined. Gastric mucosa occasionally had multifocal, mild erosion and ulceration with an underlying neutrophilic and lymphoplasmacytic gastritis. Occasionally in the submucosa of the stomach, duodenum and colon, there was formation of lymphoid follicles, but these were interpreted to pre-existing background changes associated with chronic immune stimulation of the gastrointestinal tract. The sequestration and obstruction pattern of vessels within all sections of the tract demonstrated a marked predilection for the mucosa in comparison with the underlying connective tissue of the submucosal layer, muscularis or serosa. (Figure 4.4.4.1)

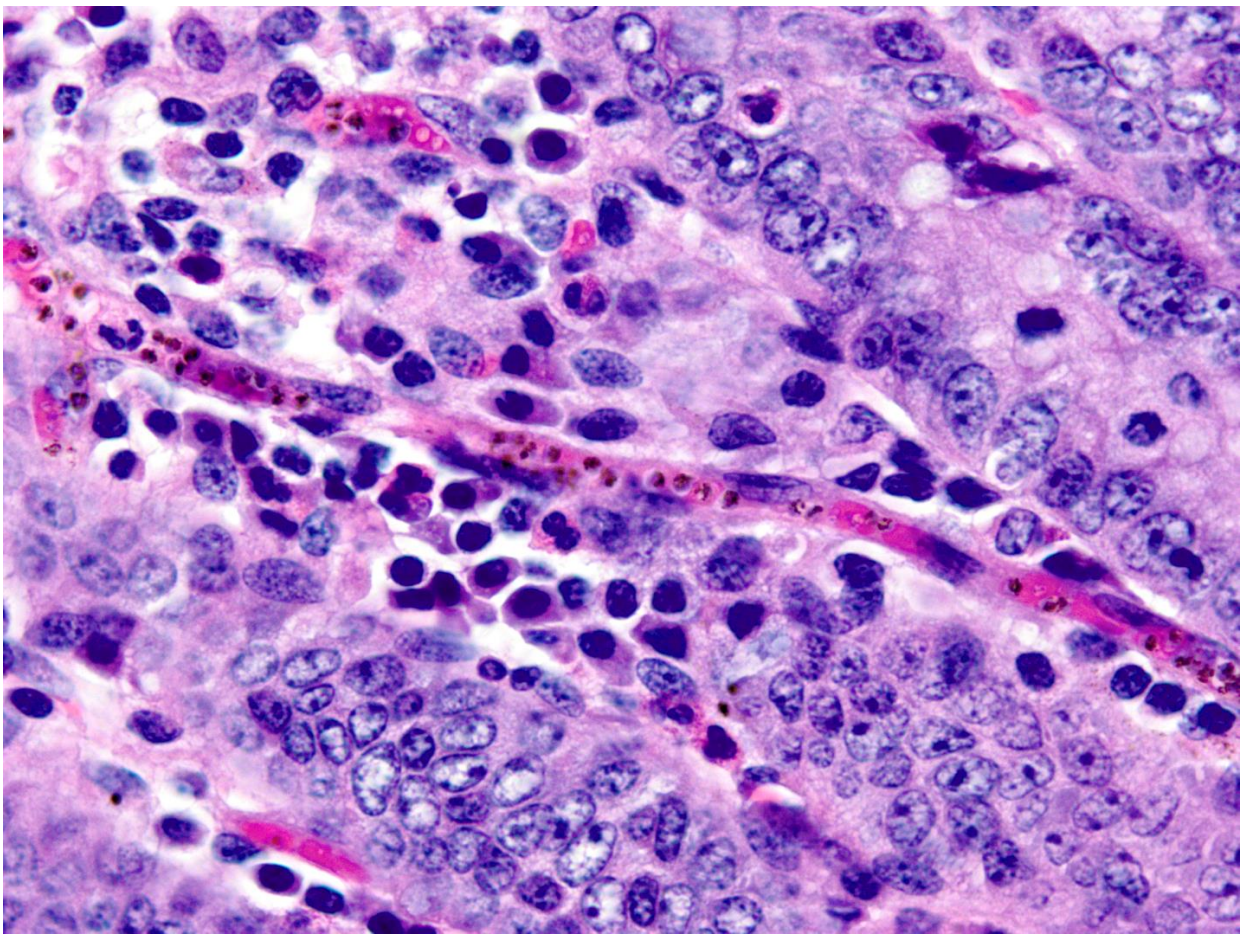

Figure 4.4.4.1: Jejunum: This image highlights the extent of sequestration observed in the gastrointestinal mucosal lamina proprial vasculature. Within this single vessel are myriad *P. coatneyi* trophozoites. (1000x HE)

4.4.5 **Liver:**

Diffusely the hepatic sinusoids were markedly expanded and congested with high numbers of iRBCs and abundant intraerythrocytic and intramonocytic hemozoin pigment. Within centrilobular tissue, there was frequent piecemeal degeneration and necrosis of individual hepatocytes. Küpffer cells were noted to be reactive and increased in number, and these often contained phagocytosed hemozoin pigment. In those few cases which were either treated or, through supportive care, survived beyond the initial insult and lived days or even weeks beyond the peak parasitemia, severe chronic lesions were observed histopathologically. These changes were comprised of marked to severe centrilobular mixed coagulative and lytic necrosis. (Figure 4.4.5.1-4) Multifocally, lost hepatocytes were replaced by loose fibrosis and, while no parasites were observed, there was often abundant residual pigment.

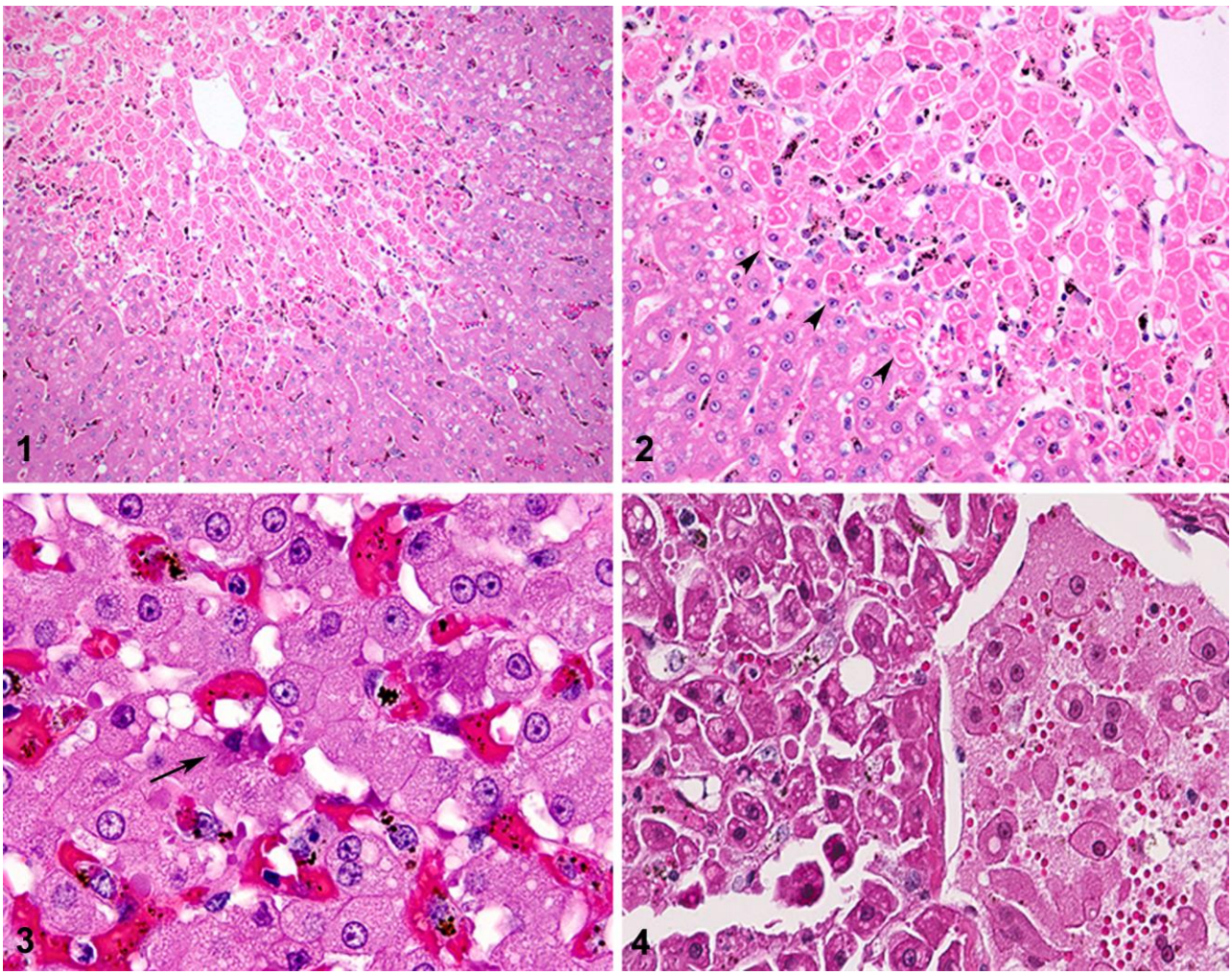

Figure 4.4.5.1-4: Liver: This plate of photomicrographs of the liver illustrates evidence of centrilobular coagulative necrosis, sinusoidal sequestration, piecemeal necrosis and disruption of the hepatic plates. 4.4.5.1 shows a low magnification of the hypereosinophilic zone surrounding a central vein. In this case there is loss of nuclear staining while retaining evidence of the prior architecture (coagulative necrosis). 200x HE. 4.4.5.2 is a higher magnification of the same centrilobular coagulative necrosis. There is a strong line of demarcation between the viable and necrotic tissue (arrowheads). 400x HE. 4.4.5.3 is a high magnification demonstrating piecemeal necrosis (arrow) and sinusoidal sequestration and congestion with infected erythrocytes. 1000x HE. 4.4.5.4 is consistent with lytic necrosis, comprised of fragmentation and loss of cells, eosinophilic cytoplasmic and nuclear debris and loss of architecture. 1000x HE.

4.4.6 **Kidney:**

The kidneys were among those organs most severely affected in all cases. All animals were found to have microscopic evidence of acute tubular necrosis. This was characterized by mild to severe degeneration, loss of the proximal tubular epithelial cell brush border on PAS staining, individual tubular epithelial cell necrosis and shedding, and formation of intratubular cellular casts, hemoglobin casts and proteinosis. (Figure 4.4.6.1). Tubular debris and red cell casts were seen within collecting tubules. These changes were in excess to post-mortem artefacts seen in control animals. Within the interstitial capillaries were high numbers of sequestered iRBC and hemozoin pigment.

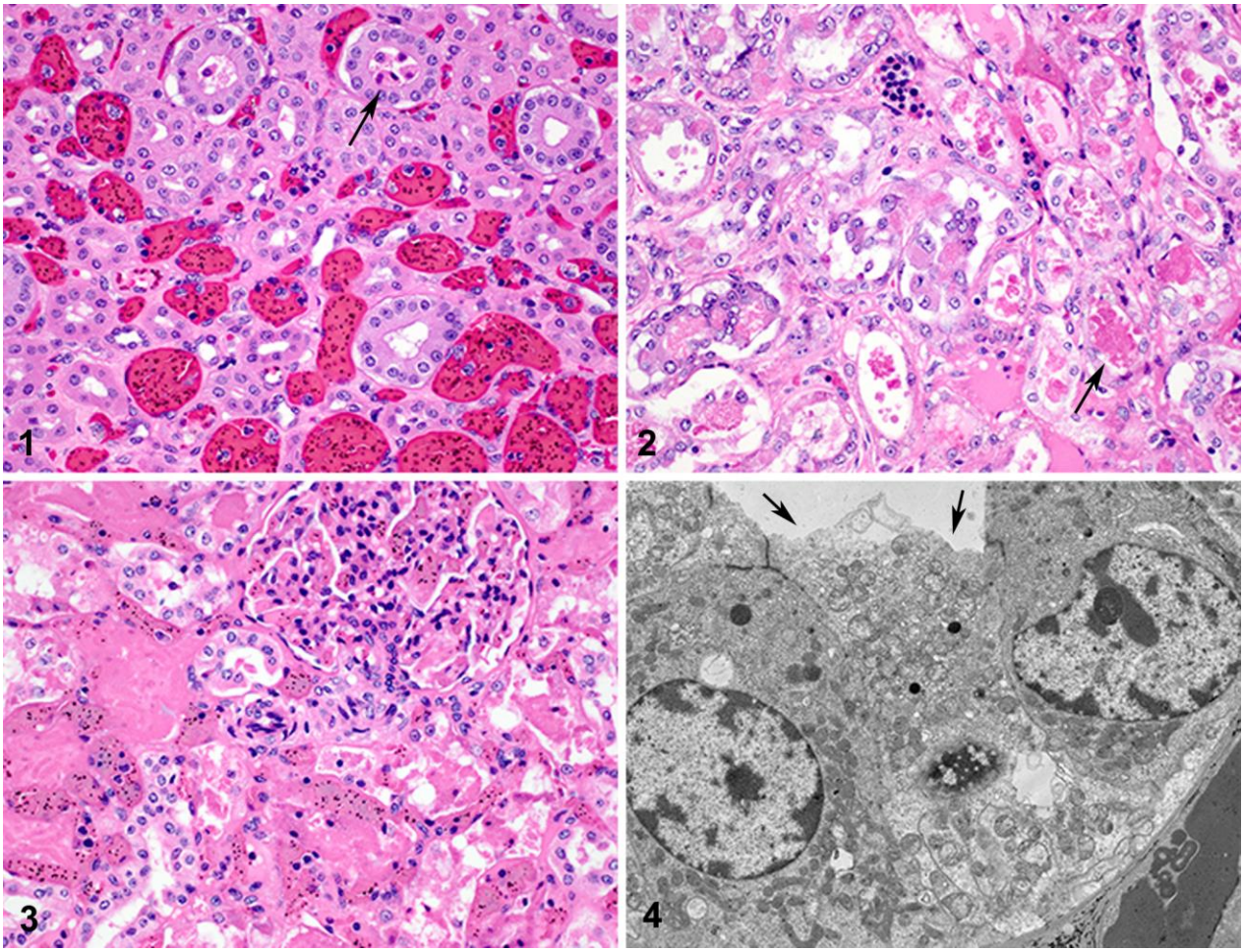

Figure 4.4.6.1-4: Kidney. This plate accentuates the various changes which were observed in the histopathological and ultrastructural evaluation of the renal tissue in severe *P. coatneyi* infection. 4.4.6.1 This photomicrograph illustrates early, subtle changes. Within the renal interstitium, vessels are markedly expanded and congested with infected erythrocytes. Frequently within the lumen of renal tubules there are sloughed, necrotic epithelial cells. (arrow) 400x HE. 4.4.6.2 A similar magnification of damage associated with a more chronic stage of the disease. In this image, there is fibrosis of the interstitium, degeneration, necrosis, regeneration and loss of the tubular epithelium, protein, cellular and hemoglobin casts (arrow) within the tubules and rare foci of inflammatory cells. 400x HE. 4.4.6.3 This photomicrograph also shows significant necrosis and loss of the renal architecture, tubular cellular and hemoglobin casts, as well as marked microvascular congestion and sequestration both within the interstitium as well as within the glomerular tuft. 400x HE. 4.4.6.4 Ultrastructural micrograph illustrates a single tubular epithelial cell undergoing necrosis (arrows)

bounded by two viable cells. There is fragmentation and rupture of the cytoplasm, swelling and vacuolization of the organelles and nuclear pyknosis. TEM 4000x.

The glomeruli were occasionally hyperlobulated and, in animals with higher parasitemias, there were focal adhesions of the glomerular tuft to the Bowman's membrane (synechiae or tip lesions) as well as abundant congestion with both iRBCs, uninfected erythrocytes and hemozoin pigment. (Figure 4.4.6.5-8) Both within the interstitial capillaries as well as within the glomerular tuft there were increased numbers of intravascular monocytes and neutrophils. However, these rarely transmigrated into the adjacent tissue and no features of a tubulointerstitial nephritis were seen to explain the clinical picture of acute tubular injury. The glomerular expansion, endocapillary leukocytes and hyperlobulation gave the appearance of a proliferative endocapillary glomerulonephritis, although no active vasculitis, destructive lesions or crescent formation was seen in any case, and no mesangiolysis. Silver and PAS staining indicated no membrane complexity, spike formation or immune complex deposition. The lack of immune complex deposition was confirmed ultrastructurally, although focal podocyte foot process effacement and proliferation was observed indicative of proteinuria.

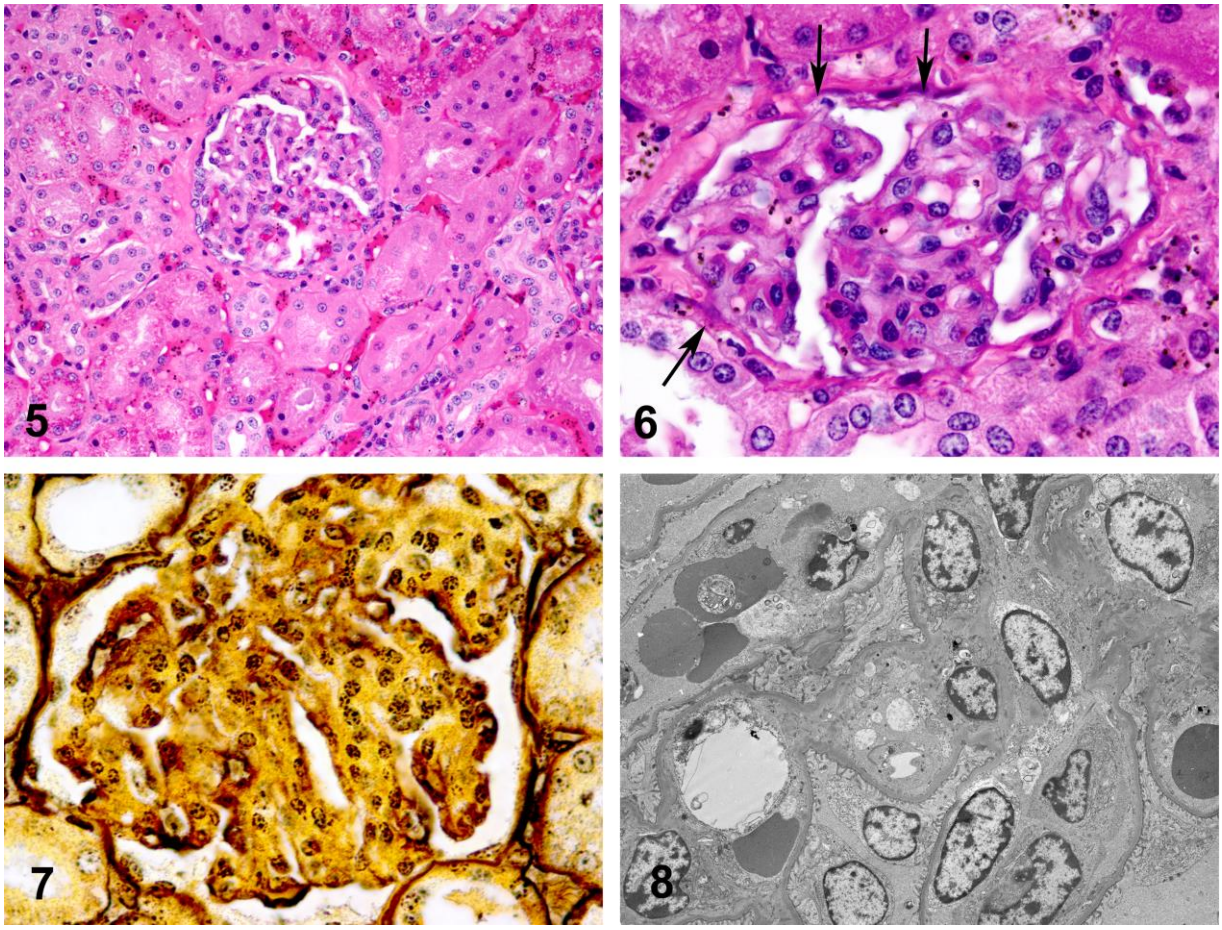

Figure 4.4.6.5-8: Kidney. This plate of histological and ultrastructural photomicrographs highlights glomerular changes within the renal tissue of *P. coatneyi* infected rhesus macaques. 4.4.6.5 demonstrates early changes in which there are only subtle changes. Aside from the changes described in the tubules in 4.4.6.1, the glomerulus in this image is beginning to adhere to the reactive parietal epithelium of the Bowman's capsule, forming synechiae (arrows). 400x HE. 4.4.6.6 is a higher magnification showing periglomerular fibrosis, more pronounced synechiae as well as dilation of the microcapillaries and low levels of interstitial mononuclear inflammatory cells. 1000x HE. 4.4.6.7 This silver stain of the glomerulus demonstrates that while there is evidence of a proliferative response in the glomerulus, that we do not observe the membranous expansion of the basement membrane as can be seen in immune mediated glomerulopathy in rare cases of *P. falciparum* and *P. malariae* induced malaria. 1000x von Kossa. 4.4.6.8 Further reinforcing the findings described in 4.4.6.7, the

glomerulus in this ultrastructural photomicrograph is essentially normal, with the exception of infected erythrocytes lodged in the microcapillaries of the glomerular tuft. TEM 2000x.

As with the liver, those animals which survived beyond the peak of infection, developed chronic lesions including severe tubular necrosis with interstitial fibrosis and glomerular sclerosis. Rarely in these animals, the microvasculature was obscured by fibrin thrombi.

4.4.7 **Heart:**

The myocardium was the tissue that displayed the greatest degree of vascular congestion, obstruction or sequestration. The interstitial capillaries were almost universally expanded by iRBC, cytoadhered uninfected erythrocytes and intraerythrocytic and intramonocytic hemozoin pigment. Both light microscopic and ultrastructural examination of the myocardium noted that there was only scant haemorrhage, and that the vast majority of the infected erythrocytes were intravascular. Commonly the perivascular connective tissue was expanded by edema. One feature not previously reported, but consistently observed within this study, was an increased degree of microscopic pathology within the cardiomyocytes of the myocardium. Overall 71% of the experimental animals were noted to have some degree of damage to the cardiomyocytes, although rarely did the severity exceed a ranking of mild. That was increasingly evident when comparing the population of retrospective animals, many of which had lower peak parasitemias, with the prospective cases. Affected cardiomyocytes were either swollen with microvacuoles (degenerative) or shrunken, hypereosinophilic and angular, with contraction bands and nuclear fragmentation or loss (necrosis). (Figure 4.4.7.1-4). This was typically noted to occur in a piecemeal fashion, and coalescing areas of necrotic tissue or neutrophil/monocyte reactive infiltrates were not observed. The rest of the cardiovascular system was less affected. However, at high magnification changes to the endothelium are observed in vasculature throughout the body. Frequently the endothelium of obscured and sequestered microvasculature was swollen and vacuolated (degenerative) or occasionally fragmented

(necrotic). Ultrastructurally, the endothelium occasionally formed membrane bound pseudopodia which interdigitated with the cytoadhered iRBC.

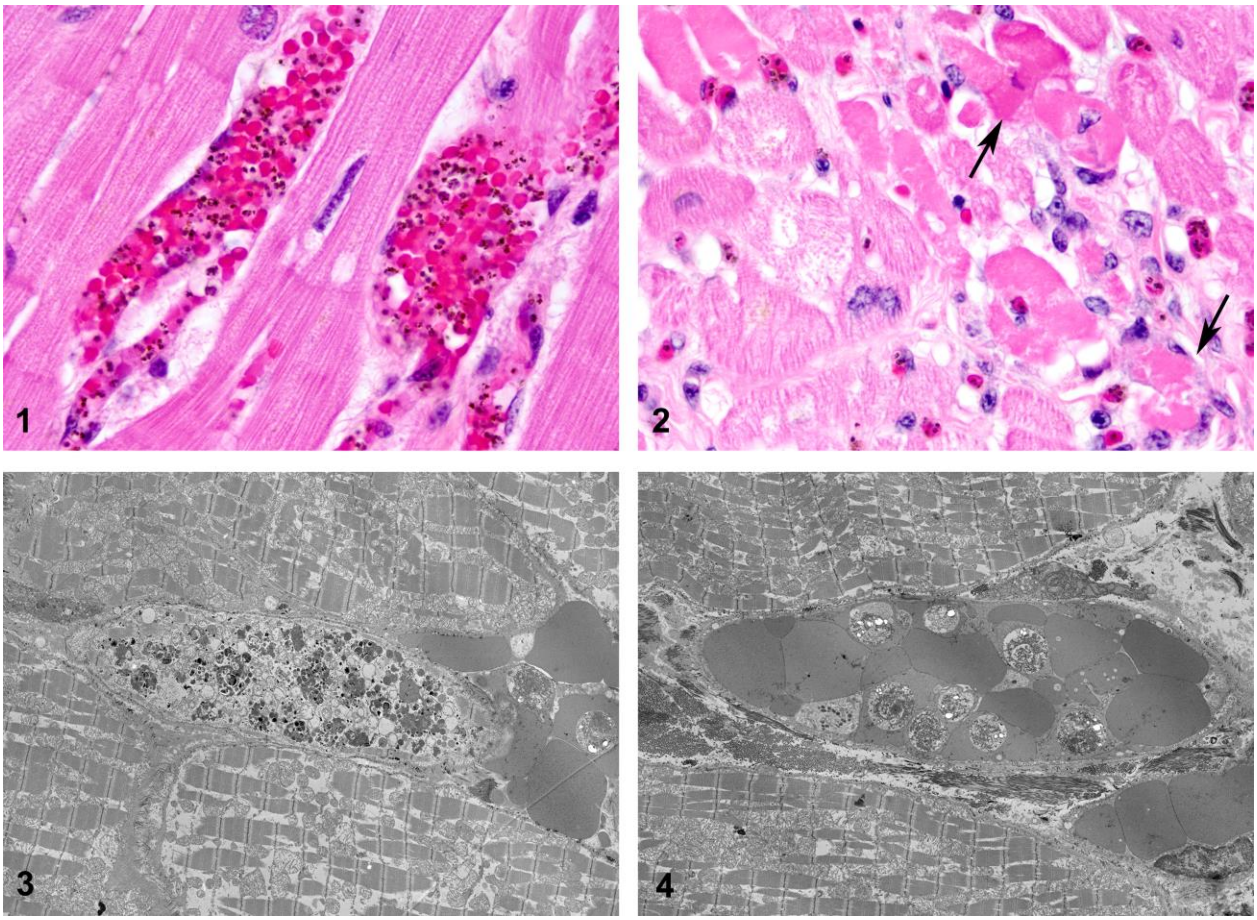

Figure 4.4.7.1-4: **Heart**. This plate illustrates the severe sequestration observed microscopically in the cardiac interstitial microvasculature and the cardiomyocytic piecemeal necrosis, degeneration and loss noted in most of the infected animals. These findings were relatively subtle and rarely did the changes coalesce, however they were consistent and contrasted with the cardiac tissue of the control animals. 4.4.7.1 High magnification of markedly expanded interstitial capillaries, congested with innumerable *P. coatneyi* infected erythrocytes. Furthermore, the perivascular space is expanded by proteinaceous material or clear space interpreted to be edema. 1000x HE. 4.4.7.2 This photomicrograph illustrates a field in which the majority of the cardiomyocytes are either swollen, pale and vacuolated (degenerate) or hypereosinophilic, angular and fragmented with condensed nuclei and loss of structural integrity (necrotic) (arrow). 1000x HE. 4.4.7.3 This ultrastructural

photomicrograph demonstrates a necrotic cardiomyocyte adjacent to a vessel containing iRBCs. TEM 1500x. 4.4.7.4 In this instance the image shows a couple of cardiac microvessels in which there is margination of iRBCs with cytoadhereance to the endothelium and a degree of autoagglutination. TEM 2000x.

4.4.8 **Lung:**

The model exhibited plentiful infected erythrocyte sequestration within pulmonary microvessels, but a minimal degree of histopathological signs of resultant pulmonary injury. The lungs were typically affected by expansion of the alveolar septae by sequestered iRBC and uninfected erythrocytes, with variable increases in host leukocyte numbers, some of which contained phagocytosed hemozoin pigment (Figure 4.4.8.1-4). Occasional animals had an interstitial histiocytic pneumonitis, but there was no significant pulmonary edema in any animal, nor was there marked inflammatory destruction of the parenchyma and no development of hyaline membranes to suggest diffuse alveolar damage or incipient ARDS. Of note however, was that in larger pulmonary vessels, histocytes and other leukocytes were often noted to be pavementing along the endothelium. Potentially, this finding might represent a precursor to a greater degree of pulmonary disease should the animals have survived into a chronic stage.

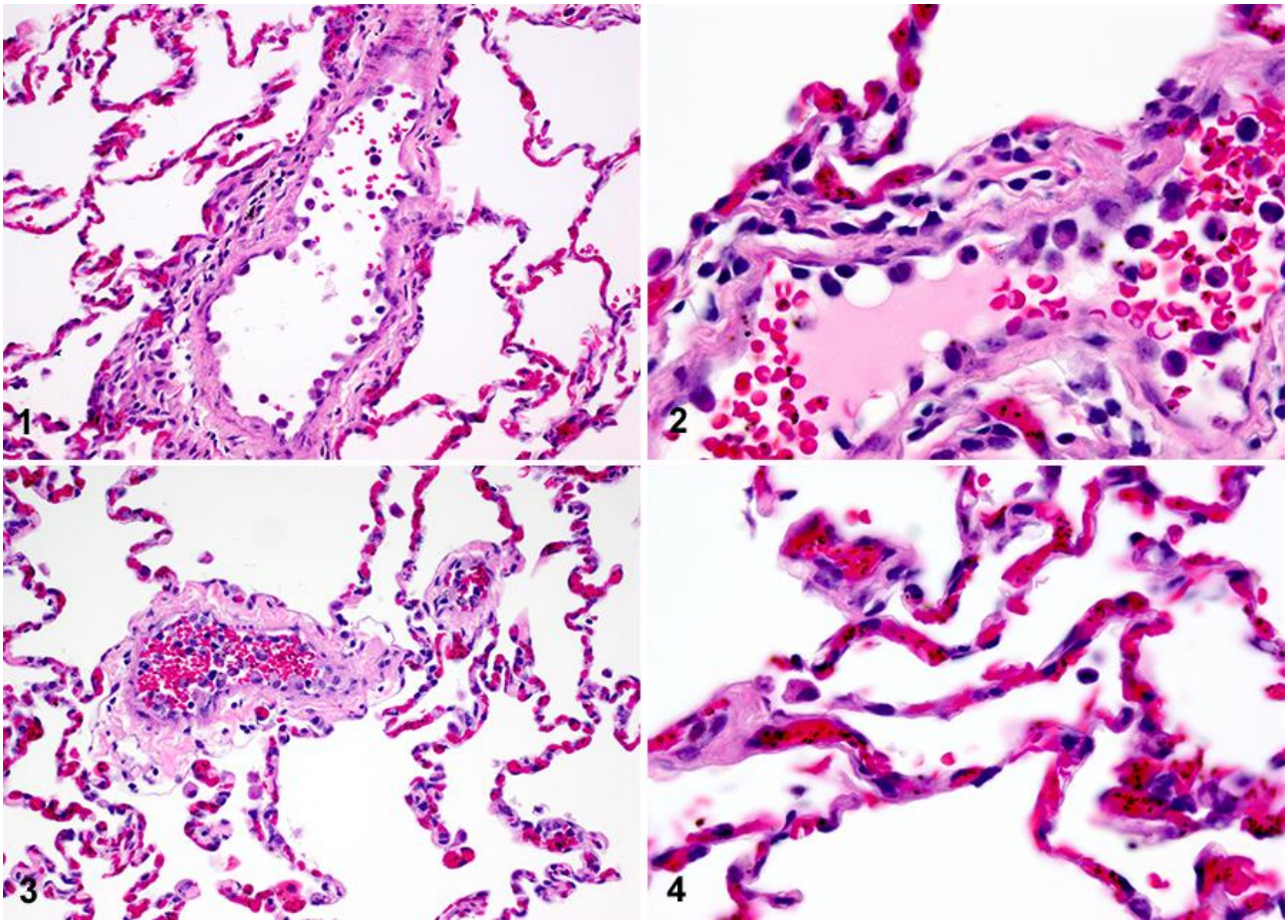

Figure 4.4.8.1-4: Lung. This plate illustrates subtle early changes within the pulmonary interstitium, as well as the complete absence of alveolar edema in this model. 4.4.8.1 is a low magnification photomicrograph with margination of mononuclear leukocytes. 400x HE. 4.4.8.2 illustrates a higher magnification of the same phenomenon. 1000x HE. 4.4.8.3 serves to describe the sequestration of the alveolar wall capillaries with high numbers of infected erythrocytes. Additionally, there are rare alveolar macrophages within the alveolar space, however these are not noted to be in excess of normal background numbers. 400x HE. 4.4.8.4 Similarly, this high magnification photomicrograph shows the fact that all vessels are packed with plasmodium infected erythrocytes. 1000x HE.

4.4.9 **Spleen:**

In the select few cases in which splenectomized animals were found at autopsy to have a daughter spleen (splenunculum), these were examined. In all cases, the red pulp was markedly

expanded by high numbers of iRBC and monocytes, both of which contained abundant hemosiderin or hemozoin pigment (Figure 4.4.9.1-2). Additionally, there was a significant amount of erythrophagocytosis observed throughout the sections, and rarely splenic vasculature contained fibrin thrombi.

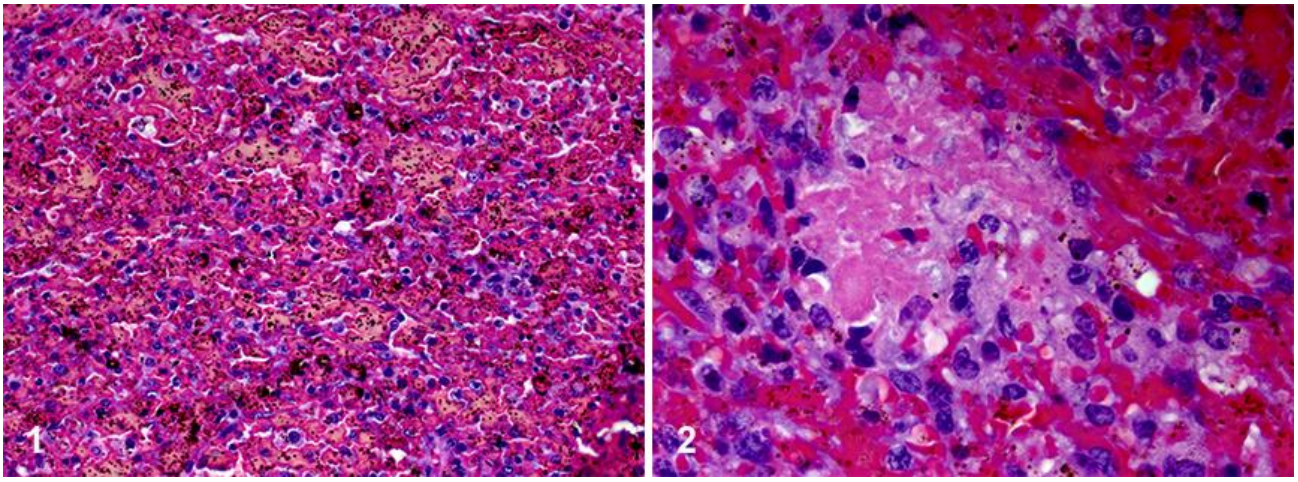

Figure 4.4.9.1-2: Spleen. In the rare cases in which there was splenic material available for examination, the degree of concentration of infected erythrocytes, hemozoin and hemosiderin within the sinusoids was significant as is demonstrated in 4.4.9.1. 400x HE. Furthermore, when rare fibrin thrombi were noted, they were most often observed within the splenic tissue as in 4.4.9.2. 400x HE.

4.4.10 **Endocrine system:**

a. Pituitary gland: Within the pars anterior there was a high degree of vascular sequestration with intravascular abundance of hemozoin pigment. Rare mononuclear macrophages were observed phagocytozing the hemozoin-laden food vacuoles. No significant changes were observed in the parenchymal tissue of the pituitary. However, the sequestration density was more pronounced in the pars anterior than in the pars intermedia (pars nervosa).

b. Adrenal gland: The only significant changes observed in the adrenal glands consisted of a high degree of cortical congestion with medullary vessels being packed with iRBC and hemozoin.

c. <u>Pancreas</u>: Sequestration was seen with greater density within the endocrine pancreas versus the exocrine tissue. However, no other tissue changes were noted. (Figure 4.4.10.1)

d. <u>Thyroid and parathyroid glands</u>: No tissue-specific histopathologic findings were noted in any of the affected animals.

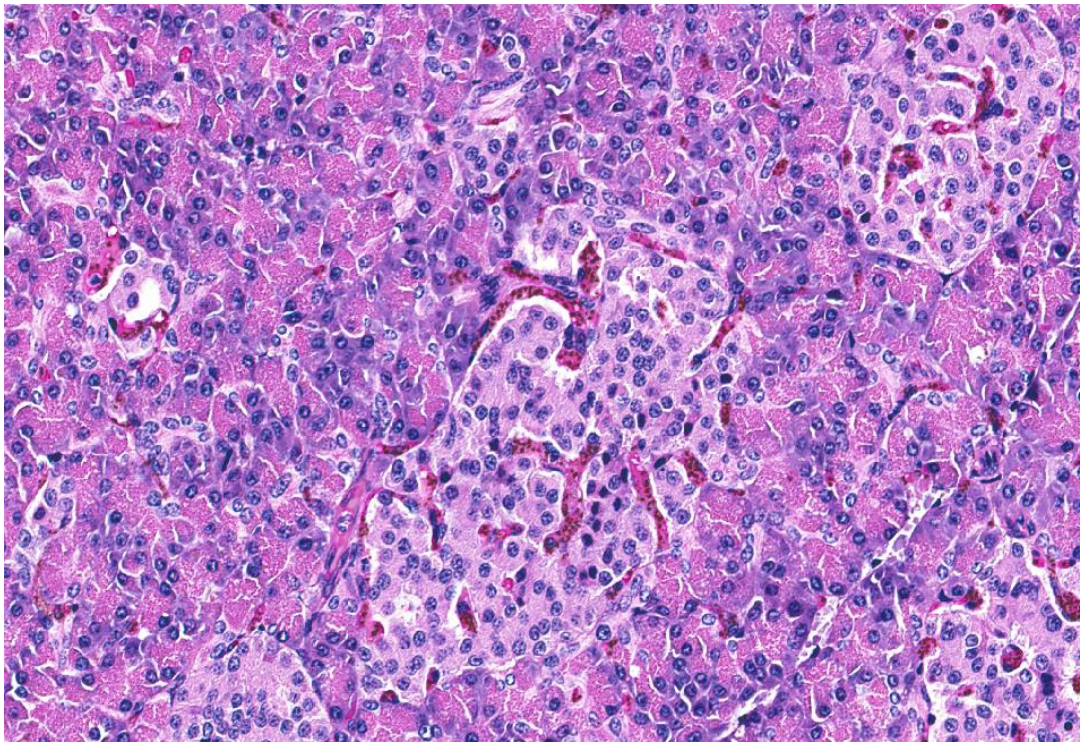

Figure 4.4.10.1: Pancreas. Throughout the endocrine tissue, potentially associated with the increased vascularity, the microvasculature was markedly expanded, congested and sequestered with infected erythrocytes and hemozoin pigment. This photomicrograph shows two central islets of Langerhans (endocrine pancreas) in contrast with the surrounding exocrine pancreatic tissue. No significant tissue specific pathology was noted in any of the endocrine tissues. 200x HE.

4.4.11 **<u>Bone marrow</u>**:

The changes in the bone marrow in response to the regenerative anemia which occurs secondary to the intense destruction of both infected and uninfected erythrocytes has been well described by Moreno and colleagues in their studies in the *P. coatneyi*/rhesus model, albeit under different experimental conditions. (Moreno 2013) Bone marrow was only available in 10 of the

prospective animals. Evaluation consisted primarily of establishing a Myeloid to Erythroid ratio within sections of sternal marrow. Additionally, the average number of megakaryocytes were assessed in 10 high powered fields. Other than those two quantitative criteria, qualitative examination included the maturity of the megakaryocytes, the condition of the stroma, degree of mitotic activity and features associated with the destruction of iRBC or systemic damage. The average ME ratio of those animals was approximately 5.4:1. Megakaryocyte numbers ranged from 1.5 to 10 per high powered field, and frequently these were noted to be immature. In about 30% of the cases there was an increase in mitotic activity in the hematopoietic elements. No significant change was noted in the stroma, but in almost all of the animals, pigment accumulation was observed. This was interpreted to be a combination of both hemozoin pigment and hemosiderin, as there was also frequent evidence of erythrophagocytosis. Additionally, in 2 cases fibrin thrombi were observed in the marrow samples. (Figure 4.4.11.1)

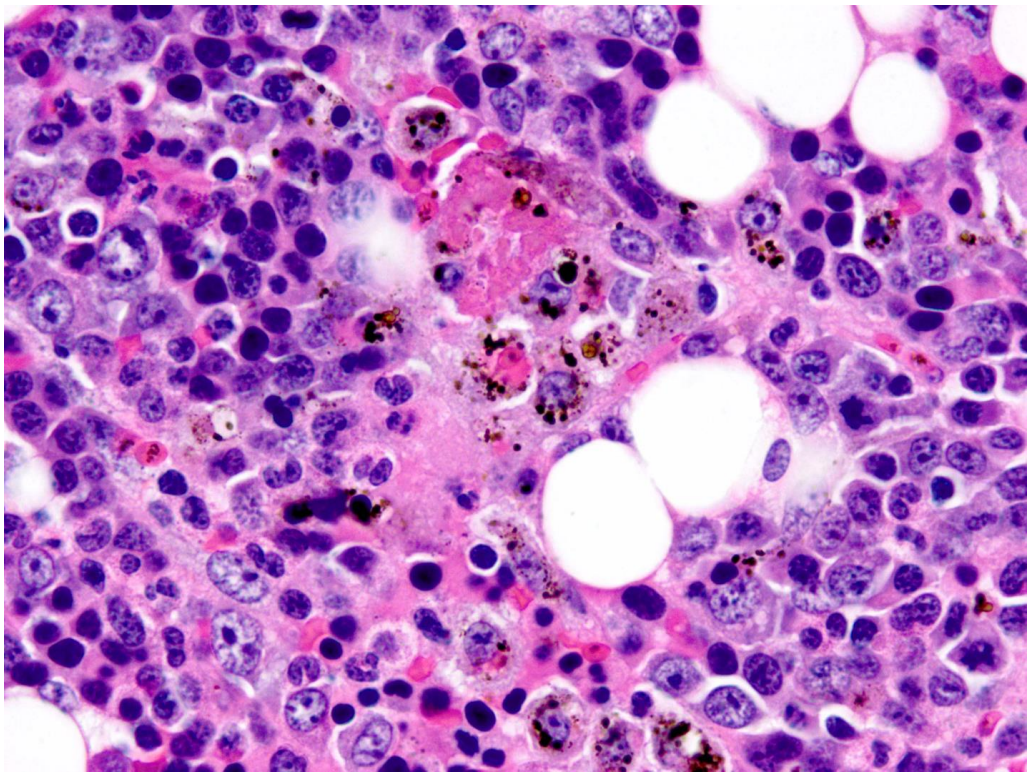

Figure 4.4.11.1: Bone marrow. As with the splenic tissue, the bone marrow fibrin thrombi were rarely observed within sections of bone marrow hematopoietic tissue. Phagocytes within the marrow were often replete with ingested erythrocytes and both hemosiderin and malaria pigment. 1000x HE.

4.4.12 **Other tissues:**

Other tissues were variably available from retrospective and control animals, but collected comprehensively in prospective cases. Sections were examined from skin, mesenteric and subcutaneous adipose, lymph nodes (including mesenteric, inguinal, axillary, submandibular and visceral), abdominal aorta, skeletal muscle (diaphragm and thigh), trachea, larynx, thymus, salivary glands, gallbladder, ears, urinary bladder, testes, epididymides, uterus, ovaries, fallopian tubes and cervix.

In all of these tissues, the capillaries contained varying amounts of sequestered erythrocytes (infected and uninfected) as well as hemozoin malaria pigment, some of which appeared free and some phagocytosed by host leukocytes. No specific pathology was noted in the majority of examined samples, apart from a select few animals (n=4) which developed a form of severe, neutrophilic, necrotizing dermatitis and inflammation of the testes. This appeared associated with a coagulopathy, and may represent a leukocytoclastic vasculitis related to DIC as evidenced by thrombosis most notably within the haired skin, testes and scrotum. In one animal which survived into the chronic phase, the superficial necrosis progressed to the point of loss of the nasal planum and several digits.

4.5 **Discussion:**

Prior to this study, which incorporated a significant number of animals within relatively controlled parameters, there has not been a comprehensive description of pathology in this animal model. Histopathological examinations of autopsy samples from *P. coatneyi*-infected rhesus macaques are reported in the literature. However, with the exception of recent work examining the dyserythropoeisis in the bone marrow (Moreno 2013) and several elegant studies of placental

pathology (Davison 1998; Davison 2000), these descriptions were typically limited. They were conducted in only a select few animals and targeted to specific organs, such as the brain and the heart, in order to confirm particular aspects of the pathophysiology such as rosette formation (Aikawa 1992; Tegoshi 1993; Udomsangpetch 1991), deep vascular sequestration (Desowitz 1969) or knob formation. (Aikawa 1992; Kawai 1993; Kawai 1998; Tegoshi 1993; Udomsangpetch 1991) Furthermore, interpretation of these reports is complicated by the heterogeneous populations of experimental animals, variable levels of parasitemia, splenic status and whether curative treatment had been given.

As such, the scale and relative uniformity of this study represents a unique attempt at characterizing the microscopic tissue changes in the splenectomized rhesus macaque/*P. coatneyi* model of severe malaria. Additionally, this study includes many organs and tissues, such as the spinal cord, in which the pathology of *P. coatneyi* infection had not been previously evaluated, and yet may be critically important in the pathophysiology of the disease. The results from this research demonstrate the pathology of *P. coatneyi* in the rhesus macaque and allow more comprehensive comparison with the reported lesions in human patients afflicted with *P. falciparum*-induced disease. The relative heterogeneity of the monkeys in these studies performed over more than two decades, mirrors the diversity of human populations suffering from malaria and appears to underscore the importance of the host response.

P. falciparum infection in humans has been associated with a range of severe life-threatening complications to include cerebral malaria (CM), severe anemia, metabolic acidosis, hepatic insult with accompanying jaundice, acute kidney injury (AKI), acute respiratory distress syndrome (ARDS), disseminated intravascular coagulopathy (DIC), malaria retinopathy and cardiac disease. (WHO 2014) These syndromes are almost universally seen as part of a spectrum of lesions that are interconnected rather than independently responsible for disease. Using the kidneys as an example, falciparum induced disease has been reported to present with various histopathologic appearances to include acute tubular injury, mild endocapillary but non-immune complex mediated glomerulonephritis and

inflammatory interstitial host leukocyte infiltrates, although without classical tubulointerstitial nephritis. (Barsoum 2000; Elsheikha 2007; Ngaungsangiam 2007; Thanachartwet 2013; Trang 1992) The histopathological features of renal disease are found to be closely recapitulated in this model, with resultant AKI in some cases. In this review of the histologic lesions in the rhesus, we have described acute tubular injury with a proliferative glomerulopathy, but lacking in a significant inflammatory response. This raises the question as to variability in disease presentation, and underscores the fact that no perfect model exists.

While the *P. coatneyi*/rhesus macaque model appears to be very appropriate for the study of multi-organ involvement, there is still significant variability in comparison with human disease in that the pathology was not replicated equally in every organ system. This is particularly underscored by the lack of pneumonitis and pulmonary edema in the lungs, or with the rarity of significant cerebral hemorrhage. Just as some of the histopathologic features of human disease are absent in the animal model, there are findings in the rhesus which are not typical of human disease. Examples of this include the cardiac findings which are relatively novel and may be similar to human cases with algid malaria. However, in those cases, the myocytic damage noted in the rhesus is predominantly absent. Hepatic injury in these animals is likewise more pronounced than in human cases, and the zonal necrosis described here is only rarely reported to occur in humans.

One of the main pathophysiological questions arising from clinico-pathological investigations of severe falciparum malaria in humans is the relative role of parasitized erythrocyte sequestration in causing end organ damage. Some investigators believe this to be an epiphenomenon, and that severe disease is a consequence of host immune response (Hu 2014; Ladhani 2002; Storm 2014), while others support concepts of alternative mechanisms such as an apoptosis-driven pathogenesis. (Lackner 2007; Pino 2003; Toure 2008) Much of this data arises from the murine experimental models of cerebral or severe malaria (Craig 2012; Schmidt 2011; Sun 2003; Xu 2001; White 2010) although the relevance of this model to human CM has been questioned due to the lack of iRBC sequestration in the brain in murine models. In addition, neurological signs following *P. berghei*, *P. yoellii* and *P.*

chabaudi infection in a variety of host murine strains are clearly related to an inflammatory and immune-mediated encephalitis which does not recapitulate the pathological features of human disease.

The Rhesus-*P. coatneyi* model has been used to study the chronic effects of repeated infection on bone marrow function (and subsequent anemia). (Moreno 2013) The splenectomized model allows higher parasitemias (up to 50%) which is associated with multi-organ severe disease. (Aikawa 1992; Lombardini 2015) Whilst earlier studies used this model to study the effects of cytoadhesion-dependent sequestration in the brain as a model of CM (Aikawa 1992), the degree of secondary neuropathological changes observed here are limited. There were practically no microhemorrhages, some perivascular but limited gross edema, limited cellular inflammatory responses or platelet deposition within microvessels, but definite astroglial activation, and mild axonal injury which is most apparent in the brainstem and spinal cord, rather than the cortical white matter.

There was evidence for sequestration of iRBC in all organs. In the brain this caused microvascular obstruction which was mediated both by cytoadhesion to endothelial cells (as shown on EM) but also by the marker degree of autoagglutination and rosetting in this parasite species. The degree of sequestration is in excess of that expected in a free mixing model. Calculation of the sequestration index (SI) confirmed this although the peripheral parasitemia was higher than might be expected in natural infection of these animals, due to splenectomy, so the SI is probably an underestimate of the preferential sequestered parasite burden leading to tissue disease. In human studies SI in the brain can approach 20 (Silamut 1999) due to lower relative circulating parasitemia, and in kidney may be in the range of 1.5-2. Using adjuvant markers of parasite biomass to investigate the relationship between tissue burden and disease is indicated, although *P. coatneyi* does not produce HRP-2 which is commonly used in *P. falciparum.* (Ly 2010; Parra 1991) However, use of 18S DNA within serum may offer another useful adjuvant marker. (Imwong 2014)

The neuropathological feature of the model which is notably different to the human pathology is the relative lack of cerebral ring hemorrhages which are reported to be a common diagnostic feature in advanced cases of cerebral malaria. (Milner 2014; Turner 1997) While only 12 cases of cerebral hemorrhage were observed in our experimental animals, and of those, only one case was severe, brain stem and spinal cord hemorrhage was found with a relatively high incidence (44% of the animals). Additionally, morphological evidence of axonal injury was more common in the brain stem and the spinal cord than in the rest of the central nervous system. The retinas were examined in all of the prospective animals and in those sporadic retrospective cases in which the eyes had been collected. In no case were retinal hemorrhages noted although these lesions are a field of significant interest in children with cerebral malaria. (Beare 2006; Maude 2009) Histopathological features of severe or cerebral malaria have not been reported in the spinal cord.

Cardiac changes represented one of the more consistent findings in infected animals and, while the histopathological changes were subtle, their significance cannot be overlooked. The question which needs to be addressed is what the role of sequestration is in causing myocyte necrosis, especially in the absence of a significant inflammatory myocarditis. Although the histopathologic lesions are piecemeal or in multifocal clusters with few infiltrating inflammatory cells, the interstitial microvasculature is severely congested with iRBC. Does sequestration directly contribute to primary cardiogeneic shock? There is certainly information available on cardiac complications of severe malaria. However, in those instances in which humans succumb to disease and are autopsied, it is infrequent that the microscopic examination of the heart demonstrates any direct evidence of ischemic injury to the cardiomyocytes. (Costanero 2011; Dudgeon 1917; Mohsen 2001; Sprague 1946; Wichmann 2003)

Comparative analysis of this model is of most use to understand changes which may be age related and normal. (Chamanza 2012; Lowenstine 2003) While the model shows strong correlations with human pathology in many organs (such as the kidneys and to a lesser extent, the heart), there are also areas in which the *P. coatneyi*/rhesus macaque model differs from human disease. The

degree of liver damage varied, however in 47% of the animals the histopathological lesions consisted of either centrilobular coagulative necrosis or a degree of hepatocellular degeneration and necrosis warranting a severity score of moderate, marked or severe. This is interpreted to be much more than is typically observed in human disease, which is characterised by liver function abnormalities and a mild inflammatory “hepatitis’ (Saya 2012) but rarely presents with frank zonal necrosis.

The relative absence of any severe lung pathology, such as alveolar edema, fulminant pneumonitis or diffuse alveolar damage/hyaline membrane formation, is discordant with the observations in humans with severe malaria. (Taylor 2012; Ampawong 2015) This is despite the presence in the monkeys of host leukocyte collections, pigment-laden macrophages and iRBC as have been described in the human lung. The causal link between these pathological features and specific clinical syndromes such as ARDS is therefore likely to be dependant both on the species-parasite combination and the individual infected.

Finally, whilst increased numbers of circulating monocytes and polymorphonuclear leukocytes were observed in infected animals, there was a relative absence of inflammation in affected tissues. In particular, there was almost no evidence for collections of platelets, fibrin-platelet thrombi and related microvascular injury in the brain, which has been described in pediatric cases of CM. (Dorovini-Zis 2011; White VA 2001)

The utility of any animal model depends on both the similarities and differences to the disease in humans which is being modelled. But for optimal use and interpretation, it is essential for investigators to be aware of the differences from, as well as the similarities to, human disease as they apply a specific model to the investigation of therapies, vaccines or pathophysiology.

4.6 Summary:

The in-depth evaluation of the histopathology in this model is unparalleled in the simian and the human literature of malaria. While this may seem to be a highly presumptuous assertion, the fact is that the scope of this study outstrips the majority of autopsy examinations in terms of the systemic investigation and the relative uniformity of the study population in terms of age, body condition, disease history, lack of co-morbidities and criteria of infection. Furthermore, this dissertation represents the only review of malaria induced spinal cord, endocrine, retinal and respiratory pathology in any species, as well as providing significant details on features of disease in all body systems and in quantifying the pathology therein. In doing so, this study describes the effect of *P. coatneyi* in those tissues which parallel falciparum induced disease in humans, as well as highlighting those areas in which the two diseases deviate from one another. An example of the former is seen in the kidneys which show synchrony of acute tubular injury without glomerulonephritis, while the latter is most evident in the lungs, which in the *P. coatneyi*/rhesus macaque model lacks the significant pulmonary edema observed in humans. The primary benefit of this study is in having enough conformity of experimental disease, and an adequate animal population so as to be able to demonstrate consistent changes which directly relate to the clinical syndromology, as well as to the hematology, clinical chemistry and autopsy findings.

Chapter 5: Studying Secondary Neuropathological Changes in the Brain of the Rhesus Macaque/*P. coatneyi* Severe Malaria Model

5.1 **Introduction:**

Cerebral malaria (CM) is one of the most crucial manifestations of severe falciparum malaria resulting not only in significant numbers of deaths in victims of infection, but also often resulting in a spectrum of neuropathology in surviving patients. The greatest challenge for care providers for CM patients is in the treatment and management of both the symptomology of active disease as well as in the survival and recovery phases due to the severity of damage to the central nervous system. It is important to underscore the fact that the clinical presentation of disease in *P. coatneyi*-infected rhesus macaques does not mimic that observed in humans as there is the absence of coma. However, early ultrastructural studies of the model proposed that it may represent a good model for sequestration-dependent cerebral pathology. (Aikawa 1992; Maeno 1993) The histopathological findings described in the previous chapter provided some concordance of pathology between that described in humans and that in the rhesus macaque model (eg. the high levels of sequestration, widespread astroglial responses but a relative lack of host leukocyte responses) whereas other features showed some differences (such as the relative lack of cerebral hemorrhages, significant brain edema or morphological evidence of axonal injury).

In the last 20 years more comprehensive immunohistochemical studies of human brain tissue from fatal CM cases (Brown 1999a; 1999b; Dorovini-Zis 2011; Medana 2002; Medana 2011; Ponsford 2012; Turner 1994), and CSF studies in living patients on BBB function, cytokine and neurological injury markers (Brown 2000; Brown 2001; Dittrich 2015; Medana 2005) have expanded our understanding of processes such as astroglial activation, BBB breakdown and edema in mediating secondary neuropathological injury in CM. Cellular inflammatory infiltrates, which are widely

described in murine models of CM are much less marked in human studies, although some authors have proposed both leukocyte (Patnaik 1994) and platelet adhesion (Grau 2003) as mediators of endothelial injury in CM. Another recent article describing the inflammatory response in children with fatal HIV and malaria coinfections does confirm a monocyte/macrophage predominant inflammatory response. The study examined ionized calcium binding adapter molecule 1 (Iba1) which is an immunohistochemical marker specific for the monocyte lineage that includes macrophages, monocytes and microglia. Additionally, that particular study examined Cluster of Differentiation 61 (CD61), a platelet glycoprotein, and neutrophil elastase (NE), a serine protease found specifically in the granules of neutrophils. (Hochman 2015) Other case reports of cerebral malaria in humans describe a macrophage- and monocyte-driven inflammation, but those instances relied on histopathology without the adjunct diagnostic of IHC. (Boonpucknavig 1988; Porta 1993) In general there have been emerging differences proposed for the microvascular pathology of CM in pediatric African cases and adult Southeast Asian patients, not all of which have been based on detailed histopathological studies (summarized in Turner & Millner 2014).

Previous studies have used a range of animal models to attempt to elucidate the pathophysiology of cerebral and severe malaria, with specific focus on the impact of disease on the BBB. (Gitau 2005; Hunt 1992; Migasena 1968; Neill 1992; Rénia, 2012; Thumwood 1988) Early studies in rhesus examined the integrity of the BBB in *P. knowlsei* infections by determining the degree of albumin passage from the cerebral microvasculature. (Migasena 1968) That study utilized *P. knowlsei* which does not have a predilection for the central nervous system in non-human primates. Rather, sequestration concentrates in the liver and gastrointestinal tract in contrast to *P. falciparum*. (Gitau 2005)

As corollary to these human studies, and the histopathological evaluation of the experimental animals in both the retrospective and prospective populations in this study, as reported in Chapter 3, further studies were performed using immunohistochemistry and studies of peri-mortem CSF

samples, focusing specifically on the secondary neuropathology of the central nervous system in the prospective animals, compared with a range of control animals.

These studies were designed to examine the following potential pathways of CNS damage previously identified in human CM, namely:

1. **Blood-brain barrier leakage:** Immunohistochemical analysis of fibrinogen leakage and astrocyte foot process GFAP expression, measurement of the Blood/CSF Albumin index as a marker of BBB breakdown and histological observation of hemorrhages and edema.
2. **Host Leukocyte and Platelet Localization**: Immunohistochemical quantitation of host leukocytes including CD3+ T-cells, CD20+ B-cells, CD68+ monocyte/macrophages and CD61+ platelets in and around cerebral microvessels.
3. **Axonal Injury**: Morphology and immunohistochemistry for β-amyloid precursor protein (β-APP) accumulation in axon
4. **Apoptosis**: Morphology and immunohistochemistry for Cleaved caspase-3
5. **CSF Measurement of** β-APP **and Tau protein, as marker for neuroaxonal injury**
6. **Multiplex ELISA measurement of CSF cytokine signatures.** These were conducted in a limited number of *P. coatneyi*-infected animals to generate a preliminary description of the immune response in the brain.

5.2 **<u>Immunohistochemical Markers background</u>:**

A range of immunohistochemical markers were employed and assessed in sections of the cerebrum and brain stem of the prospective animals. These included amyloid precursor protein Beta (β-APP), fibrinogen, glial fibrillary acidic protein (GFAP), CD3 for T-cells, CD20 for B-cells, CD61 for thrombocytes, CD68 for monocyte/macrophages, Amyloid Precursor Protein (β-APP) for axonal injury and Cleaved caspase 3 as a marker of early apoptosis. The markers were selected in an attempt i) to identify and, to a certain extent, quantify the predominant inflammatory cells involved in the

pathology observed in the brain, ii) to determine if there was compromise of the blood brain barrier, and if so to characterize and compare the immunohistochemical features of the insult, and iii) to identify and describe the degree of neuronal and astrocytic damage associated with severe CNS disease associated with *P. coatneyi* in the rhesus model.

5.2.1 **GFAP:** GFAP is an intermediate filament protein expressed by a range of different cell types within the central nervous system to include ependymal cells and astrocytes, where it is upregulated on astrocyte foot processes following damage to the BBB, or leakage of serum proteins into the perivascular (Virchow-Robin) space. The protein plays a significant role in a variety of different CNS processes including cellular mitosis through the adjustment of the filament network, as well as being crucial in blood brain barrier function and cell to cell communication. Examination of the importance of GFAP in CNS function has been studied in a murine knockout model in which the affected animals succumb to a range of neurodegenerative disorders associated with atypical myelination, deficiencies in the function of the blood brain barrier and white matter degradation. (Liedtke 1996) GFAP is theorized to play a significant part in the molecular pathways associated with astrocytic communication and interaction with neurons. (Weinstein 1991)

Of critical importance to this study is the role of GFAP in exhibiting both astroglial activation and repair mechanisms in the CNS following injury. The protein has been shown to make up a significant portion of glial scars observed in the brain following insult. (Paetau 1985) In the *P. berghei* murine model of cerebral malaria, GFAP expression in perivascular spaces in the CNS has been evaluated to demonstrate the adaptive response of astrocytes to malaria-induced injury. The marker was also used to highlight increased numbers of clustering astrocytes observed microscopically in the affected animals in comparison with controls. (Ampawong 2014; Ma 1997)

5.2.2 **Fibrinogen**: This is a serum protein which, at 340Kda is normally barred from passing into the brain through the function of the intact blood-brain barrier. In cerebral malaria in humans, impairment of the blood-brain barrier is implicated in the pathophysiology of the disease, with increased permeability described as a feature following parasitized erythrocyte binding to cerebral endothelial cells. (Brown 1999) Histopathological and ultrastructural evidence of cerebral edema in victims of cerebral malaria was often associated with different fibrinogen staining patterns associated with vascular endothelial injury and/or fibrin thrombi. Additionally, in some cases the fibrinogen leakage was observed without overt signs of damage to the microvasculature. (Dorovini-Zis 2011; Medana 2011)

5.2.3 **CD3:** 'CD' stands for cluster of differentiation, which defines a collection of antibodies which taken together define a specific antigen. CD3 corresponds to the pan-T-cell co-receptor which is integral to the activation of cytotoxic T-cells. It is a protein complex which is comprised of four distinct chains and is initially expressed in the cytoplasm of pro-thymocytes, the stem cells from which T-cells arise in the thymus. At later stages of development, once the pro-thymocytes have differentiated into medullary thymocytes, the CD3 antigen is localized in the cell membrane and is relatively unique to mature T-cells. As such, the immunohistochemical marker is highly useful and specific to the identification of T-cells in tissue. (Leong 2003) In the case of falciparum malaria infection, the cell-mediated immune response hinges upon Natural Killer cell-, γδT cell- or Th1-derived interferon γ (IFN-γ) driven activation of macrophages resulting in enhanced phagocytosis and destruction of infected erythrocytes, as well as the inhibition by CD8+ cytotoxic and IFN-γ-producing T cells of intrahepatocyte parasitic growth and development. (Artavanis-Tsakonas 2003)

5.2.4 **CD20:** This is a B-lymphocyte antigen which is expressed on the surface of all B cells, and increases in concentration through maturation. Studies in murine malaria models have demonstrated that malaria infections can suppress the upregulation response of B cells, thereby stunting the patient's ability to mount immunological memory to the parasite. (Liu 2012) *P. falciparum* infections in endemic areas elicit antibody-mediated immunity, however its development is very slow. While the reasons behind this delayed acquisition of immunity remains poorly understood, theories include the significant genetic diversity of *P. falciparum* antigens as well as the clonality of the parasites reorganizing the genetic makeup of the antigens expressed on the surface of infected erythrocytes. (Portugal 2014)

5.2.5 **CD61**: CD61 is the Integrin beta-3 (β3) which are associated primarily with platelets/ thrombocytes as well as being expressed by a wide range of other cells, including leukocytes, endothelial and smooth muscle cells as well as having been noted to be useful as a marker for certain malignancies. (Meehan 2003; Merono 2002) In human cerebral malaria, the pathogenesis of disease has been theorized to be associated with microthrombi composed of plasmodium infected erythrocytes adhered to thrombocytes causing occlusion of the microvasculature as well as cytoadhesion to and activation of the endothelium. (Cox 2010) In renal transplantation studies, microscopic CD61 immunoreactivity detection was observed in cases of capillary platelet activation without evidence of light microscopic thrombi. (Meehan 2003) CD61 has been used in the study of cerebral malaria in humans and in murine models of cerebral malaria (Grau 2003; Hochman 2015; Oo 1987; Patnaik 1994; Porta 1993; Sun 2003; Wassmer 2003; White 2009) but as yet, we were not able to find any relevant non-human primate studies.

5.2.6 **CD68:** CD68 represents a glycoprotein widely expressed on monocytes/macrophages (and more weakly in some activated lymphocytes) is found in cytoplasmic granules within a range of hematopoetic cells. The immunohistochemical marker for the glycoprotein is used extensively to identify cells within the macrophage lineage. Macrophages play a crucial role in the control and elimination of malaria infections. However, in humans the disease has been demonstrated to inhibit macrophage function. One theory involves an inhibitory role of malaria pigment or hemozoin. (Nielsen 1986) Researchers have observed that phagocytosis by macrophages of low numbers of infected erythrocytes (iRBCs) containing hemozoin inhibits additional phagocytosis of both iRBCs or other associated material. Additionally, studies have noted that the actual process of intracellular destruction of the pathogens was also interrupted in those macrophages consuming hemozoin in comparison with monocytes which phagocytozed erythrocytes in earlier stages of infection. (Schwartzer 1996)

5.2.7 **Cleaved caspase-3**: Cleaved caspase-3 is a caspase protein that interacts with caspase-8 and caspase-9. The caspases are a family of endoproteases involved in cell regulatory networks which are in turn associated with inflammation, apoptosis and cell death. Sequential activation of caspases cascades to initiate cellular apoptosis. In Alzheimer's disease, the predominant caspase involved in the cleavage of amyloid-beta 4A precursor protein is Cleaved caspase 3. Amyloid-beta 4A is then associated with neuronal cell death. (McIlwain 2013) In malaria, studies have shown that Cleaved caspase 3 (and a variety of other apoptosis-associated molecules) are upregulated. In the brain, this appears to be driven by TNF activation and subsequent platelet binding to the endothelium. The apoptosis of vascular endothelial cells during malaria infection contributes to the compromise of the blood-brain barrier and the resulting cerebral edema. (Baton 2008)

5.2.8 **Beta - Amyloid precursor protein (β-APP):** β-APP is expressed in the synapses of neurons. While the primary purpose remains unknown, the integral membrane protein is theorized to play a regulatory role in neural plasticity (Turner 2003), synapse formation (Priller 2006), and iron export. (Duce 2010) The protein has been studied extensively due to its posited activity as the precursor molecule through which proteolysis forms beta amyloid (Aβ) whose amyloid fibrillar form is the primary component of the amyloid plaques observed in the cerebrum of patients with Alzheimer's disease. β-APP is observed extensively in synaptic repair and formation, and its expression has been observed to be upregulated both during neuronal development and response to injury. β-APP is an immunohistochemical marker of axonal injury, the expression of which was originally thought to be limited to trauma such as diffuse axonal injury, but has subsequently been shown to increase as a marker or axonal injury in infectious diseases as well. Inhibition of fast axonal transport causes beads of the protein to localize in damaged axons, allowing their demonstration in tissue sections, and was first described in CM by Medana et al (2002) and subsequently in pediatric fatal malaria cases. (Dorovini-Zis 2011)

In this part of the study, as well as using negative control tissues (taken from animals dying of noninfectious causes from the same colony), there was an opportunity to study a limited number of animals infected with a chimeric Human Immunodeficiency Virus Envelope-expressing Simian Immunodeficiency Virus (SHIV). (Shedlock 2009) This particular model is being employed at AFRIMS in the examination of early CNS infection in HIV. It was hoped that the SHIV infected animals would provide a good positive control for subtle neuropathological changes compared to *P. coatneyi* malaria infection, as it is generally represented by an early viral parenchymal CNS infection without marked neuropathology and without centralization of the pathological process in the vascular and perivascular compartment.

5.3 **Immunohistochemical Results**:

Control staining of brain sections was performed on animals either sacrificed for normal colony control or dying of non-CNS disease including malignancy, or of trauma due to inter-animal fighting. These controls showed basal amounts of CD68+ monocyte staining, particularly on CD68+ subsets of pericytes which are a normal functional part of the Virchow-Robin space. Basal levels of T and B-cells were minimal, and no CD61+ platelet staining was seen in controls. Likewise, β-APP showed minimal staining in normal brain sections and Cleaved caspase 3 was predominantly non-diagnostic and as such only permits speculation without substantiation. In all cases, the immunohistochemical substrate was chosen based on red staining so as to allow for differentiation with the brown color of both the hemozoin malaria pigment as well as instances of hemosiderin accumulation within phagocytes. (Ramos-Vara 2014)

In general, immunostaining for the cellular immune subsets showed low numbers of CD3 positive T-cells, but focally increased, and in some cases appreciable numbers of both intravascular and perivascular CD68 positive monocyte/macrophages. GFAP staining and Fibrinogen staining, indicating perivascular leakage, was also increased in malaria animals. Some of the CD68+ intravascular monocytes showed intracytoplasmic granules of phagocytosed malaria hemozoin pigment, were a response to vascular sequestration. (Figure 5.3.1-4)

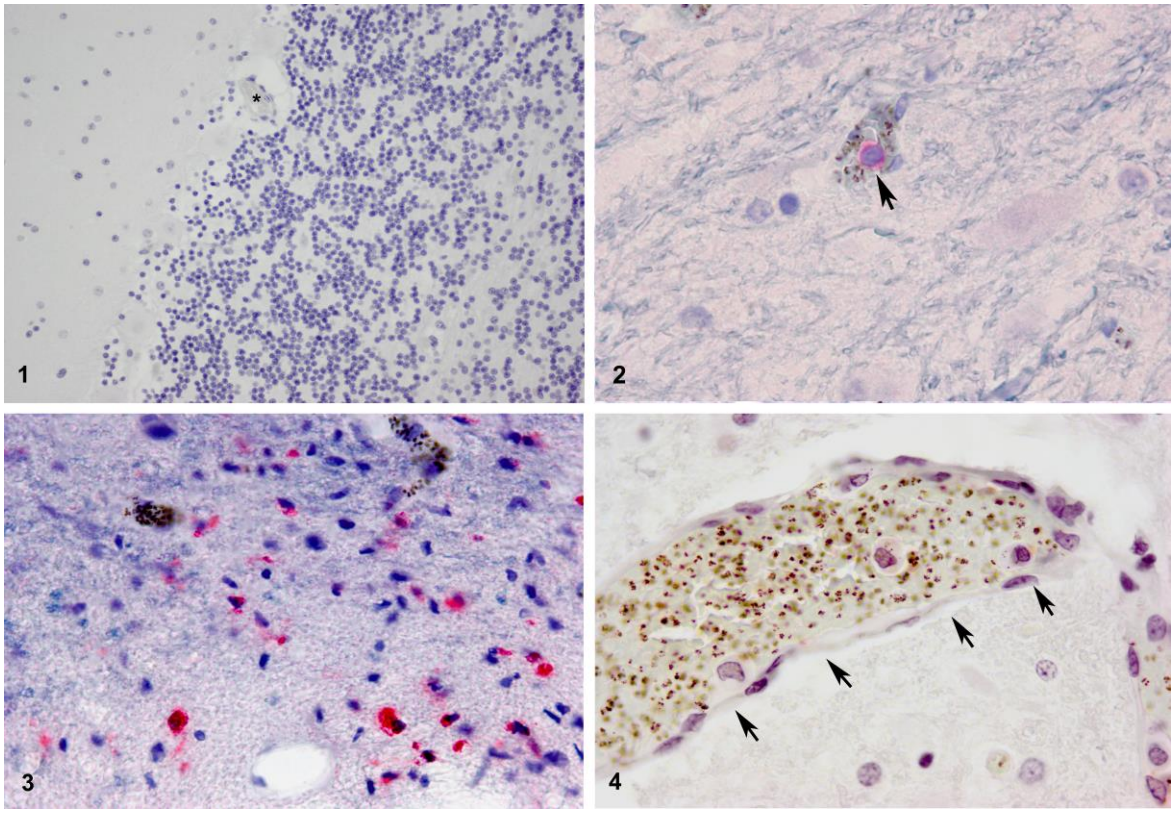

Figure 5.3.1-4. This plate of immunohistochemical photomicrographs includes examples of the different antibodies evaluated in the present study. 5.3.1. This image is a representative negative control image from the cerebellum. There is a small caliber blood vessel bounded by endothelium on the periphery of the granular layer (asterix). CD68 400x. 5.3.2. This photomicrograph demonstrates a single CD3 positive T cell (arrow) within a cerebral microvessel in which hemozoin pigment is observable. CD3 1000x. 5.3.3. is an image in the brain stem in which there are myriad CD68 immunoreactive cells scattered throughout the neuropil. CD68 1000x. 5.3.4. A blood vessel containing innumerable infected erythrocytes with scant CD61 positive platelets and no evidence of fibrin thrombus formation or thrombocyte adherence to the endothelium (vessel outlined by arrows). While there is no immunoreactivity noted within the photomicrograph, strong positive immunostaining was observed in control slides. CD61 1000x.

Immunohistochemical Marker	BS CTRL	C CTRL	BS Exp	C Exp	C Exp 2	Mean C Exp 1&2
CD3	8	2	NA	19	5	
	0	0	NA	25	10	
	6	4	NA	10	5	
	5	1	15	2	2	
	NA	NA	16	6	0	
	NA	NA	8	2	1	
	NA	NA	21	4	NA	
	NA	NA	16	9	NA	
	NA	NA	28	4	NA	
Mean	**4.75**	**1.75**	**17.33**	**9**	**3.83**	**6.93**
CD20	0	0	NA	0	0	
	NA	2	NA	1	NA	
	0	2	NA	1	NA	
	0	0	2	0	0	
	NA	NA	0	0	0	
	NA	NA	1	0	0	
	NA	NA	1	0	NA	
	NA	NA	0	0	NA	
	NA	NA	0	0	NA	
Mean	**0**	**1**	**0.67**	**0.22**	**0**	**0.15**
CD68	22	5	NA	30	1	
	23	5	NA	2	2	
	0	0	NA	21	NA	
	NA	NA	NA	1	NA	
	NA	NA	102	7	0	
	NA	NA	91	25	39	
	NA	NA	137	47	NA	
	NA	NA	190	22	NA	
	NA	NA	120	5	NA	
	NA	NA	146	35	NA	
Mean	**15**	**3.33**	**131**	**19.5**	**10.5**	**16.93**
Fibrinogen*	0	0	NA	1	1	
	NA	0	NA	2	3	
	0	0	NA	3	2	
	0	0	4	3	1	
	NA	0	4	2	1	
	NA	NA	4	2	2	
	NA	NA	5	2	NA	

	NA	NA	4	1	NA	
	NA	NA	4	1	NA	
Mean	**0**	**0**	**4.17**	**1.89**	**1.67**	**1.8**
GFAP**	0	0	NA	3	4	
	NA	0	NA	2	1	
	0	0	NA	2	2	
	0	0	2	2	3	
	NA	0	2	3	2	
	NA	NA	2	3	2	
	NA	NA	2	2	NA	
	NA	NA	2	2	NA	
	NA	NA	3	1	NA	
Mean	**0**	**0**	**2.17**	**2.22**	**2.33**	**2.27**

* Fibrinogen: Overall impression is that microcapillaries are more susceptible to leakage than larger vessels. Additionally, there is uptake of fibrin by perivascular and parenchymal monocytes.

** GFAP: Qualitative/ Loss of fine architecture, swelling, process blunting and increased staining.

Key: BS = Brain Stem; C = Cerebrum; CTRL = Control; Exp = Experimental; NA = Not Available

Table 5.3.1 Quantitative and semi-quantitative analysis of multiple immunohistochemical stains of central nervous system tissues from *P. coatneyi* infected rhesus macaques.

This table contains the data from the evaluation of the CD3, CD20, CD68, GFAP and Fibrinogen immunohistochemical studies. CD61 has been omitted as the results were negative across all experimental animals. In the case of the various cluster of differentiation stains, the numbers represent absolute counts of immunoreactive cells over 20 high powered fields (defined as 400x). The GFAP and Fibrinogen severity scores are primarily qualitative and through assessment of a range of microscopic changes in comparison with control samples, a semi-quantitative score was assessed to each sample. The five-point scoring system consisted of gradation in severity of changes to the neurons, axons and dendrites within a given section in contrast with normal controls as described in Chapter 2. In all cases, stains were conducted in both the brain stem and the cerebrum, however each evaluated animal had two samples stained from the midbrain and as such, mean scores were

analyzed in order to regularize the data. From these, P values were then calculated using the Mann-Whitney test in order to determine statistical significance of both brain stem and cerebral scores in comparison with control and between experimental brain stem samples and experimental cerebral samples.

5.4 **Immunohistohemical Results Interpretation**:

5.4.1 **GFAP:** The immunostaining of GFAP was characterized in tissue from experimental animals in comparison with similar sections of the cerebrum and brain stem in the control animals. The evaluation was primarily qualitative and assessed the fine architecture of the astrocytes and the neuronal processes. Neuronal/axonal injury was characterized based on swelling of the cytoplasm/neuroplasm, dendrites and axons with blunting of the processes and increased uptake of stain. (Figure 5.4.1.1-4)

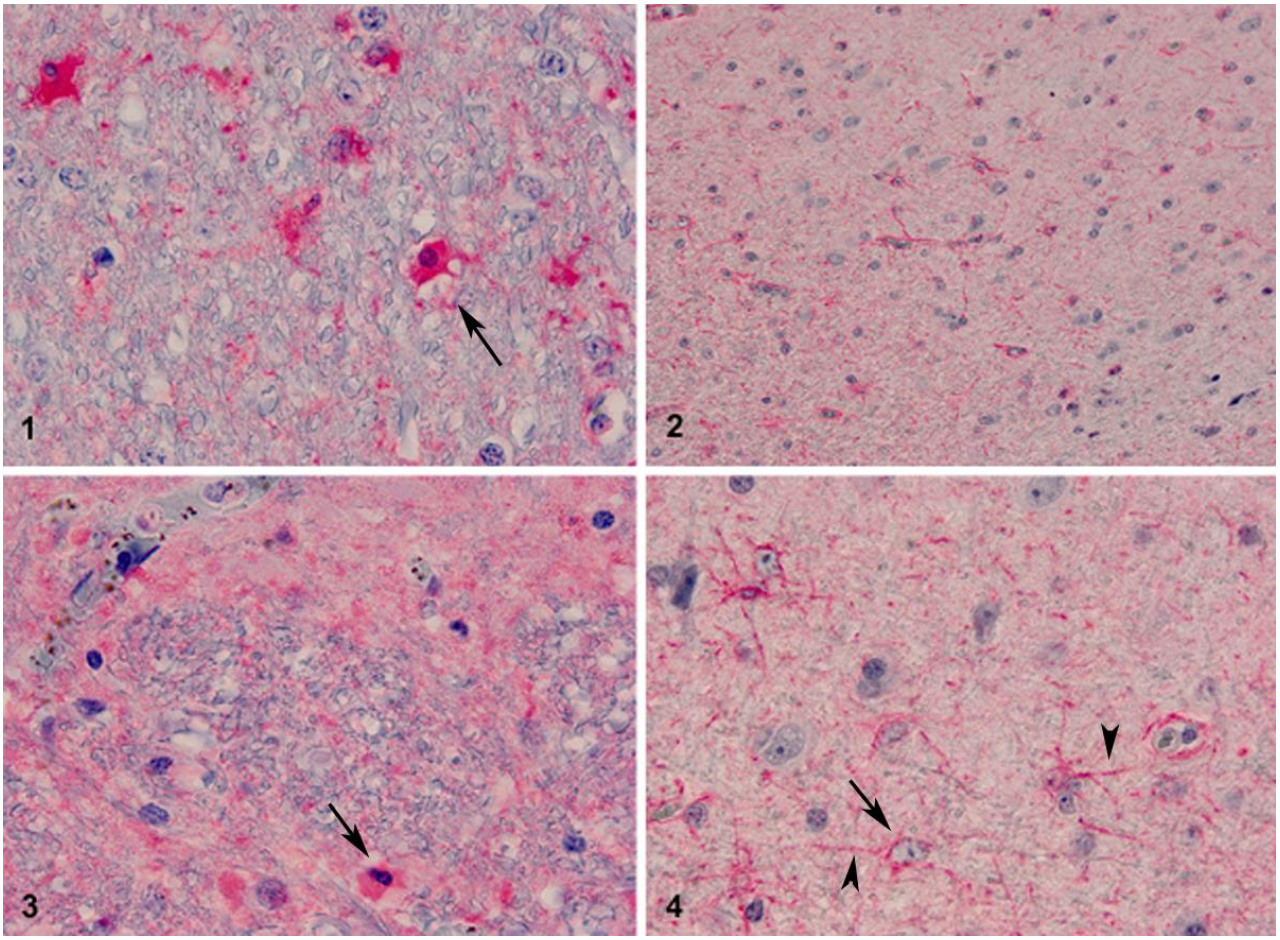

Figure 5.4.1.1-4: GFAP immunostaining patterns. 5.4.1.1 This immunohistochemical photomicrograph of the cerebrum of a P. coatneyi infected rhesus macaque illustrates the loss of the axonal and dendritic fine architecture (arrow), the globular swelling of the soma, blebbing of the cytoplasm and pericellular edema. GFAP 1000x; 5.4.1.2. This is contrasted with the fine fibrillary architecture of a cerebral sample from a control macaque. GFAP 400x. 5.4.1.3. Similarly, in the brain stem, experimental samples stained with GFAP also displayed similar pathological changes to the neurons (arrow). GFAP 1000x; 5.4.1.4. Juxtaposed with control samples of brain stem in which the soma of neurons contains a small amount of uniform cytoplasm (arrow) and thin, interconnecting dendrites (arrowheads). GFAP 1000x.

In all experimental samples, the qualitative observations demonstrated a highly significant change in the fine structure, with loss of detail in the experimental animals suggestive of degenerative, apoptotic or even early necrotic changes. In the case of degeneration, the neurons became swollen with loss of fine processes. There was frequent evidence of peri-cellular neuropil clearing interpreted to be edema. Although apoptosis is primarily an ultrastructural diagnosis, GFAP-stained cells were interpreted to be apoptotic when there was nuclear condensation combined with cytoplasmic blebbing and increased GFAP staining. (Saraste 1999) Finally, those cells characterized as necrotic were typically fragmented, shrunken and angulated with loss of processes. These findings were observed consistently among the experimental animals and a semi-quantitative assessment of the examined sections revealed a significant degree of damage in the infected animals in comparison with the normal control rhesus which represented a baseline. (Figure 5.4.2)

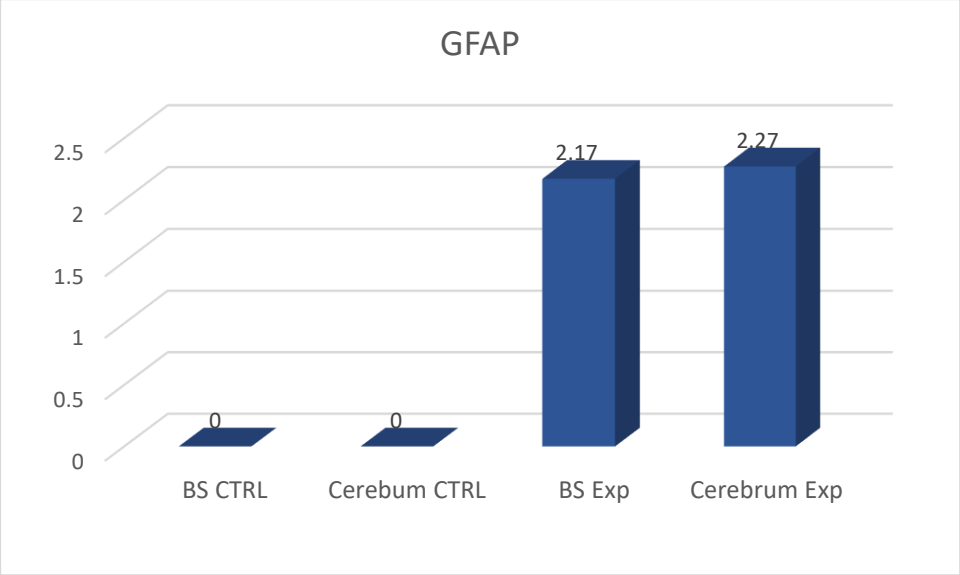

Table Analyzed	GFAP	Table Analyzed	GFAP	Table Analyzed	GFAP
Column B	BS Exp	Column D	C Exp	Column D	C Exp
vs.	vs.	vs.	vs.	vs.	vs.
Column A	BS CTRL	Column C	C CTRL	Column B	BS Exp
Mann Whitney test		Mann Whitney test		Mann Whitney test	
P value	0.0119	P value	0.0005	P value	0.8785
Exact or approximate P value?	Exact	Exact or approximate P value?	Exact	Exact or approximate P value?	Exact
P value summary	*	P value summary	***	P value summary	ns
Significantly different (P < 0.05)?	Yes	Significantly different (P < 0.05)?	Yes	Significantly different (P < 0.05)?	No
One- or two-tailed P value?	Two-tailed	One- or two-tailed P value?	Two-tailed	One- or two-tailed P value?	Two-tailed
Sum of ranks in column A, B	6, 39	Sum of ranks in column C, D	15, 90	Sum of ranks in column B, D	46.5, 73.5
Mann-Whitney U	0	Mann-Whitney U	0	Mann-Whitney U	25.5
Difference between medians		Difference between medians		Difference between medians	
Median of column A	0, n=3	Median of column C	0, n=5	Median of column B	2, n=6
Median of column B	2, n=6	Median of column D	2, n=9	Median of column D	2, n=9
Difference: Actual	2	Difference: Actual	2	Difference: Actual	0
Difference: Hodges-Lehmann	2	Difference: Hodges-Lehmann	2	Difference: Hodges-Lehmann	0

Figure 5.4.2 GFAP staining. Semi-quantitative assessment of the presence of suspected neuronal damage ranked on a severity scale of 0-5 based on a mean calculation of all sections evaluated qualitatively and semi-quantitatively. The criteria involved in the scoring included loss of fine architecture, neuroplasmic swelling, blebbing or fragmentation, process blunting, loss and increased GFAP staining intensity. There was equivalent severity of changes observed in the cerebrum and the brainstem.

Statistical investigation was conducted for each of the immunohistochemical stains using the Mann-Witney U test, 2 tailed, nn parametric, with significance scored as $p<0.05$. In the case of the GFAP, analysis revealed a significant increase in the degree of GFAP expression in experimental animals in both the brain stem ($p<0.001$) and cerebrum ($P<0.012$) in comparison with control samples, however no difference was seen between GFAP expression in the brain stem and the cerebrum within the experimental cohort ($p= 0.878$).

5.4.2 **Fibrinogen:** Fibrinogen staining revealed a similar pattern and was assessed in comparison with the normal controls both qualitatively and semi-quantitatively. Normal control animals had fibrinogen staining uniquely restricted to the lumen of the microvasculature and in no instance extending into the adjacent perivascular space or the neuropil. Conversely, in the experimental SM animals there was consistent and significant fibrinogen staining of cells around the affected vessels, as well as free fibrinogen in the perivascular space and dissecting the neuropil. The staining pattern of fibrinogen in the experimental animals indicated definitive blood-brain barrier leakage when compared with the normal controls. (Figure 5.4.3.) The findings were more significant in the brain stem than in the cerebrum which is consistent with the histopathological findings that severity of pathological features was also greater in the brain stem and the spinal cord than in the cerebrum or cerebellum. (Figure 5.4.4.)

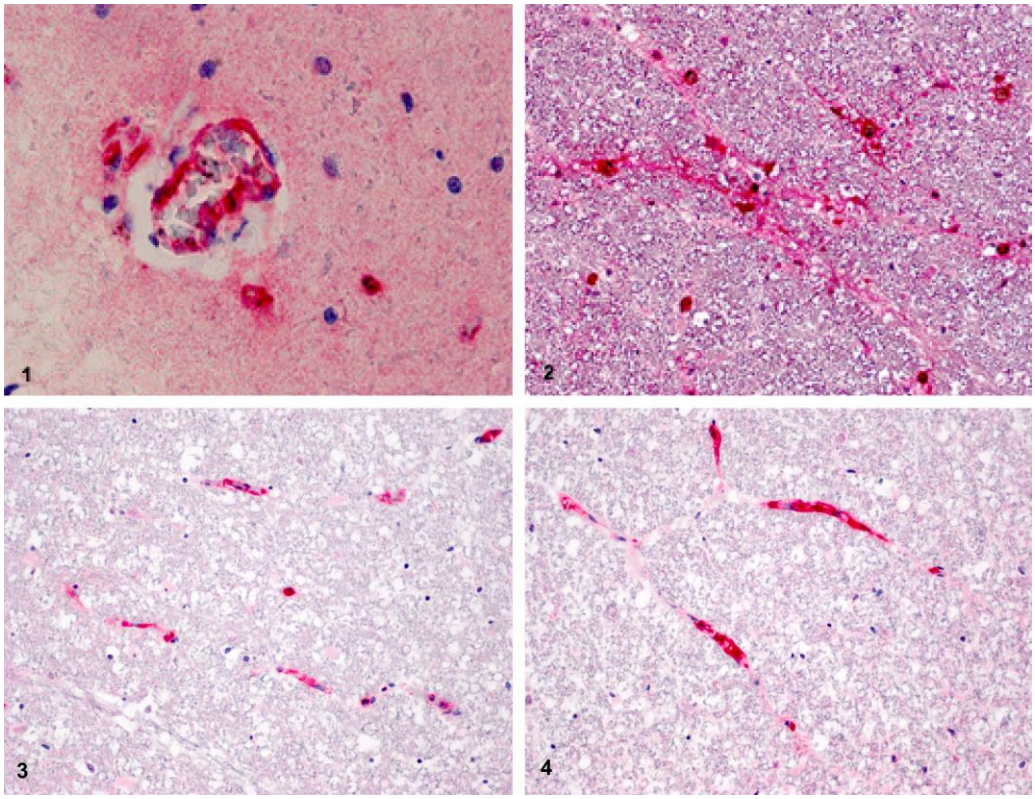

Figure 5.4.3.1-4: Fibrinogen immunostaining patterns. 5.4.3.1. This photomicrograph demonstrates the fibrinogen leakage in a cerebral section from an experimental animal. There is increased generalized neuropil staining as well as immunoreactivity within the endothelium and cells interpreted to be phagocytic cells within the periphery of the leaking vessel. Fibrinogen 1000x. 5.4.3.2. In this sample from the brain stem, there is similar increased immunoreactivity in a generalized, background fashion as well as highlighting the perivascular area and within neighboring cells interpreted to be monocytes/macrophages. Fibrinogen 400x. These two experimental samples are contrasted with controls, 5.4.3.3. in the cerebrum and 5.4.3.4 in the brain stem. Fibrinogen 400x.

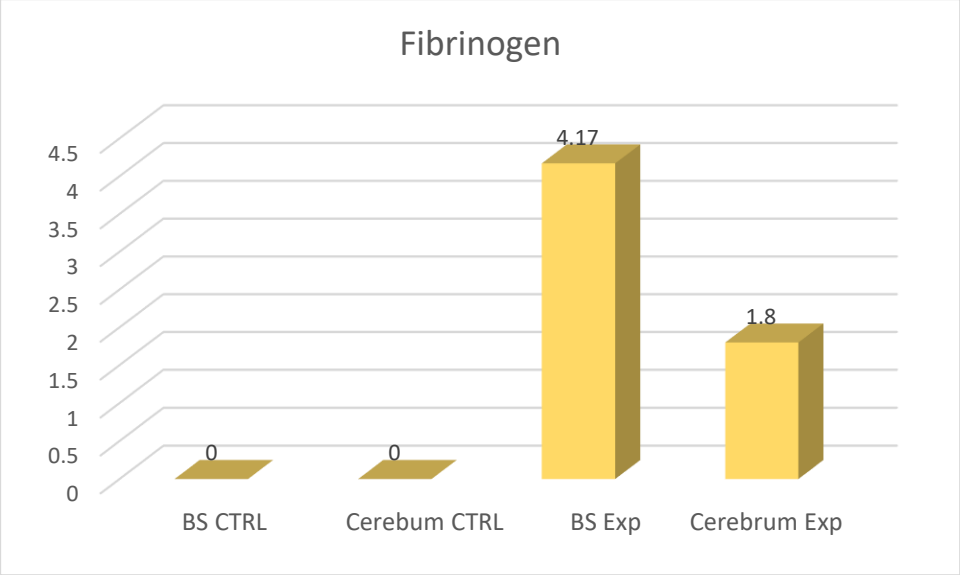

Table Analyzed	Fibrinogen		Table Analyzed	Fibrinogen		Table Analyzed	Fibrinogen
Column B	BS Exp		Column D	C exp		Column D	C exp
vs.	vs.		vs.	vs.		vs.	vs.
Column A	BS ctrl		Column C	C ctrl		Column B	BS Exp
Mann Whitney test			Mann Whitney test			Mann Whitney test	
P value	0.0119		P value	0.0010		P value	0.0002
Exact or approximate P value?	Exact		Exact or approximate P value?	Exact		Exact or approximate P value?	Exact
P value summary	*		P value summary	***		P value summary	***
Significantly different (P < 0.05)?	Yes		Significantly different (P < 0.05)?	Yes		Significantly different (P < 0.05)?	Yes
One- or two-tailed P value?	Two-tailed		One- or two-tailed P value?	Two-tailed		One- or two-tailed P value?	Two-tailed
Sum of ranks in column A, B	6, 39		Sum of ranks in column C, D	15, 90		Sum of ranks in column B, D	75, 45
Mann-Whitney U	0		Mann-Whitney U	0		Mann-Whitney U	0
Difference between medians			Difference between medians			Difference between medians	
Median of column A	0, n=3		Median of column C	0, n=5		Median of column B	4, n=6
Median of column B	4, n=6		Median of column D	2, n=9		Median of column D	2, n=9
Difference: Actual	4		Difference: Actual	2		Difference: Actual	-2
Difference: Hodges-Lehmann	4		Difference: Hodges-Lehmann	2		Difference: Hodges-Lehmann	-2.5

Figure 5.4.4 Fibrinogen staining. Semi-quantitative assessment of the integrity of the blood brain barrier, ranked on a scale of 0-5, within the cerebrum and the brain stem when compared with normal control sections. There was increased leakage (and theorized associated injury) noted in the brainstem in comparison with the cerebrum. Calculations of P values demonstrated statistical significance between brain stem and controls, cerebrum and controls as well as demonstrating increased fibrinogen leakage in the brain stem in comparison with the cerebrum.

5.4.3 **CD3:** CD3 staining demonstrated a predilection for T-cell localization in the brain stem in comparison with the cerebrum. However, the mean number of CD3-positive cells in the evaluated experimental sections was significantly higher in both the cerebrum and the brain stem when contrasted with the normal background levels in the central nervous system of the rhesus macaque control animals. The highest count was 28 cells (per 20 HPF) observed to be immunoreactive in one of the brain stems of the experimental animals.

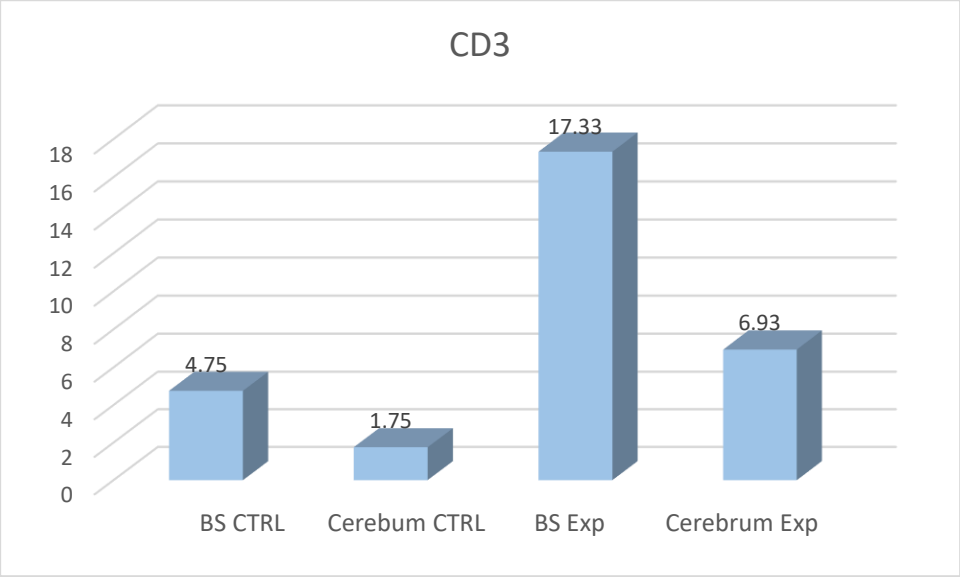

Table Analyzed	CD3	Table Analyzed	CD3	Table Analyzed	CD3
Column B	BS Exp	Column D	C exp	Column D	C exp
vs.	vs.	vs.	vs.	vs.	vs.
Column A	BS ctrl	Column C	C ctrl	Column B	BS Exp
Mann Whitney test		Mann Whitney test		Mann Whitney test	
P value	0.0143	P value	0.0573	P value	0.0108
Exact or approximate P value?	Exact	Exact or approximate P value?	Exact	Exact or approximate P value?	Exact
P value summary	*	P value summary	ns	P value summary	*
Significantly different (P < 0.05)?	Yes	Significantly different (P < 0.05)?	No	Significantly different (P < 0.05)?	Yes
One- or two-tailed P value?	Two-tailed	One- or two-tailed P value?	Two-tailed	One- or two-tailed P value?	Two-tailed
Sum of ranks in column A, B	10.5, 44.5	Sum of ranks in column C, D	15.5, 75.5	Sum of ranks in column B, D	69, 51
Mann-Whitney U	0.5	Mann-Whitney U	5.5	Mann-Whitney U	6
Difference between medians		Difference between medians		Difference between medians	
Median of column A	5.5, n=4	Median of column C	1.5, n=4	Median of column B	16, n=6
Median of column B	16, n=6	Median of column D	4, n=9	Median of column D	4, n=9
Difference: Actual	10.5	Difference: Actual	2.5	Difference: Actual	-12
Difference: Hodges-Lehmann	11	Difference: Hodges-Lehmann	3.25	Difference: Hodges-Lehmann	-12

Figure 5.4.5 CD3 staining. Quantitative assessment of the number of CD3-positive cells counted in experimental and control sections of the brain stem and the cerebrum over 20 high powered fields (400x). There was statistical significance in the increased infiltration of CD3 immunoreactive cells within the *P. coatneyi*-infected animals in the brain stem but not in the cerebrum. Furthermore, there was an almost 3-fold higher number in the brain stem in comparison to the cerebrum in experimental animals.

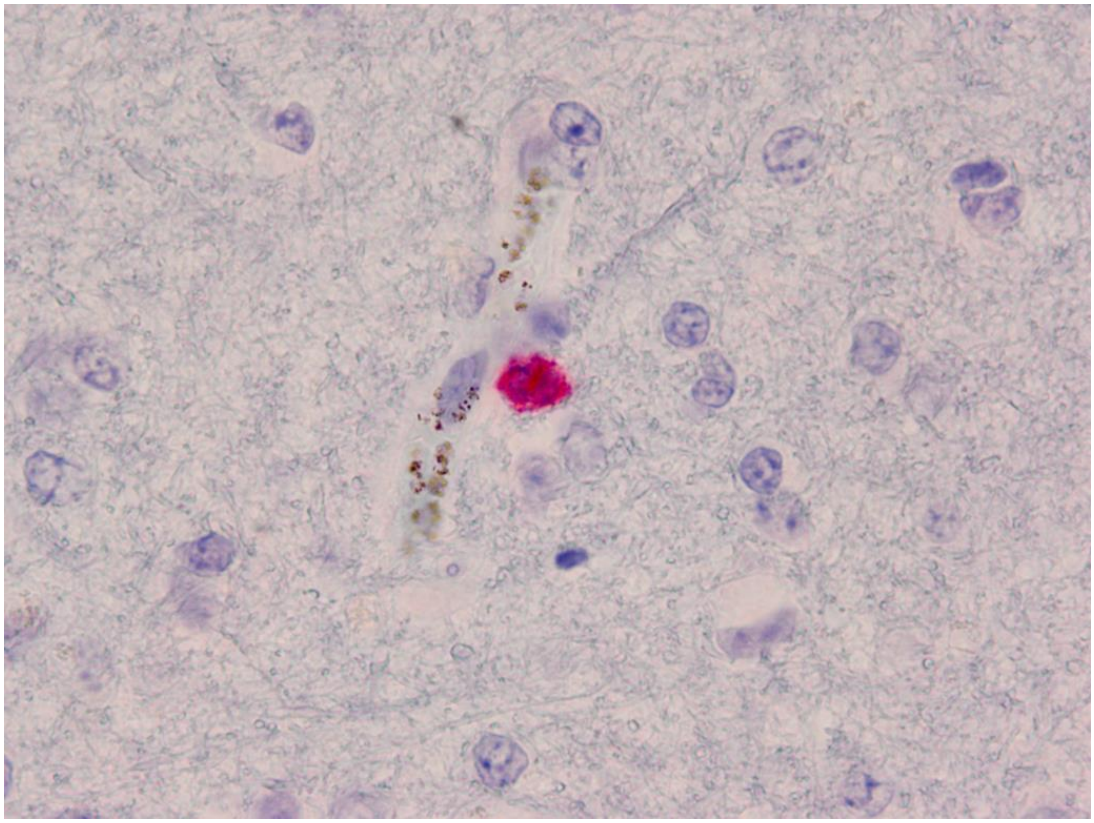

Figure 5.4.6 CD3 immunostaining patterns. CD3 immunohistochemical photomicrograph demonstrating a strongly immunoreactive cell adjacent to a cerebral capillary with notable infected erythrocyte sequestration. CD3 1000x.

5.4.4 **CD20:** Quantitative assessment of the number of CD20-positive cells counted in experimental and control sections of the brain stem and the cerebrum over 20 high powered fields (400x). There

was no significant difference in the frequency of CD20 immunoreactive cells between tissues of control and experimental animals. In both cases, the maximum number of CD20 immunoreactive cells observed over 20 high powered fields was 2, and in most instances no cells were positive for the marker. No statistically significant difference was calculated between experimental or control animals in either the brain stem or the cerebrum. CD20 staining demonstrated that B cells do not show any increase within brain microvessels, which is a common feature with both human and murine disease. In the macaque model, there were only rare cells observed to be immunoreactive, and in those cases there was no significant difference between experimental and control animals nor between the brain stem and the cerebrum.

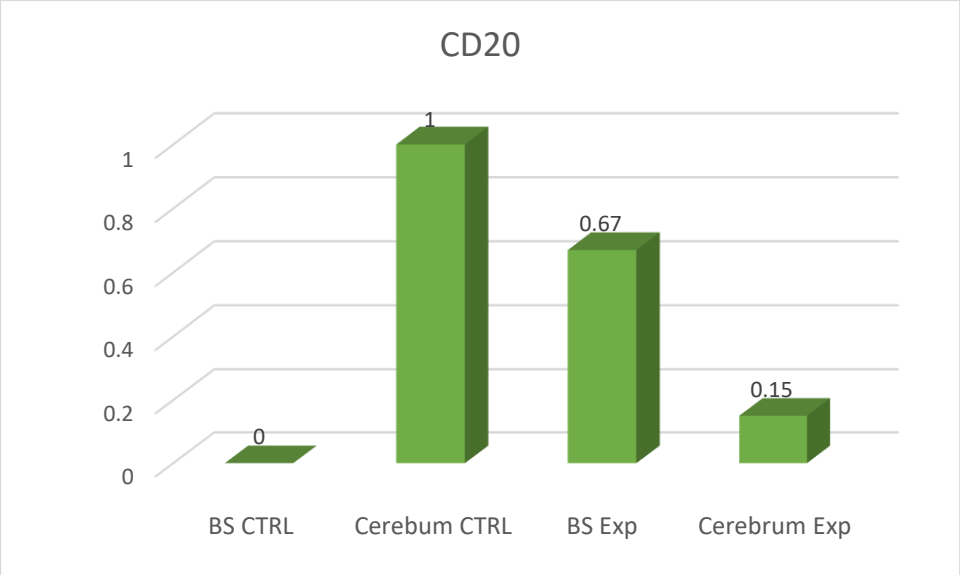

Table Analyzed	CD20		Table Analyzed	CD20		Table Analyzed	CD20
Column B	BS Exp		Column D	C Exp		Column D	C Exp
vs.	vs.		vs.	vs.		vs.	vs.
Column A	BS CTRL		Column C	C CTRL		Column B	BS Exp
Mann Whitney test			Mann Whitney test			Mann Whitney test	
P value	0.3929		P value	0.2783		P value	0.2328
Exact or approximate P value?	Exact		Exact or approximate P value?	Exact		Exact or approximate P value?	Exact
P value summary	ns		P value summary	ns		P value summary	ns
Significantly different (P < 0.05)?	No		Significantly different (P < 0.05)?	No		Significantly different (P < 0.05)?	No
One- or two-tailed P value?	Two-tailed		One- or two-tailed P value?	Two-		One- or two-tailed P value?	Two-

				tailed			tailed
Sum of ranks in column A, B	10.5, 34.5		Sum of ranks in column C, D	35, 56		Sum of ranks in column B, D	56.5, 63.5
Mann-Whitney U	4.5		Mann-Whitney U	11		Mann-Whitney U	18.5
Difference between medians			Difference between medians			Difference between medians	
Median of column A	0, n=3		Median of column C	1, n=4		Median of column B	0.5, n=6
Median of column B	0.5, n=6		Median of column D	0, n=9		Median of column D	0, n=9
Difference: Actual	0.5		Difference: Actual	-1		Difference: Actual	-0.5
Difference: Hodges-Lehmann	0.5		Difference: Hodges-Lehmann	-0.5		Difference: Hodges-Lehmann	0

Figure 5.4.7 CD20 staining. Quantitative assessment of the number of CD20-positive cells counted in experimental and control sections of the brain stem and the cerebrum over 20 high powered fields (400x). There was no statistical significance as to increased infiltration of CD20 immunoreactive cells within the *P. coatneyi*-infected animals in the brain stem or the cerebrum in the samples evaluated.

5.4.5 **CD61:** CD61 immunoreactivity, within the microvasculature of the cerebrum, cerebellum, brain stem and spinal cord, was negative in both control and experimental animals in all cases examined. This was consistent with the preponderance of cases in which there were no observable aggregates of thrombocytes or fibrin thrombi in the central nervous system. Those cases in which thrombi were noted in the brain during histopathological examination, they were observed as correlating with mural fibrinoid vasculitis. Considering the low numbers of total cases examined with immunohistochemistry, the few cases with such pathology were excluded from immunohistochemical analysis to avoid skewing the results.

5.4.6 **CD68:** CD68 immunohistochemistry demonstrated a notable increase of CD68 positive cells observed within the central nervous system of experimental animals in comparison with control animals. As with CD3, immunoreactivity of CD68-positive cells in infected monkeys appeared to have a proclivity for the brain stem, with one animal having a count of 190 immunoreactive cells in 20 high powered fields (400x). This resulted in a 10-fold increase in immunoreactive cells in the brain stem of *P. coatneyi* infected animals in contrast with controls. The calculated P value demonstrated statistical

significance. While the cerebrum had significantly fewer cells which were positive for the marker in comparison with the brain stem, there was still a 5-fold difference between the control and experimental animals, however calculation of the p value demonstrated that there was no statistical significance in the cerebrum. These findings suggest strong evidence that within the brain stem, CD68 positive monocytes/macrophages play an important role in the neuropathology of *P. coatneyi* induced disease in rhesus macaques.

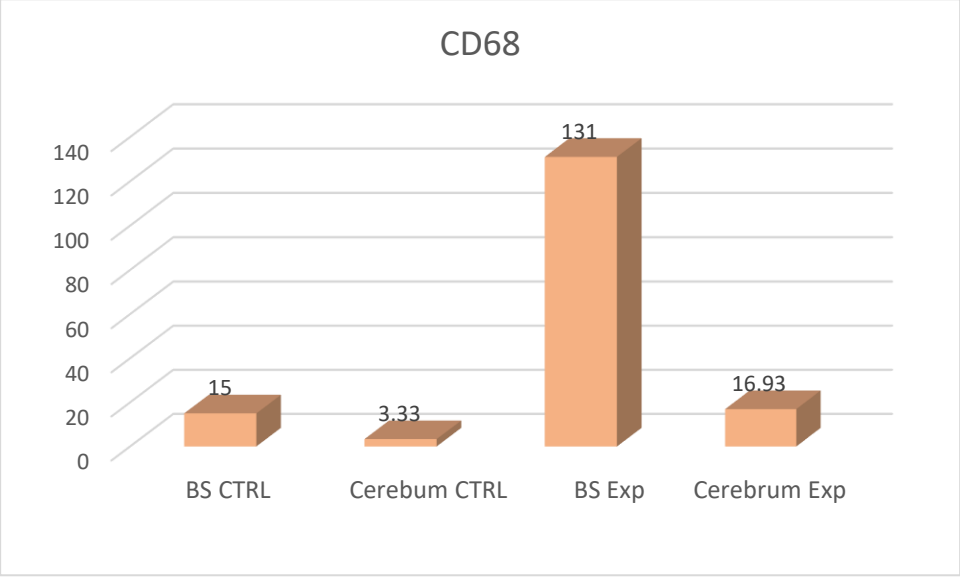

Table Analyzed	CD68	Table Analyzed	CD68	Table Analyzed	CD68
Column B	BS Exp	Column D	C Exp	Column D	C Exp
vs.	vs.	vs.	vs.	vs.	vs.
Column A	BS CTRL	Column C	C CTRL	Column B	BS Exp
Mann Whitney test		Mann Whitney test		Mann Whitney test	
P value	0.0238	P value	0.2203	P value	0.0002
Exact or approximate P value?	Exact	Exact or approximate P value?	Exact	Exact or approximate P value?	Exact
P value summary	*	P value summary	ns	P value summary	***
Significantly different (P < 0.05)?	Yes	Significantly different (P < 0.05)?	No	Significantly different (P < 0.05)?	Yes
One- or two-tailed P value?	Two-tailed	One- or two-tailed P value?	Two-tailed	One- or two-tailed P value?	Two-tailed
Sum of ranks in column A, B	6, 39	Sum of ranks in column C, D	13, 78	Sum of ranks in column B, D	81, 55
Mann-Whitney U	0	Mann-Whitney U	7	Mann-Whitney U	0
Difference between medians		Difference between medians		Difference between medians	
Median of column A	22, n=3	Median of column C	5, n=3	Median of column B	128.5, n=6
Median of column B	128.5, n=6	Median of column D	18.25, n=10	Median of column D	18.25, n=10
Difference: Actual	106.5	Difference: Actual	13.25	Difference: Actual	-110.3
Difference: Hodges-Lehmann	114.5	Difference: Hodges-Lehmann	15.75	Difference: Hodges-Lehmann	-108

Figure 5.4.8 CD68 staining. Quantitative assessment of the number of CD68-positive cells counted in experimental and control sections of the brain stem and the cerebrum over 20 high powered fields (400x). There was statistical significance in the increased infiltration of CD68 immunoreactive cells within the *P. coatneyi*-infected animals in the brain stem but not in the cerebrum. Furthermore, there was an approximately 8-fold increase of immunoreactive cells in the brain stem in comparison to the cerebrum in experimental animals.

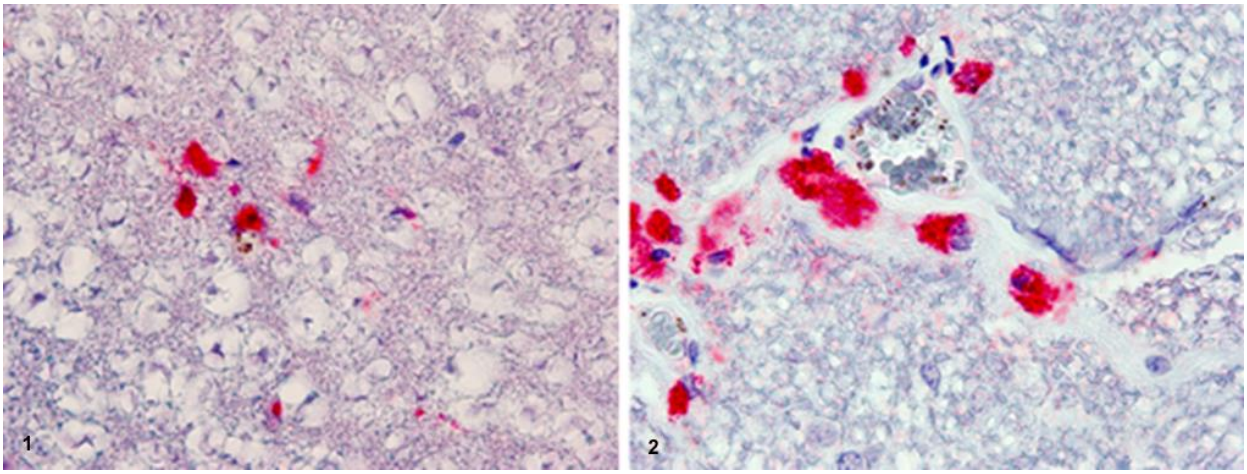

Figure 5.4.9.1-2: CD68 immunostaining patterns. These CD68 immunohistochemical photomicrographs demonstrate aggregates of immunoreactive cells in the brain stem adjacent to a small focus of hemozoin pigment (left) and a high number of strongly immunoreactive cells adjacent to a cerebral capillary with notable infected erythrocyte sequestration (right). CD68 1000x.

5.4.7 **B-APP**: Only a select few samples stained with βAPP and Cleaed caspase 3 were considered to be diagnostic. In those instances, there was observable evidence of cellular staining with both antigens. However due to the small sample size it is not possible to infer statistical significance. As such, for the purpose of this dissertation, the valuation of both antigens must be limited to a qualitative assessment.

βAPP staining was far more intense and frequent in those sections evaluated from experimental animals in comparison with controls. Staining was most frequently cytoplasmic and the most powerful immunoreactivity was noted in the neurons and the Purkinje cells, which correlates well to the histopathological observations which noted a significant increase in damage in these cells in comparison with the control animals. (Figure 5.4.10.1-4)

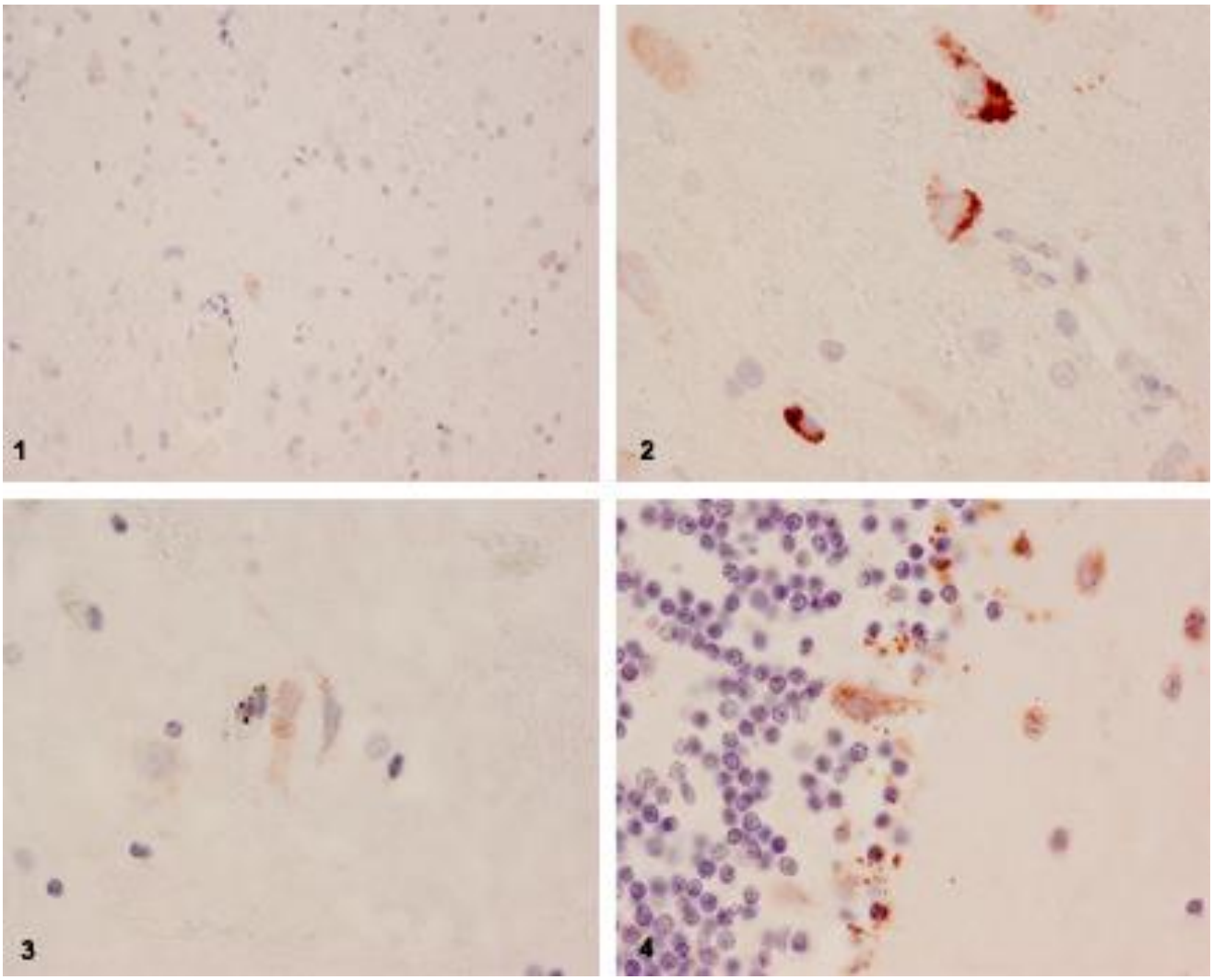

Figure 5.4.10.1-4: βAPP immunostaining patterns: This immunohistochemical photomicrographic plate illustrates βAPP staining in multiple locations within the central nervous system. 5.4.10.1. Cerebrum, control. Background staining was typically very faint as can be noted in the cerebral control sample. βAPP 200x; 5.4.10.2. In this image from the cerebrum of an infected animal, multiple neurons are strongly immunoreactive, suggestive of injury. βAPP 400x. 5.4.10.3. This

photomicrograph demonstrates immunoreactivity in the brain stem of an experimental sample. βAPP 400x. 5.4.10.4. In contrast with the control animal, the immunoreactivity of the Purkinje cells and astrocytes from the cerebellum of an experimental animal is extremely pronounced. This photomicrograph, combined with those from other segments of the central nervous system in contrast with the control demonstrate βAPP staining consistent with significant neuronal and Purkinje cell injury and the histopathological observations. βAPP 1000x.

5.4.8 **Cleaved caspase 3**: Cleaved caspase 3 staining was only successful in a select few animals and as such it is even less significant that the βAPP immunohistochemistry. In the few cases in which staining was successful, scattered cells, often adjacent to microvasculature with iRBC sequestration, demonstrated the intense immunoreactivity. (Figure 5.4.11)

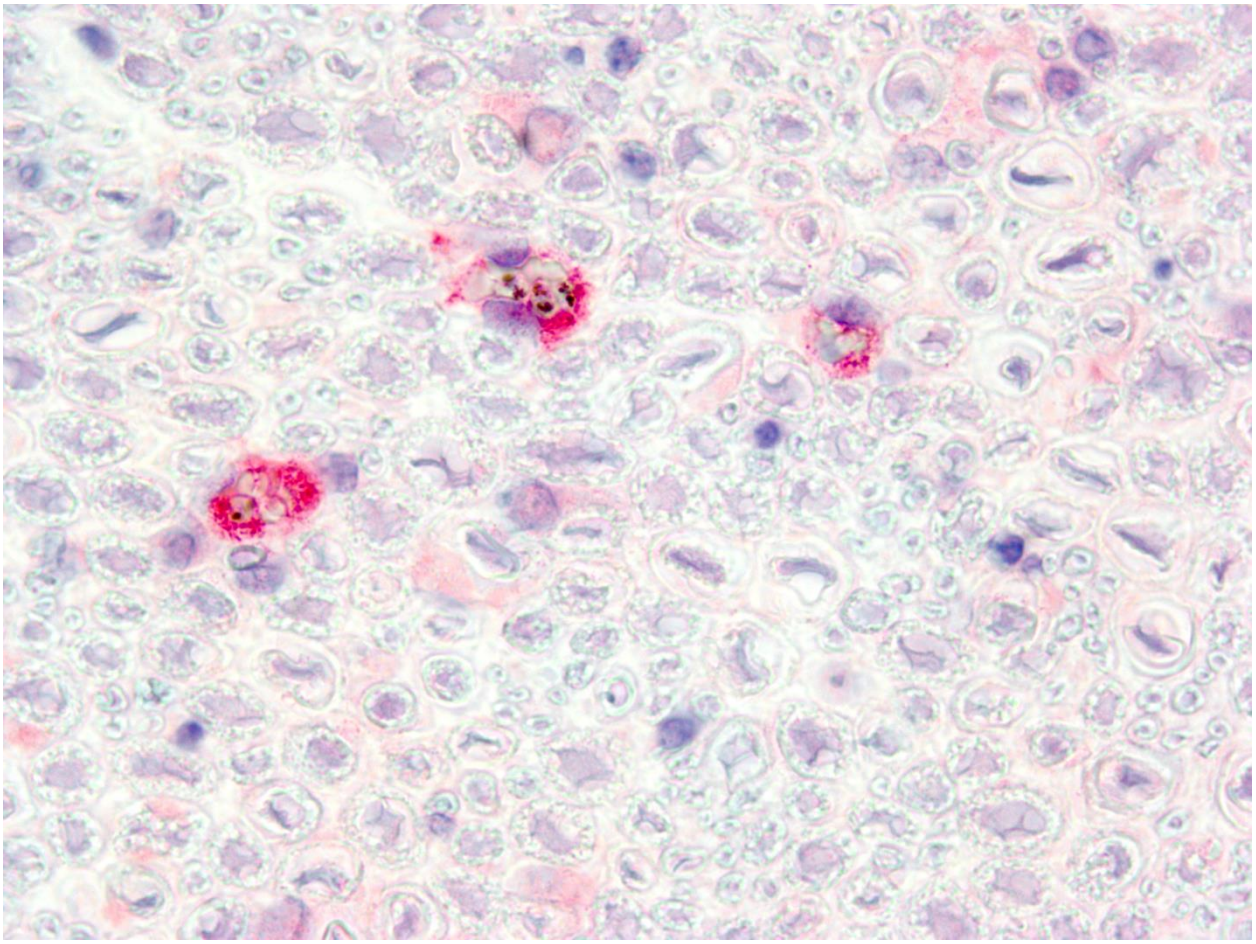

Figure 5.4.11: Cleaved caspase 3 immunostaining patterns. In this photomicrograph, several cells conforming to the periphery of brain stem capillaries are immunoreactive to Cleaved caspase 3. The limited number of successful immunoreactive slides precludes definitive statements as to the value of these findings, or even to the qualitative significance. Cleaved caspase 3 is intended on highlighting those cells undergoing apoptotic change due to its role in DNA fragmentation and in chromatin condensation, and as such it may be posited that the illustrated cells which appear to be vascular endothelium are injured cells undergoing apoptosis, however the nuclei appear to be within normal limits and as such do not conform to the typical microscopic findings that are correlated with apoptosis. As such, this is purely speculation due to the low numbers of cases in which Cleaved caspase 3 was considered to be diagnostic. The image is included purely to illustrate the need for further evaluation and elucidation of this immunohistochemical marker and of the role of apoptosis in *P. coatneyi* pathogenesis in general. Cleaved caspase 3 1000x.

5.5 **CSF Measurement of Blood-Brain Barrier integrity and Tau protein release**:

As an adjunct to the immunohistochemical analyses, we examined the ratio of albumin in cerebrospinal fluid (CSF) to serum, thereby establishing an albumin index (AI) which served as a measure of BBB permeability in the *P. coatneyi* infected macaques. The use of AI to measure BBB permeability is well established in a number of different CNS diseases, and has been used to study BBB function in both adult and pediatric CM cases. (Brown 2000; Brown 2001) CSF (and serum) taken from *P. coatneyi* infected macaques at post mortem was compared with control animals and a cohort of Simian Human Immunodeficiency Virus (SHIV)-infected animals from a collaborator's study.

5.5.1 Blood-brain barrier integrity and brain injury in *P. coatneyi*-infected monkeys:

The ratio of albumin in cerebrospinal fluid to serum served as an albumin index determining BBB permeability in infected monkeys. The CSF and serum albumin levels were evaluated using an albumin ELISA kit. As described above, we employed three cohorts of macaques: control group (n=2), 12-week post SHIV-infection Indian origin rhesus macaques from the same AFRIMS colony (n=12), and *P. coatneyi*-infected monkeys (n=12). The control animals were normal rhesus macaques who were euthanized due to non-infectious disease or trauma. The SHIV-infected monkeys were euthanized at 12 weeks post-inoculation, and immediately post-euthanasia serum and CSF samples were collected. For *P. coatneyi*-infected monkeys, nine out of 12 monkeys were derived from the methylene blue clinical trial study described in Chapter 7, in which the animals were euthanized once 15% parasitemia and pre-determined clinical symptomology and clinical pathologic criteria were reached. As with the SHIV and control animals, serum and CSF samples were collected immediately after euthanasia. The AI and albumin concentrations in CSF and serum are shown in Table 5.5.1. The normal range of AI is $\leq 5 \times 10^{-3}$. All monkeys in control and SHIV groups (median 1.115×10^{-3}, interquartile range $1.65\text{-}3.49 \times 10^{-3}$) were in the control range (median 0.975×10^{-3}, interquartile range $0.74\text{-}1.21 \times 10^{-3}$). Only one *P. coatneyi*-infected monkey had an abnormal albumin ratio calculated at 10.99×10^{-3}. However, the AI of *P. coatneyi*-infected monkeys (median 2.45×10^{-3}, interquartile range $1.65\text{-}3.49 \times 10^{-3}$) was significantly higher in comparison with that in SHIV-infected monkeys using Kruskal-Wallis test, one-way ANOVA multiple comparison as shown in Figure 5.5.2.1. While the majority of the *P. coatneyi* infected animals had CSF albumin index levels that were empirically higher than those observed in the two control animals, these findings were not statistically significant using the Kruskal-Wallis test. While, this would appear to fail to support the immunohistochemical fibrinogen analyses which demonstrated visual evidence of BBB leakage and suggested potential injury to the microvascular endothelium, the statistically significant variance between the SHIV animals and the *P. coatneyi* animals appears to lend support, especially in light of having only two control animals. If nothing else, the AI study bears repeating with greater numbers of samples.

Monkey group	Monkey ID	Methylene blue treatment (mg/kg of monkey weight)	Serum albumin (μg/ml)	CSF albumin (μg/ml)	AI (10^{-3})	Tau (total) (pg/ml)
Control	R541	none	39600	48	1.212	298
	R626	none	37600	28	0.745	139
P. coatneyi	DA831	none	42400	96	2.264	622
	DA923	none	36800	138	3.750	410
	R519	none	38000	82	2.158	730
	R130	6	29200	80	2.740	286
	R453	6	40800	28	0.686	168
	R761	6	28000	74	2.643	198
	DA977	10	30800	84	2.727	348
	R420	10	32400	124	3.827	520
	R711*	10	30400	334	10.987	294
	R121	16	36800	80	2.174	462
	R338	16	28400	42	1.479	1435
	R745	16	31200	34	1.090	242
SHIV	R323		40000	34	0.850	174
	R333		43600	32	0.734	ND
	R441		32800	36	1.098	171
	R450		44400	50	1.126	242
	R514		44400	26	0.586	ND
	R522		45600	40	0.877	268
	R546		31600	102	3.228	ND
	R607		39200	50	1.276	197
	R629		44000	26	0.591	185
	R708		35200	40	1.136	209
	R731		36000	88	2.444	168
	R759		45200	58	1.283	196

AI =Albumin index; ND = not determined due to inadequate sample volume. *AI of this monkey (R711) was abnormal.

Table 5.5.1 Albumin index and CSF Tau levels in monkeys by disease or control groups.

5.5.2 <u>CSF Tau (total) protein measurement as a biomarker for neuro-axonal degeneration</u>:

Tau proteins stabilize microtubules, with a specific function relating to axonal microtubules. The proteins are abundant in neurons of the central nervous system, while being expressed at much lower levels in oligodendrocytes and astrocytes. Certain neuropathologies of humans such as Alzheimer's disease have been reported to cause Tau proteins to undergo transformative pathologies

resulting in an inability to properly stabilize microtubules. Due to the relative specificity of Tau to the neurons within the CNS, the protein is an excellent marker for neuronal damage.

Nine CSF samples of SHIV-infected monkeys were available as a comparative diseased cohort for the Tau assay. The CSF Tau concentration in *P. coatneyi*-infected monkeys (median 379 pg/ml, interquartile range 253-597 pg/ml) was significantly increased in comparison to the SHIV groups (median 196 pg/ml, interquartile range 172-226 pg/ml), but interestingly were not significantly different when compared with the control cohort (median 219 pg/ml, interquartile range 139-298 pg/ml) as described in Figure 5.5.2.

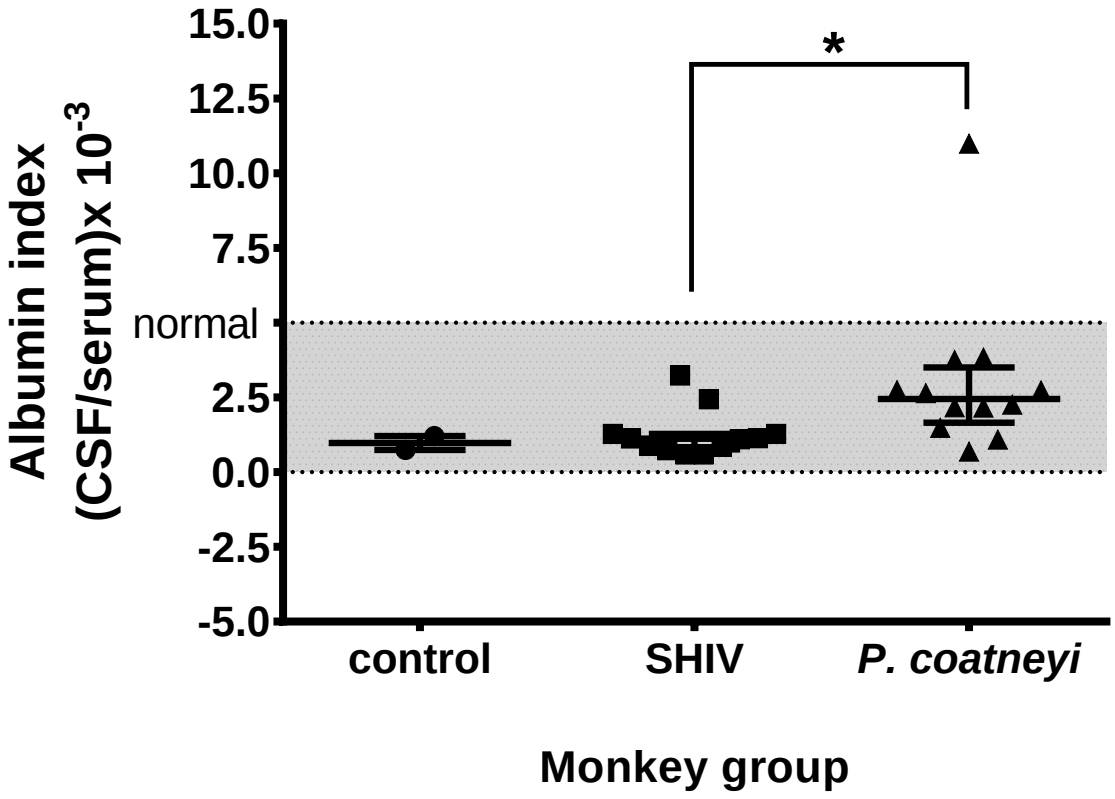

Figure 5.5.2.1 Albumin index (AI) as a measure of blood-brain barrier function in different groups of monkeys. Middle lines indicate median; error bars represent interquartile range (IQR). Each dot represents an individual monkey. Shaded area shows normal values of AI. Asterisk (*) indicates significant difference at $p \leq 0.05$ by Kruskal-Wallis test.

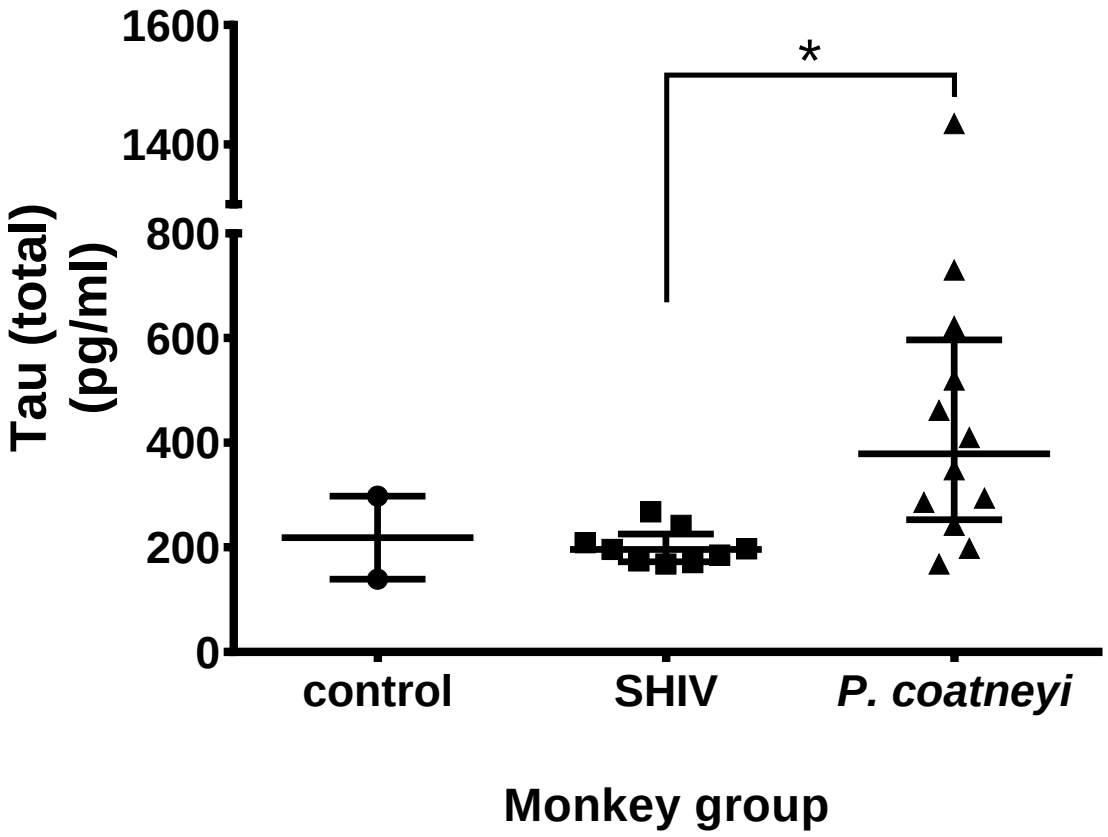

Figure 5.5.2.2 Tau (total) protein in different groups of monkeys. Middle lines indicate median; error bars represent interquartile range (IQR). Each dot represents an individual monkey. (*) indicates significant difference at $p \leq 0.05$ by Kruskal-Wallis test.

5.5.3 Pro-inflammatory cytokine response in the central nervous system of *P. coatneyi*-infected rhesus macaques:

As a preliminary study to identify the spectrum of cytokine release into the CSF during experimental severe malaria, a panel of cytokine levels was measured using multiplex ELISA on cerebrospinal fluid from (n=3) *P. coatneyi*-infected monkeys and compared with the same controls and SHIV-infected animals used in the determination of an albumin index.

In order to evaluate the pro-inflammatory response in the central nervous system in *P. coatneyi*-infected rhesus, 23 cytokines were evaluated using multiplex assays. Six cytokines, including G-CSF, IL-6, IL-8, IL-15, MCP-1, TGF-α, were found to be expressed in greater amounts in comparison with both control and SHIV-infected macaque specimens which were run concurrently (Figure 5.5.3.1; Table 5.5.3.1). The levels of G-CSF, IL-8, MCP-1 and TGF-α in *P. coatneyi*-infected rhesus were markedly increased in comparison to both control and SHIV-infected monkey groups, as well as there being a very large increase in IL-6 and IL-15 noted between *P. coatneyi* and SHIV groups. Statistical significance was assessed between the different groups when possible using the Kruskal-Wallis test, however based on the number of samples for both the controls and SHIV groups that were out of range (OOR) as well as the very small sample size for the *P. coatneyi* cohort, the significance needs to be taken with a high degree of caution.

This preliminary cytokine profile demonstrated a range of interesting findings suggestive of activation of angiogenic pathways (TGF-alpha, IL-8) suggestive of endothelial injury, proinflammatory and specific inflammatory cell proliferation pathways (IL-6, IL-15 and MCP-1) and bone marrow stimulation (G-CSF). Of note is that several of the cytokine which demonstrated increased profiles are either produced by macrophages and/or T-cells (IL-6, IL-8, TGF-alpha), are chemoattractants for macrophages (MCP-1) or are involved in proliferation of cells observed to be involved in the pathogenesis of *P. coatneyi* induced disease (IL-15: Induces NK cell and T-cell proliferation). These findings support the data elucidated in the earlier portion of this chapter relating to the Immunohistochemical profiles which noted increases in CD68 and CD3 positive cells.

This data provides an initial foundation and while these preliminary findings are of interest, significantly more intensive study is required prior to contributing to the comparative description of *P. coatneyi* and its correlation to severe and cerebral malaria in humans.

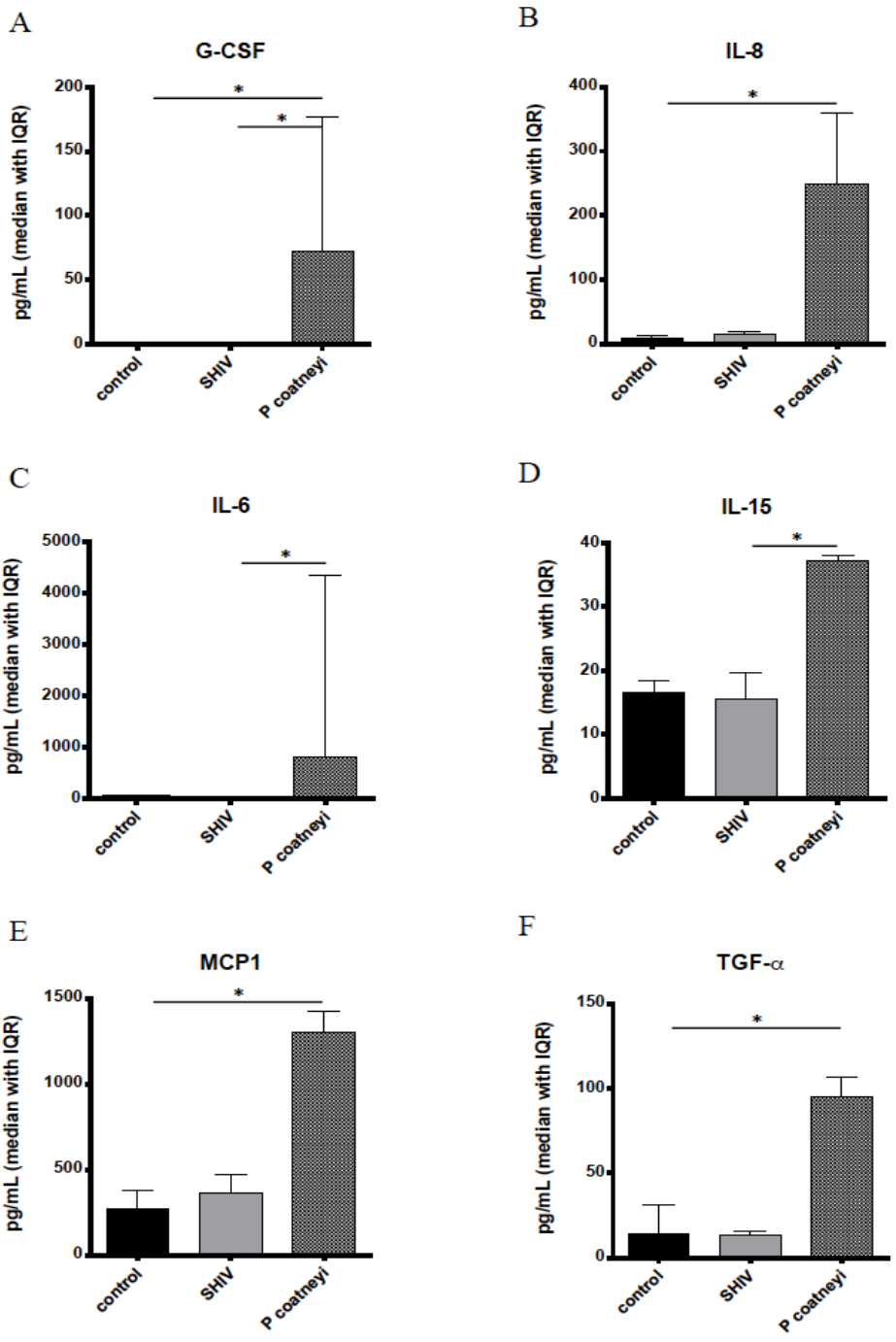

Figure 5.5.3.1. Pro-inflammatory cytokine responses in the CSF of different disease groups. Bar graphs represent median; error bars represent interquartile range (IQR). (*) indicates significant difference at $p \leq 0.05$ by Kruskal-Wallis test.

Monkey group	Monkey ID	G-CSF (pg/ml)	IL-6 (pg/ml)	IL-8 (pg/ml)	IL-15 (pg/ml)	MCP-1 (pg/ml)	TGF-α (pg/ml)
Control	R541	OOR	2.47	13.22	12.20	274.91	13.88
	R616	OOR	OOR	5.61	18.54	223.84	12.35
	R626	OOR	OOR	7.06	16.61	379.01	31.02
Median (IQR)		0 (0-0)	18 (16-24)	7.06 (5.61-13.22)	16.61 (12.2-18.54)	274.9 (223.8-379)	12.35 (12.35-31.02)
P. coatneyi	DA831	13.19	107.985	141.50	23.75	742.51	74.10
	DA923	72.43	98.655	247.99	37.29	1427.98	94.65
	R519	176.57	500.765	359.96	38.05	1302.24	106.40
Median (IQR)		72.43 (13.19-176.6)	795 (688-4354)	248 (141.5-360)	37.29 (23.75-38.05)	1302 (742.5-1428)	94.65 (74.1-106.4)
SHIV	R323	OOR	OOR	13.68	14.63	428.48	13.33
	R333	OOR	OOR	18.53	29.17	523.89	22.91
	R441	OOR	OOR	7.61	14.13	305.32	11.59
	R450	OOR	2.47	18.41	12.97	603.61	11.87
	R514	OOR	2.59	12.56	20.02	397.37	26.74
	R522	OOR	OOR	8.70	17.33	294.00	14.15
	R546	OOR	OOR	11.30	21.18	299.38	10.51
	R607	OOR	OOR	18.97	18.81	360.33	15.43
	R629	OOR	2.24	17.67	15.73	482.84	11.33
	R708	OOR	2.24	12.64	14.80	331.90	15.93
	R731	OOR	OOR	9.76	12.47	364.17	9.48
	R759	OOR	3.26	16.61	15.29	283.64	12.82
Median (IQR)		0 (0-0)	2.47 (2.24-2.925)	13.16 (10.15-18.23)	15.51 (14.26-19.72)	362.3 (300.9-469.3)	13.08 (11.4-15.81)

OOR = Out of range; G-CSF = Granulocyte-colony stimulating factor; IL-6 = Interleukin-6; IL-8 = Interleukin-8; IL-15 = Interleukin-15; MCP-1 = Monocyte chemoattractant protein-1; TGF-α = Transforming growth factor alpha.

Table 5.5.3.1. CSF cytokine levels in monkeys by disease groups. Comparison of 6 cytokines in the SHIV animal cohort, compared with 3 animals from the *P. coatneyi* study and contrasting those with samples from normal controls.

5.6 **Discussion**:

The histopathological findings described in the previous chapter, and those which will be subsequently illustrated in the chapter on ultrastructure, set the stage regarding the hypothesis of multifactorial nervous system injury in the *P. coatneyi*-Rhesus macaque model. The subtle changes associated with perivascular edema, neuronal degeneration, necrosis, rare hemorrhage and slight

leukocytic infiltrates required confirmation. The overall analysis of Blood Brain Barrier integrity through the immunohistochemical study of fibrinogen and GFAP, combined with the preliminary work conducted into the molecular mechanisms of confirmation of the hypothesis of neuronal injury as well as the immunohistochemical assessment of different populations of leukocytes in the central nervous system have shed light on the pathogenesis of the disease, and reinforced the findings from the other modalities we employed.

CD3, CD20, CD61 and CD68 immunostaining allowed for characterization of the immunological profile of those leukocytes which are involved in acute *P. coatneyi* severe malaria. The analysis identified an increase in CD3 positive T-cells as well as a marked increase in the CD68 positive monocyte/macrophage response. T-cells have been reported to drive pathogenesis in murine cerebral malaria as have monocytes (Finley 1982; Grau 1986), however with the exception of the occasional finding of Dürck's granulomas in the white matter of the brain, inflammation is not a significant part of the histopathology in humans. (Boonpucknavig 1990; Hunt 2006; Medana 2001; Turner 1997)

Furthermore, CD20 positive B-cells and CD61 positive platelets were minimal and were consistent with background findings in control animals. As such, the immunological profile of *P. coatneyi* appears to deviate somewhat from that observed in humans. Additionally, while microvascular fibrin thrombi have been described in histopathological studies of cerebral malaria in humans (Boonpucknavig 1990; Krishnan 2004; MacPherson 1985), other studies have posited that the immune system's response to malarial infection may include a suppression of plasminogen activation and therefore, a decrease of thrombotic activity. (Pongponratn 1985; Thuma 2011) The absence of a significant platelet driven response in macaques may correlate to this hypothesized pathogenesis in humans.

Difficulties with β-APP restricted the degree with which we can interpret the findings in the few cases that were diagnostic, however in those instances, there was a notable and marked increase in immunoreactivity in neurons, astrocytes and Purkinje cells in comparison with control animals.

Further investigation of the degree of axonal injury and neuronal damage is warranted based on these preliminary findings. Furthermore, the retina is a tissue which was not examined in this study, but which, due to the histopathological findings of ganglion cell loss, merits additional evaluation with β-APP immunohistochemistry. The problems associated with refining the protocol for use of β-APP in the macaque limited the number of samples which could be examined and as such no retinal samples were evaluated.

GFAP and fibrinogen immunostaining showed marked increases based on qualitative assessment of the fine architecture in the former and presence of fibrinogen immunoreactivity outside of the vessels and within phagocytic cells in the latter, both of which imply damage to the blood brain barrier and a degree of vascular leakage. This finding is theoretically supported by the ELIZA Albumin Index study in which there was an understated increase in the severe malaria cohort in comparison with the SHIV group and empirically in comparison with the two control animals. The increase, while subtle, demonstrated significance when contrasted with the other disease cohort. This is similar to what has been reported in humans, where the BBB changes as judged by AI were increased in malaria patients compared to controls, but much less than other infectious diseases characterized by massive inflammatory destruction to the BBB, such as tuberculosis, Cryptococcosis and acute bacterial meningitis. (Brown 2000; Gitau 2005; Mturi 2008)

There has been significant research examining the cytokine responses associated with the immunopathology of Plasmodial infections. (Aubouy 2002; Baptista 1997; Brown 1999; Day 1999; de Kossodo 1993; el Nashar 2002; Kern 1989; Peyron 1994; Prakash 2006; Newton 1998; Rodrigues-da-Silva 2014) Unfortunately there remains a substantial amount of debate as to the specific correlation of the cytokine levels and their association with the pathophysiology of observed disease in humans. Severe malaria resulting from *P. falciparum* infection has been proposed to be modulated by the increases in circulating TNF-α, IL-1 and IL-6 and IL-8. (Akanmori 2000; Brown 1999) TNF-α levels in *P. falciparum* infections have been demonstrated to be higher in cases of fatal cerebral malaria than in those cases that are not fatal. (Grau 1989; Kwiatkowski 1990) Interferon-gamma responses are felt to

be key to development of cerebral symptoms in murine experimental CM (Hunt 2014), but the relevance of this to human disease is not established. The attempted reversal of circulating cytokine levels in both murine models and humans, using specific anti-TNF antibodies, has not been successful in a limited clinical setting. Additionally, high plasma levels of TNF-α, IL-1 and IL-6 have been described in human patients with uncomplicated malaria, which underscores the remaining need to understand the specific role of these cytokines in the pathogenesis of disease. (Baptista 1997)

Chemokines have not been as intensely examined as cytokines in severe malaria, but there is still abundant work that has been conducted examining the association between increased chemokine production and severe malaria. In particular, these have examined T cell expressed and secreted RANTES, monocyte chemotactic protein (MCP)-1, macrophage inflammatory protein (MIP)-1α, MIP-1β, and IL-8 among others. These are theorized to play important roles in the pathogenesis of malaria induced disease as they are powerful chemoattractants for monocytes which in turn generate increased production and secretion of TNF-α and IL-6. (Armah 2007)

While the sample size was quite small, it is notable that the CSF samples from *P. coatneyi*-infected rhesus yielded no difference in concentration in the majority of the cytokines assessed in the Multiplex assay. Specifically, TNF-α, VEGF, IL-1b, IL-2, IL-4, IL-5, IL-12, IL-13, IL-17a, IL-18, MIP-1a and MIP-b did not show any differentiation of expression between control, SHIV and *P. coatneyi* cohorts. Interferon-gamma, IL-1a and IL-15 demonstrated very slight increases but lacked statistical significance, while a single *P. coatneyi*-infected animal was noted to have an elevation of IL-10. Overall, these findings are surprising due to the fact that TNF-α has been implicated in the neuropathology of a range of diseases to include severe and cerebral malaria. Interpretation is difficult since the cytokine appears to have both physiological roles in the normal brain and pathological roles in the diseased central nervous system. (Montgomery 2012; Olmos 2014) Under pathological conditions, large amounts of TNF-α can be secreted from microglia and astrocytes which significantly contribute to the neuroinflammatory response that is associated with several neurological disorders. (Montgomery 2012; Wyss-Coray 2002) Two different mechanisms have been

elucidated in which TNF-α potentiates glutamate-mediated cytotoxicity. This can occur either indirectly through the inhibition of glutamate transport on astrocytes, or directly through the increase of glutamate receptor localization to synapses. (Olmos 2014) In malaria, TNF-α is theorized to be formed and secreted by host cells subsequent to exposure to a range of plasmodial antigens. This increase in the secretion of TNF-α is felt to be associated with overexpression of adhesion molecules, potentiating the sequestration phenomenon and augmenting the severity of disease. (Gimenez 2003; Shaffer 1991)

There is little literature examining the CSF cytokine profiles of severe malaria; rather, most studies have evaluated the serum profiles. In one of the few studies that included CSF, Ghanaian children were sampled and wide range of cytokines were evaluated. The results found that IL-1ra, IL-8, IP-10, PDGFbb, MIP-1beta, Fas-L, sTNF-R1, and sTNF-R2 were significantly increased in the cohort of children that had died of cerebral malaria in comparison with both those who died of severe malaria and a control group who died of causes unrelated to malaria. (Armah 2007) As such, the current findings in CSF of the experimental rhesus model may represent an alternate profile for severe malaria disease presentation, although the correlation with human disease appears to be piecemeal with MCP-1, IL-6 and IL-8 being the most consistent parallels to human falciparum disease. Increases in IL-1ra and INF-γ, while not statistically significant, are worth noting and considered for further study.

5.7 **Summary**:

The synopsis of immunohistochemical findings in the dissertation consisted of the following: There was significantly greater evidence of pathology observed in the brain stem than comparable studies in the cerebrum, a finding which was consistent with the observations noted in the histopathology chapter. Furthermore, in comparison with control animals, *P. coatneyi* infected animals had increased numbers of CD-68 positive monocyte/macrophages/glial cells within the

central nervous system. This was also observed to be the case in the increased numbers of CD-3 positive T cells. However, and of interest, was the fact that there were no significant increases in CD-20 B cells or CD-61 platelets observed in the CNS.

Brain blood barrier injury was demonstrated through both the increased fibrinogen leakage, with perivascular uptake and astrocyte end feet absorption. The strong GFAP immunoreactivity and highlighting of marked structural changes also argues for a degree of BBB injury, which parallels that which has been demonstrated in autopsy samples from humans having succumbed to *P. falciparum* induced cerebral malaria. The remaining two immunohistochemical assays proved difficult to manage and as such, the limited data only permits speculation rather than assertion. Beta APP immunoreactivity demonstrated initial evidence of focal axonal injury within brainstem and spinal cord, while cleaved Caspase 3 suggested in those rare instances in which the staining worked that there was evidence of apoptotic endothelium in CNS samples.

Additional examination of the blood brain barrier integrity was performed through the CSF/Plasma Albumin index in which the *P. coatneyi* infected animals were compared with both normal controls and SHIV chimera infected rhesus. There was a statistically significant increase over SHIV chimera cohort, and empirical evidence of an increased in comparison with control animals, further supporting the hypothesis of BBB injury in *P. coatneyi* infection.

Chapter 6: Ultrastructural Studies

6.1 **Introduction**:

From the initial description of the parasite as part of a survey of blood parasites in cynomolgus macaques (*Macaca fascicularis*) in the Philippines (Eyles 1962), there has been significant interest in the use of the plasmodium as a comparative model for severe *P. falciparum* induced malaria, and those varied studies have described the morphological and ultrastructural features of the parasite and the infected erythrocyte. (Aikawa 1992; Aikawa 1992; Coatney 1971; Eyles 1963; Kawai 1993; Maeno 1993, Moreno 2013; Tegoshi 1993) While these reports have described the ultrastructure of the *P. coatneyi* parasite, they were typically conducted in a very limited number of animals, and the focus remained on the phenotypic alterations of the infected erythrocyte without describing the parasite host interaction or the tissue specific pathology of the disease. As such, there is a dearth of comparative information relating the pathogenesis of *P. coatneyi* with the tissue pathology observed and described in *P. falciparum*.

Ultrastructural pathology studies in human patients dying of *P. falciparum* were the first to detail the close interaction of parasitized erythrocytes with vascular endothelial cells via electron dense knob protein structures on the infected erythrocyte surface. (Luse 1971) Subsequently EM studies were used to quantitate sequestration within different organs, in order to link post mortem patterns of organ specific sequestration with pre-mortem clinical symptoms, such as coma, renal failure, liver and lung dysfunction. (Aikawa 1988; MacPerson 1985; Pongponratn 2003; Nakazawa 1995; Nguangsangiam 2007; Sein 1993)

P. coatneyi has a range of biological features that it shares with *P. falciparum* as well as several important distinguishing phenotypic traits. There is evidence of microvascular cytoadherence, with the formation of rosettes between infected erythrocytes and uninfected red blood cells and several early reports have described the development of electron dense knobs on the cell surface of infected erythrocytes which have been purported to be involved in cytoadhesion and have been

described ultrastructurally. (Aikawa 1992; Kilejian 1977; Lombardini 2015) Both *P. falciparum* and *P. coatneyi* undergo deep vascular sequestration of red blood cells infected with trophozoites and schizonts. (Desowitz 1969; MacPherson 1985; Pongponratn 1991; Sein & Brown 1993; Smith 1996)

P. coatneyi has been reported as causing both natural and experimentally-induced disease in a variety of non-human primate species. (Kawai 1993; Kawai 1998; Lombardini 2015; Moreno 2013; Sein & Brown 1993; Smith 1996) The cynomolgus macaque is described as being one of the natural hosts of the parasite and it is theorized may have coevolved resulting in reduced clinical disease in comparison with experimental infections in the rhesus or Japanese macaques. (Kawai 1993; Kawai 1995; Kawai 1998; Lombardini 2015; Moreno 2013) Tissue pathology associated with *P. coatney*i infection in the rhesus macaque is variable and likely is dependent on the genetic heterogenicity of the infected population, degree of blood parasitemia, coinfection with other agents, immune status, age and overall health of the animals. (Lombardini 2015)

In this part of the thesis, the ultrastructural features of *P. coatneyi* infected red blood cells and their in-situ interaction with host tissues were examined and compared to that of *P. falciparum* infections in humans. Following novel observations of the type of knob structures identified in vivo, further examination of the surface of the *P. coatneyi* infected erythrocyte were conducted using both scanning and atomic force microscopy. These techniques allow closer examination and quantitative studies on the knob and calveolar structures on the infected red cell surface. (Aikawa 1997)

6.2 **Results**:

6.2.1 **Light microscopic findings**:

Microscopically, the earliest stage identified in tissue was the ring stage present in the cytoplasm of infected erythrocytes. As the parasite matured, the more spherical trophozoite stage could be identified comprised of a single nucleus and a food vacuole often containing hemozoin crystals. Trophozoite growth in *P. coatneyi* is associated with nuclear division followed by schizogony which results in the formation of 16 to 20 merozoites. The mature schizonts appeared to occur

primarily in the deep vasculature. This process is termed sequestration and involves cytoadherence of the infected erythrocytes to both the vascular endothelium and/or to other infected and uninfected erythrocytes. These features are similar to those described of *P. falciparum.* (Aikawa 1975; Aikawa 1983; Aikawa 1985; Aikawa 1988; Aikawa 1988; Atkinson 1990; Bannister 2000; Barnwell 1990; Carlson 1993; Handunnetti 1989; Kilejian 1977)

6.2.2 **Ultrastructural findings in Post Mortem Tissues**:

Examination of a minimum of five grids per animal from three selected tissues (brain, kidney and heart) from multiple experimental animals (n=15), using transmission electron microscopy, allowed for evaluation of the distribution of infected red blood cells (iRBC) within the deep microvasculature. There was very strong synchrony of parasite stage of maturation and as such, the vast majority of the observed parasites were trophozoites at various stages of development. Only a relatively few mature schizonts and ring forms were observed. In all three tissues, iRBCs were identified in both large and small blood vessels with no obvious difference in the number of iRBCs between tissues (Fig 1a-c). Similar appearances were recorded in the three tissues examined with large numbers of iRBCs observed within the blood vessels of the heart, kidney and brain in all animals examined (Fig 1a, b, c).

The smaller blood vessels were typically tightly packed with a mixture of uninfected and infected erythrocytes (Fig 1a-c). While the majority of infected cells had a single parasite, a number had two or more parasites (Fig 1c). The parasites were located within a parasitophorous vacuole limited by a unit membrane. Trophozoites appeared to increase in size, developing from stages with a single nucleus (Fig 1e) to stages with multiple nuclei and finally into mature schizonts (Fig 3a). Food vacuoles were initially small but increased in size into large vacuoles containing a number of hemozoin crystals (Fig 2b, 3a). The few mature schizonts observed were comprised of multiple merozoites, with apical rhoptries and a posterior nucleus, centered around a body of residual cytoplasm containing food vacuoles filled with hemozoin crystals (Figure 3a). The erythrocytic

cytoplasm frequently contained numbers of circular or curved bilayered channels interpreted as serpentine cleft-like vesicular structures with a narrow electron lucent lumen (Figure 2b insert). However, the stereotypical Maurer's clefts running parallel to the RBC plasmalemma were not observed. Erythrocyte infection is associated with profound changes in the shape of the iRBCs. The majority of iRBCs within small blood vessels were more spherical in shape with a relatively regular outline (Fig 2a, b). However, others show marked deformation of shape consisting of irregular cytoplasmic protrusions giving the infected cells a more flattened, crenated appearance (Figure 3b, c). The surface of the less deformed cells appeared relatively smooth (Fig 2a, b). A feature of all iRBCs was the presence of a number of caveolae, small circular invaginations with an electron dense coating which measured approximately 90nm in diameter (Fig 2a, b, c). Additionally, in the more distorted cells there appeared to be a variable number of blebs or excrescences consistent with knob formation. These knob-like structures are approximately 70-90 nm in diameter (Fig 2c, e, h). On closer inspection, while some possessed some electron dense material beneath the plasmalemma as previously described (Fig 2c), the majority appeared to lack the clearly defined sub-plasma membrane electron dense material (Fig 2e, f). However, there did appear to be plaques of electron dense material associated with the iRBC plasmalemma but lacking the protuberance (Fig 2d). The majority of iRBCs appeared to have relatively few knobs, and those that were noted were randomly distributed.

In small vessels, there was often a tight association between the iRBC and the endothelial cells (Fig 2b), which resulted in evidence of margination of iRBCs along the luminal wall of the affected vessels. When examined in detail there appeared to be close apposition between the iRBC plasmalemma and the plasmalemma of the endothelial cells with possible areas showing connection via proteinaceous material (Fig 2b, g). While in the majority of cases, knob-like protuberances were absent from such areas, they were observed on occasion and in these cases, proteinaceous material connecting the knob to the surface was observed (Fig 2h) Also, there was evidence of limited microvillus formation by the endothelial cells with the cytoplasmic process protruding into

invaginations of the iRBC surface (Fig 2f). In the larger vessels, where the RBCs were more loosely packed, it was often possible to observe features consistent with posited auto-agglutination (Fig 3b) and rosette formation (Fig 3c). This was characterized by adhesion between both iRBCs and between RBCs and iRBCs. The iRBCs in this situation showed more severe shape changes which allowed for increased interdigitation between cells. Interestingly, there was less evidence of cytoadherence between iRBCs and the endothelium in such vessels. While both ultrastructural and light microscopic evaluation of the tissues noted perivascular edema, and a small degree of perivascular hemorrhage in cerebral samples, no examples of vessel rupture were observed by electron microscopy, although several endothelial cells showed some degenerative changes. There did appear to lucent and vacuolated areas around cerebral vessels which was interpreted to be edema. Within the vessels, a number of macrophages and neutrophils were observed and certain macrophages appear to have phagocytised packets of malarial pigment (Fig 3d). This was consistently observed in the renal samples with a concentration noted in glomeruli. However, there was no evidence of electron dense deposits within the basement membrane or other pathological changes observed in the glomeruli (Fig 1c).

Frequently, the close association between the iRBCs and either the endothelium or other infected erythrocytes or uninfected cells, which was interpreted as cytoadherence, resulted in the occlusion of microvasculature which is proposed to represent one of the most significant aspects of the pathogenesis of cerebral malaria. The cytoadherance to the endothelium was often observed as margination of infected erythrocytes (Fig 4a), resulting in a decreased vascular lumen and suspected disruption of blood flood. When compounded by the distortion of the infected erythrocytes and either autoagglutination or rosette formation (Fig 4b), the resultant sludging of the blood and promotion of Virchow's triad (Factors leading to thrombosis, including hypercoagulability, hemodynamic changes such as stasis or increased turbulence and endothelial injury or dysfunction) lends to a hypothesis of decreased oxygen delivery and hypoxic and/or anoxic tissue injury. SEM

images of blood from the infected animals also demonstrated binding between infected and uninfected erythrocytes (Fig 4c and 4d).

6.2.3 **Structure of iRBCs from ex vivo blood samples in both Splenectomized and Spleen-intact Animals**:

The observation of anomalies on the structure of the knobs described above in splenectomized animals was unexpected. Therefore, to see if this was a phenomenon arising from the use splenectomized experimental animals (eg. modulation of cytoadherence within an infection due to the lack of selection for splenic clearance), blood was obtained from two spleen intact animals infected with *P. coatneyi* and was examined by both TEM and SEM. These animals underwent cure and thus survived infection. In these blood samples, it was observed that the iRBCs could be identified by a markedly irregular outline (Fig 1a, e). By TEM and SEM, the surface of the iRBCs showed the formation of variable numbers of caveolae and knob-like structures (Fig 5a, e). The structure of the caveolae with the invagination of the plasmalemma with underlying electron dense material could be seen by TEM (Fig 5d) and appeared as surface pores by SEM (Fig 5f). Detailed examination of the knob-like structures revealed circular electron dense plaques beneath the plasmalemma shown in longitudinal section (Fig 5b) and tangential section (Fig 5c). The knobs could be identified in SEM as slightly raised circular electron lucent structures (Fig 5e, f). The SEM images illustrated the relatively random distribution of the knob (Fig 5e, f).

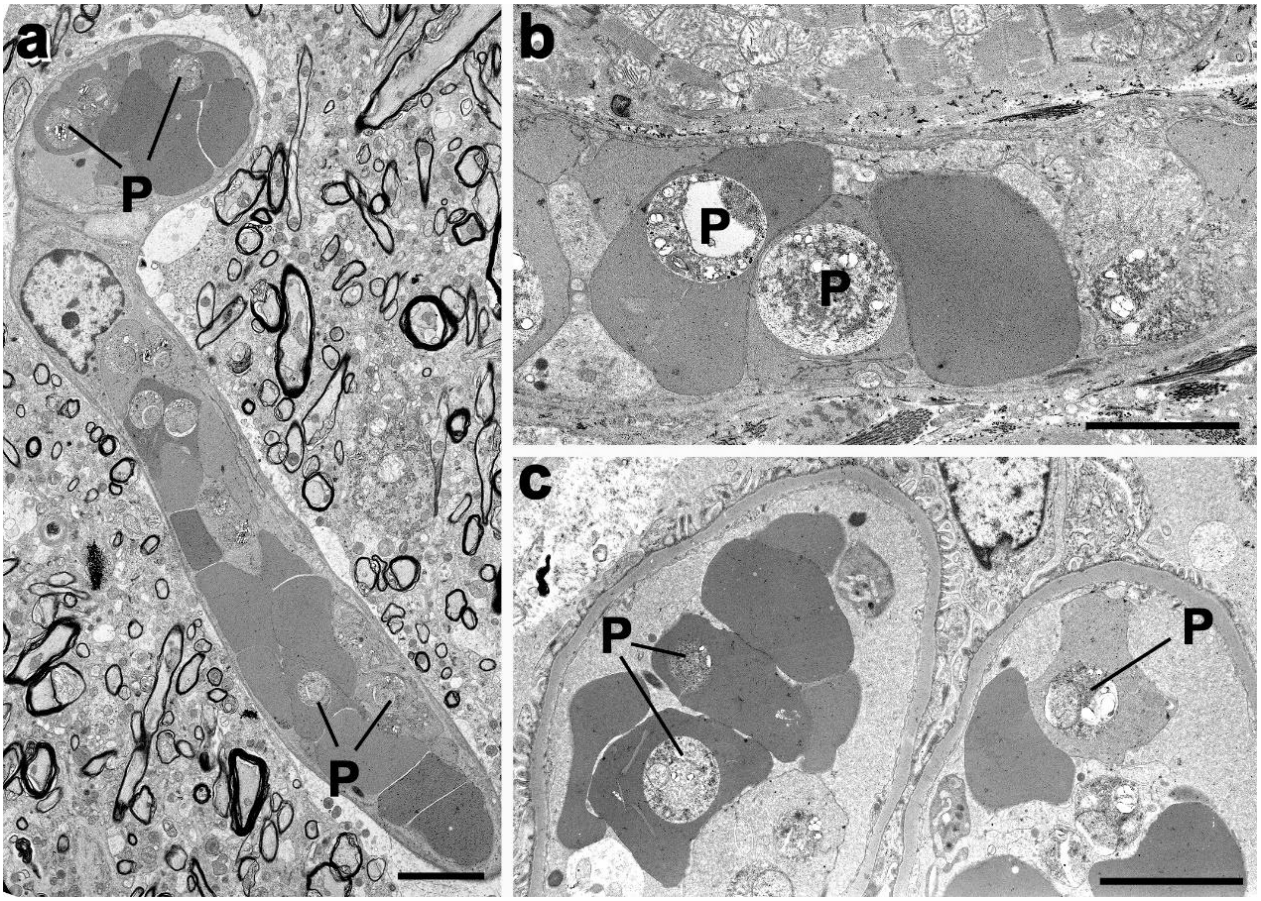

Figure 6.2.3.1a-1c:

Electron micrographs of *P. coatneyi* infected rhesus macaque tissues. The phenotypic structure of the parasites (P) and the infected erythrocytes were similar in the three tissues examined (1a. Brain; 1b. Heart; 1c. Kidney). Microvasculature was often tightly packed with both infected and uninfected erythrocytes. Infected erythrocytes typically contained a single parasite, however two or more parasites in a single red blood cell was not an uncommon finding (1c). Trophozoites appeared to increase in size, developing from stages with a single nucleus (Fig 1c) to stages with multiple nuclei and finally into mature schizonts (Fig 3a). Bar is 10 µm.

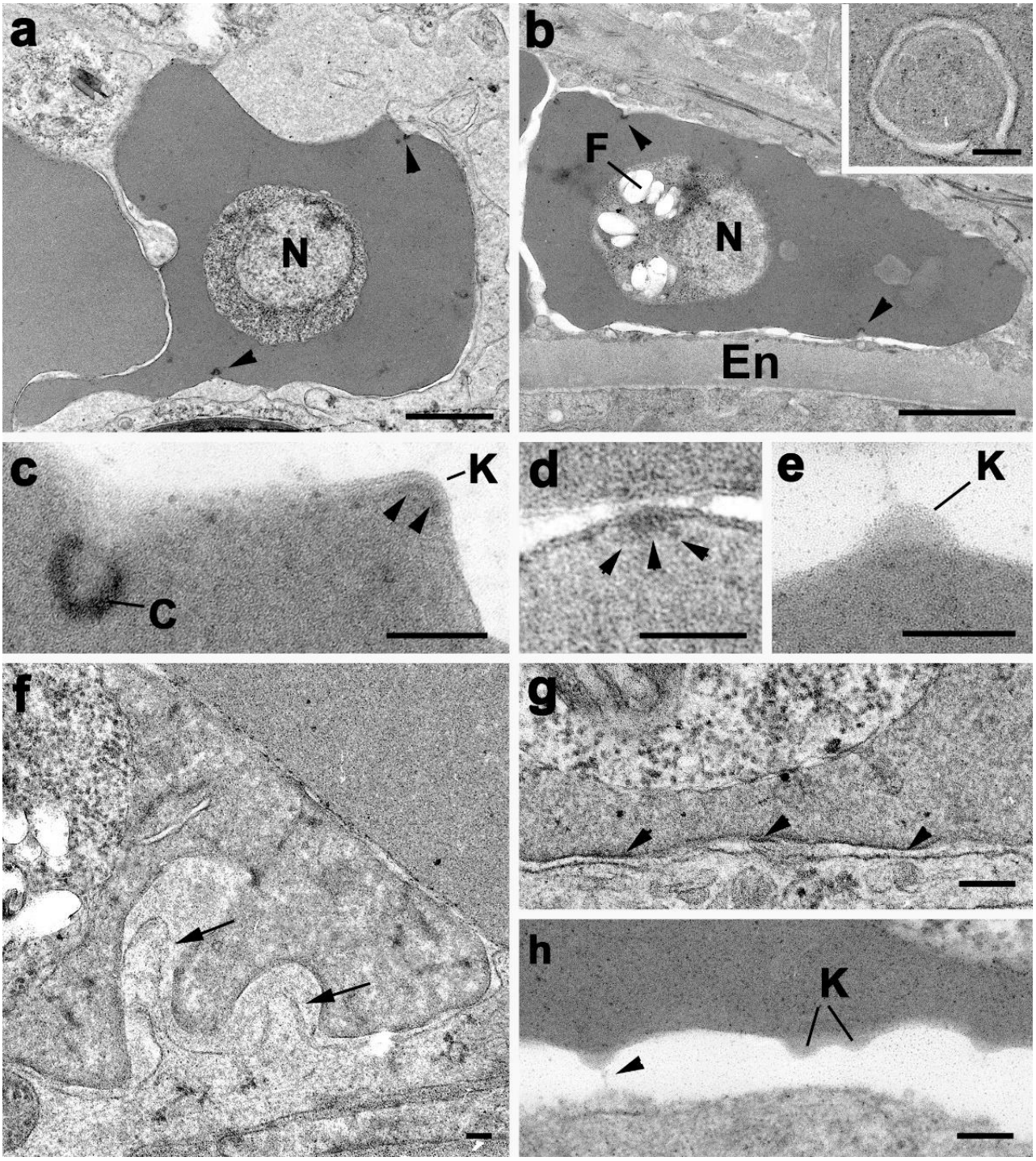

Figure 6.2.2.2a-2h: Transmission electron micrographs of *P. coatneyi* infected rhesus macaque tissues.

a. Section through an iRBC showing a trophozoite with a centrally located nucleus (N). Note the surface of the iRBC exhibits caveola formation (arrowheads). Bar represents 1µm.

b. iRBC with a trophozoite displaying hemozoin crystals in the food vacuole (F). Note the tight apposition of the iRBC plasmalemma with caveola (arrowheads) with the endothelial cells (En) lining the vessel. Bar is 1 µm.

Insert: Part of an iRBC cytoplasm showing the double membraned cleft-like structure. Bar is 100nm.

c. Detail from the surface of an iRBC showing an invagination of the plasmalemma to form a caveola (C) with underlying electron dense material and knob (K) with underlying dense material (arrowheads). Bar is 100nm.

d. Detail from the surface of an iRBC in which electron dense material (arrowheads) is associated with the plasmalemma of an iRBC but in the absence of any protrusion. Bar is 100nm

e. Detail from the surface of an iRBC showing a knob that appears to lack underlying dense material. Bar is 100 nm.

f. Section through the junction between an iRBC and an endothelial cell showing two microvilli from the endothelial cell protruding into folds in the iRBC (arrows). Bar is 1µm.

g. Enlargement of the junction between iRBC and endothelial cell with no evidence of knob formation but proteinaceous material appearing to connect the plasma membranes (arrowheads). P – parasite. Bar is 100nm.

h. Detail of junction between iRBC and endothelial cell where the iRBC appears to form knobs (K). Note the proteinaceous connecting the knob to the endothelial cell. Bar is 100nm.

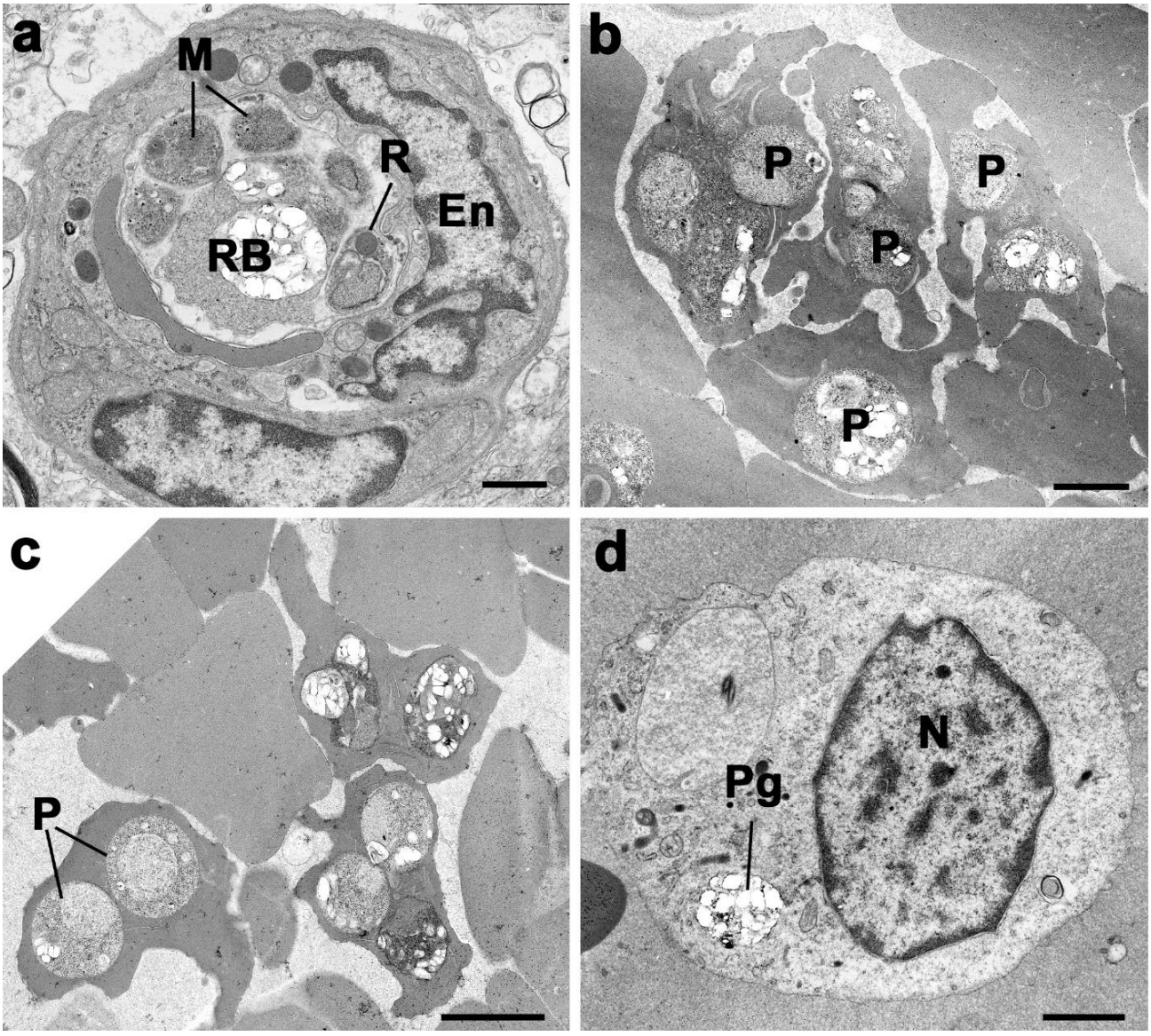

Figure 6.2.2.3a-3d:

Transmission electron micrographs of *P. coatneyi* infected rhesus macaque tissues.

a. Cross section through a small blood vessel showing an iRBC with a mature schizont containing merozoites (M) with electron dense rhoptries (R) around a residual mass (RB). En -endothelial cell. Bar is 1µm

b. Low power from a large vessel showing a number of iRBCs interacting with each other to form an auto-agglutinate- like structure. P – parasite. Bar is 1µm.

c. Part of a vessel in which iRBCs are interacting with RBCs to form rosette-like structures. Bar is 1µm.

d. Section through a vessel showing macrophage that had phagocytise a packet of pigment (Pg). Bar is 1 µm.

Transmission electron micrographs of blood from *P. coatneyi* infected, spleen intact rhesus macaques.

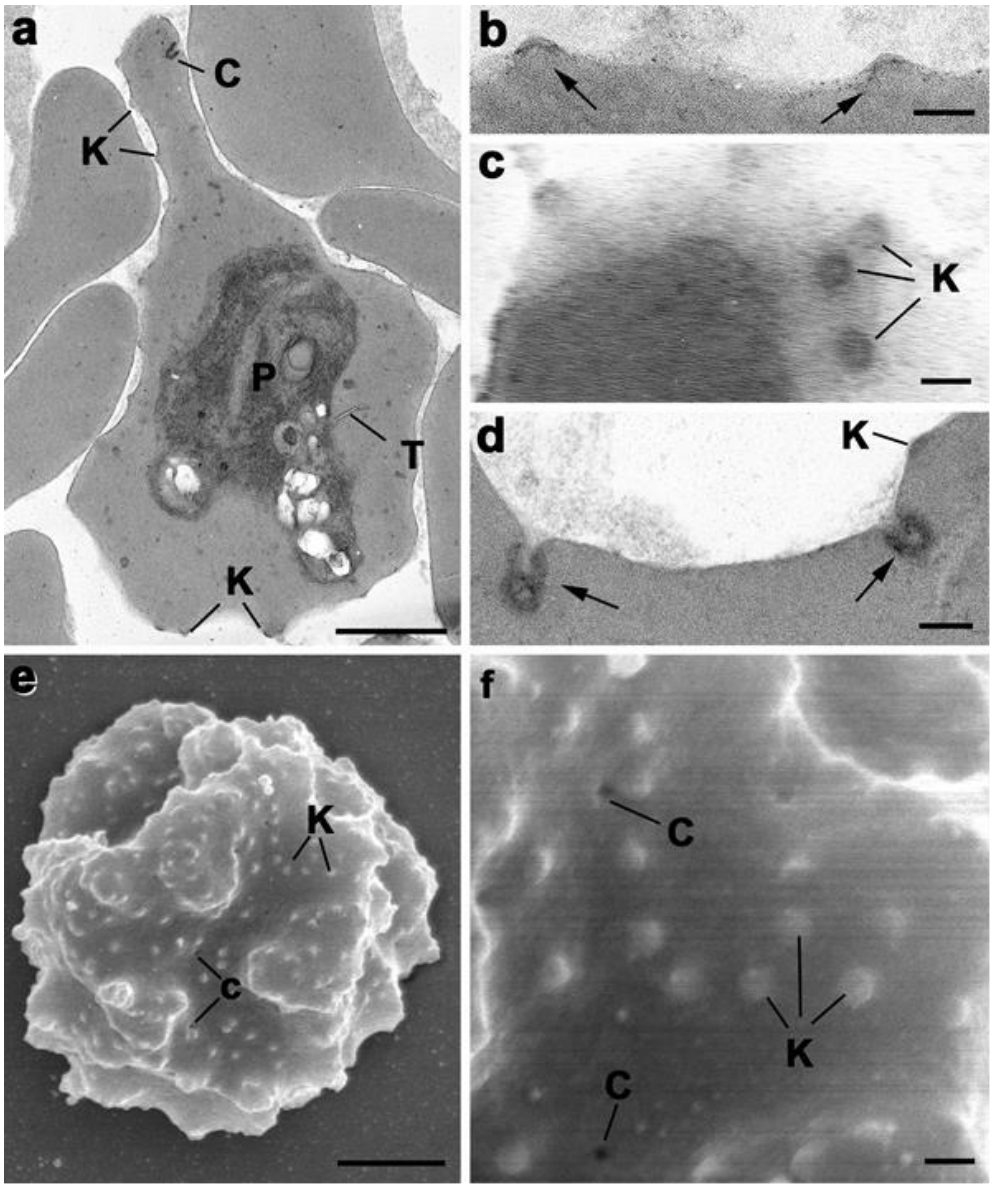

Figure 6.2.2.4a-4f

a. Low power image showing an iRBC containing a mid-stage trophozoite (P) in which tubular or cleft-like structures (T), caveolae (C) and knobs (K) can be identified. Bar represents 1µm.

b. Longitudinal section through two knobs showing the underlying dense material (arrows). Bar is 100nm

c. Tangential section through the surface of an iRBC showing knobs (K) with the circular appearance of the underlying dense material. Bar is 100nm.

d. Longitudinal section showing the caveolae formed by the invagination of the iRBC plasmalemma with underlying dense material (arrows). K – knob. Bar is 100nm.

e. Low power scanning electron micrograph of an iRBC showing the irregular (lumpy) surface appearance in which randomly distributed knobs (K) and caveolae (C) can be identified. Bar is 1µm.

f. Detail of the surface of the iRBC showing the circular slightly raised electron lucent knobs (K) and the openings of the caveolae (C). Bar is 100nm.

6.3 **Host tissue changes**:

Ultrastructural tissue pathology associated with *P. coatneyi* infection has yet to be described. This study examined samples from a range of host target tissues allowing for an evaluation of the damage in the acute phase of the disease at high parasitemia.

In general terms, the parasite-host interaction has been well described earlier in this chapter as well as by other authors (Aikawa 1992; Desowitz 1967; Desowitz 1969; Eyles 1963; Kawai 1998; Kawai 2003; Sein 1993), however the specific changes to tissue remains to be evaluated.

Samples collected in glutaraldehyde during the autopsy of the 15 prospective animals included a focus on the central nervous system (cerebrum, cerebellum, brain stem, spinal cord), heart, and kidney in all animals and the liver, retina, pituitary gland, and lung in a select few. Baseline changes are described above and include perivascular edema, which was most pronounced in the brain, microvascular obstruction in all tissues with margination of infected erythrocytes, rosette formation and auto-agglutination.

In all tissues, the formation of pseudopod like structures occurred on occasion between the endothelium and the infected erythrocytes, and the endothelial cells occasionally were noted to have

evidence of cytoplasmic proteolysis correlating with acute cellular swelling. In those cases, there were swollen mitochondria and dilatation of the cisternae in the endoplasmic reticulum and fragmentation, forming vesicles. (Figure 6.3.1-2)

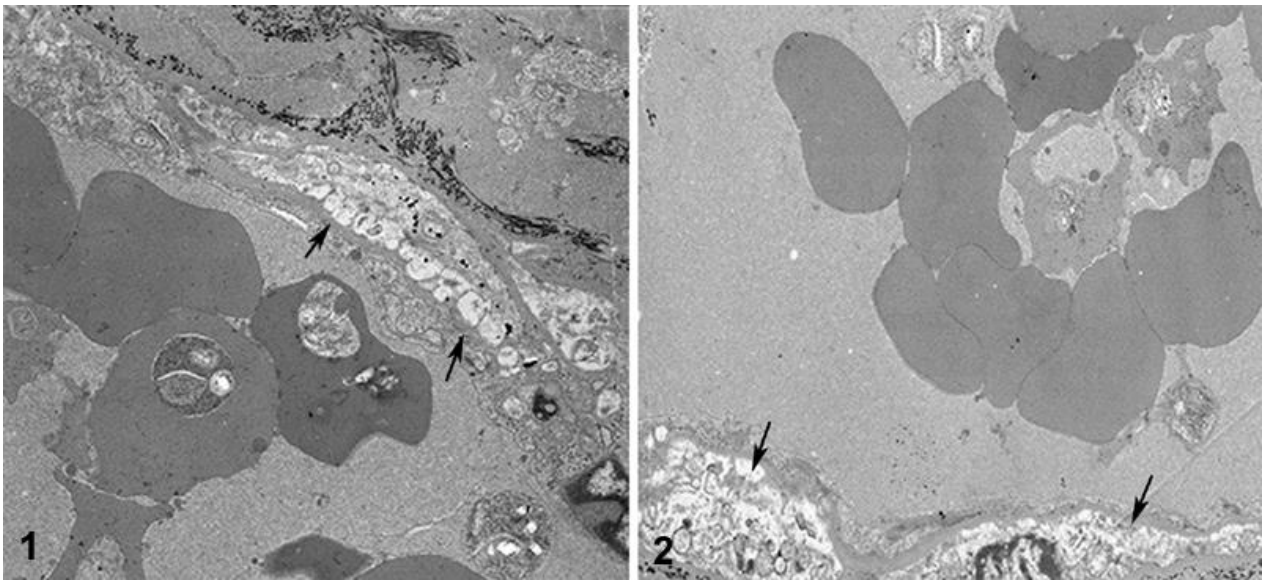

Figure 6.3.1-2: These ultrastructural photomicrographs highlight the endothelial degeneration (arrows) observed in some of the microvasculature in which there are either cytoadherent infected cells, rosette formation or autoagglutination. 6.3.1 TEM 4000x; 6.3.2 TEM 2500x.

6.3.1 <u>Central Nervous System (CNS)</u>: Changes in the brain were relatively consistent between the various sections examined, with perivascular edema being a prominent feature. This finding occasionally extended into the adjacent neuropil, widely separating and displacing the matrix. Rarely neurons were observed to have evidence of early neuronal chomatolysis, with preliminary stages of cellular swelling and proteolysis affecting the dendrites and extending into the perikaryon, interpreted as acute cellular injury and reversible degenerative changes (Figure 6.3.3).

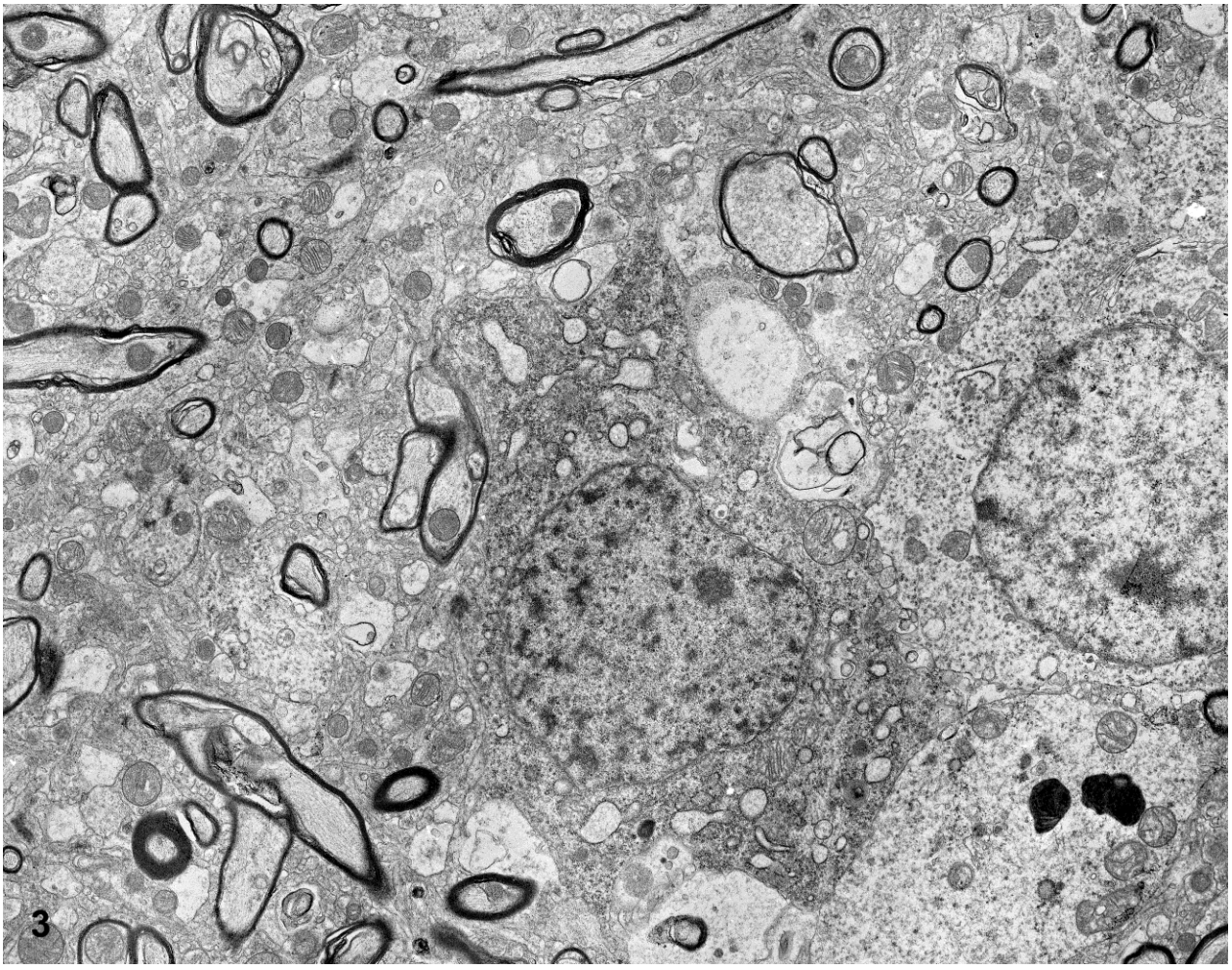

Figure 6.3.3: Cerebrum. The neuron central to this photomicrograph displays evidence of organelle swelling and vacuolation. There is loss of dendritic processes and the beginning of neuroplasmic angulation, suggestive of degenerative changes. TEM 3000x.

In rare instances, there was evidence of irreversible acute cellular swelling, with loss of the nucleolus and the chromatin and angular consolidation of the nucleus. Cytoplasmic changes consistent with cellular necrosis included the accumulation of residual bodies, lipid and vacuoles and necrotic debris. The plasma membrane, when identifiable was undulant and fragmented (Figure 6.3.4).

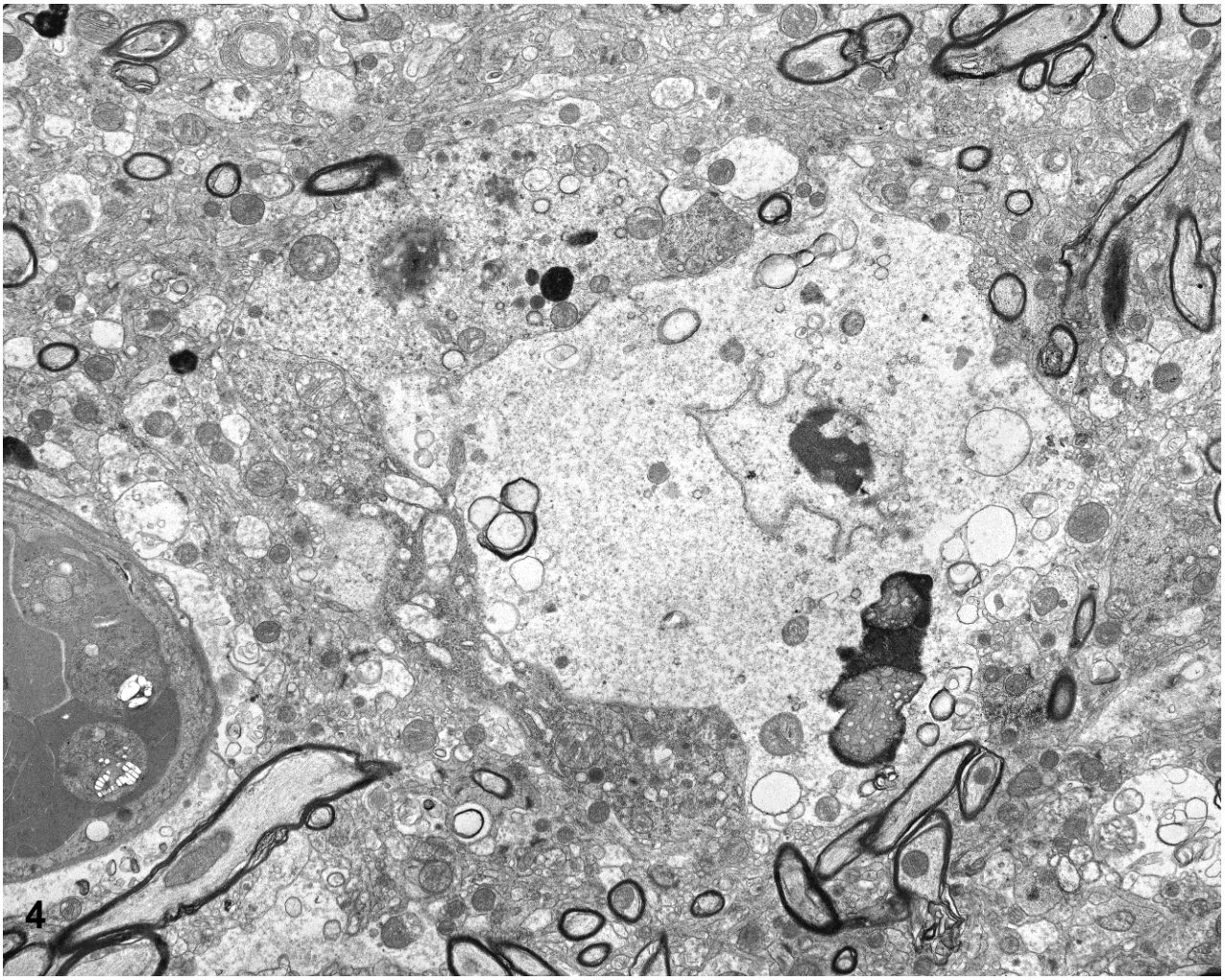

Figure 6.3.4: Cerebrum. In this case, the neuron is necrotic, with loss of structural architecture, pyknosis and fragmentation of the nucleus, rupture of the plasma membrane and loss or swelling of the organelles. TEM 2500x.

In one instance, assessment of a section of brain stem from an experimental animal revealed a focus of hemorrhage. The extravasated erythrocytes separated and surrounded myelin fibers and the disrupted neuropil. (Figure 6.3.5.)

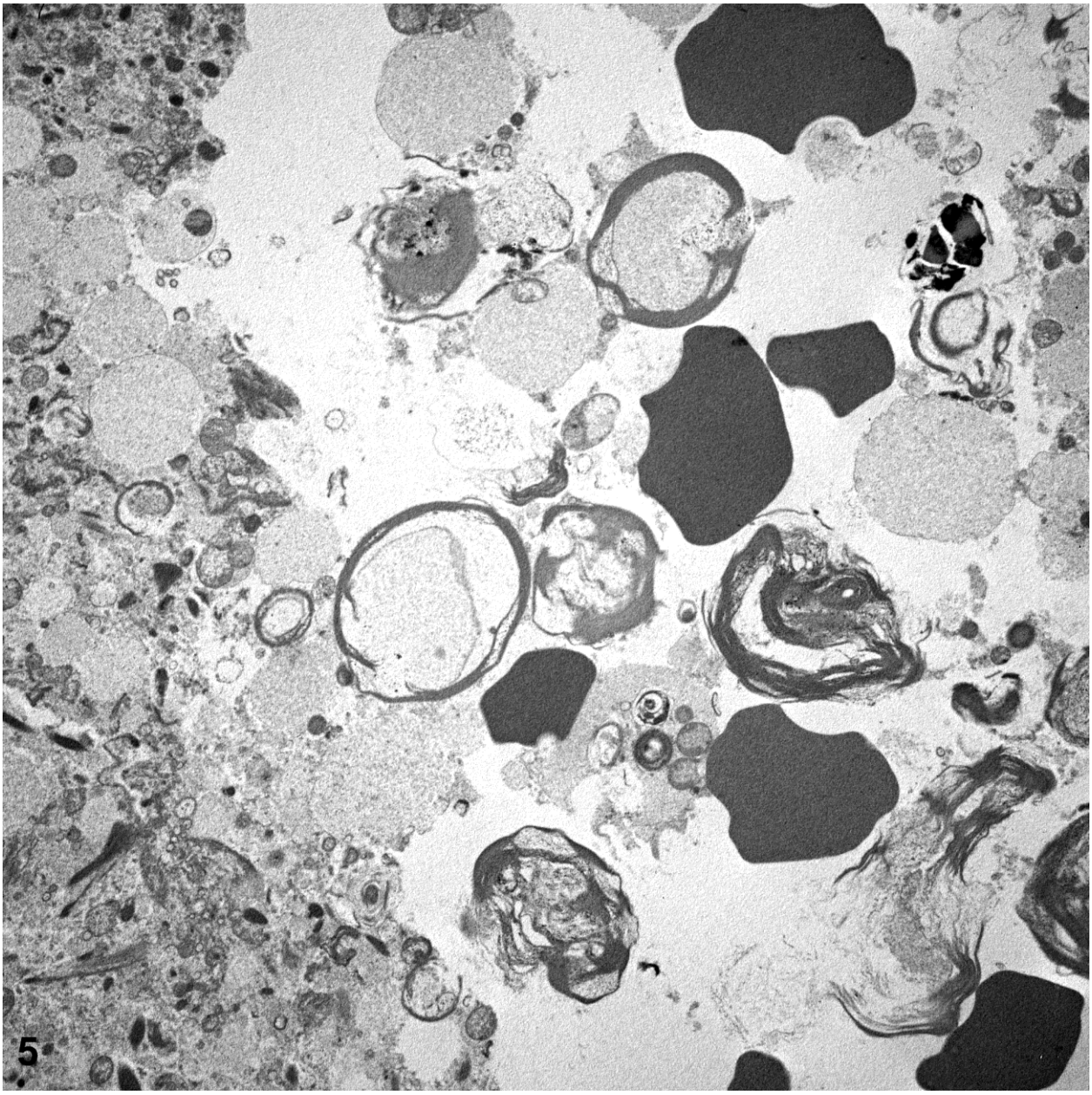

Figure 6.3.5: Brain stem. This ultrastructural photomicrograph illustrates an example of hemorrhage which occurred with greater frequency in the brain stem and spinal cord in comparison with the cerebrum or cerebellum. There is loss of neuropil, and replacement with extravasated erythrocytes, proteinaceous material and clear space. TEM 4000x.

The literature concerning *P. falciparum* has described perivascular edema in correlation with sequestration and alterations of the cerebral microvascular endothelium (reviewed in Medana and Turner 2006). Furthermore, cerebral disease in humans is illustrated by the typical ring hemorrhages

observed due to microvascular rupture. (Pongponratn 2003) While light microscopy did observe hemorrhaging in the CNS in the *P. coatneyi* experimental animals, it was predominantly noted in the spinal cord and the brain stem and did not assume the pattern described in deaths associated with *P. falciparum*.

6.3.2 <u>Kidney</u>: Renal ultrastructural pathology consisted of all of those host-parasite interactions, in addition to significant observable injury to both the distal and the proximal tubules. In the former, individual or aggregates of tubular epithelium were either degenerate or necrotic, characterized by a continuum of cytoplasmic swelling, with proteolysis of the cytoplasmic elements, observable primarily as swelling of the mitochondria, chromatolysis and condensation of the nuclei and fragmentation of the plasma membrane with extrusion of organelles into the tubular lumen (Figure 6.3.6-7).

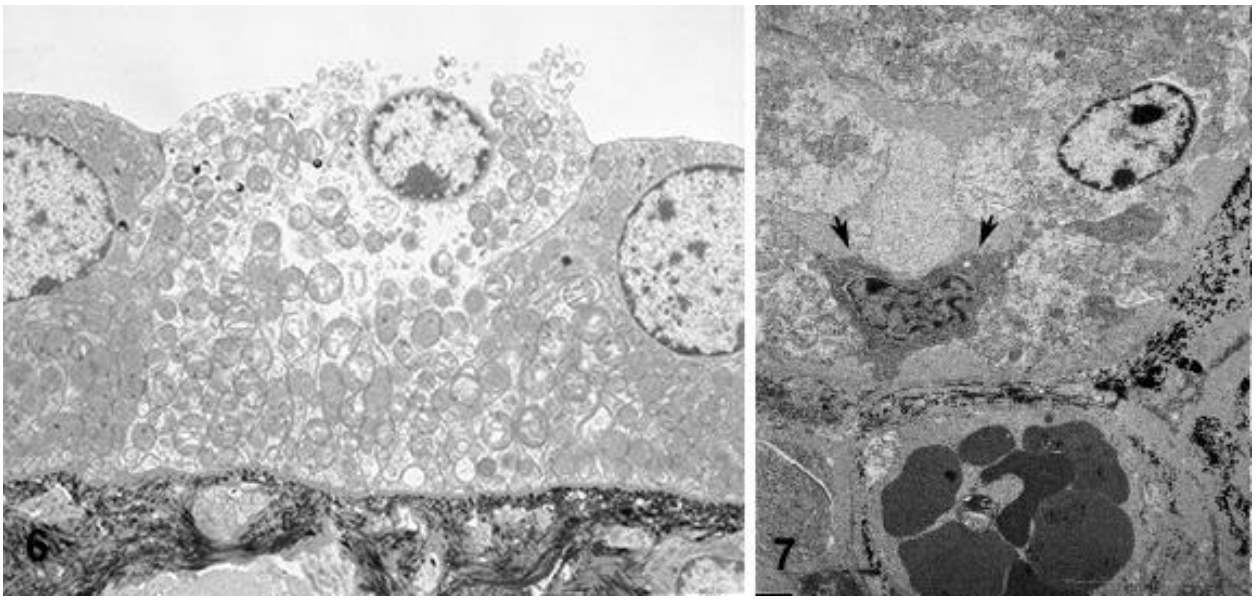

Figure 6.3.6-7: This plate of ultrastructural photomicrographs demonstrates two different tubular epithelial cells undergoing necrotic change. In 6.3.6, the nucleus while shrunken, still maintains vestiges of its architecture, in spite of complete rupture of the apical plasma membrane. TEM 3000x. On the other hand, the cell represented in 6.3.7 illustrates angulation and chromatolysis of the nucleus with condensation of the cytoplasm (arrows). Adjacent cells demonstrate various stages of

cytoplasmic vacuolization, and organelle swelling suggestive of earlier degenerative changes. Additionally, the tubule lumen is obscured by protein and cellular debris. TEM 4000x.

Proximal tubular pathology was comprised of similar findings as those observed in the distal tubular epithelium with the addition of changes to the apical surface microvilli. The condensed, fragmented necrotic cells demonstrated either a blunting and fusion of the microvilli or complete loss. As with the distal tubules, the affected cells were noted to undergo an initial injury consisting of cytoplasmic and organelle swelling followed by nuclear condensation, fragmentation and extrusion of cellular elements into the tubular lumen. (Figure 6.3.8-9)

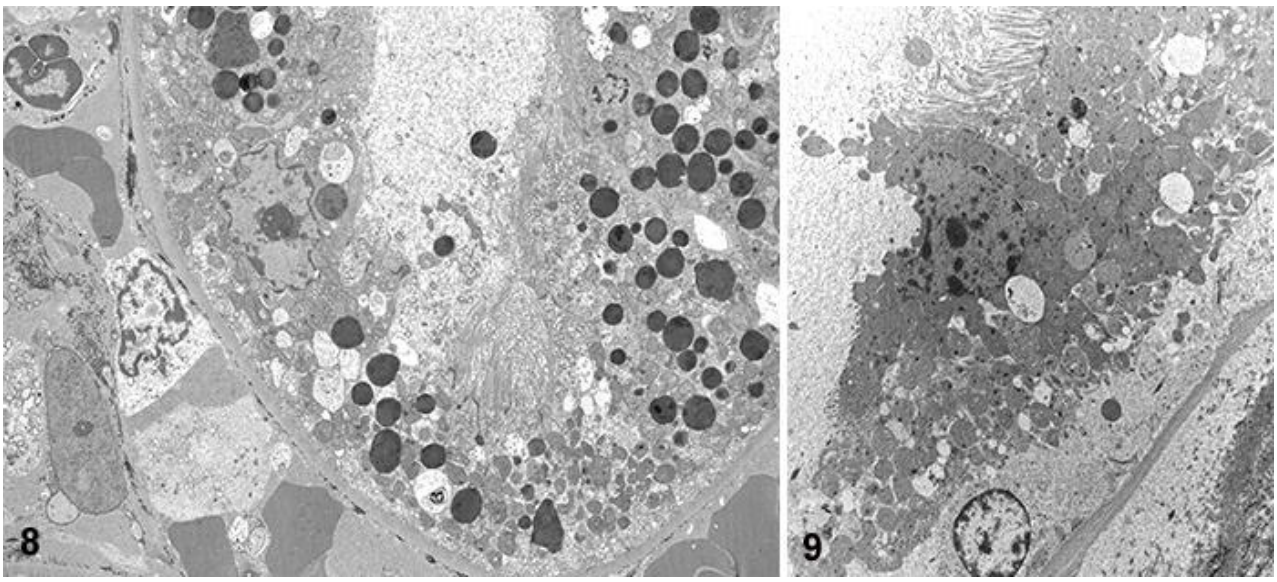

Figure 6.3.8-9: These two figures are of proximal tubular epithelium undergoing similar necrotic changes to those described in the prior figures. 6.3.8 TEM 2000x; 6.3.9 TEM 5000x.

Ultrastructural changes in the glomeruli were subtle, and unlike the description of a membranoproliferative glomerulonephritis with abnormal deposits described in early human and *P. berghei* mouse model studies (Bhamarapravati 1973; Boonpucknavig 1976), the changes in the glomeruli of the affected rhesus macaques were not the predominant lesions observed. Histologically in this study, the glomeruli were typically hypercellular, occasionally hypersegmented,

with glomerular capillaries often occluded by infected erythrocytes and high numbers of polymorphonuclear cells interpreted as neutrophils, as well as frequent macrophages containing phagocytosed debris. These were interpreted to be extrinsic host monocytes which are recruited due to the occlusion and sequestration of the glomerular tuft microvasculature. The macrophages often contained cellular debris and hemozoin fragments suggestive of clearance of ghosted erythrocytes, a feature described in *P. falciparum* induced disease in humans. (Pongponratn 2003)

Additionally, there was significant evidence under light microscopy of synechial attachment of the glomerular tuft to the Bowman's membrane (Figure 6.3.10-11).

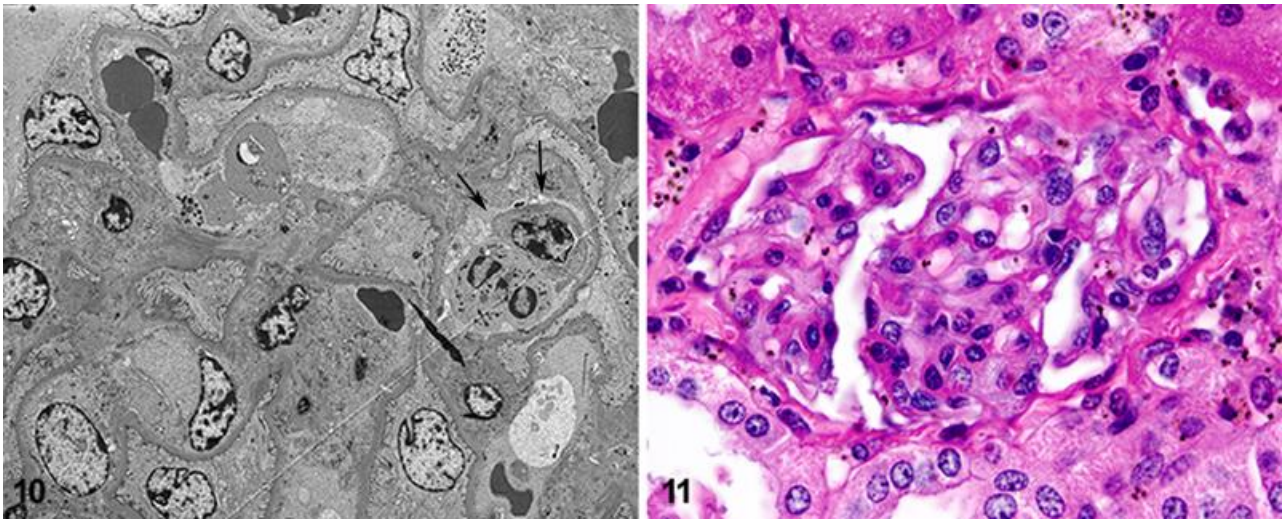

Figure 6.3.10-11: 6.3.10 is an ultrastructural photomicrograph of a glomerulus with an example of the frequent accumulation of polymorphonuclear cells observed within the glomerular tuft microvasculature (arrow). TEM 1500x. The photomicrograph demonstrates the hypersegmentation, ectasia of the vasculature and the frequent synechiae to the parietal epithelium of Bowman's capsule. HE 400x.

Occasionally the foot processes of the podocytes, were mildly hypertrophic with evidence of fusion (Figure 6.3.12).

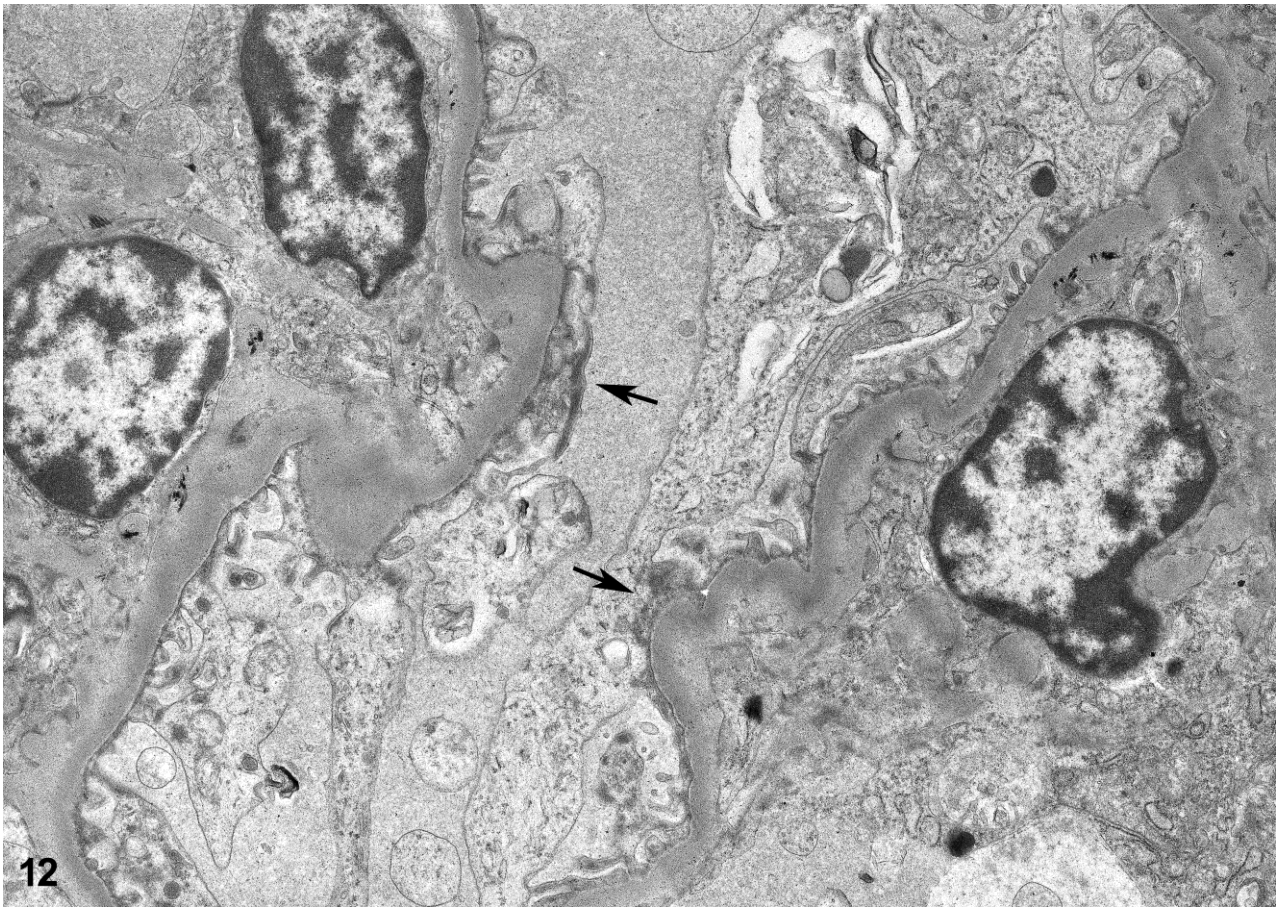

Figure 6.3.12: This ultrastructural photomicrograph of the glomerulus in an *P. coatneyi* infected rhesus, notes some of the subtle changes which were occasionally observed. In this instance, there is periodic fusion of the podocyte foot processes (arrows) as well as some increased electron lucency, and swelling suggestive of damage to the glomerulus. TEM 4000x.

In humans infected with *P. falciparum,* ultrastructural examination of the glomeruli suggested that the basement membrane was either multifocally absent or asymmetrical in thickness. Furthermore, depending on the study, mesangial cells have been described as being either proliferative and containing electron-dense deposits suggestive of an immune complex nephritis (el-Shoura 1994) or a posited absence of immune complex glomerulonephritis as a feature of acute renal failure in *P. falciparum* malaria infection. (Nguansangiam 2007) A third study suggested that glomerulopathy was only observed in one fifth of autopsied victims of *P. falciparum* and in those

cases, the histopathology and ultrastructural evaluation of the tissues noted a prominent mesangial proliferation with only minimal basement membrane electron microscopic changes. (Barsoum 2000) Intensive examination of the images generated from the *P. coatneyi* infected macaques did not reveal reliably reproducible evidence of immune complex deposition in the subendothelial tissues. Rather, the basement membrane underlying the podocyte foot processes was typically uniform in thickness and in electron density. (Figure 6.3.13). The brevity of the experimental infection (up to approximately 6-10days) in the rhesus may not permit adequate time for the formation of the subepithelial deposits, or the pathogenesis of the disease may simply not involve an immune complex deposition as a significant factor. Considering there is still some debate as to the presence or absence of an immune-complex driven pathogenesis in the acute renal failure in *P. falciparum*, the lack of lesions in the macaques may simply be a supportive characteristic of the commonality of *P. coatneyi* and *P. falciparum* driven disease.

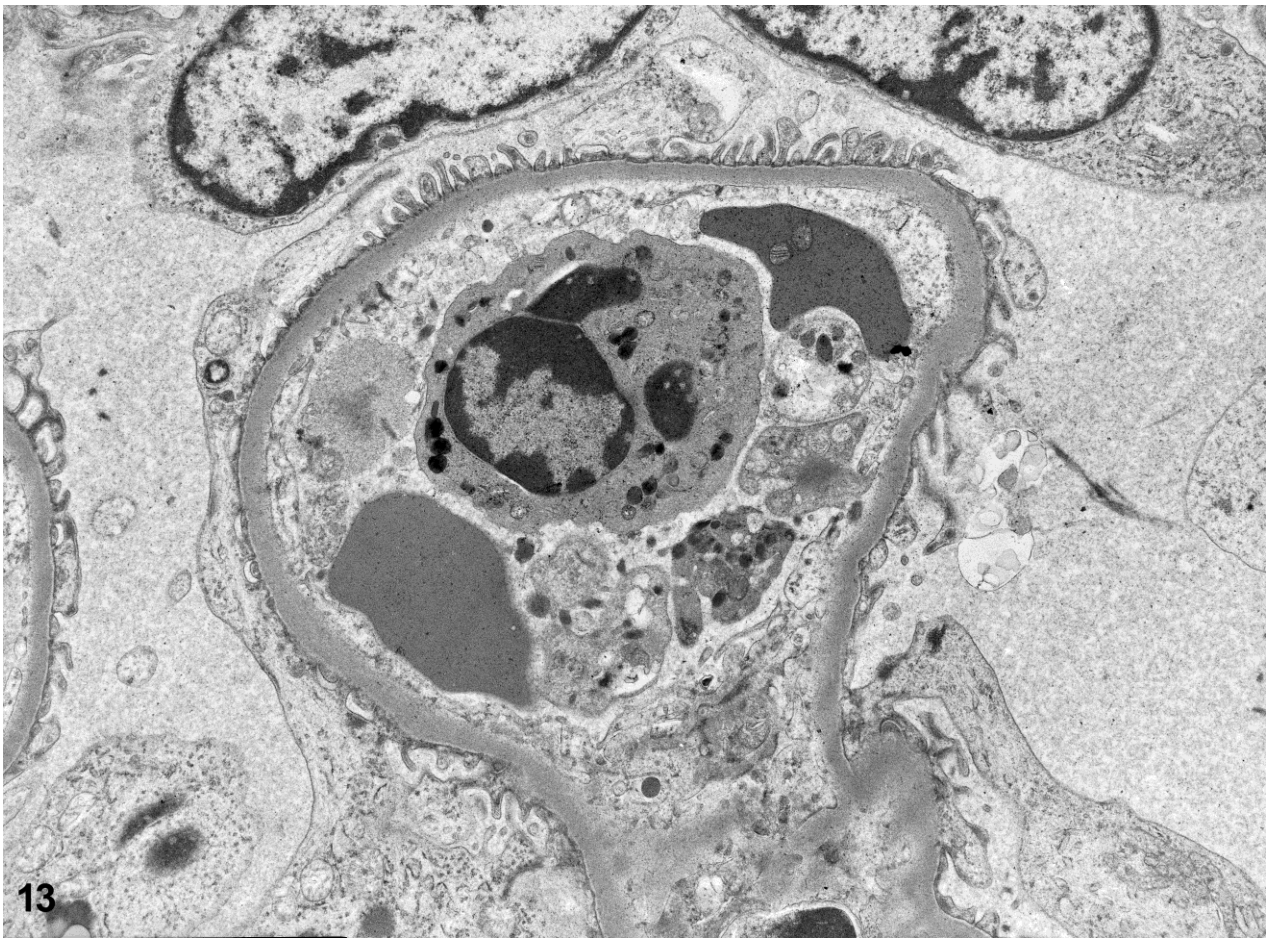

Figure 6.3.13: This ultrastructural photomicrograph illustrates the typical glomerulus imaged during this study, in which the basement membrane is of uniform thickness and the food processes are typically individualized. In this instance, the capillary lumen is replete with ghost erythrocytes, polymorphonuclear leukocytes and both infected and uninfected erythrocytes. TEM 4000x.

6.3.3 <u>Heart</u>: Cardiac ultrastructural pathology consists predominantly of degeneration and necrosis of the cardiomyocytes, accumulation of interstitial edema and debris, significant occlusion and sequestration of the parasitized erythrocytes within the microvasculature, without a significant inflammatory response.

Under both light microscopy and electron microscopy, the degree of microvascular sequestration was overwhelming, with almost 100% of visible vessels being occluded. (Figure 6.3.14) Ultrastructurally, the parasitized erythrocytes were frequently marginated and cytoadhered to the endothelium (Figure 6.3.15). The interstitium, especially in proximity to occluded vessels contained varying amounts of electron lucent edema. Degenerative changes consisted of cellular hypertrophy with distinct loss of thick (myosin) filaments, as well as streaming and clumping of Z bands. Progressively with increased severity, affected cells became condensed and fragmented, with extensive myofibrillar lysis and loss of T tubules. Cytoplasmic organelles such as the mitochondria and the sarcoplasmic reticulum were swollen and electron lucent. Occasional cardiomyocytes contained electron dense bodies and were separated from adjacent cells, having lost intracellular connections. (Figure 6.3.16-17)

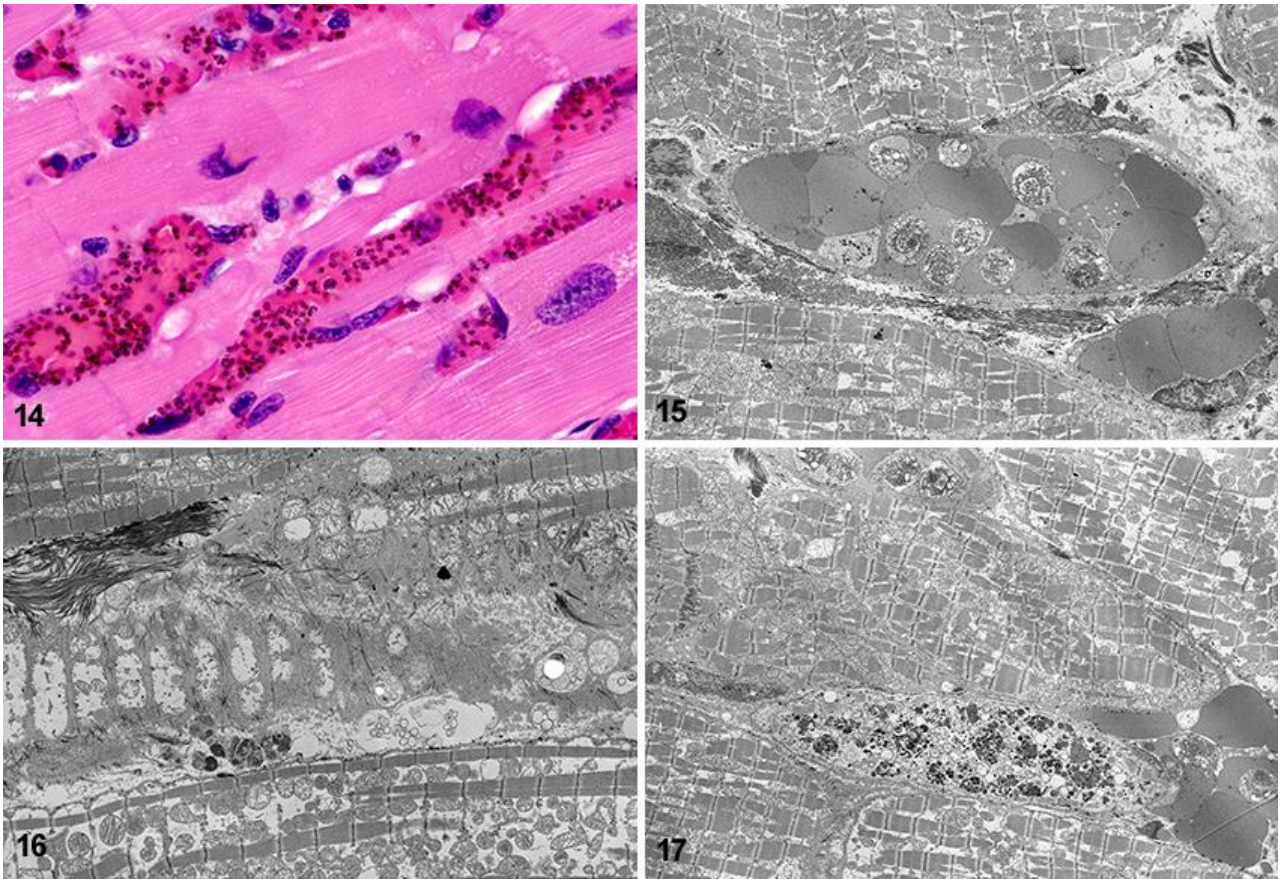

Figure 6.3.14-17: This plate is comprised of tissue changes observed in the cardiac tissue of *P. coatneyi* infected rhesus macaques. 6.3.14 is a photomicrograph underscoring the extraordinary amount of parasitism and sequestration of infected erythrocytes in the myocardial microvasculature. HE 1000x. 6.3.15 shows the margination of the infected erythrocytes and illustrates the degree of cytoadherence and sequestration at an ultrastructural level. TEM 4000x. Both 6.3.16 (TEM 2000x) and 6.3.17 (TEM 1500x) are examples of either severe degeneration or piecemeal myocardial necrosis with fragmentation of the myofibers, swelling of the organelles and rupture of the cells.

There are only scant ultrastructural descriptions of cardiac injury in *P. falciparum* induced disease, and those reports that are in the literature typically concentrate on the microvasculature rather than a description of the cardiomyocytes themselves (Luse 1971; Pongponratn 1991), or are single case reports which describe either ischemic pathology secondary to the sequestration and occlusion of cardiac microvasculature (Chopra 2013), a lymphocytic myocarditis in humans or

determined cardiac disease based on ante-mortem clinical findings. (Costenaro 2011; Mohsen 2001) Additionally, this is the first study to directly focus on the cardiac tissue in *P. coatneyi*. Given the high levels of parasitized erythrocyte sequestration and clinical picture of terminal metabolic derangement and shock, it may be that direct parasite induced cardiomyopathy contributes to the cause of death in this model, similar to the mechanisms of shock postulated over a century ago in human post mortem studies of 'algid' malaria. (Dudgeon 1917)

6.3.4 <u>Lung and liver</u>: While only a few experimental animals' lungs and livers were evaluated, the ultrastructural changes observed were consistent with the histopathological findings described in Chapter 4. In the pulmonary interstitium, the microvasculature was occluded by infected erythrocytes admixed with frequent monocytes, however there was no discernible inflammatory response and the alveolar space was not impaired by edema or other proteinaceous infiltrates. Resident alveolar macrophages were present in the alveolar space, but not in significant numbers and not outside of the realm of normal. Pulmonary pathology is strongly associated with morbidity in severe falciparum induced malaria in humans, and the absence of significant lung pathology in the rhesus macaque model is an important discrepancy in the applicability of this animal model to human disease. (Duarte 1985) A possible consideration is that the microanatomy of the rhesus lung is more durable and resistant to leakage than that of the human, potentially resulting in the macaque being refractory to malaria induced pulmonary disease.

The hepatic samples were frequently difficult to interpret due to a significant degree of dissociation, degeneration and necrosis of the hepatocytes. Individual cells often were expanded by lipid and intracytoplasmic vacuoles. As with other tissues, there was evidence of a continuum of degeneration to necrosis with consistent cytoplasmic and nuclear changes.

P. falciparum infection in adults commonly causes liver function abnormalities and jaundice, although this is multifactorial and not necessarily due to widespread hepatic necrosis (Kochar 2003; Prommano 2005), and is not typically associated with the degree of hepatic injury observed here in the rhesus

model (especially when considering the light microscopic findings of centrilobular coagulative necrosis, which may be secondary both to sequestration and host immune responses in the hepatic sinuses and the microvasculature, resulting in hypoxic insult).

6.3.5 Retina: Attempts to examine retinal pathology with EM were unsuccessful. Preparation technique impaired the ability to adequately interpret changes in the retinal samples as the delicate sections frequently folded over themselves and compromised diagnostic capacity.

6.4 **Atomic Force Microscopy (AFM)**:

In conjunction with an experimental anti-malarial drug trial of methylene blue in the *P. coatneyi*/Rhesus macaque model for severe malaria, blood smears were taken from multiple untreated animals at various degrees of parasitemia in order to conduct a more widespread descriptive analysis of the surface ornamentation in *P. coatneyi* and to compare those with descriptions of *P. falciparum* studies undertaken at the National University of Singapore (NUS), Vivax malaria laboratory.

Atomic Force Microscopy was employed to further describe the structural modifications which occur in *P. coatneyi* infected erythrocytes. The findings included confirmation and description of the presence of knob-like protuberances as well as the common finding of caveolae on the cell surface. The diameter and overall density of knobs and caveolae observed on *P. coatneyi* were compared and contrasted with those of *P. falciparum.* Initially, the infected erythrocyte was staged using Giemsa staining to identify the parasite within the erythrocyte. (Figure 6.4.1.)

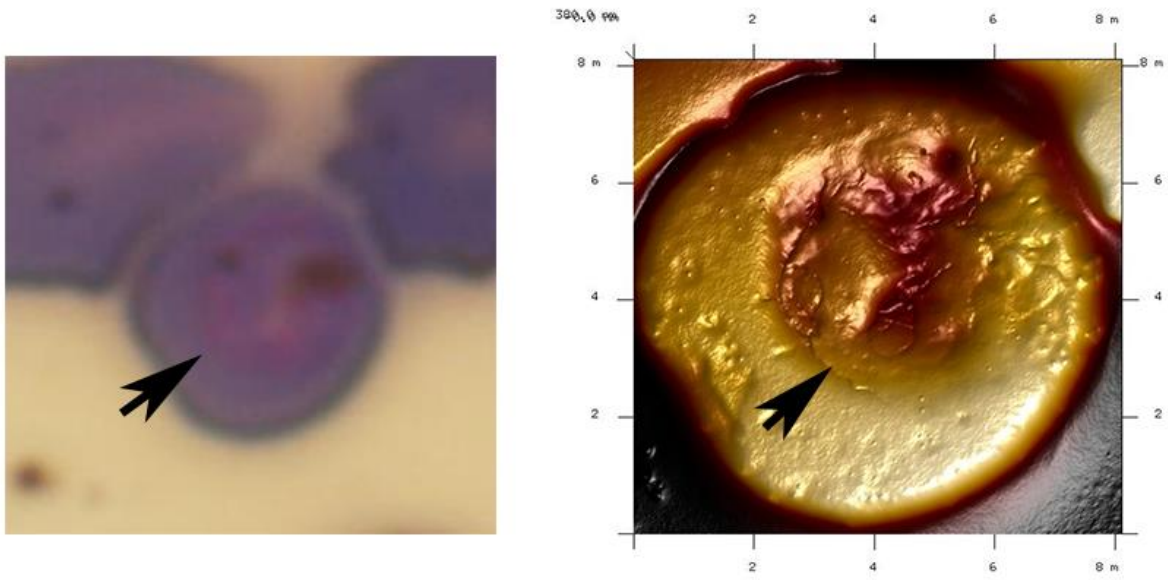

Figure 6.4.1: Identification of the *P. coatneyi* parasitophorous vacuole (arrow) within the infected cell to demonstrate that the selected cell is, in fact, parasitized. The same cell examined using Giemsa staining was then scanned using AFM. Giemsa 1000x.

6.4.1 **AFM Results**:

P. coatneyi infected erythrocyte surface morphology was described using TEM, SEM and AFM.

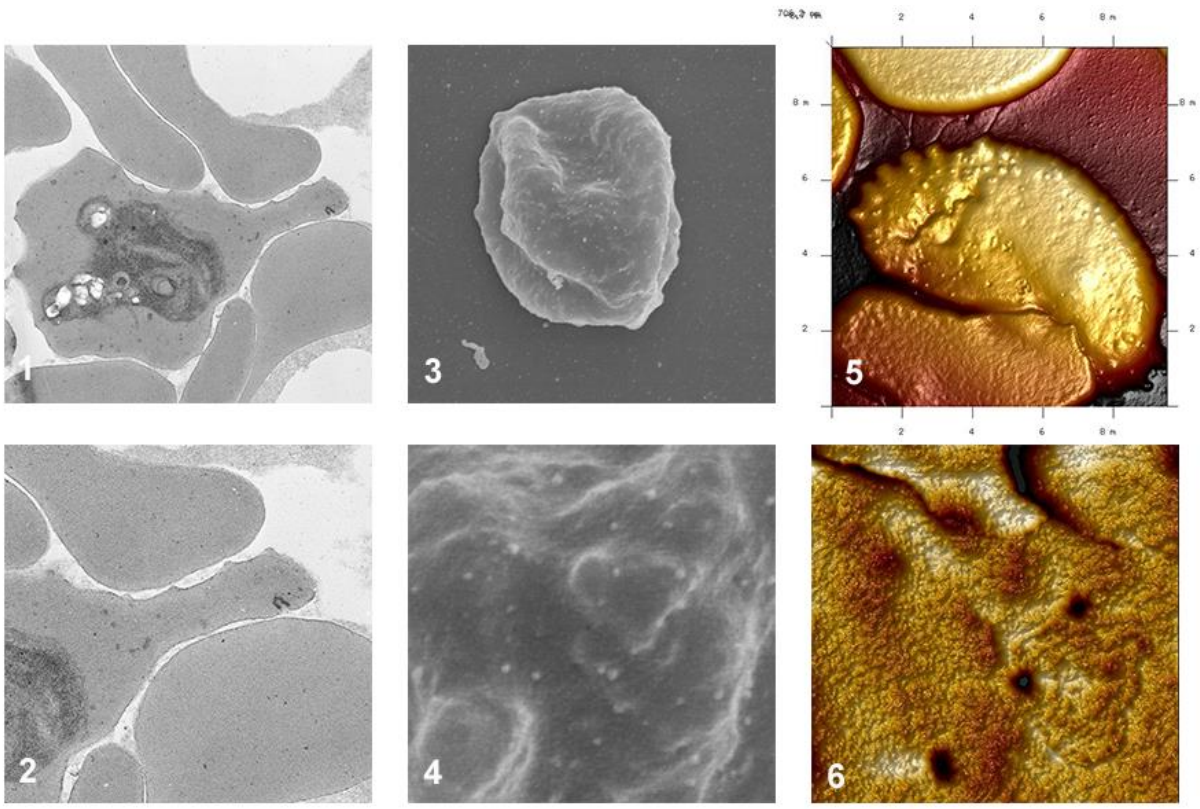

Figure 6.4.2.1-6: This panel of images demonstrates the nanostructural surface ornamentation using each diagnostic modality at lower and higher magnification with evidence of both caveolae and knobs. 1,2 Transmission Electron Microscopy (TEM), 3,4 Scanning Electron Microscopy (SEM) and 5,6 Atomic Force Microscopy.

Knob-like excrescences which are a critical feature of *P. falciparum* infection, are observed infrequently in the prospective experimental animals in this study, which we posit is the result of the macaques from which the SEM and AFM samples were derived being splenectomized. This is consistent with observations made in a case of fatal *P. falciparum* malaria in a splenectomized human and in *P. knowlsei* infected, splenectomized cynomolgus macaques. (Barnwell 1982; Barnwell 1983; Pongponratn 2000) In this study, in samples derived from the prospective population of

splenectomized experimental rhesus macaques, caveolae were observed with increased frequency and both knob-like structures and caveolae were measured using AFM. (Figure 6.4.3.)

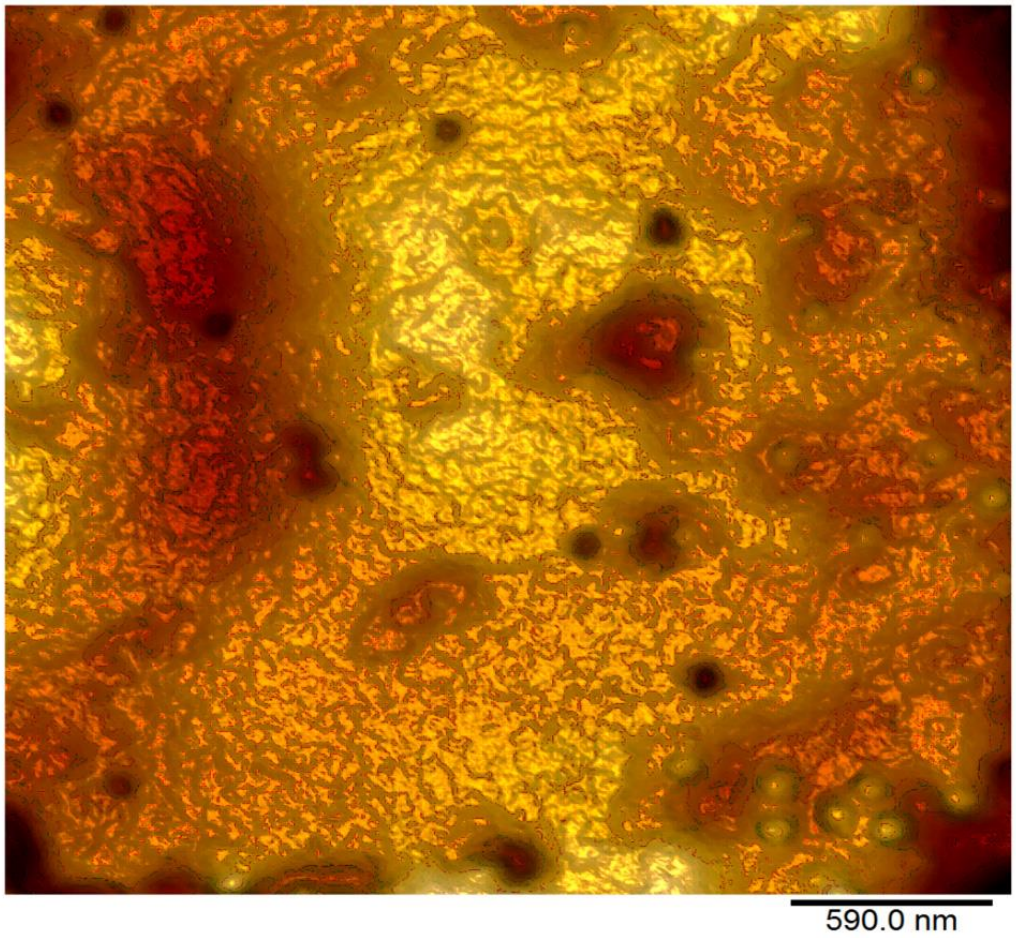

Figure 6.4.3: *P. coatneyi* infected erythrocyte atomic force microscopic scan illustrating regular and uniform invaginations in the cell membrane which are interpreted to be caveolae.

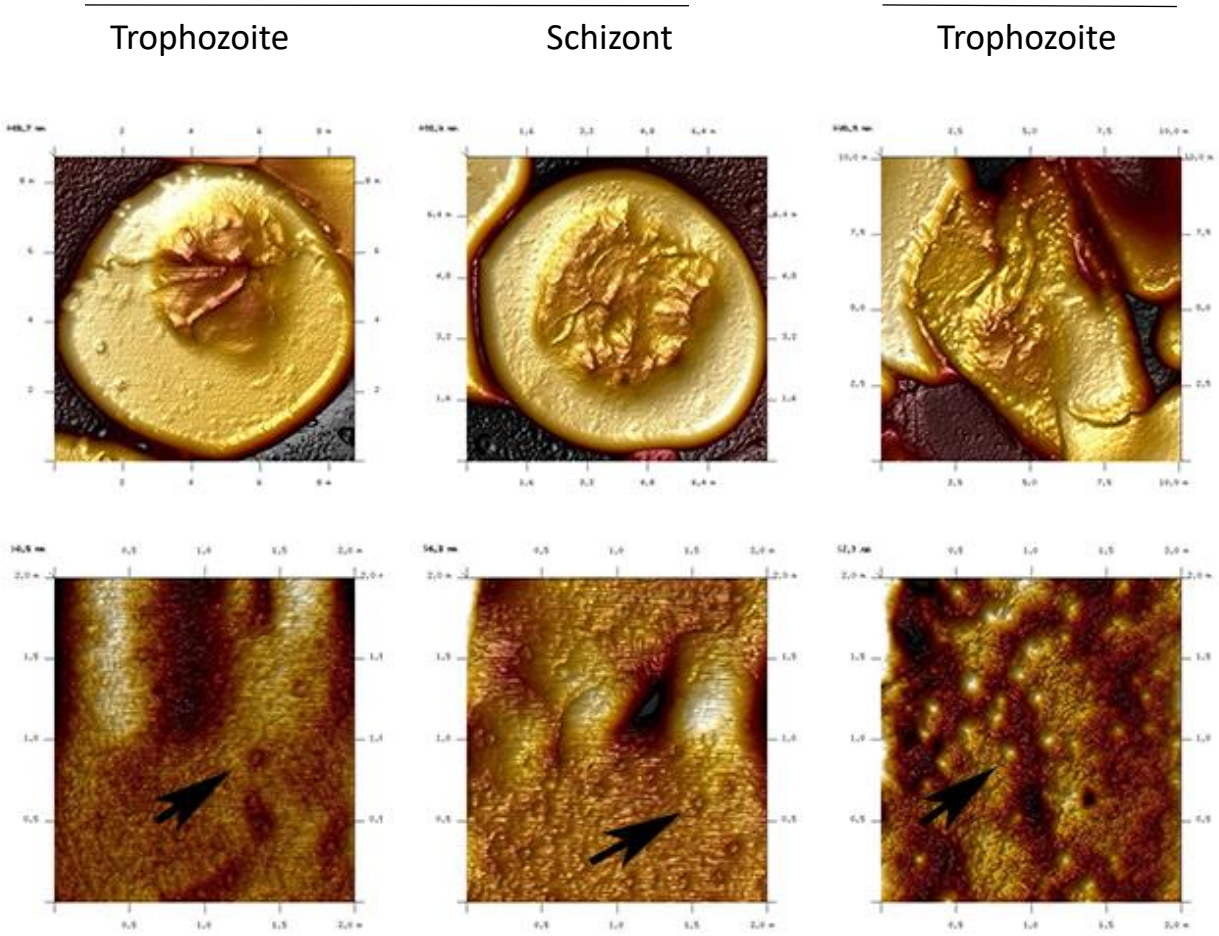

Figure 6.4.4.1: Comparative AFM images showing slight differences in the diameter of the knobs between *P. falciparum* and P. *coatneyi*.

The knob density was measured by calculating the number of knobs per μm^2. Five knobs per cell were randomly chosen, and the diameter of each knob was measured NanoScope Analysis (version 1.40). In the former, we measured more five knobs randomly chosen from 11 trophozoite infected erythrocytes and five knobs on the surface of 11 cells containing schizonts. As knobs were scarce in *P. coatneyi* infected red blood cells in the samples examined, five random knobs were

measured from two infected cells containing *P. coatneyi* trophozoites. The *P. coatneyi*-infected cell (bottom right), containing a trophozoite is covered with dense excrescences (mean diameter: 92 nm), which are morphologically distinct from the smaller knobs measured on *P. falciparum* trophozoite infected red cell (mean diameter: 64 nm) (bottom left). *P. falciparum* schizont associated knobs are slightly larger than those on cells infected with *P. falciparum* trophozoites, however the diameter of knobs on *P. coatneyi* infected cells is larger than those from the human plasmodium (Figure 6.4.4.2). Knob density was not statistically significant due to the low numbers of *P. coatneyi* infected cells having knob-like protuberances as surface ornamentation. Examination of knob density involved counting the total number of excrescences over the scanned surface of the cell. The availability of only a select few *P. coatneyi* cells displaying knob-like structures was consistent with the transmission electron microscopy findings, and limits the value of the comparison of knob density (Figure 6.4.4.3).

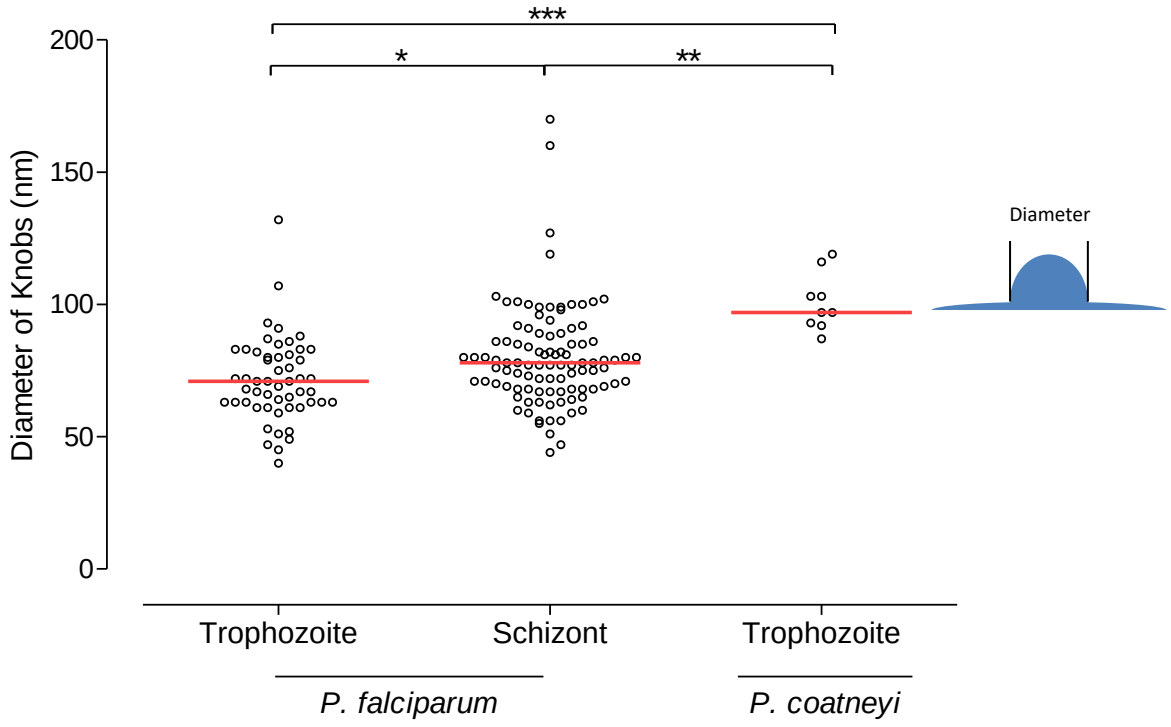

Figure 6.4.4.2: Graphed data of knob diameter measurements which show a slightly larger knob occurring on the *P. coatneyi* infected cells in comparison with those from *P. falciparum*. (* P ≤ 0.05; ** P ≤ 0.01; *** P ≤ 0.001)

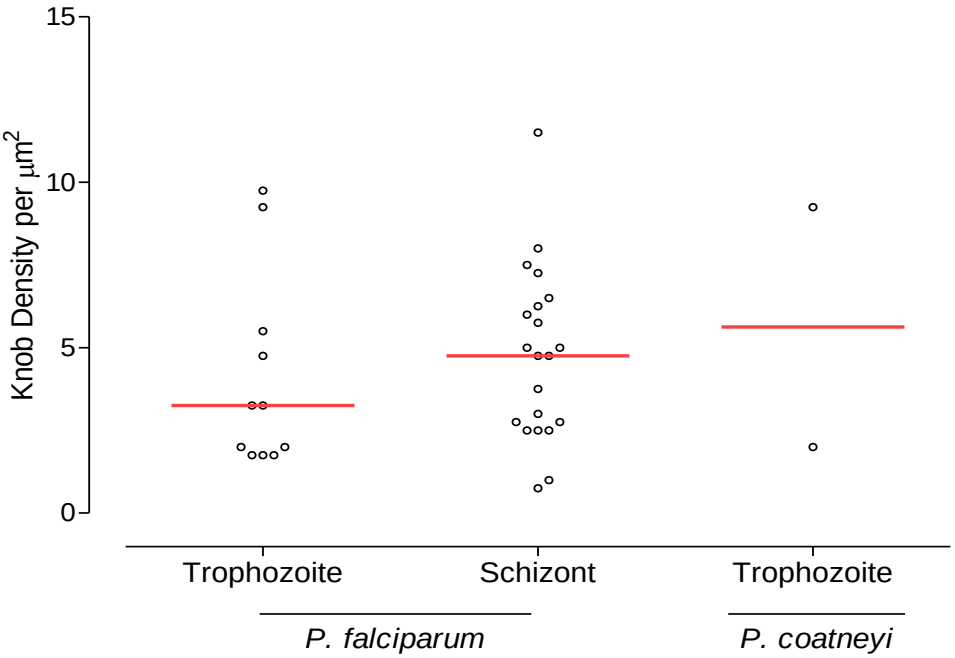

Figure 6.4.4.3: Graphed data of comparative knob density measurements which unfortunately due to the limited number of *P. coatneyi* knobs, limited any significant analysis of knob density in comparison with those from *P. falciparum*.

A relatively surprising finding noted during the ultrastructural analyses of the *P. coatneyi* infected erythrocytes consisted of the frequency of caveolae observed on the surface of the iRBCs. While a single author has described ultrastructural evidence of caveolae in association with *P. coatneyi* (Aikawa 1975; Aikawa 1977), no elucidation of the purpose of the structure was proffered. P. vivax has similar surface ornamentation which has been posited to be involved in protein trafficking from the parasite parasitophorous vacuole to the erythrocyte surface. (Aikawa 1988; Atkinson 1990) Using

AFM, we were able to conduct evaluations of the diameter of the caveolae (Figure 6.4.5.2) as well as of their density (Figure 6.4.5.3), however as this feature is not found on *P. falciparum*, no comparison was possible. Future research would be of interest in comparing these nanostructural features with those described in *P. vivax*, *P. ovale*, *P. fragile* and *P. cynomolgi*.

P. coatneyi

Trophozoite

Schizont

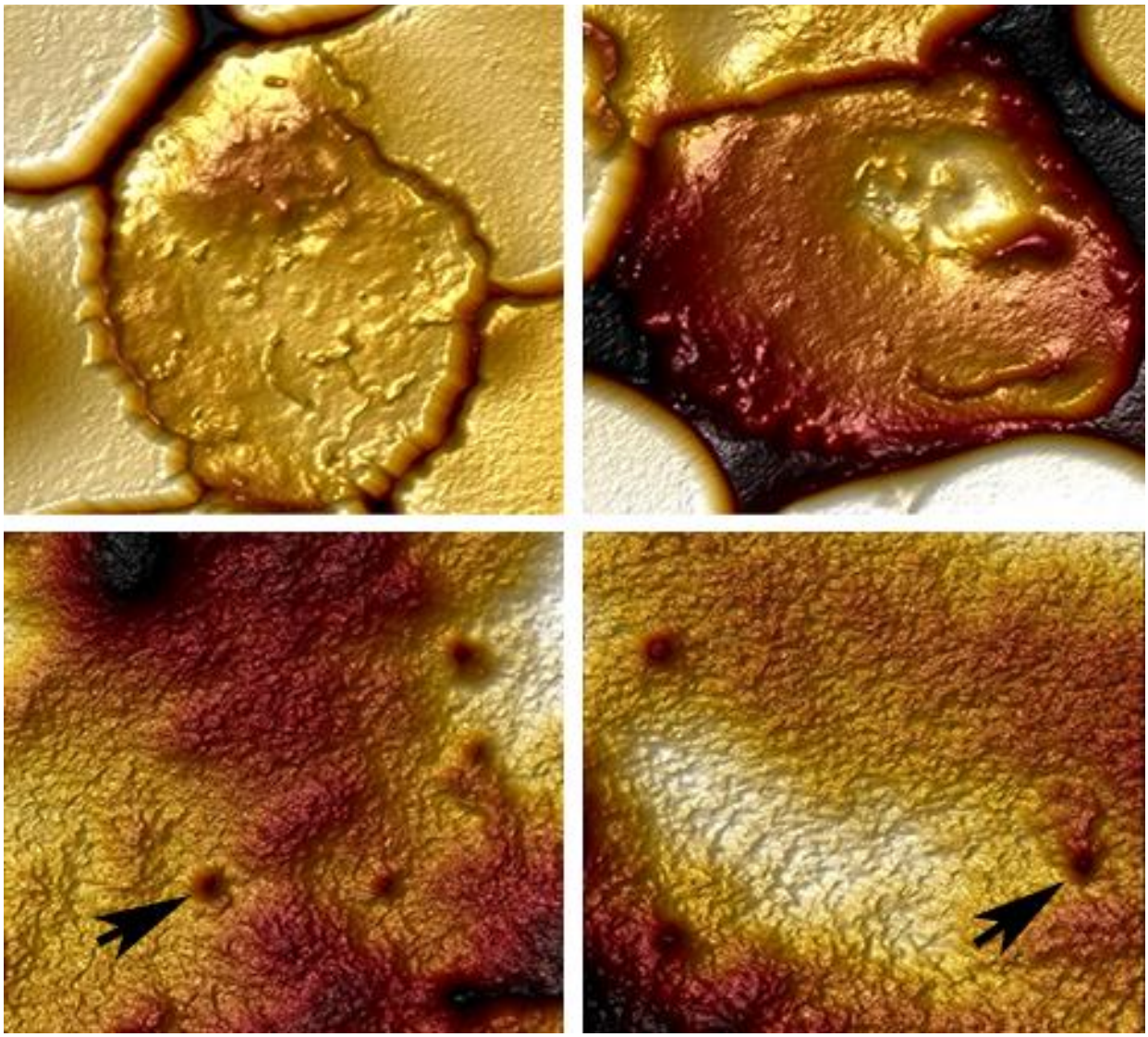

Figure 6.4.5.1: Caveolae were much more commonly observed using TEM, SEM and AFM, and as such, analysis holds greater statistical strength. The specific role of the caveolae in protein trafficking or in adhesion in *P. coatneyi* is unknown.

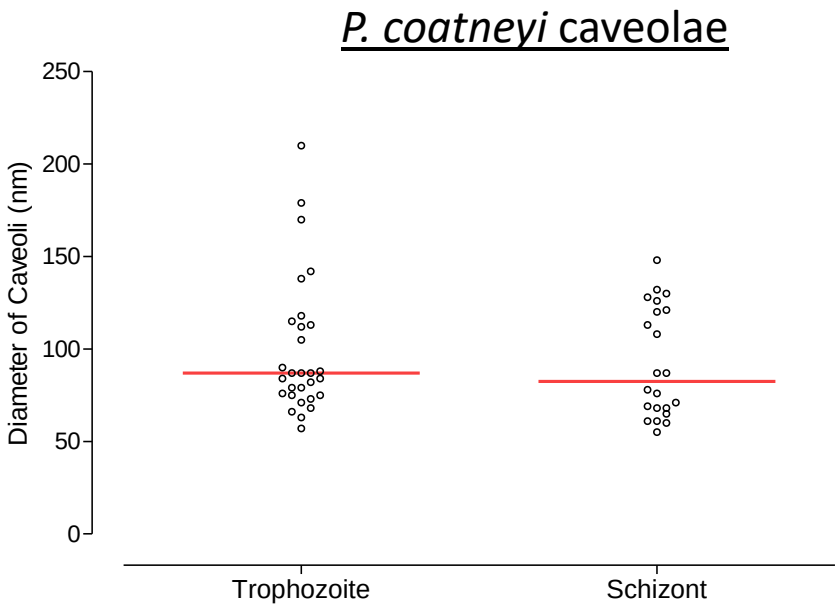

Figure 6.4.5.2: Graph demonstrating the mean diameter of caveolae. This did not differ significantly between trophozoites and schizonts. As with the knobs, five caveolae per cell were randomly chosen, and the diameter of each was measured using NanoScope Analysis (version 1.40)

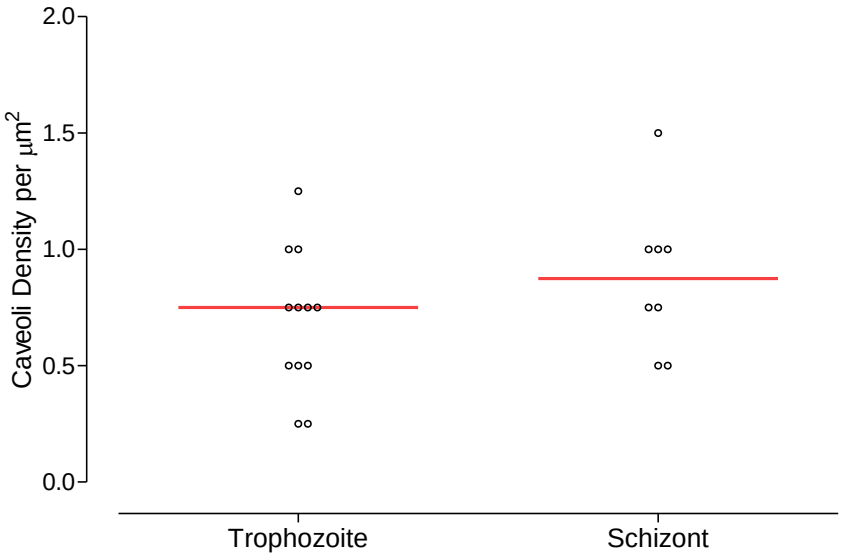

Figure 6.4.5.3: The density of caveolae on the plasma membrane was measured by calculating the number of knobs per μm^2. Again, this did not differ significantly between trophozoites and schizonts.

6.5 **Flow and binding dynamics**:

Preliminary analyses were undertaken using micropipette technology to measure the binding strength of the interaction between *P. coatneyi*-infected erythrocytes and uninfected normal RBC within rosette structures, as were evaluations of microfluidics in which flow dynamics of *P. coatneyi* were evaluated using flow grids designed with 2 and 4 µm channels intended on replicating the microvascular microstructure of the spleen (Figure 6.5.1-4). However, this was an initial pathfinding study and the resultant data, generated in only single experiments, are not within the scope of this dissertation.

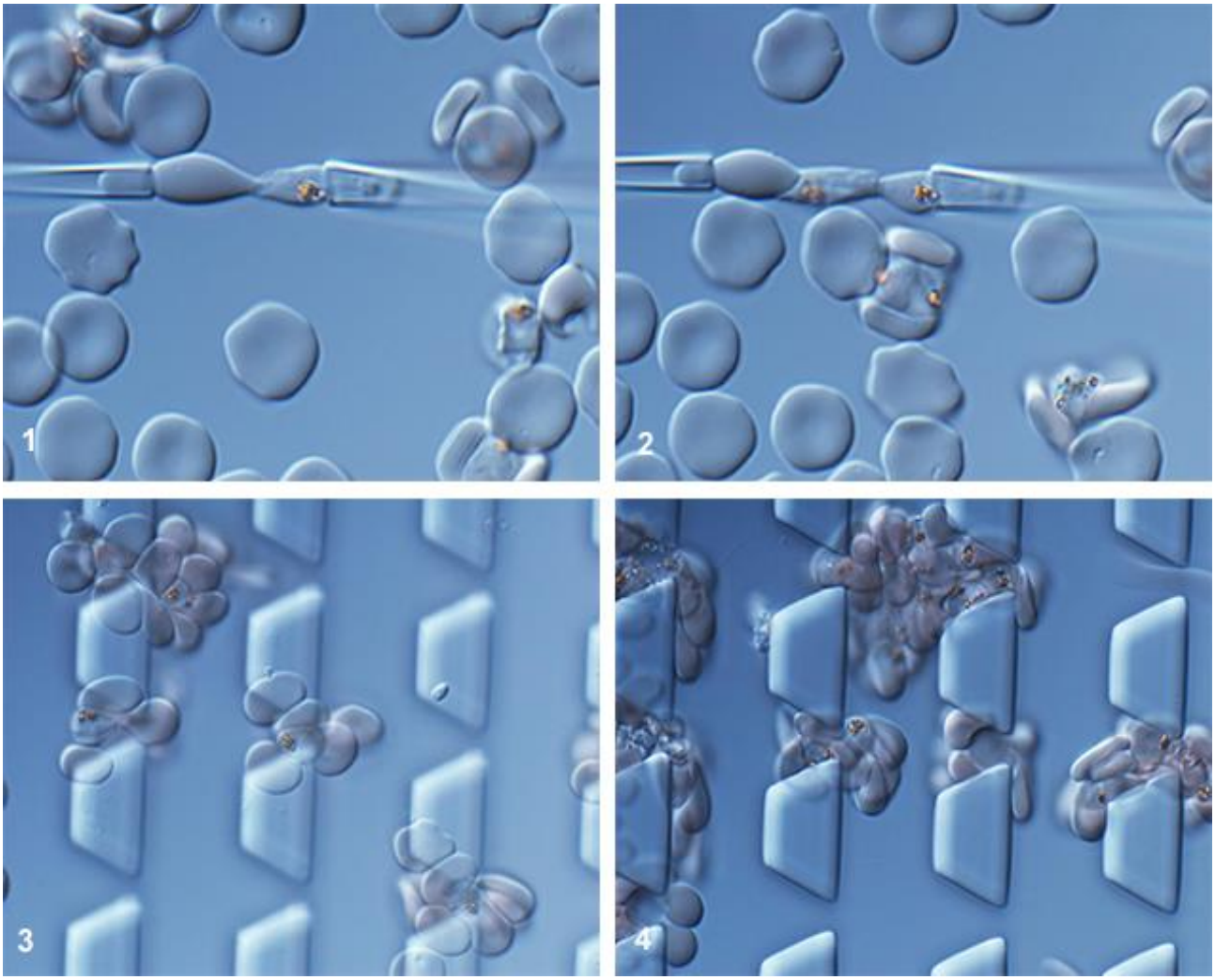

Figure 6.5.1-4: The micropipette images demonstrate the binding strength between Fig 1. an uninfected erythrocyte and an infected RBC, Fig 2. rosette cells consisting of 2 infected erythrocytes and an uninfected cell binding to each other. Fig 3. and Fig 4. are illustrations of the flow dynamics of *P. coatneyi* using flow grids to simulate the microvascular sludging resulting from the formation of rosettes.

6.6 **Discussion**:

The pathogenesis of both *P. falciparum* and *P. coatneyi* is proposed to be critically dependent on the capability to remodel the surface membrane of the infected erythrocyte and in doing so insert a range of adhesion proteins which are crucial to both the survival and pathogenicity of the parasites.

Mature mammalian erythrocytes lack endogenous molecules which permit a mechanism of protein trafficking, and as such the plasmodiae have evolved their own specialized mechanisms, which are extended beyond the parasitophorous vacuole of the malaria parasite into the host cell cytoplasm and then into the plasma membrane. (Akinyi 2012; Kats 2014) These adhesins molecules have been well described and are members of the protein family *P. falciparum* erythrocyte membrane protein 1, PfEMP1. (Leech 1984; Craig 2001; Quadt 2012) These molecules have been shown to be involved in the mediation of high-affinity interaction with an array of host vascular receptors. The library of parasite derived molecules expands daily however the main categories remain as 1. knob-inducing protein or "KAHRP"; 2. knob-associated cytoadherent proteins such as PFEMP-1; and 3. knob-associated structural proteins. (Sharma 1991; Tilley 2011) Phenotypically these can present as the nanostructural modifications which are observed as knobs or knob-like excrescences in *P. falciparum* and in *P. coatneyi* or as caveolae which are seen in *P. coatneyi* and in a select few other plasmodiae such as *P. vivax* and *P. ovale*.

Atomic force microscopy (AFM) is a technology which has showed extraordinary diversity in its application and has been used to successfully map the ultrastructural topography of malaria infected erythrocytes for various different plasmodial entities, to include select human parasites: *P. falciparum* (Aikawa 1996; Aikawa 1997; Akaki 2002; Garcia 1997; Li 2013; Nagao 2000; Olliaro 1997; Quadt 2012), *P. malariae* (Li 2010), *P. vivax* (Malleret 2015) and rodent parasites: *P. yoelli* (Claser 2014).

Knobs (or some variant thereof), caveolae, caveola-vesicle complexes, cytoplasmic clefts, and electron-dense material have all been described in plasmodium infected erythrocyte plasma membranes using various ultrastructural techniques. (Atkinson 1990) We focused on two important forms of surface ornamentation which are expressed on the plasma membrane of *Plasmodium* spp. infected primate erythrocytes. These structures vary in association with the specific species of plasmodium causing the infection. Knobs, or knob like protuberances, have been well described in *P.*

falciparum and *P. malariae* (Aikawa 1996; Aikawa 1997; Aikawa 2002; Li 2010) as well as in *P. coatneyi* (Aikawa 1992), while caveolae are seen on the surface of *P. vivax*, *P. ovale*, *P. fragile*, *P. cynomolgi* and rare reports of the structure observed in *P. coatneyi*. (Aikawa 1975; Aikawa 1977) There are sporadic reports which describe knobs on *P. ovale* (Matsumoto 1986) and portrayals of caveolae on the surface of *P. malariae* infected erythrocytes. (Atkinson 1990; Mackenstedt 1989) Both of these characteristic morphological alterations have been primarily described through the use of transmission electron microscopy and scanning electron microscopy.

P. coatneyi infected Rhesus macaques and Japanese macaques have been employed as animal models for severe and cerebral malaria associated by *P. falciparum*. (Aikawa 1992; Davison 1998; Kawai 1993; Lombardini 2015; Moreno 2013) *P. coatneyi* shares a range of pathophysiological, pathological and ultrastructural features with *P. falciparum*, as well as several distinguishing phenotypic characteristics. Both species of plasmodium have 48 hour intraerythrocytic development cycles, subsequent to which, schizogony occurs. The newly released merozoites undergo reinvasion of uninfected erythrocytes and the host has a resultant febrile spike. Both *P. falciparum* and *P. coatneyi* develop rosettes comprising one or multiple infected red blood cells which recruit uninfected erythrocytes (Doumbo 2009; Lombardini 2015; Moreno 2013), they both have well documented microvascular cytoadherence and both parasites appear to share some variation of knob-like structure on the cell surface hypothesized to be involved in the pathogenesis of cytoadhesion. The knobs on erythrocytes infected with mature asexual forms of *P. falciparum* are posited to allow the infected cells to cytoadhere to the vascular endothelium under shear flow conditions and thus avoid splenic clearance. (Malleret 2015)

Atomic Force Microscopy analysis of multiple *P. coatneyi* infected rhesus macaque erythrocytes demonstrated and confirmed the presence of both knob-like structures and caveolae on the modified cell wall of the infected erythrocytes. The surface ornamentation was analyzed for density per millimeter as well as for the overall diameter of the structures, and in the case of the

knob-like structures, were compared to similar structures on *P. falciparum* infected human erythrocytes. There appears to be a relative similarity in knob diameter, and while the data relating to density does not hold statistical significance, the mean data of the two *P. coatneyi* cells analyzed suggest similarity in density as well.

The subtleties as to the specific role in pathogenesis of *P. falciparum* malaria as well as the temporal dynamics of PfEMP1 and other malaria induced adhesion molecules have been extensively studied (Acharya 2012; Baruch 2002; Cooke 2004; Gruenberg 1983; Horrocks 2005; Leech 1984; Li 2006; Quadt 2012; Raventos-Suarez 1985; Su 1995), but beyond a few initial studies, the adhesion mechanisms of *P. coatneyi* infected erythrocytes remain poorly described. (Aikawa 1975; Aikawa 1988)

P. falciparum knob presentation appears to have maturation and temporal dependent mechanism as well as being linked to specific clones of PfEMP1 and chemical factors such as hemoglobin. (Allred 1986; Gruenberg 1983; Quadt 2012; Subramani 2015). All of the experimental animals in this study, in addition to being splenectomized were closely synchronized as to parasite stage of development. As such the resultant data is limited by being a single snapshot in the surface phenotype of the infected cells, and provides a foundation for further temporal descriptions.

Again, taking into account the fact that the present study is temporally static, caveolae appear to be the predominant surface ornamentation observed with *P. coatneyi*. (Aikawa 1975; Aikawa 1988; Barnwell 1990) These, described either as caveolae or as caveola-vesicle complex structures, are described in *P. cynomolgi*, *P.* vivax and P. *ovale* (Aikawa 1975; Aikawa 1977; Akinyi 2012; Barnwell 1990; Matsumoto 1986). The structures in *P. vivax* are predominantly a pit in the membrane surface which ultrastructurally appear as flask-shaped indentations of the erythrocytic membrane. In the case of vivax malaria, these structures are typically associated with membrane vesicles and as such have been termed as caveola–vesicle complexes (CVCs). In some cases, the

vesicles are described as being alveolar, while in other instances they are elongated and tubular (Aikawa 1975). In our description of the ultrastructural appearance of *P. coatneyi* infected erythrocytes, there appears to be a network of cleft-like vesicular structures which are distinct from Maurer's clefts, and which form intricate serpentine structures within the plasma membrane. While we have not been able to describe a specific link between the observed caveolae and these structures, they likely play a role in protein trafficking between the parasite and the erythrocyte plasma membrane.

It is fascinating to note that *P. coatneyi*, being a relatively young plasmodium in phylogenetic terms, shares phenotypic features which have been associated with *P. falciparum* and *P. vivax*. This study confirmed the ability of *P. coatneyi* to cytoadhere to host vascular endothelium and other cells in vivo, causing microvascular obstruction similar to that seen in human studies of *P. falciparum*. In addition, *P. coatneyi* shares a propensity for rosette formation with vivax (Chotivanich 1998) which may reflect phenotypic similarities in caveolae, which have been shown in *P. vivax* to co-localize with CD71 (transferrin receptor) expression on the infected reticulocyte surface and mediates adhesion to CD236 (Glycophorin) on uninfected RBC during rosette formation (Lee 2014). Whether this high rate of rosetting observed *in vitro* contributes to microvascular obstruction *in vivo* remains unclear.

6.7 **Summary**:

The ultrastructural studies examining the primarily the brain, kidneys and heart asserted the fact that P. coatneyi is a sequestering model, with strong evidence of infected erythrocytic cytoadherence through direct binding to the endothelium through the surface ornamentation as well as through a process of interdigitation and pseudopodia formation. Furthermore, there was abundant evidence of autoagglutination and rosette formation, although this proved to be excessive to that described in P. falciparum. Of crucial importance was the description by transmission electron microscopy, scanning

electron microscopy and atomic force microscopy of the surface ornamentation which proved to deviate from *P. falciparum* in the lack of regularity of the electron dense knobs with were scattered on the surface of erythrocytes infected with mature trophozoites, and the fact that *P. coatneyi* infected erythrocytes are also adorned by high numbers of caveolae, a feature more in common with *P. vivax*. Finally, instead of having Maurer's clefts, the infected RBCs contained single lamellar coiled vesicular structures throughout the cytoplasm. All of these findings were confirmed in spleen intact samples. The use of atomic force microscopy allowed for the actual measurement of both the knobs and the caveolae as well as an assessment of the density of the structures throughout the observed surface of the infected cells. In addition to describing the parasite-host cell interaction and the changes which occur secondary to the maturation of the parasite, this study permitted the ultrastructural description of the tissue pathology, observations of which have not been conducted to date with the *P. coatneyi* model.

Finally, and of substantial interest, were initial studies in micropipette measurements of binding strength, as well as rheology studies of adhesion which were conducted using matrices which mimic the splenic microvasculature. While the data derived from these studies is only preliminary, there remains a wealth of information to be derived from the further development of this technology and its use in describing *P. coatneyi* infection.

Chapter 7: The use of the Rhesus – *P. coatneyi* model in a treatment study of Methylene Blue in severe malaria

7.1 **Introduction**:

The World Health Organization assessed the human malaria burden worldwide in 2012 to be greater than 200 million cases of infection, 90% of which were caused by *Plasmodium falciparum*. (WHO 2014) *P. falciparum* infections are responsible for the preponderance of the deaths due to complications associated with the symptomology and pathology of severe malaria. The current crisis, which is becoming more and more apparent, is the escalating development of drug resistance by some strains of human malaria parasites, to include much of the world's *P. falciparum* strains. (Anderson 2010; Bhumiratana 2013; Kim 2013; Noedl 2010; Verdrager 1986; WHO 2014) There is ongoing investigation into the use of intravenous artesunate (AS) and several different phenothiazines as therapeutics for severe malaria. At present, the only United States Food and Drug Administration approved regimen for severe malaria is intravenous (IV) Quinidine, which has a narrow therapeutic index and severe potential side effects. A complication of this drug is that, due to the fact that the compound is no longer used in its primary form as an anti-arrhythmic agent, due to safer alternatives, many hospitals in the US have stopped carrying this medicine.

In the ongoing struggle to identify and test new potential anti-malarial drugs, there is significant concern relating to the very limited number of severe malaria animal models and their relevancy to human disease. Primate malaria models are justifiable to the extent that they can more closely predict human responses to anti-malarial drugs. It is a valid observation in malaria drug efficacy studies that the more phylogenetically similar the animal model, the more accurate the prediction of human responses. This has been previously described in the *P. coatneyi*-rhesus model for intravenous Artesunate. (Maeno 1993)

7.2 **Materials and Methods**:

7.2.1 **Methylene Blue**:

Mefloquine, halofantrine, and doxycycline are products of the U.S. Army's drug development program. One of the ongoing efforts is to develop a parenteral drug for severe malaria to replace quinidine; the only FDA approved parenteral anti-malarial currently available in the United States. Quinidine, an antiarrhythmic drug, has significant potential side effects, and is no longer carried in many U.S. hospitals as it has been replaced by newer and safer antiarrhythmic drugs. Most mortality from severe malaria occurs in the first 24-48 hours. Artemisinin derivatives differ from quinine/quinidine, the traditional treatments of severe malaria, in that they kill parasites much more rapidly. IV AS has been shown to reduce mortality in severe malaria when compared with quinine in two prior large Phase III trials. (Dondrop 2010, Seaquamat 2005) These agents can be given orally, intrarectally, intramuscularly, and intravenously. (Cao 1997) However, bioavailability and absorption variability are important limitations of oral agents as well as intramuscular artemether and artesunate (AS) suppositories. (Sabchareon 1998) Oral Artesunate-lumifantrine is available in the US for treatment of uncomplicated malaria, and parenteral AS is currently under evaluation by the FDA for use in the US for severe malaria, but it has not yet been approved. Furthermore, the cost and availability of the parenteral artemesinins may limit the availability of these drugs. Artesunate for injection (IV AS), is produced without internationally recommended Good Manufacturing Practices (GMP) by the Chinese (Guilin Pharmaceutical Factory #2, Guangxi, China), and currently is the only commercially available non-bulk pharmaceutical formulation. It is packaged by Atlantic Pharmaceutical Co. in Bangkok and is marketed in Thailand and other parts of Southeast Asia. The currently marketed AS formulation is a freeze-dried preparation which requires mixing with a sodium bicarbonate solution at the bedside, and then diluted with dextrose in water (Package Insert, AS for Injection, Atlantic Pharmaceutical Co., Bangkok). No non-bulk GMP parenteral artemisinin product is available. The US Army Medical Research and Materiel Command (USAMRMC) is developing a GMP

formulation of IV AS for use in the USA; at present however, IV AS is available in the USA via Investigational New Drug (IND). Additionally, oral artemisinin combinations for uncomplicated malaria are now the standard of care worldwide. They are also widely sold over the counter as single agents in non-curative regimens. The incredible drug pressure applied will ultimately result in drug resistance to artemisinins if patterns seen with all other anti-malarial drugs are followed. Resistance has been reported on the border regions between Thailand and both Cambodia and Myanmar. (Noedl 2010; Rooney 1992; Sermwittayawong 2015; Wongsrichanalai 2001) Efficacious alternatives to AS should, therefore, be investigated for the treatment of severe malaria.

Methylene Blue (MB) is commercially available as an IV formulation that is produced under GMP conditions as an U.S. Food and Drug Administration approved drug. It is used for the treatment of acquired and idiopathic methemoglobinemia (Devine 1983; Ellenhorn 1988; Gennaro 1990; Krogh 1993; Meissner 2006) and as a tissue dye in diagnostic procedures as a bacteriological stain (Devine 1983; Gennaro 1990; Krogh 1993), as a dye in diagnostic procedures such as fistula detection, and for the selective staining of certain body tissues during surgery. (Devine 1983; Krogh 1993) Its most commonly used brand name is Urolene Blue. MB has also been used off label for cases of septic shock, where it has been found to stabilize blood pressure and decrease vascular permeability. This is thought to largely be due to its ability to inhibit guanylate cyclase and the production of cGMP, which in turn decreases levels of TNF. (Harbrecht 1995; Kirov 2001) High levels of TNF have also been found to be an independent risk factor for severe *P. falciparum* cerebral malaria. (Day 1999; McCall 2010)

MB combines with nicotinamide adenine dinucleotide phosphate reduced (NADPH), in the presence of NADPH-methemoglobin reductase, to produce leukoMB; leukoMB then reduces methemoglobin to hemoglobin. (Curry 1982; Ellenhorn 1988; Krogh 1993; Yusim 2007) In high concentrations, MB oxidizes the ferrous iron of hemoglobin to the ferric state, facilitating the conversion of hemoglobin to methemoglobin. (Curry 1982; Devine 1983; Gennaro 1990; Krogh 1993; Meissner 2006) It has a 70% bioavailability in oral form (Walter-Sack 2009), is rapidly reduced to

leukoMB (Curry 1982; Gennaro 1990), and is excreted in the urine (Curry 1982; Ellenhorn 1988; Krogh 1993) and bile, primarily as leukoMB, although some unchanged drug is also excreted in the urine.

MB has long been recognized as an anti-malarial, being first described as one of many different phenothiazine compounds by Guttman and Ehrlich in 1891. (Guttman 1891; Guttmann 1960; Greenwood 1995) It has demonstrated activity against all malarial blood and gametocyte stages. German researchers working with modifications of the basic side chains on MB eventually were able to synthesize the first synthetic anti-malarial, pamaquine, and later synthesized a less toxic analog, primaquine. (Greenwood 1995; Olliaro 1995) Primaquine is still used to eradicate refractory hypnozoites of *P. vivax* and *P. ovale*. MB has recently been compared with other phenothiazine dyes and demonstrated a notably higher potency and selectivity in its anti-malarial activity. (Vennerstrom 1995) More recently, MB and some of its derivatives demonstrated an ability to bind haem/ferriprotoporphyrin IX (FP) and appear to have anti-malarial mechanisms that are similar to those of chloroquine, in that their activities are partially correlated with their abilities to inhibit β-haematin formation. (Atamna 1996)

MB also kills Plasmodia species via an increase in Plasmodial oxidants. Increase in oxidants can be due to inhibition of plasmodial glutathione reductase (so that oxidants are not removed) or by being a subversive substrate of the reductase (so that more oxidants are created). MB has demonstrated in vitro anti-malarial activity with a mean ED50 of 0.97 ng/mL against an in vitro panel of seven parasites. (Ohrt ILIR 2003, unpublished) No cross-resistance with other anti-malarial drugs has been identified. (Ademowo 2007; Pascual 2011) Combinations of AS and MB have demonstrated synergism when used in vitro. (Ohrt ILIR 2002, unpublished) This synergism has been confirmed in both rat and mouse/*P. berghei* models where 3-day intravenous regimens of both compounds resulted in cure, whereas AS or MB alone resulted only in parasite clearance with recrudescence. (Li, unpublished) Additionally, MB given as combination therapy with AS appeared to increase the rate of reduction of malaria parasites relative to AS given as a single drug therapy. (Xie, unpublished) An

earlier AFRIMS study compared IV AS and IV MB in the rhesus/*P. cynomolgi* model and found both to clear parasite loads rapidly, with some synergistic effects when the agents were combined. (Barker, et al unpublished) Similar findings were noted when comparing IV AS and IV MB in Aotus monkeys infected with *P. falciparum*. (Ohrt, unpublished) Several human clinical studies have been conducted in Burkina Faso, using MB to treat mild to moderate cases of *P. falciparum*. MB has demonstrated significant efficacy in clearing blood stage parasitemia using oral doses of 6-12 mg/kg twice daily for three days, regardless of chloroquine resistance. (Meissner 2006) MB has also been proven to be an effective addition to other anti-malarial medications including AS and Malarone, increasing rate of clearance. (Zoungrana 2008) By itself, MB as is true with AS, will clear blood stage parasitemia, but will show a high rate of recrudescence with only three days of therapy, demonstrating its need to be partnered with a longer acting agent to affect a cure.

With parenteral dosage forms in humans, MB should be administered by intravenous injection only; either subcutaneous or intrathecal injection may result in tissue necrosis or neural damage (Krogh 1993), respectively. Usual adult and adolescent parenteral dosage forms for methemoglobinemia are given as 1 to 2 mg per kg of body weight (Curry 1982; Ellenhorn 1988; Gennaro 1990; Krogh 1993; Yusim 2007), or 25 to 50 mg per square meter of body surface area (Ellenhorn 1988), administered over 5 minutes. The dose may be repeated after one hour if needed. The usual adult prescribing limit is 7.5 mg per kg of body weight. (Ellenhorn 1988) Pharmacokinetic (PK) data for MB in humans, dogs and rats has been published (Aeschlimann 1996; Aeschlimann 1998; Disanto 1972a; Disanto 1972b; Disanto 1972c; Peter 2000; Walter-Sack 2009; White 1999), and has been evaluated in non-malaria infected rhesus monkeys at 2.5, 5, 10, and 20 mg/kg in a prior AFRIMS experiment. Data from rhesus monkeys shows similar peak concentration properties to humans, however it is metabolized about 3.5 times more rapidly, resulting in a smaller AUC. (Barker, et al unpublished) The usual commercially available formulation is a generic at 10 mg per mL prepared and

packaged under GMP conditions as a 1% USP solution in water. Sodium chloride 0.9% is compatible for dilution of MB.

MB has demonstrated the ability to rapidly decrease parasitic load. If proven non-inferior to IM Quinine, IV MB would make a welcome addition to the severe malaria drugs, given that it appears to be safer than IV quinidine, and IV AS is not readily available worldwide at this time. It will also be useful to have an alternative treatment available in the event that resistance develops to IV AS.

7.2.2 **Dose Formulations Stability and Storage Conditions**:

1. Methylene Blue: Methylene blue was packaged as a USP 1% solution in water for injection at 10 mg/mL in that has already been pH adjusted with sodium hydroxide and/or hydrochloric acid. The injectable solution was stored in the dark at controlled room temperature (15° - 30°C).

7.2.3 **Drug inoculation**:

Animals were randomly assigned to three experimental groups which were: MB 6 mg/kg IV twice daily (cohort 1), MB 10 mg/kg IV twice daily (cohort 2) or MB 17 mg/kg IV twice daily (cohort 3). Based on these groups, evaluation of the efficacy of methylene blue was achieved at low, medium and high doses.

7.3 **Donor Animals**:

P. coatneyi was inoculated from one rhesus to another through a blood challenge of infected erythrocytes. Inoculation began in an infected donor by intravenous inoculation of freshly thawed cryopreserved *P. coatneyi* strain infected blood. The stabilate stock (maintained at AFRIMS) has been tested and confirmed negative for Herpes B virus, SRV, SIV and STLV-1 to ensure no possibility of

adventitious virus transmission into the monkey colony. One cc aliquot of a thawed stabilate of *P. coatneyi* infected RBCs was administered intravenously into a peripheral vein of the donor monkey as described below. Blood smears were prepared to detect malaria parasites starting on Day 0 before inoculation and continued daily.

Once the blood smear was noted to be positive, either white blood cell (WBC) and/or red blood cell (RBC) counts were performed daily to determine a parasite density (parasitemia). After the parasitemia had reached > 50,000 parasitized RBCs per µL, 10-20 mL of blood was drawn into a heparinized tube, diluted with sterile PBS solution to a concentration of $5x10^6$ infected erythrocytes per 1 mL suspension, and divided into equal 1 mL aliquots. The 1 mL aliquots were subsequently used to infect the study animals and to prepare additional cryopreserved stabilates for future use.

After completion of the blood draws, curative treatment was given with CQ 10 mg/kg, PO daily for 7 days. The donor monkeys were considered to be off-study once blood donation had been completed and animals were cleared of parasites.

7.4 **Experimental Animals**:

A total of nine monkeys in this portion of the study were randomly assigned to each of 3 experimental groups with three monkeys in per group. A prior model refinement study involving 6 untreated animals served as controls. Experimental animals (not including donors) were euthanized upon treatment failure or on day six after initiation of treatment. The ultimate goal of this study was to provide efficacy data for the selection of an optimal dose of MB for use in planned phase II human clinical trials, and to support the U.S. Army anti-malarial research program.

The MB drug dosing schedule, euthanasia date, peak parasitemia and terminal parasitemias are described in Table 7.2. Due to the intensity of blood sampling, parasitemia assessment, clinical

monitoring and eventual autopsy, the three MB groups were staggered by a week, and an individual donor macaque was randomly assigned to each group.

The study selected nine splenectomized, chair trained, Indian origin rhesus macaques ranging in age from seven to 13 years old, from the AFRIMS closed colony. Both genders were represented and all animals were evaluated for prior experimental history to ensure that none of the animals had been exposed to *P. coatneyi* previously. Additionally, three spleen intact donor Indian origin rhesus macaques were selected and randomly assigned to each dosage group. The nine experimental animals were splenectomized in accordance with AFRIMS surgical protocols, injected with a microchip temperature recording device (telemetry) in the subcutaneous tissues between the shoulder blades and recovered for one month prior to being infected by peripheral vein inoculation with *P. coatneyi*-blood stage parasites (approximately 1 mL of 5x106 infected RBCs) drawn from the donor monkeys.

Throughout the study, blood draws were calculated using a reference point of a 6.8kg animal as the least common denominator. However, with larger animals, under the purview of the attending veterinarian, blood draws were increased based on their body weight and permissible blood draws per SOP. All blood drawn was used in accordance with the testing described in the IACUC approved protocol amendments.

7.4.1 **Ethics**:

Research was conducted in compliance with the Animal Welfare Act and other federal statutes and regulations relating to animals and experiments involving animals, and adhered to principles stated in the Guide for the Care and Use of Laboratory Animals, NRC Publication, 2011 edition. The protocol was approved by AFRIMS 12-08.

7.5 **Clinical parasitology**:

Blood smears were conducted beginning on ID-0 before the parasite inoculation and continued three times daily until positive parasitemias exceeding 5000 per cu mm are measured, typically on day five to six. Beginning on day six, parasitemia assessments increased to eight times daily until the treatment criteria were reached and for several subsequent days (typically day six through day 10). Once a smear was positive, WBC and/or RBC counts were performed on an increasing schedule both to determine parasite density and percent parasitemias (calculations per AFRIMS Standard Operating Procedures: Malarial Parasite Count for Quantifying Parasitemia in Experimental Animal's Infected Blood), as well as for clinical chemistry evaluation and complete blood count (CBC).

Blood smear samples on glass slides were fixed in methanol and stained with Giemsa. They were examined for the presence or absence of parasites under the oil-immersion objective as well as parasite staging. If no parasites are found in 50 microscopic oil-immersion thick fields or approximately per 1000 white blood cells (WBCs), the smear were considered negative. The parasitemia level was reported as number of parasites per 1µl or mm^3 of whole blood and converted to a percentage. Parasites were counted per number of WBCs or red blood cells (RBCs), i.e., per 100 –300 WBCs or 500 – 10,000 RBCs. Parasitemia levels were calculated by the appropriate total blood cell count (white or red) per mm^3.

7.6 **Study endpoints and Treatment Outcome Definitions**:

Response to treatment was characterized as a continuum based on parasite suppression, clearance and clinical symptomology. Success was determined as a combination of a parasitemia decline by $\geq$ 75% at 48 hours with clinical improvement, combined with parasitemia clearance >99% at the third day after treatment initiation, and an absence of moribund behavior, stable respiratory

status, and stable blood pressure. Study Failure, on the other hand, included a parasitemia decline of less than 75% at 48 hours with clinical deterioration, failure to clear parasitemia by 99% by day 3 after treatment initiation, or moribund behavior, unstable respiratory status, or unstable blood pressure at the end of three days of therapy.

Further treatment failure was determined by the attending veterinarian in association with the Principal Investigator and the infected monkeys were considered as having reached study endpoints if the parasitemia failed to decrease and any three predetermined clinical criteria were reached during the post treatment period. These included: symptomology associated with persistently elevated temperatures, severely suppressed mentation, sustained anorexia, chemistry associated with hepatic or renal failure, coagulopathies or respiratory distress.

It was expected, in this severe malaria model, that the animals would display signs of severe malaria at the initiation of therapy, and it was anticipated that they would continue to show these signs during the first 24 hours of therapy regardless of the medication dose used. Anticipated clinical signs included combinations of the above listed clinical criteria, however these were expected to be transient and reversible once treatment was initiated. Additionally, clinical chemistry and hematological findings were expected to demonstrate organ pathology. These included hypoglycemia, metabolic acidosis, severe anemia, high blood lactate and/or renal impairment (elevated BUN and Creatinine).

7.7 **Temperatures and clinical symptomology**:

Temperatures and clinical signs were monitored throughout the study with frequency increasing in synchrony with the rising parasitemia to a peak of every other hour over 24 hour cycles. Temperatures were recorded via rectum as well as by using a subcutaneous transponder that was injected under the skin between the shoulder blades in all animals.

Clinical signs were collected a minimum of 7 times daily and a maximum of 12 times daily. These were in conjunction with collection of a drop of blood for parasitemia assessment and were noninvasive.

Criteria evaluated and scored included the assessment of activity level as determined by moving around the cage and the response to the presence of a veterinarian or a technician; mentation which was evaluated as a response to stimuli outside the cage; menace response in which an animal will blink or withdraw when a sudden movement occurs close to the eyes; breathing, to include both the quantitative number of breaths as well as the quality: labored, shallow, gasping…etc; skin color to include any signs of hemorrhage, jaundice or cyanosis; presence of vomitus; skin turgor as a sign of hydration status; urine color and both quantitative and qualitative assessment of the urine captured in the pans under the cage; and appetite. All signs were graded, with a maximum score of 24. A normal animal would score 0.

All animals had terminal blood, cerebrospinal fluid and urine collected. Complete autopsy was performed in all animals with weighing of select organs (brain, lungs, heart, liver), collection of all tissues in 10% buffered formalin, selected tissues in Glutaraldehyde and RNA-later, as well as photography of all significant lesions.

7.8 **Histopathology**: In the 15 animals enrolled in various elements of the study, widespread tissue sampling was performed at post mortem, and the histopathology evaluated both by a board certified veterinary pathologist (EDL) and medical pathologist (GDHT). Tissue pathology was categorized in comparison with both AFRIMS archival tissue from normal control rhesus macaques as well as noting those changes that have been associated with normal aging or background variation. (Chamanza 2012)

7.9 **Results**:

Infected animals typically began to develop clinical symptomology around day 7 post inoculation, although decreased appetite or anorexia was often noted around day 4 to 5. Initial signs were often found to be associated with activity level and mentation. These were closely aligned with the first significant increases in temperature. At this stage, an animal would typically have a total score of around 7, consisting of anorexia (3), some degree of hematuria (1-3), moderate to marked reduction in activity (1-2) and decreased mentation (1). When the hematuria became more significant, changes in skin turgor would typically follow. Immediately prior to death or euthanasia, animals had severely decreased mentation with loss of the menace response. Animals were recumbent in their cages and non-responsive to external stimuli without reaching human criteria of true coma. Animals would typically have been anorexic for 2 days, and at some point would have vomited. Occasionally, there were episodes of dysuria, and in all animals varying degrees of hematuria was observed. By day 7, most animals were showing signs of dehydration, and in a couple of the animals, prior to death there was evidence of dyspnea.

Animals in cohort 1, at the point of euthanasia, while being slightly depressed, had normalized their clinical signs. All three animals had regained their appetites, had improved urination and were normothermic. 2 of the 3 animals in cohort 2 were noted to be vomiting, have decreased mentation, be anorexic or have dysuria at euthanasia, while the third had normalized. In cohort 3, 2 animals also had severe clinical signs at euthanasia, to include epistaxis, vomiting, sustained anorexia, decreased mentation. The third animal had normalized.

In normal adult animals from the AFRIMS colony, baseline temperatures measured rectally fluctuate between 99.5° F to 102° F (37.5° C to 38.9° C) depending on a range of physiological factors to include gender, feeding schedule, stress, handling time, concurrent procedures.

Experimentally, following the initial temperature spike at day 7, which would often be around 104° Fahrenheit (F) or 40° Celsius (C), the temperature would remain higher than baseline, with peak temperatures reaching up to 107° F or 41.7° C, but fluctuating until death or euthanasia.

Beginning on day 1 post inoculation, there was an observable parasitemia which subsequently decreased and by the beginning of day 3 was no longer significant. By the 3rd sampling on day 3, the parasitemia had undergone an initial spike in the range of 10,000 to 30,000 parasites/mm^3 red blood cells. The cycle continued and the parasitemia again decreased, rising again by the end of day 5 at which point the values ranged from 200,000 to 350,000 parasites/mm^3 red blood cells. A subsequent decrease over day 6 with an expected spike by the end of day 7 resulted in calculated parasitemia in excess of 1 million parasites/mm^3 red blood cells. In the control animals, the parasitemia remained sustained at that threshold until death or euthanasia which never exceeded day 8 without some form of medical intervention.

Parasite life cycle stage was a crucial feature employed for a complete understanding of the disease progression. The parasitemia spike on day 5 represented a peak of ring stages followed by a predictable increase and peak in trophozoites on day 6 leading to a small spike in schizonts. This was closely followed by the day 6 (evening) increase in ring forms, a smaller increase in trophozoites and then a schizont increase on day 7. This was followed closely by a dramatic increase in ring forms, which as it began to taper off, yielded to the significant increase in trophozoites at the beginning of day 8. The animals in the refinement protocol (untreated controls) typically did not survive beyond this peak, and were euthanized or died naturally. Animals in the MB dosage groups showed similar initial parasitemia curves, but once the treatment window was achieved, the parasitemias were significantly controlled, decreased and eventually cleared in most of the drug study animals. (Figures 7.9.1-3)

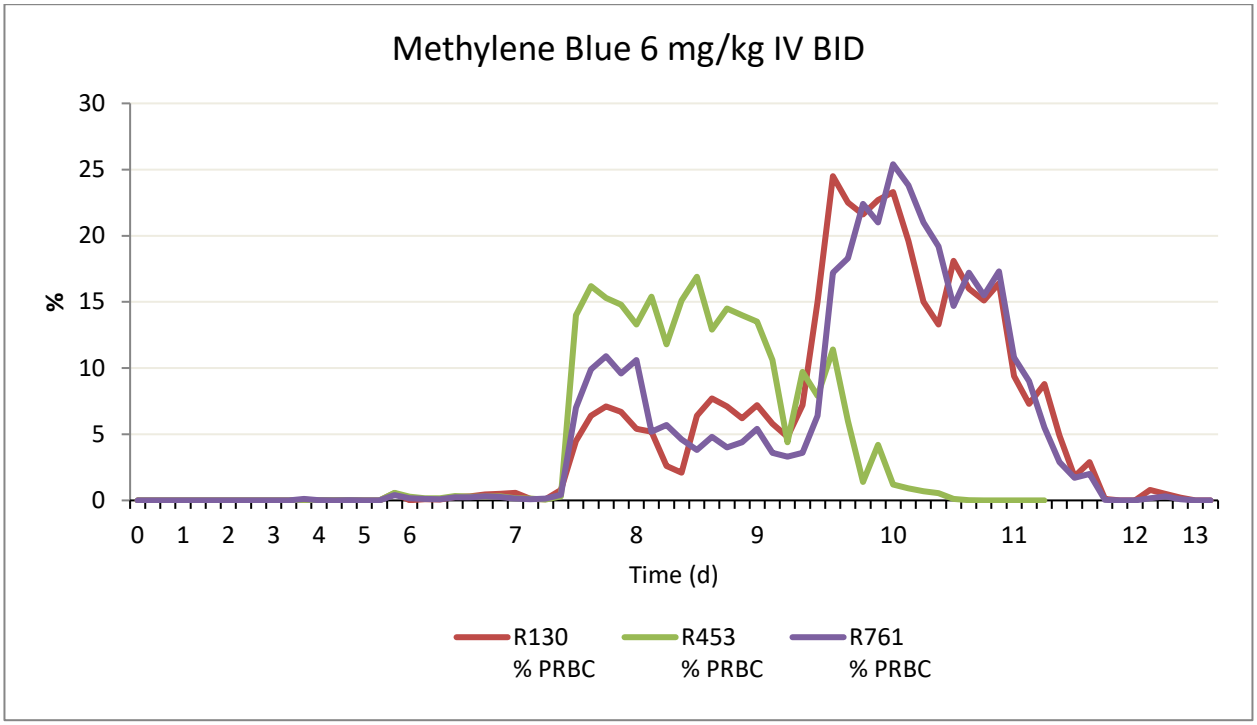

Figure 7.9.1: Parasitemia curves cohort 1

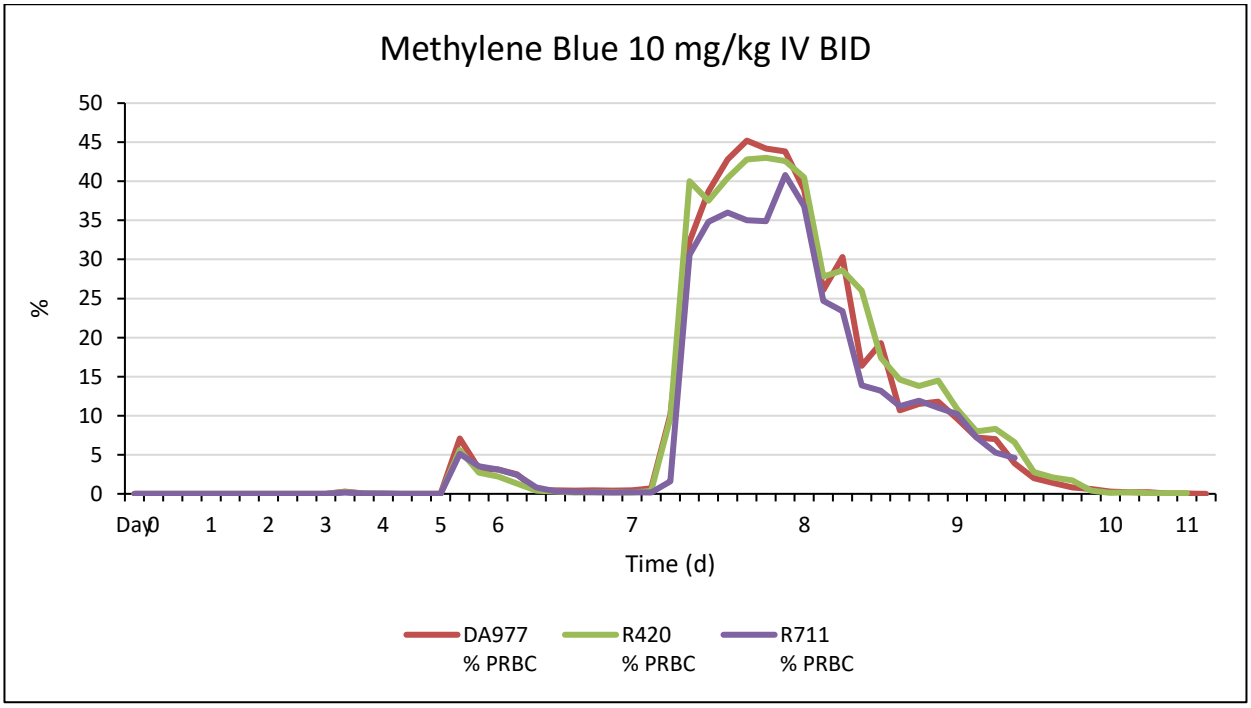

Figure 7.9.2: Parasitemia curves cohort 2

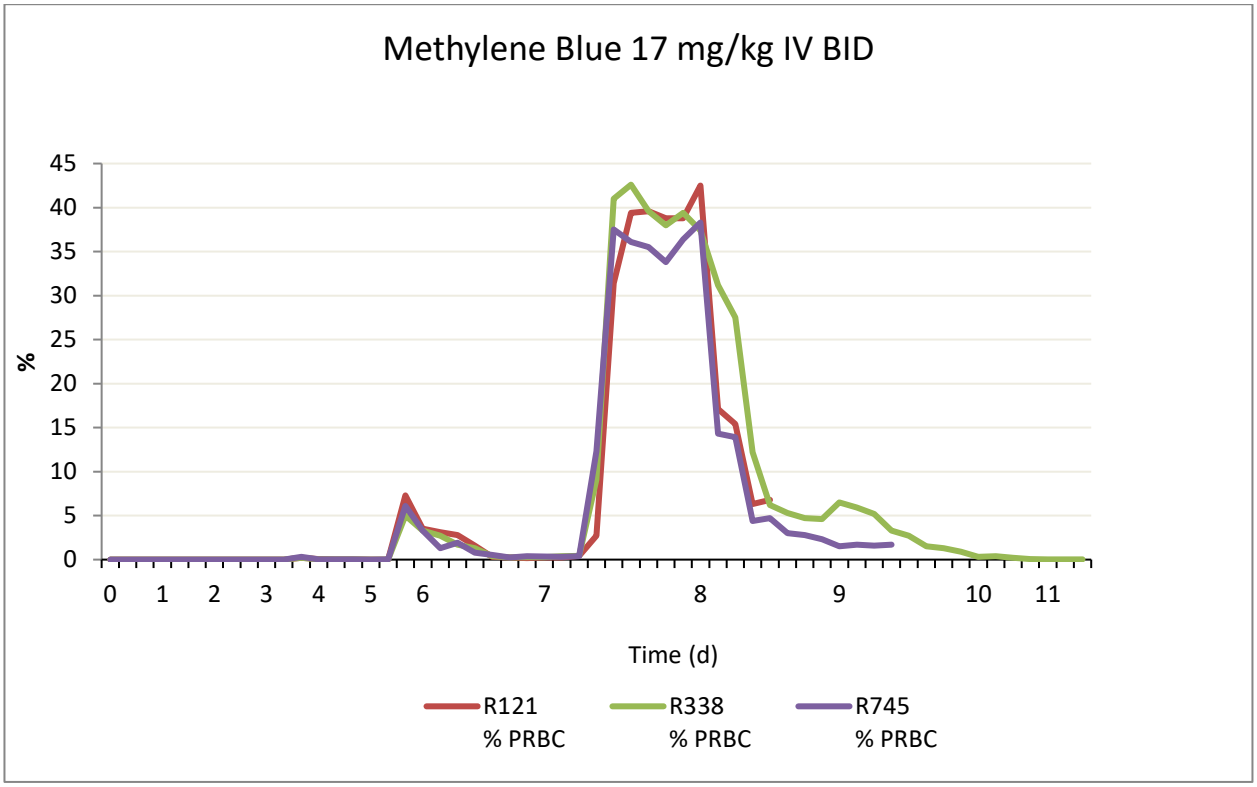

Figure 3: Parasitemia curves cohort 3

7.9.1 **Drug-treated animals**:

The efficacy of each dose of MB is shown in Table 7.3. MB at all doses was relatively effective in terms of parasite clearance. Three animals did not fully clear as the full treatment regimen could not be administered due to severity of clinical signs. In those three animals (1 from cohort 2 and 2 from cohort 3) the parasitemia was trending towards clearance at euthanasia. 6mg/kg BID MB was the most effective cohort, however peak parasitemias in those animals remained at 25% or below, while cohorts 2 and 3 reached parasitemias which peaked at between 38-45%. Due to severe vomiting and dysuria in cohorts 2 and 3, furosemide and cimetidine were administered in some animals concurrently with MB treatment.

For those animals who demonstrated treatment success, clearance times ranged from two to three days. The increased severity of clinical signs in animals from cohorts 2 and 3 must be considered in the context of both the increasing drug dose and therefore a potential toxicity as well

as the markedly higher peak parasitemias and associated clinical signs and tissue pathology. As the infected control animals were also noted to have evidence of acute renal, hepatic and cardiac injury, we posit that the degree of parasitemia was the driving force requiring early euthanasia in 3 of the experimental animals rather than potential toxicity of MB.

7.9.2 **Gross findings**:

The primary macroscopic findings in control animals were associated with hemozoin deposition in tissues. This presented as a dark brown discoloration of the parenchymal organs. Liver, heart, lungs and kidneys all were severely darkened by the presence of the malaria pigment, admixed with the blue tinge of MB. (Figure 4) Additionally, there was enlargement of multiple organs with the liver being the primary organ demonstrating megaly.

Macroscopic findings in experimental animals was primarily dependent on the duration of treatment and the survival period beyond peak parasitemia. Findings ranged from lesions consistent with those described in the *P. coatneyi* infected control animals to tissues appearing only slightly discolored when compared with archival normal control animals. Additionally, MB appeared to concentrate in specific tissues, resulting in a light blue tinge being noted in the grey matter of the spinal cord, brain stem, the pars intermedia of the pituitary gland (Figure 5), the prostate gland, the gallbladder, urinary bladder and the renal medullae.

Figure 7.9.2.1: Kidney. MB treated *P. coatneyi* Rhesus macaque. The renal parenchyma is markedly discolored, with concentration of the methylene blue within the cortex and the medullary pyramids.

Figure 7.9.2.2: Cerebrum, cerebellum, brain stem and pituitary gland. MB treated *P. coatneyi* Rhesus macaque demonstrating the dramatic blue tinge seen in various tissues throughout the body of

treated animals, but which was most significant within the endocrine tissues, the kidneys and the central nervous system.

7.9.3 **Histopathology**:

In the control animals, there was significant microvascular sludging with parasitized erythrocytes and hemozoin pigment noted in all tissues, with increased evidence noted in the central nervous system, heart, hepatic sinusoids, the renal glomeruli and endocrine tissues such as the pancreatic islets of Langerhans, the adrenal glands and the pituitary gland. This appeared to be resulting in a degree of microvascular obstruction, interpreted due to an increased congested appearance to many vessels and increased numbers of vessels observed per section. Due to the detail required for confirmation, sequestration was confirmed using transmission electron microscopy. Additionally, in all affected tissues, there was abundant hemozoin pigment observed.

Tissue histopathology in the experimental cohorts ranged in severity, correlating both with peak parasitemia levels and survival period post treatment. (Table 7.1) The treated animals lacked any observable sequestration, and with the exception of the presence of free and phagocytosed hemozoin and hemosiderin pigments, there was no remnant evidence of the malaria infection. However, the lingering effect of the insult of severe malaria was evident in many of the tissues. (Figure 7.9.3.1-4) Occasionally, liver samples would have evidence of zonal coagulative or lytic necrosis while sections from the kidneys would have significant epithelial regeneration as well as ongoing evidence of residual damage. Cardiac pathology was typified by piecemeal loss of cardiomyocytes, periodic fibrosis and single cell hypertrophic changes suggestive of reactive changes. The central nervous system had fewer lesions in comparison with experimental control animals and often there would be an absence of acute pathology, while there was a slight increase in more chronic evidence of injury such as degenerative changes to the neurons. Other changes consisted of

expected chronic effects of the systemic erythrocyte damage, such as lymph node and (when available) splenunculum erythrophagocytosis and hemozoin pigment admixed with hemosiderin.

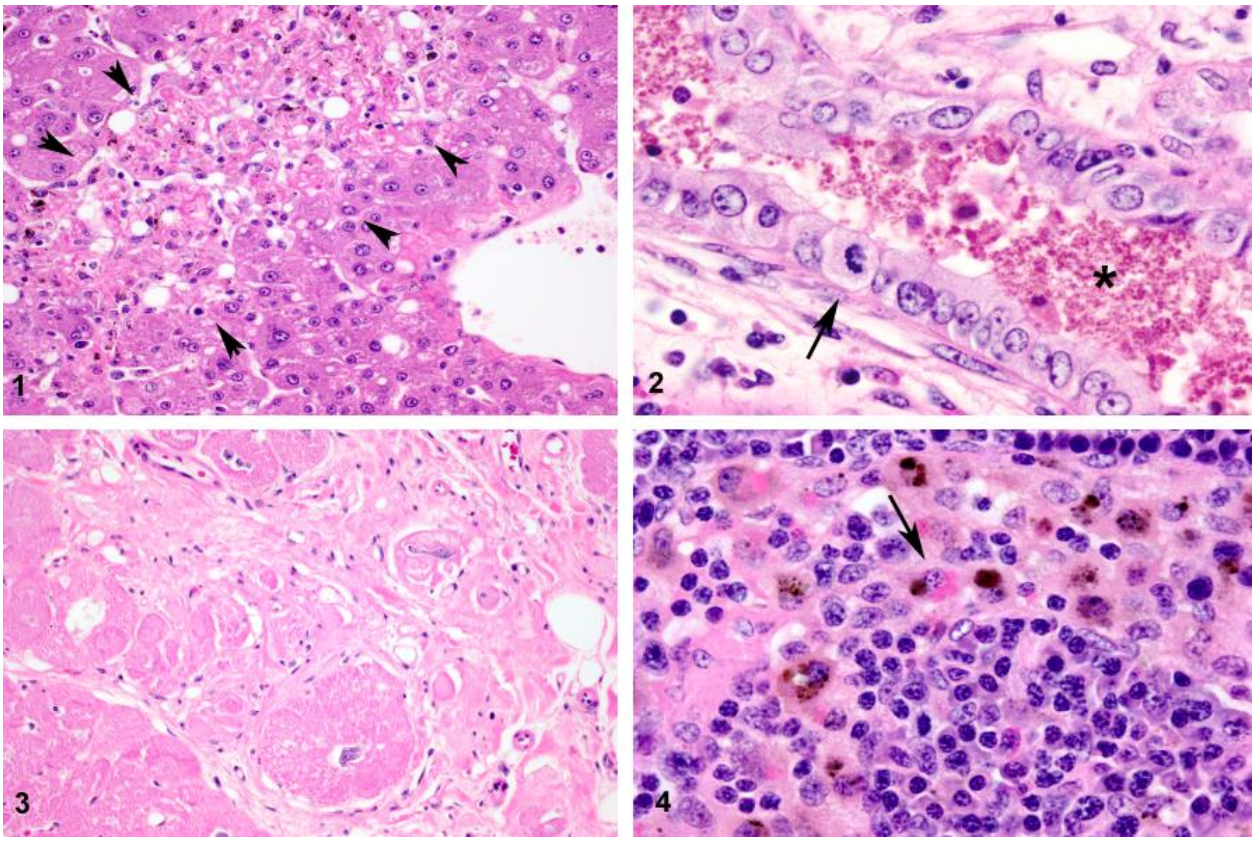

Figure 7.9.3.1-4 Example photomicrographs of residual severe malaria pathology in MB treated macaques. 7.9.3.1 This image demonstrates an example of a focus of hepatocellular necrosis (arrowheads). In this instance the lesion is near the central vein and while in this plane of section it is not contiguous with the centrilobular zone, there was a noted zonality hypothesized to be associated with hypoxic injury. HE 400x. 7.9.3.2 This photomicrograph illustrates a renal tubule with luminal hemoglobin pigment (asterix) and necrotic cells. The epithelium lining the tubule demonstrates evidence of regeneration with mitotic activity (arrow), cellular piling and cells with a high nuclear to cytoplasmic ratio. Additionally, there are scattered leukocytes infiltrating the interstitium. HE 1000x. 7.9.3.3 This photomicrograph of the myocardium shows evidence of fibrosis and cardiomyocyte loss as well as reactive changes comprised of cellular hypertrophy and megakaryosis. HE 400x. 7.9.3.4 This image is a high magnification of the sinus of a paratracheal lymph node. In this image, there is a sinus

histiocytosis with abundant phagocytosed hemosiderin pigment and abundant erythrophagocytosis. (arrow) HE 1000x.

Animal #	Drug dose	Terminal parasitemia	Parasite sequestration severity	CNS hemorrhage severity and location	CNS edema severity	Cerebellum Purkinje cell degen	Axonal/neuronal injury severity and location	Renal injury severity	Hepatic injury severity	Cardiac injury severity	Vasculitis Y/N
15-264	Cohort 1	16.90%	0	3/2; brain stem/spinal cord	2	3	3/2; cerebrum/spinal cord	2	3	1	N
15-265	Cohort 1	24.50%	0	0	3	3	3/2; cerebrum, brain stem/spinal cord	4	4	3	N
15-266	Cohort 1	25.40%	0	0	1	1	1; cerebrum, brain stem	3	2	1	N
15-274	Cohort 2	42.80%	0	0	3	3	3/2; cerebrum/spinal cord	4	4	3	N
15-275	Cohort 2	45.20%	0	0	2	1	2/1; spinal cord/cerebrum	3	2	3	Y
15-272	Cohort 2	40.80%	0	1; spinal cord	2	1	1; cerebrum; brain stem	5	2	1	Y
15-271	Cohort 3	42.50%	0	3/2; spinal cord/brain stem	1	1	3; spinal cord	5	2	1	Y
15-273	Cohort 3	38.30%	0	0	2	0	2; cerebrum	5	2	3	N
15-276	Cohort 3	42.60%	0	1; spinal cord	2	1	1; cerebrum, brain stem	2	3	2	Y
Mean	**Cohort 1**	**22.30%**	**0**	**1**	**2**	**2.3**	**2.3**	**3**	**3**	**1.7**	
Mean	**Cohort 2**	**42.90%**	**0**	**0.33**	**2.3**	**1.7**	**2**	**4**	**3.3**	**2.3**	
Mean	**Cohort 3**	**41.10%**	**0**	**1.3**	**1.7**	**0.7**	**2**	**4**	**2.3**	**2**	
13-106	Control	13.60%	5	3; spinal cord	3	1	3/2; cerebrum/spinal cord	2	2	2	Y
13-107	Control	10.50%	5	3; spinal cord	3	3	3; spinal cord	2	2	2	Y
13-108	Control	7.50%	5	3; spinal cord	3	1	2; cerebrum, spinal cord	2	3	2	Y
14-198	Control	34.80%	5	2; brain stem/cerebrum	3	3	2/1; cerebrum/spinal cord, brain stem	3	3	2	N
14-199	Control	39.20%	5	1; spinal cord	3	3	2/1; cerebrum/spinal cord, brain stem	3	3	2	N
14-200	Control	34.20%	5	2; spinal cord	3	2	2/1; cerebrum/spinal cord, brain stem	2	3	2	Y
Mean	**Control**	**23.30%**	**5**	**2.3**	**3**	**2.2**	**2.3**	**2.3**	**2.7**	**2**	

Table 7.1: Comparative histopathology control animals versus methylene blue treated. Scores are semi-quantitative based on assessment by both EDL and GDHT. The severity score was based on a scale of 0 to 5, and then the data was averaged by cohort to achieve a mean value per group. The same was conducted for the experimental controls, thereby allowing comparison.

Specifically, experimental animals did have pathology which was hypothesized to be attributed to hypoxic injury secondary to the previous sequestration. In cohort 1, hepatic pathology extended from zonal glycogenosis and lipidosis to one animal having moderate, portal bridging coagulative necrosis of the hepatocytes. In that particular animal, there was also evidence of hemorrhage within the brain stem. Cohort 2 was observed to have similar degree of hepatic severity as cohort 1 while cohort 3 had milder amounts of hepatic insult, and those were typically limited to a zonal glycogenosis, and piecemeal necrosis rather than large scale coagulative necrosis. In all of the

groups, there was a degree of acute renal damage which correlated with clinical chemistry findings. The methylene blue treated animals displayed slightly increased severity of renal pathology than control animals which appears to be a paradoxical finding. MB has been used in a range of studies as a reno-protective drug due to its inhibition of the Nitric Oxide (NO) pathway with the downstream formation of cyclic guanosine monophosphate (cGMP) through the binding of the soluble guanylate cyclase (sGC) heme moiety. Combined, these results in lipopolysaccharide-associated proximal tubular renal toxicity. (Heemskerk 2008) As discussed previously in the chapter, MB is capable of binding sGC, which thereby blocks the production of cGMP. Furthermore, MB scavenges NO as well as having the capability of inhibiting NO synthases. (Harbrecht 1995; Kirov 2001; Mayer 1993) We hypothesize that the severity of the renal pathology correlated to several interrelated factors to include the degree of parasitemia and the extended survival of the MB treated animals prior to euthanasia (average 4 days longer) in comparison with infected controls, allowing for development of more significant lesions in the kidneys.

In the kidney samples, there was a histiocytic and lymphoplasmacytic interstitial nephritis observed in most cases, combined with a lesser neutrophilic tubulitis, as well as the presence of hemoglobin, cellular and protein casts. Renal samples also had evidence of epithelial degeneration and necrosis, as well as a lesser degree of membranoproliferative glomerulopathy with synechiae. The myocardium was observed to have a moderate amount of pericyte hyperplasia, with cardiomyocyte degeneration, necrosis and karyomegaly suggestive of reactive changes. In rare cases in which the lung was affected, a histiocytic, lymphoplasmocytic and neutrophilic interstitial and perivascular pneumonitis was observed. Rare fibrin thrombi were noted in certain animals, as well as a minimal amount of alveolar edema.

It is important to note that while MB treatment resulted in trends towards parasite clearance, there was residual histopathologic and clinical chemical evidence of ongoing damage to a range of organ systems. Beyond suppression of vomiting and application of diuretics to promote urination, no

supportive care was given to the experimental animals. There is the potential that with fluid therapy and other avenues of care, that the degree of clinical symptomology which per protocol required euthanasia, would have been suppressed allowing for validation of complete parasite clearance at all drug doses.

Animal #	Cohort #	Treatment Day	Euthanasia day	Peak parasit. %	Terminal parasit. %
R130	1	9	14	24.5	0.00
R453	1	7	13	16.9	0.00
R761	1	9	14	25.4	0.00
DA977	2	7	12	45.2	0.01
R420	2	7	11	42.8	0.06
R711	2	7	9	40.8	4.6
R121	3	7	8	39.6	6.8
R338	3	7	12	42.6	0.01
R745	3	7	9	38.3	1.7

Table 7.2: Treatment schedule, peak parasitemia and terminal parasitemia.

	Cohort 1	Cohort 2	Cohort 3
Dose (mg/kg/BID):	6 mg/kg	10 mg/kg	17 mg/kg
No. animals:	3	3	3
No. animals cleared:	3	2	1
No. animals euthanized prior to clearance (*):	0	1	2

*Clearance defined as less than 0.1% parasitemia

Table 7.3: Efficacy of IV MB at each dose in *P. coatneyi* infected Rhesus macaques.

7.10 **Discussion**:

This study evaluated the use of IV methylene blue as a potential therapeutic compound for use in the radical cure of severe malaria in splenectomized rhesus macaques infected with *P. coatneyi* as part of the strategy to combat the spread of artemisinin resistance beyond Southeast Asia.

The rhesus macaque is one of the hardiest of the established primate malaria models and therefore is considered to be optimal in its ability to tolerate the required procedures for drug evaluation protocols. The rhesus is superior to the New World Aotus monkey because sufficient blood volumes can be collected for adequate analysis without causing an adverse iatrogenic anemia in addition to the high predilection of background renal disease which can confound findings of severe malaria in these species. (Chalifoux 1981; Gozalo 1992; Hunt 1993) The model that appears to mimic human severe malaria most closely is the rhesus monkey/*Plasmodium coatneyi* model. (Aikawa 1992; Lombardini 2015; Maeno 1993; Moreno 2007; Moreno 2013)

The use of intravenous MB as an anti-malarial would be highly advantageous as the compound is already approved throughout the world for use in humans as a treatment for methemoglobinemia and therefore could be used off label rather than needing to go through the entire prolonged process of FDA or similar agency approval.

Several clinical trials have now been conducted using MB either in uncomplicated malaria in African children, or in combination with artemesinin based therapy (Bountogo 2010; Coulibaly 2009; Coulibaly 2015; Fall 2015; Meissner 2006; Müller 2013; Zoungrana 2008), where in both settings, the compound was noted to have strong gametocidal activity, as well as transmission-blocking properties, both of which are potential advantages in preventing spread and which therefore in aiding in avoiding drug resistance to the artemesinins. (Adjalley 2011; Coulibaly 2009) The mode of action of MB in regards to plasmodiae, while not completely understood, is posited to act through the inhibition of the activity of the antioxidant glutathione reductase. (Buchholz 2008) In one study, MB therapy resulted in mean male gametocyte exflagellation inhibition values which were greater than 98%, in comparison with female gametocytes in which inhibition of activation was less than 11% suggesting that there are significant differences in the drug action on the different sex of gametocytes. (Delves 2013) MB has also been evaluated in-vitro against both vivax and falciparum isolates (Ademowo 2007; Adjalley 2011; Pascual 2011; Suwanarusk 2015; Wirjanata 2015) and as an anti-malarial in murine models of cerebral malaria (Atamna 1996; Dormoi 2013; Dormoi 2013b; Orht 2014; Mwangi 2016; Nneji 2013) in which the drug has been shown to be highly effective in preventing cerebral malaria and in markedly decreasing mortality rates. A single prior study of methylene blue efficacy has been conducted in non-human primates and was evaluated in the *P. cynomolgi*/rhesus macaque model at AFRIMS and in Aotus monkeys infected with *P. falciparum* at the WRAIR overseas laboratory in Peru as well as in *P. berghei* infected rats. The study noted that in the rhesus and in the rat models, intravenous MB was of equal efficacy as intravenous artesunate, and that combination protocols were superior to either compound used as a single agent treatment. (Orht 2014)

Based on the foundation work already conducted, the interest was in determining the efficacy of the compound in the *P. coatneyi*/rhesus macaque model of severe malaria. Our hypothesis was that IV MB given twice daily for 3 days at the point of development of severe malaria would have therapeutic efficacy and thus might represent a viable alternative to IV AS. As such, we initiated the examination of IV MB in the *P. coatneyi*/rhesus macaque model of severe malaria. In Rhesus macaques infected with *P. coatneyi*, IV MB was tested at varying doses dose (6 mg/kg/BID, 10 mg/kg/BID and 17 mg/kg/BID) once the experimental animals reached a treatment threshold of greater than 15% parasitemia.

MB efficacy at parasite clearance was noted at all doses, however, there was significant morbidity noted in the two cohorts at higher doses, which required euthanasia of the experimental animals. At the lower dose, MB appeared to result in 100% clearance of parasitemia as well as resolution of clinical signs in animals meeting the criteria of severe malaria while having peak parasitemias no greater than 26%. Clearance was observed in both the mid-range and high dose cohorts which coincidentally also achieved greater peak parasitemias, however those animals also displayed more severe symptomology.

Macroscopic and microscopic pathologic evaluation of all tissues found that, while the parasites were trending towards clearance in all cases, those animals which had suffered the highest parasitemias (30-40%) typically demonstrated evidence of marked acute renal, hepatic and cardiac injury. Additionally, the histopathological evidence of *P. coatneyi* induced injury was consistent with the signs of severe malaria observed in all of three drug dose cohorts. The parasite clearance data was fundamentally similar to the efficacy studies conducted in murine models, and superior to those described in the prior WRAIR non-human primate study in which only a few of each MB treated group cleared. (Orht 2014) It is important to recognize that certain murine studies noted almost total suppression of cerebral malaria symptoms in treated cohorts with practically complete parasite clearance. (Dormoi 2013; Dormoi 2013b)

Whilst encouraged by the preliminary findings in this study, the sponsors recommend that subsequent trials be undertaken in which both supportive care is provided to the experimental animals and the post treatment period be extended, so as to determine the viability, not only in clearing the parasites, but also in terms of survivability of the treated animals beyond the acute infection and treatment period.

7.11 **Summary**:

Our study culminated with the application of methylene blue, a compound with known anti-malarial properties to this severe malaria model.

The outcome was extremely encouraging, both in that MB proved to be highly parasitocidal to *P. coatneyi*, but also due to the prolonged survival of animals in comparison with untreated infected controls. Of significant interest was the fact that the treated animals survived beyond day 7, correlating to the killing of the parasites by methylene blue, but in exchange and largely due to the fact that no supportive care was provided to the infected animals, this extended survival period allowed for the emergence of more severe clinical symptomatology. This was in evidence in increased levels of hepatic and renal injury which were biochemically comparable to nontreated infected animals. However, we feel that the clinical symptoms of severe malaria experienced by the treated animals would have potentially been reversible with supportive care, and should be considered as part of the protocol for future studies.

Equally importantly, the methylene blue appears to both protect against metabolic acidosis and to off a moderate degree of neuroprotection based on our comparable histopathologic examination of all of the infected animals, both treated and untreated.

As such, this arm of the dissertation was paramount in that it both confirmed the validity, reproducibility and applicability of the *P. coatneyi*/Rhesus macaque model as a platform for anti-malarial drug studies as well as demonstrating the potential use of methylene blue as an anti-malarial compound in cases of severe falciparum malaria.

Chapter 8: Conclusion

8.1 **Introduction**:

Our understanding and discovery of the mysteries of malaria expand daily. However, and crucially, the arms race for effective prophylaxis, treatment therapeutics and vaccines, looms large in the present, especially as plasmodiae develop drug resistance to the few effective compounds which remain in our armamentarium. It is sobering to remember that malaria is one of the most significant infectious diseases on the planet, affecting in excess of 200 million people yearly and resulting in over 600,000 annual deaths, most of which are children under the age of five. (WHO 2015; Winzeler 2014)

Since the 1990s, the ongoing battle against malaria has suffered significant setbacks, centered upon the expanding drug resistance against some of our most utilized anti-malarial compounds. Chloroquine and sulfadoxine-pyrimethamine in particular were seriously compromised and the epicenters of this development were in regions in which malaria was endemic and where people were at the greatest risk. With the advent of artemisinin derivatives as effective anti-malarials, there was a brief reprieve in those regions hardest hit. (Ashley 2014) The widespread use of artemisinin based drugs and combination protocols was crucial in the significant drop in deaths associated in particular with falciparum malaria observed over the past 2 decades. However, for a range of reasons, artemisinin resistance in *P. falciparum* has developed, with an epicenter in South East Asia. This threatens to overturn all of the recent gains in combating malaria and in decreasing the morbidity and mortality rates of at risk populations. (Ashley 2014; Dondorp 2009; Dondorp 2010; Fairhurst 2012; Price 1998; White 2016; Wongsrichanalai 2001)

P. falciparum, responsible for most of the severe malaria syndromes and for the vast majority of the mortality associated with malarial infections, has developed drug resistance to practically all of the anti-malarial pharmacological agents at our disposal. This has resulted in regional spikes of child mortality, correlated first with resistance to chloroquine and subsequently to sulfadoxine-

pyrimethamine and mefloquine. Artemisinin-based Combination Therapies (ACT) became the recommended treatment for severe malaria employing artemisinin or an artemisinin derivative such as artesunate, artemether, or dihydroartemisinin in combination with another anti-malarial compound such as mefloquine, piperaquine or others. (Fairhurst 2012; Saunders 2014; Trape 2001; WHO 2015)

Unfortunately, the same trends held, in spite of combination therapies, and artemisinin resistance began to expand its range, spreading from the forested Thai-Cambodian and Thai-Myanmar borders, to recently include areas close to the Myanmar-Indian border. (Tun 2015; White 2016; WHO 2015) This latest trend of resistance was first identified in Western Cambodia due to markedly increased ACT failure rates. (Dondorp 2009; Noedl 2008) While research continues in the search for novel therapeutics (White 2016), and the use of preventive measures such as insecticide-treated bed nets have proven efficacy in the control of malaria, there is no licensed vaccine which provides fully-protective immunity. Thus, chemotherapy remains one of the most important mechanisms to ward off death and decrease morbidity. As such, the mounting drug resistance adds urgency to the need for a clearer understanding of the genetic determinants of parasite resistance (Imwong 2010; Sidhu 2006; Winzeler 2014), for the elucidation of the pathophysiology of the disease in humans and, critically, for the development of reliable, replicable, applicable and fully-described animal model platforms in which to evaluate potential chemotherapeutics and candidate vaccines.

Animal models of severe malaria fall primarily into one of two camps, murine and non-human primate models. (Craig 2012; deSouza 2010; Hunt 2010; Langhorne 2011; White 2010) Debate over their appropriateness and utility continues. Champions of each have launched to their defense in the literature and have provided abundant reasoning for each respective camp, and certainly there are legitimate arguments to be made for both. The debate as to the applicability and relevance of murine models in the study of human immunopathology has extended well beyond the domain of malaria and remains a topic of significant argument. (Gillespie 2014, Hagan 2013; Seok 2103; Takao and

Miyakawa 2015; Takao 2015; Warren 2015) To understand the current status of this dispute, it bears examining its foundation, especially as this particular project emerged due to a recognition of the debate and the need for well-considered non-human primate models of severe and cerebral malaria.

Murine models have become the mainstay of malaria research over the past 20 years, and with so much work having been conducted in murine models of human disease in general, there is a vast wealth of crucial knowledge that is available for comparison. Equally, with the recent advances in genomics and advent of knockout, transgenic animals and humanized mice, the potential for study appears limitless.

There are certain inherent benefits to using rodents in medical research. First of all, the ability to use large numbers of inbred or outbred strains of laboratory rodents permits far greater statistical power in the analyses of such studies. Furthermore, the cost of standard strains of laboratory mice is far less than that of non-human primates. This is obviously not the case with many of the genetically engineered animals. However, for large scale studies using standard strains, the cost requirements are far reduced in comparison with the use of monkeys. Space, which is always at a premium, is significantly condensed with rodents. Standard mice are typically far easier to manage and present only minor physical risks to the laboratory staff. And, critically, public opinion is logarithmically different toward the use of laboratory rodents versus so called “higher” vertebrates and in particular non-human primates, although in many ways this is an arbitrary distinction based on a quagmire of cultural, moral and societal criteria that may have little basis in science.

From the genetic perspective, both the mouse and the rhesus genomes have been sequenced. We are able to compare them with humans, and there is significant research demonstrating gaps in the genetic overlap of mice and of men. 75% of mouse genes have been shown to have an equivalent counterpart in humans, while approximately 90% of the mouse genome can be correlated with a region on the human genome and 99% of mouse genes appear to have a human analogue. However, although these percentages appear to support a relatively close genetic

homology between murine models and humans, it is only partially the case once one considers chromosomal shuffling of genes, the overall base pair difference in the mouse and human genome, and the effects of evolutional changes to the actual genes themselves. In fact, from the strict point of view of genetic homology, there is only 5% preservation of the genome between mice and humans. (Church 2009; Gunter 2002; Spencer 2002)

Sequencing of the rhesus macaque genome has demonstrated 93% shared genetic material with humans although the macaque and human chromosomes are mosaics of one another resulting from genetic rearrangement over the 21 million years of divergence between the species. (Gibbs 2007; SoRelle 2007) Therefore the same evolutionary arguments can just as easily be lodged against the non-human primate modelers as against murine modelers. Nonetheless, due to the robust similarities with humans, bridging genetic, developmental, physiologic, behavioral and immunologic domains, the rhesus macaque remains a critical platform for a diverse spectrum of biomedical research. (Vallender 2013)

It would, however, be disingenuous to not mention the myriad difficulties along with the benefits in working with the rhesus macaque. First and foremost, the macaque is a large non-human primate and is extremely strong. The positive aspect of this is that the individual animal's blood volume permits far greater sample collection than smaller primates such as the Aotus or the much smaller murine animals. The negative aspect is in terms of safety. The rhesus macaque is capable of inflicting significant traumatic damage to a handler and, critically, is also a reservoir for the cases of potentially fatal macacine herpesvirus which have occurred in laboratory workers. (Huff 2003; Sabin 1934) Additional zoonoses of import include *Mycobacterium tuberculosis*, monkeypox, benign epidermal monkeypox, Yaba virus, molloscum contagiosum and Marburg virus to name a few. (Parrott 2014) This represents the double-edged sword associated with the similarity of the genome between humans and the rhesus which allows for this degree of zoonotic disease transmission.

Additional challenges in working with a macaque model are associated with the cost and management of housing. One mechanism through which the risk of zoonoses is mitigated is through the maintenance of a closed colony such as the one at AFRIMS. There is an extremely high cost associated with establishing and maintaining such a population. The animals which are available through vendors are typically Chinese-origin rhesus, as opposed to the Indian-origin macaques used in this study, and there are subtle but significant immunological differences between the populations. The primary distinction is associated with differences in immune responses specifically correlating to the MHC alleles. An example of this is seen in patterns of T-cell activation as well as in other hematological and blood chemistry differences. (Champoux 1996) Chinese-origin rhesus are described as having greater variability in the MHC region than is seen in Indian origin macaques. This can result in greater immunological variance when using the Chinese-origin animals as opposed to the Indian-origin monkeys. (Kanthaswamy 2004) An example of this important difference is seen in Simian Immunodeficiency Virus (SIV) studies in which Chinese-origin macaques are noted to be far more resistant to disease than rhesus of Indian-origin. (Ling 2002; Trichel 2002)

Specifically evaluating the validity and applicability of the *P. coatneyi*/rhesus macaque model of severe and cerebral malaria in humans, there are areas which demonstrate a strong correlation with human disease. These provide ample substantiation for the use of the macaque model, but there are other areas which do not perfectly mimic human disease.

The first area requiring consideration is in the use of a splenectomized model. Splenectomy allows for development of high circulating parasitemias, and in contrast to the spleen intact model used in the studies of Moreno et al, as discussed previously, this allows a shorter and more severe host malaria disease phenotype, mimicking the course of severe falciparum malaria in humans. Case report studies of splenectomized human cases of *P. falciparum* malaria (including pathological reports on fatal cases) have shown that whilst circulating parasitemia is higher, which may in analogy to this model cause more severe disease due to loss of control of total parasite biomass, there is an

accompanying modulation of cytoadherence. Parasitized erythrocytes in splenectomized patients show decreased knob expression and cytoadherence, probably because of the lack of immunological pressure to avoid splenic clearance. In this study, ultrastructural examination of *P. coatneyi*-infected RBC from spleen intact donor animals confirmed the presence of Knob proteins, and both the histological and ultrastructural studies provided ample evidence that cytoadhesion and resultant sequestration was maintained. However, the loss of the spleen in these animals may cause immunological modulation in response to infection which will contrast to the normal human.

The second area where the course of natural infection will be different to the human is the use of live blood stage inoculation as a mode of transmission, meaning that the initial stage of natural falciparum infection (the intra-hepatic stage) is bypassed. Again, this will lead to a different temporal challenge to the host immune system and inevitably a difference in the presentation of parasite antigen which guides the development of any protective, or disease ameliorating immune response. Disease patterns in endemic areas in humans are crucially determined by immune status, as shown by the eventual development of protective immunity to severe disease amongst populations in hyper endemic areas. The animals used in the prospective studies were selected to be naïve to any previous challenge with *P. coatneyi*. However, the use of animals in a maintained colony for multiple research studies may result in some animals having been involved in previous experimental protocols, including vaccine trials, other pathogen exposures, etc, which could significantly affect their immune status. This may be responsible for some elements of heterogeneity in disease response, something which is in reality probably more relevant to a human population than the use of genetically inbred strains of mice.

A comparative review of the use of this model as described in the literature bears discussion. Historically, the *P. coatneyi*/rhesus macaque model was initially represented as a strong model of cerebral malaria. This view depends heavily on the fact that it is a sequestering model (Desowitz 1969; Nakano 1996; Sein 1993; Smith 1996), based on the ultrastructural features (Aikawa 1992;

Kilejian 1977; Miller 1972; Rudzinska 1968), rosetting characteristics in both rhesus and Japanese macaques (Kawai 1995; Tegoshi 1993; Udomsangpetch 1991), and the *P. falciparum*-like lifecycle of the parasite. (Eyles 1963) In all of these studies, the study populations were small, frequently consisted of different species or subspecies of macaque, had markedly different criteria for quantitating parasitemia levels, and the evaluation of the pathophysiology was typically limited to a very finite range of diagnostic criteria. While in principle, all of the studies have valid and defensible points, it was deemed probable that the study of a larger number of animals would reveal an inter-animal variation more closely paralleling that found in humans infected with *P. falciparum*.

A select few studies employed larger numbers of animals and have maintained stricter criteria for the specific use of the model. These included the examination of *P. coatneyi* as a model for severe pregnancy malaria in humans (Davison 1998; Davison 2000), as a relapsing model for severe anemia and metabolic disturbance (Moreno 2007; Moreno 2013) and for use as a platform for a drug trial based on the prior assertions of validity as a model. (Maeno 1993)

Unfortunately, with the exception of the studies by Davison and those by Moreno, much of the use of the model has been based upon the hypothesis that the *P. coatneyi*/rhesus macaque model was a strong correlate to sequestration dependent human cerebral malaria, which the clinical and pathological evidence from this current study suggests that it is, in fact, not perfectly parallel to human disease. The authors of those studies carried the hypothesis forward, derived their data and observations and drew conclusions based upon them. Aspects of the model certainly do replicate pathology observed in CM, while others deviate from the strict definition of cerebral malaria. Examples include the fact that whilst sequestration does occur, the incidence of neurological symptoms, fitting and secondary neuropathological changes in the brain is less severe than that observed in humans. This in itself is a very interesting finding, because it allows for argument that cerebral parasitized erythrocyte sequestration is in itself not sufficient to cause coma.

What was lacking in the prior studies was a comprehensive description of all of the different aspects of the pathophysiology of the disease in a larger population of rhesus, to include the ante-mortem clinical symptomology, hematology, blood chemistry and cytokine profile, as well as the post mortem histopathology, ultrastructure and immunohistochemistry. This study has attempted to remedy the lack of a comprehensive description and evaluation of the model, allowing determination of its validity and applicability as a model of severe human malaria.

8.2 **Clinical synopsis**:

Focusing on the in-depth clinical data collected in the prospective studies, comprised of the 15 animals described in Chapter 7, we have clarified both areas of confluence and divergence with human falciparum induced disease. It is important to note that, especially in comparison with the statistical strength of murine studies, an n of 15 is still quite small in order to show variance. However, it is an adequate number to demonstrate reproducibility of the model and is an important addition to the existing literature. Furthermore, the effective, reproducible and comparable demonstration of the use of the model in a clinical drug trial is invaluable in the ongoing arms race with the malarial plasmodiae and especially *P. falciparum*.

It is important to reiterate and underscore that the *P. coatneyi*/rhesus macaque model employed in this series of studies was specifically geared towards an understanding, first and foremost, of its validity as a model of cerebral malaria which has been the primary focus of the literature to date. Secondarily, and with the benefit of hindsight, we were able to examine the model and its applications in terms of the study of severe malaria, and the spectrum of symptomology and pathophysiologies associated with the wider definition of severe malaria. Fundamentally, the *P. coatneyi*/rhesus macaque model is a sequestering model of malaria, and one which does still demonstrate many facets of pathology and pathophysiology which mimic aspects of human disease.

It is also important to note that the terms “severe malaria” and “cerebral malaria” are themselves used variably, in the literature both in research describing *P. coatneyi*, and in human medical studies. This compounds the difficulties in attempting to specifically correlate this model with human disease. The patterns of severe disease associated with *P. falciparum* infection differ between children and adults. Marked socioeconomic factors also impact the characterization of human diseases, as the malaria prevalence is highest in the most impoverished regions of the planet, where disease diagnosis and documentation is most unreliable. (WHO 2014) Add to this, the confusion and concealment of severe malaria created by concurrent etiologies of febrile disease such as dengue, chikungunya or a vast panoply of other tropical diseases. Furthermore, prior infection, immune status, and partial treatment can impact both diagnosis and severity of disease, and thus lead to an extremely heterogeneous pool of data in humans.

The WHO uses the following broad criteria for the definition of severe malaria: “Severe malaria by definition is associated with a high mortality. From a clinical perspective, there is a continuum from asymptomatic malaria to uncomplicated illness through to severe and lethal malaria…In a patient with a *P. falciparum* asexual parasitemia and no other confirmed cause for their symptoms or signs, the presence of one or more of the clinical or laboratory features in Table 1 classifies that patient as suffering from severe malaria.” (WHO 2014)

Table 1, referred to in the above quotation includes the following clinical indicators which are subdivided into prognostic value based on the age of the patient be they adult or children: impaired consciousness, respiratory distress, convulsions, prostration, shock, pulmonary edema (diagnosed radiologically), abnormal bleeding and jaundice. These are combined with hematological and biochemical parameters including severe anemia, hypoglycemia, acidosis, hyperlactatemia, renal impairment suggestive of acute renal injury and hyperparasitemia. (WHO 2014) The specific laboratory criteria for inclusion have been continuously refined as taken directly from Table 4, Epidemiological and research definition of severe falciparum malaria. (WHO 2014):

1. Impaired consciousness: A Glasgow Coma Score of less than 11 of 15 in adults.
2. Severe acidosis: Manifests clinically as respiratory distress – rapid, deep and labored breathing.
3. Hypoglycemia: Blood or plasma glucose 8 meq/l or, if unavailable, a plasma bicarbonate of 5 mM.
4. Renal impairment (acute kidney injury): Plasma or serum creatinine >265 µM (3 mg/dl) or blood urea >20 mM.
5. Jaundice: Plasma or serum bilirubin >50 lM (3 mg/dl) as well as a parasite count >100 000/ll.
6. Pulmonary edema: Radiologically confirmed, or oxygen saturation 30/min, often with chest in-drawing and crepitation on auscultation.
7. Significant bleeding: Including recurrent or prolonged bleeding from nose gums or venipuncture sites; hematemesis or melena.
8. Shock: Compensated shock is defined as capillary refill ≥3 s or temperature gradient on leg (mid to proximal limb), but no hypotension. Decompensated shock is defined as systolic blood pressure <70 mm Hg in children or <80 mm Hg in adults with evidence of impaired perfusion (cool peripheries or prolonged capillary refill)
9. Hyperparasitemia: *P. falciparum* parasitemia >10%

Compounding the lack of clarity in the simian studies conducted over the past 50 years using the *P. coatneyi*/rhesus macaque model, these have employed a range of defining characteristics for "severe" and "cerebral" malaria not covered by a range of criteria similar to those in place for human disease. As described previously, the model has been used in focused descriptive studies consisting of a limited number of animals. (Aikawa 1992; Davis 1993; Desowitz 1967; Desowitz 1969; Kilejian 1977; Nakano 1996; Sein 1993; Smith 1996; Udomsangpetch 1991) The studies have used different macaque species or subspecies, (Aikawa 1992; Eyles 1962; Kawai 1993; Migot-Nabias 1999; Smith 1996), have had differing definitions and ranges of parasitemia (Davison 1998; Moreno 2013; Smith

1996), and have included both spleen-intact and splenectomized animals. (Aikawa 1993; Desowitz 1967; Desowitz 1969; Kawai 1993; Lombardini (unpublished); Maeno 1993; Moreno 2013, Smith 1982) Further, treatment regimens were sometimes given in between legs of a study or prior to reaching severe and potentially irreversible symptomology. (Moreno 2013) While the wide range of *P. coatneyi*-focused studies have contributed to our understanding of the parasite and the host pathophysiology (and indeed the impetus for this dissertation grew from that foundation), what was necessary was an in-depth examination of all of the available material so as to establish parameters for the model and through which subsequent studies can be evaluated and compared with human disease.

It should be noted that these criticisms can equally be made against the use of murine models, and indeed, of many human clinical studies where clinical criteria are variable. Murine studies tend to use specific strains of mice to represent disease syndromes, mimicking those observed in humans. Examples of which include, an anemia prone mouse model or 'cerebral' combination of mouse and host parasite, or mice which have been selected for a specific end organ complication such as lung disease. Given that an autoimmune meningo-encephalitis can induce lethargy, severe systemic illness and symptoms interpreted as 'coma' or decreased consciousness, it is also tempting to wonder whether some published models are in fact just severely ill mice with prostration, rather than a specific cerebral syndrome.

8.3 **Pathology Synopsis**:

The major clinico-pathological findings derived from the prospective animals in this study, which concurs with the material available in the retrospective animals and the literature, includes multi-organ systemic disease with varying severity. Pathology was concentrated in the urinary tract, the central nervous system, the hepatic system and the hematopoietic system.

The parasitemia curves examined in this study demonstrated a cycling similar to that seen in falciparum malaria with a relative absence of mature stages in the peripheral circulation, implying deep vascular sequestration of trophozoite and schizonts stages. This, combined with the fever cycles and clinical symptomology in the *P. coatneyi* model, all of which are clearly parasite density dependent and very reproducible, are significant benefits in the use of this model for drug or vaccine trials.

The most significant correlation of the model with human disease appears to be with the *P. coatneyi*-induced, acute kidney injury observed in the rhesus monkeys. Findings parallel those in humans at the levels of the symptomology (hematuria, dysuria, anuria), blood chemistry (elevated creatinine and blood urea nitrogen), and pathology as observed with both light and transmission electron microscopy. Renal disease in malaria is under-recognized in pediatric cases, but has been commonly reported in the adult, and is characterized by acute tubular injury. A model such as this, which would allow studies or adjuvant reno-protective drugs or better characterization of early markers of renal injury, would be of great utility.

The central nervous system findings are more difficult to interpret, in large part due to the fact that the rhesus macaque does not appear to develop coma as defined by the criteria set forth by the WHO. (WHO 2014) The definition of cerebral malaria is described by the WHO as “a clinical syndrome characterized by coma at least 1 hour after termination of a seizure or correction of hypoglycemia, asexual forms of *Plasmodium falciparum* parasites on peripheral blood smears and no other cause to explain the coma.” (WHO 2000; WHO 2014) The clinical hallmark of cerebral malaria is reported by some as impaired consciousness, with coma being the most severe manifestation. (Idro 2011) To a certain extent, the World Health Organization’s strict definition conflicts with other reports in the literature which, for example, define cerebral malaria as a manifestation of CNS dysfunction in a victim with symptomology to include disruption of consciousness (confusion, delirium, obtundation, stupor, or coma), convulsions, focal neurologic deficit, and/or psychosis.

(Misra 2011) The definition of cerebral malaria based on coma may be open to revision, as there has been significant discussion into the cause of coma in humans, and the literature reports the hypothesis that cerebral malarial coma is the result of four distinct but associated syndromes and not specifically a sequela of cerebral edema. These syndromes are comprised of a prolonged post-ictal state, covert status epilepticus, severe metabolic derangement and a primary neurological syndrome. (Idro 2011; Marsh 1996; Medana 2011) However, for the sake of clarity, this study assumed the WHO's definition and, as such, the rhesus macaque does not replicate the clinical symptomology of human disease. Additionally, clinical symptoms of epileptic seizures or status epilepticus were absent, retinal abnormalities appeared mild or absent, and both neuropathological and CSF studies implied that the degree of secondary neurological injury in this model was limited.

Anecdotally, discussion by the author with upwards of 20 clinical veterinarians, specializing in non-human primates, was not able to uncover a single instance of strict coma as defined by the medical literature as a prolonged or indefinite state of deep unconsciousness in which the patient was non-responsive to noxious stimuli. The veterinary literature contains subjective examples of coma in small animals (dogs and cats), however the clinical definition applied in those cases appears to be extremely variable. Experimental cases of ischemic coma involving cardiac arrest have been reported (Ching 2013; Gurvitch 1974), and attempts to modify the Glasgow Coma score for use in small animals have been published. (Platt 2001) The point at which most animals would qualify for a strict definition of the term coma is typically peri-mortem, due primarily to severe head trauma, severe intracranial pressure, anesthetic death, or severe hypothermia. Regarding rhesus macaques, there is even less information available relating to coma in this species. The only report in the literature appears to derive from malaria researchers examining the potential use *of P. knowlsei* in rhesus macaques. One group reported coma as occurring just prior to death (Ibimoye 1993), however an earlier study which examined 12 animals infected with *P. knowlsei* does not give adequate information as to the peri-mortem state of consciousness. (Spangler 1978) As such, the

application of the WHO clinical criterium of coma to the rhesus macaque or realistically to any animal model, may be forced, and not bear the degree of importance that we and other researchers in both camps have placed on the concept of coma. Likely, the severely decreased mentation, decreased withdrawl and menace responses and severe obtundation observed in all of the *P. coatneyi* infected animals serves as an adequate correlate to the concept of coma in humans. However, as previously stated, and for the sake of conformity to human disease criteria, we adopted the WHO symptomology for comparative purposes throughout the study.

In the prospective study, the animals were monitored during illness on an hourly basis up until euthanasia or death. While the animals became markedly moribund, had severely depressed mentation, had a decreased menace response, and were lethargic and recumbent, at no time did they completely lose their ability to respond to noxious stimuli such as a pinch withdrawl test. Thus, the WHO's definition of coma was not met. Additionally, subsequent to autopsy, additional features show incongruence with those described in human cerebral malaria. The pathology in adult human cerebral malaria has been reported to be related to parasite sequestration in the brain (Turner 1997), and histopathology and electron microscopy confirmed that the same holds true in the *P. coatneyi*-rhesus macaque model. However, in spite of this, the rhesus macaque appears to be less susceptible to major neuropathological evidence of the types of injury described in humans such as cerebral hemorrhages or severe swelling of the brain. The blood brain barrier dysfunction which has been elucidated using immunohistochemistry in this study appears to be in line with that observed in leukocyte mediated immune responses described in the severe malaria of children. (Idro 2011)

Preliminary retinal findings suggest that there may be some damage in these animals, but that it deviates from the pathologic findings in certain ways. Human criteria for malarial retinopathy include: retinal whitening, vessel changes, retinal hemorrhages, and papilledema. (Beare 2006) While, several of these signs were described in the retinal imaging conducted in the few prospective animals examined, the very small sample size, the absence of histopathological retinal hemorrhaging and the

lack of control animals prohibits making any definitive statements as to significance in the macaque. This remains an area which warrants further controlled study to elucidate these preliminary findings of retinal injury.

The severity of hepatic dysfunction observed in these animals was somewhat variable, and the animals that demonstrated severe evidence of coagulative necrosis typically had survived the initial insult. However, there was a consistent spike in the hepatic enzymes trailing peak parasitemia observed in the majority of the prospective animals (in common with findings of a 'biochemical malarial hepatitis' in adult falciparum malaria, especially in South and Southeast Asia) and as such, the finding is clinically relevant and may be interpreted as a potential feature of the systemic multi-organ dysfunction observed. (Kochar 2003; Shah 2009) Similar studies in children do not appear to show significant hepatopathy associated with falciparum malaria. (Whitten 2011) Jaundice was reported in *P. coatneyi* infected macaques as a feature in many of the retrospective pathology reports evaluated in this study, however the brown tinge in most organ systems associated with hemozoin accumulation in the prospective studies masked the presence of jaundice if present. Additionally, as the course of disease was so rapid in these animals, they lacked the chronicity of illness likely required for significant jaundice to develop.

One interesting area of difference between humans and rhesus macaques with severe malaria was that cardiac pathology was noted consistently, if at low levels, in the 15 prospective animals, as well as in the majority of the retrospective animals examined microscopically and ultrastructurally. Several of the prospective animals underwent electrocardiograms at various stages of infection, and while preliminary evaluation of the results does not appear to demonstrate a global cardiac dysfunction, the presence of reproducible single cell necrosis of cardiomyocytes combined with the severity of parasite sequestration in the heart is of interest. There are a few reports in the literature which highlight *P. falciparum*-induced cardiac injury in humans and recommend a reevaluation of the potential for damage to the heart with falciparum malaria. (Costenaro 2011)

While anemia was noted in several animals, the rapid onset and severity of disease in this model do not make it an ideal model to evaluate severe anemia of malaria. This contrasts with the low parasitemia, recurrent infection model which Moreno et al. have described using the spleen-intact, *P. coatneyi*/rhesus macaque model. (Moreno 2013) In their report, the animals underwent repeated bouts of *P. coatneyi* infection at a lower parasitemia levels and, with the increased chronicity of disease, demonstrated marked changes in the bone marrow which were not found in this severe model. Their study suggests a likely immunopathogenesis associated with chronicity, while our prospective animals succumbed too rapidly to severe malaria to elicit the same immune-driven chronic changes.

Hyperlactatemia was observed in the prospective animals associated with the model refinement portion of the study in which the animals achieved high levels of parasitemia without treatment. Those animals consistently demonstrated a spike in lactate which followed after the spike in parasitemia. The same did not hold true for the treated animals in the methylene blue study. The latter animals did not develop acidosis and the lactate levels remained stable (in normal range) throughout the clinical trials, suggesting the possibility that the drug had a protective effect not only in terms of parasite clearance but also in managing the clinical symptomology of disease. In the affected animals which displayed hyperlactatemia, the specific mechanism remains unclear. However, hyperlactatemia has been reported in human malaria to be associated with the destruction or deformation of erythrocytes, as well as potentially with the degree of hemozoin accumulation and the resultant immune response, or as a sign of microvascular endothelial dysfunction due to sequestration. (Casals-Pascual 2006; Day 2000; Hanson 2015; Ishioka 2016) Additional experimental research would be necessary to confirm mechanisms in the rhesus macaque model.

Another difference from severe falciparum malaria in humans, was the absence of pulmonary edema in these animals, either in the retrospective or prospective groups, despite marked sequestration of infected erythrocytes, host leukocytes and pigmented ghosted erythrocytes in the

alveolar interstitial microcapillaries. The animals are often dyspneic, but based on the histopathological observations, this is not due to mechanical obstruction of the airways. Rather it is theorized to be a feature of cardiovascular shock leading to death. This finding, taken together with the relative integrity of the blood-brain barrier and predominant absence of cerebral hemorrhages, may suggest that the rhesus macaque has a greater degree of endothelial 'resistance' to malaria-induced injury following direct cytoadherence of iRBC than humans. Alternatively, it may reflect immune modulation of pathogenetic pathways in this model in contrast to the human. Perhaps there is a genetic component, suggested by the fact that the macaque is not naturally susceptible to severe disease from this parasite. There is no current literature to support or negate either of these theories. Emerging differences in microvascular pathology between adult and pediatric CM in the human include the extent of platelet mediated injury and dysregulated hemostatic mechanisms in CNS microvessels. iRBC cytoadhesion is mediated via a number of different host receptors on cerebral endothelial cells, of which ICAM-1 appears to be important in the brain. (Turner 1994) More recently described, is the Endothelial Protein C receptor (Ho 2014), binding to which induces harmful hemostatic dysregulation via von WIllebrand factor and Tissue factor release, and is a receptor for certain parasite lines expressing specific PfEMP-1 variants. ICAM-1 and EPRC can act as co-receptors on brain endothelial cells (Avril 2016) so it seems likely that even if parasites sequester in a microvessel, it is both the type of parasite variant, the site of sequestration and the host response to this which may determine patterns of organ specific damage in clinical disease.

The various microscopic modalities that were used in this study (histopathology, immunohistochemistry, transmission Electron Microscopy, scanning EM and Atomic Force Microscopy) all served to carefully and more fully examine the impact of *P. coatneyi* infection in a large number of infected rhesus macaques. It was important to examine ultrastructural host-parasite interactions and tissue-specific injuries in the light of the sparse existing literature examining the model's relevance to human disease. As was discussed, the animals do not mimic the clinical and

neuropathologic features of human disease. That is, while the macaques are obtunded and demonstrate severe mentation deficits in the final stages, they neither develop coma or fitting clinically, nor cerebral edema or ring hemorrhages with any significance and frequency histologically. There is subtler evidence of neuropathology in the affected monkeys, especially at the ultrastructural level, however the observed injuries are less extensive than the lesions that have been described in humans and in particular in children.

While this may be a controversial statement, it is important to note that the human literature is also markedly underscored by its own heterogeneity. Few reported human autopsy studies have examined the brain stem (one exception being a neurotoxicity study of artemether by Hien & colleagues 2003) and none have described spinal cord pathology in any depth. Comparisons of pathology between different areas of the brain such as the cerebrum versus the cerebellum are limited. (Sien 1993) Additionally, while over the past century, there have been many autopsy studies in both adults and children (Dorovini-Zis 2011; Dudgeon 1917; Galatioto 1995; Kean 1944; Manning 2012; Turner 1997), the histopathology studies in the human literature have significant limitations. Humans who are infected and succumb from *P. falciparum* will have undergone variable degrees of clinical support and treatment, will be from different geographic regions, ages and susceptibility, have a variable immunological response and pre-existing immunity to both infection and disease, and may suffer from concurrent diseases. In addition to host factors, patients may be infected by different strains of the plasmodium parasite, and finally, the results may have been evaluated by pathologists of differing experience. These variables all influence the data that is derived from the study of these cases and interpretation of larger human autopsy based pathological studies. (Aikawa 1992; Clark 1949; Dorvini-Zis 2011; Dudgeon 1917; Ewing 1902; Iano-Wossinetsky 1938; Kean 1944; MacPherson 1985; Marchaifava 1894; Oo 1987; Ponsford 2012; Spitz 1945; Taylor 2003; Toro 1978) In a fashion, the human literature is just as unfocussed as those studies in animals. It is crucial to recognize that

one of the benefits of a controlled animal study, be it in mice or monkeys, is that it allows for a degree of homogeneity or standardization which is absent from human autopsy studies.

While there is also significant heterogeneity evidenced in this study, certain factors hold. Firstly, the same *P. coatneyi* strain was used throughout. In the prospective cohorts, we were therefore able to control the inoculation dose, key aspects of the genetic and immunologic background of the hosts, the treatment protocol, data collection, the overall signalment (demographics) of the animals used, and the pathologists examining the material. One area of potential heterogeneity in this study related to the prior experimental history in both retrospective and prospective macaques. All of the animals were exposed to *P. cynomolgi* and often to the dengue virus at various points in their history, and while we attempted to regularize the study by selecting experimental animals that had similar backgrounds, the lack of malaria-naïve animals raises questions which require further study.

Host/parasite interaction bears many parallel features between *P. coatneyi* in rhesus and *P. falciparum* in humans. Binding interactions have been illustrated ultrastructurally through the margination of infected erythrocytes, rosetting and autoagglutination, as well as the phenotypical expression of knob structures on the infected RBC cell surface, notwithstanding the structural differences in knobs which the EM study showed. These features of cytoadherence were demonstrated in the histopathology of multiple organs (heart, brain, glomeruli, hepatic sinusoids, endocrine tissues) in which sequestration is severe.

There has been discussion as to the role of iRBC binding in *P. falciparum* infection in vivo, especially as cytoadherence phenotypes have been proven to be associated with increased risk of severe disease, such as rosetting in cerebral malaria (Rowe 1995), but have not been observed ultrastructurally as contributing directly to tissue pathology in human pathology studies. (Pongponrat 2003) This potentially means that the more vivax-like rosetting behavior of *P. coatneyi* in the splenectomized rhesus model has a more significant contribution to tissue injury and microvascular

obstruction in this model than perhaps does *P. falciparum* in the human. The presence of numerous calveolae is also fascinating as it is a feature more typically associated with *P. vivax*, a parasite which is in fact genetically more closely related to *P. coatneyi* than to *P. falciparum*. Binding has been further confirmed through the preliminary micropipette and biofluidics assays, supporting a similar pathogenesis of disease. The hypothesis of severe and cerebral malaria being partially modulated by the blood flow disruption in humans infected with *P. falciparum* appears equally valid for *P. coatneyi* in rhesus macaques.

As to specific organ systems, there is room for debate as to the correlation of the CNS histopathology based on the prior discussion of case heterogeneity in humans. We have confirmed via histopathology, TEM and immunohistochemistry that the *P. coatneyi*/rhesus macaque model is definitively associated with extensive sequestration, neuronal injury and significant Purkinje cell damage, along with a T-cell-driven inflammatory response which was observed early in the infection (at d7-10). Also observed were collections of macrophages/monocytes both within and around vessels, limited perivascular edema, and only rare instances of perivascular punctate and ring hemorrhages similar to those which have been described as characteristic in the cerebrum of both adult and pediatric CM in humans. Although the cerebrum was only infrequently affected in the monkeys, hemorrhages were observed in the brain stem and spinal cord and with greater severity and frequency, a finding which is important and novel. Axonal injury was limited, and platelet deposition almost nonexistent. These observations combined with the severe decrease in mentation in the end stages of disease, demonstrates relative conformity with human disease in spite of the absence of true coma as defined by the WHO. These similarities in CNS microscopic and ultrastructural pathology between the monkey and human disease, was a parallel not observed in the retinal histopathology of monkeys and humans. Additional work is necessary before conclusions are drawn in this regard, especially as retinal findings in adult humans are also not uniform. (Maude 2009)

The light microscopic, ultrastructural and clinical pathological evidence of renal pathology described in detail in this model is significant and correlates well with human disease, rendering it a useful tool for better understanding of falciparum malaria-induced, acute renal injury. This is crucial in that one of the important non-human primate models of falciparum malaria and one which is used as a platform for drug discovery and vaccine trials is the Aotus. Owl monkeys or night monkeys have a significant deficit in their use in these trials, specifically relating to the kidneys. Various species of owl monkeys, namely *Aotus nancymae*, *Aotus vociferans* and *Aotus trivirgatus*, have commonly described chronic renal lesions, such as an immune-mediated glomerulonephritis which has been shown to be associated with hemolytic anemia. (Chalifoux 1981) Additionally, a large scale retrospective study conducted at the Peruvian Primatological Project breeding center noted chronic nephropathy in 10% of all necropsied *A. vociferans* and *A. nancymae* owl monkeys examined. (Gozalo 1992) These descriptions of significant background renal disease in these species of New World monkey, unrelated to malaria, represents a significant confounding factor in the study of malarial nephropathy. This fact may unfortunately require some reevaluation of previous studies which have employed these species for malaria studies specific to the kidneys. (Iseki 1990; Nagatake 1992; Weller 1992) Given the large cohort of animals examined in our study, the acute nature of the lesions described, and confirmed ultrastructurally and the concurrent clinical pathology, allow for a high degree of confidence in the veracity of this predominantly tubular, rather than glomerular pathology as a parallel to acute renal injury in falciparum malaria. Additional areas which would warrant examination would include immunohistochemistry of the immune response within the kidneys, the apoptotic versus necrotic nature of epithelial and endothelial damage in the kidney, and immunoglobulin markers specifically targeting the glomeruli to assess the presence of deposits. Furthermore, studies examining the chronic impact of cured or repeated *P. coatneyi* infections and the ability of the macaques to recover from nephropathy would be of interest as an adjunct to clinical drug studies.

As discussed in earlier chapters, both cardiac and hepatic injuries have been described in scattered cases of *P. falciparum* infection in adults, although these do not appear to be universal features of disease. While the cardiac findings in the macaque were relatively mild in most instances, we theorize that the observed pathology is associated with widespread microvascular sequestration, occlusion and resultant hypoxia. Hepatic lesions tend to have a zonal pattern often localized around a central vein which further supports the concept of injury secondary to dysregulation of vascular blood flow. However, to place all responsibility on the cytoadherent infected erythrocytes would be naïve. Systemically, the fact that animals undergo significant febrile episodes over the parasitemia cycle, combined with the presence of abundant hemozoin pigment in tissues and other parasite-associated antigens, monocytic inflammation and both direct erythrocytic and endothelial cell degeneration and necrosis, all combine theoretically to initiate a cytokine storm. The likelihood is that, as with human disease, macaques infected with *P. coatneyi*, succumb to a complex combination of factors, all of which contribute to the progressive collapse of tissues at the cellular and eventually at the whole organ level.

Patterns of injury in human falciparum malaria vary significantly as evidenced in the heterogeneity of case diversity as well as in the recent flood of studies comparing adults and children. In the large autopsy study of children in Malawi with cerebral malaria, histopathology of the brain was characterized first and foremost by significant iRBC sequestration in the cerebral microvasculature, a finding which is wholly consistent with this study in rhesus. Children in the Malawi study were subdivided into groups based on the presence of perivascular and intravascular pathology, but all cases were noted to have sequestration. (Dorovini-Zis 2011) In addition to the sequestration of iRBCs, the children's brains were often described as being edematous at autopsy. While we did not conduct a comparative study between normal and *P. coatneyi*-infected brain weights to account for the influx of edema, histopathologic and ultrastructural examination of the CNS in the macaques noted perivascular edema in the sections evaluated. This was further supported

by the fibrinogen immunohistochemistry which demonstrated leakage from the microvasculature. One other area of confluence between the Malawi study and this one was in the immunohistochemical identification of perivascular and intraparenchymal monocytes, which were observed at a mean ratio of 131:15 (infected:control) in the brain stem and 19:3 in the cerebrum, suggesting a significant monocytosis similar to cerebral disease in African children (although a significant number of the cases in the Malawi study are also HIV co-infected and this may influence immune responses in the brain). Monocytosis has also been reported in morphological and immunohistochemical studies of adult with cerebral malaria. (Porta 1993; Patnaik 1994) The primary divergent feature was in the relatively few cases of thrombosis and vascular obliteration with subsequent hemorrhage in the macaques. Platelet associated pathology appears to be a prominent feature in children with falciparum malaria while only 12 (27%) of the 45 animals in our study had fibrin thrombi in any tissue. 27% of the animals (combined retrospective and prospective) were noted to have minimal or mild hemorrhaging in the cerebrum. However, 60% had evidence of some degree of hemorrhage in the spinal cord.

The immunohistochemical data in our study supports the histopathologic and ultrastructural descriptive evidence described in their respective chapters, but the IHC evaluation was limited to the central nervous system. It did provide evidence for similar changes in blood-brain barrier function, which are actually milder in CM than other CNS infections involving destruction of the BBB such as viral encephalitis or meningitis. (Brown 2000) This was mirrored by evidence of mild, perivascular cerebral edema and fibrinogen leakage, limited microscopic axonal injury and minimal evidence for widespread neuroaxonal damage in the CSF studies. However, a unique immunological response to CNS infection is occurring in this monkey model, as evidenced by the preliminary work describing the CSF cytokine signature. Many of these findings are still not fully elucidated in human studies, but the results in this thesis imply that the model is a potential platform for doing so, and perhaps for using

some of these markers as surrogate measures for neuroprotection in any studies of adjuvant treatments for neuro/vascular protection in the future.

Fundamentally, the data garnered throughout the study suggest that the model has valid, reproducible and correlatable application as a model for severe *P. falciparum*-induced malaria in humans. The findings emphasize the importance of a thorough understanding of the basic clinical and pathological aspects of any animal model. Thus, while the central nervous system pathology is similar, but lesser in degree to that in humans, the clinical picture of coma as defined by the WHO and fitting in human CM are not present. However, the model offers an opportunity to observe sequestration dependent end organ damage at high parasitemia, particularly in acute renal, hepatic and cardiac injury, and parallels severe human disease with reproducible waves of parasitemia, systemic metabolic disturbance and fatal outcome.

8.4 **Future potential uses of the model**:

This dissertation represents an in-depth evaluation of the model, which to date was lacking. Our work has definitively established the model as a platform upon which to continue to elucidate the pathology and pathophysiology of *P. coatneyi* in the rhesus macaque. As such, there are certain areas where additional work needs to be conducted. As shown, this is a sequestering model, and the present body of work, as well as satellite projects that have arisen, will allow for an accurate interpretation of the impact of parasite burden on the overall severity of disease and the observed patterns of end organ disease.

As mentioned there has been considerable interest in using plasma HRP-2 measurement as an indirect measure of parasite biomass reflecting sequestered parasite burden better than a simple peripheral parasitemia. (Dondorp 2005; Hendriksen 2013) As part of this thesis we had hoped to use a similar approach to quantitate parasite burden in the Rhesus model, but faced a problem in that *P.*

coatneyi does not produce an analogue of HRP-2. One alternative to HRP-2 has recently been described, which is the measurement of soluble DNA released from the malaria parasite into serum. (Imwong 2015) At present, collaborators at the Mahidol Oxford Research Unit (led by Dr. Malika Imwong) are developing a quantitative real time PCR (qPCR) based on 18S rRNA in order to quantify the parasite biomass in *P. coatneyi* infections in the splenectomized rhesus macaque. This explorational work has thus far succeeded in establishing a protocol with both high sensitivity and specificity for *P. coatneyi*, using cryopreserved blood samples from the prospective experimental animals described in this study. It is hoped that this will eventually lead us to be able to correlate parasitemia data, and histopathological evidence of organ sequestration, to correlate clinical symptomatology with parasite burden both systemically and in an organ specific manner. In this manner, it may be possible to prove quantitatively whether organ specific complications such as renal disease correlate with sequestration is a particular organ, or overall parasitemia, as has been attempted in the human in the brain and kidney. (Ngaungsangiam 2007; Pongponratn 2003)

The second major area in which samples from this study will be used in the future is projected to be in collaboration with the National University of Singapore's Vivax Laboratory and Dr. Laurent Renia's team at Singapore's Agency for Science, Technology and Research (A*STAR). We are in the preliminary stages of conducting whole RNA sequencing (RNA-seq), also referred to as whole transcriptome shotgun sequencing (WTSS) on tissue samples selected from the CNS, kidney and heart tissues from the prospective animals in this study and will be compared with control animals. The intent will be to assess the activity level and specific quantity of a diverse array of RNA in the sample at the time of peak parasitemia in the animals.

The tissues were selected based on the specificity of disease observed in other areas of this project, and with the recognition that gene expression is variable between organs and cells. Recognizing that gene expression is time dependent and that the transcriptome changes throughout the course of disease, it would be fascinating to be able to conduct this experiment at various time-points

throughout infection. However, our sample collection timeline as well as the ethics governing animal use in this study, required minimizing the total number of animals used to focus on our study objectives. Bioinformatics will be conducted so as to make sense of the huge volume of data that this will generate. Subsequently, the data will be compared with similar work which has been conducted by Dr. Turner and his collaborators at MORU on human tissues. Finally, our preliminary assessment of the biofluidics and micropipette binding strength assays discussed in Chapter 6 will be expanded upon in collaboration with Dr. Bruce Russell and his team.

As with all science, the act of discovery merely opens the doors to more questions, and this study has shed light on a range of fascinating problems that need to be addressed. Examples include the need to fully clarify the cardiac injury in these animals. Evaluation of the cardiac specific marker, troponin, over the course of the infection may provide a great mechanism with which to substantiate the histopathologic and ultrastructural findings that we have described. Combining troponin with examination of B-type natriuretic peptide (BNP) or N-terminal pro B-type natriuretic peptide (NT-proBNP) as mechanisms to identify the theorized low grade cardiac ischemia would be of significant interest.

Another area that still remains a mystery is the actual mechanism of death in these animals which appear to succumb to circulatory shock. It is theorized to be due to massive sequestration of parasitized RBCs, resulting in decreased blood perfusion to tissues. The resultant hypoxia, anoxia, subsequent cellular injury, and multi-organ failure is posited to cause the death of these animals. This theory is based on the clinical symptomology of dyspnea, lethargy and decreased mentation, renal failure, and bleeding disorders (as noted by the ecchymoses and petechiae) that occur in some animals. Furthermore, the clinical pathology finding of hyperlactatemia in the untreated macaques, suggestive of acidosis, abnormalities reflecting renal and hepatic injury, and the onset of anemia, all support the theory of circulatory insufficiency, however this remains to be confirmed. Histopathologic and ultrastructural evaluation of all tissues demonstrate piecemeal necrosis of cells

rather than wholesale death of organs. This is significant in that it supports a systemic pathology relating to the microvasculature. The knowledge that this foundational work has generated would be further strengthened by confirming these hypotheses. Blood pressure monitoring, real time imaging of tissue perfusion or tracer techniques including functional MRI imaging, throughout the course of an experimental infection would be difficult, but are possible with an animal model while not being feasible in humans. They may allow confirmation of some of these theories, which have been muted for years in relation to human disease without a suitable model to test them on.

8.5 **Final Summary**:

The successful use of the model, in conducting the methylene blue drug study, confirms the fact that *P. coatneyi* in splenectomized rhesus macaques can be effectively employed as a platform for the evaluation of anti-malarial compounds. While the model has limitations in the study of pulmonary injury, retinal hemorrhage and chronic malarial anemia, as well as not mirroring the clinical picture of cerebral malaria perfectly, it has concrete and definite applicability in the study of malaria induced acute kidney injury, cardiac and hepatic pathology. Practically, the model is extremely labor intensive, although this varies with individual study designs. Furthermore, the model is expensive unless the research group has a rhesus colony or such facilities at their disposal. However, and crucially, we have demonstrated that the model offers significant potential in treatment studies, post-infection therapeutic and supportive care studies and a range of further pathophysiology studies.

When considering the models currently available, and comparing the validity and applicability of *P. coatneyi* induced disease with the *P. berghei* ANKA or *P. yoelii* mouse models, the rhesus macaque provides a mechanism to examine the clinical course and pathology of malaria in a controlled manner not possible in human studies, but with direct correlation to the same. In

comparison with murine models, the macaque model has the advantage of a high degree of homology to the human immune system. Furthermore, unlike the murine models, there are opportunities in the macaque to engineer functional studies to evaluate metabolic and physiologic changes which are fundamentally difficult or impossible to perform in human malaria patients such as with intracranial pressure monitoring, functional MRI imaging, laser video microscopy of flow and EEG. In comparison with the non-sequestration dependent, immunologically mediated encephalitis of experimental murine cerebral malaria, the similarities of the pathophysiological tapestry of *P. coatneyi* to human falciparum malaria make its results more medically relevant.

Therefore, the use of this dissertation and its accompanying studies provides malaria investigators with a significantly more profound understanding of the animal model with direct relevance to the falciparum malaria of humans. Additionally, the work accomplished herein validates the use of the *P. coatneyi*/Rhesus macaque model as an applicable, reproducible and effective animal model for use in anti-malarial drug trials for severe malaria. This work provides the most comprehensive pathologic assessment of the *P. coatneyi*/rhesus macaque model to date, with in-depth description of the parasite and host-parasite interactions at all levels from the macroscopic to the nanostructural and molecular. Furthermore, and fundamentally, this study has taken the model from the conceptual to the practical through the successful demonstration of the model's use in practice with methylene blue. With this greater understanding of the model, its proven efficacy and replicability translates to enormous potential for practical application as a useful platform for both basic science studies of malaria pathophysiology and the development of anti-malarial drugs, adjuvant therapies and vaccines.

Chapter 9: References

Chapter 1: Introduction

Abu Sayeed A, Maude RJ, Hasan MU, Mohammed N, Hoque MG, Dondorp AM, Faiz MA. Malarial retinopathy in Bangladeshi adults. Am J Trop Med Hyg. 2011; 84:141-147.

Aikawa M, Brown AE, Smith CD, et al. A primate model for human cerebral malaria: Plasmodium coatneyi–infected rhesus monkeys. Am J Trop Med Hyg. 1992; 46:391-397.

Aikawa M, Iseki M, Barnwell JW, Taylor D, Oo MM, Howard RJ. The pathology of human cerebral malaria. Am J Trop Med Hyg. 1990; 43:S30-S37.

Aikawa M, Rabbege JR, Udeinya I, Miller LH. Electron microscopy of knobs in Plasmodium falciparum-infected erythrocytes. J Parasitol. 1983; 69:435-437.

Almelli T, Ndam NT, Ezimegnon S, Alao MA, Ahouansou C, Sagbo G, Amoussou A, Deloron P, Tahar R. Cytoadherence phenotype of Plasmodium falciparum-infected erythrocytes is associated with specific pfemp-1 expression in parasites from children with cerebral malaria. Malar J. 2014; 13:333-342.

Anstey N, Douglas NM, Poespoprodjo JR, Price RN. Plasmodium vivax: clinical spectrum, risk factors and pathogenesis. Adv Parasitol. 2012; 80:151-201.

Arekul S, Kanakakorn K, Kasemsuthi R. Mechanism of haemolysis in monkeys infected with Plasmodium coatneyi. Southeast Asian J Trop Med Pub Hlth. 1971; 2:261-262.

Arekul S. Plasmodium coatneyi: Alterations of transcapillary escape rate and capillary permeability to fibrinogen in rhesus monkeys. Exp Parasitol. 1986; 61:304-310.

Ashley EA, Dhorda M, Fairhurst RM, et al. Spread of artemisinin resistance in Plasmodium falciparum malaria. N Engl J Med. 2014; 371:411-423.

Barber BE, William T, Grigg MJ, Menon J, Auburn S, Marfurt J, Anstey NM, Yeo TW. A prospective comparative study of knowlesi, falciparum and vivax malaria in Sabah, Malaysia: high proportion with severe disease from Plasmodium knowelsi and Plasmodium vivax but no mortality with early referral and artesunate therapy. Clin Infect Dis. 2013; 56(3):383-97.

Beare NA, Taylor TE, Harding SP, Lewallen S, Molyneux ME. Malarial retinopathy: a newly established diagnostic sign in severe malaria. Am J Trop Med Hyg. 2006; 75:790–797.

Beare NA, Lewis DK, Kublin JG, Harding SP, Zijlstra EE, Molyneux ME. Retinal changes in adults with cerebral malaria. Ann Trop Med Parasitol. 2003; 97:313–315.

Beignon AS, Le Grand R, Chapon C. In vivo imaging in NHP models of malaria: Challenges, progress and outlooks. Parasitol Int. 2014; 63(1):206-215.

Bhumiratana A, Intarapuk A, Sorosjinda-Nunthawarasilp P, Maneekan P, Koyadun S. Border malaria associated with multidrug resistance on Thailand-Myanmar and Thailand-Cambodia borders: Transmission dynamic, vulnerability, and surveillance. Biomed Res Int. 2013; 2013:363417.

Binnig G, Quate CF, Gerber C. Atomic-Force Microscope. Physical Review Letters. 1986; 56: 930-933.

The non-human primate in nonclinical drug development and safety assessment. Bluemel J, Korte S, Schenck E, Weinbauer GF. Eds. First edition, Academic press, London, UK; 2015.

Bray RS. Studies on malaria in chimpanzees. VI. Laverania falciparum. Am J Trop Med Hyg. 1958; 7:20-24.

Bruce-Chwatt LJ. The Malaria Parasites. In. Essential Malariology. Ed. Bruce-Chwatt LJ. second edition, William Heinemann medical books Ltd, London, UK. Pp 38-39; 1985.

Bruneel F, Hocqueloux L, Alberti C, et al. The clinical spectrum of severe imported falciparum malaria in the intensive care unit: report of 188 cases in adults. Am J Respir Crit Care Med. 2003; 167:684-689.

Buffet PA, Safeukui I, Deplaine G, Brousse V, Prendki V, Theillier M, Turner GD, Mercereau-Puijalon O. The pathogenesis of Plasmodium falciparum malaria in humans: insights from splenic physiology. Blood. 2011; 117(2):381-392.

Carrara VI, Lwin KM, Phyo AP, Ashley E, Wiladphaingern J, Sriprawat K, Rijken M, Boel M, McGready R, Proux S, Chu C, Singhasivanon P, White N, Nosten F. Malaria Burden and Artemisinin Resistance in the Mobile and Migrant Population on the Thai–Myanmar Border, 1999-2011: An Observational Study. PLoS Med. 2013; 10:e1001398.

Chittichai P, Chierakul N, Davis TM. Peripheral gangrene in nonfatal pediatric cerebral malaria: a report of two cases. SE Asian J Trop Med. 1991; 22:190-194.

Clark IA, Rockett KA. The cytokine theory of Cerebral Malaria. Parasitol Today. 1994; 10(10):410-412.

Coatney GR, Collins WE, Warren M, Contacos PG. The Primate Malarias. Washington, D.C.: U.S. Government Printing Office; Pp. 289–299; 1971.

Combes V, Coltel N, Faille D, Wassmer SC, Grau GE. Cerebral malaria: role of microparticles and platelets in alterations of the blood-brain barrier. Int J Parasitol. 2006; 36(5):541-546.

Cox-Singh J, Culleton R. Plasmodium knowlesi: from severe zoonosis to animal model. Trends Parasitol. 2015; 31(6):232-238.

Cox-Singh J, Davis TM, Lee KS, Shamsul SS, Matusop A, Ratnam S, Rahman HA, Conway DJ, Singh B. Plasmodium knowlesi malaria in humans is widely distributed and potentially life threatening. Clin Infect Dis. 2008; 46:165-171.

Cox-Singh J, Hui J, Lucas SB, Divis PC, Zulkarnaen M, Chandran P, Wong KT, Adem P, Zaki SR, Singh B, Krishna S. Severe malaria- a case of fatal Plasmodium knowlesi infection with post-mortem findings: a case report. Malar J. 2010; 9:10.

Craig AG, Grau GE, Jansse C, Barnwell J, Kazura JW, Milner D, Turner GD, Langhorne J, on behalf of the participants of the Hinxton Retreat meeting on ‘‘Animal Models for Research on Severe Malaria’’. The Role of Animal Models for Research on Severe Malaria. PLoS Pathog. 2012; 8(2):e1002401.

Craig, AG, Grau GE, Janse C, Kazura JW, Milner D, Barnwell JW, Turner GD, Langhorne J. The role of animal models for research on severe malaria. PLoSPathog. 2012; 8:1-9.

Collins WE. Major animal models in malaria research: Simian. *In*: Malaria: Principles and Practice of Malariology. Eds. Wernsdofer WH and McGregor. Edinburgh: Churchill Livingstone. Pp. 1473-501; 1988.

Cox-Singh J, Culleton R. Plasmodium knowlesi: from severe zoonosis to animal model. Trends Parasitol. 2015; 31(6):232-236.

Davis TM, Brown AE, Smith CD. Metabolic disturbances in Plasmodium coatneyi-infected rhesus monkeys. Int J Parasitol. 1993; 23:557-563.

Davison BB, Cogswell FB, Baskin GB, Falkenstein KP, Henson EW, Tarantal AF, Krogstad DJ. Plasmodium coatneyi in the rhesus monkey (Macaca mulatta) as a model of malaria in pregnancy. Am J Trop Med Hyg. 1998; 59:189-201.

Davison BB, Cogswell FB, Baskin GB, Falkenstein KP, Henson EW, Krogstad DJ. Placental changes associated with fetal outcome in the Plasmodium coatneyi/rhesus monkey model of malaria in pregnancy. Am J Trop Med Hyg. 2000; 63:158-173.

Deschamps S, Maynadier M, Wein S, Gannoun-Zaki L, Marechal E, Vial HJ. Rodent and non-rodent malaria parasites differ in their phospholipid metabolic pathways. J Lipid Res. 2009; 51:81-96.

de Souza JB, Hafalla JCR, Riley EM, Couper KN. Cerebral malaria: why experimental murine models are required to understand the pathogenesis of disease. Parasitology. 2010; 137:755-772.

Desowitz RS, Miller LH, Buchanan RD, Yuthasastrkosol V, Permpanich B. Comparative studies on the pathology and host physiology of malarias. I. Plasmodium coatneyi. Ann Trop Med Parasitol. 1967; 61:365-374.

Desowitz RS, Miller LH, Buchanan RD, Permpanich B. The sites of deep vascular schizogony in Plasmodium coatneyi malaria. Trans R Soc Trop Med Hyg. 1969; 63:198-202.

Desowitz RS, Pavanand K. A vascular-permeability-increasing factor in the serum of monkeys infected with primate malarias. Ann Trop Med Parasitol. 1967; 61:128-133.

Dondorp AM, Lee SJ, Faiz MA, Mishra S, Price R, Tjitra E, Than M, Htut Y, Mohanty S, Yunus EB, Rahman R, Nosten F, Anstey NM, Day NP, White NJ. The relationship between age and the manifestations of and mortality associated with severe malaria. Clin Infect Dis. 2008; 12:151-157.

Dondorp AM, Desakorn V, Pongtavornpinyo W, Sahassananda D, Silamut K, Chotivanich K, Newton PN, Pitisuttithum P, Smithyman AM, White NJ, Day NPJ. Estimation of the total parasite biomass in acute falciparum malaria from plasma PfHRP2. PLoS Med. 2005; 2:e204.

Dondorp AM, Desakorn V, Pongtavornpinyo W, Sahassananda D, Silamut K, et al. Estimation of the total parasite biomass in acute falciparum malaria from plasma PfHRP2. PloS Med. 2005; 2: e204.

Dorovini-Zis K, Schmidt K, Huynh H, Fu W, Whitten RO, Milner D, Kamiza S, Molyneux M, Taylor TE. The neuropathology of fatal cerebral malaria in Muuj8talawian children. Am J Pathol. 2011; 178:2146–2158.

Escalante AA, Barrio E, Ayala FJ. Evolutionary origin of human and primate malarias: Evidence from the circumsporozoite protein gene. Mol Biol Evol. 1995; 12:616–626.

Escalante AA, Freeland DE, Collins WE, Lal AA. The evolution of primate malaria parasites based on the gene encoding cytochrome b from the linear mitochondrial genome. Proc Natl Acad Sci USA. 1998; 95:8124–8129.

Epiphanio S, Campos MG, Pamplona A, Carapau D, Pena AC, Ataíde R, Monteiro CA, Félix N, Costa-Silva A, Marinho CR, Dias S, Mota MM. VEGF promotes malaria-associated acute lung injury in mice. PLoS Pathog. 2010; 6:e1000916.

Essuman VA, Ntim-Amponsah CT, Astrup BS, et al. Retinopathy in severe malaria in Ghanaian children - overlap between fundus changes in cerebral and non-cerebral malaria. Malar J. 2010; 9:232.

Eyles DE. The species of simian malaria: taxonomy, morphology, lifecycle and geographical distribution of the monkey species. J Parasit. 1963; 49:866-867.

Eyles DE, Dunn F, Warren McW, Guinn E. Plasmodium coatneyi from the Philippines. J Parasit. 1963; 49:1038.

Eyles DE, Fong YL, Warren McW, Guinn E, Sandosham AA, Wharton RH. Plasmodium coatneyi, a new species of primate malaria from Malaya. Am J trop Med Hyg. 1962; 11:597-604.

Eyles DE, Laing ABG, Warren M, et al. Malaria parasites of the Malayan leaf monkeys of the genus Presbytis. Med J Malaya. 1962; 17:85-86.

Field JW, Shute PG. The microscopic diagnosis of human malaria. II A morphological study of the erythrocytic parasites. Inst Med Res, Fed Malaya. 1956; 24:251.

Fooden J. Malaria in macaques. Int J Primatol. 1994; 15:573-596.

Fujioka H, Millet P, Maeno Y, Nakazawa S, Ito Y, Howard RJ, Collins WE, Aikawa M. A non-human primate model for human cerebral malaria: rhesus monkeys experimentally infected with Plasmodium fragile. Exp Parasitol. 1994; 78(4):371-376.

Furst T, Raso G, Acka CA, Tschannen AB, N'Goran EK, Utzinger J. Dynamics of socioeconomic risk factors for neglected tropical diseases and malaria in an armed conflict. PLoSntds. 2009; 3:1-10.

Garamszegi LZ. Patterns of co-speciation and host switching in primate malaria parasites. Malar J. 2009; 8:110-125.

Ghafoor SZA, MacRae EA, Harding KG, Patel GK. Symmetrical peripheral digital gangrene following severe Plasmodium falciparum malaria-induced disseminated intravascular coagulopathy. Int Wound J. 2010; 7:418-422.

Giessibl FJ. Advances in atomic-force microscopy. Reviews of Modern Physics. 2003; 75(3):949–983.

Gonçalves RM, Salmazi KC, Santos BA, Bastos MS, Rocha SC, Boscardin SB, Silber AM, Kallás EG, Ferreira MU, Scopel KK. CD4+CD25+Foxp3+regulatory T cells, dendritic cells, and circulating cytokines in uncomplicated malaria: Do different parasite species elicit similar host responses? Infect Immun. 2010; 78:4763-4772.

Guimarães LO, Bajay MM, Wunderlich G, Bueno MG, Röhe F, Catão-Dias JL, Neves A, Malafronte RS, Curado I, Kirchgatter K. The genetic diversity of Plasmodium malariae and Plasmodium brasilianum from human, simian and mosquito hosts in Brazil. Acta Trop. 2012; 124:27-32.

Grau GE, Mackenzie CD, Carr RA, Redard M, Pizzolato G, Allasia C, Cataldo C, Taylor TE, Molyneux ME. Platelet accumulation in brain microvessels in fatal pediatric cerebral malaria. J Infect Dis. 2003; 187:461-466.

Handunnetti SM, David PH, Perera KL, Mendis KN. Uninfected erythrocytes form "rosettes" around Plasmodium falciparum infected erythrocytes. Am J Trop Med Hyg. 1989; 40:115-118.

Hayakawa T, Culleton R, Otani H, Horii T, Tanabe K. Big Bang in the Evolution of Extant Malaria Parasites. Mol Biol Evol. 2008; 25:2233-2239.

Hellgren O, Krizanauskiene A, Hasselquist D, Bensch S. Low Haemosporidian and one key-host species in a bird malaria community on a mid-Atlantic island (Sao Miguel, Azores). J Wildl Dis. 2011; 47:849-859.

Hempelmann E, Krafts K. Bad Air, amulets and mosquitoes. Malar J. 2013; 12:1-18.

Hendriksen IC, White LJ, Veenemans J, Mtove G, Woodrow C, Amos B, Saiwaew S, Gesase S, Nadjm B, Silamut K, Joseph S, Chotivanitch K, Day NP, von Seidlein L, Verhoef H, Reyburn H, White NJ, Dondopr AM. J Infect Dis. 2013; 207(2):351-361.

Hidayat AA, Nalbandian RM, Sammons DW, Fleischmann JA, Johnson TE. The diagnostic histopathologic features of ocular malaria. Ophthalmology. 1993; 100:1183-1186.

Hora R, Kapoor P, Thind KK, Mishra PC. Cerebral malaria-clinical manifestations and pathogenesis. Metab Brain Dis. 2016; 31(2):225-237.

Howard RJ, Gilladoga AD. Molecular studies related to the pathogenesis of cerebral malaria. Blood. 1989; 74:2603-2618.

Howe L, Castro IC, Schoener ER, Hunter S, Barraclough RK, Alley MR. Malaria parasites (Plasmodium spp.) infecting introduced, native and endemic New Zealand birds. Parasitol Res. 2012; 100:913-923.

Hueck IS, Rossiter K, Artmann GM, Schmid-Schönbein GW. Fluid shear attenuates endothelial pseudopodia formation into the capillary lumen microcirculation. 2008; 15:531–542.

Hunt NH, Ball HJ, Hansen AM, Khaw LT, Guo J, Bakmiwewa S, Mitchell AJ, Combes V, Grau GE. Cerebral Malaria: gamma-interferon redux. Front Cell Infect Microbiol. 2014; 4:113.

Hunt NH, Grau GE, Engwerda C, Barnum SR, van der Heyde H, Hansen DS, Schofield L, Golenser J. Murine cerebral malaria: the whole story. Trends Parasitol. 2010; 26:272–274.

Hviid L, Marinho CR, Staalsoe T, Penha- Goncalves C. Of mice and women: rodent models of placental malaria. Trends Parasitol. 2010; 26:412-419.

Jaff MS, McKenna D, McCann SR. Platelet Phagocytosis: A Probable mechanism of Thrombocytopenia in Plasmodium falciparum Infection. J ClinPathol. 1985; 38:1318-1319.

John CC, Kutumba E, Mugarura K, Opaka RO. Adjunctive therapy for cerebral malaria and other severe forms of Plasmodium falciparum malaria. Expert Rev Anti Infect Ther. 2010; 8(9):997-1008.

Lanzer M, Wickert H, Krohne G, Vincensini L, Breton CB. Maurer's clefts: A novel multi-functional organelle in the cytoplasm of Plasmodium falciparum-infected erythrocytes. Int J Parasitol. 2006; 36:23-36.

Kaiser K, Texier A, Ferraniz J, Buguet A, Meillier A, Latour C, Peyron F, Cespuglio R, Picot S. Recombinant human erythropoietin prevents the death of mice during cerebral malaria. J Infect Dis. 2006; 193(7):987-995.

Kawai S, Aikawa M, Kano S, Suzuki M. A primate model for severe human malaria with cerebral involvement: Plasmodium coatneyi-infected Macaca fuscata. Am J Trop Med Hyg. 1993; 48:630-636.

Kawai S, Aikawa M, Suzuki M, Matsuda H. A nonhuman primate model for severe human malaria: Plasmodium coatneyi-infected Japanese macaque (Macaca fuscata). Tokai J Exp Clin Med. 1998; 23:101-102.

Kawai S, Ikeda E, Sugiyama M, Matsumoto J, Higuchi T, Zhang H, Khan N, Tomiyoshi K, Inoue T, Yamaguchi H, Katakura K, Endo K, Matsuda H, Suzuki M. Enhancement of splenic glucose metabolism during acute malarial infection: Correlation of findings of FDG-PET imaging with pathological changes in a primate model of severe human malaria. Am J Trop Med Hyg. 2006; 74:353-360.

Kawai S, Sugiyama M. Imaging analysis of the brain in a primate model of cerebral malaria. Acta Trop. 2010; 114:152-156.

Kawai S, Yoshinari M, Matsumoto J, Kirinoki M, Aikawa M, Minami M. Plasmodium coatneyi-infected erythrocytes bind to C32 amelanotic melanoma cells under static and flow conditions. J Vet Med Sci. 2003; 65:375-380.

Kilejian A, Abati A, Trager W. Plasmodium falciparum and Plasmodium coatney: immunogenicity of "knob-like protrusions" on infected erythrocyte membrane. Exp Parasitol. 1977; 42:157-164.

Kyle DE, Corcoran KD, Young GD, et al. Plasmodium coatneyi exhibits innate resistance to mefloquine in rhesus monkeys (Macaca mulatta) and in vitro {abstract #394}. Annual Meeting of the American Society of Tropical Medicine and Hygiene, Pp.257; 1994

Langhorne J, Buffet P, Galinski M, Good M, Harty J, Leroy D, Mota MM, Pasini E, Renia L, Riley E, Stins M, Duffy P. The relevance of non-human primate and rodent malaria models for humans. Malar J. 2011; 10:23-27.

Lawrence C, Olson JA. Birefringent hemozoin identifies malaria. Am J Clin Pathol. 1986; 86:360-363.

Leclerc MC, Hugot JP, Durand P, Renaud F. Evolutionary relationships between 15 Plasmodium species from New and Old World primates (including humans): a 18S rDNA cladistic analysis. Parasitology. 2004; 129:677-684.

Lee K-S, Divis PCS, Zakaria SK, Matusop A, Julin RA, Conway DJ, Cox-Singh J, Singh B. Plasmodium knowlesi: Reservoir hosts and tracking the emergence in humans and macaques. PLoS Pathog. 2011; 7:e1002015.

Levine ND. The protozoan phylum Apicomplexa. CRC Press, Boca Raton (FL); 1988.

Lewallen S, Bakker H, Taylor TE, Wills BA, Courtright P, Molyneux ME. Retinal findings predictive of outcome in cerebral malaria. Trans R Soc Trop Med Hyg. 1999; 90:144-146.

Lewallen S, White VA, Whitten RO, Gardiner J, Hoar B, Lindley J, Lochhead J, McCormick A, Wade K, Tembo M, Mwenechanyana J, Molyneux ME, Taylor TE. Clinical-Histopathological Correlation of the Abnormal Retinal Vessels in Cerebral Malaria. Arch Ophthalmol. 2000; 118:924-928.

Liechti ME, Zumsteg V, Hatz CF, Herren T. Plasmodium falciparum cerebral malaria complicated by disseminated intravascular coagulation and symmetrical peripheral gangrene: case report and review. Eur J Clin Microbiol Infect Dis. 2003; 22:551-554.

Looareesuwan S, Warrell DA, White NJ, Sutharasamai P, Chanthavanich P, Sundaravej K, Juel-Jensen BE, Bunnag D, Harinasuta T. Do patients with cerebral malaria have cerebral oedema? A computed tomography study. Lancet. 1983; 1:434-437.

Looareesuwan S, Wilairatana P, Krishna S, Kendall B, Vannaphan S, Viravan C, White NJ. Magnetic resonance imaging of the brain in patients with cerebral malaria. Clin Infect Dis. 1995; 21:300-309.

Lou J, Lucas R, Grau GE. Pathogenesis of cerebral malaria: Recent experimental data and possible applications for humans. Clin Microbiol Rev. 2001; 14:810-820.

Lovegrove FE, Gharib SA, Peña-Castillo L, Patel SN, Ruzinski JT, Hughes TR, Liles WC, Kain KC. Parasite burden and CD36-mediated sequestration are determinants of acute lung injury in an experimental malaria model. PLoS Pathog. 2008; 4:e1000068.

MacPherson GG, Warrell MJ, White NJ, Looareesuwan S, Warrell DA. Human Cerebral Malaria: A Quantitative ultrastructural analysis of parasitized erythrocyte sequestration. Am J Pathol. 1985; 119:385-401.

Maeno Y, Brown AE, Smith CD, Tegoshi T, Toyoshima T, Ockenhouse CF, Corcoran KD, Ngampochjana M, Kyle DE, Webster HK, et al. A non-human primate model for cerebral malaria: effects of artesunate (qinghaosu derivative) on rhesus monkeys experimentally infected with Plasmodium coatneyi. Am J Trop Med Hyg. 1993; 49:726-734.

Matsumoto J, Kawai S, Terao K, Kirinoki M, Yasutomi Y, Aikawa M, Matsuda H. Malaria infection induces rapid elevation of the soluble Fas ligand level in serum and subsequent T lymphocytopenia: Possible factors responsible for the differences in susceptibility of two species of Macaca monkeys to Plasmodium coatneyi infection. Infect Immun. 2000; 68:1183-1186.

Mbale EW, Moxon CA, Mukaka M, Chagomerana M, Glover S, Chisala N, Omar S, Molyneux M, Seydel K, Craig AG, Taylor T, Heyderman RS, Mallewa M. HIV coinfection influences the inflammatory response but not the outcome of cerebral malaria in Malawian children. J Infect. 2016 Jun 14. pii: S0163-4453(16)30097-4. doi: 10.1016/j.jinf.2016.05.012. [Epub ahead of print]

McGouran RC, Emmerson GA. Symmetrical peripheral gangrene. Br Heart J. 1977; 39:569-572.

Medana IM, Day NPJ, Hien TT, Mai NT, Bethell D, Phu NH, Farrar J, Esiri MM, White NJ, Turner GD. Axonal injury in Cerebral Malaria. Am J Pathol. 2002; 160: 655-666.

Medana IM, Day NPJ, Hien TT, White NJ, Turner GDH. Erythropoietin and its receptor in the Brainstem of Adults with Fatal Falciparum Malaria. Malar J. 2009; 8:261.

Medana IM, Turner GDH. Human cerebral malaria and the blood-brain barrier. Int J Parasitol. 2006; 36:555-568.

Medana IM, Turner GD. Plasmodium falciparum and the blood-brain barrier--contacts and consequences. J Infect Dis. 2007; 195(7):921-923.

Mendiratta DK, Bhutada K, Narang R, Narang P. Evaluation of different methods for diagnosis of P. falciparum malaria. Indian J Med Microbiol. 2006; 24:49-51.

Migot-Nabias F, Ollomo B, Dubreuil G, Morelli A, Domarle O, Nabias R, Georges AJ, Millet P. Plasmodium coatneyi: differential clinical and immune responses of two populations of Macaca fascicularis from different origins. Exp Parasitol. 1999; 91:30-39.

Miller LH. Distribution of mature trophozoites and schizonts of Plasmodium falciparum in the organs of Aotus trivirgatus, the night monkey. Am J Trop Med Hyg. 1969; 18:860-865.

Milner DA, Jr. Rethinking cerebral malaria pathology. Curr Opin Infect Dis. 2010; 23:456-463.

Mitsui H, Arisue N, Sakihama N, Inagaki Y, Horii T, Hasegawa M, Tanabe K, Hashimoto T. Phylogeny of Asian primate malaria parasites inferred from apicoplast genome-encoded genes with special emphasis on the positions of Plasmodium vivax and P. fragile. Gene. 2010; 450:32-38.

Mohanty D, Marwaha N, Ghosh K, Chauhan AP, Shah S, Sharma S, Das KC. Vascular occlusion and disseminated intravascular coagulation in falciparum malaria. Br Med J (Clin Res Ed). 1985; 290:115-116.

Moreno A, Cabrera-Mora M, Garcia A, et al. Plasmodium coatneyi in rhesus macaques replicates the multisystemic dysfunction of severe malaria in humans. Infect Immun. 2013; 81:1889-1904.

Moreno A, García A, Cabrera-Mora M, Strobert E, Galinski MR. Disseminated intravascular coagulation complicated by peripheral gangrene in a rhesus macaque (Macaca mulatta) experimentally infected with Plasmodium coatneyi. Am J Trop Med Hyg. 2007; 76:648-654.

Nagatake T, Hoang VT, Tegoshi T, Rabbege J, Ann TK, Aikawa M. Pathology of falciparum malaria in Vietnam. Am J Trop Med Hyg. 1992; 47:259-264.

Nakano Y, Fujioka H, Luc KD, Rabbege JR, Todd GD, Collins WE, Aikawa M. A correlation of the sequestration rate of P. coatneyi- infected erythrocytes in cerebral and subcutaneous tissue of a rhesus monkey. Am J Trop Med Hyg. 1996; 55:311-314.

Newton CR, Kirkham FJ, Winstanley PA, Pasvol G, Peshu N, Warrell DA, Marsh K. Intracranial pressure in African children with cerebral malaria. Lancet. 1991; 337:573-576.

Ng OT, Ooi EE, Lee CC, Lee PJ, Ng LC, Pei SW, Tu TM, Loh JP, Leo YS. Naturally acquired human Plasmodium knowlesi infection, Singapore. Emerg Infect Dis. 2008; 14:814-816.

Olliaro P. Mortality associated with severe Plasmodium falciparum malaria increases with age. Clin Infect Dis. 2008; 12:158–160.

Oquendo P, Hundt E, Lawler J, Seed B. CD36 directly mediates cytoadherence of Plasmodium falciparum parasitized erythrocytes. Cell. 1989; 58:95–101.

Pacheco MA, Reid MJ, Schillaci MA, Lowenberger CA, Galdikas BM, Jones-Engel L, Escalante AA. The origin of malarial parasites in orangutans. PLoS One. 2012; 7:1-11.

Perkins SL, Austin C. Four new species of Plasmodium from New Guinea lizards: Integrating morphology and molecules. J Parasitol. 2009; 95:424-433.

Phyo AP, Nkhoma S, Stepniewska K, Ashley EA, Nair S, McGready R, ler Moo C, Al-Saai S, Dondorp AM, Lwin KM, Singhasivanon P, Day NP, White NJ, Anderson TJ, Nosten F. Emergence of artemisinin-resistant malaria on the western border of Thailand: a longitudinal study. Lancet. 2012; 379:1960–1966.

Picot S, Bienvenu AL, Konate D, Sissoko S, Barry A, Diarra E, Bamba K, Djimde A, Doumbo OK. Safety of epoietin beta-quinine drug combination in children with cerebral malaria in Mali. Malar J. 2009 8:169

Poharkar A, Reddy PA, Gadge VA, Kolte S, Kurkure N, Shivaji S. Is Malaria the Cause for Decline in the Wild Population of the Indian White-Backed Vulture (Gyps bengalensis). Curr Sci. 2009; 96:553-559.

Poinar G. Plasmodium dominicana n. sp. (Plasmodiidae: Haemospororida) from Tertiary Dominican amber. Syst Parasitol. 2005; 61:47-52.

Ponsford MJ, Medana IM, Prapansilp P, Hien TT, Lee SJ, Dondorp AM, Esiri MM, Day NP, White NJ, Turner GD. Sequestration and Microvascular Congestion Are Associated with Coma in Human Cerebral Malaria. J Infect Dis. 2012; 205:663-671.

Ramiro RS, Reece SE, Obbard DJ. Molecular evolution and phylogenetics of rodent malaria parasites. BMC Evol Biol. 2012; 12:219-230.

Roberts DD, Scherwood JA, Spitalnik SL, Panton LJ, Howard RJ, Dixit VM, Frazier WA, Miller LH, Ginsburg V. Thrombospondin binds falciparum malaria parasitized erythrocytes and may mediate cytoadherence. Nature. 1985; 318:64-66.

Rogers EE, Bonifacio SL, Glass HC, Juul SE, Chang T, Maycock DE, Durand DJ, Song D, Barkovisg AJ, Ballard RA, Wu YW. Erythropoeitin and hypothermia for hypoxic-ischameic encephalopathy. Paediatr Neurol. 2014; 51(5):657-662.

Rogers WO, Weiss WR, Kumar A, Aguiar JC, Tine JA, Gwadz R, Harre JG, Gowda K, Rathore D, Kumar S, Hoffman SL. Protection of rhesus macaques against lethal Plasmodium knowlesi malaria by heterologous DNA priming and poxvirus boosting immunization regimen. Infect Immun. 2002; 70:4329-4335.

RTS,S Clinical Trials Partnership. Efficacy and safety of the RTS,S/AS01 malaria vaccine during 18 months after vaccination: a phase 3 randomized, controlled trial in children and young infants at 11 African sites. PloS Med. 2014; 11:e1001685

Rug M, Prescott SW, Fernandez KM, Cooke BM, Cowman AF. The role of KAHRP domains in knob formation and cytoadherence of P falciparum-infected human erythrocytes. Blood. 2006; 108:370-378.

Sá JM, Twu O, Hayton K, Reyes S, Fay MP, Ringwald P, Wellems TE. Geographic patterns of Plasmodium falciparum drug resistance distinguished by differential responses to amodiaquine and chloroquine. PNAS. 2009; 106:1-7.

Sabbatani S, Fiorino S, Manfredi R. The emerging of the fifth malaria parasite (Plasmodium knowlesi): a public health concern? Braz J Infect Dis. 2010; 14:299-309.

Schmidt EP, Lee LW, Zemans RL, Yamashita C, Downey GP. On, around, and through: Neutrophil-endothelial interactions in innate immunity. Physiol. 2011; 26:334–347.

Seethamchai S, Putaporntip C, Malaivijitnond S, Cui L, Jongwutiwes S. Malaria and Hepatocystis species in wild macaques, southern Thailand. Am J Trop Med Hyg. 2008; 78:646-653.

Sein KK, Brown AE, Maeno Y, Smith CD, Corcoran KD, Hansukjariya P, Webster HK, Aikawa M. Sequestration pattern of parasitized erythrocytes in cerebrum, mid-brain and cerebellum of Plasmodium coatneyi-infected rhesus monkeys (Macaca mulatta). Am J Trop Med Hyg. 1993; 49:513-519.

Semenya AA, Sullivan JS, Barnwell JW, Secor WE. Schistosoma mansoni infection impairs antimalaria treatment and immune responses of rhesus macaques infected with mosquito-borne Plasmodium coatneyi. Infect Immun. 2012; 80:3821-3827.

Seydel KB, Kampondeni SD, Valim C, Potchen MJ, Milner DA, Muwalo FW, Birbeck GL, Bradley WG, Fox LL, Glover SJ, Hammond CA, Heyderman RS, Chilingulo CA, Molyneux ME, Taylor TE. Brain swelling and death in children with cerebral malaria. N Engl J Med. 2015; 372(12):1126-1137.

Sharma BD, Gupta B. Peripheral gangrene in a case of complicated falciparum malaria. J Indian Acad Clin Med. 2002; 3:297-299.

Smith LP, Hunter KW, Oldfield EC, Strickland GT. Murine Malaria: Blood Clearance and Organ Sequestration of Plasmodium yoelii-infected Erythrocytes. Infect Immun. 1982; 38:162-167.

Smith CD, Brown AE, Nakazawa S, Fukioka H, Aikawa M. Multi-organ erythrocyte sequestration and ligand expression in rhesus monkeys infected with Plasmodium coatneyi malaria. Am J Trop Med Hyg. 1996; 55:379-383.

Smith JD, Craig AG, Kriek N, Hudson-Taylor D, Kyes S, Fagan T, Pinches R, Baruch DI, Newbold CI, Miller LH. Identification of a Plasmodium falciparum intercellular adhesion molecule-1 binding domain: a parasite adhesion trait implicated in cerebral malaria. Proc Natl Acad Sci U S A. 2000; 97:1766-1771.

Sokoli A, Groebel K, Hoelzle K, Hoelzle K, Amselgruber WM, Mateos JM, Schneider MK, Ziegler U, Felder KM, Hoelzle LE. Mycoplasma suis infection results endothelial cell damage and activation: new insight into the cell tropism and pathogenicity of hemotrophic mycoplasma. Vet Res. 2013; 44:6-18.

Sri-Hidajati, BS. Molecular and Immunological Aspects of Anemia in Malaria. Folia Medica Indonesiana. 2005; 41:240-247.

Stevenson MM, Gros P, Olivier M, Fortin A, Serghides L. Cerebral malaria: human versus mouse studies. Trends Parasitol. 2010; 26:274-275.

Spangler WL, Grible D, Abildgaard C, Harrison J. Plasmodium knowlesi malaria in the rhesus monkey. Vet Pathol. 1978; 15:83-91.

Storm J, Craig AG. Pathogenesis of cerebral malaria--inflammation and cytoadherence. Front Cell Infect Microbiol. 2014; 4:100.

Sullivan JS, Bounngaseng A, Stewart A, Sullivan JJ, Galland GG, Fleetwood H, William EC. Infection of Saimiri boliviensis monkeys with Plasmodium coatneyi. J Parasitol. 2005; 91:479-481.

Tegoshi T, Udomsangpetch R, Brown A, Nakazawa S, Webster HK, Aikawa M. Ultrastructure of rosette formation by Plasmodium coatneyi-infected erythrocytes of rhesus. Parasitol Res. 1993; 79:611-613.

Tongren JE, Yang C, Collins WE, Sullivan JS, Lai AA, Xiao L. Expression of Proinflammatory Cytokines in four regions of the brain in Macaque mulatta (Rhesus) monkeys infected with Plasmodium coatneyi. Am J Trop Med Hyg. 2000; 62:530–534.

Turner GDH. Cerebral Malaria. Brain Pathol. 1997; 7(1):569-582.

Udomsangpetch R, Brown AE, Smith CD, Webster HK. Plasmodium coatneyi infected erythrocytes form erythrocyte rosettes. Am J Trop Med Hyg. 1991; 44:399-401.

Udomsangpetch R, Wahlin B, Carlson J, et al. Plasmodium falciparum-infected erythrocytes form spontaneous erythrocyte rosettes. J Exp Med. 1989; 169:1835-1840.

Vythilingam I. Plasmodium knowlesi in humans: a review on the role of its vectors in Malaysia. Trop Biomed. 2010; 27:1–12.

Vythilingam I, NoorAzian YM, Huat TC, Jiram AI, Yusri YM, Azahari AH, Norparina I, Noorrain A, Lokmanhakim S. Plasmodium knowlesi in humans, macaques and mosquitoes in peninsular Malaysia. Parasit Vectors. 2008; 1:26-36.

Vythilingam I, Lim YA, Venugopalan B, Ngui R, Leong CS, Wong ML, Khaw L, Goh X, Yap N, Sulaiman WY, Jeffery J, Zawiah AG, Nor Aszlina I, Sharma RS, Yee Ling L, Mahmud R. Plasmodium knowlesi malaria an emerging public health problem in Hulu Selangor, Selangor, Malaysia (2009-2013): epidemiologic and entomologic analysis. Parasit Vectors. 2014; 7:436.

Vythilingam I, Wong ML, Wan-Yussof WS. Current status of Plasmodium knowlesi vectors: a public health concern? Parasitology. 2016 May 25:1-9. [Epub ahead of print]

Wahlgren M, Carlson J, Helmby H, Hedlund I, Treutiger CJ. Molecular mechanisms and biological importance of Plasmodium falciparum erythrocyte rosetting. Mem Inst Oswaldo Cruz, Rio de Janeiro. 1992; 87(Suppl. III):323-329.

Warren McW, Wharton RH. The vectors of simian malaria: identity, biology and geographical distribution. J Parasit. 1963; 49:892-904.

White VA, Lewallen S, Beare N, Kayira K, Carr RA, et al. Correlation of retinal haemorrhages with brain haemorrhages in children dying of cerebral malaria in Malawi. Trans R Soc Trop Med Hyg. 2001; 95:618-621.

White NJ, Turner GDH, Medana IM, Dondorp AM, Day NP. The murine cerebral malaria phenomenon. Trends Parasitol. 2010; 26:11-15.

World Health Organization (WHO): Severe malaria Trop Med Int Health. 2014; 19(suppl S1):7-131.

Wilson M. Laboratory diagnosis of malaria: Conventional and rapid diagnostic methods. Arch Pathol Lab Med. 2013; 137:805-811.

Woodworth BL, Atkinson CT, Lapointe DA, et al. Host population persistence in the face of introduced vector-borne diseases: Hawaii amakihi and avian malaria. Proc Natl Acad Sci USA. 2005; 102:1531-1536.

World Malaria Report 2013. In WHO (ed.). World Health Organization, Switzerland; 2013.

Yacoub S, Lang HJ, Shebbe M, et al. Cardiac function and hemodynamics in Kenyan children with severe malaria. Crit Care Med. 2010; 12:940-945.

Yan G, Zhang G, Fang X, et al. Genome sequencing and comparison of two nonhuman primate animal models, the cynomolgus and Chinese rhesus macaques. Nat Biotechnol. 2011; 29:1019-1023.

Yang C, Xiao L, Tongren JE, Sullivan J, Lal AA, Collins WE. Cytokine production in Rhesus monkeys infected with Plasmodium coatneyi. Am J Trop Med Hyg. 1999; 61:226-229.

Yu WA, Yu MC, Young PA. Ultrastructural changes in the cerebrovascular endothelium induced by a diet high in linoleic acid and deficient in vitamin E. Exp Mol Pathol. 1974; 21:289-299.

Chapter 2: Materials and Methods

Ademowo OG, Nneji CM, Adedapo AD. In vitro anti-malarial activity of methylene blue against field isolates of Plasmodium falciparum from children in Southwest Nigeria, Indian J Med Res. 2007; 126:45-49.

Aeschlimann C, Cerny T, Kűpfer A. Inhibition of (mono) amine oxidase activity and prevention of ifosfamide encephalopathy by methylene blue. Drug Metab Dispos. 1996; 24(12):1336-1339.

Aeschlimann C, Kűpfer A, Schefer H, Cerny T. Comparative pharmacokinetics of oral and intravenous ifosfamide/mesna/methylene blue therapy. Drug Metab Dispos. 1998; 26(8):883-890.

Aikawa M. Human cerebral malaria. Am J Trop Med Hyg. 1988; 39:3-10.

Aikawa M, Iseki M, Barnwell JW, Taylor D, Oo MM, Howard RJ. The pathology of human cerebral malaria. Am J Trop Med Hyg. 1990; 43:S30-S37.

Aikawa M, Brown AE, Smith CD, Tegoshi T, Howard RJ, Hasler TH, Ito Y, Perry G, Collins WE, Webster K. A primate model for human cerebral malaria: Plasmodium coatneyi–infected rhesus monkeys. Am J Trop Med Hyg. 1992; 46:391-397.

Atamna H, Krugliak M, Shalmiev G, Deharo E, Pescarmona G, Ginsburg H. Mode of anti-malarial effect of methylene blue and some of its analogues on Plasmodium falciparum in culture and their inhibition of P. vinckei petteri and P. yoelii nigeriensis in vivo. Biochem Pharmacol. 1996; 51(5):693-700.

Benitz WE and Tatro DS. The pediatric Drug Handbook, 3rd ed. St. Louis, MO: Mosby-YearBook, Inc; 1995

Cao XT, Bethell DB, Pham TP, Ta TT, Tran TN, Nguyen TT, Pham TT, Nguyen TT, Day NP, White NJ. Comparison of artemisinin suppositories, intramuscular artesunate and intravenous quinine for the treatment of severe childhood malaria. Trans R Soc Trop Med Hyg. 1997; 91(3):335-342.

Coatney GR, Collins WE, Warren McW, Contacos PG. The Primate Malarias. Bethesda, MD: National Institute of Allergy and Infectious Diseases; 1971.

Collins WE. Major animal models in malaria research: Simian. In: Malaria: Principles and Practice of Malariology. Eds. Wernsdofer WH and McGregor. Edinburgh: Churchill Livingstone. Pp. 1473-501; 1988.

Collins WE, Warren M, Sullivan JS, Galland GG. Plasmodium coatneyi: observations on periodicity, mosquito infection, and transmission to Macaca mulatta monkeys. Am J Trop Med Hyg. 2001; 64:101-110.

Craig, AG, Grau GE, Janse C, et al. The role of animal models for research on severe malaria. PLoS Pathog. 2012; 8:1-9.

Curry S. Methemoglobinemia. Ann Emerg Med. 1982; 11:214-221.

Davison BB, Cogswell FB, Baskin GB, et al. Plasmodium coatneyi in the rhesus monkey (Macaca mulatta) as a model of malaria in pregnancy. Am J Trop Med Hyg. 1998; 59:189-201.

Dawson AH, Whyte IM. Management of dapsone poisoning complicated by methaemoglobinemia. Med Toxicol Adverse Drug Exp. 1989; 4:387-392.

Day, NPJ, Hien TT, Schollaardt T, Loc PP, Chuong LV, Chau TT, Mai NT, Phu NH, Sinh DX, White NJ, Ho M. The Prognostic and Pathophysiologic Role of Pro- and Antiinflammatory Cytokines in Severe Malaria. JID. 1999; 180:1288-1297.

De Souza JB, Hafalla JCR, Riley EM, Couper KN. Cerebral malaria: why experimental murine models are required to understand the pathogenesis of disease. Parasitology. 2010; 137:755-772.

Deschamps S, Maynadier M, Wein S, Gannoun-Zaki L, Marechal E, Vial HJ. Rodent and non-rodent malaria parasites differ in their phospholipid metabolic pathways. J Lipid Res. 2009; 51:81-96.

Devine RM, van Heerden JA, Grant CS, Muir JJ. The role of methylene blue infusion in the management of persistent or recurrent hyperparathyroidism. Surgery. 1983; 94:916-918.

DiSanto AR, Wagner JG. Pharmacokinetics of highly ionized drugs I: Methylene blue-whole blood, urine, and tissue assays. J Pharm Sci. 1972a; 61(4):598-601.

DiSanto AR, Wagner JG. Pharmacokinetics of highly ionized drugs II: Methylene blue – absorption, metabolism, and excretion in man and dog after oral administration. J Pharm Sci. 1972b; 61(7):1086-1090.

DiSanto AR, Wagner JG. Pharmacokinetics of highly ionized drugs III: Methylene blue–blood levels in the dog and tissue levels in the rat following intravenous administration. J Pharm Sci. 1972c; 61(7):1090-1094.

Dittrich S, Sunyakumthorn P, Phetsouvanh R, Rattanavong S, Phetsouvanh R, Panyanivong P, Sengduangphachanh A, Phoumin P, Anantatat T, Chanthongthip A, Lee SJ, Dubot-Peres A, Day NPJ, Paris DH, Newton PN, Turner GDH. Blood -Brain barrier function and CSF biomarkers in Rickettsial versus other Neurological infections in Laos. Am J Trop Med Hyg. 2015; 93(2):232-237.

Dondorp AM, et al, for the AQUAMAT group. 2010, Artesunate versus quinine in the treatment of severe falciparum malaria in African children (AQUAMAT): an open-label, randomised trial. Lancet Vol 376:1647-1657.

Eizirik E, Murphy WJ, O'Brien SJ. Molecular dating and biogeography of the early placental mammal radiation. J Heredity. 2001; 92:212-219.

Ellenhorn MJ, Barceloux DG. Medical toxicology. Diagnosis and treatment of human poisoning. New York: Elsevier. Pp. 829-835, 844-852; 1988.

Fujioka H, Millet P, Maeno Y, Nakazawa S, Ito Y, Howard RJ, Collins WE, Aikawa M. A non-human primate model for human cerebral malaria: rhesus monkeys experimentally infected with Plasmodium fragile. Exp Parasitol. 1994; 78(4):371-376.

Gennaro AR. Remington's pharmaceutical sciences. 18th ed. Easton, PA: Mack Publishing Company. Pp. 829-830; 1990.

Greenwood D. Conflicts of interest: the genesis of synthetic anti-malarial agents in peace and war. J Antimicrob Chemothe. 1995; 36:857-872.

Guttmann P, Ehrlich P. Uber die Wirkung des Methylenblau bei Malaria. Berl Klin Wochenschr. 1891; 28:953-956.

Guttmann P, Ehrlich P. On the action of methylene blue in malaria. The Collected Papers of Paul Ehrlich. London: Pergamon Press. Pp. 15-20; 1960.

Harbrecht BG, Wang SC, Simmons RL, Billiar TR. Cyclic GMP and guanylate cyclase mediate lipopolysaccharide-induced Kupffer cell tumor necrosis factor-a synthesis. J Leukoc Biol. 1995; 57: 297-302.

Howard RJ, Gilladoga AD. Molecular studies related to the pathogenesis of cerebral malaria. Blood 1989; 74:2603-2618.

Hunt NH, Grau EG, Engwerda C, et al. Murine Cerebral Malaria: The Whole Story. Trends Parasitol. 2010; 26:272-274.

Kawai S, Aikawa M, Suzuki M, Matsuda H. A nonhuman primate model for severe human malaria: Plasmodium coatneyi-infected Japanese macaque (Macaca fuscata). Tokai J Exp Clin Med. 1998; 23:101-102.

Kearney TE, Manoguerra AS, Dunford JV. Chemically induced methemoglobinemia from aniline poisoning. West J Med. 1984; 140:282-286.

Krogh CME. CPS Compendium of pharmaceuticals and specialties. 28th ed. Ottawa: Canadian Pharmaceutical Association, Pp. 717; 1993.

Laney RF, Hoffman RS. Methemoglobinemia secondary to automobile exhaust fumes. Am J Emerg Med. 1992; 10:426-428.

Langhorne J, Buffet P, Galinski M, et al. The relevance of non-human primate and rodent malaria models for humans. Malar J. 2011; 10:23-27.

Lombardini ED, Gettayacamin M, Turner GD, Brown AE. A Review of Plasmodium coatneyi-Macaque Models of Severe Malaria. Vet Pathol. 2015; 52(6):998-1011.

Luk G, Riggs D, Luque M. Severe methemoglobinemia in a 3-week-old infant with a urinary tract infection. Crit Care Med. 1991; 19:1325-1357.

Kirov MY, Evgenov OV, Evgenov NV, Egorina EM, Sovershaev MA, Sveinbjørnsson B, Nedashkovsky EV, Bjertnaes LJ. Infusion of methylene blue in human septic shock: a pilot, randomized, controlled study. Crit Care Med. 2001; 29(10):1860-1867.

Kumar S, Hedges SB. A timescale for vertebrate evolution. Nature. 1998; 392:917-920.

Maeno Y, Brown AE, Smith CD, Tegoshi T, Toyoshima T, Ockenhouse CF, Corcoran KD, Ngampochjana M, Kyle DE, Webster HK, et al. A nonhuman primate model for human cerebral malaria: effects of artesunate (qinghaosu derivative) on rhesus monkeys experimentally infected with Plasmodium coatneyi. Am J Trop Med Hyg. 1993;49(6):726-34.

Malleret B, Xu F, Mohandas N, Suwanarusk R, Chu C, Leite JA, Low K, Turner C, Sriprawat K, Zhang R, Bertrand O, Colin Y, Costa FT, Ong CN, Ng ML, Lim CT, Nosten F, Rénia L, Russell B. Significant Biochemical, Biophysical and Metabolic Diversity in Circulating Human Cord Blood Reticulocytes. PLoS ONE. 2013; 8(10):e76062.

Mansouri A. Review: methemoglobinemia. Am J Med Sci. 1985; 289:200-209.

Mansouri A, Lurie AA. Concise review: methemoglobinemia. Am J Hematol. 1993; 42:7-12.

McCall MBB, Sauerwein RW. Interferon-gamma, central mediator of protective immune responses against the pre-erythrocytic and blood stage of malaria. J Leukoc Biol. 2010; 88:1131-1143.

McErney JK, McEnerney LN. Unfavorable neonatal outcome after Intraamniotic injection of methylene blue. Obstet Gynecol 1983; 6:35S-37S.

Meissner PE, Mandi G, Coulibaly B, Witte S, Tapsoba T, Mansmann U, Rengelshausen J, Schiek W, Jahn A, Walter-Sack I, Mikus G, Burhenne J, Riedel KD, Schirmer RH, Kouyaté B, Müller O. Methylene blue for malaria in Africa: results from a dose-finding study in combination with chloroquine. Malar J. 2006; 5:84.

Mestas J, Hughes CC. Of mice and not men: differences between mouse and human immunology. J Immunol. 2004; 172:2731-2738.

McInnes EF. Background Lesions in Laboratory Animals. A Color Atlas. Elsevier, Philadelphia, PA. Pp. 1-16; 2012.

Miller LH. Distribution of mature trophozoites and schizonts of Plasmodium falciparum in the organs of Aotus trivirgatus, the night monkey. Am J Trop Med Hyg. 1969; 18:860-865.

Moreno A, Cabrera-Mora M, Garcia A, et al. Plasmodium coatneyi in rhesus macaques replicates the multisystemic dysfunction of severe malaria in humans. Infect Immun. 2013; 81:1889-1904.

National Research Council. Guide for the Care and use of Laboratory Animals. 8th edition. Washington DC: National Academies Press; 2011.

Nguansangiam S, Day NPJ, Hien TT, Main NTH, Chaisri U, Riganti M, Dondorp AM, Lee SJ, Phu NH, Turner GDH, White NJ, Ferguson DJP, Pongponratn E. Quantitative Ultrastructural Study of Renal pathology in fatal P. falciparum Malaria. Trop Med Int Health. 2007; 12(9):1037-1050.

Noedl H, Se Y, Sriwichai S, Schaecher K, Teja-Isavadharm P, Smith B, Rutvisuttinunt W, Bethell D, Surasri S, Fukuda M, Socheat D, Thap L. Artemisinin Resistance in Cambodia: A Clinical Trial Designed to Address an Emerging Problem in Southeast Asia. CID. 2010; 51(11):e82-9.

Olliaro PL, Trigg PI. Status of anti-malarial drugs under development. Bull World Health Organ. 1995; 73: 565-571.

Page SL, Goodman M. Catarrhine phylogeny: Noncoding DNA evidence for a diphyletic origin of the mangabeys and for a human-chimpanzee clade. Mol Phylogenet Evol. 2001; 18:14-25.

Pascual A, Henry M, Briolant S, Charras S, Baret E, Amalvict R, Huyghues des Etages E, Feraud M, Rogier C, Pradines B. In Vitro Activity of Proveblue (Methylene Blue) on Plasmodium falciparum Strains Resistant to Standard Anti-malarial Drugs. Antimicrob Agents Chemother. 2011; 55(5):2472-2474.

Perlman RL. Mouse models of human disease: An evolutionary perspective. Evol Med Public Health. 2016; 2016(1):170-176.

Peter C, Hongwan D, Kűpfer A, Lauterburg BH. Pharmacokinetics and organ distribution of intravenous and oral methylene blue. Eur J Clin Pharmacol. 2000; 56:247-250.

Ponponrat E, Turner GDH, Day NPJ, Phu NH, Simpson JA, Stepniewska K, Mai NTH, Viriyavjakul P, Looaresuwan S, Hien TT, Ferguson DJ, White NJ. An ultrastructural study of the brain in fatal Plasmodium falciparum malaria. Am J Trop Med Hyg. 2003; 69(4):345-359.

Prommano O, Chaisri U, Turner GDH, Wilairatana P, Ferguson D, Viriyavejakul P, White NJ, Pongponratn E. A Quantitative Ultrastructural Study of the Pathology of Fatal Falciparum Malaria in the Liver and Spleen. SE Asian J Trop Med Publ Health. 2005; 36(6):1359-1370.

Prophet EB, Mills B, Sobin LH (eds): Armed Forces Institute of Pathology Laboratory Methods in Histotechnology. American Registry of Pathology, Washington, DC; 1992.

Rhesus macaque genome sequencing and analysis consortium. Evolutionary and Biomedical Insights from the Rhesus Macaque Genome. Science. 2007; 13 April:222-234.

Rooney W. Dynamics of multi-drug resistance in Plasmodium falciparum in Thailand. Southeast Asian J Trop Med Public Health. 1992; 23(Suppl 4):131-137.

Sabchareon A, Attanath P, Chanthavanich P, Phanuaksook P, Prarinyanupharb V, Poonpanich Y, Mookmanee D, Teja-Isavadharm P, Heppner DG, Brewer TG, Chongsuphajaisiddhi T. Comparative clinical trial of artesunate suppositories and oral artesunate in combination with mefloquine in the treatment of children with acute falciparum malaria. Am J Trop Med Hyg. 1998; 58(1):11-16.

Sermwittayawong N, Nishibuchi M, Sawangjaroen N, Vuddhakul V. Characterization of malaria infection at two border areas of Thailand adjoining with Myanmar and Malaysia. Southeast Asian J Trop Med Public Health. 2015; 46(4):551-557.

South East Asian Quinine Artesunate Malaria Trial (SEAQUAMAT) group. Artesunate versus quinine for treatment of severe falciparum malaria: a randomised trial, Lancet. 2005; 366:717-725.

Stevenson MM, Gros P, Olivier M, Fortin A, Serghides L. Cerebral malaria: human versus mouse studies. Trends Parasitol. 2010; 26:274-275.

Stewart CB, Disotell TR. Primate evolution-in and out of Africa. Current Biology. 1998; 8:R582-R588.

Vennerstrom JL, Makler MT, Angerhofer CK, Williams JA. Anti-malarial Dyes Revisited: Xanthenes, Azines, Oxazines, and Thiazines. Antimicrob Agents Chemother. 1995; 39(12):2671-2677.

Walter-Sack I, Rengelshausen J, Oberwittler H, Burhenne J, Mueller O, Meissner P, Mikus G. High absolute bioavailability of methylene blue given as an aqueous oral formulation Eur J Clin Pharmacol 2009; 65:179–189.

White NJ. Cerebral perfusion in cerebral malaria. Crit Care Med. 1999; 27(3):478-479.

White NJ, Turner GDH, Medana IM, Dondorp AM, Day NP. The murine cerebral malaria phenomenon. Trends Parasitol. 2010; 26:11-15.

World Malaria Report 2013. In WHO (ed.). World Health Organization, Switzerland; 2013.

Wongsrichanalai C, Sirichaisinthop J, Karwacki JJ, Congpuong K, Miller RS, Pang L, Thimasarn K. Drug resistant malaria on the Thai-Myanmar and Thai-Cambodian borders. Southeast Asian J Trop Med Public Health. 2001; 32(1):41-49.

Yaffe SJ, Aranda JV. Pediatric pharmacology. Therapeutic principles in practice. Second ed. Philadelphia: W.B. Saunders Company: Pp. 587-588; 1992.

Yusim Y, et al. Blue dyes, blue people: the systemic effects of blue dyes when administered via different routes. Journal of Clinical Anesthesia. 2007; 19:315–321.

Zoungrana, A, et al. Safety and Efficacy of Methylene Blue Combined with Artesunate or Amodiaquine for Uncomplicated Falciparum Malaria: A Randomized Controlled Trial from Burkina Faso. PLoS ONE 2008; 3(2): e1630.

Chapter 3: Clinical and Gross Pathology

Agbenyega T, Angus BJ, Bedu-Addu G, Baffoe-Bonnie B, Guyton T, Stacpoole PW, Krishna S. Glucose and lactate kinetics in children with severe malaria. J CLin Endocrinol Metab. 2000; 85(4):1569-1576.

Barsoum RS. Malarial Acute Renal Failure. J Am Soc Nephrol. 2000; 11: 2147-2154.

Beare NA, Lewallen S, Taylor TE, Molyneux ME. Redefining cerebral malaria by including malaria retinopathy. Future Microbiol. 2011; 6(3):349-355.

Buffet PA, Safeukui I, Deplaine G, Brousse V, Prendki V, Thellier M, Turner GD, Mercereau-Puijalon O. The pathogenesis of Plasmodium falciparum malaria in humans: insights from splenic physiology. Blood. 2011; 117(2):381-392.

Casals-Pascual C, Kai O, Lowe B, English M, Williams TN, Maitland K, Newton CR, Peshu N, Roberts DJ. Lactate levels in severe malarial anaemia are associated with haemozoin-containing neutrophils and low levels of IL-12. Malar J. 2006; 5:101.

Carvalho LJ de M, Moreira A da S, Daniel-Ribeiro CT, Martins YC. Vascular dysfunction as a target for adjuvant therapy in cerebral malaria. Memórias do Instituto Oswaldo Cruz. 2014; 109(5):577-588.

Chang KH, Tam M, Stevenson MM. Inappropriately low reticulocytosis in severe malarial anemia correlates with suppression in the development of late erythroid precursors. Blood. 2004; 103:3727-3735.

Chen Y, Qin S, Ding Y, Wei L, Zhang J, Li H, Bu H, Lu Y, Cheng J. Reference values of clinical chemistry and hematology parameters in rhesus monkeys (Macaca mulatta). Xenotransplantation. 2009; 16(6):496-501.

Chianura L, Errante IC, Travi G, Rossotti R, Puoti M. Hyperglycemia in Severe Falciparum Malaria: A Case Report. Case Reports in Critical Care. 2012; 2012:312458.

Clark IA, Awburn MM, Harper CG, Liomba NG, Molyneux ME. Induction of HO-1 in tissue macrophages and monocytes in fatal falciparum malaria and sepsis. Malar J. 2003; 2(1):41.

Coatney GR, Collins WE, Warren M, Contacos PG. The Primate Malarias. Washington, D.C.: U.S. Government Printing Office; Pp. 289-299; 1971.

Das BS. Renal failure in malaria. J Vector Borne Dis. 2008; 45: 83-97.

Davison BB, Cogswell FB, Baskin GB, Falkenstein KP, Henson EW, Tarantal AF, Krogstad DJ. Plasmodium coatneyi in the rhesus monkey (Macaca mulatta) as a model of malaria in pregnancy. Am J Trop Med Hyg. 1998; 59:189-201.

Davison BB, Cogswell FB, Baskin GB, Falkenstein KP, Henson EW, Krogstad DJ. Placental changes associated with fetal outcome in the Plasmodium coatneyi/rhesus monkey model of malaria in pregnancy. Am J Trop Med Hyg. 2000; 63:158-173.

Davison BB, Kaack MB, Rogers LB, Rasmussen KK, Rasmussen T, Henson EW, Montenegro S, Henson MC, Mzwaek F, Krogstad DJ. Alterations in the profile of blood cell types during malaria in previously unexposed primigravid monkeys. J Infect Dis. 2005; 191(11):1940-1952.

Day NP, Phu NH, Mai NT et al. The pathophysiologic and prognostic significance of acidosis in severe adult malaria. Crit Care Med. 2000; 28:1833–1840

Desowitz RS, Miller LH, Buchanan RD, Yuthasastrkosol V, Permpanich B. Comparative studies on the pathology and host physiology of malarias. I. Plasmodium coatneyi. Ann Trop Med Parasitol. 1967; 61:365-374.

Dörmer P, Dietrich M, Kern P, Horstmann RD. Ineffective erythropoiesis in acute human P. falciparum malaria. Ann Hematol. 1983; 46:279-288.

Dungan KM, Braithwaite SS, Preiser JC. Stress hyperglycaemia. Lancet. 2009; 373:1798-1807.

English M, Sauerwein R, Waruiru C, Mosobo M, Obiero J, Lowe B, Marsh K. Acidosis in severe childhood malaria. Qjm. 1997; 90:263-270.

Francischetti IMB. Does activation of the blood coagulation cascade have a role in malaria pathogenesis? Trends Parasitol. 2008; 24:258-263.

Ghosh K, Shetty S. Blood coagulation in falciparum malaria: a review. Parasitol Res. 2008; 102:571-576.

Grau GE, Mackenzie CD, Carr RA, et al. Platelet accumulation in brain microvessels in fatal pediatric cerebral malaria. J Infect Dis. 2003; 187(3):461–466.

Gupta BK, Gupta A, Nehra HR, Balotia HR, Meena SL, Kumar S. Clinical Profile and Prognostic Indicators in Adults Hospitalized with Severe Malaria Caused by Different Plasmodium Species. Infect Dis (Auckl). 2015; 8:45-50.

Hanson J, Phu NH, Hasan MU, Chaunwatthana P, Plewes K, Maude RJ, Prapansilp P, Kingsto HW, Mishra SK, Mohanty S, Price RN, Faiz MA, Dondopr AM, White NJ, Hien TT, Day NP. The clinical implications of thrombocytopaenia in adults with severe falciparum malaria: a retrospective analysis. BMC Med. 2015; 13:97.

Helbok R, Lackner P, Schmutzhard E. Severe Plasmodium falciparum malaria with peripheral gangrene. Lancet Infect Dis. 2008; 8:400.

Hochman SE, Madaline TF, Wassmer SC, Mbale E, Choi N, Seydal KB, Whitten RO, Varughese J, Grau GE, Kamiza S, Molyneux ME, Taylor TE, Lee S, Milner DA Jr, Kim K. Fatal Pediatric Cererbal Malaria Is Associated with Intravascular Monocytes and Platelets That Are Increased with HIV coinfection. MBio. 2015; 6(5): e1390-15.

Ishioka H, Ghose A, Charunwatthana P, Maude R, Plewes K, Kingston K, et al. Sequestration and Red Cell Deformability as Determinants of Hyperlactatemia in Falciparum Malaria. J Infect Dis. 2016; 213(5):788-793.

Kakati S, Doley, B, Barman B, Devi A. Symmetric peripheral gangrene and Falciparum malaria. J Assoc Physicians India. 2004; 52:498-499.

Kawai S, Aikawa M, Kano S, Suzuki M. A primate model for severe human malaria with cerebral involvement: Plasmodium coatneyi-infected Macaca fuscata. Am J Trop Med Hyg. 1993; 48:630-636.

Kawai S, Aikawa M, Suzuki M, Matsuda H. A nonhuman primate model for severe human malaria: Plasmodium coatneyi-infected Japanese macaque (Macaca fuscata). Tokai J Exp Clin Med. 1998; 23:101-102.

Kirchgatter K, Del Portillo HA. Clinical and molecular aspects of severe malaria. An Acad Bras Cienc. 2005; 77(3):455-475.

Lerolle N, Borgel D, Diehl JL. Coagulation intravasculaire disséminée en réanimation: physiopathologie, épidémiologie, diagnostic et prise en charge thérapeutique. Hématologie. 2007; 13:409-420. (Article in French)

Liechti ME, Zumsteg V, Hatz CF, Herren T. Plasmodium falciparum cerebral malaria complicated by disseminated intravascular coagulation and symmetrical peripheral gangrene: case report and review. Eur J Clin Microbiol Infect Dis. 2003; 22:551-554.

McKenzie FE, Prudhomme WA, Magill AJ, Forney JR, Permpanich B, Lucas C, Gasser RA Jr., Wongsrichanalai C. White Blood Cell Counts and Malaria. J Infect Dis. 2005; 192(2):323–330.

Maitland K, Newton CR. Acidosis of severe falciparum malaria: heading for a shock? Trends Parasitol. 2005; 21(1):11-16.

Maitland K, Marsh K. Pathophysiology of severe malaria in children. Acta Tropica. 2004; 90:131-140.

Marik PE, Bellomo R. Stress hyperglycemia: an essential survival response! Critical Care. 2013; 17(2):305.

Maude RJ, Beare NA, Abu Sayeed A, Chang CC, Charunwatthana P, Faiz MA, Hossain A, Yunus EB, Hoque MG, Hasan MU, White NJ, Day NP, Dondorp AM. The spectrum of retinopathy in adults with Plasmodium falciparum malaria. Trans R Soc Trop Med Hyg. 2009; 103(7):665-671.

Matsumoto J, Kawai S, Terao K, Kirinoki M, Yasutomi Y, Aikawa M, Matsuda H. Malaria infection induces rapid elevation of the soluble Fas ligand level in serum and subsequent T lymphocytopenia: possible factors responsible for the differences in susceptibility of two species of Macaca monkeys to Plasmodium coatneyi infection. Infect Immun. 2000; 68(3):1183-1188.

Milner DA, Jr., Whitten RO, Kamiza S, Carr R, Liomba G, Dzamalala C, Seydel KB, Molyneux ME, Taylor TE. The systemic pathology of cerebral malaria in African children. Front Cell Infect Microbiol. 2014; 4:104.

Mirsky IA, Nelson N, Elgart S. Diabetic acidosis and coma in the monkey. Science. 1941; 93(2424):576.

Moreno A, Cabrera-Mora M, Garcia A, Orkin J, Strobert E, et al. Plasmodium coatneyi in rhesus macaques replicates the multisystemic dysfunction of severe malaria in humans. Infect Immun. 2013; 81:1889-1904.

Moreno A, García A, Cabrera-Mora M, Strobert E, Galinski MR. Disseminated intravascular coagulation complicated by peripheral gangrene in a rhesus macaque (Macaca mulatta) experimentally infected with Plasmodium coatneyi. Am J Trop Med Hyg. 2007; 76:648-654.

Musoke C, Ssendikadiwa C, Babua C, Schwartz JI. Severe falciparum malaria associated with massive pulmonary embolism. Ann Afr Med. 2014; 13(1):47-49.

O'Sullivan JM, Preston RJ, O'Regan N, O'Donnell JS. Emerging roles for hemostatic dysfunction in malaria pathogenesis. Blood. 2016; 127(19):2281-2288.

Osier FH, Berkley JA, Ross A, Sanderson F, Mohammed S, Newton CR. Abnormal blood glucose concentrations on admission to a rural Kenyan district hospital: Prevalence and outcome. Arch Dis Child. 2003; 88:621-625.

Perkins DJ, Were T, Davenport GC, Kempaiah P, Hittner JB, Ong'echa JM. Severe malarial anemia: innate immunity and pathogenesis. Int J Biol Sci. 2011; 7(9):1427-1442.

Planche T, Dzeing A, Ngou-Milama E, Kombila M, Stacpoole PW. Metabolic complications of severe malaria. Curr Top Microbiol Immunol. 2005; 295:105-136.

Planche T, Krishna S. Severe malaria: metabolic complications. Curr Mol Med. 2006; 6(2):141-153.

Sasi P, Burns SP, Waruiru C, English M, Hobson CL, King CG, Mosobo M, Beech JS, Iles RA, Boucher BJ, Cohen RD. Metabolic acidosis and other determinants of hemoglobin-oxygen dissociation in severe childhood Plasmodium falciparum malaria. Am J Trop Med Hyg. 2007; 77(2):256-260.

Singh Y, Joshi SC, Satyawali V, Gupta A. A case of severe falciparum malaria presenting with hyperglycemia. J Med Trop. 2014; 16:39-41.

Sirivichayakul C, Chanthavanich P, Chokejindachai W, Pengsaa K, Kabkaew K, Saelim R. Pleural effusion in childhood falciparum malaria. Southeast Asian J Trop Med Public Health. 2000; 31:187-189.

Taylor WR, Cañon V, White NJ. Pulmonary manifestations of malaria: recognition and management. Treat Respir Med. 2006; 5(6):419-428.

Tessier-Marteau A, Cruguel Sl, Grand F, Asfar P, Zandecki M, Macchi L. [DIC and peripheral gangrene in a severe Plasmodium falciparum malaria: the coagulation-inflammation cycle with Plasmodium falciparum as a model]. [Article in French] Ann Biol Clin (Paris). 2009; 67(5):569-572.

Thanachartwet V, Krudsood S, Wilairatana P, Phumratanaprapin W, Silachamroon U, Looareesuwan S. Peripheral gangrene in patients with severe falciparum malaria: Report of 3 cases. Korean J Parasitol. 2006; 44:139-143.

Tobón-Castaño A, Mesa-Echeverry E, Miranda-Arboleda AF. Leukogram Profile and Clinical Status in vivax and falciparum Malaria Patients from Colombia. J Trop Med. 2015:796182.

Trampuz A, Jereb M, Muzlovic I, Prabhu RM. Clinical review: Severe malaria. Critical Care. 2003; 7(4):315-323.

Tombe M, Bhatt KM, Obel AO. Clinical surprises and challenges of severe malaria at Kenyatta National Hospital, Kenya. East Afr Med J. 1993; 70:117-119.

von Seidlein L, Olaosebikan R, Hendriksen IC, Lee SJ, Adedoyin OT, Agbenyega T, Nguah SB, Bojang K, Deen JL, Evans J, Fanello CI, Gomes E, Pedro AJ, Kahabuka C, Karema C, Kivaya E, Maitland K, Mokuolu OA, Mtove G, Mwanga-Amumpaire J, Nadjm B, Nansumba M, Ngum WP, Onyamboko MA, Reyburn H, Sakulthaew T, Silamut K, Tshefu AK, Umulisa N, Gesase S, Day NP, White NJ, Dondorp AM. Predicting

the clinical outcome of severe falciparum malaria in African children: findings from a large randomized trial. Clin Infect Dis. 2012; 54:1080-1090

World Health Organization (WHO): Severe malaria Trop Med Int Health. 2014; 19 suppl S1 p 7-131.

Zaki SA, Shanbag P. Atypical manifestations of malaria. Res Rep Trop Med. 2011; 2:9-22.

Chapter 4: Cytological pathology and Histopathology

Aikawa M, Brown AE, Smith CD, Tegoshi T, Howard RJ, et al. A primate model for human cerebral malaria: Plasmodium coatneyi–infected rhesus monkeys. Am J Trop Med Hyg. 1992; 46:391-397.

Ampawong S, Chaisri U, Viriyavejkul P, Prapansilp P, Grau GE, Turner GDH. Pongonratn E. A potential role for interleukin-33 and γ-epithelium sodium channel in the pathogenesis of human malaria associated lung injury. Malar J. 2015; 14(1):389.

Arekul S, Kanakakorn K, Kasemsuthi R. Mechanism of haemolysis in monkeys infected with Plasmodium coatneyi. Southeast Asian J Trop Med Pub Hlth. 1971; 2:261-262.

Barsoum RS. Malarial acute renal failure. J Am Soc Nephrol. 2000; 11:2147-2154.

Beare NA, Taylor TE, Harding SP, Lewallen S, Molyneux ME. Malarial retinopathy: a newly established diagnostic sign in severe malaria. Am J Trop Med Hyg. 2006; 75:790-797.

Brewster DR, Kwiatkowski D, White NJ. Neurological sequelae of cerebral malaria in children. Lancet. 1990; 336:1039–1043.

Brown H, Mai NTH, Day N, Chuong LV, Chau TTH, et al. Evidence of Blood-Brain Barrier Dysfunction in Human Cerebral Malaria. Neuropathol Appl Neurobiol. 1999; 25:331-340.

Brown HC, TTH Chau, NTH Mai, NPJ Day, DX Sinh, et al. Blood-brain barrier function in cerebral malaria and CNS infections in Vietnam. Neurology. 2000; 55:104-111.

Burel-Vandenbos F1, Effa'a C, Alunni V, Cardot-Leccia N, Haudebourg J, et al. A histologic study of brain in fatal cerebral malaria. Ann Pathol. 2008; 28:495-497.

Carlson J. Erythrocyte rosetting in Plasmodium falciparum malaria-with special reference to the pathogenesis of cerebral malaria. Scand J Infect Dis Suppl. 1993; 86:1-79.

Chamanza R. Non-human primates: Cynomolgus (Macaca fascicularis) and rhesus (Macaca mulatta) macaques and the common marmoset (Callithrix jacchus). *In.* Background Lesions in Laboratory Animals: A Color Atlas. Elizabeth F. McInnes ed., Saunders (Elsevier), Edinburgh; pg 1-16; 2012

Chen Q, Schlichtherle M, Wahlgen M. Molecular Aspects of Severe Malaria. Clin Microbiol Rev. 2000; 13:439-450.

Clark IA, Alleva LM. Is human malarial coma caused, or merely deepened, by sequestration? Trends Parasitol. 2009; 25:314–318.

Costanero P, Benedetti P, Facchin C, Mengoli C, Pellizzer G. Fatal myocarditis in course of Plasmodium falciparum infection: Case report and review of cardiac complications in malaria. Case Reports in Medicine, 2011:202083.

Craig AG, Grau GE, Jansse C, Barnwell J, Kazura JW, et al. The Role of Animal Models for Research on Severe Malaria, on behalf of the participants of the Hinxton Retreat meeting on ‘‘Animal Models for Research on Severe Malaria’’. PLoS Pathog; 2012; 8(2):e1002401.

Davis TM, Brown AE, Smith CD. Metabolic disturbances in Plasmodium coatneyi-infected rhesus monkeys. Int J Parasitol. 1993; 23:557-563.

Davison BB, Cogswell FB, Baskin GB, Falkenstein KP, Henson EW, et al. Plasmodium coatneyi in the rhesus monkey (Macaca mulatta) as a model of malaria in pregnancy. Am J Trop Med Hyg. 1998; 59:189-201.

Davison BB, Cogswell FB, Baskin GB, Falkenstein KP, Henson EW, et al. Placental changes associated with fetal outcome in the Plasmodium coatneyi/rhesus monkey model of malaria in pregnancy. Am J Trop Med Hyg. 2000; 63:158-173.

Deaderick WH. A practical study of malaria. Saunders, Philadelphia PA; 1909

Desowitz RS, Miller LH, Buchanan RD, Yuthasastrkosol V, Permpanich B. Comparative studies on the pathology and host physiology of malarias. I. Plasmodium coatneyi. Ann Trop Med Parasitol. 1967; 61:365-374.

Desowitz RS, Miller LH, Buchanan RD, Permpanich B. The sites of deep vascular schizogony in Plasmodium coatneyi malaria. Trans R Soc Trop Med Hyg. 1969; 63:198-202.

Desowitz RS, Pavanand K. A vascular-permeability-increasing factor in the serum of monkeys infected with primate malarias. Ann Trop Med Parasitol. 1967; 61:128-133.

Dorovini-Zis K, Schmidt K, Huynh H, Fu W, Whitten RO, et al. The neuropathology of fatal cerebral malaria in malawian children. Am J Pathol. 2011; 178:2146-2158.

Dudgeon LS, Clarke C. A contribution to the microscopical histology of malaria. Lancet. 1917; Aug:153-156.

Dudgeon LS, Clarke C. An Investigation on Fatal Cases of Pernicious Malaria caused by Plasmodium falciparum in Macedonia. Q J Med. 1919; 12:372-390.

Elsheikha HM, Sheashaa HA. Epidemiology, pathophysiology, management and outcome of renal dysfunction associated with plasmodia infection. Parasitol Res. 2007; 101:1183-1190.

Eyles DE, Dunn F, Warren McW, Guinn E. Plasmodium coatneyi from the Philippines. J Parasit. 1963; 49:1038.

Eyles DE, Fong YL, Warren McW, Guinn E, Sandosham AA, et al. Plasmodium coatneyi, a new species of primate malaria from Malaya. Am J trop Med Hyg. 1962; 11:597-604.

Harnagel EE, Florence V, Rhudy FV. Falciparum Malaria-Report of a Fatal Case and Autopsy Findings. Calif Med. 1954; 81:89-91.

Ho M, Davis TM, Silamut K, Bunnag D, White NJ. Rosette formation of Plasmodium falciparum-infected erythrocytes from patients with acute malaria. Infect Immun. 1991; 59:2135-2139.

Hu WC. Human immune responses to Plasmodium falciparum infection: molecular evidence for a suboptimal THalphabeta and TH17 bias over ideal and effective traditional TH1 immune response. Malar J. 2013; 12:392-411.

Idro R, Jenkins NE, Newton CR. Pathogenesis, clinical features, and neurological outcome of cerebral malaria. Lancet Neurol. 2005; 4:827-840.

Imwong M, Woodrow CJ, Hendriksen ICE, Veenemans J, Verhoef H, et al. Plasma concentration of parasite DNA as a measure of disease severity in falciparum malaria. J Infect Dis. 2014; 211:1128-1133.

Kawai S, Aikawa M, Kano S, Suzuki M. A primate model for severe human malaria with cerebral involvement: Plasmodium coatneyi-infected Macaca fuscata. Am J Trop Med Hyg. 1993; 48:630-636.

Kawai S, Aikawa M, Suzuki M, Matsuda H. A nonhuman primate model for severe human malaria: Plasmodium coatneyi-infected Japanese macaque (Macaca fuscata). Tokai J Exp Clin Med. 1998; 23:101-102.

Kawai S, Yoshinari M, Matsumoto J, Kirinoki M, Aikawa M, et al. Plasmodium coatneyi-infected erythrocytes bind to C32 amelanotic melanoma cells under static and flow conditions. J Vet Med Sci. 2003; 65:375-380.

Kean BH, Smith JA. Death due to estivo-autumnal malaria. A resume of one hundred autopsy cases, 1925-1942. Am J Trop Med. 1944; 24:317–322.

Kirchgatter K, Del Portillo HA. Clinical and molecular aspects of severe malaria. An Acad Bras Cienc. 2005; 77:455-75.

Ladhani S, Lowe B, Cole AO, Kowuondo K, Newton CR. Changes in white blood cells and platelets in children with falciparum malaria: relationship to disease outcome. Br J Haematol. 2002; 119:839-847.

Lackner P, Burger C, Pfaller K, Heussler V, Helbok R, et al. Apoptosis in experimental cerebral malaria: spatial profile of cleaved caspase-3 and ultrastructural alterations in different disease stages. Neuropathol Appl Neurobiol. 2007; 33:560-571.

Lombardini ED, Gettayacamin M, Turner GDH, Brown AE. A Review of *Plasmodium coatneyi*-macaque models of severe and cerebral malaria. Vet Pathol. 2015; 52:998-1011.

Lombardini ED, Imerbsin R, Weina P, Brown AE, Turner GDH. 2014. Renal pathology in the rhesus macaque/Plasmodium coatneyi model for severe malaria. Paper and poster presented at the ASTMH annual conference, New Orleans, LA. Abstract retrieved from http://www.astmh.org/AM/Template.cfm?Section=Abstracts_and_Education1&Template=/CM/ContentDisplay.cfm&ContentID=6134

Lowenstine LJ. A Primer of Primate Pathology: Lesions and Nonlesions. Tox Path. 2003; 31(Suppl.):92-102.

Ly AB, Tall A, Perry R, Baril L, Badiane A, et al. Use of HRP-2-based rapid diagnostic test for Plasmodium falciparum malaria: assessing accuracy and cost-effectiveness in the villages of Dielmo and Ndiop, Senegal. Malar J. 2010; 9:153.

Maeno Y, Brown AE, Smith CD, Tegoshi T, Toyoshima T, et al. A non-human primate model for cerebral malaria: effects of artesunate (qinghaosu derivative) on rhesus monkeys experimentally infected with Plasmodium coatneyi. Am J Trop Med Hyg. 1993; 49:726-734.

Matsumoto J, Kawai S, Terao K, Kirinoki M, Yasutomi Y, et al. Malaria infection induces rapid elevation of the soluble Fas ligand level in serum and subsequent T lymphocytopenia: Possible factors

responsible for the differences in susceptibility of two species of Macaca monkeys to Plasmodium coatneyi infection. Infect Immun. 2000; 68:1183-1186.

Maude RJ, Dondorp AM, Abu Sayeed A, Day NP, White NJ, et al. The eye in cerebral malaria: what can it teach us? Trans R Soc Trop Med Hyg. 2009; 103:661–664.

Medana IM, Day NPJ, Hien TT, Mai NT, Bethell D, Phu NH, Farrar J, Esiri MM, White NJ, Turner GD. Axonal injury in Cerebral Malaria. Am J Pathol. 2000; 160: 655-666.

Medana IM, Day NPJ, Sachanonta N, Mai NTH, Dondorp AM, Pongponratn E, Hien TT, White NJ, Turner GD. Cerebral Edema in Fatal Adult Human Malaria is Not Associated with Coma. Malar J. 2011; 10(267):1-14.

Menezes RG, Pant S, Kharoshah MA, Senthilkumaran S, Arun M, Nagesh KR, Bhat NB, Mahadeshwara Prasad DR, Karki RK, Subba SH, Fazil A. Autopsy discoveries of death from malaria. Leg Med (Tokyo). 2012; 14:111-115.

Migot-Nabias F, Ollomo B, Dubreuil G, Morelli A, Domarle O, et al. Plasmodium coatneyi: differential clinical and immune responses of two populations of Macaca fascicularis from different origins. Exp Parasitol. 1999; 91:30–39.

Milner D Jr, Factor R, Whitten R, Carr RA, Kamiza S, et al. Pulmonary pathology in pediatric cerebral malaria. Hum Pathol. 2013; 44:2719-2726.

Milner DA, Whitten R, Kamiza S, Carr R, Liomba G, et al. The systemic pathology of cerebral malaria in African children. Front Cell Infect Microbiol. 2014; 4:1-13.

Mohsen AH, Green ST, McKendrick MW, West JN. Myocarditis associated with Plasmodium falciparum malaria: a case report and a review of the literature. J Travel Med. 2001; 8:219–220.

Moreno A, Cabrera-Mora M, Garcia A, Orkin J, Strobert E, et al. Plasmodium coatneyi in rhesus macaques replicates the multisystemic dysfunction of severe malaria in humans. Infect Immun. 2013; 81:1889-1904.

Moreno A, García A, Cabrera-Mora M, Strobert E, Galinski MR Disseminated intravascular coagulation complicated by peripheral gangrene in a rhesus macaque (Macaca mulatta) experimentally infected with Plasmodium coatneyi. Am J Trop Med Hyg. 2007; 76:648-54.

Moxon CA, Wassmer SC, Milner DA, Chisala NV, Taylor TE, et al. Loss of endothelial protein C receptors links coagulation and inflammation to parasite sequestration in cerebral malaria in African children. Blood. 2013; 122:842-851.

Nagatake T, Hoang VT, Tegoshi T, Rabbege J, Ann TK, et al. Pathology of falciparum malaria in Vietnam. Am J Trop Med Hyg. 1992; 47:259-264.

Nakano Y, Fujioka H, Luc KD, Rabbege JR, Todd GD, et al. A correlation of the sequestration rate of P. coatneyi- infected erythrocytes in cerebral and subcutaneous tissue of a rhesus monkey. Am J Trop Med Hyg. 1996; 55:311-314.

Nguansangiam S, Day NPJ, Hien TT, Main NTH, Chaisri U, et al. Quantitative Ultrastructural Study of Renal pathology in fatal *P. falciparum* Malaria. Trop Med Int Health. 2007; 12:1037-1050.

Olsson RA, Johnston EH. Histopathologic changes and small bowel absorption in falciparum malaria. Am J Trop Med Hyg. 1969; 18:355-359.

Parra ME, Evans CB, Taylor DW. Identification of Plasmodium falciparum histidine-rich protein 2 in the plasma of humans with malaria. J Clin Microbiol. 1991; 29:1629-1634.

Patel DN, Pradeep P, Surti MM, Agarwal SB. Clinical manifestations of complicated malaria-An overview. JIACM. 2003; 4:323-331.

Pino P, Vouldoukis I, Kolb JP, Mahmoudi N, Desportes-Livage I, et al. Plasmodium falciparum-infected erythrocyte adhesion induces caspase activation and apoptosis in human endothelial cells. J Infect Dis. 2003; 187:1283-1290.

Rowe JA, Claessens A, Corrigan RA, Arman M. Adhesion of Plasmodium falciparum-infected erythrocytes to human cells: molecular mechanisms and therapeutic implications. Expert Rev Mol Med. 2009; 11:e16, 1-29.

Sato J, Doi T, Kanno T, Wako Y, Tsuchitani M, et al. Histopathology of Incidental Findings in Cynomolgus Monkeys (Macaca Fascicularis) Used in Toxicity Studies. J Toxicol Pathol. 2012; 25:63-101.

Saya RP, Debabrata G, Saya GK. Malarial Hepatopathy and Its Outcome in India. North Am J Med Sci. 2012; 4:449-452.

Schmidt KE, Schumaka B, Spechta S, Dubbena B, Limmerb A, et al. Induction of pro-inflammatory mediators in Plasmodium berghei infected BALB/c mice breaks blood-brain-barrier and leads to cerebral malaria in an IL-12 dependent manner. Microb Infect. 2011; 13:828–836.

Sein KK, Brown AE, Maeno Y, Smith CD, Corcoran KD, et al. Sequestration pattern of parasitized erythrocytes in cerebrum, mid-brain and cerebellum of Plasmodium coatneyi-infected rhesus monkeys (Macaca mulatta). Am J Trop Med Hyg. 1993; 49:513-519.

Semenya AA, Sullivan JS, Barnwell JW, Secor WE. Schistosoma mansoni infection impairs antimalaria treatment and immune responses of rhesus macaques infected with mosquito-borne Plasmodium coatneyi. Infect Immun. 2012; 80:3821-3827.

Silamut K, Phu NH, Whitty C, Louwrier K, Turner GDH, et al. A quantitative analysis of the microvascular sequestration of malaria parasites in the human brain. Am J Pathol. 1999; 155:395-410.

Smith CD, Brown AE, Nakazawa S, Fukioka H, Aikawa M. Multi-organ erythrocyte sequestration and ligand expression in rhesus monkeys infected with Plasmodium coatneyi malaria. Am J Trop Med Hyg. 1996; 55:379-383.

Spitz S. The pathology of acute falciparum malaria. Military Surg. 1946; 99:555-572.

Sprague HB. The effect of malaria on the heart. Am Heart J. 1946; 31:426-430.

Storm J, Craig AG. Pathogenesis of cerebral malaria-inflammation and cytoadherence. Front Cell Infect Microbiol. 2014; 4:100.

Sun G, Chang WL, Li J, Berney SM, Kimpel D, et al. Inhibition of platelet adherence to brain microvasculature protects against severe Plasmodium berghei malaria. Infect Immun. 2003; 71:6553-6561.

Taylor WRJ, Dondorp A, Hanson J, Turner GDH, White NJ. Respiratory manifestations of malaria. Chest. 2012; 142:492-505.

Taylor TE, Fu WJ, Carr RA, Whitten RO, Mueller JS, et al. Differentiating the pathologies of cerebral malaria by post-mortem parasite counts. Nat Med. 2004; 10:143-145.

Tegoshi T, Udomsangpetch R, Brown A, Nakazawa S, Webster HK, et al. Ultrastructure of rosette formation by Plasmodium coatneyi-infected erythrocytes of rhesus. Parasitol Res. 1993; 79:611-613.

Thanachartwet V, Desakorn V, Sahassananda D, Kyaw Win KK, Supaporn T. Acute Renal Failure in Patients with Severe Falciparum Malaria: Using the WHO 2006 and RIFLE Criteria. Int J Nephrol. 2013(3):841518.

Tongren JE, Yang C, Collins WE, Sullivan JS, Lai AA, et al. Expression of Proinflammatory Cytokines in four regions of the brain in Macaque mulatta (Rhesus) monkeys infected with Plasmodium coatneyi. Am J Trop Med Hyg. 2000; 62:530-534.

Toro G, Roman G. Cerebral malaria. A disseminated vasculomyelinopathy. Arch Neurol. 1978; 35:271-5.

Touré FS, Ouwe-Missi-Oukem-Boyer O, Bisvigou U, Mousa O, Rogier C, et al. Apoptosis: a potential triggering mechanism of neurological manifestation in Plasmodium falciparum malaria. Parasite Immunol. 2008; 30:47-51.

Trang TT, Phu NH, Vinh H, Hien TT, Cuong BM, et al. Acute renal failure in patients with severe falciparum malaria. Clin Infect Dis. 1992; 15:874-880.

Turner G. Cerebral Malaria. Brain Pathol. 1997; 7:569–582.

Udomsangpetch R, Brown AE, Smith CD, Webster HK. Plasmodium coatneyi infected erythrocytes form erythrocyte rosettes. Am J Trop Med Hyg. 1991; 44:399-401.

White VA, Lewallen S, Beare N, Kayira K, Carr RA, et al. Correlation of retinal hemorrhages with brain hemorrhages in children dying of cerebral malaria in Malawi. Trans R Soc Trop Med Hyg. 2001; 95:618-621.

White NJ, Silamut K. Postmortem brain smear assessment of fatal malaria. J Infect Dis. 2005; 192:547.

White NJ, Turner GDH, Medana IM, Dondorp A, Day NP. The Murine Cerebral Malaria Phenomenon. Trends Parasitol. 2010; 26:11-15.

Wichmann O, Loscher T, Jelinek T. Fatal malaria in a German couple returning from Burkina Faso. Infection. 2003; 31:260-262.

Wilairatana P, Riganti M, Puchadapirom P, Punpoowong B, Vannaphan S, et al. Prognostic significance of skin and subcutaneous fat sequestration of parasites in severe falciparum malaria. Southeast Asian J Trop Med Public Health. 2000; 31, 203-212.

World Health Organization. Trop Med Int Health. 2014; 19 suppl:7-131.

Xu X, Sumita K, Feng C, Xiong X, Shen H, et al. Down-regulation of IL-12 p40 gene in Plasmodium berghei-infected mice. J Immunol. 2001; 167:235-241.

Yang C, Xiao L, Tongren JE, Sullivan J, Lal AA, et al. Cytokine production in Rhesus monkeys infected with Plasmodium coatneyi. Am J Trop Med Hyg. 1999; 61:226–229.

Chapter 5: Immunohistochemistry

Akanmori BD, Kurtzhals JA, Goka BQ, Adabayeri V, Ofori MF, Nkrumah FK, Behr C, Hviid L. Distinct patterns of cytokine regulation in discrete clinical forms of Plasmodium falciparum malaria. Eur Cytokine Netw. 2000; 11:113–118.

Ampawong S, Chaisri U, Viriyavejakul P, Nontprasert A, Grau GE, Pongponratn E. Electron microscopic features of brain edema in rodent cerebral malaria in relation to glial fibrillary acidic protein expression. Int J Clin Exp Pathol. 2014; 7(5):2056-2067.

Areekul S. Plasmodium coatneyi: alterations of transcapillary escape rate and capillary permeability to fibrinogen in rhesus monkeys. Exp Parasitol. 1986; 61:304-310.

Armah HB, Wilson NO, Sarfo BY, Powell MD, Bond VC, Anderson W, Adjei AA, Gyasi RK, Tettey Y, Wiredu EK, Tongren JE, Udhayakumar V, Stiles JK. Cerebrospinal fluid and serum biomarkers of cerebral malaria mortality in Ghanaian children. Malar J. 2007; 6:147.

Artavanis-Tsakonas K, Tongren JE, Riley EM. The war between the malaria parasite and the immune system: immunity, immunoregulation and immunopathology. Clin Exp Immunol. 2003; 133(2):145-152.

Aubouy A, Deloron P, Migot-Nabias F. Plasma and in vitro levels of cytokines during and after a Plasmodium falciparum malaria attack in Gabon. Acta Trop. 2002; 83:195–203.

Baptista JL, Vanham G, Wery M, van Marck E. Cytokine levels during mild and cerebral falciparum malaria in children living in a mesoendemic area. Trop Med Int Health. 1997; 2:673–679.

Baton LA, Warr E, Hoffman SA, Dimopoulos G. Chapter 7: Programmed cell death during malaria parasite infection of the vertebrate host and mosquito vector. In. Programmed Cell Death in Protozoa. Ed. Jose Perez-Martin. Molecular Biology Intelligence Unit. Springer, New York, NY. Pp. 74-84; 2008.

Boonpucknavig V, Boonpucknavig S. The histopathology of malaria. In Malaria, Principles and Practice of Malariology. Edited by Wernsdorfer WH, McGregor I. London, Churchill Livingstone. Pp 673-707; 1988.

Boonpucknavig V, Boonpucknavig S, Udomsangpetch R, Nitiyanant P. An immunofluorescence study of cerebral malaria: a correlation with histopathology. Arch Pathol Lab Med. 1990; 114:1028-1034.

Brown HC, Chau TTH, Mai NTH, Day NPJ, Sinh DX, White NJ, Hien TT, Farrar J, Turner GDH. Blood-brain barrier function in cerebral malaria and CNS infections in Vietnam. Neurology. 2000; 55(1):104-11

Brown H, Mai NTH, Day N, Chuong LV, Chau TTH, Phu NH Farrar J, Bethell D, Gatter K, Hien TT, White N, Turner G. Evidence of Blood-Brain Barrier Dysfunction in Human Cerebral Malaria. Neuropathol Appl Neurobiol. 1999; 25(4):331-340.

Brown H, Rogerson S, Taylor T, Tembo M, Mwenechanya J, Molyneux M, Turner G. Blood-Brain Barrier Function in Cerebral Malaria in Malawian Children. Am J Trop Med Hyg. 2001; 64(3):207–213.

Brown HC, Turner GDH, Rogerson S, Tembo M, Mwenechanya J, Molyneux MM, Taylor T. Cytokine Expression in the Brain in Human Cerebral Malaria. J Infect Dis. 1999; 180(5):1742-1746.

Cox D, McConkey S. The role of platelets in the pathogenesis of cerebral malaria. Cell Mol Life Sci. 2010; 67(4):557-568.

Day NP, Hien TT, Schollaardt T, Loc PP, Chuong LV, Chau TT, Mai NT, Phu NH, Sinh DX, White NJ, Ho M. The prognostic and pathophysiologic role of pro and antiinflammatory cytokines in severe malaria. J Infect Dis. 1999; 180:1288-1297.

de Kossodo S, Grau GE. Role of cytokines and adhesion molecules in malaria immunopathology. Stem Cells. 1993; 11(1):41-48.

Dittrich S, Sunyakumthorn P, Phetsouvanh R, Rattanavong S, Phetsouvanh R, Panyanivong P, Sengduangphachanh A, Phoumin P, Anantatat T, Chanthongthip A, Lee SJ, Dubot-Peres A, Day NPJ, Paris DH, Newton PN, Turner GDH. Blood -Brain barrier function and CSF biomarkers in Rickettsial versus other Neurological infections in Laos. Am J Trop Med Hyg. 2015; 93(2):232-237.

Dorovini-Zis K, Schmidt K, Huynh H, Fu W, Whitten RO, Milner D, Kamiza S, Molyneux M, Taylor TE. The neuropathology of fatal cerebral malaria in Malawian children. Am J Pathol. 2011; 178:2146-2158.

Duce JA, Tsatsanis A, Cater MA, James SA, Robb E, Wikhe K, Leong SL, Perez K, Johanssen T, Greenough MA, Cho HH, Galatis D, Moir RD, Masters CL, McLean C, Tanzi RE, Cappai R, Barnham KJ, Ciccotosto GD, Rogers JT, Bush AI. Iron-export ferroxidase activity of β-amyloid precursor protein is inhibited by zinc in Alzheimer's disease. Cell. 2010; 142(6):857-867.

el-Nashar TM, el-Kholy HM, el-Shiety AG, Al-Zahaby AA. Correlation of plasma levels of tumor necrosis factor, interleukin-6 and nitric oxide with the severity of human malaria. J Egypt Soc Parasitol. 2002; 32:525–535.

Finley RW, Mackey LJ, Lambert PH. Virulent P. berghei malaria: prolonged survival and decreased cerebral pathology in T-cell-deficient nude mice. J Immunol. 1982; 129:2213–2218.

Flanders KC, Ren RF, Lippa CF. Transforming growth factor-betas in neurodegenerative disease. Prog Neurobiol 1998; 54:71-85.

Gitau EN, Newton CR. Review Article: blood-brain barrier in falciparum malaria. Trop Med Int Health. 2005; 10(3):285-292.

Grau GE, Mackenzie CD, Carr RA. Platelet accumulation in brain microvessels in fatal paediatric cerebral malaria. J Infect Dis. 2003; 187:461-466.

Grau GE, Piguet PF, Engers HD, et al. L3T4+ T lymphocytes play a major role in the pathogenesis of murine cerebral malaria. J Immunol. 1986; 137:2348-2354.

Grau GE, Taylor TE, Molyneux ME, et al. Tumor necrosis factor and disease severity in children with falciparum malaria. N Engl J Med. 1989; 320:1586-1591.

Greiner J, Dorovini-Zis K, Taylor TE, Molyneux ME, Beare NA, Kamiza S, White VA. Correlation of hemorrhage, axonal damage, and blood-tissue barrier disruption in brain and retina of Malawian children with fatal cerebral malaria. Front Cell Infect Microbiol. 2015; 5:18.

Gimenez F, Barraud de Lagerie S, Fernandez C, Pino P, Mazier D. Tumor necrosis factor alpha in the pathogenesis of cerebral malaria. Cell Mol Life Sci. 2003; 60(8):1623-1635.

Hunt NH, Ball HJ, Hansen AM, Khaw LT, Guo J, Bakmiwewa S, Mitchell AJ, Combed V, Grau GE. Cerebral Malaria: gamma-interferon redux. Front Cell Infect Microbiol. 2014; 4:113.

Hunt NH, Golenser J, Chan-Ling T, Parekh S, Rae C, Potter S, Medana IM, Miu J, Ball HJ. Immunopathogenesis of cerebral malaria. Int J Parasitol. 2006; 36(5):569-582.

Kaur B, Rutty GN, Timperley WR. The possible role of hypoxia in the formation of axonal bulbs. J Clin Pathol. 1999; 52(3):203-209.

Kern P, Hemmer CJ, van Damme J, Gruss HJ, Dietrich M. Elevated tumor necrosis factor alpha and interleukin-6 serum levels as markers for complicated Plasmodium falciparum malaria. Am J Med. 1989; 87:139-143.

Krishnan A, Karnad DR, Limaye U, Siddharth W. Cerebral venous and dural sinus thrombosis in severe falciparum malaria. J Infect. 2004; 48:86-90.

Kwiatkowski D, Hill AV, Sambou I, et al. TNF concentration in fatal cerebral, non-fatal cerebral, and uncomplicated Plasmodium falciparum malaria. Lancet. 1990; 336:1201-1204.

Lackner AA, Marx PA, Lerche NW, Gardner MB, Kluge JD, Spinner A, Kwang HS, Lowenstine LJ. Asymptomatic infection of the central nervous system by the macaque immunosuppressive type D retrovirus, SRV-1. J Gen Virol. 1989; 70:1641-1651.

Leong, Anthony S-Y; Cooper, Kumarason; Leong, F Joel W-M. Manual of Diagnostic Cytology (2 ed.). Greenwich Medical Media, Ltd. pp. 63–64; 2003.

Liedtke W, Edelmann W, Bieri PL, Chiu FC, Cowan NJ, Kucherlapati R, Raine CS. GFAP is necessary for the integrity of CNS white matter architecture and long-term maintenance of myelination. Neuron. 1996; 17(4):607-615.

Liu XQ, Stacey KJ, Horne-Debets JM, Cridland JA, Fischer K, Narum D, Mackay F, Pierce SK, Wykes MN. Malaria infection alters the expression of B-cell activating factor resulting in diminished memory antibody responses and survival. Eur J Immunol. 2012; 42(12):3291-3301.

Ma N, Madigan MC, Chan-Ling T, Hunt NH. Compromised blood-nerve barrier, astrogliosis, and myelin disruption in optic nerves during fatal murine cerebral malaria. Glia. 1997; 19(2):135-151.

MacPherson GG, Warrell MJ, White NJ, Looareesuwan S, Warrell DA. Human cerebral malaria: A quantitative ultrastructural analysis of parasitized erythrocyte sequestration. Am J Pathol. 1985; 119:385–401.

Maegraith B. Other pathological processes in malaria. Bull World Health Organ. 1974; 50(3-4):187-193.

Medana IM, Chaudhri G, Chan-Ling T, Hunt NH. Central nervous system in cerebral malaria: 'Innocent bystander' or active participant in the induction of immunopathology? Immunol Cell Biol. 2001; 79(2):101-120.

Medana IM, Day NP, Hien TT, Mai NT, Bethell D, Phu NH, Farrar J, Esiri MM, White NJ, Turner GD. Axonal injury in cerebral malaria. Am J Pathol. 2002; 160(2):655-666.

Medana IM, Day NPJ, Hien TT, Mai NTH, Bethell D, Phu NH, Farrar J, White NJ, Turner GDH. Cellular Stress and Injury Responses in the Brains of Adult Vietnamese Patients with Fatal Plasmodium falciparum malaria. Neuropathol Appl Neurobiol. 2001; 27(6):421-433.

Medana IM, Day NP, Sachanonta N, Mai NT, Dondorp AM, Pongponratn E, Hien TT, White NJ, Turner GD. Coma in fatal adult human malaria is not caused by cerebral oedema. Malar J. 2011; 10:267.

Medana IM, Lindert RB, Wurster U, Hien TT, Day NP, Phu NH, Mai NT, Chuong LV, Chau TT, Turner GD, Farrar JJ, White NJ. Cerebrospinal fluid levels of markers of brain parenchymal damage in Vietnamese adults with severe malaria. Trans R Soc Trop Med Hyg. 2005; 99(8):610-617.

Meehan SM, Limsrichamrern S, Manaligod JR, Junsanto T, Josephson MA, Thistlethwaite JR, Haas M. Platelets and capillary injury in acute humoral rejection of renal allografts. Hum Pathol. 2003; 34(6):533-540.

Merono A, Lucena C, López A, Garrido JJ, Pérez de LL, Llanes D. Immunohistochemical analysis of beta3 integrin (CD61): expression in pig tissues and human tumors. Histol Histopathol. 2002; 17:347-352.

Milner DA Jr, Lee JJ, Frantzreb C, Whitten RO, Kamiza S, Carr RA, Pradham A, Factor RE, Playforth K, Liomba G, Dzamalala C, Seydel KB, Molyneux ME, Taylor TE. Quantitative Assessment of Multiorgan Sequestration of Parasites in Fatal Pediatric Cerebral Malaria. J Infect Dis. 2015; 212(8):1317-1321.

Migasena P, Maegraith BG. The movement of the dye (disulphine blue) from blood into brain tissue examined by dye method in normal and Plasmodium berghei infected mice. Med J Malaya. 1968; 22(3):252.

Montgomery SL, Bowers WJ. Tumor necrosis factor-alpha and the roles it plays in homeostatic and degenerative processes within the central nervous system. Journal of Neuroimmune Pharmacology, vol. 7, no. 1, pp. 42–59; 2012.

Mturi N, Keir G, MacLennan CA, et al. Cerebrospinal Fluid Studies in Kenyan Children with Severe Falciparum Malaria. Open Trop Med J. 2008; 1:56-62.

Neill AL, Hunt NH. Pathology of fatal and resolving Plasmodium berghei cerebral malaria in mice. Parasitology. 1998; 105(Pt 2):165-175.

Newton CRJC, Krishna S. Severe falciparum malaria in children: current understanding of pathophysiology and supportive treatment. Pharmacol Ther. 1998; 79:1–53.

Nielsen H, Kharazmi A, Theander TG: Suppression of blood monocyte and neutrophil chemotaxis in acute human malaria. Parasite Immunol. 1986; 8:541-550.

Olmos G, Lladó J. Tumor Necrosis Factor Alpha: A Link between Neuroinflammation and Excitotoxicity, Mediators of Inflammation, vol. 2014, Article ID 861231, 12 pages; 2014.

Oo MM, Aikawa M, Than T, Aye TM, Myint PT, Igarashi I, Schoene WC. Human cerebral malaria: a pathological study. J Neuropathol Exp Neurol 1987; 46:223-231.

Paetau A, Elovaara I, Paasivuo R, Virtanen I, Palo J, Haltia M. Glial filaments are a major brain fraction in infantile neuronal ceroid-lipofuscinosis. Acta Neuropathologica. 1985; 65(3-4):190-194.

Patnaik JK, Das BS, Mishra SK, Mohanty S, Satpathy SK. Vascular clogging, mononuclear cell margination, and enhanced vascular permeability in the pathogenesis of human cerebral malaria. Am J Trop Med Hyg. 1994; 51:642-647.

Petzold A. CSF biomarkers for improved prognostic accuracy in acute CNS disease. Neurol Res. 2007; 29:691-708.

Peyron F, Burdin N, Ringwald P, Vuillez JP, Rousset F, Banchereau J. High levels of circulating IL-10 in human malaria. Clin Exp Immun. 1994; 95:300-303.

Pongponratn E, Riganti M, Harinasuta T, Bunnag D. Electron microscopy of the human brain in cerebral malaria. Southeast Asian J Trop Med Public Health. 1985; 16:219-227.

Ponsford M, Medana IM, Prapansilp P, Hein TT, Lee SJ, Dondorp AM, Esiri M, Day NPJ, White NJ, Turner GDH. Sequestration and Microvascular Congestion are associated with coma in Human Cerebral Malaria. J Infect Dis. 2012; 205(4):663-671.

Porta J, Carota A, Pizzolato GP, Wildi E, Widmer MC, Margairaz C, Grau GE: Immunopathological changes in human cerebral malaria. Clin Neuropathol. 1993; 12:142-146

Portugal S, Pierce SK, Crompton PD. Young Lives Lost as B Cells Falter: What We're Learning about Antibody Responses in Malaria. J Immunol. 2013; 190(7):3039-3046.

Prakash D, Fesel C, Jain R, Cazenave PA, Mishra GC, Pied S. Clusters of cytokines determine malaria severity in Plasmodium falciparum-infected patients from endemic areas of Central India. J Infect Dis. 2006; 194(2):198-207.

Priller C, Bauer T, Mitteregger G, Krebs B, Kretzschmar HA, Herms J. Synapse formation and function is modulated by the amyloid precursor protein. J Neurosci. 2006; 26(27):7212-7221.

Ramos-Vara, JA; Miller MA. When tissue antigens and antibodies get along: revisiting the technical aspects of immunohistochemistry--the red, brown, and blue technique. Vet Pathol. 2014; 51(1):42-87.

Rénia L, Wu Howland S, Claser C, Gruner AC, Suwanarusk R, Teo TH, Russell B, Ng L. Cerebral malaria: Mysteries at the blood-brain barrier. Virulence. 2012; 3(2):193-201.

Rodrigues-da-Silva RN, Lima-Junior J da C, Fonseca B de PF e, et al. Alterations in cytokines and haematological parameters during the acute and convalescent phases of Plasmodium falciparum and Plasmodium vivax infections. Memórias do Instituto Oswaldo Cruz. 2014; 109(2):154-162.

Saraste A. Morphologic criteria and detection of apoptosis. Herz. 1999; 24(3):189-195.

Schwarzer E, Arese P: Phagocytosis of malarial pigment hemozoin inhibits NADPH-oxidase activity in human monocyte derived macrophages. Biochim Biophys Acta. 1996; 1316:169-175.

Shaffer N, Grau GE, Hedberg K, Davachi F, Lyamba B, Hightower AW, Breman JG, Phuc ND. Tumor necrosis factor and severe malaria. J Infect Dis. 1991; 163(1):96-101.

Shedlock DJ, Silvestri G, Weiner DB. Monkeying around with HIV vaccines: using rhesus macaques to define 'gatekeepers' for clinical trials. Nat Rev Immunol. 2009; 9(10):717-728.

Sun G, Chang WL, Li J, Berney SM, Kimpel D, van der Heyde HC. Inhibition of platelet adherence to brain microvasculature protects against severe Plasmodium berghei malaria. Infect Immun. 2003; 71(11):6553-6561.

Thuma PE, van Dijk J, Bucala R, et al. Distinct Clinical and Immunologic Profiles in Severe Malarial Anemia and Cerebral Malaria in Zambia. J Infect Dis. 2011; 203(2):211-219.

Turner GDH. Cerebral malaria. Brain Pathol. 1997; 7:569-582.

Turner GDH. Severe malaria (WHO). Section 8: Pathology of Severe falciparum Malaria. Turner GDH. Milner DA Jr, in "Severe Malaria". Trop Med Int Health. 2014; 19(suppl S1):7-131.

Turner GDH, Morrison H, Jones M, Davis TME, Looareesuwan S, Buley ID, Gatter KC, Newbold CI, Pukritayakamee S, Nagachinta B, White NJ, Berendt AR. An Immunohistochemical Study of the Pathology of Fatal Malaria: Evidence for Widespread Endothelial Activation and a Potential Role for Intercellular Adhesion Molecule-1 in Cerebral Sequestration. Am J Pathol. 1994; 145(5):1057–1069.

Turner PR, O'Connor K, Tate WP, Abraham WC. Roles of amyloid precursor protein and its fragments in regulating neural activity, plasticity and memory. Prog Neurobiol. 2003; 70(1):1-32.

Wassmer SC, Combes V, Grau GE. Pathophysiology of cerebral malaria: role of host cells in the modulation of cytoadhesion. Ann N Y Acad Sci. 2003; 992:30-38.

Weinstein DE, Shelanski ML, Liem RK. Suppression by antisense mRNA demonstrates a requirement for the glial fibrillary acidic protein in the formation of stable astrocytic processes in response to neurons. J Cell Biol. 1991; 112(6):1205-1213.

White VA, Lewallen S, Beare NAV, Molyneux ME, Taylor TE. Retinal Pathology of Pediatric Cerebral Malaria in Malawi. PLoS ONE. 2009; 4(1):e4317.

Wikoff WR, Pendyala G, Siuzdak G, Fox HS. Metabolomic analysis of the cerebrospinal fluid reveals changes in phospholipase expression in the CNS of SIV-infected macaques. J Clin Invest. 2008; 118(7):2661-2669.

Wyss-Coray T, Mucke L. Inflammation in neurodegenerative disease-a double-edged sword. Neuron. 2002; 35(3):419-432.

Chapter 6: <u>Ultrastructure</u>

Acharya P, Chaubey S, Grover M, Tatu U. An Exported Heat Shock Protein 40 Associates with Pathogenesis-Related Knobs in Plasmodium falciparum Infected Erythrocytes. PLoS One. 2012; 7:e44605.

Aikawa M. Variations in structure and function during the life cycle of malarial parasites. Bull World Health Organ. 1977; 55(2-3):139-156.

Aikawa M. Studies on falciparum malaria with atomic-force and surface-potential microscopes. Ann Trop Med Parasitol. 1997; 91(7):689-692.

Aikawa M. Human cerebral malaria. Am J Trop Med Hyg. 1988; 39:1-10.

Aikawa M. Morphological changes in erythrocytes induced by malarial parasites. Biol Cell. 1988; 64(2):173-181.

Aikawa M, Brown AE, Smith CD, Tegoshi T, Howard RJ, Hasler TH, Ito Y, Collins WE, Webster HK. Plasmodium coatneyi-infected rhesus monkeys: a primate model for human cerebral malaria. Inst Oswaldo Cruz. 1992; 87(Suppl 3):443-447.

Aikawa M, Kamanura K, Shiraishi S, et al. Membrane knobs of unfixed Plasmodium falciparum infected erythrocytes: new findings as revealed by atomic force microscopy and surface potential spectroscopy. Exp Parasitol. 1996; 84(3):339-343.

Aikawa M, Miller LH, Rabbege J. Caveola--vesicle complexes in the plasmalemma of erythrocytes infected by Plasmodium vivax and P cynomolgi. Unique structures related to Schüffner's dots. Am J Pathol. 1975; 79(2):285-300.

Aikawa M, Rabbege JR, Udeinya I, Miller LH. Electron microscopy of knobs in Plasmodium falciparum-infected erythrocytes. J Parasitol. 1983; 69:435-437.

Aikawa M, Udeinya IJ, Rabbege J, Dayan M, Leech JH, Howard RJ, Miller LH. Structural alteration of the membrane of erythrocytes infected with Plasmodium falciparum. J Protozool. 1985; 32(3):424-429.

Akaki M, Nagayasu E, Nakano Y, Aikawa M. Surface charge of Plasmodium falciparum merozoites as revealed by atomic force microscopy with surface potential spectroscopy. Parasitol Res. 2002; 88(1):16-20.

Akinyi S, Hanssen E, Meyer EV, Jiang J, Korir CC, Singh B, Lapp S, Barnwell JW, Tilley L, Galinski MR. A 95 kDa protein of Plasmodium vivax and P. cynomolgi visualized by three-dimensional tomography in the caveola-vesicle complexes (Schüffner's dots) of infected erythrocytes is a member of the PHIST family. Mol Microbiol. 2012; 84(5):816-831.

Allred DR, Gruenberg JE, Sherman IW. Dynamic rearrangements of erythrocyte membrane internal architecture induced by infection with Plasmodium falciparum. J Cell Sci. 1986; 81:1-16.

Anderson DC, Lapp SA, Akinyi S, Meyer EV, Barnwell JW, Korir-Morrison C, Galinski MR. Plasmodium vivax trophozoite-stage proteomes. J Proteomics. 2015; 115:157-176.

Atkinson CT, Aikawa M, Rock EP, Marsh K, Andrysiak PM, Campbell GH, Collins WE, Howard RJ. Ultrastructure of the erythrocytic stages of Plasmodium malariae. J Protozool. 1987; 34(3):267-274.

Atkinson CT, Aikawa M. Ultrastructure of malaria-infected erythrocytes. Blood Cells. 1990; 16(2-3):351-368.

Bannister LH, Hopkins JM, Fowler RE, Krishna S, Mitchell GH. A brief illustrated guide to the ultrastructure of Plasmodium falciparum asexual blood stages. Parasitol Today. 2000; 16(10):427-433.

Barnwell JW, Howard RJ, Miller LH. Altered expression of Plasmodium knowlesi variant antigen on the erythrocyte membrane in splenectomized rhesus monkeys. J Immunol. 1982; 128(1):224-226.

Barnwell JW, Howard RJ, Miller LH. Influence of the spleen on the expression of surface antigens on parasitized erythrocytes. Ciba Found Symp. 1983; 94:117-136.

Barnwell JW, Ingravallo P, Galinski MR, Matsumoto Y, Aikawa M. Plasmodium vivax: malarial proteins associated with the membrane-bound caveola-vesicle complexes and cytoplasmic cleft structures of infected erythrocytes. Exp Parasitol. 1990; 70(1):85-99.

Barsoum RS. Malarial acute renal failure. J Am Soc Nephrol. 2000; 11:2147–2154.

Baruch, D. I., Rogerson, S. J. & Cooke, B. M. Asexual blood stages of malaria antigens: cytoadherence. Chem Immunol. 2002; 80:144–162.

Bhamarapravati N. Boonpucknavig S, Boonpucknavig V, Yaemboonruang C. Glomerular changes in acute plasmodium falciparum infection. An immunopathologic study. Arch Pathol. 1973; 95(5):289-293.

Boonpucknavig S, Wongsawang S, Boonpucknavig V, Bhamarapravati N. Serum-soluble malaria antigens and immun complex nephritis in Plasmodium berghei berghei infected mice. J Trop Med Hyg. 1976; 79(6):116-119.

Carlson J. Erythrocyte rosetting in Plasmodium falciparum malaria-with special reference to the pathogenesis of cerebral malaria. Scand J Infect Dis Suppl. 1993; 86:1-79.

Carlson J, Helmby H, Hill AV, Brewster D, Greenwood BM, Wahlgren M. Human cerebral malaria: association with erythrocyte rosetting and lack of anti-rosetting antibodies. Lancet. 1990; 336(8729):1457-1460.

Chopra P, Ray R, Saxena. Chapter 8: Myocarditis. In. An Illustrated Textbook of Cardiovascular Pathology. CRC Press. Pp. 116; 2013.

Chotivanich KT, Pukrittayakamee S, Simpson JA, White NJ, Udomsangpetch R. Characteristics of Plasmodium vivax-infected erythrocyte rosettes. Am J Trop Med Hyg. 1998; 59(1):73-76.

Claser C, Malleret B, Peng K, Bakocevic N, Gun SY, Russell B, Ng LG, Rénia L. Rodent Plasmodium-infected red blood cells: imaging their fates and interactions within their hosts. Parasitol Int. 2014; 63(1):187-194.

Coatney GR, Collins WE, Warren McW, Contacos PG. The Primate Malarias. Washington, DC: U.S. Government Printing Office; 1971.

Cooke BM, Mohandas N, Coppel RL. Malaria and the red blood cell membrane. Semin Hematol. 2004; 41(2):173-188.

Coatney GR, Collins WE, Warren M, et al. The Primate Malarias. Washington, D.C.: U.S. Government Printing Office; Pp. 289-299; 1971.

Costenaro P, Benedetti P, Facchin C, Mengoli C, Pellizzer G. Fatal Myocarditis in Course of Plasmodium falciparum Infection: Case Report and Review of Cardiac Complications in Malaria. Case Reports in Medicine, 2011; 2011:202083.

Craig A, Scherf A. Molecules on the surface of the Plasmodium falciparum infected erythrocyte and their role in malaria pathogenesis and immune evasion. Mol Biochem Parasitol. 2001; 115(2):129-143.

David PH, Handunnetti SM, Leech JH, Gamage P, Mendis KN. Rosetting: a new cytoadherence property of malaria-infected erythrocytes. Am J Trop Med Hyg. 1988; 38(2):289–297.

Davis TM, Pongponratan E, Supanaranond W, Pukrittayakamee S, Helliwell T, Holloway P, White NJ. Skeletal muscle involvement in falciparum malaria: biochemical and ultrastructural study. Clin Infect Dis. 1999; 29(4):831-835.

Davison BB, Cogswell FB, Baskin GB, Falkenstein KP, Henson EW, Tarantal AF, Krogstad DJ. Plasmodium coatneyi in the rhesus monkey (Macaca mulatta) as a model of malaria in pregnancy. Am J Trop Med Hyg. 1998; 59(2):189-201.

Desowitz RS, Miller LH, Buchanan RD, Permpanich B. The sites of deep vascular schizogony in Plasmodium coatneyi malaria. Trans R Soc Trop Med Hyg. 1969; 63:198-202.

Desowitz RS, Miller LH, Buchanan RD, Yuthasastrkosol V, Permpanich B. Comparative studies on the pathology and host physiology of malarias. I. Plasmodium coatneyi. Ann Trop Med Parasitol. 1967; 61:365-374.

Doumbo OK, Thera MA, Koné AK, Raza A, Tempest LJ, Lyke KE, Plowe CV, Rowe JA. High levels of Plasmodium falciparum rosetting in all clinical forms of severe malaria in African children. Am J Trop Med Hyg. 2009; 81(6):987-993.

Duarte MI, Corbett CE, Boulos M, Amato Neto V. Ultrastructure of the lung in falciparum malaria. Am J Trop Med Hyg. 1985; 34(1):31-35.

Dudgeon LS, Clark C. A contribution to the microscopical histology of malaria. Lancet. 1917; 190(4901):153-156.

el-Shoura SM. Falciparum malaria in naturally infected human patients: X. Ultrastructural pathological alterations of renal glomeruli. Parasite. 1994; 1(3):205-210.

Escalante AA, Barrio E, Ayala FJ. Evolutionary origin of human and primate malarias: evidence from the circumsporozoite protein gene. Mol Biol Evol. 1995; 12(4):616-626.

Eyles DE. The species of simian malaria: taxonomy, morphology, life cycle, and geographical distribution of the monkey species. J Parasitol. 1963; 49:866-887.

Eyles DE, Fong YL, Warren McW, Guinn EG, Sandosham AA, Wharton RH. Plasmodium coatneyi, a new species of primate malaria from Malaya. Am J Trop Med Hyg. 1962; 11:597-604.

Fernandez V, Wahlgren M. Rosetting and autoagglutination in Plasmodium falciparum. Chem Immunol. 2002; 80:163-187.

Garcia CR, Takeuschi M, Yoshioka K, Miyamoto H. Imaging Plasmodium falciparum-infected ghost and parasite by atomic force microscopy. J Struct Biol. 1997; 119(2):92-98.

Gruenberg J, Allred DR, Sherman IW. Scanning electron microscope-analysis of the protrusions (knobs) present on the surface of Plasmodium falciparum-infected erythrocytes. J Cell Biol. 1983; 97(3):795-802.

Gutierrez Y, Aikawa M, Fremount HN, Sterling CR. Experimental infection of Aotus monkeys with Plasmodium falciparum Light and electron microscopic changes. Ann Trop Med Parasitol. 1976; 70(1):25-44.

Hasler T, Handunnetti SM, Aguiar JC, van Schravendijk MR, Greenwood BM, Lallinger G, Cegielski P, Howard RJ. In vitro rosetting, cytoadherence, and microagglutination properties of Plasmodium

falciparum-infected erythrocytes from Gambian and Tanzanian patients. Blood. 1990; 76(9):1845-1852.

Handunnetti SM, David PH, Perera KL, Mendis KN. Uninfected erythrocytes form "rosettes" around Plasmodium falciparum infected erythrocytes. Am J Trop Med Hyg. 1989; 40(2):115-118.

Ho M, Davis TM, Silamut K, Bunnag D, White NJ. Rosette formation of Plasmodium falciparum-infected erythrocytes from patients with acute malaria. Infect Immun. 1991; 59(6):2135-2139.

Hochman SE, Madaline TF, Wassmer SC, Mbale E, Choi N, Seydel KB, Whitten RO, Varughese J, Grau GE, Kamiza S, Molyneux ME, Taylor TE, Lee S, Milner DA Jr, Kim K. Fatal Pediatric Cerebral Malaria Is Associated with Intravascular Monocytes and Platelets That Are Increased with HIV Coinfection. MBio. 2015; 6(5):e01390-15.

Horrocks P, Pinches RA, Chakravorty SJ, Papakrivos J, Christodoulou Z, Kyes SA, Urban BC, Ferguson DJ, Newbold CI. PfEMP1 expression is reduced on the surface of knobless Plasmodium falciparum infected erythrocytes. J Cell Sci. 2005; 118(Pt 11):2507-2518.

Kats LM, Fernandez KM, Glenister FK, Herrmann S, Buckingham DW, Siddiqui G, Sharma L, Bamert R, Lucet I, Guillotte M, Mercereau-Puijalon O, Cooke BM. An exported kinase (FIKK4.2) that mediates virulence-associated changes in Plasmodium falciparum-infected red blood cells. Int J Parasitol. 2014; 44(5):319-328.

Kawai S, Aikawa M, Kano S, Suzuki M. A primate model for severe human malaria with cerebral involvement: Plasmodium coatneyi-infected Macaca fuscata. Am J Trop Med Hyg. 1993; 48:630-636.

Kawai S, Kano S, Suzuki M. Rosette formation by Plasmodium coatneyi-infected erythrocytes of the Japanese macaque (Macaca fuscata). Am J Trop Med Hyg. 1995; 53(3):295-299.

Kawai S, Aikawa M, Suzuki M, et al. A nonhuman primate model for severe human malaria: Plasmodium coatneyi-infected Japanese macaque (Macaca fuscata). Tokai J Exp Clin Med. 1998; 23:101-102.

Kawai S, Matsumoto J, Aikawa M, Matsuda H. Increased plasma levels of soluble intercellular adhesion molecule-1 (sICAM-1) and soluble vascular cell molecule-1 (sVCAM-1) associated with disease severity in a primate model for severe human malaria: Plasmodium coatneyi-Infected Japanese macaques (Macaca fuscata). J Vet Med Sci. 2003; 65(5):629-631.

Kennedy SJ. Ultrastructure of normal monkey liver. Lab Anim. 1979; 13(2):125-129.

Kilejian A, Abati A, Trager W. Plasmodium falciparum and Plasmodium coatneyi: immunogenicity of "knob-like protrusions" on infected erythrocyte membranes. Exp Parasitol. 1977; 42(1):157-164.

Kochar DK, Singh P, Agarwal P, Kochar SK, Pokharna R, Sareen PK. (2003) Malaria Hepatitis. J Assoc Physicians India. 2003; 51:1069-1072.

Lanners HN. Ultrastructure of erythrocytes from Aotus trivirgatus and Saimiri sciureus monkeys infected by Plasmodium vivax. Parasitol Res. 1991; 77(5):395-401.

Leclerc MC, Hugot JP, Durand P, Renaud F. Evolutionary relationships between 15 Plasmodium species from new and old world primates (including humans): an 18S rDNA cladistic analysis. Parasitology. 2004; 129(Pt 6):677-684.

Lee WC, Malleret B, Lau YL, Mauduit M, Fong MY, Cho JS, Suwanarusk R, Zhang R, Albrecht L, Costa FT, Preiser P, McGready R, Renia L, Nosten F, Russell B. Glycophorin C(CD236R) mediated vivac malaria parasite rosetting to normocytes. Blood. 2014; 123(18):e100-109.

Leech JH, Barnwell JW, Miller LH, Howard RJ. Identification of a strain-specific malarial antigen exposed on the surface of Plasmodium falciparum-infected erythrocytes. J Exp Med. 1984; 159: 1567–1575.

Li A, Russell B, Renia L, Lek-Uthai U, Nosten F, Lim CT. High density of 'spiky' excrescences covering the surface of an erythrocyte infected with Plasmodium malariae. Br J Haematol. 2010; 151(1):1.

Li A, Mansoor AH, Tan KS, Lim CT. Observations on the internal and surface morphology of malaria infected blood cells using optical and atomic force microscopy. J Microbiol Methods. 2006; 66(3):434-439.

Li A, Rénia L, Lim CT, Russell B. Atomic force microscopy of Plasmodium-infected red blood cells: detecting and localizing single molecular recognition events. Methods Mol Biol. 2013; 923:299-305.

Li A, Rénia L, Lim CT, Russell B. Atomic Force Microscopy of Plasmodium-Infected Red Blood Cells: Detecting and Localizing Single Molecular Recognition Events. *In*. Malaria : Methods and Protocols. Ed. Robert Ménard Volume: 923, pp:299-305; 2012.

Lombardini ED, Gettayacamin M, Turner GDH, Brown AE. A Review of *Plasmodium coatneyi*-macaque models of severe and cerebral malaria. Vet Pathol. 2015; 52:998-1011

Luse SA, Miller LH. Plasmodium falciparum malaria. Ultrastructure of parasitized erythrocytes in cardiac vessels. Am J Trop Med Hyg. 1971; 20(5):655-660.

MacPherson GG, Warrell MJ, White NJ, Looareesuwan S, Warrell DA. Human cerebral malaria. A quantitative ultrastructural analysis of parasitized erythrocyte sequestration. Am J Pathol. 1985; 119(3):385-401.

Maeno Y, Brown AE, Smith CD, Tegoshi T, Toyoshima T, Ockenhouse CF, Corcoran KD, Ngampochjana M, Kyle DE, Webster HK, Aikawa M: A nonhuman primate model for human cerebral malaria: effects of artesunate (qinghaosu derivative) on rhesus monkeys Experimentally infected with Plasmodium coatneyi. Am J Trop Med Hyg. 1993; 49:726-734.

Malleret B, Xu F, Mohandas N, Suwanarusk R, Chu C, Leite JA, Low K, Turner C, Sriprawat K, Zhang R, Bertrand O, Colin Y, Costa FT, Ong CN, Ng ML, Lim CT, Nosten F, Rénia L, Russell B. Significant biochemical, biophysical and metabolic diversity in circulating human cord blood reticulocytes. PLoS One. 2013; 8(10):e76062.

Matsumoto Y, Matsuda S, Yoshida Y. Ultrastructure of human erythrocytes infected with Plasmodium ovale. Am J Trop Med Hyg. 1986; 35(4):697-703.

Mackenstedt U, Brockelman CR, Mehlhorn H, Raether W. Comparative morphology of human and animal malaria parasites. I. Host-parasite interface. Parasitol Res. 1989;75(7):528-Miller LH, Fremount HN, Luse SA. Deep vascular schizogony of Plasmodium knowlesi in Macaca mulatta. Distribution in organs and ultrastructure of parasitized red cells. Am J Trop Med Hyg. 1971; 20(6):816-824.

Medana IM, Turner GDH. Human Cerebral Malaria and the Blood-Brain Barrier. Int J Parasitol. 2006; 36(5): 555-568

Miller LH, Chien S, Usami S. Decreased deformability of Plasmodium coatneyi-infected red cells and its possible relation to cerebral malaria. Am J Trop Med Hyg. 1972; 21:133-137.

Mohsen AH, Green ST, McKendrick MW, West JN. Myocarditis associated with Plasmodium falciparum malaria: a case report and a review of the literature. J Travel Med. 2001; 8(4):219-220.

Moreno A, Cabrera-Mora M, Garcia A, Orkin J, Strobert E, et al. Plasmodium coatneyi in rhesus macaques replicates the multisystemic dysfunction of severe malaria in humans. Infect Immun. 2013; 81:1889-1904.

Nagao E, Kaneko O, Dvorak JA. Plasmodium falciparum-infected erythrocytes: qualitative and quantitative analyses of parasite-induced knobs by atomic force microscopy. J Struct Biol. 2000; 130(1):34–44.

Nakazawa S, Looareesuwan S, Fujioka H, Pongponratn E, Luc KD, Rabbege J, Aikawa M. A correlation between sequestered parasitized erythrocytes in subcutaneous tissue and cerebral malaria. Am J Trop Med Hyg. 1995; 53(5):544-546.

National Research Council: Guide for the Care and use of Laboratory Animals. Washington DC: National Academies Press; 2011.

Neill AL, Chan-Ling T, Hunt NH. Comparisons between microvascular changes in cerebral and non-cerebral malaria in mice, using the retinal whole-mount technique. Parasitology. 1993; 107(5):477-487.

Nguansangiam S, Day NP, Hien TT, Mai NT, Chaisri U, Riganti M, Dondorp AM, Lee SJ, Phu NH, Turner GD, White NJ, Ferguson DJ, Pongponratn E. A quantitative ultrastructural study of renal pathology in fatal Plasmodium falciparum malaria. Trop Med Int Health. 2007; 12(9):1037-1050.

Olliaro P, Castelli F. Plasmodium falciparum: an electronmicroscopy study of caveolae and trafficking between the parasite and the extracellular medium. Int J Parasitol. 1997; 27(9):1007-1012.

Pongponratn E, Riganti M, Punpoowong B, Aikawa M. (1991) Microvascular sequestration of parasitized erythrocytes in human falciparum malaria: a pathological study. Am J Trop Med Hyg. 1991; 44:168–175.

Pongponratn E, Viriyavejakul P, Wilairatana P, Ferguson D, Chaisri U, Turner G, Looareesuwan S. Absence of knobs on parasitized red blood cells in a splenectomized patient in fatal falciparum malaria. Southeast Asian J Trop Med Public Health. 2000; 31(4):829-835.

Pongponratn E, Turner GD, Day NP, Phu NH, Simpson JA, Stepniewska K, Mai NT, Viriyavejakul P, Looareesuwan S, Hien TT, Ferguson DJ, White NJ. An ultrastructural study of the brain in fatal Plasmodium falciparum malaria. Am J Trop Med Hyg. 2003; 69(4):345-359.

Pongponratn E, Prommano O, Chaisri U, Viriyavejakul P, Wilairatana P. Plasmodium malariae-infected erythrocytes in the peripheral blood, liver, stomach and duodenum: an ultrastructural study. Southeast Asian J Trop Med Public Health. 2012; 43(5):1080-1086.

Prommano O, Chaisri U, Turner GD, Wilairatana P, Ferguson DJ, Viriyavejakul P, White NJ, Pongponratn E. A quantitative ultrastructural study of the liver and the spleen in fatal falciparum malaria. Southeast Asian J Trop Med Public Health. 2005; 36(6):1359-1370.

Quadt KA, Barfod L, Andersen D, Bruun J, Gyan B, Hassenkam T, Ofori MF, Hviid L. The density of knobs on Plasmodium falciparum-infected erythrocytes depends on developmental age and varies among isolates. PLoS One. 2012; 7(9):e45658.

Raventos-Suarez, C., Kaul, D. K., Macaluso, F. & Nagel, R. L. Membrane knobs are required for the microcirculatory obstruction induced by Plasmodium falciparum-infected erythrocytes. Proc Natl Acad Sci USA. 1985; 82:3829-3833.

Roberts DJ, Pain A, Kai O, Kortok M, Marsh K. Autoagglutination of malaria-infected red blood cells and malaria severity. Lancet. 2000; 355(9213):1427-1428.

Rudzinska MA, Trager W. The fine structure of trophozoites and gametocytes in Plasmodium coatneyi. J Protozool. 1968; 15(1):73-88.

Sachanonta N, Chotivanitch K, Chaisri U, Turner GDH, Ferguson DJP, Day NPJ, Ponponratn E. Ultrastructural and Real-Time Microscopic changes in P. falciparum-infected red blood cells following treatment with Anti-malarial Drugs. Ultrastructural Pathol 2011; 35(5):214-225.

Sein KK, Brown AE, Maeno Y, et al. Sequestration pattern of parasitized erythrocytes in cerebrum, mid-brain and cerebellum of Plasmodium coatneyi-infected rhesus monkeys (Macaca mulatta). Am J Trop Med Hyg. 1993; 49:513-519.

Sein KK, Maeno Y, Thuc HV, Anh TK, Aikawa M. Differential sequestration of parasitized erythrocytes in the cerebrum and cerebellum in human cerebral malaria. Am J Trop Med Hyg. 1993; 48(4):504-511.

Sharma YD. Knobs, knob proteins and cytoadherence in falciparum malaria. Int J Biochem. 1991; 23(9):775-789.

Smith CD, Brown AE, Nakazawa S, et al. Multi-organ erythrocyte sequestration and ligand expression in rhesus monkeys infected with Plasmodium coatneyi malaria. Am J Trop Med Hyg. 1996; 55:379-383.

Sommer JR, Waugh RA. Ultrastructure of heart muscle, a review. Environ Health Perspect. 1978; 26:159-167.

Su XZ, Heatwole VM, Wertheimer SP, Guinet F, Herrfeldt JA, Peterson DS, Ravetch JA, Wellems TE. The large diverse gene family var encodes proteins involved in cytoadherence and antigenic variation of *Plasmodium falciparum*-infected erythrocytes. Cell. 1995; 82:89-100.

Subramani R, Quadt K, Jeppesen AE, Hempel C, Petersen JE, Hassenkam T, Hviid L, Barfod L. Plasmodium falciparum-infected erythrocyte knob density is linked to the PfEMP1 variant expressed. MBio. 2015; 6(5):e01456-15.

Tegoshi T, Udomsangpetch R, Brown A, Nakazawa S, Webster HK, Aikawa M. Ultrastructure of rosette formation by Plasmodium coatneyi-infected erythrocytes of rhesus. Parasitol Res. 1993; 79(7):611-613.

Thumwood CM, Hunt NH, Clark IA, Cowden WB. Breakdown of the blood-brain barrier in murine cerebral malaria. Parasitology. 1988; 96(3):579-589.

Tilley L, Dixon MW, Kirk K. The Plasmodium-infected red blood cell. Int J Biochem Cell Biol. 2011; 43(6):839-842.

Udomsangpetch R, Brown AE, Smith CD, Webster HK. Rosette formation by Plasmodium coatneyi-infected red blood cells. Am J Trop Med Hyg. 1991; 44(4):399-401.

Udomsangpetch R, Wåhlin B, Carlson J, Berzins K, Torii M, Aikawa M, Perlmann P, Wahlgren M. Plasmodium falciparum-infected erythrocytes form spontaneous erythrocyte rosettes. J Exp Med. 1989; 169(5):1835-1840.

Wahlgren M, Carlson J, Udomsangpetch R, Perlmann P. Why do Plasmodium falciparumm-infected erythrocytes form spontaneous erythrocyte rosettes? Parasitol Today. 1989; 5(6):183-185.

Watermeyer JM, Hale VL, Hackett F, Clare DK, Cutts EE, Vakonakis I, Fleck RA, Blackman MJ, Saibil HR. A spiral scaffold underlies cytoadherent knobs in Plasmodium falciparum-infected erythrocytes. Blood. 2016; 127(3):343-351.

Chapter 7: <u>Methylene Blue study</u>

Ademowo OG, Nneji CM, Adedapo AD. In vitro anti-malarial activity of methylene blue against field isolates of Plasmodium falciparum from children in Southwest Nigeria. Indian J Med Res. 2007; 126(1):45-49.

Adjalley SH, Johnston GL, Li T, Eastman RT, Ekland EH, Eappen AG, Richman A, Sim BK, Lee MC, Hoffman SL, Fidock DA. Quantitative assessment of Plasmodium falciparum sexual development reveals potent transmission-blocking activity by methylene blue. Proc Natl Acad Sci USA. 2011; 108(47):E1214-1223.

Aeschlimann C, Cerny T, Küpfer A. Inhibition of (mono)amine oxidase activity and prevention of ifosfamide encephalopathy by methylene blue. Drug Metab Dispos. 1996; 24:1336–1339.

Aeschlimann C, Küpfer A, Schefer H, Cerny T. Comparative pharmacokinetics of oral and intravenous ifosfamide/mesna/methylene blue therapy. Drug Metab Dispos. 1998; 26(9):883-890.

Aikawa M, Brown AE, Smith CD, Tegoshi T, Howard RJ, Hasler TH, Ito Y, Perry G, Collins WE, Webster K. A primate model for human cerebral malaria: Plasmodium coatneyi–infected rhesus monkeys. Am J Trop Med Hyg. 1992; 46:391-397.

Andersen T, Nair S, Nkhoma S, Williams JT, Imwong M, Yi P, Socheat D, Das D, Chotivanich K, Day NP, White NJ, Dondorp AM. High Heritability of Malaria Parasite Clearance Rate Indicates a Genetic Basis for Artemisinin Resistance in Western Cambodia. J Infect Dis. 2010; 201:1326–1330.

Ashley EA, Dhorda M, Fairhurst RM, Amaratunga C, Lim P, et al. Tracking Resistance to Artemisinin Collaboration (TRAC) Spread of artemesinin resistance on Plasmodium falciparum malaria. N Engl J Med. 2014; 371(5):411-423.

Atamna H, Krugliak M, Shalmiev G, Deharo E, Pescarmona G, Ginsburg H. Mode of anti-malarial effect of methylene blue and some of its analogues on Plasmodium falciparum in culture and their inhibition of P. vinckei petteri and P. yoelii nigeriensis in vivo. Biochem Pharmacol. 1996; 51(5): 693-700.

Bhumiratana A, Intarapuk A, Sorosjinda-Nunthawarasilp P, Maneekan P, Koyadun S. Border malaria associated with multidrug resistance on Thailand-Myanmar and Thailand-Cambodia borders: transmission dynamic, vulnerability, and surveillance. Biomed Res Int. 2013; 2013:363417.

Bountogo M, Zoungrana A, Coulibaly B, Klose C, Mansmann U, Mockenhaupt FP, Burhenne J, Mikus G, Walter-Sack I, Schirmer RH, Sié A, Meissner P, Müller O. Efficacy of methylene blue monotherapy in semi-immune adults with uncomplicated falciparum malaria: a controlled trial in Burkina Faso. Trop Med Int Health. 2010; 15(6):713-717.

Buchholz K, Schirmer RH, Eubel JK, Akoachere MB, Dandekar T, Becker K, Gromer S. Interactions of methylene blue with human disulfide reductases and their orthologues from Plasmodium falciparum. Antimicrob. Agents Chemother. 2008; 52:183–191.

Cao XT, Bethell DB, Pham TP, Ta TT, Tran TN, Nguyen TT, Pham TT, Nguyen TT, Day NP, White NJ. Comparison of artemisinin suppositories, intramuscular artesunate and intravenous quinine for the treatment of severe childhood malaria. Trans R Soc Trop Med Hyg. 1997; 91(3):335-342.

Chamanza R. Non-human primates: Cynomolgus (Macaca fascicularis) and rhesus (Macaca mulatta) macaques and the common marmoset (Callithrix jacchus). *In.* Background Lesions in Laboratory Animals: A Color Atlas. Elizabeth F. McInnes ed., pg 1-16. Saunders (Elsevier), Edinburgh; 2012

Chalifoux LV, Bronson RT, Sehgal P, Blake BJ, King NW: Nephritis and hemolytic anemia in owl monkeys (*Aotus trivirgatus*). Vet Pathol. 1981; 18(Suppl 6):23-37.

Collins WE. Major animal models in malaria research: Simian. In: Malaria: Principles and Practice of Malariology. Eds. Wernsdofer WH and McGregor. Edinburgh: Churchill Livingstone. Pp. 1473-501; 1988.

Coulibaly B, Pritsch M, Bountogo M, Meissner PE, Nebié E, Klose C, Kieser M, Berens-Riha N, Wieser A, Sirima SB, Breitkreutz J, Schirmer RH, Sié A, Mockenhaupt FP, Drakeley C, Bousema T, Müller O. Efficacy and safety of triple combination therapy with artesunate-amodiaquine-methylene blue for falciparum malaria in children: a randomized controlled trial in Burkina Faso. J Infect Dis. 2015; 211(5):689-697.

Coulibaly B, Zoungrana A, Mockenhaupt FP, Schirmer RH, Klose C, Mansmann U, Meissner PE, Müller O. Strong gametocytocidal effect of methylene blue-based combination therapy against falciparum malaria: a randomised controlled trial. PLoS One. 2009; 4(5):e5318.

Craig, AG, Grau GE, Janse C, et al. The role of animal models for research on severe malaria. PLoSPathog. 2012; 8:1-9.

Curry S. Methemoglobinemia. Ann Emerg Med. 1982; 11(4):214-221.

Davison BB, Cogswell FB, Baskin GB, et al. Plasmodium coatneyi in the rhesus monkey (Macaca mulatta) as a model of malaria in pregnancy. Am J Trop Med Hyg. 1998; 59:189-201.

Day NPJ, Hien TT, Schollaardt T, Loc PP, Chuong LV, Chau TT, Mai NT, Phu NH, Sinh DX, White NJ, Ho M. The Prognostic and Pathophysiologic Role of Pro- and Antiinflammatory Cytokines in Severe Malaria. JID. 1999; 180:1288-1297.

Delves MJ, Ruecker A, Straschil U, Lelièvre J, Marques S, López-Barragán MJ, Herreros E, Sinden RE. Male and female Plasmodium falciparum mature gametocytes show different responses to anti-malarial drugs. Antimicrob Agents Chemother. 2013; 57(7):3268-3274.

Deschamps S, Maynadier M, Wein S, Gannoun-Zaki L, Marechal E, Vial HJ. Rodent and non-rodent malaria parasites differ in their phospholipid metabolic pathways. J Lipid Res. 2009; 51:81-96.

De Souza JB, Hafalla JCR, Riley EM, Couper KN. Cerebral malaria: why experimental murine models are required to understand the pathogenesis of disease. Parasitology. 2010; 137:755-772.

Desowitz RS, Miller LH, Buchanan RD, Permpanich B. The sites of deep vascular schizogony in Plasmodium coatneyi malaria. Trans R Soc Trop Med Hyg. 1969; 63:198-202.

Devine RM, van Heerden JA, Grant CS, Muir JJ. The role of methylene blue infusion in the management of persistent or recurrent hyperparathyroidism. Surgery. 1983; 94:916-918.

DiSanto AR, Wagner JG. Pharmacokinetics of highly ionized drugs. I. Methylene blue--whole blood, urine, and tissue assays. J Pharm Sci. 1972; 61(4):598-602.

DiSanto AR, Wagner JG. Pharmacokinetics of highly ionized drugs. II. Methylene blue--absorption, metabolism, and excretion in man and dog after oral administration. J Pharm Sci. 1972; 61(7):1086-1090.

DiSanto AR, Wagner JG. Pharmacokinetics of highly ionized drugs. 3. Methylene blue--blood levels in the dog and tissue levels in the rat following intravenous administration. J Pharm Sci. 1972; 61(7):1090-1094.

Dondorp A, Fanello CI, Hendriksen IC, Gomes E, Seni A, et al. Artesunate versus quinine in the treatment of severe falciparum malaria in African children (AQUAMAT):an open-label, randomised trial. Lancet. 2010; 376:1647-1657.

Dormoi J, Briolant S, Desgrouas C, Pradines B. Efficacy of proveblue (methylene blue) in an experimental cerebral malaria murine model. Antimicrob Agents Chemother. 2013; 57(7):3412-3414.

Dormoi J, Briolant S, Desgrouas C, Pradines B. Impact of methylene blue and atorvastatin combination therapy on the apparition of cerebral malaria in a murine model. Malar J. 2013; 12:127.

Ellenhorn MJ, Barceloux DG. Medical toxicology. Diagnosis and treatment of human poisoning. New York: Elsevier, 829-835, 844-852; 1988.

Fall B, Camara C, Fall M, Nakoulima A, Dionne P, Diatta B, Diemé Y, Wade B, Pradines B. Plasmodium falciparum susceptibility to standard and potential anti-malarial drugs in Dakar, Senegal, during the 2013-2014 malaria season. Malar J. 2015; 14:60.

Gennaro AR. Remington's pharmaceutical sciences. 18th ed. Easton, PA: Mack Publishing Company, 829-830; 1990.

Gozalo A, Dagle GE, Montoya E, Weller RE, Malaga CA: Spontaneous cardiomyopathy and nephropathy in the owl monkey (*Aotus* sp.) in captivity. J Med Primatol. 1992; 21:279-284.

Greenwood D. Conflicts of interest: the genesis of synthetic anti-malarial agents in peace and war. J Antimicrob Chemothe. 1995; 36:857-872.

Guttmann P, Ehrlich P. Uber die Wirkung des Methylenblau bei Malaria. Berl Klin Wochenschr 1891; 28:953-956.

Guttmann P, Ehrlich P. On the action of methylene blue in malaria. The Collected Papers of Paul Ehrlich. London: Pergamon Press, 15-20; 1960.

Harbrecht BG, Wang SC, Simmons RL, Billiar TR. Cyclic GMP and guanylate cyclase mediate lipopolysaccharide-induced Kupffer cell tumor necrosis factor-a synthesis. J Leukoc Biol. 1995; 57:297-302.

Heemskerk S, van Haren FMP, Foudraine NA, WHM Peters, van der Hoeven JG, Russel FGM, Masereeuw R, Pickkers P. Short-term beneficial effects of methylene blue on kidney damage in septic shock patients. Intensive Care Medicine. 2008; 34(2):350-354.

Hunt RD, Blake BJ: Glomerulonephritis, owl monkeys. *In*: Nonhuman Primates II, ed. Jones TC, Mohr U, Hunt RD, pp. 143-147. Springer-Verlag, Berlin, Germany; 1993

Hunt NH, Grau EG, Engwerda C, et al. Murine Cerebral Malaria: The Whole Story. Trends Parasitol. 2010; 26:272-274.

Kawai S, Aikawa M, Suzuki M, Matsuda H. A nonhuman primate model for severe human malaria: Plasmodium coatneyi-infected Japanese macaque (Macaca fuscata). Tokai J Exp Clin Med. 1998; 23:101-102.

Kim Y, Schneider KA: Evolution of Drug Resistance in Malaria Parasite Populations. Nature Education Knowledge. 2013; 4(8):6.

Kirov MY, Evgenov OV, Evgenov NV, Egorina EM, Sovershaev MA, Sveinbjørnsson B, Nedashkovsky EV, Bjertnaes LJ. Infusion of methylene blue in human septic shock: a pilot, randomized, controlled study. Crit Care Med. 2001; 29(10):1860-1867.

Krogh CME. CPS Compendium of pharmaceuticals and specialties. 28th ed. Ottawa: Canadian Pharmaceutical Association, 717; 1993.

Langhorne J, Buffet P, Galinski M, et al. The relevance of non-human primate and rodent malaria models for humans. Malar J. 2011; 10:23-27.

Lombardini ED, Gettayacamin M, Turner GD, Brown AE. A Review of Plasmodium coatneyi-Macaque Models of Severe Malaria. Vet Pathol. 2015; 52(6):998-1011.

Maeno Y, Brown AE, Dahlem Smith C, Tegoshi T, Toyoshima T, Ockenhouse CF, Corcoran KD, Ngampochjana M, Kyle DE, Webster HK, Aikawa M. A nonhuman primate model for human Cerebral malaria: effects of artesunate (qinghaosu derivative) on rhesus monkeys Experimentally infected with plasmodium coatneyi. Am J Trop Med Hyg. 1993; 49(6):726-734.

Mayer B, Brunner F, Schmidt K. Inhibition of nitric oxide synthesis by methylene blue. Biochem Pharmacol. 1993; 45:367-374.

McCall MBB, Sauerwein RW. Interferon-gamma, central mediator of protective immune responses against the pre-erythrocytic and blood stage of malaria. J Leukoc Biol. 2010; 88:1131-1143.

Moreno A, Cabrera-Mora M, Garcia A, et al. Plasmodium coatneyi in rhesus macaques replicates the multisystemic dysfunction of severe malaria in humans. Infect Immun. 2013; 81:1889-1904.

Moreno A, García A, Cabrera-Mora M, Strobert E, Galinski MR. Disseminated intravascular coagulation complicated by peripheral gangrene in a rhesus macaque (Macaca mulatta) experimentally infected with Plasmodium coatneyi. Am J Trop Med Hyg. 2007; 76:648-654.

Meissner PE, Mandi G, Coulibaly B, Witte S, Tapsoba T, Mansmann U, Rengelshausen J, Schiek W, Jahn A, Walter-Sack I, Mikus G, Burhenne J, Riedel KD, Schirmer RH, Kouyaté B, Müller O. Methylene

blue for malaria in Africa: results from a dose-finding study in combination with chloroquine. Malar J. 2006; 5:84.

Müller O, Mockenhaupt FP, Marks B, Meissner P, Coulibaly B, Kuhnert R, Buchner H, Schirmer RH, Walter-Sack I, Sié A, Mansmann U. Haemolysis risk in methylene blue treatment of G6PD-sufficient and G6PD-deficient West-African children with uncomplicated falciparum malaria: a synopsis of four RCTs. Pharmacoepidemiol Drug Saf. 2013; 22(4):376-385.

Mwangi VI, Mumo RM, Kiboi DM, Omar SA, Ng'ang'a ZW, Ozwara HS. Methylene blue inhibits lumefantrine-resistant Plasmodium berghei. J Infect Dev Ctries. 2016; 10(6):635-642.

National Research Council. Guide for the Care and use of Laboratory Animals. Washington DC: National Academies Press; 2011.

Nneji CM, Adaramoye OA, Falade CO, Ademowo OG. Effect of chloroquine, methylene blue and artemether on red cell and hepatic antioxidant defense system in mice infected with Plasmodium yoelii nigeriensis. Parasitol Res. 2013; 112(7):2619-2625.

Noedl H, Se Y, Sriwichai S, Schaecher K, Teja-Isavadharm P, et al. Artemisinin Resistance in Cambodia: A Clinical Trial Designed to Address an Emerging Problem in Southeast Asia. Clin Infect Dis. 2010; 51:e82-e89.

Olliaro PL, Trigg PI. Status of anti-malarial drugs under development. Bull World Health Organ. 1995; 73:565-571.

Ohrt C, Li Q, Obaldia N, Im-erbsin R, Xie L, Berman J. Efficacy of intravenous methylene blue, intravenous artesunate, and their combination in preclinical models of malaria. Malar J. 2014; 13:415.

Pascual A, Henry M, Briolant S, et al. In Vitro Activity of Proveblue (Methylene Blue) on Plasmodium falciparum Strains Resistant to Standard Anti-malarial Drugs. Antimicrob Agents Chemother. 2011; 55(5):2472-2474.

Peter C, Hongwan D, Küpfer A, Lauterburg BH. Pharmacokinetics and organ distribution of intravenous and oral methylene blue. Eur J Clin Pharmacol. 2000; 56(3):247-250.

Rooney W. Dynamics of multi-drug resistance in Plasmodium falciparum in Thailand. Southeast Asian J Trop Med Public Health. 1992; 23(Suppl 4):131-137.

Sabchareon A, Attanath P, Chanthavanich P, Phanuaksook P, Prarinyanupharb V, Poonpanich Y, Mookmanee D, Teja-Isavadharm P, Heppner DG, Brewer TG, Chongsuphajaisiddhi T. Comparative clinical trial of artesunate suppositories and oral artesunate in combination with mefloquine in the treatment of children with acute falciparum malaria. Am J Trop Med Hyg. 1998; 58(1):11-16.

SEAQUAMAT group. Artesunate versus quinine for treatment of severe falciparum malaria: a randomised trial. Lancet. 2005; 366:717-725.

Sermwittayawong N, Nishibuchi M, Sawangjaroen N, Vuddhakul V. Characterization of malaria infection at two border areas of Thailand adjoining with Myanmar and Malaysia. Southeast Asian J Trop Med Public Health. 2015; 46(4):551-557.

Stevenson MM, Gros P, Olivier M, Fortin A, Serghides L. Cerebral malaria: human versus mouse studies. Trends Parasitol. 2010; 26:274-275.

Suwanarusk R, Russell B, Ong A, Sriprawat K, Chu CS, PyaePhyo A, Malleret B, Nosten F, Renia L. Methylene blue inhibits the asexual development of vivax malaria parasites from a region of increasing chloroquine resistance. J Antimicrob Chemother. 2015; 70(1):124-129.

Urolene Blue label http://www.drugs.com/mmx/urolene-blue.html. Accessed August 28, 2016.

Vennerstrom JL, Makler MT, Angerhofer CK and Williams JA. Anti-malarial Dyes Revisited: Xanthenes, Azines, Oxazines, and Thiazines. Antimicrob Agents Chemother. 1995, 39(12):2671-2677.

Verdrager J. Epidemiology of the emergence and spread of drug-resistant falciparum malaria in South-East Asia and Australasia. J Trop Med Hyg. 1986; 89(6):277-289.

Walter-Sack I, Rengelshausen J, Oberwittler H, Burhenne J, Mueller O, Meissner P, Mikus G. High absolute bioavailability of methylene blue given as an aqueous oral formulation. Eur J Clin Pharmacol. 2009; 65(2):179-189.

White NJ, Turner GDH, Medana IM, Dondorp AM, Day NP. The murine cerebral malaria phenomenon. Trends Parasitol. 2010; 26:11-15.

Wirjanata G, Sebayang BF, Chalfein F, Prayoga, Handayuni I, Trianty L, Kenangalem E, Noviyanti R, Campo B, Poespoprodjo JR, Möhrle JJ, Price RN, Marfurt J. Potent Ex Vivo Activity of Naphthoquine and Methylene Blue against Drug-Resistant Clinical Isolates of Plasmodium falciparum and Plasmodium vivax. Antimicrob Agents Chemother. 2015; 59(10):6117-6124.

WHO. World Malaria Report. Geneva: World Health Organization; 2014.

Wongsrichanalai C. Rapid diagnostic techniques for malaria control**.** Trends Parasitol. 2001; 17(7):307-309.

Yusim Y, Livingstone D, Sidi A. Blue dyes, blue people: the systemic effects of blue dyes when administered via different routes. J Clin Anesthesia. 2007;19:315-321.

Zoungrana A, Coulibaly B, Sié A, Walter-Sack I, Mockenhaupt FP, Kouyaté B, Schirmer RH, Klose C, Mansmann U, Meissner P, Müller O. Safety and efficacy of methylene blue combined with artesunate or amodiaquine for uncomplicated falciparum malaria: a randomized controlled trial from Burkina Faso. PLoS One. 2008; 3(2):e1630.

Chapter 8: Discussion

Aikawa M, Iseki M, Barnwell JW, Taylor D, Oo MM, Howard RJ. The pathology of human cerebral malaria. Am J Trop Med Hyg. 1990; 43(2 Pt 2):30–37.

Aikawa M, Brown A, Smith CD, Tegoshi T, Howard RJ, Hasler TH, Ito Y, Perry G, Collins WE, Webster K. A primate model for human cerebral malaria: Plasmodium coatneyi-infected rhesus monkeys. Am J Trop Med Hyg. 1992; 46(4):391-397.

Aikawa M, Brown AE, Smith CD, Tegoshi T, Howard RJ, Hasler TH, Ito Y, Collins WE, Webster HK. Plasmodium coatneyi-infected rhesus monkeys: a primate model for human cerebral malaria. Mem Inst Oswaldo Cruz. 1992; 87(Suppl 3):443-447.

Ashley E.A, Dhorda M, Fairhurst R.M, Amaratunga C, Lim P, Suon S, Sreng S, Anderson J.M, Mao S, Sam B, Sopha C, Chuor C.M, Nguon C, et al. Spread of Artemisinin Resistance in Plasmodium falciparum Malaria. N Engl J Med. 2014; 371(5):411-423.

Avril M, Bernabeu M, Benjamin M, Brazier AJ, Smith JD. Interaction between Endothelial Protein C Receptor and Intercellular Adehsion Molecule 1 to Mediate Binding of Plasmodium falciparum Infected Erythrocytes to Endothelial Cells. MBio. 2016; 7(4):e00615-16.

Bach O, Baier M, Pullwitt A, et al. Falciparum malaria after splenectomy: a prospective controlled study of 33 previously splenectomized Malawian adults. Trans R Soc Trop Med Hyg. 2005; 99(11):861-867.

Beare NAV, Taylor TE, Harding SP, Lewallen S, Molyneux ME. Malarial retinopathy: A newly established diagnostic sign in severe malaria. Am J Trop Med Hyg. 2006; 75(5):790-797.

Buffet PA, Safeukui I, Deplaine G, et al. The pathogenesis of Plasmodium falciparum malaria in humans: insights from splenic physiology. Blood. 2011; 117(2):381-392.

Bull PC, Marsh K. The role of antibodies to Plasmodium falciparum–infected erythrocyte surface antigens in naturally acquired immunity to malaria. Trends Microbiol. 2002; 10(2):55–58.

Casals-Pascual C, Kai O, Lowe B, English M, Williams TN, Maitland K, Newton CR, Peshu N, Roberts DJ. Lactate levels in severe malarial anaemia are associated with haemozoin-containing neutrophils and low levels of IL-12. Malar J. 2006; 5:101.

Chalifoux LV, Bronson RT, Sehgal P, Blake BJ, King NW: Nephritis and hemolytic anemia in owl monkeys (Aotus trivirgatus). Vet Pathol. 1981; 18 (Suppl 6):23-37.

Champoux MK, Kriete F, Higley JD, Suomi SJ. CBC and serum chemistry differences between Indian-derived and Chinese–Indian hybrid rhesus monkey infants. Am J Primatol. 1996; 39:79–84.

Ching S, Liberman MY, Chemali JJ, Westover MB, Kenny JD, Solt K, Purdon PL, Brown EN. Real-time closed-loop control in a rodent model of medically induced coma using burst suppression. Anesthesiology. 2013; 119(4):848-860.

Chotivanich K, Udomsangpetch R, McGready R, et al. Central role of the spleen in malaria parasite clearance. J Infect Dis. 2002; 185(10):1538-1541.

Church DM, Goodstadt L, Hillier LW, Zody MC, Goldstein S, She X, et al. Lineage-Specific Biology Revealed by a Finished Genome Assembly of the Mouse. PLoS Biol. 2009; 7(5):e1000112.

Clark H, Tomlinson W. The pathological anatomy of malaria. In: Boyd MF. ed. Malariology. WB Saunders: Philadelphia, Pp. 874-903; 1949.

Costenaro P, Benedetti P, Facchin C, Mengoli C, Pellizzer G Fatal Myocarditis in Course of Plasmodium falciparum Infection: Case Report and Review of Cardiac Complications in Malaria. Case Rep Med. 2011; 2011:202083.

Craig AG, Grau GE, Janse C, et al. The Role of Animal Models for Research on Severe Malaria. Rall GF, ed. PLoS Pathogens. 2012; 8(2):e1002401.

Davis TM, Brown AE, Smith CD. Metabolic disturbances in Plasmodium coatneyi-infected rhesus monkeys. Int J Parasitol.1993; 23:557-563.

Davison BB, Cogswell FB, Baskin GB, Falkenstein KP, Henson EW, Tarantal AF, Krogstad DJ. Plasmodium coatneyi in the rhesus monkey (Macaca mulatta) as a model of malaria in pregnancy. Am J Trop Med Hyg. 1998; 59(2):189-201.

Davison BB, Cogswell FB, Baskin GB, Falkenstein KP, Henson EW, Krogstad DJ. Placental changes associated with fetal outcome in the Plasmodium coatneyi/rhesus monkey model of malaria in pregnancy. Am J Trop Med Hyg. 2000; 63(3-4):158-173.

Day NP, Phu NH, Mai NT et al. The pathophysiologic and prognostic significance of acidosis in severe adult malaria. Crit Care Med. 2000; 28:1833–1840

de Souza JB, Hafalla JC, Riley EM, Couper KN. Cerebral malaria: why experimental murine models are required to understand the pathogenesis of disease. Parasitology. 2010; 137:755-772.

Desowitz RS, Miller LH, Buchanan RD, Yuthasastrkosol V, Permpanich B. Comparative studies on the pathology and host physiology of malarias. I. Plasmodium coatneyi. Ann Trop Med Parasitol. 1967; 61:365-374.

Desowitz RS, Miller LH, Buchanan RD, Permpanich B. The sites of deep vascular schizogony in Plasmodium coatneyi malaria. Trans R Soc Trop Med Hyg. 1969; 63(2):198-202.

Dondorp AM, Nosten F, Yi P, et al. Artemisinin resistance in Plasmodium falciparum malaria. N Engl J Med. 2009; 361:455-467.

Dondorp AM, Yeung S, White L, Nguon C, Day NP, Socheat D, von Seidlein L. Artemisinin resistance: current status and scenarios for containment. Nat Rev Microbiol. 2010; 8: 272.

Dorovini-Zis K, Schmidt K, Huynh H, et al. The Neuropathology of Fatal Cerebral Malaria in Malawian Children. Am J Pathol. 2011; 178(5):2146-2158.

Dudgeon L and Clark C. An Investigation On Fatal Cases of Pernicious Malaria Caused by Plasmodium Falciparum in Macedonia. Q J Med. 1919; 12:372-390.

Ewing J. Contribution to the pathological anatomy of malaria fever. J Exp Med 1902; 6:119-180.

Eyes DE, Dunn FL, Warren M, Guinn E. Plasmodium coatneyi from the Philippines. J Parasitol. 1963; 49:1038.

Fairhurst RM, Nayyar GM, Breman JG, Hallett R, Vennerstrom JL, Duong S, Ringwald P, Wellems TE, Plowe CV, Dondorp AM. Artemisinin-resistant malaria: research challenges, opportunities, and public health implications. Am J Trop Med Hyg. 2012; 87(2):231-241.

Galatioto S. Neuromalaria: neuropathological study of 3 cases and review of the literature. Pathologica. 1995; 87(2):121-124. (Article in Italian)

Gibbs RA, Rogers J, Katze MG, Bumgarner R, Weinstock GM, Mardis ER, Remington KA, Strausberg RL, et al (Rhesus Macaque Genome Sequencing and Analysis Consortium). Evolutionary and biomedical insights from the rhesus macaque genome. Science. 2007; 316(5822):222-234.

Gillespie SH, Crook AM, McHugh TD, Mendel CM, Meredith SK, Murray SR, Pappas F, Phillips PP, Nunn AJ; REMoxTB Consortium. Four-month moxifloxacin-based regimens for drug-sensitive tuberculosis. N Engl J Med. 2014; 371(17):1577-1587.

Gozalo A, Dagle GE, Montoya E, Weller RE, Malaga CA: Spontaneous cardiomyopathy and nephropathy in the owl monkey (Aotus sp.) in captivity. J Med Primatol.1992; 21:279-284.

Gunter C, Dhand R. Human biology by proxy. Nature. 2002; 420:509.

Gurvitch AM. Determination of the depth and reversibility of post-anoxic coma in animals. Resuscitation. 1974; 3(1):1-26.

Hagan CE. New York Times article misleads on the value of mouse models. Mo Med. 2013 May-Jun;110(3):206.

Hien TT, Turner GD, Mai NT, Phu NH, Bethell D, Blakemore WF, Cavanagh JB Dayan A, Medana I, Weller RO, Day NP, White NJ. Neuropathological assessment of artemether-treated severe malaria. Lancet. 2003; 362(9380):295-296.

Ho M. EPRC: holy grail of malaria cytoadhesion? Blood. 2014; 123(2):163-167.

Huff JL, Barry PA. B-Virus (Cercopithecine herpesvirus 1) Infection in Humans and Macaques: Potential for Zoonotic Disease. Emerg Infect Dis. 2003; 9(2):246–250.

Hunt NH, Grau GE, Engwerda C, Barnum SR, van der Heyde H, et al. Murine cerebral malaria: the whole story. Trends Parasitol. 2010; 26:272-274.

Ibiwoye MO, Howard CV, Sibbons P, Hasan M, van Velzen D. Cerebral malaria in the rhesus monkey (Macaca mulatta): observations on host pathology. J Comp Pathol. 1993; 108(3):303-310.

Idro R, Marsh K, John CC, Newton CR. Cerebral Malaria; Mechanisms of Brain Injury And Strategies For Improved Neuro-Cognitive Outcome. Pediatr Res. 2010; 68(4):267-274.

Imwong M, Dondorp AM, Nosten F, Yi P, Mungthin M, Hanchana S, Das D, Phyo AP, Lwin KM, Pukrittayakamee S, Lee SJ, Saisung S, Koecharoen K, Nguon C, Day NP, Socheat D, White NJ. Exploring the contribution of candidate genes to artemisinin resistance in Plasmodium falciparum. Antimicrob Agents Chemother. 2010; 54:2886-2892.

Imwong M, Woodrow CJ, Hendriksen IC, Veenemans J, Verhoef H, Faiz MA, Mohanty S, Mishra S, Mtover G, Gesase S, Seni A, Chhaganlal KD, Day NP, Dondorp AM, White NJ. Plasma concentration of parasite DNA as a measure of disease severity in falciparum malaria. J Infect Dis. 2015: 211(7):1128-1133.

Iseki M, Broderson JR, Pirl KG, Igarashi I, Collins WE, Aikawa M. Renal pathology in owl monkeys in Plasmodium falciparum vaccine trials. Am J Trop Med Hyg. 1990; 43(2):130-138.

Ishioka H, Ghose A, Charunwatthana P, Maude R, Plewes K, Kingston K, et al. Sequestration and Red Cell Deformability as Determinants of Hyperlactatemia in Falciparum Malaria. J Infect Dis. 2016; 213(5):788-793.

Kanthaswamy S, Smith DG. Effects of geographic origins on captive Macaca mulatta mitochondrial DNA variation. Comp Med. 2004; 54:193–201.

Kawai S, Aikawa M, Suzuki M, Matsuda H. A nonhuman primate model for severe human malaria: Plasmodium coatneyi-infected Japanese macaque (Macaca fuscata). Tokai J Exp Clin Med. 1998; 23:101-102.

Kawai S, Kano S, Suzuki M. Rosette formation by Plasmodium coatneyi-infected erythrocytes of the Japanese macaque (Macaca fuscata). Am J Trop Med Hyg. 1995; 53(3):295-299.

Kean B, Smith J. Death due to Estivo-Autumnal Malaria. Am J Trop Med Hyg. 1944; 24:317-322.

Kilejian A, Abati A, Trager W. Plasmodium falciparum and Plasmodium coatneyi: immunogenicity of "knob-like protrusions" on infected erythrocyte membranes. Exp Parasitol. 1977; 42(1):157-164.

Kochar DK, Singh P, Agarwal P, Kochar SK, Pokharna R, Sareen PK. Malarial hepatitis. J Assoc Physicians India. 2003; 51:1069-1072.

Langhorne J, Buffet P, Galinski M, Good M, Harty J, et al. The relevance of non-human primate and rodent malaria models for humans. Malar J. 2011; 10:23.

Ling B, Veasey RS, Luckay A, Penedo C, Xu K, Lifson JD et al. SIVmac pathogenesis in rhesus macaques of Chinese and Indian origin compared with primary HIV infections in humans. AIDS. 2002; 16:1489-1496.

MacPherson GG, Warrell MJ, White NJ, Looareesuwan S, Warrell DA. Human cerebral malaria: a quantitative ultrastructural analysis of parasitized erythrocyte sequestration. Am J Pathol. 1985; 119: 385-401.

Maeno Y, Brown AE, Smith CD, Tegoshi T, Toyoshima T, Ockenhouse CF, Corcoran KD, Ngampochjana M, Kyle DE, Webster HK, et al. A nonhuman primate model for human cerebral malaria: effects of artesunate (qinghaosu derivative) on rhesus monkeys experimentally infected with Plasmodium coatneyi. Am J Trop Med Hyg. 1993; 49(6):726-734.

Manning L, Rosanas-Urgell A, Laman M, et al. A histopathologic study of fatal paediatric cerebral malaria caused by mixed Plasmodium falciparum/Plasmodium vivax infections. Malar J. 2012; 11:107.

Marchiafava E, Bignami A. “On Summer-Autumnal Malaria Fever”. In: Malaria and the parasites of malaria fevers. London: The New Sydenham Society 150;1-234; 1894.

Marsh K, English M, Crawley J, Peshu N. The pathogenesis of severe malaria in African children. Ann Trop Med Parasitol. 1996; 90:395-402.

Maude RJ, Beare NA, Abu Sayeed A, Chang CC, Charunwatthana P, Faiz MA, Hossain A, Yunus EB, Hoque MG, Hasan MU, White NJ, Day NP, Dondorp AM. The spectrum of retinopathy in adults with Plasmodium falciparum malaria. Trans R Soc Trop Med Hyg 103(7): 665-671.

Medana IM, Day NP, Sachanonta N, Mai NT, Dondorp AM, Pongponratn E, Hien TT, White NJ, Turner GD. Coma in fatal adult human malaria is not caused by cerebral oedema. Malar J. 2011; 10:267.

Migot-Nabias F, Ollomo B, Dubreuil G, et al. Plasmodium coatneyi: differential clinical and immune responses of two populations of Macaca fascicularis from different origins. Exp Parasitol. 1999; 91:30-39.

Miller LH, Chien S, Usami S. Decreased deformability of Plasmodium coatneyi-infected red cells and its possible relation to cerebral malaria. Am J Trop Med Hyg. 1972; 21(2):133-137.

Misra UK, Kalita J, Prabhakar S, Chakravarty A, Kochar D, Nair PP. Cerebral malaria and bacterial meningitis. Ann Indian Acad Neur. 2011; 14(Suppl1):S35-S39.

Moreno A, Cabrera-Mora M, Garcia A, Orkin J, Strobert E, Barnwell JW, Galinski MR. Plasmodium coatneyi in rhesus macaques replicates the multisystemic dysfunction of severe malaria in humans. Infect Immun. 2013; 81(6):1889-1904.

Moreno A, García A, Cabrera-Mora M, Strobert E, Galinski MR. Disseminated intravascular coagulation complicated by peripheral gangrene in a rhesus macaque (Macaca mulatta) experimentally infected with Plasmodium coatneyi. Am J Trop Med Hyg. 2007; 76(4):648-654.

Nagatake T, Broderson JR, Tegoshi T, Collins WE, Aikawa M. Renal pathology in owl monkeys vaccinated with Plasmodium falciparum asexual blood-stage synthetic peptide antigens. Am J Trop Med Hyg. 1992; 47(5):614-620.

Nakano Y, Fujioka H, Luc KD, Rabbege JR, Todd GD, Collins WE, Aikawa M. A correlation of the sequestration rate of Plasmodium coatneyi-infected erythrocytes in cerebral and subcutaneous tissues of a rhesus monkey. Am J Trop Med Hyg. 1996; 55(3):311-314.

Noedl H, Se Y, Schaecher K, Smith BL, Socheat D, Fukuda MM. Evidence of artemisinin-resistant malaria in western Cambodia. N Engl J Med. 2008; 359:2619-2620.

Oo MM, Aikawa M, Than T, Aye TM, Myint PT, Igarashi I, Schoene WC. Human cerebral malaria: a pathological study. J Neuropathol Exp Neurol. 1987; 46(2):223-231.

Parrott T. Viral Diseases of Nonhuman Primates. In. Merck Veterinary Manual. Ed. Aiello SE. 2014. http://www.merckvetmanual.com/mvm/index.html. Accessed 24 May 2016.

Platt SR, Radaelli ST, McDonnell JJ. The prognostic value of the modified Glasgow Coma Scale in head trauma in dogs. J Vet Intern Med. 2001; 15(6):581-584.

Porta J, Carota A, Pizzolato GP, Wildi E, Widmer MC, Margairaz C, Grau GE. Immunopathological changes in human cerebral malaria. Clin Neuropathol. 1993; 12(3):142-146.

Price R, van Vugt M, Nosten F, Luxemburger C, Brockman A, Phaipun L, Chongsuphajaisiddhi T, White N. Artesunate versus artemether for the treatment of recrudescent multidrug resistant falciparum malaria. Am J Trop Med Hyg. 1998; 59:883–888.

Rowe A, Obeiro J, Newbold CI, Marsh K. Plasmodium falciparum rosetting is associated with malaria severity in Kenya. Infect Immun. 1995; 63(3):2323-2326.

Rudzinska MA, Trager W. The fine structure of trophozoites and gametocytes in Plasmodium coatneyi. J Protozool. 1968; 15(1):73-88.

Sabin AB, Wright WM Acute ascending myelitis following a monkey bite, with the isolation of a virus capable of reproducing the disease. J Exp Med. 1934; 59:115-136.

Saunders DL, Vanachayangkul P, Lon C: Dihydroartemisinin-piperaquine failure in Cambodia. New Engl J Med. 2014; 371:484-485.

Sein KK, Brown AE, Maeno Y, Smith CD, Corcoran KD, Hansukjariya P, Webster HK, Aikawa M. Sequestration pattern of parasitized erythrocytes in cerebrum, mid-brain, and cerebellum of Plasmodium coatneyi-infected rhesus monkeys (Macaca mulatta). Am J Trop Med Hyg. 1993; 49(4):513-519.

Seok J, Warren HS, Cuenca AG, Mindrinos MN, Baker HV, et al. Genomic responses in mouse models poorly mimic human inflammatory diseases. Proc Natl Acad Sci U S A. 2013; 110(9):3507-3512.

Shah S, Ali L, Sattar RA, Aziz T, Ansari T, Ara J. Malarial hepatopathy in falciparum malaria. J Coll Physicians Surg Pak. 2009; 19(6):367-370.

Sidhu AB, Uhlemann AC, Valderramos SG, Valderramos JC, Krishna S, Fidock DA. Decreasing pfmdr1 copy number in Plasmodium falciparum malaria heightens susceptibility to mefloquine, lumefantrine, halofantrine, quinine, and artemisinin. J Infect Dis. 2006; 194:528-535.

Simpson JA, Aarons L, Collins WE, Jeffery GM, White NJ. Population dynamics of untreated Plasmodium falciparum malaria within the adult human host during the expansion phase of the infection. Parasitology. 2002; 124(Pt 3):247–263.

Smith CD, Brown AE, Nakazawa S, Fujioka H, Aikawa M. Multi-organ erythrocyte sequestration and ligand expression in rhesus monkeys infected with Plasmodium coatneyi malaria. Am J Trop Med Hyg. 1996; 55(4):379-383.

Snow RW, Trape JF, Marsh K. The past, present and future of childhood malaria mortality in Africa. Trends Parasitol. 2001; 17:593-597.

SoRelle R. “DNA sequence of Rhesus macaque has evolutionary, medical implications" (Press release). Human Genome Sequencing Center. 13 April 2007. Accessed 24 May 2016

Spangler WL, Gribble D, Abildgaard C, Harrison J. Plasmodium knowlesi malaria in the Rhesus monkey. Vet Pathol. 1978; 15(1):83-91.

Spencer G. The Mouse Genome and The Measure of Man. 2002 https://www.genome.gov/page.cfm?pageID=10005831. Accessed 24 May 2016

Spitz S. Pathology of acute falciparum malaria. Military Medicine 1946; 99:555-572.

Stevenson MM, Riley EM. Innate immunity to malaria. Nat Rev Immunol. 2004; 4(3):169–180.

Su X-Z, Heatwole VM, Wertheimer SP, et al. The large diverse family var encodes proteins involved in cytoadherence and antigenic variation of Plasmodium falciparum–infected erythrocytes. Cell. 1995; 82(1):89-100

Takao K, Miyakawa T. Genomic responses in mouse models greatly mimic human inflammatory diseases. Proc Natl Acad Sci U S A. 2015 Jan 27;112(4):1167-1172.

Takao K, Hagihara H, Miyakawa T. Reply to Warren et al. and Shay et al.: Commonalities across species do exist and are potentially important. Proc Natl Acad Sci U S A. 2015; 112(4):E347-E348.

Tegoshi T, Udomsangpetch R, Brown A, Nakazawa S, Webster HK, Aikawa M. Ultrastructure of rosette formation by Plasmodium coatneyi-infected erythrocytes of rhesus. Parasitol Res. 1993; 79(7):611-613.

Toro G, Roman G. Cerebral malaria. A disseminated vasculomyelinopathy. Arch Neurol. 1978; 35(5):271-275.

Trape J. The public health impact of chloroquine resistance in Africa. Am J Trop Med Hyg. 2001; 64 (1-2 Suppl):12–17.

Trichel AM, Rajakumar PA, Murphy-Good M. Species-specific variation in SIV disease progression between Chinese and Indian subspecies of rhesus macaques. J Med Primatol. 2002; 31:171-178.

Tun KM, Imwong M, Lwin KM, Win AA, Hlaing TM, Hlaing T, Lin K, Kyaw MP, Plewes K, Faiz MA, Dhorda M, Cheah PY, Pukrittayakamee S, Ashley EA, Anderson TJ, Nair S, McDew-White M, Flegg JA, Grist EP, Guerin P, Maude RJ, Smithuis F, Dondorp AM, Day NP, Nosten F, White NJ, Woodrow CJ. Spread of artemisinin-resistant Plasmodium falciparum in Myanmar: a cross-sectional survey of the K13 molecular marker. Lancet Infect Dis. 2015; 15(4):415-421.

Turner G. Cerebral malaria. Brain Pathol. 1997; 7(1):569-582.

Udomsangpetch R, Brown AE, Smith CD, Webster HK. Rosette formation by Plasmodium coatneyi-infected red blood cells. Am J Trop Med Hyg. 1991; 44(4):399-401.

Vallender EJ, Miller GM. Nonhuman primate models in the genomic era: a paradigm shift. ILAR J. 2013; 54(2):154-165.

Warren HS, Tompkins RG, Moldawer LL, Seok J, Xu W, Mindrinos MN, Maier RV, Xiao W, Davis RW. Mice are not men. Proc Natl Acad Sci U S A. 2015; 112(4):E345.

Weller RE, Collins WE, Buschbom RL, Malaga CA, Ragan HA. Impaired renal function in owl monkeys (Aotus nancymai) infected with Plasmodium falciparum. Mem Inst Oswaldo Cruz. 1992; 87 Suppl 3:435-442.

White NJ. Can new treatment developments combat resistance in malaria? Expert Opin Pharmacother. 2016 May 18. [Epub ahead of print]

White NJ, Turner GD, Medana IM, Dondorp AM, Day NP. The murine cerebral malaria phenomenon. Trends Parasitol. 2010; 26:11–15.

Whitten R, Milner DA, Yeh MM, Kamiza S, Molyneux ME, Taylor TE. Liver pathology in Malawian children with fatal encephalopathy. Hum Pathol. 2011; 42:1230-1239.

Winzeler EA, Manary MJ. Drug resistance genomics of the anti-malarial drug artemisinin. Genome Biol. 2014; 15(11):544.

World Health Organization Severe falciparum malaria. World Health Organization, communicable diseases cluster. Trans R Soc Trop Med Hyg. 2000; 94:S1-90.

World Health Organization 2014. Tropical Medicine and International Health, John Wiley & Sons., 19 (Suppl. 1), pp. 7-131; 2014.

World Health Organization. Guidelines for the treatment of malaria. Geneva; 2015.

Wongsrichanalai C, Sirichaisinthop J, Karwacki JJ, Congpuong K, Miller RS, Pang L, Thimasarn K. Drug resistant malaria on the Thai-Myanmar and Thai-Cambodian borders. Southeast Asian J Trop Med Public Health. 2001; 32(1):41-49.